Ontario
Ministry of
Northern Development
and Mines

Mines and
Minerals
Division

Geoscience Research Grant Program
Summary of Research
1987-1988

Ontario Geological Survey
Miscellaneous Paper 140

edited by
V.G. Milne

1988

89-02301/

©Queen's Printer for Ontario, 1988
ISSN 0704-2752 (Series)
Printed in Ontario, Canada
ISSN 0225-5316 (Sub-series)

Publications of the Ontario Geological Survey, Ministry of Northern Development and Mines, are available from the following sources. Orders for publications should be accompanied by cheque or money order payable to the *Treasurer of Ontario.*

Reports, maps, and price lists (personal shopping or mail order):

Public Information Centre, Ministry of Natural Resources
Room 1640, Whitney Block, Queen's Park
Toronto, Ontario M7A 1W3

Reports and accompanying maps only (personal shopping):

Ontario Government Bookstore
Main Floor, 880 Bay Street
Toronto, Ontario M7A 1N8

Reports and accompanying maps (mail order or telephone orders):

Publications Services Section, Ministry of Government Services
5th Floor, 880 Bay Street
Toronto, Ontario M7A 1N8
Telephone (local calls) 965-6015
Toll-free long distance 1-800-268-7540
Toll-free from Area Code 807 0-ZENITH-67200

Every possible effort is made to ensure the accuracy of the information contained in this report, but the Ministry of Northern Development and Mines does not assume any liability for errors that may occur. Source references are included in the report and users may wish to verify critical information.

Parts of this publication may be quoted if credit is given. It is recommended that reference be made in the following form:

Moritz, R.P., Crocket, J.H., and Dickin, A.P.
1988: Lead Isotope Study of Gold Mineralization in the Dome Mine Quartz-Fuchsite Vein; Grant 280, p.56-67 *in* Geoscience Research Grant Program, Summary of Research, 1987-1988, edited by V.G. Milne, Ontario Geological Survey, Miscellaneous Paper 140, 251p.

If you wish to reproduce any of the text, tables or illustrations in this report, please write for permission to the Director, Ontario Geological Survey, Ministry of Northern Development and Mines, 11th floor, 77 Grenville Street, Toronto, Ontario, M7A 1W4.

Scientific Editors: Sally Elliott-Meadows and Bojan Sifrer
1000-88-Maracle

Contents

Introductory Remarks, *V.G. Milne* 2

Grant 225—Genesis of Pegmatites in the Quetico Gneiss Belt of Northwestern Ontario—Pegmatites and Associated Granitoids of the Pine Portage Area, *S.A. Kissin and D.L. Archibald* 4

Grant 249—Geochemical Studies of Formation Waters, Southwestern Ontario, Canada, and Southern Michigan, U.S.A., *P. Dollar, S.K. Frape, R.H. McNutt, P. Fritz, and R.W. Macqueen* 14

Grant 265A—Mineralogy and Surface Chemistry of Iron Oxides Associated with Bacteria in Acidic Sediments, *F.G. Ferris, K. Tazaki, and W.S. Fyfe* 29

Grant 265B—Retardation of Toxic Heavy Metal Dispersion From U, and Cu-Ni Mine Tailings, Elliot Lake and Sudbury Districts, Ontario: Role of Acidophilic Microorganisms, *H. Mann, K. Tazaki, W.S. Fyfe, and M. Wiseman* 34

Grant 275—Deformation of the Sudbury Structure, *W.S. Shanks and W.M. Schwerdtner* 46

Grant 280—Lead Isotope Study of Gold Mineralization in the Dome Mine Quartz-Fuchsite Vein, *R.P. Moritz, J.H. Crocket, and A.P. Dickin* 56

Grant 286—The Geochemistry, Origin, and Economic Potential of Platinum Group Element Bearing Rocks of the Lac Des Iles Complex, Northwestern Ontario, *J.M. Sweeny and A.D. Edgar* 68

Grant 288—Petrogenesis of Archean Trondhjemite-Tonalite-Granodiorite (TTG) Intrusions and Their Relationships to Gold Mineralization, Renabie and Magino Areas, Wawa, *R.A. Jemielita, N.J. Callan, and E.T.C. Spooner* 78

Grant 290—Maximal Simplicity Gravity Interpretation with Continuous Density Models, *R.C. Bailey and S.W. Reford* 94

Grant 291—Evaluation of Geobotanical Remote Sensing as an Aid to Mineral Exploration in Northeastern Ontario, *A.E. Beswick, P.J. Beckett, G.M. Courtin, and G.O. Tapper* 103

Grant 294—Quaternary Geology and Geochemical Exploration in the Matheson Area, *M.B. McClenaghan, O.P. Lavin, I. Nichol, and J. Shaw* 112

Grant 295—Karst Episodes and Permeability Development, Silurian Reef Reservoirs, Ontario, *L. Smith, D.J. Grimes, and S. Charbonneau* 124

Grant 298—The Geological Setting of Gold Deposits in the Porcupine Mining Camp, *R. Mason, D.I. Brisbin, and S. Aitken* 133

Grant 300—The Genesis of Silver Vein Deposits in the Thunder Bay Area, Northwestern Ontario, *S.A. Kissin and T.C. McCuaig* 146

Grant 301—Computer Software for Micro-PIXE Analysis of Mineralogical Specimens, *J.L. Campbell, J.A. Maxwell, and W.J. Teesdale* 157

Grant 305—Metamorphic Petrology of the White River Gold Prospect, Hemlo Area, Ontario, *Y. Pan and M.E. Fleet* 164

Grant 307—Light Minerals and Specialty Sand in Southern Ontario, *J.W. Butler and S.R. Hicock* 177

Grant 310—Application of Surface Radar Sounding Techniques in Peatland Inventories, Southern Ontario: Preliminary Results, *B.G. Warner and D.C. Nobes* 182

Grant 312—Subsurface Quaternary Stratigraphy Using Borehole Geophysics, *P.F. Karrow, J.P. Greenhouse, and M.B. Dusseault* 188

Grant 313—Magmatic-Hydrothermal and Wall Rock Alteration Petrology at the Lake Shore Gold Deposit, Kirkland Lake, Ontario, *K.D. Hicks and K. Hattori* 192

Grant 316—Placer Formation in Braided River Systems, *J.P. Burton and P.W. Fralick* 205

Grant 319—Gypsum Deposits of Southern Ontario, *S.J. Haynes, R. Boland, and J. Hughes-Pearl* 217

Grant 322—Physical and Chemical Processes of Archean Subaqueous Pyroclastic Rocks, *J. Stix and M.P. Gorton* 231

Grant 323—Lithogeochemistry and Light Stable Isotope (Carbon, Oxygen, and Sulphur) Geochemistry of Hydrothermal Alteration and Breccia Veins from the Cameron Lake Gold Deposit, Northwestern Ontario, *D.R. Melling, R.P. Taylor, and D.H. Watkinson* 239

CONVERSION FACTORS FOR MEASUREMENTS IN ONTARIO GEOLOGICAL SURVEY PUBLICATIONS.

CONVERSION FROM SI TO IMPERIAL			CONVERSION FROM IMPERIAL TO SI		
SI Unit	*Multiplied by*	*Gives*	*Imperial Unit*	*Multiplied by*	*Gives*
			LENGTH		
1 mm	0.039 37	inches	1 inch	**25.4**	mm
1 cm	0.393 70	inches	1 inch	**2.54**	cm
1 m	3.280 84	feet	1 foot	**0.304 8**	m
1 m	0.049 709 7	chains	1 chain	20.116 8	m
1 km	0.621 371	miles (statute)	1 mile (statute)	**1.609 344**	km
			AREA		
1 cm^2	0.155 0	square inches	1 square inch	**6.451 6**	cm^2
1 m^2	10.763 9	square feet	1 square foot	**0.092 903 04**	m^2
1 km^2	0.386 10	square miles	1 square mile	2.589 988	km^2
1 ha	2.471 054	acres	1 acre	0.404 685 6	ha
			VOLUME		
1 cm^3	0.061 02	cubic inches	1 cubic inch	**16.387 064**	cm^3
1 m^3	35.314 7	cubic feet	1 cubic foot	0.028 316 85	m^3
1 m^3	1.308 0	cubic yards	1 cubic yard	0.764 555	m^3
			CAPACITY		
1 L	1.759 755	pints	1 pint	0.568 261	L
1 L	0.879 877	quarts	1 quart	1.136 522	L
1 L	0.219 969	gallons	1 gallon	**4.546 090**	L
			MASS		
1 g	0.035 273 96	ounces (avdp)	1 ounce (avdp)	28.349 523	g
1 g	0.032 150 75	ounces (troy)	1 ounce (troy)	**31.103 476 8**	g
1 kg	2.204 62	pounds (avdp)	1 pound (avdp)	**0.453 592 37**	kg
1 kg	0.001 102 3	tons (short)	1 ton (short)	**907.184 74**	kg
1 t	1.103 311	tons (short)	1 ton (short)	**0.907 184 74**	t
1 kg	0.000 984 21	tons (long)	1 ton (long)	**1016.046 908 8**	kg
1 t	0.984 206 5	tons (long)	1 ton (long)	**1.016 046 908 8**	t
			CONCENTRATION		
1 g/t	0.029 166 6	ounce (troy)/ ton (short)	1 ounce (troy)/ ton (short)	34.285 714 2	g/t
1 g/t	0.583 333 33	pennyweights/ ton (short)	1 pennyweight/ ton (short)	1.714 285 7	g/t

OTHER USEFUL CONVERSION FACTORS

1 ounce (troy) per ton (short)	20.0	pennyweights per ton (short)
1 pennyweight perton (short)	0.05	ounces (troy) per ton (short)

Note. Conversion factors which are in bold type are exact. The conversion factors have been taken from or have been derived from factors given in the Metric Practice Guide for the Canadian Mining and Metallurgical Industries, published by the Mining Association of Canada in cooperation with the Coal Association of Canada.

Geoscience Research Grant Program
Summary of Research 1987-1988

---

edited by
V.G. Milne

Director, Ontario Geological Survey

INTRODUCTORY REMARKS

The Ontario Geoscience Research Grants Program was initiated in 1978 to encourage geoscience research at Ontario universities. By supporting mission-oriented geological projects, a program of research was established which would complement the work of the Ontario Geological Survey through its mandate:

> To stimulate exploration for, and facilitate sound planning in, all matters related to mineral and other earth resources by providing an inventory and analysis of the geology and mineral deposits of Ontario.

The program supports applied studies of up to three years duration towards: mineral deposit characterization involving studies of specific occurrences or groups of occurrences within Ontario; petrology, rock geochemistry, structural geology, stratigraphy, and geochronology studies; field and laboratory studies leading to the development of new geophysical or geochemical concepts and techniques; engineering and environmental geology studies; and methods for improving automated or manual processing, and facilitating the interpretation of geoscience data.

In order to receive funding, applications must be forwarded to the Ontario Geological Survey by November 15. Project proposals are subject to review by a committee which reports to the Director of the Ontario Geological Survey. This committee advises the Minister of Northern Development and Mines concerning geoscience research priorities at Ontario universities and of the scientific merit and relevance of proposals submitted to the Ontario Geoscience Research Grants Program. The committee consists of three representatives from the minerals industry, three representatives from the university community, four representatives from the Ontario Geological Survey, and a chairman from either industry or a university. Members of the 1987-88 committee include:

Dr. D.J. Misener, Chairman; Paterson, Grant and Watson Limited

Mr. C.L. Baker; Ontario Geological Survey

Dr. A.E. Beswick; Laurentian University

Dr. G. Cargill; Utah Mines Ltd

Dr. M. E. Cherry; Ontario Geological Survey

Dr. W. Coker; Geological Survey of Canada

Dr. J.E. Hanneson; Ontario Geological Survey

Dr. J. Legault; University of Waterloo

Dr. R. Mitchell; Lakehead University

Dr. H. Wallace; Ontario Geological Survey

Successful grant recipients are expected to submit reports for publication in the annual Summary of Research and participate in the Mines and Minerals Symposium held annually in December.

Publication in other scientific journals is encouraged and a final report summarizing the research will be released as an Ontario Geological Survey Open File Report. Open File Reports concerning the Ontario Geoscience Research Grant Program are released from time to time and are available at the Mines Library, 77 Grenville Street, Toronto, or at Ministry of Northern Development and Mines regional offices. The following research projects partially or wholly funded by this Program during 1987-88 are due for release as Open File Reports (only principal applicant's name listed):

Grant 249: Geochemical Studies of Formation Waters and Diagenetic Cements, Paleozoic Strata, Southwestern Ontario; S.K. Frape, Universtiy of Waterloo.

Grant 265: Metal Accumulation in Microorganisms with Emphasis on U-Au-Ag-Cu-Zn-Fe; W.S. Fyfe, University of Western Ontario.

Grant 286: The Geochemistry, Origin, and Economic Potential of Platinum Group Element Bearing Rocks of the Lac des Iles Intrusion, Northwestern Ontario; A.D. Edgar, University of Western Ontario.

Grant 301: Software Development for Micro-PIXIE Analysis of Mineralogical Specimens; J.L. Campbell, University of Guelph.

Grant 312: Subsurface Quaternary Stratigraphy Using Borehole Geophysics; P.F. Karrow, University of Waterloo.

Grant 316: Placer Formation in Braided River Systems; P.W. Fralick, Lakehead University.

During 1987-88, 25 projects were funded under the program. Of these, 13 were renewal projects.

University	Value of Grants	No. of Grants
Brock	$15,930.00	1
Carleton	24,850.00	1
Lakehead	2,950.00	1
Laurentian	14,950.00	1
McMaster	69,515.00	4
Ottawa	23,040.00	1
Queen's	165,838.00	6
Toronto	80,704.00	4
Waterloo	29,347.00	2
Western	72,876.00	4
TOTAL	$500,000.00	25

The undersigned would like to thank Dr. D.J. Misener, who acted as Committee Chairman, and the Review Committee Members who gave freely of their time. The efforts of the researchers are of course fundamental and are acknowledged. The following people are also acknowledged for their participation in producing this volume; R.L.W. McKnight, who served as Grants Administrator and Secretary to the Committee, staff geologists who reviewed the papers, and Sally Elliott-Meadows, Bojan Sifrer, Tammy Hoey, and Ron Steenstra, who acted as scientific editors for this publication.

V.G. Milne

Director

Ontario Geological Survey

Grant 225 Genesis of Pegmatites in the Quetico Gneiss Belt of Northwestern Ontario—Pegmatites and Associated Granitoids of the Pine Portage Area

S.A. Kissin and D.L. Archibald

Department of Geology, Lakehead University, Thunder Bay

ABSTRACT

The Pine Portage area lies at the southern end of Lake Nipigon where Archean rocks of the Quetico Gneiss Belt are exposed in a window in Proterozoic cover rocks. Granitoids constitute the Pine Portage Intrusion, which consists of two-mica leucogranites displaying the characteristics of peraluminous S-type granites. Tonalitic sills or dikes and northeast-striking simple pegmatite dikes cut the leucogranites. Some 2 to 3 km to the east of the Pine Portage Intrusion, rare-element pegmatites cut metasediments in northeast-striking dikes. The muscovite and perthitic microcline of the simple pegmatites and the perthitic microcline and Ta-Nb oxide minerals of the rare-element pegmatites were analyzed for evaluation of fractionation trends. The simple and rare-element pegmatites appear to lie on a trend of increasing fractionation, implying that the latter were derived from the former. The two-mica leucogranites appear to be parental to the rare-element pegmatites as well as to the simple pegmatites, as evidenced by extensive fractionation in terms of high K/Ba, Ba/Sr, and Rb/Sr ratios, and low K/Rb, Ba/Rb, and Mg/Li ratios. The tonalitic dikes or sills may be A-type granitoids emplaced late in the intrusive history of the area.

INTRODUCTION

The Pine Portage rare-element pegmatite field lies within a window in Proterozoic diabase sills, exposing Archean granitoids and metasediments along the east and west sides of Forgan Lake, an arm of Lake Nipigon (Figure 225.1). A granitic pluton on the west side of Forgan Lake is in contact with overlying diabase and metasediments. These contacts were more precisely located during the course of the past year's field studies. While simple pegmatites occur within the granitic intrusion, rare-element pegmatites occur on the east side of Forgan Lake, where they intrude metasediments.

The Pine Portage area was mapped by Pye (1965) and the field relationships of the pegmatites described. The objective of this year's work was to supply additional information on the geochemistry and petrology of the pegmatites, and to investigate their possible relationship to granitic rocks of the area and to the Georgia Lake Pegmatite Field lying to the east (Kissin and Zayachkivsky 1985; Kissin *et al.* 1986).

METHODOLOGY

Whereas whole rock analysis is adequate for the homogeneous granitoids, separate analyses of pegmatite alkali feldspar, muscovite, and Ta-Nb oxide minerals were carried out due to pegmatite inhomogeneity. Granitoids were analyzed for SiO_2, Al_2O_3, TiO_2, K_2O, CaO, MgO, total iron as Fe_2O_3, Rb, Sr, Zr, Y, and Ba by X-ray fluorescence spectrometry (XRF). FeO was determined by titration, and MnO, Na_2O, Pb, and Li were determined by atomic absorption spectrophotometry (AA). P_2O_5 was determined by ultraviolet spectrophotometry, and CO_2 and H_2O were determined on a carbon hydrogen-nitrogen analyzer (CHN).

AA was used in the partial analysis of perthitic microcline for K_2O, CaO, Na_2O, Li, and Pb, and in the partial analysis of muscovite for Na_2O and Li. Rb, Sr, and Ba in perthitic microcline, and K_2O, CaO, MgO, and total iron as FeO in muscovite were determined by XRF. Rb in muscovite was determined by inductively coupled argon plasma emission spectroscopy techniques, using dissolutions from the AA analyses. Sr analyses were corrected for radiogenic Sr using a method devised by Clark and Cerny (1987).

Analyses of the Ta-Nb oxide minerals were determined on a Hitachi scanning electron microscope with a Tracor Northern TN2000 energy dispersive analyzer (SEM-EDA). The standardless software routine SQ from Tracor Northern program 5502 was utilized in obtaining analyses, which were automatically normalized to near 100 percent. Complete details of all analytical procedures are given by Archibald (1987).

GRANITOIDS

GEOLOGICAL SETTING

The granitoids of the Pine Portage area constitute the Pine Portage Intrusion of McCrank *et al.* (1981). The northern and southeastern margins of the intrusion are delineated by sharp contacts with Quetico metasediments. Extrapolation of the southeastern contact beneath Forgan Lake suggests that the eastern margin of the intrusion does not lie far from the western shore of Forgan Lake (Figure 225.1). The granitoids are covered to the west and southwest by Proterozoic diabases, but mapping some 4 km to the south by Coates (1972) indicates the presence of metasediments at the southern margin of the diabase sill. Therefore, while the Pine Portage Intrusion may extend a considerable distance to the west beneath diabase, its southern extent is constrained.

Near the northern margin of the Pine Portage Intrusion is a zone of tonalite, contrasting with the leucogranites of the remainder of the intrusion. Although the contact between the tonalite and leucogranites is not exposed, the occurrence of the tonalites in a linear east-trending zone suggests that they are tabular hypabyssal intrusions similar to the tonalites of the Georgia Lake area (Kissin and Zayachkivsky 1985).

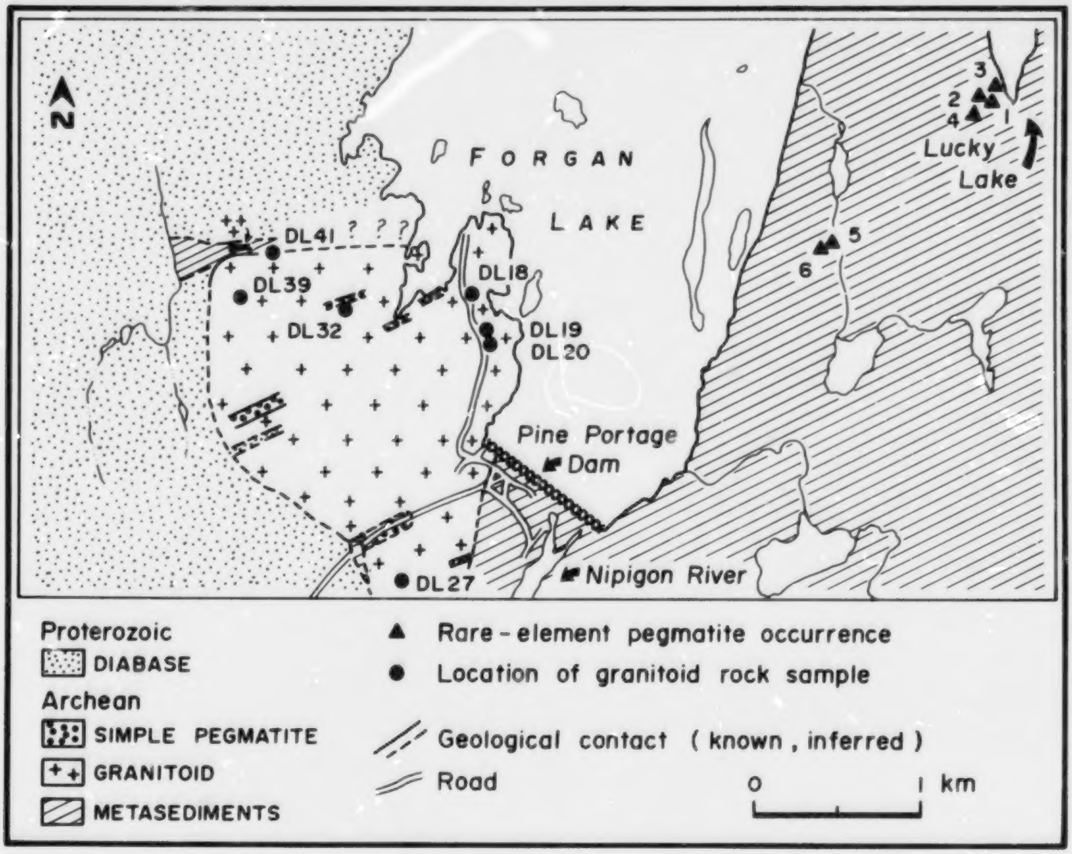
N
FORGAN
LAKE
Lucky Lake
1
2
3
4
5
6
DL41
? ? ?
DL39
DL32
DL18
DL19
DL20
Pine Portage Dam
Nipigon River
DL27
Proterozoic
DIABASE
Archean
SIMPLE PEGMATITE
GRANITOID
METASEDIMENTS
▲ Rare-element pegmatite occurrence
● Location of granitoid rock sample
Geological contact (known , inferred)
Road
0
1 km

Figure 225.1. The Pine Portage area showing the regional geology of the study area and the granitoid rock sample locations.

PETROGRAPHY

The major exposed portion of the Pine Portage Intrusion consists of homogeneous two-mica leucogranites of medium grain size. Accessory minerals are absent except for traces of apatite and garnet crystals up to 1 mm in diameter, which occur at locality DL18 (Figure 225.1). The muscovite to biotite ratio in the leucogranites appears to be at a maximum in the north, and decreases to the south.

The tonalites are leucotonalites (trondhjemites), which generally contain both biotite and muscovite, the former predominating. Apatite is a ubiquitous accessory mineral. The texture of the rock varies from equigranular to porphyritic.

GEOCHEMISTRY

Whole rock major and trace element analyses from sample locations indicated in Figure 225.1 are given in Table 225.1. The data support the distinction made on petrographical grounds between the two-mica leucogranites and the tonalites in that both major and trace elements differ significantly in many respects. However, both rock types have normative corundum >1 percent and $Al_2O_3/(CaO+Na_2O+K_2O)$ (A/CNK) ratios ≥1.1, both indicators of peraluminous S-type granitoids (Chappel 1978; Hine *et al.* 1978). The two-mica leucogranites have significantly higher normative corundum and A/CNK ratios than the tonalites, in most cases. The two-mica leucogranites are enriched in Rb and depleted in Sr, Ba, and Zr with respect to the tonalites, yielding high K/Ba, Ba/Sr, and Rb/Sr ratios and low K/Rb and Ba/Rb ratios. These abundance patterns suggest that the two-mica leucogranites may be parental to the rare-element pegmatites according to criteria established by Goad and Cerny (1981) and Trueman and Cerny (1982). The one element that fails to conform to this pattern is Li, which is anomalously low in the two-mica leucogranites. Based on the small area sampled and the limited number of samples, little significant difference in degree of fractionation is apparent within the two-mica leucogranites and the tonalites.

PEGMATITES

GEOLOGICAL SETTING

The pegmatites of the Pine Portage area are of two types: simple pegmatites, which occur within the Pine Portage Intrusion; and rare-element pegmatites, which

TABLE 225.1. ANALYSIS OF PINE PORTAGE GRANITOIDS.

	leucogranites				tonalites		
Sample	**DL18**	**DL19**	**DL20**	**DL27**	**DL32**	**DL39**	**DL41**
SiO_2(wt.%)	73.70	75.63	72.78	73.86	71.05	72.71	73.07
TiO_2	≤0.01	≤0.01	≤0.01	≤0.01	≤0.01	≤0.01	≤0.01
Al_2O_3	14.91	14.68	15.06	15.22	17.21	16.85	16.13
Fe_2O_3	0.76	0.64	1.06	1.09	0.32	0.32	0.65
FeO	0.17	0.13	0.17	0.15	0.49	0.33	0.25
MnO	0.01	0.00	0.01	0.00	0.19	0.01	0.01
MgO	0.00	0.00	0.00	0.00	0.19	0.09	0.00
CaO	0.25	0.20	0.00	0.17	2.38	1.30	1.70
Na_2O	4.29	4.50	2.64	4.30	5.63	5.74	5.71
K_2O	4.36	3.07	7.77	4.43	1.59	1.60	1.50
P_2O_5	0.55	0.40	0.21	0.00	0.12	0.12	0.09
CO_2	0.34	0.57	0.34	0.34	0.23	0.11	0.68
H_2O	0.45	0.45	0.45	0.36	0.45	0.45	0.36
Total	99.79	100.27	100.04	99.92	99.67	99.63	100.15
FeO/Fe_2O_3	0.22	0.20	0.16	0.14	1.53	1.03	0.38
A/(CNK)*	1.22	1.32	1.18	1.25	1.12	1.25	1.14
c**	4.03	4.58	2.82	3.07	2.21	3.63	2.26
Pb(ppm)	94	59	69	54	65	62	62
Li	3.6	3.6	2.2	4.0	87	61	44
Rb	214	177	379	279	44	77	41
Sr	≤5	≤5	≤5	≤5	577	410	424
Ba	251	436	276	0.13	620	767	751
Zr	≤3	≤3	≤3	≤3	65	27	9
Y	≤3	≤3	≤3	≤3	2	≤3	≤3
K/Rb	84.6	72.0	85.1	65.9	150.0	86.2	151.8
K/Ba	72.1	29.2	116.8	-	10.7	8.7	8.3
K/Sr	-	-	-	-	11.4	16.2	14.7
Ba/Rb	1.2	2.5	0.73	-	1.1	1.9	1.8
Ba/Sr	-	87.2	-	-	0.1	0.2	0.1
Rb/Sr	-	35.4	-	-	0.0	0.2	0.1
Mg/L1	0.0	0.00	0.00	0.00	21.8	14.8	0.0

*A/(CNK) = $Al_2O_3/(CaO + Na_2O + K_2O)$

**c = normative corundum

+ Corrected for the presence of radiogenic Sr

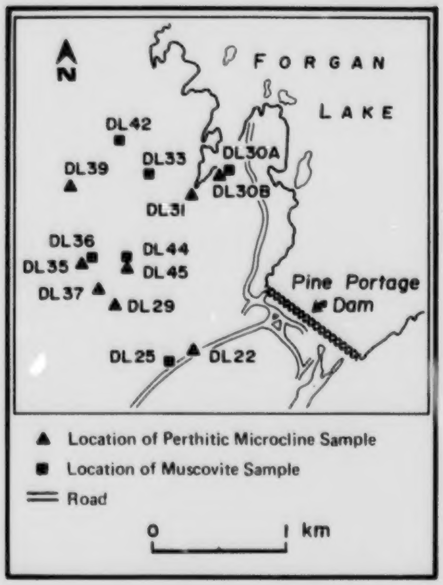
N
FORGAN
LAKE
DL42
DL39
DL33
DL30A
DL30B
DL31
DL36
DL35
DL44
DL45
DL37
DL29
Pine Portage
Dam
DL25
DL22
▲ Location of Perthitic Microcline Sample
■ Location of Muscovite Sample
═ Road
0
1 km

Figure 225.2. *Sample locations for simple pegmatites within the Pine Portage Intrusion (cf. Figure 225.1).*

are hosted in metasediments and lie 2 to 3 km to the east of the Pine Portage Intrusion (Figure 225.1). All of the pegmatites occur as near-vertical dikes which strike in a northeasterly direction. There are 6 rare-element pegmatite dikes, but Occurrences No. 5 and 6 were not studied due to their very poor exposure.

PETROGRAPHY

The simple pegmatites are dominantly composed of blocky pink and white perthitic microcline, with lesser muscovite and quartz. The microcline occurs as euhedra with maximum dimensions in the range 2.5 to 10 cm, and muscovite is present as books up to 2 cm thick.

The rare-element pegmatites are generally similar in mineralogical constitution and contain, in order of decreasing abundance, microcline, spodumene, quartz, sucrosic albite, muscovite, and accessory amounts of Ta-Nb oxide minerals and apatite. Microcline is coarse-grained to very coarse-grained, with some individual grains exceeding 30 cm in maximum dimension. The spodumene crystals are greenish with a prismatic habit. The texture of the pegmatite is formed by poorly oriented microcline and spodumene in a matrix of microcline, quartz, and muscovite. Ta-Nb oxide minerals seem to be limited to disseminations in a sucrosic albite host. These minerals are less than 1 cm in long axis and can be easily overlooked.

GEOCHEMISTRY

The compositional characteristics of perthitic microcline from simple pegmatites (locations shown on Figure 225.2) and from rare-element pegmatites (locations shown on Figure 225.3) are given in

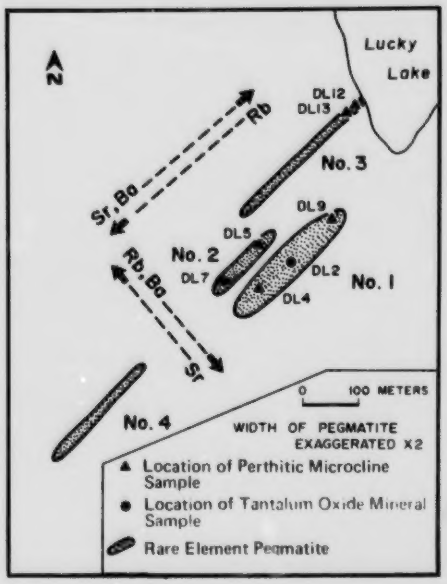
N
Lucky
Lake
DL12
DL13
Rb
Sr, Ba
No. 3
DL9
DL5
No. 2
DL7
DL2
No. 1
DL4
Rb, Ba
Sr
No. 4
0
100 METERS
WIDTH OF PEGMATITE EXAGGERATED X2
▲ Location of Perthitic Microcline Sample
● Location of Tantalum Oxide Mineral Sample
Rare Element Pegmatite

Figure 225.3. *Sample locations for rare-element pegmatites near Lucky Lake. Arrows indicate the directions of increasing Sr, Rb, and Ba concentrations in perthitic microcline.*

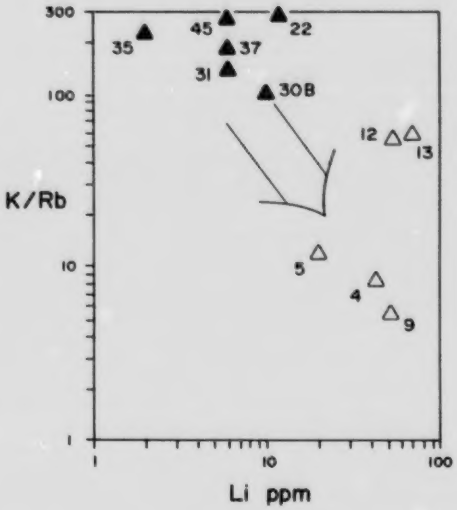

Figure 225.4. *K/Rb versus Li in perthitic microclines from the Pine Portage area. Solid symbols indicate simple pegmatites, while open symbols indicate rare-element pegmatites. The arrow indicates the expected trend for increasing fractionation.*

TABLE 225.2. PARTIAL CHEMICAL ANALYSIS OF PERTHITIC MICROLINE FROM SIMPLE PEGMATITES.

Sample	DL22	DL30B	DL31	DL35	DL37	DL45
wt.%						
K_2O	10.34	8.73	9.47	9.87	9.62	10.95
CaO	0.06	0.03	0.05	0.01	0.02	0.03
Na_2O	2.61	2.46	9.47	1.78	1.89	1.87
ppm						
Rb	297	723	564	362	431	332
Sr*	≤5	≤5	≤5	≤5	87	27
Ba	317	210	198	298	402	293
Li	12	10	6	2	6	6
Pb	79	77	70	65	63	87
K/Rb	289	100	139	226	185	274
K/Ba	271	345	397	275	199	310
K/Sr	-	-	-	-	918	3367
Rb/Sr	-	-	-	-	4.95	12.3
Rb/Ba	0.93	3.4	2.8	1.21	1.1	1.1
Ba/Sr	-	-	-	-	4.62	10.9

*data corrected for radiogenic Sr

TABLE 225.3. PARTIAL ANALYSIS OF PERTHITIC MICROLINE FROM RARE-ELEMENT PEGMATITES.

Sample	DL4	DL5	DL9	DL12	DL13
wt.%					
K_2O	10.51	4.07	4.32	10.34	11.37
CaO	0.05	0.13	0.07	0.07	0.09
Na_2O	0.64	7.53	2.37	2.76	2.40
ppm					
Rb	10431	2844	8154	1489	1577
Sr+	13	153	122	68	91
Ba	326	245	381	666	770
Li	43	20	52	54	70
Pb	77	82	87	77	73
K/Rb	8.36	11.88	4.40	57.65	59.85
K/Ba	267	138	94.1	129	123
K/Sr	6712	220	294	1262	1037
Rb/Sr	802	18.6	66.8	21.9	17.3
Rb/Ba	31	12	21	2.2	2.1
Ba/Sr	25	1.6	3.1	9.8	8.5

+ Data corrected for radiogenic Sr

TABLE 225.4. PARTIAL CHEMICAL ANALYSIS OF MUSCOVITE FROM SIMPLE PEGMATITES.

Sample	DL25	DL29	DL30A	DL33
wt.%				
K_2O	9.36	9.38	8.95	8.37
Na_2O	0.67	n.a.	0.74	n.a.
CaO	0.09	0.00	0.06	0.00
MgO	0.07	0.18	0.37	0.01
FeO(total)	2.11	2.05	n.a.	2.75
ppm				
Li	138	n.a.	18	n.a.
Rb	2166	n.a.	2175	n.a.
K/Rb	57.4	-	34.2	-
Mg/Li	3.06	-	10.1	-
Sample	**DL36**	**DL39**	**DL42**	**DL44**
wt.%				
K_2O	8.80	7.21	8.66	9.50
Na_2O	0.81	0.74	0.83	1.02
CaO	0.03	0.10	0.04	0.01
MgO	0.12	0.49	0.25	0.20
FeO(total)	2.27	n.a.	4.58	2.44
ppm				
Li	74	200	288	78
Rb	1354	1100	2877	1337
K/Rb	54.0	54.4	25.0	59.0
Mg/Li	9.78	14.8	5.24	15.5

n.a. = not analyzed
- = not detected

Tables 225.2 and 225.3, respectively. Insufficient muscovite is present in the rare-element pegmatites for analysis; however, muscovite grains from the simple pegmatites (Figure 225.2) were partially analyzed (Table 225.4). The microcline of rare-element pegmatites shows a pronounced enrichment in Rb and Li as compared to that of the simple pegmatites. However, rare-element pegmatites are also slightly enriched in Sr and Ba, elements in which they should suffer depletion if they have a common origin with the simple pegmatites. The most effective measure of the degree of fractionation is a plot of K/Rb versus Li; a plot of the data from the perthitic microclines of the simple and rare-element pegmatites is given in Figure 225.4. The rare-element pegmatites plot in an area expected by the trend of increasing fractionation of the simple pegmatites and are thus permissibly derived from them. However, there are significant differences in geochemistry among the rare-element pegmatites, as indicated by the clustering of points of DL4, DL5, and DL9 from Occurrences No. 1 and 2 and of DL12 and DL13 from Occurrence No. 3.

The simple pegmatites exhibit no clear trend of increasing fractionation either in the microcline analyses or the muscovite analyses (Figure 225.5). In the latter, a normal trend toward DL42 or an anomalous low-Li trend toward DL30A are possible, but more data are required for substantiation.

Two types of Ta-Nb oxide minerals were found in the rare-element pegmatites. In Occurrence No. 1, sample DL2 was found to be compositionally zoned with a ferrotantalite core and a ferrocolumbite rim, with marginal areas of a complex and inhomogeneous alteration product (Table 225.5). These zones are clearly distinguishable in a back-scattered electron image (Photo 225.1). Figure 225.6 illustrates the locations of analyzed points in the grain. The core to rim variation (Figure 225.7) defines a normal fractionation trend for the columbite-tantalite group, as established by Cerny *et al.* (1985; 1986).

Sample DL7 from Occurrence No. 2 has the composition of fersmite, $(Ca,REE,Na)(Nb,Ta,Ti)_2(O,OH,F)$, a late-stage replacement of such Nb-Ta oxides as microlite or pyrochlore in granitic pegmatites (Foord 1982). As in the case of the columbite-tantalite grain, appreciable Si appears to have substituted for Ta (Table 225.6).

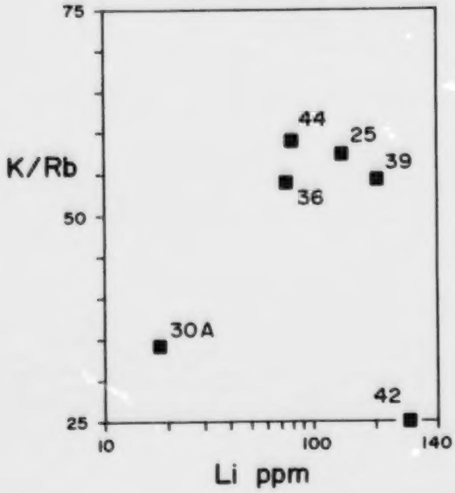

Figure 225.5. K/Rb versus Li in muscovite from simple pegmatites, Pine Portage area. There is no clear trend of increasing fractionation in these analyses.

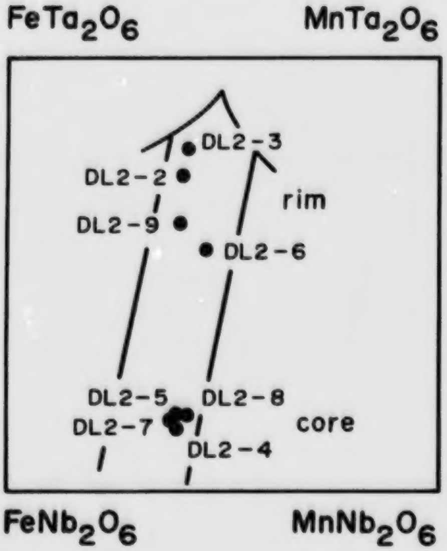

Figure 225.7. Tantalite-columbite composition quadrilateral showing the fractionation trend from core to rim in sample DL2.

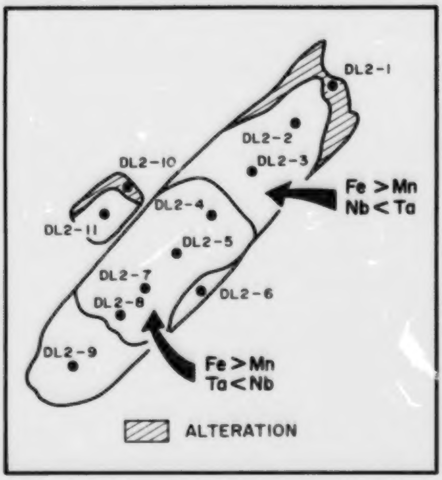
DL2-1
DL2-2
DL2-3
DL2-10
DL2-11
DL2-4
DL2-5
DL2-6
DL2-7
DL2-8
DL2-9
Fe > Mn
Nb < Ta
Fe > Mn
Ta < Nb
ALTERATION

Figure 225.6. Diagram of the grain in Photo 225.1 showing the locations of analyzed points and the trends in compositional variation.

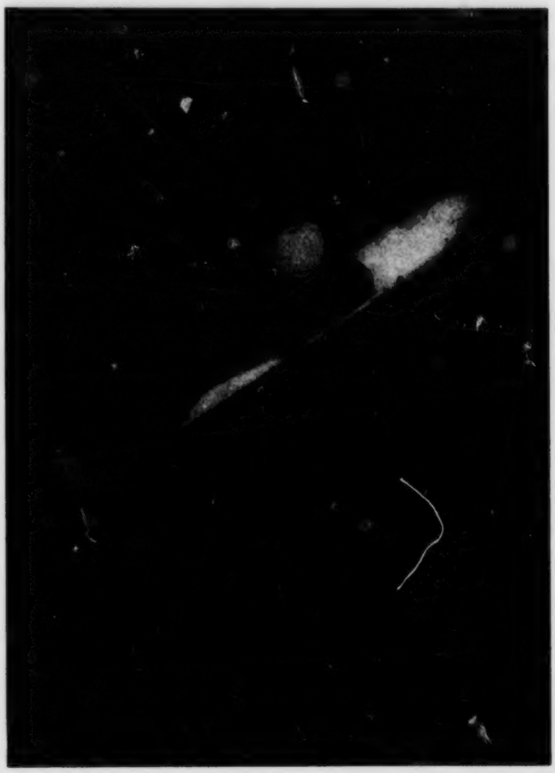

Photo 225.1. Back-scattered electron image of zoned ferrotantalite (core)–ferrocolumbite (rim) grain from Occurrence No. 1. Magnification x200.

TABLE 225.5(A). SEM-EDA ANALYSES OF POINTS IN COLUMBITE-TANTALITE GRAIN FROM OCCURRENCE NO. 1.

Sample	DL2-1	DL2-2	DL2-3	DL2-4	DL2-5	DL2-6
wt%						
Na_2O	2.57	—	1.02	0.86	—	0.94
CaO	8.09	—	0.06	—	—	0.47
K_2O	1.62	—	—	0.11	—	—
Al_2O_3	5.10	—	—	—	—	—
SiO_2	26.51	—	—	4.87	0.96	—
MnO	0.20	5.36	5.43	8.26	8.41	6.60
FeO	1.12	8.14	7.56	13.38	12.91	7.75
Ta_2O_5	51.26	70.54	73.53	16.80	21.00	56.88
Nb_2O_5	3.43	15.56	12.07	55.09	56.16	25.83
TiO_2	0.12	0.43	0.36	0.68	0.66	0.58
Total	100.02	100.03	100.03	100.05	100.04	100.05

Sample	DL2-7	DL2-8	DL2-9	DL2-10	DL2-11
wt%					
Na_2O	—	—	0.43	1.91	—
CaO	—	0.20	—	7.63	—
K_2O	—	—	—	0.69	—
Al_2O_3	—	—	—	2.87	—
SiO_2	7.86	12.35	5.82	0.38	5.32
MnO	13.13	9.31	8.94	1.25	9.63
FeO	2.07	1.87	—	20.85	—
Nb_2O_5	0.64	0.48	0.34	0.16	0.40
Ta_2O_5	56.86	55.70	22.96	9.02	22.86
Total	100.05	100.05	100.02	100.02	100.02

— not detected

DISCUSSION

As noted earlier, the two-mica leucogranites of the Pine Portage Intrusion have most of the characteristics of "fertile" granitoids and appear to be the likely parent of the rare-element pegmatites of the Pine Portage area. The relationship of the Pine Portage Intrusion to other granitic intrusions in the area is unfortunately unknown due to large areas of intervening Proterozoic cover.

The tonalites, which appear to cut the Pine Portage Intrusion in east-striking dikes or sills, have remarkable similarities to the tonalites of the Georgia Lake area, as described by Kissin and Zayachkivsky (1985). The regional relationship of these intrusions, emplaced late in dilatent structures, as well as their petrographical and geochemical characteristics, suggests that they may be A-type (anorogenic) granitoids, as described by Whalen *et al.* (1986). A model for the generation of A-type granitoids proposes that they have formed by partial melting of F- and/or Cl-enriched dry granulitic residue remaining after the extraction of orogenic granites. Thus, the S-type Pine Portage Intrusion may represent the orogenic granite, with some sort of reactivation producing the A-type tonalites.

The pegmatites of the Pine Portage area appear to lack the gradational zoning from simple "barren" types to rare-element types as discussed in theories of pegmatite zonation (*see* Trueman and Cerny 1982). The simple pegmatites occurring within the Pine Portage Intrusion, however, are separated from the rare-element pegmatites near Lucky Lake by both Forgan Lake and areas of very poor exposure. Thus, the presence of intermediate types, for example, beryl-bearing pegmatites, cannot be excluded.

The patterns of trace element fractionation do suggest that the simple pegmatites and rare-element pegmatites may be genetically related. The rare-element pegmatites are permissibly derivable by fractionation of a simple pegmatite parental source. Moreover, the strong structural control as evidenced by the consistent northeast strike of the pegmatite dikes suggest that all the pegmatites were emplaced at the same time in a zone of regional fracturing.

TABLE 225.5(B). STRUCTURAL FORMULAE FOR POINTS ANALYZED IN (A).

Sample	DL2-2	DL2-3	DL2-4	DL2-5	DL2-6
atomic props.*					
Na	0.00	0.16	0.10	0.00	0.13
Ca	0.00	0.01	0.00	0.00	0.04
K	0.00	0.00	0.01	0.00	0.00
Al	0.00	0.00	0.00	0.00	0.00
Fe	0.53	0.50	0.65	0.64	0.47
Mn	0.35	0.36	0.41	0.42	0.40
Total	0.88	1.03	1.17	1.06	1.04
Ta	1.48	1.57	0.26	0.34	1.11
Nb	0.54	0.42	1.44	1.50	0.87
Ti	0.03	0.02	0.03	0.03	0.03
Total	2.05	2.01	2.01	1.98	2.01

Sample	DL2-7	DL2-8	DL2-9	DL2-11
atomic props.*				
Na	0.00	0.00	0.00	0.00
Ca	0.00	0.00	0.00	0.00
K	0.00	0.00	0.00	0.00
Al	0.00	0.00	0.00	0.00
Fe	0.66	0.45	0.55	0.60
Mn	0.40	0.63	0.36	0.34
Total	1.06	1.08	0.97	0.94
Ta	0.32	0.33	1.23	1.25
Nb	1.54	1.52	0.77	0.77
Si	0.12	0.00	0.00	0.00
Ti	0.03	0.02	0.02	0.00
Total	2.01	1.99	2.02	2.03

* based on six oxygens

CONCLUSIONS

The past year's work supports the following conclusions:

1. The Pine Portage Intrusion is a potentially fertile granitoid body, which is the probable source of rare-element pegmatites in the Pine Portage area.
2. Tonalitic intrusions in the Pine Portage and Georgia Lake areas appear to be later than two-mica leucogranites. They have the characteristics of A-type granitoids.
3. Traces of Ta-Nb oxide mineralization in the rare-element pegmatites of the Pine Portage area suggest that the pegmatites may warrant further examination as economic targets. In addition, missing zones of pegmatites may indicate that undiscovered bodies of possible economic interest may occur in the area.

ACKNOWLEDGMENTS

Assistance in field work was provided by Borys Zayachkivsky, S.M. Stock, and T.C. McCuaig, who also assisted with analytical work. Ain Raitsakas, K.D.L. Pringnitz, T.J. Griffith, E.A. Jensen, and A.D. Mackenzie assisted with XRF, AA, CHN, ICP, and SEM-EDA analyses. Maureen Artist-Downey provided valuable support in data processing. Thin and polished sections were prepared by Diane Crothers and A.L. Hammond. Finally, typing was due to W.C. Bons and drafting by S.T. Spivak.

REFERENCES

Archibald, D.L.
1987: Granitoids and Pegmatites of the Pine Portage Area, Northwestern Ontario; Unpublished B.Sc. Thesis, Lakehead University, Thunder Bay, 89p.

TABLE 225.6. ANALYSES OF FERSMITE FROM PEGMATITE OCCURRENCE NO. 2.

Sample	DL7-1	DL7-2		DL7-1	DL7-2
	wt%			atomic prop.*	
Na_2O	0.96	-	Na	0.12	-
CaO	8.08	14.86	Ca	0.56	0.97
Nd_2O_3	0.92	0.41	Nd	0.02	0.01
CeO	1.06	0.29	Ce	0.03	0.01
Mn	1.22	1.03	Mn	0.07	0.05
FeO	5.86	1.62	Fe	0.32	0.08
-	-	-	Total	1.12	1.12
SiO_2	3.31	2.20	Si	0.22	0.13
TiO_2	0.59	0.45	Ti	0.03	0.02
Nb_2O_5	33.58	47.33	Nb	0.98	1.30
Ta_2O_5	44.44	31.89	Ta	0.79	0.53
Total	100.02	100.08	Total	2.02	1.98

* based on six oxygens.

Cerny, P., Goad, B.E., Hawthorne, F.C., and Chapman, R.

1986: Fractionation Trends of the Nb- and Ta-Bearing Oxide Minerals in the Greer Lake Pegmatitic Granites and Its Pegmatite Aureole, Southeastern Manitoba; American Mineralogist, Volume 71, p.501-517.

Cerny, P., Meinzer, R.E., and Anderson, A.J.

1985: Extreme Fractionation in Rare-Element Granitic Pegmatites: Selected Examples of Data and Mechanisms; Canadian Mineralogist, Volume 23, p.381-421.

Chappell, B.W.

1978: Granitoids from the Moonbi District, New England Batholith, Eastern Australia; Journal of the Geological Society of Australia, Volume 25, p.267-283.

Clark, G.S., and Cerny, P.

1987: Radiogenic ^{87}Sr, Its Mobility and the Interpretation of Rb-Sr Fractionation Trends in Rare-Element Granitic Pegmatites; Geochimica et Cosmochimica Acta, Volume 51, p.1011-1018.

Coates, M.E.

1972: Geology of the Black Sturgeon River Area, District of Thunder Bay; Ontario Department of Mines and Northern Affairs, Geological Report 98, 41p.

Foord, E.E.

1982: Minerals of Tin, Titanium, Niobium and Tantalum in Granitic Pegmatites; p.187-238 *in* Granitic Pegmatites in Science and Industry, edited by P. Cerny, Mineralogical Association of Canada, Short Course Handbook, Volume 8, 555p.

Goad, B.E., and Cerny, P.

1981: Peraluminous Pegmatitic Granites and Their Pegmatite Aureoles in the Winnipeg River District, Southeastern Manitoba; Canadian Mineralogist, Volume 19, p.177-194.

Hine, R., Williams, I.S., Chappell, B.W., and White, A.R.

1978: Contrasts Between I- and S-type Granitoids of the Kosciusko Batholith; Journal of the Geological Society of Australia, Volume 25, p.219-234.

Kissin, S.A., and Zayachkivsky, B.

1985: Genesis of Pegmatites in the Quetico Gneiss Belt of Northwestern Ontario–Rare-Element Pegmatites and Associated Granitoids of the Georgia Lake Pegmatite Field; Grant 225, p.186-199 *in* Geoscience Research Grant Program, Summary of Research, 1984-1985, edited by V.G. Milne, Ontario Geological Survey, Miscellaneous Paper 127, 246p.

Kissin, S.A., Zayachkivsky, B., and Branscombe, L.A.

1986: Genesis of Pegmatites in the Quetico Gneiss Belt of Northwestern Ontario–Granitoids, "Barren" Pegmatites, and Metasediments, with Additional Data on Rare-Element Pegmatites, from the Georgia Lake Pegmatite Field; Grant 225, p.65-78 *in* Geoscience Research Grant Program, Summary of Research 1985-1986, edited by V.G. Milne, Ontario Geological Survey, Miscellaneous Paper 130, 235p.

McCrank, G.F.D., Misiura, J.D., and Brown, P.A.

1981: Plutonic Rocks in Ontario; Geological Survey of Canada, Paper 80-23, 171p.

Pye, E.G.

1965: Georgia Lake Area; Ontario Department of Mines, Geological Report 31, 113p.

Trueman, D.L., and Cerny, P.

1982: Exploration for Rare-Element Granitic Pegmatites; p.463-493 *in* Granitic Pegmatites in Science and Industry, edited by P. Cerny, Mineralogical Association of Canada, Short Course Handbook, Volume 8, 555p.

Whalen, J.B., Currie, K.L., and Chappell, B.W.

1986: A-Type Granites: Geochemical Characteristics and Discrimination; p.144 *in* Geological Association of Canada, Mineralogical Association of Canada, and Canadian Geophysical Union, May 19-21, Ottawa, Joint Annual Meeting, Program with Abstracts, Volume 11, 158p.

Grant 249 Geochemical Studies of Formation Waters, Southwestern Ontario, Canada, and Southern Michigan, U.S.A.

P. Dollar[1], **S.K. Frape**[1], **R.H. McNutt**[2], **P. Fritz**[1], **and R.W. Macqueen**[3]

[1]Department of Earth Sciences, University of Waterloo, Waterloo

[2]Department of Geology, McMaster University, Hamilton

[3]Institute of Sedimentary and Petroleum Geology, Geological Survey of Canada, Calgary, Alberta

ABSTRACT

Formation waters from Paleozoic strata in southwestern Ontario and southern Michigan were analyzed for major, minor, and trace element geochemistry; stable isotope composition of oxygen and hydrogen; tritium content; and strontium isotopic composition. Waters from approximately 120 wells from several hydrocarbon producing formations, ranging in age from Cambrian to Mississippian, were collected.

Most formation waters are brines that contain between 140 and 391 g/L Total Dissolved Solids (TDS), the only exceptions being the dilute saline and brackish waters from the Dundee Formation in southwestern Ontario. Most brines are Ca-Na-Cl in composition, although some variation in Ca/Na ratios does occur. Stable isotopes of oxygen and hydrogen indicate that all waters plot below and to the right of the Global Meteoric Water Line (GMWL) in $\delta^{18}O-\delta^{2}H$ space, typical for sedimentary basin brines. The concentrated brines from each stratigraphic horizon plot within unique narrow ranges of isotopic composition. The only exceptions are the two low salinity samples from the Dundee Formation (Devonian) in southwestern Ontario, which are depleted in $\delta^{18}O$ and $\delta^{2}H$, indicative of cooler climatic conditions. $^{87}Sr/^{86}Sr$ ratios of the waters vary from 0.7080 to 0.7112. With the exception of those of the salt units of the Salina Formation (Silurian), most strontium ratios are greater than the corresponding Paleozoic seawater values, indicative of rock water interaction. The source of the radiogenic strontium in these waters has not been identified.

INTRODUCTION

Waters with high salinities are commonly associated with oil, gas, and metallic mineral deposits in sedimentary basins. Although occurrences of these waters are well documented, the sources of the water molecules and dissolved chemical species in many basinal brines have not been unequivocally resolved, despite decades of debate (Hanor 1983). Knowledge of the origin and evolution of these waters is of considerable interest at the present time for the development of models for a) hydrocarbon source rock potential, b) Mississippi Valley Type Pb-Zn ore deposition, and c) waste disposal strategies.

Formation water chemical compositions are also important with respect to a variety of environmental and economic issues. Knowledge of formation water salinities is, for example, vital for the calibration of electric logs that are used to determine petrophysical parameters, production zones, and hydrocarbon reserves. Casing leaks from fluid-bearing horizons other than the producing zone may be identified if there is sufficient variability in the chemical and/or isotopic compositions of the two zones. Also, since mineral solubility is a function of solution composition, formation waters can play an important role in reservoir porosity and permeability distributions.

STRATIGRAPHIC AND STRUCTURAL CONTROLS

In order to appreciate the hydrogeochemical and fluid migrationary aspects of the study, it is necessary to fully understand the important stratigraphic and structural controls that might influence fluid composition and movement in the area.

The Michigan Basin is a remarkably circular feature consisting of parallel bands of subcrop or outcrop that pass from an exterior rim of Silurian carbonates to red beds of Jurassic age in the basin's centre. The area of study extends from Oxford County, Ontario, Canada, westward to Missaukee County, Michigan, U.S.A. (Figure 249.1). In the eastern part of the study area, the Phanerozoic is represented by 875 m of strata that is Late Cambrian to Late Silurian in age. The sedimentary units generally thicken towards the depocenter of the basin, where a much more complete sedimentary succession occurs (Figure 249.2). In the central portion of the basin, the Phanerozoic sequence, which is greater than 5000 m in total thickness, ranges in age from Early Cambrian to Late Jurassic. The present study determines the characteristic inorganic chemical constituents in groundwaters from several hydrocarbon-bearing horizons and two salt mines, located in southwestern Ontario and Michigan (Table 249.1).

The Michigan Basin is bounded by faulted Precambrian rocks of the Canadian Shield to the north and northeast, the Algonquin Arch to the east and southeast, the Findlay and Kankakee Arches to the south and southwest, and the Wisconsin Arch to the west (Figure 249.3). The Algonquin and Findlay Arches are broad northeast-trending Precambrian highs, separated by the Chatham Sag, that divide the Ontario Peninsula into two parts. These two positive structural features, probably introduced during Late Precambrian time, and then intermittently reactivated during the Paleozoic, form a broad platform between a more rapidly subsiding Michigan Basin to the west, and the Appalachian Basin to the southeast (Sanford *et al.* 1985). The current regional dip of the rocks to the northwest of the arches is 6 to 9 m/km into the Michigan Basin; to the southeast of the arches, the dip is 6 m/km into the Appalachian Basin (Winder and Sanford 1972). Paleozoic strata in the Chatham Sag are, for the most part, horizontal.

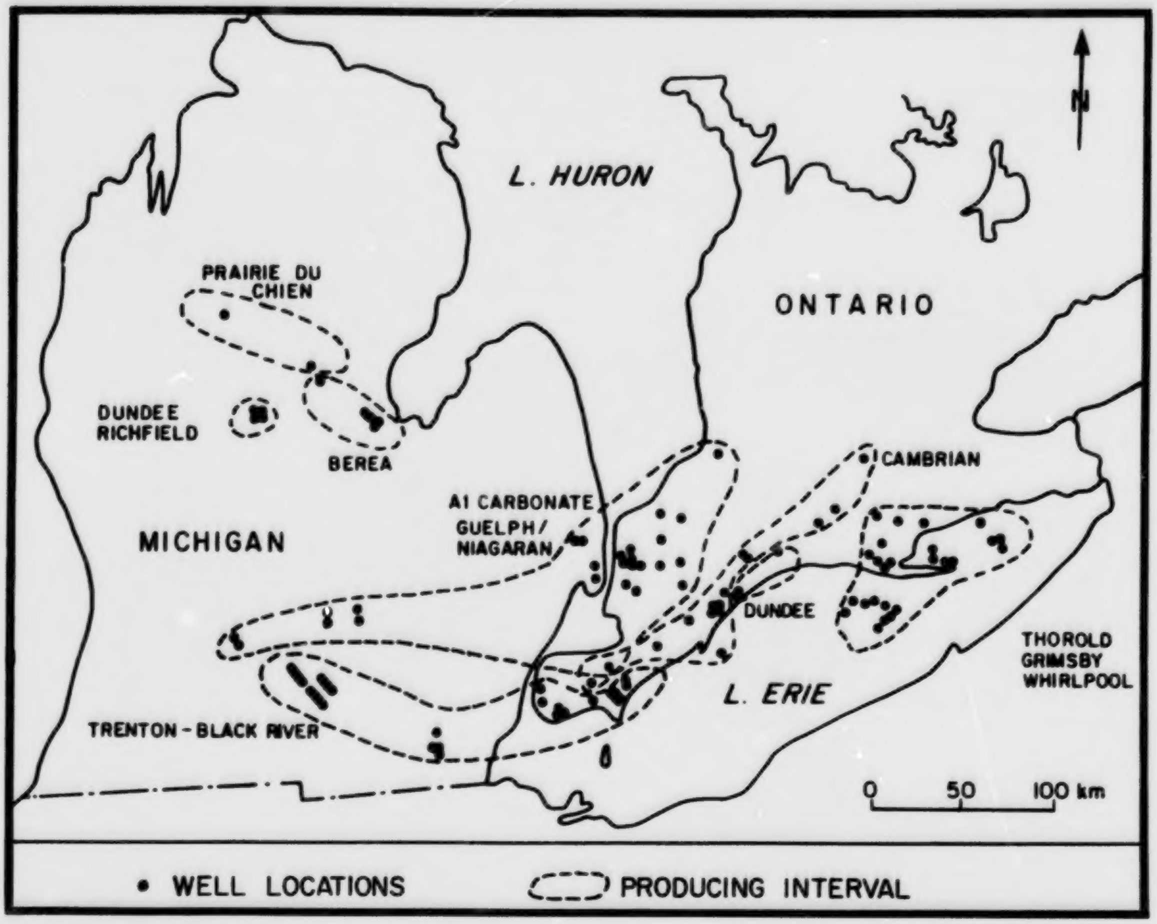

Figure 249.1. *Water sampling sites and producing intervals, southwestern Ontario, Canada, and southern Michigan, U.S.A.*

Sanford *et al.* (1985) proposed a relatively active tectonic history for southwestern Ontario. Tectonically associated fault block readjustment has provided the structural control for the origin and development of southwestern Ontario's hydrocarbon traps. The implications of such tectonic movements on the hydrodynamic/fluid migration history and salt dissolution are discussed where appropriate.

SAMPLING PROCEDURES AND ANALYTICAL METHODS

All formation water samples were collected from wells drilled in the search for petroleum. Most samples were collected from the wellhead bleeder valves of producing wells. The wellhead bleeder valve samples should provide the most representative samples, as they are collected as close to the source formation as possible. A few cable tool bailer, drill stem test, separator and production tank samples were also included for comparative purposes.

ANALYTICAL PROCEDURES

Prior to chemical analysis, samples were filtered in the laboratory through a 0.45 μm filter. A 500 mL aliquot was acidified to a pH < 2 using HCl, before analysis for cations by atomic absorption spectroscopy. A second filtered 500 mL aliquot, not acidified, was used for anion analysis by a liquid ion chromatograph. Filtered 125 mL aliquots were used for the analysis of oxygen, hydrogen, and strontium isotopic compositions, and for tritium content. Hydrogen and oxygen isotope ratios were measured by conventional gas-source mass spectrometry. The oxygen analyses were performed by long term equilibration with CO_2, while hydrogen analyses were done on water distilled from the brines at elevated temperatures ($> 400°C$) to prevent the formation of hydrated salts. Results were reported with respect to the Vienna-Standard Mean Ocean Water (V-SMOW) standard. The precision was $\pm 0.15‰$ and $\pm 2.5‰$ for ^{18}O and ^{2}H, respectively. These chemical and isotopic analyses were performed at the University of Waterloo.

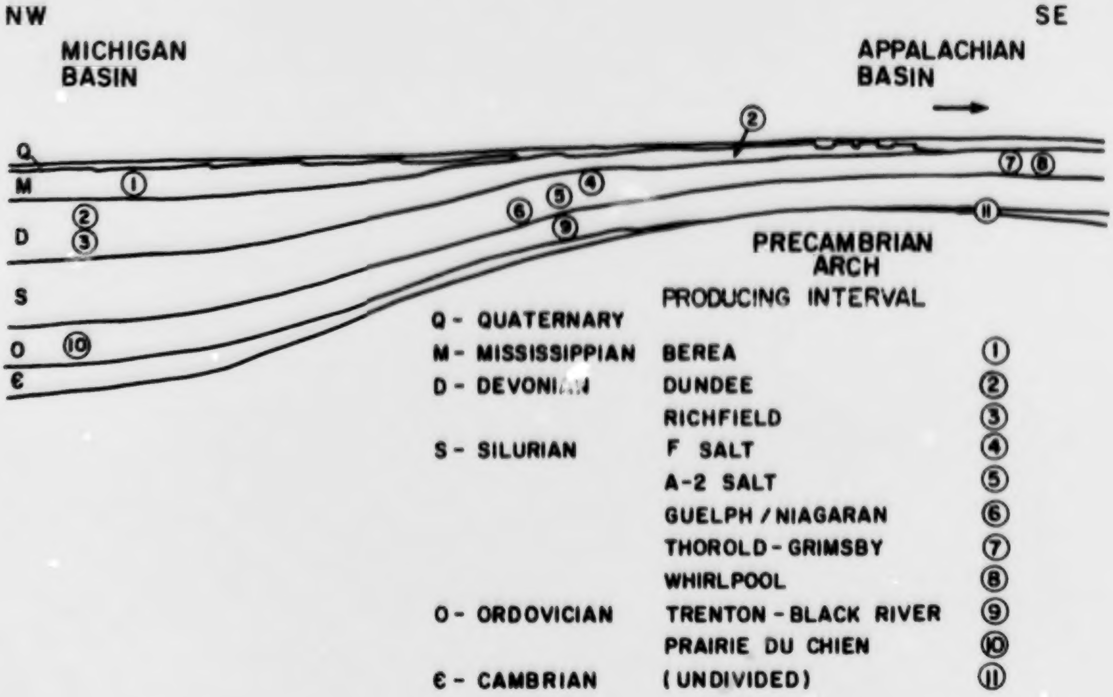
NW
SE
MICHIGAN BASIN
APPALACHIAN BASIN
Q
M
D
S
O
Є
①
②
③
④
⑤
⑥
⑦
⑧
⑨
⑩
⑪
PRECAMBRIAN ARCH
PRODUCING INTERVAL
Q - QUATERNARY
M - MISSISSIPPIAN
BEREA ①
D - DEVONIAN
DUNDEE ②
RICHFIELD ③
S - SILURIAN
F SALT ④
A-2 SALT ⑤
GUELPH / NIAGARAN ⑥
THOROLD - GRIMSBY ⑦
WHIRLPOOL ⑧
O - ORDOVICIAN
TRENTON - BLACK RIVER ⑨
PRAIRIE DU CHIEN ⑩
Є - CAMBRIAN
(UNDIVIDED) ⑪

Figure 249.2. *Schematic representation of the Paleozoic strata, eastern Michigan and northern Appalachian basins. Relative positioning of the hydrocarbon reservoirs is also shown.*

The $^{87}Sr/^{86}Sr$ ratios were measured on a VG−354 mass spectrometer, following separation by standard ion exchange techniques. Elution was carried out using 2.5 *N* HCl. The dissolution of carbonate phases was done using ultra pure 0.5 *N* HCl or acetic acid at room temperature. Gentle heating was necessary to dissolve dolomite. The dissolution of sulphate (SO_4^{2-}) was done with 6 *N* HCl. The precision between runs of a single analysis of the ratio was ±0.003 percent (2 sigma). Repeated runs of the E&A and NBS 987 standards gave average ratios of 0.70802 and 0.71022, respectively. The strontium analyses were performed at McMaster University, Hamilton, Ontario.

1. STABLE ISOTOPES: OXYGEN AND HYDROGEN

The paper briefly introduces some basic isotopic principles, and the results of analyses on waters from the Michigan and northern Appalachian Basins. The possible histories of these waters are discussed in relationship to current models of diagenetic evolution and mixing of deep-seated groundwaters in sedimentary basins.

TERMINOLOGY

δ–Notation

The results of isotopic determinations are expressed in terms of "δ" values, which are calculated as follows:

$$\delta = \frac{\text{R sample} - \text{R std}}{\text{R std}} \quad 10^3 \text{ per mil}$$

where **R** sample = ($^2H/^1H$), ($^{18}O/^{16}O$), etc., and **R** std is the corresponding ratio in the standard. By convention, the ratio (**R**) is written as the ratio of the heavy (rare) to light (common) isotope. The sign of the δ value may be either positive or negative depending on whether the sample is enriched or depleted in the heavy isotope relative to the standard.

Standard Mean Ocean Water (SMOW)

The present day stable isotopic composition of ocean water is nearly constant, varying locally within narrow limits due to dilution with fresh water, or surface evaporation. The international reference standard for oxygen and hydrogen isotopic compositions of water is Standard Mean Ocean Water or SMOW (Craig

TABLE 249.1. DOMINANT RESERVOIR LITHOLOGIES FOR STRATIGRAPHIC UNITS SAMPLED IN SOUTHWESTERN ONTARIO AND SOUTHERN MICHIGAN.

Period	Producing Interval	Location	Lithology
Mississippian	Berea	MI	Sandstone
Devonian	Dundee	ONT/MI	Carbonate
	Richfield	MI	Carbonate
Silurian	F Unit	ONT	Salt
	A2 Unit	ONT	Salt
	A1/Guelph/ Niagaran	ONT/MI	Carbonate
	Thorold/ Grimsby	ONT	Sandstone
	Whirlpool	ONT	Sandstone
Ordovician	Trenton-Black River	ONT/MI	Carbonate
	Prairie du Chien	MI	Sandstone
Cambrian	(undivided)	ONT	Sandstone

1961a). Isotopic values presented are reported as per mil (‰) deviations relative to the SMOW standard unless otherwise stated.

Meteoric Water

The stable isotopic compositions of oxygen and hydrogen in present day meteoric waters exhibit systematic variations (Taylor 1974; Fritz *et al.* 1987). Craig (1961b) has shown that the $\delta^{18}O$ and δ^2H values in meteoric waters lie close to the Global Meteoric Water Line (GMWL) described by the equation:

$$\delta^2H = 8\delta^{18}O + 10$$

The weighted mean annual isotopic composition of present day meteoric waters in southwestern Ontario and Michigan range from -7.5‰ to -10‰, and -50‰ to -70‰, for oxygen and deuterium, respectively (Fritz *et al.* 1987).

DISCUSSION

A number of mechanisms have been proposed to account for the isotopic compositions of sedimentary basin waters. These processes include: a) the evaporation of seawater or meteoric water, b) the mixing of different waters (i.e. meteoric water with connate waters), c) water–rock interaction, d) membrane filtration, and e) the release of diagenetic waters during burial diagenesis (for example, dehydration of gypsum). Each will be addressed as it applies to i) previous studies, and ii) the individual stratigraphic units of the present study.

Clayton *et al.* (1966) were the first investigators to attempt a comprehensive study of the isotopic composition of formation waters in sedimentary basins. They discovered that the subsurface waters in the Michigan Basin had isotopic signatures that were different from those of seawater, and that could be extrapolated back to the local meteoric intercept on the global meteoric water line (Figure 249.4a). As a result, they concluded that all of the primary or connate formation waters had been flushed from the system and replaced by meteoric water. Deviation from the intercept was attributed to isotopic exchange and fractionation during burial.

The deviation of these sedimentary basin water $\delta^{18}O$ and δ^2H values from the meteoric water intercept requires a mechanism that causes enrichment in both isotopic ratios relative to meteoric water. Most sedimentary basin brines display large enrichments in $\delta^{18}O$, and relatively small enrichments in δ^2H, relative to local meteoric water. The oxygen enrichment of formation waters is attributed to isotopic exchange reactions between the waters and associated carbonate minerals (Clayton *et al.* 1966; Hitchon and Friedman 1969). Deuterium exchange between water and hydrogen-bearing compounds is minimized by the overwhelming mass of formation water relative to hydrogen-bearing compounds. The enrichment of deuterium is attributed to membrane filtration for sedimentary basins with significant shale horizons (Graf *et al.* 1965; Hitchon and Friedman 1969).

Although Clayton *et al.* (1966) and Hitchon and Friedman (1969) proposed similar mechanisms for isotopic enrichment, their conclusions as to the origin and isotopic evolution of sedimentary basin waters were quite different. Hitchon and Friedman (1969) assumed seawater to be the original water composition. The seawater's isotopic composition was later modified by exchange with associated carbonate minerals and membrane filtration during burial diagenesis, resulting in the isotopic enrichment of both components (Figure 249.4b). Subsequent infiltration and mixing of isotopically depleted meteoric water with the diagenetically modified sea water was responsible for depletions in isotopic abundances of the seawater derived end member. Positioning of the waters' isotopic composition on the $\delta^{18}O$ versus δ^2H plot was a function of the relative proportions of these two end member compositions.

Recently, Knauth and Beeunas (1986) have proposed an alternative process to account for the isotopic composition of sedimentary basin waters. They have shown that the stable isotopic composition may be derived by an evaporative process similar to the model presented in Figure 249.4c (after Holser 1979).

During evaporation, water becomes progressively more enriched in $\delta^{18}O$ and δ^2H. The slope of the path taken on a $\delta^{18}O$ versus δ^2H diagram is dependent mainly on the humidity and other local climatic variables (Craig and Gordon 1965; Lloyd 1966). Arrows A and B on Figure 249.5 indicate the trajectories for high and low humidities, respectively. The enrichment of both deuterium and ^{18}O relative to SMOW during evaporation does not continue indefinitely. Once either gypsum or anhydrite begin to precipitate, isotopic enrichment ceases and the water becomes progressively more depleted, due to the removal of the heavier isotopes into precipitated mineral phases (Holser 1979; Pierre *et al.* 1984). The shape and extent of the hooked trajectory is probably controlled by factors similar to those that affected the slope of

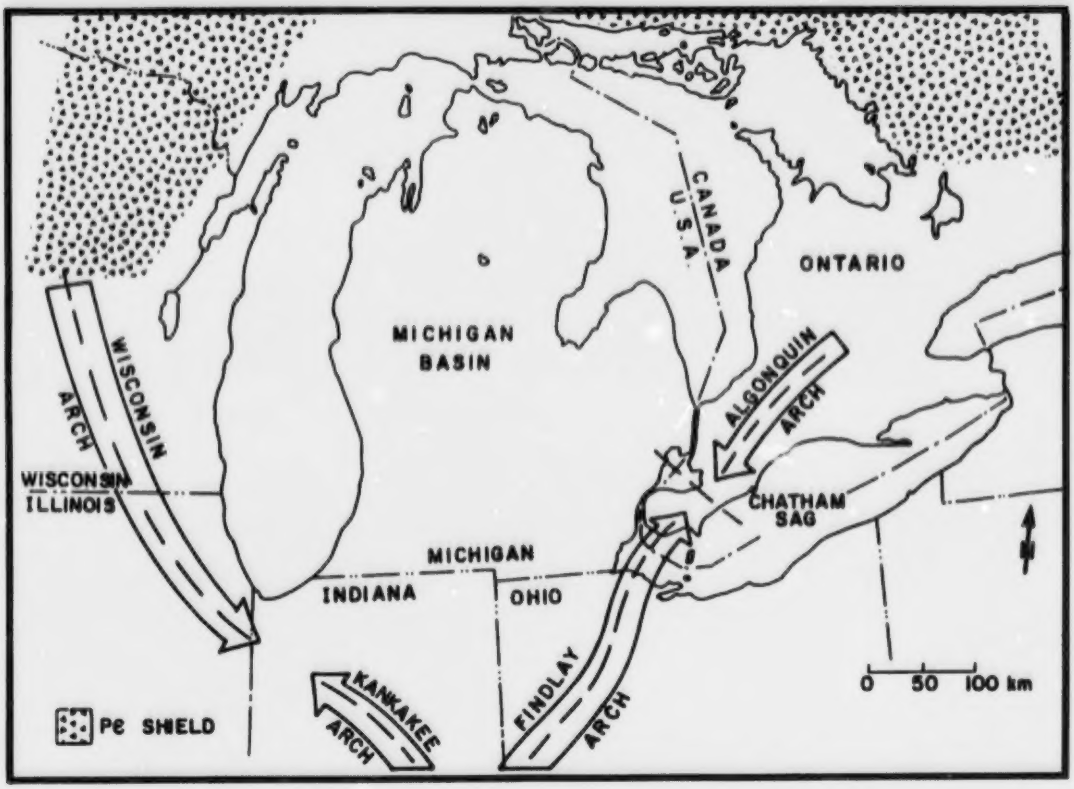

Figure 249.3. *Regional tectonic structures influencing the Paleozoic strata of southern Michigan and southwestern Ontario (modified from Ells 1969).*

the line during initial evaporation (Knauth and Beeunas 1986). This model for isotopic evolution is based on limited field and experimental data, and may not be readily applicable to complex natural systems.

The implications of this work on future stable isotopic interpretations may prove to be quite revolutionary. The negative isotopic values from previous studies are used to rule out an evaporative seawater origin (Clayton *et al.* 1966; Land and Prezbindowski 1981, 1985). Negative δ^2H and δ^{18}O values, using the evaporation model proposed by Knauth and Beeunas (1986), no longer need be interpreted as being the product of meteoric water influence, since similar results may simply be the result of the extreme evaporation of seawater following hooked trajectories.

PRESENT STUDY

All formation waters from this study plot below and to the right of the GMWL; this is typical for sedimentary basin brines (Figure 249.6). Also shown are comparable data from other studies: the Michigan Basin (Clayton *et al.* 1966); and three hydrocarbon-producing sandstone intervals from the Appalachian Basin, in Ohio (Breen *et al.* 1985). These studies all have negative δ^2H values, and positive to negative δ^{18}O values, relative to SMOW.

Traditionally, a meteoric water component has been advocated to account for such distributions (Clayton *et al.* 1966; Hitchon *et al.* 1969). The wells sampled by Clayton *et al.* (1966) are extremely biased toward younger stratigraphic units, with only five of the twenty-four samples from pre-Devonian reservoirs. The present study considers more samples, and a larger proportion from deeper horizons than the earlier study. The isotopic data in this study seriously questions the validity of the Michigan Basin line proposed by Clayton *et al.* (1966). Obviously, the system is much more complicated than previously thought, and may represent several independent hydrological systems, as indicated by the extreme dispersion of some waters from the line in Figure 249.6. Waters from the Cambrian sandstones and Ordovician carbonates, for example, are significantly enriched in δ^2H relative to the overlying units. These waters may have a meteoric component that was enriched relative to present day meteoric water.

Alternatively, this enrichment may also be explained by the membrane filtration model proposed by Bredehoeft *et al.* (1963). The waters were forced from the shale-free Cambrian and Ordovician aquifers up through the extensive overlying Ordovician shales. As these waters migrated through the semipermeable membranes, the heavy isotope of hydrogen was preferentially retarded, leaving the resid-

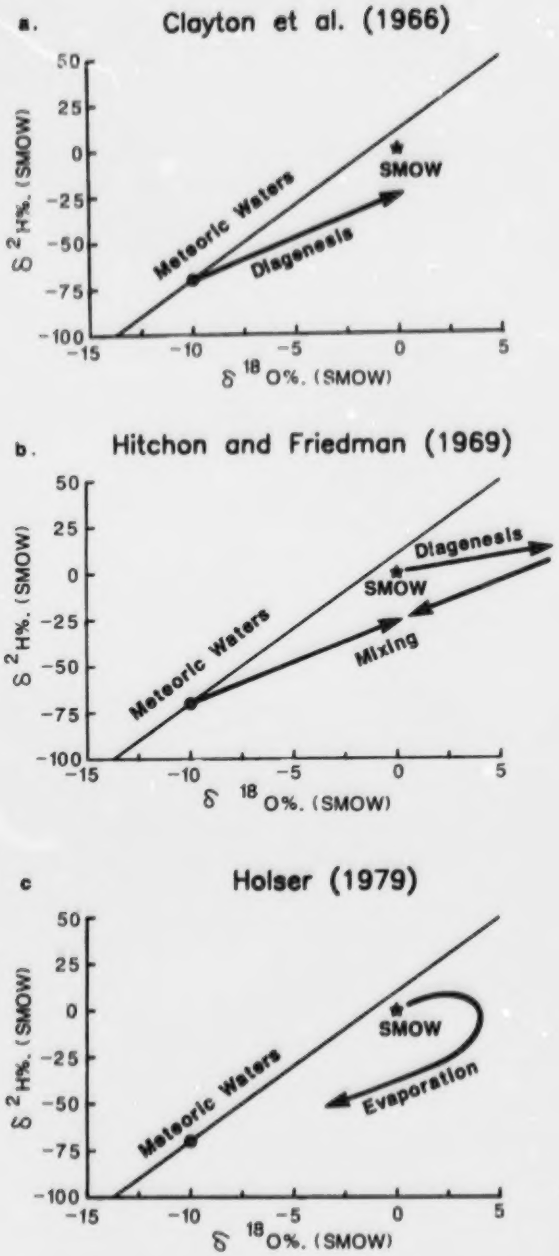

Figure 249.4. Oxygen and hydrogen isotopic interpretations by a) Clayton et al. (1966), b) Hitchon and Friedman (1969), and c) Holser (1979).

ual pore water in the Cambrian and Ordovician reservoirs isotopically enriched.

ISOTOPIC EVOLUTION OF INDIVIDUAL UNITS

Most brines from the present study plot within a narrow range of isotopic composition for the individual stratigraphic units sampled (Figure 249.7). The isotopic differences between the waters of the units sampled may indicate different origins, mixing, or different isotopic fractionation processes.

There are local groupings of isotopic composition by field and location. This regional isotopic signature with localized values possibly reflects the slight differences in temperature, individual water sources, or exchange reactions with the enclosing carbonate reservoir rocks.

The deep basin Dundee Formation sample from central Michigan plots near the centre of values on the $\delta^{18}O$ versus $\delta^{2}H$ diagram, around 0‰ and -30‰ (Figure 249.6). The waters of the Dundee Formation, from the shallow subsurface in southwestern Ontario, probably represent mixtures of original concentrated formation brines (similar to the sample mentioned above), and waters recharged under cooler climatic conditions, possibly at the end of the last period of glaciation. The possibility that these waters have been contaminated by interconnection with the overlying Pleistocene aquifer (depleted isotopic values, *see* Desaulniers *et al.* 1981) must be considered. The glacial-associated waters may not have naturally recharged into the underlying strata as previously reported in Clayton *et al.* (1966), but may result from casing leaks.

2. WATER CHEMISTRY

SUBSURFACE WATER CLASSIFICATION

A number of descriptive terms have been introduced to describe subsurface waters, based on salinity and origin (White 1957, 1965; White *et al.* 1963). One of the simplest and most widely used classification schemes is based on the Total Dissolved Solid (TDS) concentration of a water (Table 249.2).

CHEMICAL CHARACTERISTICS

The formation waters analyzed in this study vary significantly in both salinity and chemical composition between different stratigraphic units. However, waters from the same stratigraphic interval generally have similar chemical compositions across the study area. The principal ions contained in these waters are calcium, sodium, and chloride, although some variation in the Ca/Na ratios does exist between, and within, formations (Table 249.3).

Almost all groundwaters of the study area are brines, as they contain between 140 and 391 g/L TDS (Table 249.3). The only major exceptions are the dilute saline and brackish waters from the Dundee Formation in southwestern Ontario.

Several mechanisms have been proposed to account for the high salinities and chloride concentrations characteristic of many sedimentary basins. Elevated salinities are presently believed to result from one or more of the following mechanisms: a) infiltra-

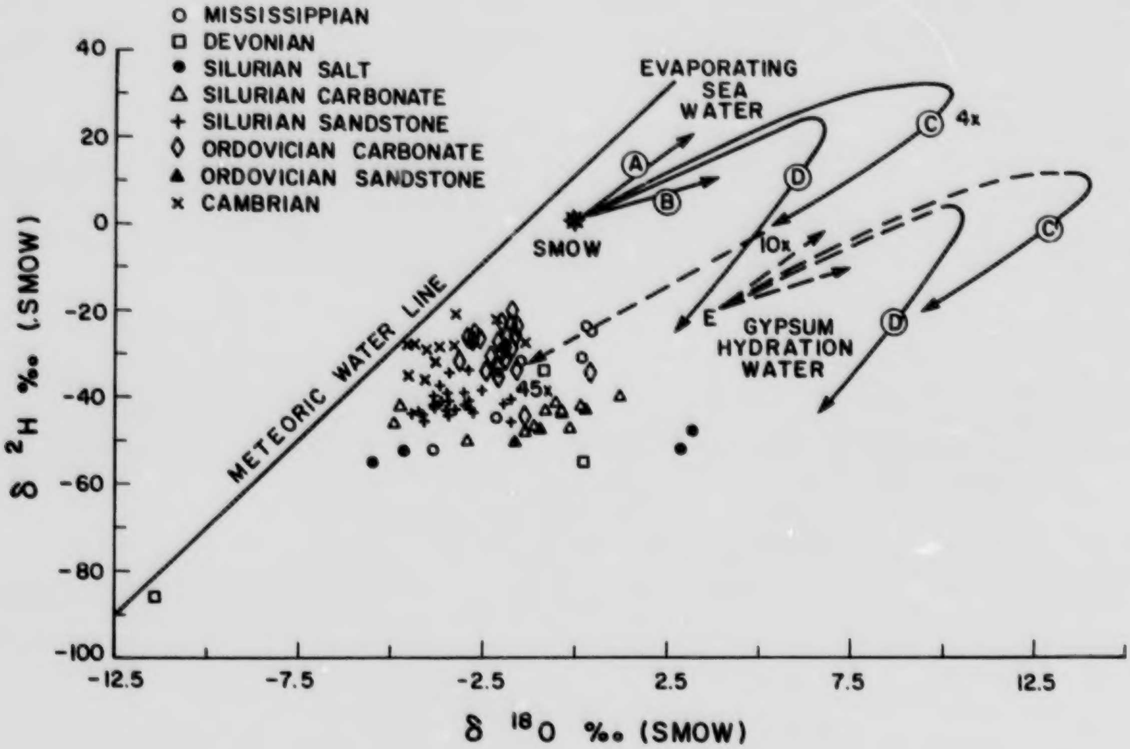

Figure 249.5. *Trajectories for seawater undergoing evaporation superimposed over data from the present study. Curve A represents initial evaporation under relatively humid conditions; curve B is for arid conditions. Curve C is Holser's (1979) estimate of evaporating seawater through a concentration of 10 times. The dashed curve extrapolation to 45 times is based on incomplete data. Curve D is given by Pierre et al. (1984). The isotopic composition of hydration water in gypsum precipitated on any point on evaporation trajectories C and D is given by curves C' and D', respectively. The solid parts of curves C' and D' correspond to gypsum precipitated in the gypsum facies during the evaporation of seawater (≅ 3 to 11 times concentration). The halite facies corresponds to a concentration of ≅ 11 to 65 times. Figure and caption are modified from Knauth and Beeunas (1986).*

tion and burial of subaerially evaporated waters (Carpenter 1978), b) the subsurface dissolution of halite (Land and Prezbindowski 1981), and c) membrane filtration (Graf 1982). Subsequent modification of waters produced by these processes may result from the mixing of different waters (for example, connate brines diluted by the influx of fresh meteoric waters), or by the interaction between the pore fluids and enclosing reservoir rocks.

The chloride concentrations for most formations do not exhibit any general tendency to increase with sample depth. The maximum observed salinities of these waters level off and never exceed values greater than 400 g/L. Several significant reversals occur in both salinity and chloride concentration within the study area. The most pronounced variations are found within the dilute waters of the Dundee Formation (near recharge areas at the basin periphery), and within the very saline and chloride enriched waters of the Guelph/Niagaran units (which are spatially related to evaporites).

DISCUSSION

The chemical composition of water within the individual units is modified by rock–water interaction, halite dissolution, mixing of waters, and membrane filtration. Several of these processes can be identified with the aid of chloride correlation plots. In most sedimentary basin hydrogeochemical systems, chloride is the dominant anion. Chloride behaves in a conservative manner, entering into precipitation/dissolution reactions at high salinities where halite precipitation occurs. For these reasons, chloride has been chosen both as the comparative species, to define the relative abundance of other chemical constituents, and as a normalizing factor to interpret possible sources of saline constituents. Chloride correlation plots allow one to determine how reactions have affected the concentration of dissolved species in these waters. Most species follow trends indicating that little or no reaction occurs between chloride and the dissolved aqueous species. Reactions produce concentrations that plot either above (dissolution), or below the general trends (precipitation). Dilution of

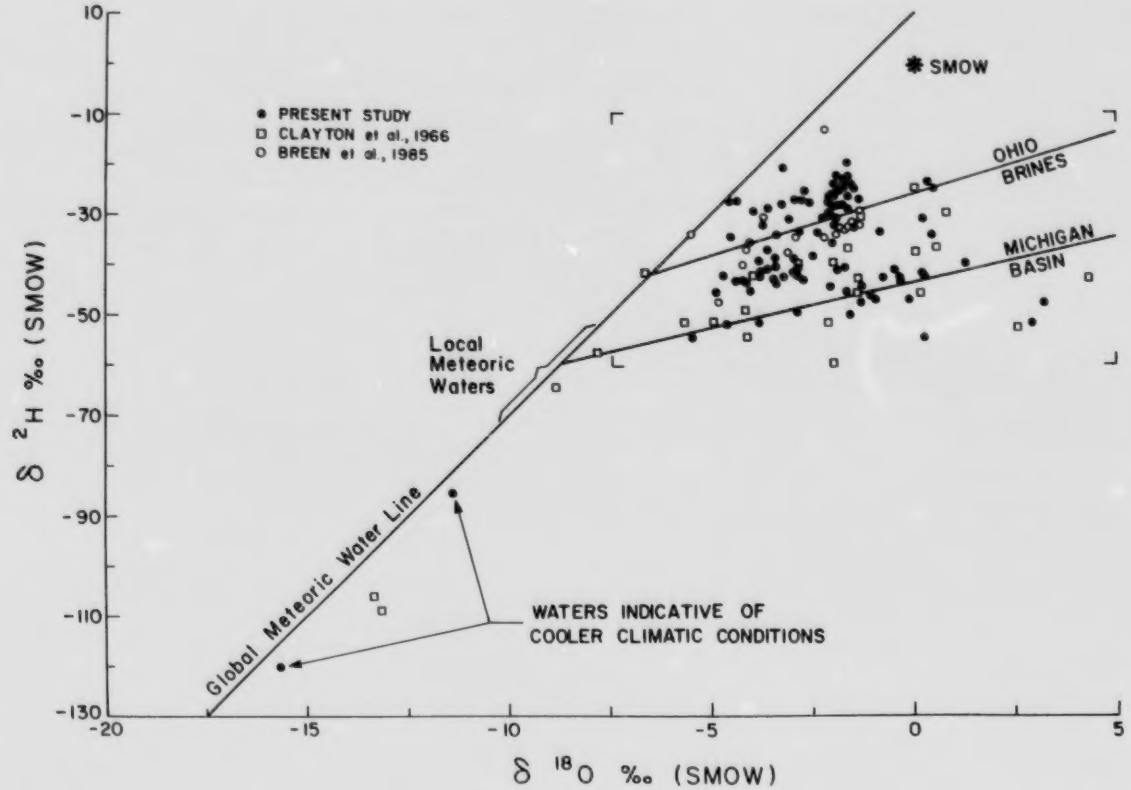

Figure 249.6. *Oxygen and hydrogen isotopic compositions of all formation waters from the present study. Data and respective basin lines for the Michigan Basin (Clayton et al. 1966) and Ohio (Breen et al. 1985) are also included.*

these chemical parameters by the input of fresher waters may also be detected.

Nesbitt (1985) has produced plots of various elemental ratios over chloride, versus chloride concentration. This allowed him to assess any chemical effects that the above mentioned processes had on formation water composition in the Illinois Basin. Similar plots have been constructed for major elements (Ca, Na, Cl) in the waters from the present study.

ALKALI METALS (SODIUM)

Sodium is the most abundant member of the alkali metal group in the waters studied, and is present in concentrations of up to 100 000 mg/L in waters associated with the Upper Silurian F Unit salt (Table 249.1). It is frequently conserved in aqueous systems, in which it is associated with chloride, until halite saturation is reached and precipitation occurs.

For most of the units studied, a constant decrease in Na/Cl ratios with increasing chloride concentration is apparent (Figure 249.8). This plot has been selected to examine the role that halite dissolution, and mixing waters of differing origins played in the formation of these concentrated brines. All of the Na/Cl ratios from the present study are much lower than the seawater value (0.57). The absolute chloride concentrations in the brines are considerably higher (up to 260 000 mg/L) than the seawater concentration of 19 000 mg/L (Krauskopf 1979). Calculations of halite dissolution chemistry show that equal molar proportions of sodium and chloride are released to solution (Na/Cl = 0.65 on a gram per gram basis; *see* Nesbitt 1985). Based on this information, the brines from the Guelph/Niagaran, Salina F Unit salt, and Richfield Zone, that plot above the generally decreasing trend, are presumed to be the product of halite dissolution.

The Silurian sandstone samples from eastern Lake Erie, and one Cambrian water sample, have constant Na/Cl ratios and variable chloride concentrations. These waters plot to the left of the trend, indicating that dilution must have occurred. Addition of fresh waters to the system serves to reduce the absolute chloride concentration, which does not alter the Na/Cl ratio provided that the waters remain saturated with respect to halite. If halite were to be dissolved, then the Na/Cl ratio would increase.

ALKALINE EARTH METALS (CALCIUM)

The correlation plot for Ca/Cl versus chloride, shown in Figure 249.9, displays a steady linear increase for most stratigraphic units. The concentration of calcium

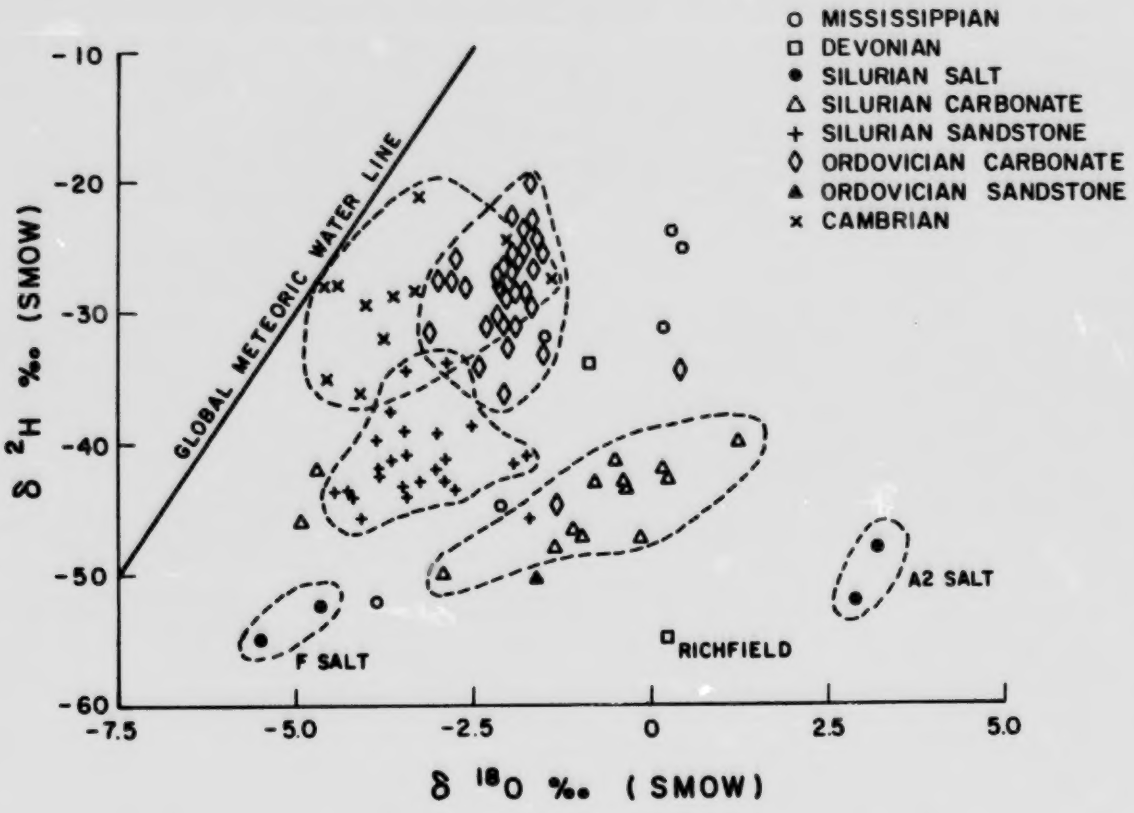

Figure 249.7. Oxygen and hydrogen isotopic compositions of brines displaying individual groupings by reservoir age.

increases with increasing chloride concentration. The only samples not to follow this trend are from the Upper Silurian F Unit salt, and the Lower Silurian sandstones under eastern Lake Erie. The F Salt waters are dominated by sodium, and as stated earlier are believed to be the product of halite dissolution. The waters from the Silurian sandstone and other units that plotted below the Na/Cl trend in Figure 249.8 (product of dilution?), plot above the Ca/Cl trend line in Figure 249.9.

3. STRONTIUM ISOTOPES

As part of a hydrogeochemical study of groundwater behaviour, strontium isotopes, in conjunction with chemical analyses and stable isotopes, are used here to assess the extent of water–rock interaction. Some aspects of this work have previously been discussed by McNutt *et al.* (1987).

BRINE SIGNATURE AND SEAWATER STRONTIUM

The $^{87}Sr/^{86}Sr$ results are shown in Figures 249.10 and 249.11 as a function of the age of the rock hosting the brine. Also shown is the curve of Burke *et al.* (1982), depicting the change in the strontium isotopic composition of seawater with time. Since strontium has a long residence time in the ocean, its concentration and isotopic composition are uniform throughout the world's oceans at any given time (Veizer and Compston 1974). Therefore, there is the potential for strontium to be used both as a geochronological tool for marine sediments, and as an indicator of the changes in chemistry that occur during diagenesis. It is the latter that is of interest in this particular study.

The strontium seawater curve varies from approximately 0.7095 to 0.7075 from the Upper Cambrian to the Mississippian, with several oscillations in the interim. If the Michigan Basin brines are the same age as their reservoir rocks, then most have $^{87}Sr/^{86}Sr$ values that are greater than seawater for the respective time period in question. The only exceptions to this are the Upper Silurian Salina Formation waters, four waters from the Middle Silurian Guelph/Niagaran reefs, and one sample from each of the Middle Ordovician Trenton Group and Mississippian Berea Formation.

Based on the above assumption, the elevated ratios imply that there has been some degree of water–rock interaction *in situ*. The radiogenic strontium would be derived from rubidium-bearing phases (mica, clay minerals, and potassium feldspar), old enough for ^{87}Rb decay to have produced measurable amounts of ^{87}Sr, resulting in ratios well above their initial seawater value.

TABLE 249.2. GROUNDWATER CLASSIFICATION BASED ON TOTAL DISSOLVED SOLIDS CONCENTRATIONS (AFTER CARPENTER (1978) MODIFIED FROM DAVIS (1964)). The TDS of seawater is approximately 35 000 mg/L.

Category	TDS (mg/L)
Fresh Water	0 - 1 000
Brackish Water	1 000 - 10 000
Saline Water	10 000 - 100 000
Brine	>100 000

If the waters are not the same age as their present reservoirs, then the interpretation becomes much more complicated. The Middle Silurian Guelph/Niagaran brines could have, for example, migrated into their present reservoir; what then appears to be water−rock interaction in Guelph time may not be the case at all (i.e. there was only fluid migration). This is possible as their strontium isotope ratios are within the expected range for Late Cambrian time. However, it seems unlikely that there would be no exchange of strontium between the solid and fluid phases.

On balance, it can be concluded that the strontium isotope ratios in the Michigan Basin brines reflect water−rock interaction and, as such, can possibly serve as a tracer for fluid migration.

MINERAL AND ROCK STRONTIUM DATA

To assess the extent of water−rock interaction between the brines and the reservoir rocks up to the present time, the rock and late stage diagenetic mineral phases coexisting with several of the brines are being analyzed.

A detailed study of the Hillman Field in southwestern Ontario has further shown the complexity of interaction between formation brines and host rock. Eleven wells were sampled for formation waters in the field. Ten brine samples, each from a producing well, were analyzed; the average $^{87}Sr/^{86}Sr$ value obtained was 0.7103 ±0.0001. The remaining well had a brine with a significantly different strontium ratio of 0.7090.

However, the preliminary analyses of the solid phases in this field add another dimension to the problem. Five matrix dolomite samples from the host rock in this field give strontium ratios of 0.7086 ±0.0002. This value is the same as the seawater curve of Burke *et al.* (1982), indicating that little change has taken place since the end of deposition and burial diagenesis. Likewise, late stage vein and vug fillings, including saddle dolomite, calcite, and anhydrite from one of the holes (brine value 0.7103), have the same strontium ratios as the host matrix dolomites. These values are consistent with the seawater value for the time period. Late stage minerals from the hole containing the anomalously low brine value (0.7090) show a very different pattern. Samples of saddle dolomite and anhydrite from this hole have ratios similar to the present day brine in the rest of the field (0.7103), and yet different from the matrix (0.7086).

TABLE 249.3. WATER CLASSIFICATION AND DOMINANT IONS.

Formation	Principal Ions (>20 g/L)	Classification	TDS (g/L)
Berea	Ca Na Cl	Brine	230-312
Dundee (Ont.)	Ca Na Cl - Na Cl	Brackish - Saline	3 - 15
Dundee (MI)	Na Ca Cl	Brine	292
Richfield	Ca Na Cl	Brine	282
F Salt	Na Cl	Brine	304 - 322
A2 Salt	Ca Na Cl	Brine	340
A1 Carbonate/ Guelph/ Niagaran	Ca Na Cl - Na Ca Cl	Brine	198 - 391
Thorold/ Grimsby Whirlpool	Na Ca Cl - Ca Na Cl	Brine	191 - 325
Trenton/ Black River	Na Ca Cl	Brine	140 - 239
Prairie du Chien	Ca Na Cl	Brine	325 - 391
Cambrian	Ca Na Cl	Brine	174 - 338

The data from these two holes present conflicting results. In one hole, the rock and secondary mineral phases have not isotopically equilibrated with the present day brine. In the other, some of the secondary mineral phases have apparently equilibrated with the dominant Hillman Field brine, even though this brine is not now present in this hole. A later brine with the 0.7090 signature is present; it appears that calcites and one sulphate sample, with ratios of 0.7087 to 0.7088, have partially equilibrated with it. The Hillman Field has had a complex history of fluid migration and diagenesis that obviously needs more study.

SUMMARY

Several conclusions can be drawn on the basis of this work.

1. Very concentrated brines (>300 g/L TDS) exist in most strata. These brines are usually Ca-Na-Cl in composition although some variability of Ca/Na does occur. The dissolved solids concentrations of these waters are derived from: a) infiltration and burial of evaporated seawater, b) subsurface dissolution of halite, and c) membrane filtration. Later modification of the chemical composition is the result of diagenesis (rock−water interaction,

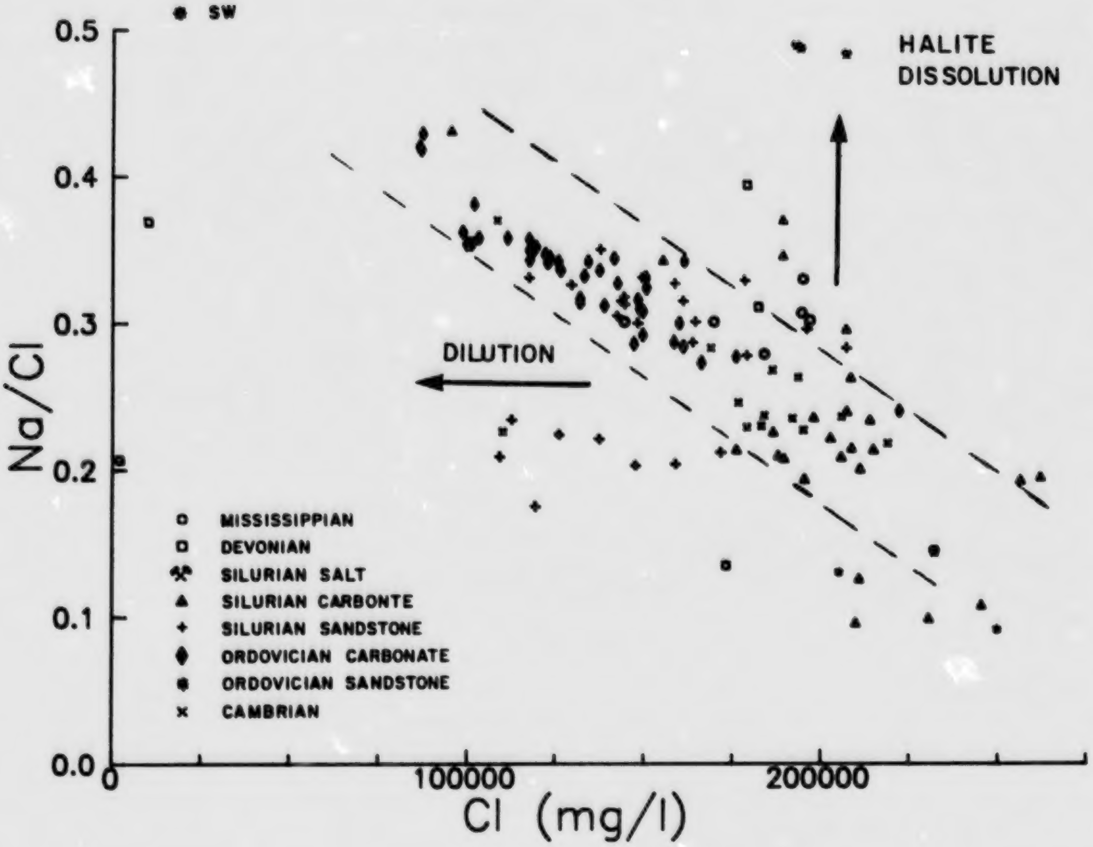

Figure 249.8. Na/Cl ratios of formation waters as a function of their chloride content.

mineral precipitation, etc.), and mixing with waters of different chemical compositions.

2. The most concentrated waters from each unit have similar isotopic and geochemical characteristics, which are distinct from the concentrated brines of the other units. Stable isotopes of oxygen and hydrogen indicate that all waters plot below and to the right of the Global Meteoric Water Line (GMWL) in $\delta^{18}O-\delta^{2}H$ space, which is typical for sedimentary basin brines. All waters have negative $\delta^{2}H$ values and positive to negative $\delta^{18}O$ values, relative to Standard Mean Ocean Water (SMOW). The concentrated brines from each stratigraphic horizon plot within unique narrow ranges of isotopic composition. The only exceptions are the two low salinity samples from the Dundee Formation (Devonian) in southwestern Ontario, which are depleted in $\delta^{18}O$ and $\delta^{2}H$, indicative of cooler climatic conditions. The differences in isotopic composition both within and between the units result from: a) differing initial isotopic compositions, b) mixing of isotopically different waters, c) membrane filtration, and d) differing isotopic fractionation processes acting on the various waters. The present day isotopic distribution is much more complicated than was previously believed, and may represent several independent hydrological systems.
3. Strontium isotope analysis of the brines shows that rock–water interaction must have occurred to explain the radiogenic $^{87}Sr/^{86}Sr$ values compared to seawater. Since strontium is a sensitive indicator of the nature and extent of rock–water interaction, it is a very useful tool for the study of mixing and migration of brines in sedimentary basins.

ACKNOWLEDGMENTS

The authors wish to thank R.A. Trevail, Chief Geologist, of the Petroleum Resources Laboratory, Ontario Ministry of Natural Resources, London, for his continued interest in the project. We would especially like to thank all the individual and corporate petroleum producers in southwestern Ontario and Michigan for allowing us access to samples. The analytical support of R. Kellerman, at the geochemistry and isotope laboratory, University of Waterloo, has been of great assistance. The technical support of I. McAndrew, D. Jones, and C. Jager at McMaster University is greatly appreciated.

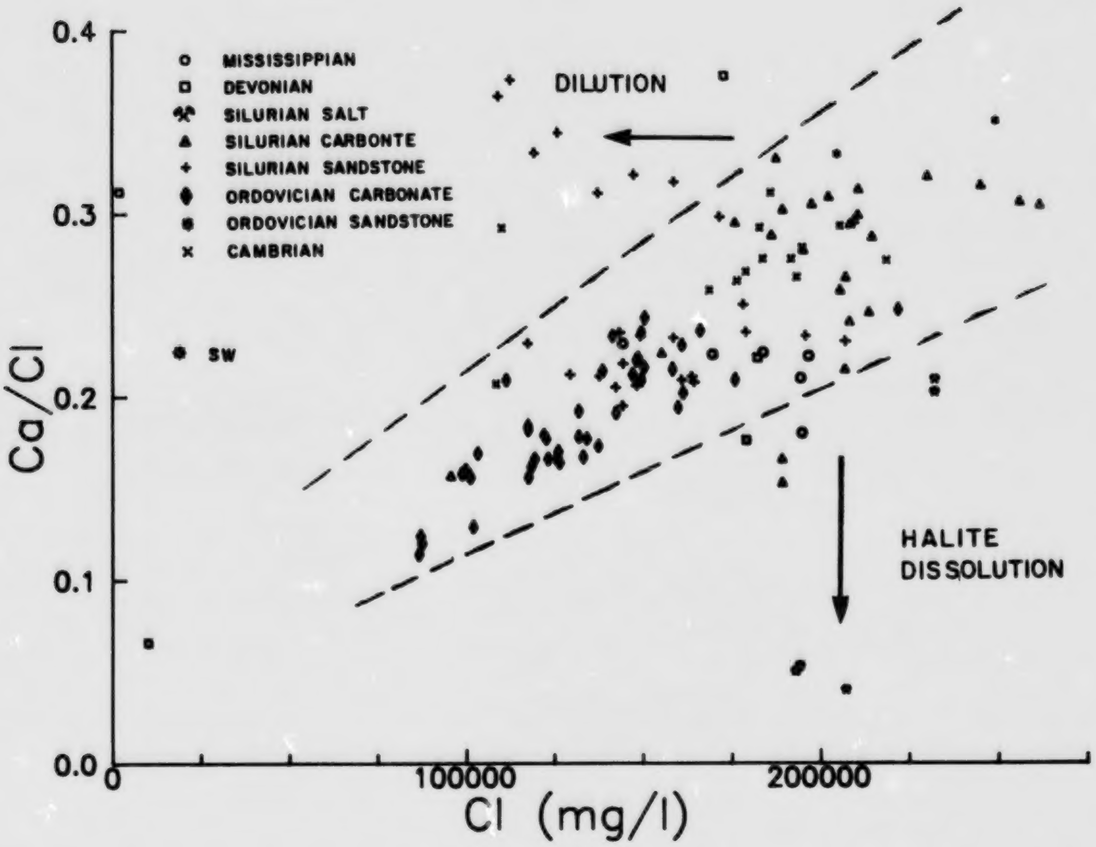

Figure 249.9. *Ca/Cl ratios of formation waters as a function of their chloride content (after Nesbitt 1985).*

REFERENCES

Bredehoeft, J.D., Blyth, C.R., White, W.A., and Maxey, G.B.

1963: Possible Mechanism for Concentration of Brines in Subsurface Formations; American Association of Petroleum Geologists, Bulletin 47, Tulsa, Oklahoma, p.257-269.

Breen, K.J, Clifford, G.A., Masters, R.W., and Sedam, R.C.

1985: Chemical and Isotopic Characteristics of Brines from Three Oil and Gas Producing Sandstones in Eastern Ohio, With Applications to the Geochemical Tracing of Brine Sources; Water Resources Investigation Report 84-4314, U.S. Geological Survey, 58p.

Burke, W.H., Denison, R.E., Hetherington, E.A., Koepnick, R.B., Nelson, H.F., and Otto, J.B.

1982: Variation of Seawater $^{87}Sr/^{86}Sr$ Throughout Phanerozoic Time; Geology, Volume 10, Number 10, p.516-519.

Carpenter, A.B.

1978: Origin and Chemical Evolution of Brines in Sedimentary Basins; p.60-77 *in* Geology of Industrial Minerals, Thirteenth Annual Forum on the Geology of Industrial Minerals, edited by K.A. Johnson and J.A. Russell, Oklahoma Geological Survey, Circular 79.

Clayton, R.N., Friedman, I., Graf, D.L., Mayeda, T.K., Meenis, W.F., and Shimp, N.F.

1966: The Origin of Saline Formation Waters—1: Isotopic Composition; Journal of Geophysical Research, Volume 71, p.3869-3882.

Craig, H.

1961a: Standard for Reporting Concentrations of Deuterium and Oxygen-18 in Natural Waters; Science, Volume 133, p.1833-1834.

1961b: Isotopic Variations in Meteoric Waters; Science, Volume 133, p.1702.

Craig, H., and Gordon, L.

1965: Deuterium and Oxygen-18 Variation in the Ocean and the Marine Atmospheres; p.9-13 *in* Stable Isotopes in Oceanographic Studies and Paleotemperatures—Spoleto 1965, CNR, Pisa.

Davis, S.N.

1964: The Chemistry of Saline Waters; A Discussion by R.A. Krieger, Ground Water, Volume 2, p.51.

Desaulniers, D.E., Cherry, J.A., and Fritz, P.

1981: Origin Age and Movement of Pore-Water in Argillaceous Quaternary Deposits in Four Sites in Southwestern Ontario; Journal of Hydrology, Volume 50, p.231-257.

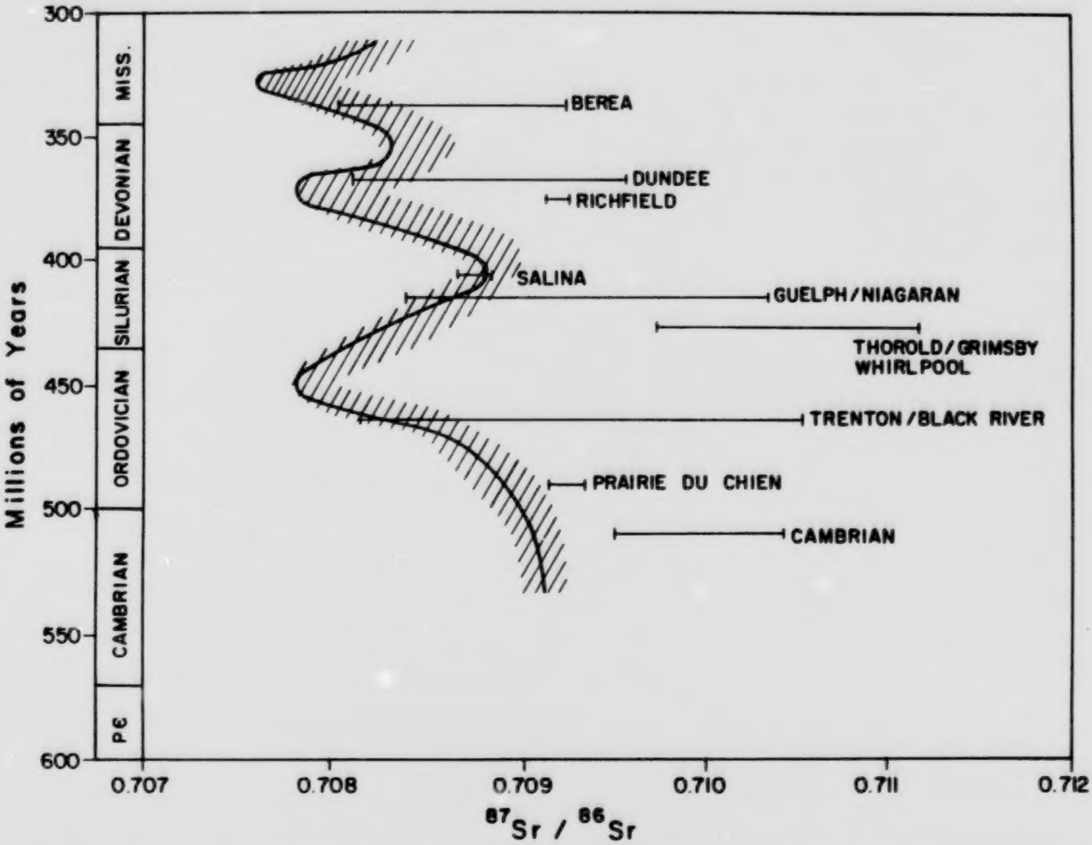

Figure 249.10. *Strontium isotopic composition of brines from the Michigan and northern Appalachian basins. The seawater curve is from Burke et al. (1982). Note that, with few exceptions, the brines are all more radiogenic with respect to seawater for the time in question.*

Ells, G.D.
1969: Architecture of the Michigan Basin; p.60-80 *in* Studies of the Precambrian of the Michigan Basin, edited by H.B. Stonehouse, Michigan Basin Geological Society, Annual Field Excursion Guidebook.

Fritz, P., Drimmie, R.J., Frape, S.K., and O'Shea, K.J.
1987: The Isotopic Composition of Precipitation and Groundwater in Canada; *in* The Use of Isotope Techniques in Water Resources Development, Proceedings of International Symposium, Symposium 299, IAEA.

Graf, D.L.
1982: Chemical Osmosis, Reverse Chemical Osmosis, and the Origin of Subsurface Brines; Geochimica et Cosmochimica Acta, Volume 46, p.1431-1448.

Graf, D.L., Friedman, I., and Meents, W.F.
1965: The Origin of Saline Formation Water—2: Isotope Fractionation by Shale Micropore Systems; Illinois Geological Survey, Circular 393, 32p.

Hanor, J.S.
1983: Fifty Years of Development of Thought on the Origin and Evolution of Subsurface Sedimentary Brines; p.99-111 *in* Revolution in the Earth Sciences: Advances in the Past Half-Century, edited by S.J. Boardman, Kendall/Hunt, Dubuque, Iowa, U.S.A.

Hitchon, B., and Friedman, I.
1969: Geochemistry and Origin of Formation Waters in the Western Canada Sedimentary Basin—1: Stable Isotopes of Hydrogen and Oxygen; Geochimica et Cosmochimica Acta, Volume 33 p.1321-1349.

Holser, W.
1979: Trace Elements and Isotopes in Evaporites; p.295-346 *in* Marine Minerals, edited by R.G. Burns, Reviews in Mineralogy, Volume 6.

Knauth, P.L., and Beeunas, M.A.
1986: Isotope Geochemistry of Fluid Inclusions in Permian Halite with Implications for the Isotopic History of Ocean Water and the Origin of Saline Formation Waters; Geochimica et Cosmochimica Acta, Volume 50, p.419-433.

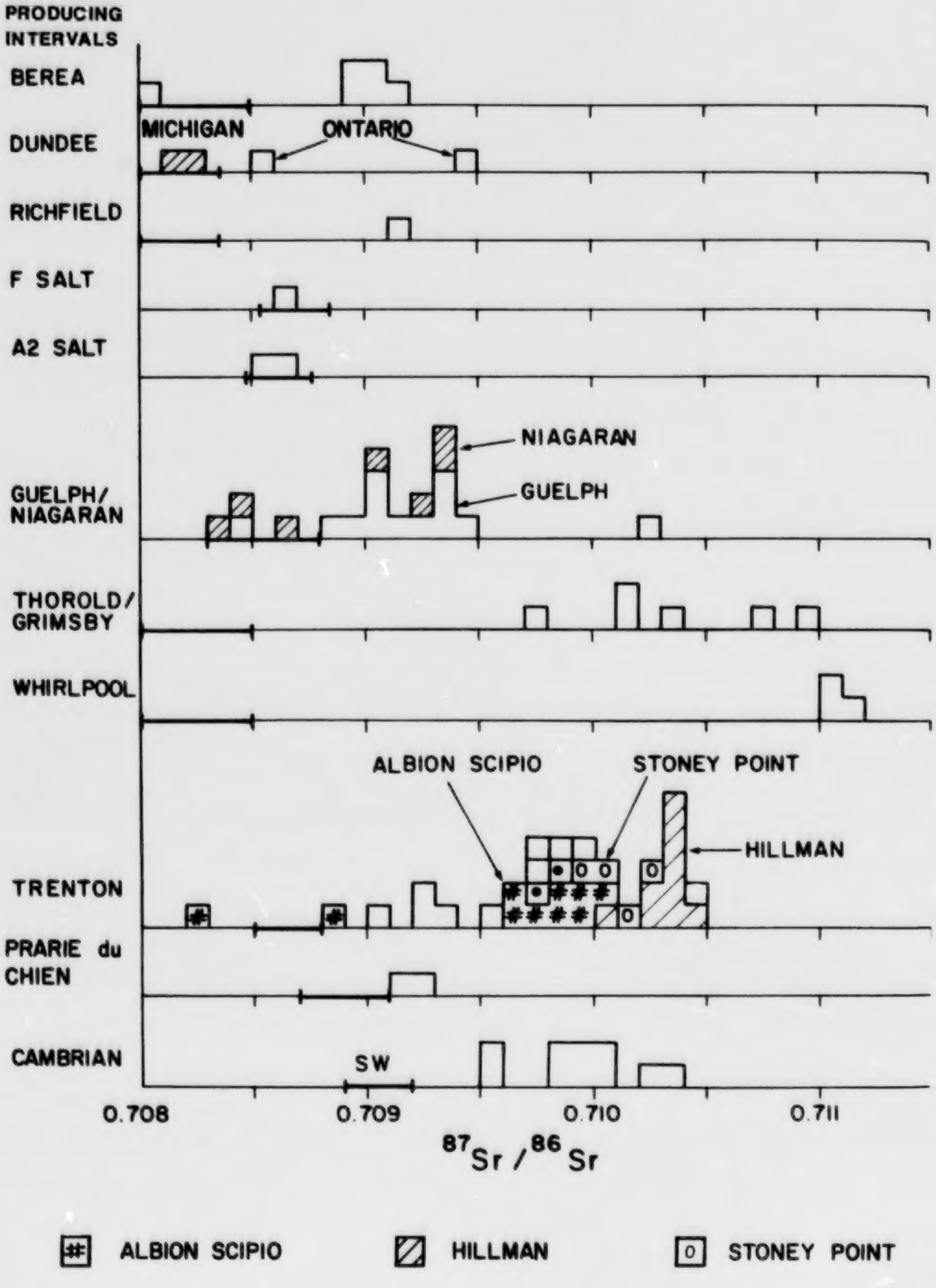

Figure 249.11. *Strontium isotopic composition versus reservoir age displaying groupings of Ordovician reservoirs by individual fields. Seawater strontium ranges are from Burke et al. (1982).*

Krauskopf, K.B.
1979: Introduction to Geochemistry, Second Edition; McGraw Hill, New York, N.Y., U.S.A., 617p.

Land, L.S., and Prezbindowski, D.R.
1981: The Origin and Evolution of Saline Formation Water, Lower Cretaceous Carbonates, Southcentral Texas, U.S.A.; Journal of Hydrology, Volume 54, p.51-74.
1985: Chemical Constraints and Origins of Four Groups of Gulf Coast Reservoir Fluids: Discussion; American Association of Petroleum Geologists, Bulletin 69, Tulsa, Oklahoma, p.119-121.

Lloyd, R.M.
1966: Oxygen Isotope Enrichment of Seawater by Evaporation; Geochimica et Cosmochimica Acta, Volume 30, p.801-814.

McNutt, R.H., Frape, S.K., and Dollar, P.
1987: The Strontium, Oxygen and Hydrogen Isotopic Composition of Brines, Michigan and Appalachian Basins, Ontario and Michigan; Applied Geochemistry, Volume 2, p.495-506.

Nesbitt, H.W.
1985: A Chemical Equilibrium Model for the Illinois Basin Formation Waters; American Journal of Science, Volume 285, p.436-458.

Pierre, C., Ortlieb, L., and Peron, A.
1984: Supratidal Evaporitic Dolomite at Ojo de Liebre Lagoon: Mineralogical and Isotopic Arguments for Primary Crystallization; Journal of Sedimentary Petrology, Volume 54, p.1049-1061.

Rittenhouse, G.
1967: Bromine in Oil Field Waters and its Use in Determining Possibilities of Origin of These Waters; American Association of Petroleum Geologists, Bulletin 51, p.2430-2440.

Sanford, B.V., Thompson, F.J., and McFall, G.H.
1985: Plate Tectonics—A Possible Controlling Mechanism in the Development of Hydrocarbon Traps in Southwestern Ontario; Bulletin of Canadian Petroleum Geology, Alberta Society of Petroleum Geologists, Volume 33, p.52-71.

Taylor, H.P.
1974: The Application of Oxygen and Hydrogen Isotope Studies to Problems of Hydrothermal Alteration and Ore Deposition; Economic Geology, Volume 69, p.843-883.

Toth, J.
1978: Gravity-Induced Cross-Formational Flow of Formation Fluids, Red Earth Region, Alberta, Canada: Analysis, Patterns, and Evolution; Water Resources Research, Volume 14, Number 5, p.805-843.

Veizer, J., and Compston, W.
1974: ^{87}Sr/^{86}Sr Composition of Seawater During the Phanerozoic; Geochimica et Cosmochimica Acta, Volume 38, p.1461-1484.

White, D.E.
1957: Magmatic, Connate, and Metamorphic Waters; Geological Society of America, Bulletin 68, p.1659-1682.
1965: Saline Waters of Sedimentary Rocks; American Association of Petroleum Geologists, Memoir 4, p.342-366.

White, D.E., Hem, J.D., and Waring, G.A.
1963: Data of Geochemistry, Sixth Edition: Chapter F, Chemical Composition of Subsurface Waters; U.S. Geological Survey Professional Paper 440-F, 67p.

Winder, C.G., and Sanford, B.V.
1972: Stratigraphy and Paleontology of Paleozoic Rocks of Southern Ontario; Excursion A45-C45, Guidebook, Twenty-fourth Session, International Geological Congress, Montreal, Quebec, Canada.

Grant 265A Mineralogy and Surface Chemistry of Iron Oxides Associated with Bacteria in Acidic Sediments

F.G. Ferris, K. Tazaki, and W.S. Fyfe

Department of Geology, University of Western Ontario, London

ABSTRACT

A variety of iron oxides were detected by X-ray diffraction in sediments receiving acid drainage from mine tailing and coal refuse impoundments. Goethite and hematite were present only in small amounts. The major iron oxide species was ferrihydrite, which gave diffuse prismatic diffraction bands at angles corresponding to d = 2.5, 2.2, and 1.5 angstroms. Main core line binding energy levels in Fe 2p and O 1s ESCA spectra were consistent with the predominance and hydrous nature of ferrihydrite. Electron microscopy also showed that individual bacterial cells promoted the formation of iron oxide mineralization similar to that present in the bulk sediment samples.

INTRODUCTION

A number of our recent studies have established that bacterial cells are capable of serving as nucleation sites for authigenic mineral formation (Beveridge *et al.* 1983; Ferris *et al.* 1986, 1987). In this investigation we report on iron oxide mineralization associated with bacteria in surface sediments from acid mine drainage environments. In these types of systems, where high levels of ferric iron (Fe^{3+}) are made available by the rapid oxidation of ferrous iron (Fe^{2+}), ferrihydrite precipitation is favoured. This poorly ordered hydrous compound is unstable and usually converts with time to more crystalline forms, such as goethite or hematite (Fischer and Schwertmann 1975; Schwertmann and Murad 1983). However, the type of mineralization that develops from ferrihydrite is strongly influenced by the physical and chemical nature of the depositional environment. For example, the conversion time for ferrihydrite increases significantly under acidic conditions (Schwertmann and Murad 1983). Similarly, inorganic anions that have a high affinity for the ferrihydrite surface tend to inhibit the formation of hematite and goethite, and suppress the crystallinity of the transformation products (Carlson and Schwertmann 1981; Brady *et al.* 1986; Cornell *et al.* 1987). Naturally occurring iron oxides therefore exhibit a broad range of morphological and crystalline states.

Because of the complex nature of iron oxides, samples examined during this investigation were characterized not only with respect to bulk mineralogy, but also in terms of surface chemistry and micromorphology. The mineral composition of the sediment samples was evaluated by X-ray diffraction (XRD); secondary ion mass spectroscopy (SIMS) was used to determine elemental distributions. Electron spectrochemical surface analysis (ESCA) was done by X-ray photoelectron spectroscopy. Bacterial associated mineralization was detected by transmission electron microscopy, and selected area electron diffraction (SAED).

METHODS

SAMPLE COLLECTION

Samples of surficial sediments were collected from seepage areas near inactive mine tailing ponds at Rossport (on the north shore of Lake Superior), Burchell Lake (west of Thunder Bay), and Cranberry Lake (northwest of Sudbury). Acidic sediment samples were also obtained near a coal refuse impoundment in Belmont County, Ohio (provided by R.G. Weise, Department of Geology, Mount Union College, Alliance, Ohio, U.S.A.). After the samples were collected, specimens were immediately fixed with 1.0 percent (volume/volume) aqueous glutaraldehyde (a biological fixative used in electron microscopy). The surficial pH values of the samples were also checked in the field with pH paper, and again in the laboratory using a Metro-Ohm pH meter equipped with a standard combination electrode.

SECONDARY ION MASS SPECTROSCOPY, X-RAY DIFFRACTION, AND X-RAY PHOTOELECTRON SPECTROSCOPY

Specimens for XRD and SIMS were ground extensively under deionized distilled water in a porcelain mortar. The resulting fine suspensions were then recovered with a pipet and dispersed on glass slides. Powder XRD spectra were obtained from these thin films of sediment using Cu Kα radiation; a mass filtered 100 μm diameter $^{16}O^-$ ion beam was used for SIMS.

Sediment samples for ESCA were mounted on copper grids and desiccated before insertion into the high vacuum chamber of the X-ray photoelectron spectrometer. A monochromatized Al Kα X-ray excitation beam was used, and specimen charging was controlled with a low energy electron flood gun. All binding energy levels were referenced to C 1s at 285.0 eV.

ELECTRON MICROSCOPY

Whole mounts and thin sections of the sediment samples were prepared as previously described (Ferris *et al.* 1987). Specimens were examined using either a JEOL EM 100C or a Philips EM 400T transmission electron microscope. Both instruments were operated at 100 kV with liquid nitrogen cooled anticontamination devices in place at all times. Selected area electron diffraction (SAED) patterns were calibrated using evaporated gold as a comparative standard.

RESULTS

SEDIMENT MINERALOGY AND CHEMISTRY

The various sediment samples generated XRD patterns with broad weak reflections suggestive of small crystal size, crystal disorder, and/or amorphous structure. The Rossport samples contained large

TABLE 265A.1. MINERAL COMPOSITION OF ACID MINE DRAINAGE SEDIMENTS AS DETERMINED BY X-RAY DIFFRACTION.

Mineral	Sediment Sample			
	Rossport	Ohio	Burchell Lake	Cranberry Lake
Hornblende	+++	-	-	-
Chlorite	+++	-	tr	-
Feldspar	+	-	-	-
Talc	+	-	-	-
Gypsum	tr	-	-	+
Quartz	+	-	+++	tr
Ferrihydrite	tr	++	+++	+++
Goethite	+	+	tr	tr
Hematite	+	+	tr	tr

tr; trace
-; not present
+; relative abundance

amounts of hornblende and chlorite with smaller amounts of quartz, feldspar, talc, gypsum, and various iron oxides (Table 265A.1). In contrast, the other samples contained an abundance of ferrihydrite which gave broad diffraction bands at angles corresponding to spacings of d = 2.5, 2.2, and 1.5 angstroms. The Burchell Lake sediment samples also contained high levels of quartz and trace amounts of chlorite, whereas gypsum was present in material from Cranberry Lake.

The surficial pH of the Cranberry Lake and Burchell Lake samples ranged from 3.0 to 3.4. Higher pH values of 4.3 to 4.8 were recorded for the Rossport and Ohio samples. A significant enrichment of C, Mg, Al, Si, and Ca was revealed by SIMS in the Rossport samples, as expected from the bulk mineralogy of the sediment; the presence of algae was revealed by light microscopy. In contrast, iron was the principal metallic element detected by SIMS in the Burchell Lake, Cranberry Lake, and Ohio samples. This paralleled the predominance of iron mineralization in these samples, as revealed by XRD. Also, silicon was found as a major nonmetallic element in material from Burchell Lake, as expected from the increased abundance of quartz in the sediment.

The Fe 2p ESCA spectra for the Burchell Lake, Cranberry Lake, and Ohio samples are shown in Figure 265A.1. Analysis of the Rossport samples was not possible because of their low iron content. The main core lines in the ESCA spectra are broad (~3 eV), and asymmetric to the high energy side, with weak satellites approximately 8 eV above the mean binding energy of the core lines. This type of energy intensity distribution is characteristic of Fe_2O_3 (711.0 eV) and FeOOH (711.9 eV; 719.9 eV) (McIntyre and Zetaruk 1977).

In the O 1s ESCA spectra, a mean core line binding energy of 532.0 eV was observed (Figure 265A.2). This is shifted 0.6 eV above the expected binding energy of 531.4 eV for hydroxyl oxygen in FeOOH, and probably reflects the presence of chemisorbed hydroxyl species in the Fe_2O_3 lattice of ferrihydrite (McIntyre and Zetaruk 1977; Wada 1981). The spectra were also broadened, and asymmetric to the low energy side of the main core line. The broadening above 532.0 eV can be attributed to adsorbed carbonyl species (i.e. organic matter), whereas the asymmetry arises from oxide oxygen in Fe_2O_3 and FeOOH (McIntyre and Zetaruk 1977). The Ohio O 1s spectrum in particular exhibited a pronounced "shoulder" around 530.0 eV which corresponds well with XRD data showing higher levels of goethite and hematite.

BACTERIAL ASSOCIATED MINERALIZATION

Direct microscopic examination of thin section samples from Burchell Lake and Cranberry Lake revealed individual bacterial cells in successive stages of mineral encrustation by ferrihydrite (Photo 265A.1). This mineralization had clearly developed in association with the bacteria, and was distinguished by a fibrous appearance. In whole mounts, these ferrihydrite precipitates generated prismatic SAED patterns with reflections at d = 2.5 and 1.5 angstroms (Photo 265A.1c). Mineralization associated with bacteria in the Rossport samples was restricted to a poorly ordered granular material which contained small hematitic microcrystals. Bacterial cells in the Ohio specimens were also encrusted by granular iron oxides, which generated goethitic SAED patterns with d-spacings of 4.2, 2.5, and 1.8 angstroms (Photo 265A.2).

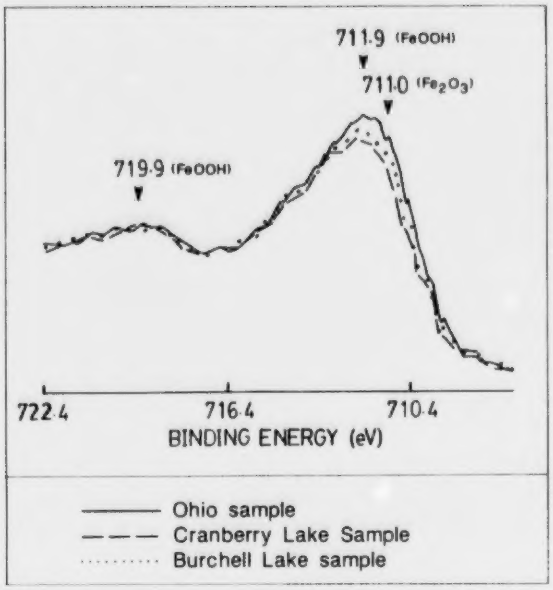

Figure 265A.1. *Fe 2p ESCA spectra of sediment samples from Ohio, Cranberry Lake, and Burchell Lake.*

DISCUSSION

A number of studies have demonstrated that ferrihydrite is commonly formed in acidic waters draining mine tailing and coal refuse impoundments (Crosby *et al.* 1983; Brady *et al.* 1986). In most natural systems, this hydrous compound serves as a precursor for the development of more stable anhydrous iron oxides, such as goethite or hematite (Carlson and Schwertmann 1981). However, low pH values tend to increase the conversion time of ferrihydrite, and decrease the crystallinity of the transformation products (Schwertmann and Murad 1983). This explains both the predominance of ferrihydrite and the formation of other poorly ordered iron oxides in our sediment samples.

Ferrihydrite appears to have a hexagonal unit cell structure which is similar to hematite (Wada 1981). However, data from infrared spectroscopic studies provide evidence of structural hydroxyl groups, and suggest a formula of $Fe_2O_3 \cdot 2FeOOH \cdot 6H_2O$ (Russel 1979). The core line binding energies in the Fe 2p ESCA spectra from our samples are consistent with the presence of both Fe_2O_3 and FeOOH species (McIntyre and Zetaruk 1977). However, comparatively small amounts of goethite and hematite were detected by XRD and electron microscopy. Furthermore, core line binding energies of 532.0 eV in the O 1s ESCA spectra are consistent with a partial replacement of lattice oxygen in Fe_2O_3 by OH^-, and suggest high levels of chemisorbed water (McIntyre and Zetaruk 1977). Thus, it seems reasonable to view ferrihydrite as a complex hydrous oxide-oxyhydroxide phase (Russel 1979).

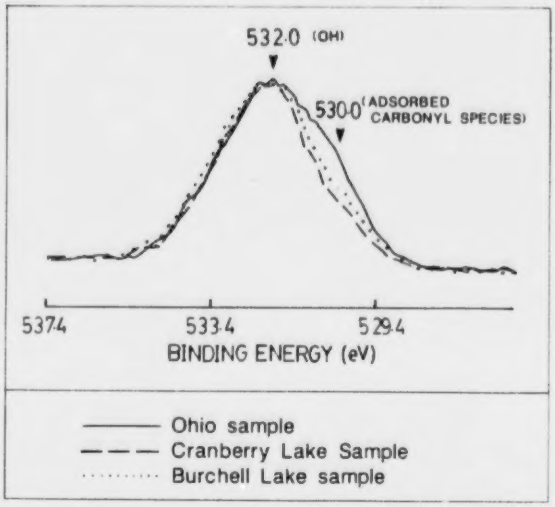

Figure 265A.2. *O 1s ESCA spectra of sediment samples from Ohio, Cranberry Lake, and Burchell Lake.*

Significant amounts of organic matter have been found in natural goethites (Yapp and Poths 1986), and in fresh ferrihydrite precipitates (Carlson and Schwertmann 1981). In the present investigation, bacterial cells were found encrusted in successive stages by ferrihydrite and other iron oxides. These bacteria not only served as nucleation sites for iron precipitation, but their remains were also trapped and incorporated into the mineral precipitates during crystal growth. The ability of bacterial cells to act as templates for mineral formation depends primarily on the inherent capacity of their anionic surface polymers to bind metallic ions (Beveridge and Fyfe 1985). Once immobilized, the metals may be precipitated by hydrolysis, a change in oxidation state, or through reacting with counter-ions in solution (Ferris *et al.* 1986, 1987). The subsequent growth of mineral precipitates formed on bacterial surfaces can then proceed via homogenous crystal nucleation reactions (Berner 1980). A similar series of events starting with the oxidation and hydrolysis of cell-bound ferrous or ferric iron accounts for the ferrihydrite mineralization we observed on bacteria present in acidic mine drainage sediments.

REFERENCES

Berner, R.A.
1980: Early Diagenesis. A Theoretical Approach; Princeton University Press, Lawrenceville, New Jersey, 241p.

Beveridge, T.J., and Fyfe, W.S.
1985: Metal Fixation by Bacterial Cell Walls; Canadian Journal of Earth Sciences, Volume 22, Number 12, p.1893-1898.

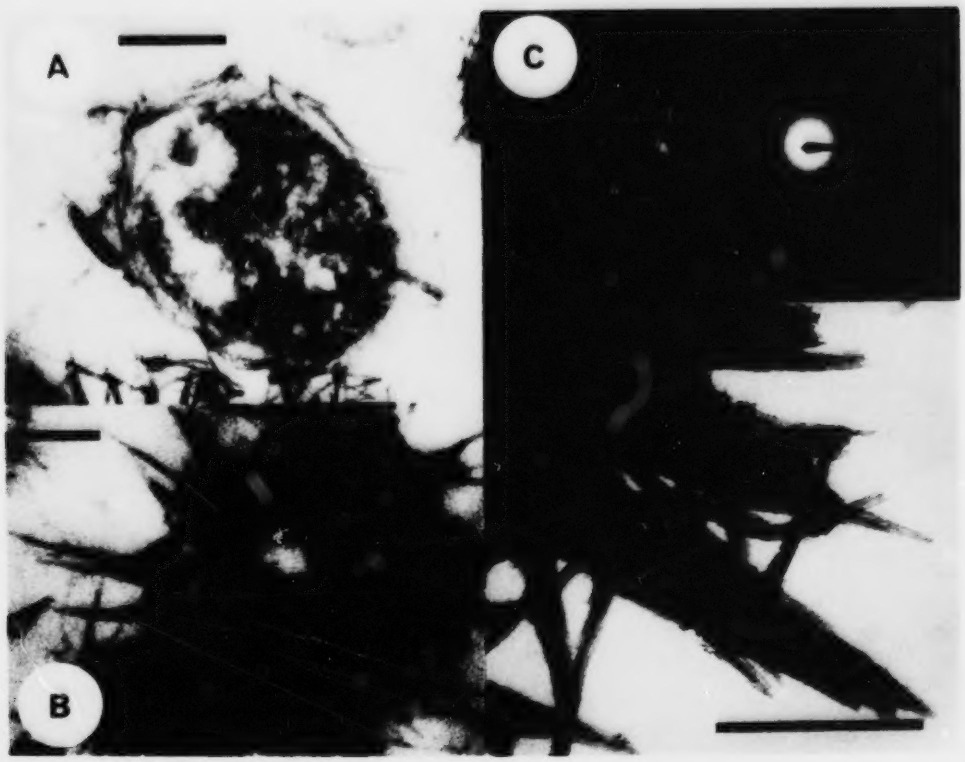

Photo 265A.1. (a and b) Thin section electron micrographs showing the progressive mineralization of bacteria by ferrihydrite in material from Cranberry Lake. (c) Fibrous ferrihydrite and the corresponding SAED pattern in a whole mount of material from Cranberry Lake (scale bar = 200 nm).

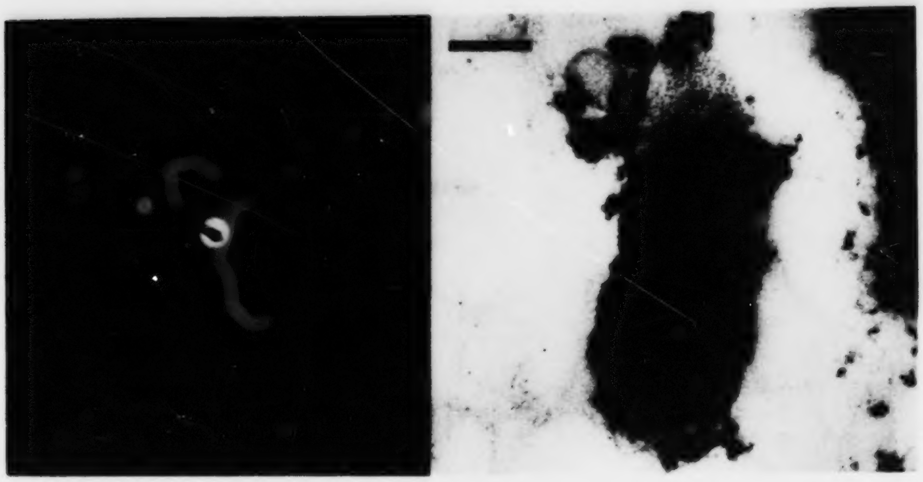

Photo 265A.2. Thin section profile showing the granular nature of bacterial associated iron mineralization in the Ohio sediment samples, and the corresponding goethite SAED pattern (scale bar = 200 nm).

Beveridge, T.J., Meloche, J.D., Fyfe W.S., and Murray, R.G.E.
1983: Diagenesis of Metals Chemically Complexed to Bacteria: Laboratory Formation of Metal Phosphates, Sulphides, and Organic Condensates; Applied and Environmental Microbiology, Volume 45, p.1094-1108.

Brady, K.S., Bigham, J.M., Jaynes, W.F., and Logan, T.J.
1986: Influence of Sulphate on Fe-Oxide Formation: Comparisons with a Stream Receiving Acid Mine Drainage; Clays and Clay Minerals, Volume 34, Number 3, p.266-274.

Carlson, L., and Schwertmann, U.
1981: Natural Ferrihydrites in Surface Deposits from Finland and Their Association with Silica; Geochimica et Cosmochimica Acta, Volume 45, p.421-429.

Cornell, R.M., Giovanoli, R., and Schindler, P.W.
1987: Effect of Silicate Species on the Transformation of Ferrihydrite into Goethite and Hematite in Alkaline Media; Clays and Clay Minerals, Volume 35, Number 1, p.21-28.

Crosby, S.A., Glasson, D.R., Cuttler, A.H., Butler, I., Turner, D.R., Whitfield, M., and Millward, G.E.
1983: Surface Areas and Porosities of Fe(III)- and Fe (II)-Derived Oxyhydroxides; Environmental Science and Technology, Volume 17, Number 12, p.709-713.

Ferris, F.G., Beveridge, T.J., and Fyfe, W.S.
1986: Iron-Silica Crystallite Nucleation by Bacteria in a Geothermal Sediment; Nature, Volume 320, Number 6063, p.609-611.

Ferris, F.G., Fyfe, W.S., and Beveridge, T.J.
1987: Bacteria as Nucleation Sites for Authigenic Minerals in a Metal-Contaminated Lake Sediment; Chemical Geology, Volume 63, Number 3/4, p.225-232.

Fischer, W.R., and Schwertmann, U.
1975: The Formation of Hematite from Amorphous Iron (III) Hydroxide; Clays and Clay Minerals, Volume 23, Number 1, p.33-37.

McIntyre, N.S., and Zetaruk, D.G.
1977: X-ray Photoelectron Spectroscopic Studies of Iron Oxides; Analytical Chemistry, Volume 49, Number 11, p.1521-1529.

Russel, J.D.
1979: Infrared Spectroscopy Studies of Ferrihydrite: Evidence for the Presence of Structural Hydroxyl Groups; Clay Minerals, Volume 14, Number 2, p.109-114.

Schwertmann, U., and Murad, E.
1983: Effect of pH on the Formation of Goethite and Hematite from Ferrihydrite; Clays and Clay Minerals, Volume 31, Number 4, p.277-284.

Wada, K.
1981: Amorphous Clay Minerals—Chemical Composition; p.385-398 *in* Developments in Sedimentology, Volume 35, edited by H. van Olphen and F. Veniale, Proceedings of the 7th International Clay Conference, Elsevier, Amsterdam, 850p.

Yapp, C.J., and Poths, H.
1986: Carbon in Natural Goethites; Geochimica et Cosmochimica Acta, Volume 50, Number 6, p.1213-1220.

Grant 265B Retardation of Toxic Heavy Metal Dispersion From U, and Cu-Ni Mine Tailings, Elliot Lake and Sudbury Districts, Ontario: Role of Acidophilic Microorganisms

H. Mann[1, 2], **K. Tazaki**[1], **W.S. Fyfe**[1], **and M. Wiseman**[3]

[1]Department of Geology, University of Western Ontario, London

[2]Department of Geological Sciences, University of Saskatchewan, Saskatoon, Saskatchewan

[3]Falconbridge Limited, Onaping

PART 1. METAL UPTAKE AND Fe, Fe–Ti OXIDE BIOMINERALIZATION BY ACIDOPHILIC MICROORGANISMS, ELLIOT LAKE

ABSTRACT

Acidic effluent containing enhanced concentrations of toxic metals discharges from a cumulative total of 104 ha of mine tailings waste in Canada. Communities of acidophilic microorganisms—specifically the unicellular alga *Euglena*—and bacteria thrive in many of the hostile low pH effluent environments which are otherwise devoid of life. The microorganisms concentrate aqueous dissolved metals onto cell walls and at intracellular sites during their life cycle, and strongly bind metals during early diagenesis. A sequence is observed in which amorphous iron and titanium concentrated at cell walls is progressively transformed into microcrystalline aggregates of goethite, ferrihydrite, maghemite, magnetite, hematite, lepidocrocite, and ilmenite. The bioprecipitated iron oxides and oxyhydroxides act as scavengers for metals such as Cu, Pb, Zn, Ni, and Th. Acidophilic microorganisms play a central role in the toxic metal budget of mine tailings waste; by efficiently sequestering aqueous metals, and by promoting the nucleation of oxide minerals whose inorganic formation is kinetically inhibited, the dispersion of toxic metals into the natural environment is retarded.

INTRODUCTION

Effluent from mine tailings waste in the Elliot Lake uranium mining district of northern Ontario is variably acidic at pH 2 to 4, and contains extremely enhanced concentrations of a number of toxic metals (Cherry *et al.* 1980; Feenstra *et al.* 1981; Mann and Fyfe 1985a, 1985b). The effluent arises from the dewatering of mine waste slurry that is hydraulically discharged into tailings impoundments, and from the infiltration of ambient precipitation into the tailings. The oxidation of pyrite (FeS_2) and other sulphide minerals in the tailings, by sulphur-oxidizing bacteria (Trudinger and Swaine 1979), generates the low pH conditions and correspondingly high concentrations of dissolved ions. Limestone slurry is generally added to the acidic wastewater from active tailings impoundments; the treated effluent subsequently confluences with the natural drainage system. In all, 100 million tonnes of mine tailings waste are present in the Elliot Lake district. The generation of acidic effluent is a more general problem in most of the mining camps throughout Canada, where tailings impoundments cumulatively amount to an area in excess of 104 ha.

RESULTS

Prolific growths of acidophilic microorganisms (Brock 1978), specifically the unicellular alga *Euglena*, and bacteria, carpet effluent channels in the Elliot Lake mining district (Mann and Fyfe 1985b), and other mining camps throughout Canada (Mann *et al.* 1986; Mann *et al.* 1987). As part of a larger study to evaluate the geochemical budget of metals released by tailings effluent, we have examined communities of the acidophilic microorganisms which populate the effluent channels that are otherwise devoid of life, and their buried remains in channel sediments.

A 0.3 m deep sediment core was bored from a discharge channel in the Stanrock tailings area (Denison Mines Limited), Elliot Lake. The core material is predominantly sand-sized quartz and feldspar derived from erosion of the tailings, with prominent layers of dark organic-rich material composed of decayed leaves and microorganisms (Mann *et al.* 1986). Discharge waters have a pH between 2.0 and 4.6, depending on the amount of precipitation, and carry enhanced concentrations of calcium, magnesium, and aluminum from the hydrolysis of aluminosilicate minerals in the tailings, as well as Fe (350 mg/mL), Zn, Mn, Ti, Ni, Cu, Pb, U, Co, and Th, at levels of up to 103 times the background solute abundances in the natural drainage of the Elliot Lake area (Mann *et al.* 1986; Mann *et al.* 1988). Relative to the average composition of the tailings, the core is characterized by variably enhanced contents of iron (5.0 to 28 weight percent), titanium (2.5 to 6.0 weight percent), and organic carbon (1.2 to 4.0 weight percent), as well as enrichments in several trace elements including Pb, Ni, Th, Cr, Co, Cu, V, and Zn (Mann *et al.* 1986; includes a map of locations).

Samples for microanalysis were taken from six positions within the core; these were placed in 1 percent (by volume) glutaraldehyde (a biological fixative used in electron microscopy), dehydrated through an ethanol-propylene oxide series, and embedded in Epan 812 epoxy resin prior to sectioning into 150 nm slices. Mineral identification in microcrystalline aggregates was conducted by selective area electron diffraction (SAED).

Cell walls of *Euglena*, and various bacteria, are ubiquitous in all sections examined from the sediment core. Identification of the bacteria has not yet been fully undertaken; however, both gram negative and gram positive varieties are present. All stages of cell wall mineralization are evident, from rod-shaped bacteria devoid of metal accumulations to intermediate stages where amorphous iron is concentrated at cell walls; to the nucleation of iron oxide and oxyhydroxide, and iron-titanium oxide minerals. In general, the microcrystalline oxide minerals are acicular in habit, forming rosette-shaped aggregates that radiate from sites on the cell wall (Photo 265B.1). A remarkable variety of iron oxide minerals are present in single sections, including goethite (α-FeOOH), ferrihydrite ($5Fe_2O_3 \cdot 9H_2O$), akaganeite (β-FeOOH), hematite (α-Fe_2O_3), magnetite (Fe_3O_4), and maghemite (γ-Fe_2O_3).

The heavily mineralized microorganisms account for the excess of iron, titanium, and carbon in the sediments over the mean concentration of these elements in the tailings (Mann *et al.* 1986). Microanalytical work is in hand to ascertain whether or not metals such as Zn, Mn, Ni, Cu, Pb, U, Co, and Th, which are present at high concentrations in bulk samples of the living microorganisms, are also present in the biologically nucleated iron and iron-titanium oxide minerals.

Researchers, such as Beveridge and Fyfe (1985), Beveridge and Murray (1985), and Mann *et al.* (1985a, 1985b, 1986), have shown from field and laboratory studies that bacteria and algae are efficient scavengers of a wide variety of aqueous metal ions. Bacterial and algal cell walls are typically anionic in character, and exhibit a profound ability to bind significant quantities of dissolved metals (Ferris and Beveridge 1985; Ferris *et al.* 1986), as well as the ability to act as templates for the nucleation of oxide and silicate minerals whose inorganic formation is kinetically inhibited. Moreover, iron oxides and oxyhydroxides are efficient scavengers of many dissolved trace metal ions (Yapp and Poths 1986; Pickering 1986); accordingly, the biomineralization of such oxides and hydroxides will promote the scavenging of metals from solution.

SUMMARY

The significance of microbiologically produced iron and titanium oxides and hydroxides in acidic mine effluent environments is that these minerals are thermodynamically stable under near surface and weathering conditions, and retain substituted trace metals. Sulphide minerals in tailings, on the other hand, are thermodynamically unstable in the terrestrial surface environment, and release toxic metals during oxidative breakdown. Biomineralization by acidophilic microorganisms acts to sequester toxic metals into stable minerals, thereby retarding metal dispersion in toxic species into the natural environment.

PART 2. STRUCTURE AND MICROANALYSIS OF BIOPRECIPITANTS, SUDBURY DISTRICT

ABSTRACT

Iron-rich sediments in the tailings effluent of the Sudbury nickel-copper mining area, northern Ontario, consist predominantly of magnetite and ferrihydrite, with subordinate amounts of akaganeite (β-FeOOH), goethite (α-FeOOH), hematite (α-Fe_2O_3), and vivianite ($Fe_3(PO_4)_2 \cdot 8H_2O$). The iron is derived from the biologically mediated oxidative breakdown of iron sulphide minerals in the mine tailings waste, which generates acidic effluent with enhanced concentrations of aqueous iron and sulphate (SO_4^{2-}). Surface analysis of the sediments (Table 265B.1) by ESCA reveals that carbon (57 atomic percent), oxygen (31 atomic percent), and iron (6.7 atomic percent) are most abundant, in accordance with the presence of ubiquitous acidophilic microorganisms and their remnants, and iron oxide and oxyhydroxide minerals. The high resolution spectra of sulphur (S 2p) indicates the partitioning of sulphur between the SH (163.4 eV), SO_3 (167.3 eV), and SO_4^{2-} oxidation states, (Figure 265B.2) with SO_4^{2-} the most abundant in the mineral gypsum ($CaSO_4$). Similarly, carbon (C 1s spectrum) is partitioned between hydrocarbon (285 eV) and carbonate (289.2 eV); and iron (Fe 2p spectrum) between FeS, $Fe(C_5H_5)(CO)_3$, $FeSO_4$, and FeOOH. Both carbon and iron spectra show a relationship between organic and inorganic compounds, suggesting that iron mineralization is linked to the microorganisms. Transmission electron micrographs revealed the ubiquitous remains of microorganisms in the sediments, heavily encrusted with iron oxide and oxyhydroxide minerals. Magnetite, maghemite, ferrihydrite, and goethite associated with cell walls and intracellular sites were identified from the d-spacings of electron diffraction patterns. The nucleation of iron oxide minerals by acidophilic microorganisms appears to be ubiquitous in acidic iron-rich tailings environments. The precise synthetic pathways of iron mineral formation are not known.

INTRODUCTION

The leaching of 600 million tonnes of mine tailings and rock waste in the Sudbury nickel-copper mining district, by the infiltration of precipitation, and by tailings dewatering, is responsible for the release of 41 000 kg of nickel and other toxic metals into tailings discharge waters annually. Mann *et al.* (1988) documented the chemical composition and pH of tailings discharge waters from various localities, and the bulk chemical composition of acidophilic microorganisms, specifically the alga *Euglena*, which thrives in this inimical, low pH, toxic metal laden environment. Bulk chemical analyses revealed extremely high concentrations of iron, nickel, and copper in the acidophilic algae, and in the sediments of the lakes in which they flourish. This signifies the role of these microorganisms in sequestering aqueous metals from solution, and in transferring these to sediments, thereby retarding toxic metal dispersion. In order to identify the nature, crystal form, and siting of the metals associated with the microorganisms, a variety of analytical techniques including X-ray diffraction (XRD), secondary ion mass spectrometry (SIMS), X-ray photoelectron spectroscopy (XPS), selective area electron diffraction (SAED), and transmission electron microscopy (TEM), were used. Below, we describe the results of microanalytical studies conducted on the algae and sediments. The study area is illustrated in Figure 265B.1

XRD

X-ray powder diffraction (XRD) was carried out with a RIGAKU (CN 2029 D/MAX-IA) instrument under standard operating conditions. Bulk samples were ground

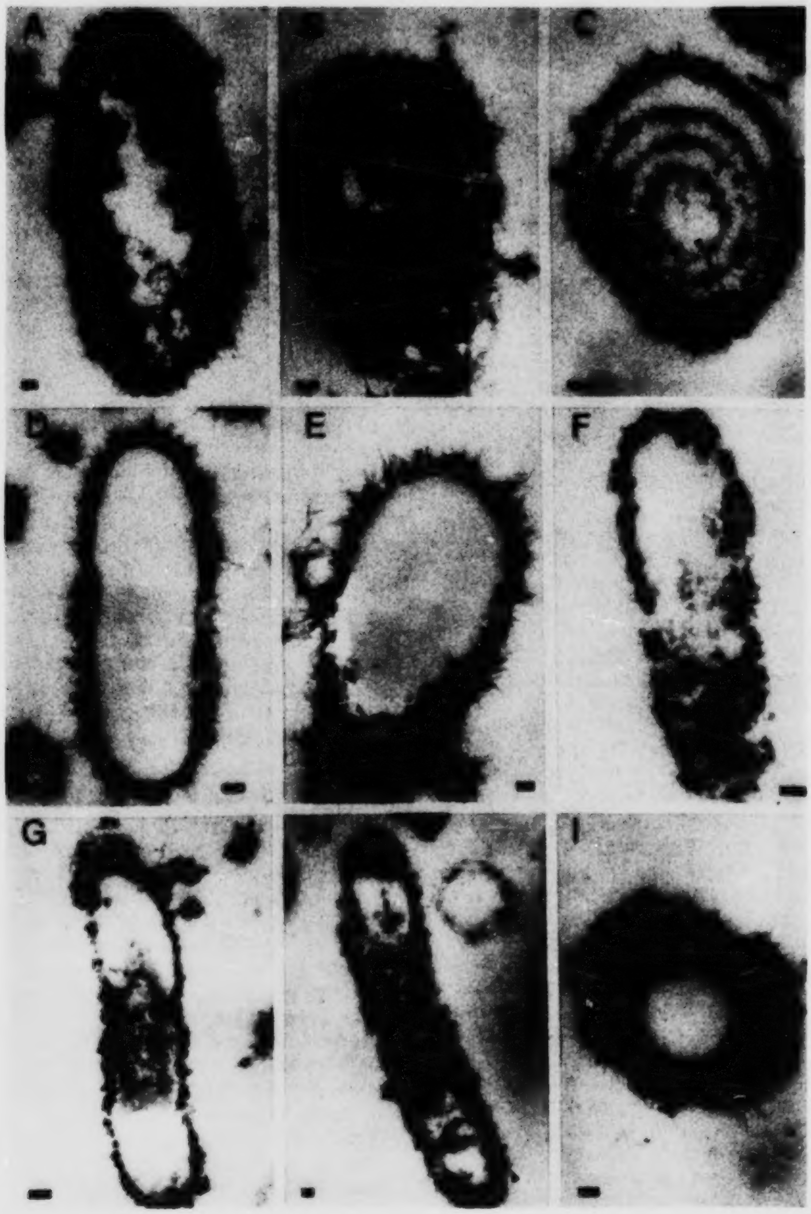

Photo 265B.1. *Montage of thin section transmission electron micrographs illustrating the variety of biologically mediated iron oxide and oxyhydroxide, and iron-titanium oxide mineralization in sediment core. (a). Mixture of well formed crystals of goethite and ferrihydrite. Arrows indicate position of the outer cell membrane. (b). Cell wall decorated by aggregates of magnetite crystals. The inner semi-circular structure (arrows) may be the remains of the nucleus. (c). Concentric zones of maghemite crystals. Concentric configuration of intracytoplasmic membranes suggestive of a Type II methanotroph bacteria. Arrows indicate membranes. (d). Rod-shaped bacterium: external surface of cell wall decorated by well formed crystals of ferrihydrite. Microcrystalline aggregate of ferrihydrite and goethite on cell wall. (e). Cell wall encrusted with acicular goethite. (f). Heavy deposition of amorphous iron on cell wall. (g). Amorphous iron on cell wall and in cytoplasm. (h). Rod-shaped bacterium with amorphous iron precipitate. Arrows indicate a few well formed goethite and ferrihydrite crystals, which are intracellular, as well as on the external cell wall surface. (i). Cell wall surrounded by a thick aggregate of ilmenite crystals.*

TABLE 265B.1. SURFACE COMPOSITION OF TAILINGS SEDIMENTS. CRANBERRY LAKE (XPS).

	Elem.	Atom %
Fe	2p3	1.93
0	1s	30.34
N	1s	1.98
C	1s	56.08
Cl	2p	0.38
S	2p	2.18
Si	2s	0.55
Fe	3p	6.56
	Total	100.00 %

under distilled water in a porcelain mortar, and the resulting suspension pipetted off and sedimented onto a glass slide.

Powder data for iron oxide minerals are taken from Towe and Bradley (1967), Chukhrov *et al.* (1973), and Brindley and Brown (1980). Because XRD data cannot adequately indicate the shape of the reflections of poorly crystalline material, it was necessary to conduct TEM with electron diffraction for each specimen (grain).

SIMS

Secondary ion mass spectrometry (SIMS) spectra were determined with a Cameca IMS-3F secondary ion mass spectrometer. The bulk specimens were analyzed with a $^{16}O^-$ primary ion beam with a beam diameter of approximately 100 nm, a 12.5 KeV primary accelerating voltage, and a +4.5 KeV secondary accelerating voltage. A mass-filtered $^{16}O^-$ primary beam produced the positive secondary ion data spectrum. Thin sections for SIMS analysis were made by the sedimentation of powders with distilled water, in the same manner as for the XRD slides.

XPS

The crystallinity of iron oxides reflects growth conditions, which depend in turn upon the environmental conditions under which the iron minerals form. It is important, therefore, to characterize the variation in compositions between Fe_2O_3 and FeOOH. This is most effectively done by X-ray photoelectron spectroscopy (XPS). XPS analyses were carried out with an SSX-100 X-ray photoelectron spectrometer (U.H.V. Instruments Canada) in custom-designed vacuum and sample treatment chambers. This system uses an exciting X-ray beam which can be focused down to a spot as small as 150 μm in diameter. A monochromatized Al K α X-ray beam was used, resulting in substantially narrower photoelectron peak widths than those obtained by a conventional XPS spectrometer.

The bulk powder samples were mounted on copper tape under grid. These were "pumped" for 5 to 6 hours before insertion into the ultra-high vacuum chamber used for the XPS experiments. Surface charging by the X-ray beam was controlled using a low energy electron flood gun. All binding energies were referenced to C 1s at 285.0 eV.

TEM

Transmission electron micrographs (TEM) were obtained with a JEOL 100 C-TEM instrument, using an accelerating voltage of 100 KeV. Bulk samples were suspended in distilled water (as for XRD) for TEM. The d-spacings of electron diffraction patterns were calibrated by using a gold standard. It is difficult to identify specific iron oxide minerals in mixed poorly crystalline aggregates; consequently, a TEM technique is required to characterize each grain.

RESULTS

MINERALOGICAL AND CHEMICAL COMPOSITION OF BULK SAMPLES

The bulk mineralogical composition from XRD is mainly magnetite and ferrihydrite with a trace amount of goethite, hematite, quartz, and gypsum. Results from electron spectrochemical surface analyses (ESCA) are then described, on the nature of sulphur, carbon, and iron compounds, and the oxidation state of these elements.

Finally, we present transmission electron micrographs of iron oxide biomineralization associated with microorganisms in the tailings sediments. X-ray diffraction analysis of the tailings sediment sample shows a predominance of magnetite and ferrihydrite. Other minerals identified were gypsum, quartz, goethite, and hematite.

The abundance of newly precipitated iron oxide and iron oxyhydroxide minerals, including magnetite, hematite, ferrihydrite, goethite, and akaganeite in the Cranberry Lake tailings sediment is in accord with the extremely enhanced levels of dissolved iron present in tailings effluent. This enhancement results from the oxidation of iron sulphide minerals in the tailings (Mann *et al.* 1988). Similarly, gypsum precipitates as the ion activity product of aqueous calcium and SO_4^{2-} is exceeded, the calcium being derived from the hydrolysis of silicate minerals, and SO_4^{2-} from the oxidation of sulphide minerals in the tailings. Phosphorus is not abundant in the tailings waters; accordingly, the iron phosphate mineral vivianite may represent a reaction between aqueous iron and phosphorus derived from the decomposition of acidophilic microorganisms.

The chemical composition of the bulk tailings sample shows high concentrations of H, O, Na, Si, S, Ca, Cu, and U, using SIMS. The surface chemical composition has been characterized quantitatively by XPS (Table 265B.1). Carbon and oxygen are predominant (56 and 30 atomic percent, respectively), with subordinate quantities of iron, nitrogen, and sulphur (8.5, 2.0, and 2.2 atomic percent, respectively). The high carbon content is in accord with the relative abundance of organic residue from decayed microorganisms, and newly formed hydrocarbon and carbonate compounds (Figure 265B.2b). Oxygen is present both within the iron oxides and hydroxides.

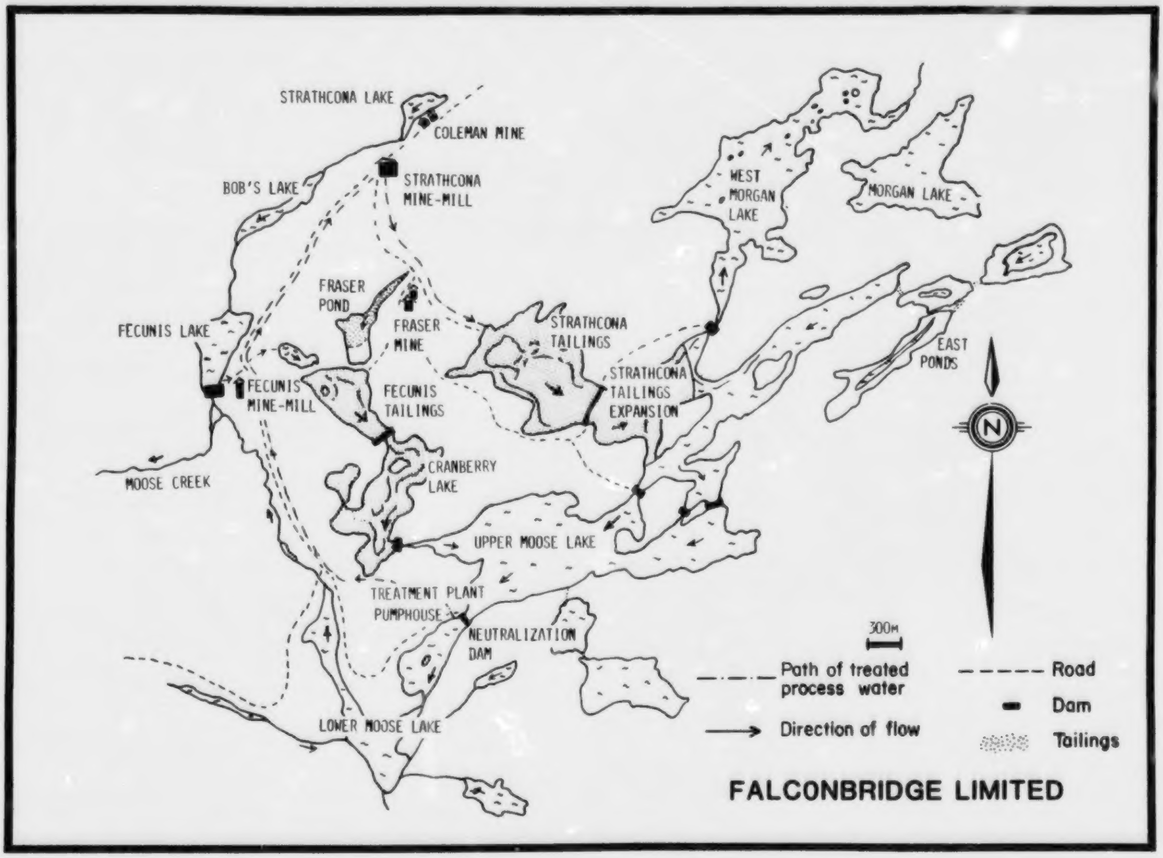
STRATHCONA LAKE
COLEMAN MINE
BOB'S LAKE
STRATHCONA MINE-MILL
WEST MORGAN LAKE
MORGAN LAKE
FRASER POND
FRASER MINE
STRATHCONA TAILINGS
FECUNIS LAKE
FECUNIS MINE-MILL
FECUNIS TAILINGS
STRATHCONA TAILINGS EXPANSION
EAST PONDS
N
CRANBERRY LAKE
MOOSE CREEK
UPPER MOOSE LAKE
TREATMENT PLANT PUMPHOUSE
NEUTRALIZATION DAM
LOWER MOOSE LAKE
300M
Path of treated process water
Road
Dam
Direction of flow
Tailings
FALCONBRIDGE LIMITED

Figure 265B.1. Simplified map of mines, tailings areas, and Moose Lake treatment system at Onaping. Dashed lines with dots represent path of recycled treated Lower Moose Lake water (process water). Arrows indicate direction of flow.

Nitrogen is presumed to be associated with the organic compounds; sulphur with gypsum ($CaSO_4$), and to a lesser extent, iron monosulphide (Figure 265B.2a, 265B.2c).

PARTITIONING OF SULPHUR, CARBON, AND IRON BETWEEN DIFFERENT COMPOUNDS

X-ray photoelectron spectroscopy (XPS) is a powerful surface analytical technique which is well suited to the characterization of reaction products on surfaces. The technique is capable of measuring the elemental composition in a layer as thin as 10 angstroms. Chemical effects can often be identified from the resulting spectrum. Measurements of electron energy shifts, resulting from chemical bonding and consequent changes in electron density near each nucleus, provide information on oxidation states and chemical compounds present.

The high resolution energy spectrum of sulphur (S 2p) in the bulk sample indicates that three types of sulphur compound are present: SH (163.4 eV; organic sulphur), SO_3 (167.3 eV), SO_4^{2-} (168.5 eV), and $SO_4^{(2p\ 1/2)}$(169.7 eV) (Figure 265B.2a). The SO_4^{2-} type is dominant in this sample at 86 percent (168.5, 169.7 eV), which is in accord with the presence of gypsum formed by the reaction of aqueous calcium with SO_4^{2-} (generated by the oxidation of sulphide minerals). The quantities of S^{2-} and SO_3 present are small (5 and 4 percent, respectively).

Similarly, the high resolution energy spectrum of carbon (C 1s) indicates that hydrocarbon (285 eV) is the dominant carbon compound; a subordinate amount of carbonate (289.2 eV) is also present (Figure 265B.2b). The high resolution energy spectrum of iron (Fe 2p) (Figure 265B.2c), shows FeS (709.0 eV), $Fe(C_5H_5)(CO)_3$ (712.4 eV), $FeSO_4$ (710.2 eV), and FeOOH (711.6 eV). The peak at 712.4 eV indicates the presence of an organic component, corroborating field observations. Both carbon (1s) and iron (2p) (Figure 265B.2b, 265B.2c) show a relationship between organic and inorganic materials, suggesting that iron mineralization is associated with microorganisms.

STEM—TEM

The whole mounts of this specimen are rich in ferrihydrite, showing two types of morphology: one with fibrous networks giving clear (electron diffraction)

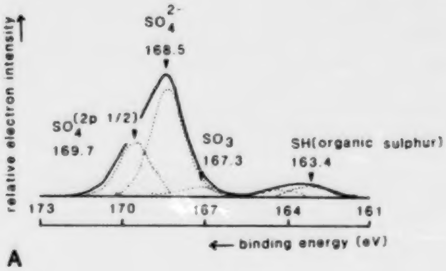

Figure 265B.2a. *High resolution energy spectra (XPS) of sulphur for a tailings sediment sample from Cranberry Lake, illustrating the partitioning of sulphur between different available sulphur compounds. Note the dominance of the sulphate (SO_4^{2-}) species at 168.5 eV.*

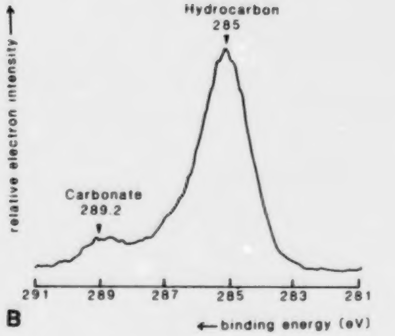

Figure 265B.2b. *High resolution energy spectra (XPS) of carbon for a tailings sediment sample from Cranberry Lake, illustrating the partitioning of carbon between different available carbon compounds. Note the dominance of hydrocarbon (285 eV), or reduced carbon compounds, over oxidized carbon (carbonate).*

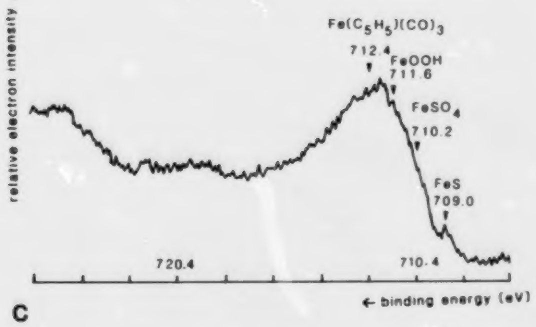

Figure 265B.2c. *High resolution energy spectra (XPS) of iron for a tailings sediment sample from Cranberry Lake, illustrating the partitioning of iron between different available iron compounds. Note the dominance of the iron hydrocarbon/carbonate compound (712.4 eV) over iron monosulphide (709.0 eV).*

rings at 2.5, 2.2, and 1.49 angstroms; the second developed in association with the bacteria, and appears as elongated fibers extending away from the cell surfaces. Fine granular iron oxide grains have been partly attached to the surface of elongated fibrous ferrihydrite.

Thin sections of material from the Fraser Mine pond revealed the remnants of microorganisms with anhydrous iron oxides heavily precipitated on outside cell membranes (ocm) (Photo 265B.2a). The deposition of finer aggregates of microcrystalline anhydrous iron oxides can be faintly detected on "cytomembranes" (cy). The "empty" areas inside the "cytomembrane" may be the remains of several contractile vacuoles (cv), found in algae.

Sediments from Lower Moose Lake, below the neutralization dam (Mann *et al.* 1988), revealed abundant microorganisms when viewed by TEM (Photos 265B.2b, 265B.3, 265B.4). These were heavily encapsulated by magnetite on both the outside and inside of cell envelopes. In the "cytoplasmic area", microcrystalline aggregates of maghemite occur with a fibrous morphology, or habit. Abundant crystals of goethite surrounding the cell wall of a microorganism were identified in a sample from Cranberry Lake (Photo 265B.5), confirming the identification of goethite from XRD analysis of the bulk samples.

DISCUSSION AND CONCLUSIONS

A prominent feature of the samples from the various tailings environments investigated at Onaping is the coexistence of a wide variety of iron oxide and iron oxyhydroxide minerals associated with the cell walls of microorganisms, including goethite, ferrihydrite, hematite, akaganeite, magnetite, and maghemite. Moreover, different morphologies of ferrihydrite crystals are present. Mann *et al.* (1986) describe amorphous iron oxyhydroxides, lepidocrocite, and magnetite biomineralization associated with the cellular remnants of acidophilic algae and bacteria, from the Elliot Lake uranium mining district of northern Ontario. The tailings environment at Elliot Lake is similar to that at Sudbury, in terms of low pH, high toxic metal loading, and specifically in terms of enhanced concentrations of dissolved iron arising from the oxidative breakdown of iron sulphide minerals in the tailings.

Ferris *et al.* (1987), and Schwertmann and Murad (1983) suggested the existence of two competitive formation processes for iron oxide synthesis: goethite by solution processes; and hematite by the internal rearrangement and dehydration within aggregates of ferrihydrite. These concepts imply that conditions favourable for the formation of goethite are unfavourable for the formation of hematite, and vice versa. The storage of ferrihydrite in aqueous suspensions at 24°C and pHs between 2.5 and 12 for three years resulted in the formation of goethite and hematite. Hematite formation was maximized between pH 7 and 8, and that of goethite between pH 14 and pH 12 (Schwertmann and Murad 1983).

In alkaline media and at 70°C, dilute suspensions of ferrihydrite transformed into goethite between pH 11.2 and 14, and to a mixture of goethite and hematite above and below this pH range. The morphology of goethite was found to be chiefly a function of the pH of the system. Acicular crystals formed at all pHs and exclusively above pH 12.2 (Cornell and Giovanoli 1985). The transformation of ferrihydrite into goethite and/or hematite in alkaline media is strongly retarded by the presence of silicate species (Cornell *et al.* 1987).

At present, the precise synthetic pathways of iron oxide and oxyhydroxide biomineralization in the tailings sediments are not fully understood. However, qualitatively, the tailings are subject to intermittent flooding and dessication, such that the activity of H_2O must fluctuate significantly. In addition, variations in Eh and pH occur on a scale of metres, according to the relative proportions of reduced carbon species, and all influence the partitioning of iron between the divalent and trivalent states. The complexity of the tailings microenvironment is interpreted to account for the variety of iron oxide minerals identified.

The significance of microbiologically mediated iron oxide mineralization is that iron oxide minerals are thermodynamically stable under terrestrial surface weathering conditions, and most natural surface environments. Sulphide minerals, on the other hand, are thermodynamically unstable under near surface aerobic conditions, and undergo biologically mediated oxidative breakdown in the tailings to generate acidic effluent with concomitant toxic metal loading, and enhanced concentrations of aqueous iron.

This study has shown that acidophilic microorganisms, especially the unicellular alga *Euglena*, and various bacteria, are ubiquitous in the low pH, toxic metal laden conditions of mine tailings environments at Sudbury. Acidophilic microorganisms are efficient scavengers of aqueous metals, promoting the nucleation of iron oxide and oxyhydroxide minerals at cell walls, and in intracellular positions. As a consequence, acidophilic microorganisms retard the dispersion of iron and other metals into the natural environment.

APPENDIX

ANALYTICAL METHODS

Algal and sediment samples were placed in 5 ml metal-free tubes containing 1 ml of 1 percent, by volume, aqueous glutaraldehyde, a biological fixative used in electron microscopy. Unfixed samples were embedded in 2 percent (by volume) noble agar (from Difco), dehydrated through an ethanol-propylene oxide series (both chemicals from Fisher), and embedded in EPON 812 (from CanEM). Sections, approximately 150 nm in thickness, were obtained using a Reichert–Jung Ultracut E ultra-microtome, and mounted on Formvar carbon-coated aluminium grids. No stains were employed for analytical electron microscopy; instead, the inherent electron scattering of metals complexed by the cells *in situ* was used for differentiation.

Specimens were examined with a Philips EM 400T TEM/STEM equipped with a goniometer stage and an EDAX energy-dispersive X-ray spectrometer. The electron microscope was operated

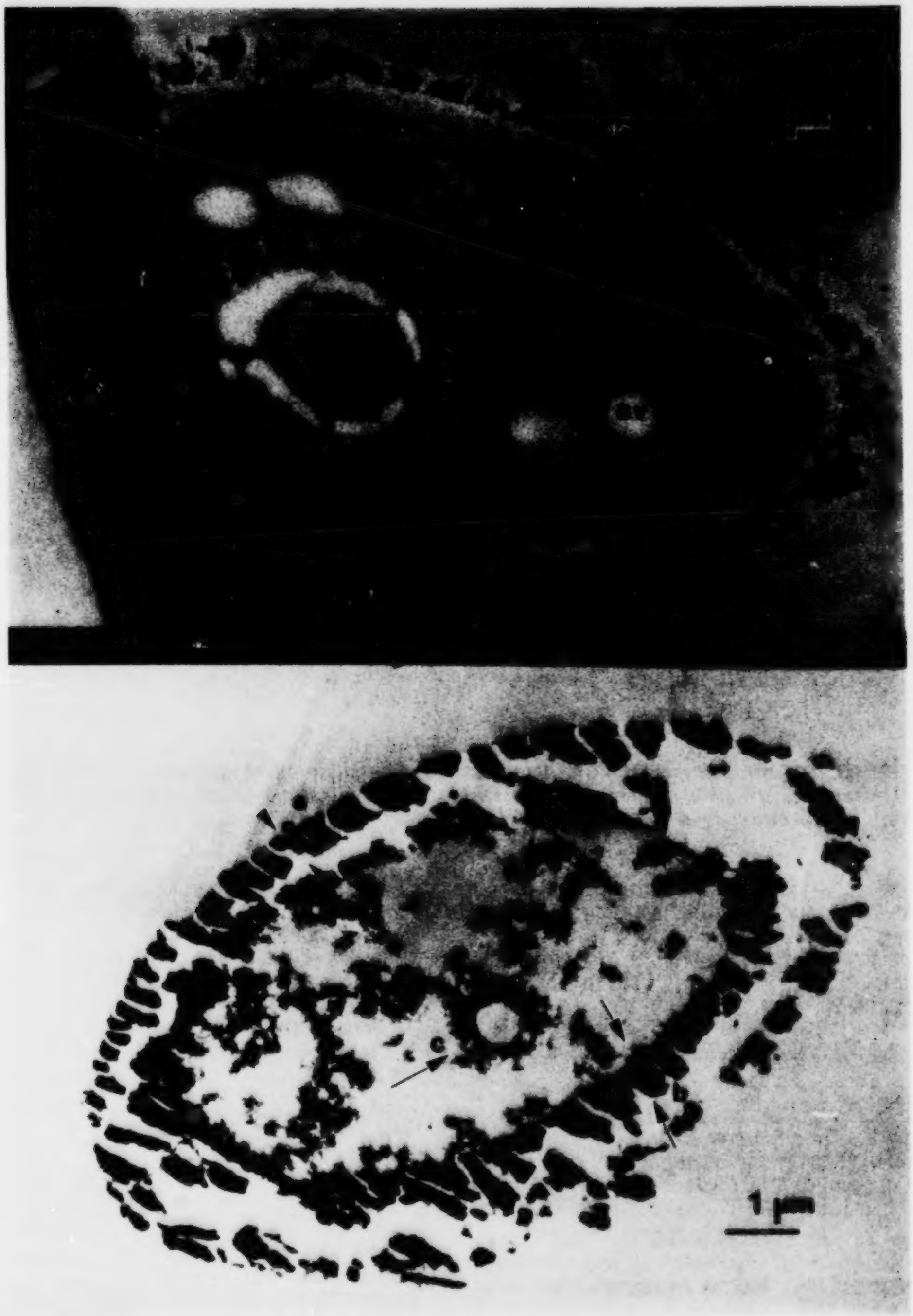

Photo 265B.2. *Remnants of microorganisms in successive stages of mineralization. (a). Transmission electron micrograph of thin-sectioned material from the Fraser Mine Pond. Microorganism with anhydrous iron oxides heavily precipitated on outside cell "membrane" (ocm). Deposition of finer aggregates of microcrystalline anhydrous iron oxides can be seen on membranes, indicated by arrows. The empty area inside the membrane may be the remains of several contractile vacuoles (cv) found in algae. (b). Transmission electron micrograph of thin-sectioned material from Lower Moose Lake, revealing abundant microorganisms: these were heavily encapsulated by magnetite on the outside (a) and inside (b) of cell envelopes. In the cytoplasmic area (c), crystals of maghemite occur.*

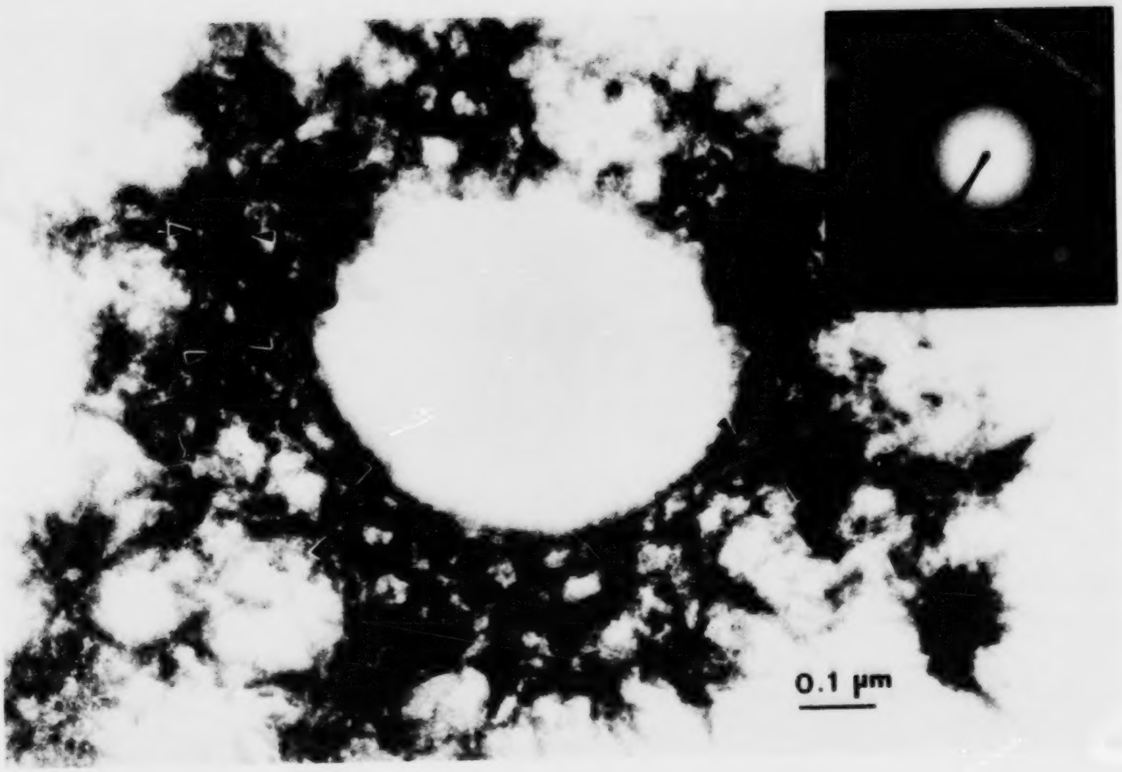

Photo 265B.3. *Transmission electron micrograph showing detail of microorganism from Photo 265B.2b (detail "c"). Remnants of the membrane can be faintly detected (arrows). Selected area electron diffraction pattern of the maghemite is inset in upper right corner.*

at 100 KeV with a liquid nitrogen-cooled anti-contamination device in place at all times. Energy-dispersive X-ray spectroscopy (EDS) was conducted with electron beam spot sizes of 100 nm or less, and counts were collected for 100 seconds (live time). Selected area electron diffraction (SAED) patterns were obtained in the transmission mode. Spacings were determined by using evaporated gold as a standard.

REFERENCES

Beveridge, T.J., and Fyfe, W.S.
1985: Metal Fixation by Bacterial Cell Walls; Canadian Journal of Earth Sciences, Volume 22, Number 12, p.1883-1898.

Beveridge, T.J., and Murray, R.G.E.
1980: Sites of Metal Deposition in the Cell Wall of Bacillus Subtilis; Journal of Bacteriology, Volume 141, p.876-887.

Brindley, G.W., and Brown, G.
1980: Crystal Structures of Clay Minerals and Their X-Ray Identification; Mineralogical Society, Monograph No. 5, London, 495p.

Brock, T.D.
1978: Thermophilic Microorganisms and Life at High Temperatures; Springer Series in Microbiology, Springer–Verlag, New York, 449p.

Cherry, J.A., Blackport, R.J., Dubrovsky, V., Gillham, R.W., Lim, T.P., Murray, D., Reardon, E.J., and Smyth, D.J.A.
1980: Subsurface Hydrology and Geochemical Evolution. Inactive Pyritic Tailings in the Elliot Lake Uranium District, Canada; p.353-385 *in* Proceedings of the Third Symposium on Uranium Tailings Management, November 24-25, Colorado State University, Fort Collins, Colorado.

Chukhrov, F.V., Zvyagin, B.B., Ermilova, L.P., and Gorshov, A.I.
1973: New Data on Iron Oxides in the Weathering Zone; p.333-341 *in* Proceedings of the 1972 International Clay Conference, edited by J.M. Serratosa, Division de Ciencias C.S.I.C., Madrid.

Cornell, R.M., and Giovanoli, R.
1985: Effect of Solution Conditions on the Proportion and Morphology of Goethite Formed from Ferrihydrite; Clays and Clay Minerals, Volume 33, Number 5, p.424-432.

Cornell, R.M., Giovanoli, R., and Schindler, P.W.
1987: Effect of Silicate Species on the Transformation of Ferrihydrite into Goethite and Hematite in Alkaline Media; Clays and Clay Minerals, Volume 35, Number 1, p.21-28.

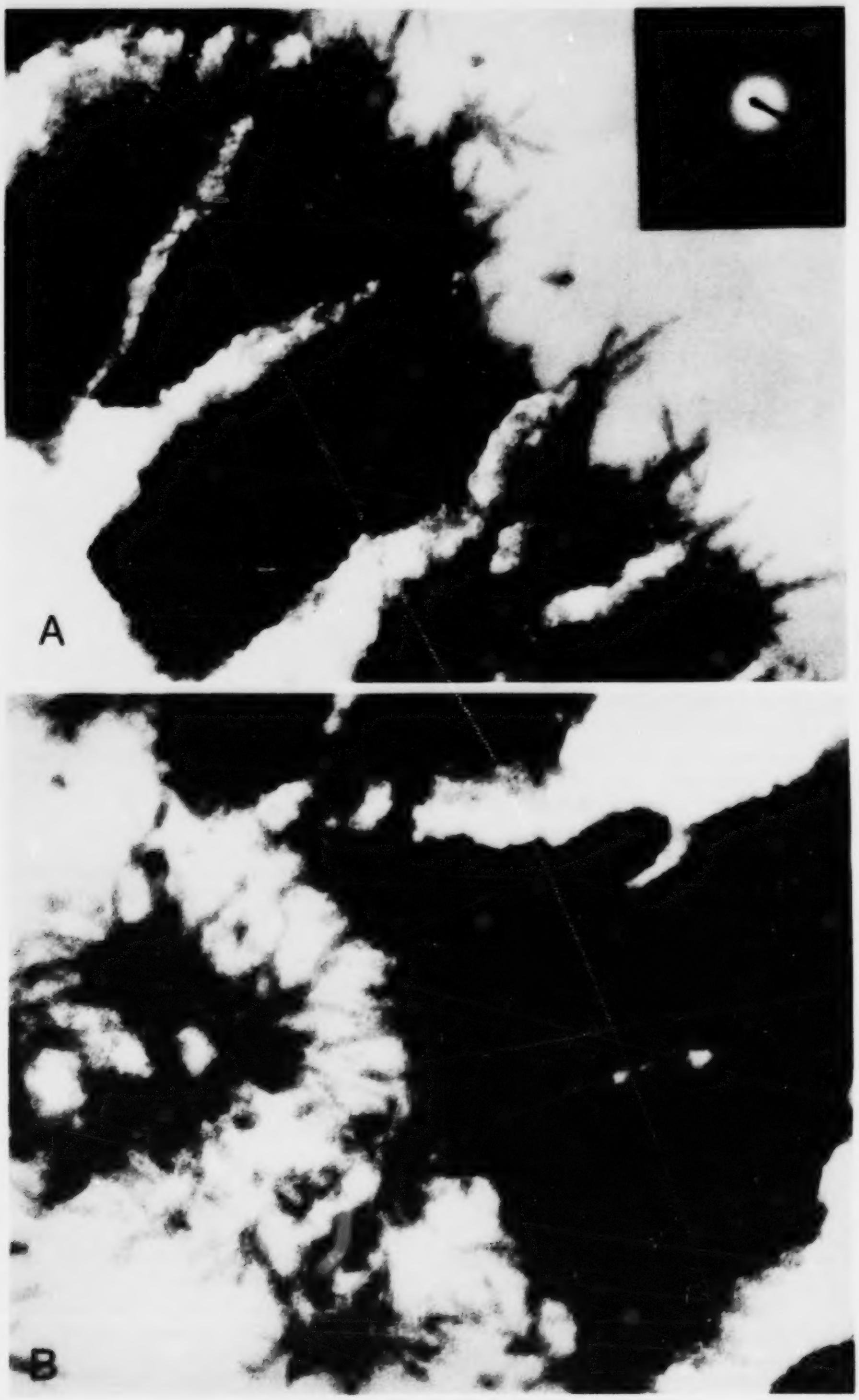

Photo 265B.4. *Transmission electron micrograph showing detail of microorganism from Photo 265B.2b. (a). Outer part of cell envelope (265B.2b, detail "a") heavily encapsulated by magnetite. Electron diffraction pattern of magnetite is inset in upper right corner. (b). Inside cell envelope (265B.2b, detail "b"), also composed of magnetite.*

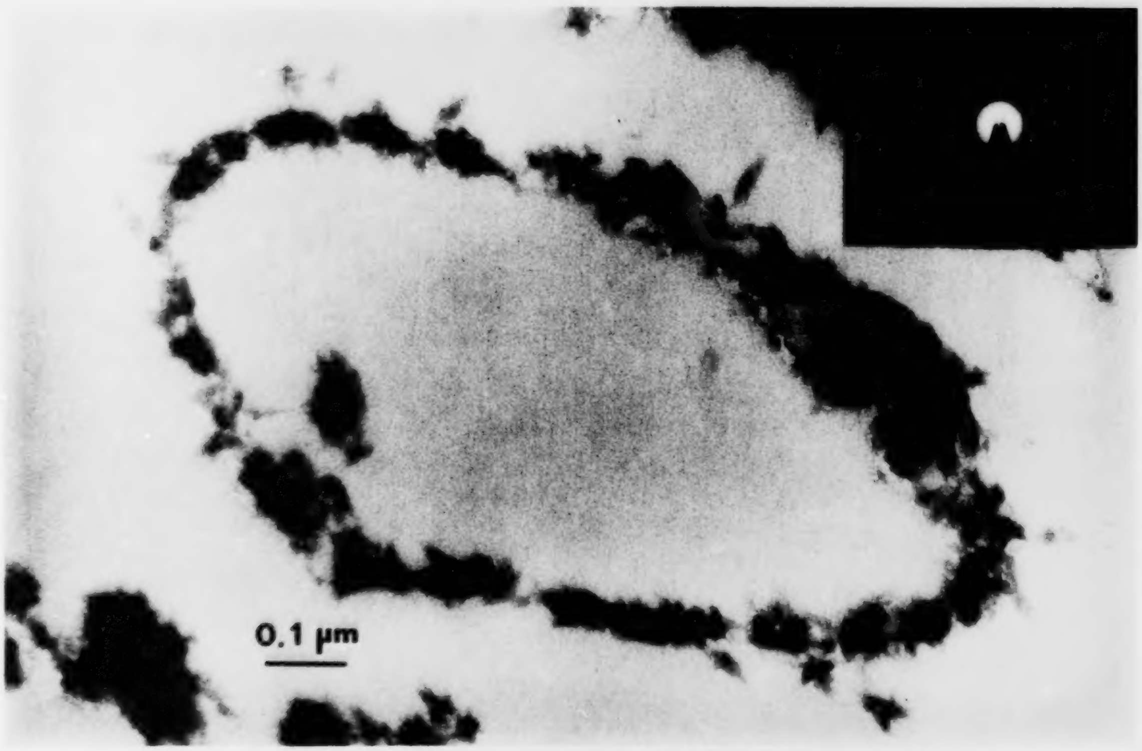

Photo 265B.5. *Transmission electron micrograph of remains of microorganism from Cranberry Lake. The microcrystalline aggregate surrounding the cell wall is goethite. Selected area electron diffraction pattern (SAED) is inset in upper right corner.*

Feenstra, S., Blair, R.D., Cherry, J.A., Chakravatti, J.L., and LaRocque, E.
1981: Hydrogeochemical Investigations of Two Inactive Tailing Areas in the Elliot Lake Uranium District, Ontario, Canada; p.367-388 *in* Proceedings of the Fourth Symposium on Uranium Mill Tailings Management, October 26-27, Colorado State University, Fort Collins, Colorado.

Ferris, F.G., and Beveridge, T.J.
1985: Functions of Bacterial Cell Surface Structures; Bioscience, Volume 35, p.172-177.

Ferris, F.G., Beveridge, T.J., and Fyfe, W.S.
1986: Iron–Silica Crystallite Nucleation by Bacteria in a Geothermal Sediment; Nature, Volume 320, Number 6063, p.609-611.

Ferris, F.G., Fyfe, W.S., and Beveridge, T.J.
1987: Bacteria as Nucleation Sites for Mineral Authigenesis; Grant 265, p.77-83 *in* Geoscience Research Grant Program, Summary of Research, 1986-1987, edited by V.G. Milne, Ontario Geological Survey, Miscellaneous Paper 136, 241p.

Mann, H., and Fyfe, W.S.
1985a: Algal Uptake of U and Some Other Metals: Implications for Global Geochemical Cycling; Precambrian Research, Volume 30, Number 4, p.337-349.

1985b: Uranium Uptake by Algae: Experimental and Natural Environments; Canadian Journal of Earth Sciences, Volume 22, Number 12, p.1899-1903.

Mann, H., Ferris, F.G., Beveridge, T.J., Fyfe, W.S., Humphrey, R., and Tazaki, K.
1986: Metal Uptake by Microorganisms: Retardation of Toxic Heavy Metal Dispersion from Tailing Environments, Elliot Lake, Timmins, and Sudbury; Grant 265, p.190-209 *in* Geoscience Research Grant Program, Summary of Research, 1985-1986, edited by V.G. Milne, Ontario Geological Survey, Miscellaneous Paper 130, 235p.

Mann, H., Tazaki, K., Fyfe, W.S., Beveridge, T.J., and Humphrey, R.
1987: Cellular Lepidocrocite Precipitation and Heavy-Metal Sorption in *Euglena* (Unicellular Algae): Implications for Biomineralization; Chemical Geology, Volume 63, Number 1/2, p.39-43.

Mann, H., Tazaki, K., Fyfe, W.S., and Wiseman, M.
1988: Retardation of Toxic Heavy Metal Dispersion from Nickel-Copper Mine Tailings, Sudbury District, Ontario: Role of Acidophilic Microorganisms. II. Structure and Microanalysis of Bioprecipitants; Journal of Biorecovery, Volume 2 (in press).

Pickering, W.F.
1986: Metal Ion Speciation, Soils and Sediments (A Review); Ore Geology Reviews, Volume 1, Number 1, p.83-146.

Schwertmann, U., and Murad, E.
1983: Effect of pH on the Formation of Goethite and Hematite from Ferrihydrite; Clays and Clay Minerals, Volume 31, Number 4, p.277-284.

Towe, K.M., and Bradley, W.F.
1967: Mineralogical Constitution of Colloidal Hydrous Ferric Oxides; Journal of Colloidal and Interface Science, Volume 4, p.384-392.

Trudinger, P.A., and Swaine, D.J.
1979: Biogeochemical Cycling of Mineral Forming Elements; Elsevier, Amsterdam, 612p.

Yapp, C.J., and Poths, H.
1986: Carbon in Natural Goethites; Geochimica et Cosmochimica Acta, Volume 50, Number 6, p.1212-1220.

Grant 275 Deformation of the Sudbury Structure

W.S. Shanks and W.M. Schwerdtner

Department of Geology, University of Toronto, Toronto

ABSTRACT

Published maps show the Sudbury Structure to be cut by a complex fault system. Our mapping shows that the present elongate form of the structure was, in part, produced by ductile strain. The Igneous Complex and the Onaping Formation within the southern part of the Sudbury Structure are cut by a large zone of reverse ductile shear, the Fairbank–Whitson Lakes Deformation Zone (FWLDZ). The zone was probably produced in the same regional stress field that produced the thrusts and reverse faults in rocks south of the Sudbury Structure.

The FWLDZ extends over much of the length of the Sudbury Structure and, to the west, cuts the southwestern footwall of the Structure. The western extent of the FWLDZ is uncertain, but it may be a branch of the Murray Fault System.

Objectives of the 1988 program are: a) to map the western extent of the FWLDZ and document the contribution of ductile shear as the main ductile deformation mechanism in the Sudbury Structure; and b) to estimate the original diameter ratio of the unstrained Sudbury Structure. Estimation of the magnitude of northwest-southeast shortening across the Sudbury Structure depends upon the availability of natural strain gauges. Laboratory research will therefore be directed toward assessing the usefulness of existing gauges including igneous fabrics, concretions, and various fragment types.

INTRODUCTION

The paper focuses on the ductile deformation of the southern portion of the Sudbury Structure and summarizes the progress after seven and a half months of field work and follow-up laboratory analysis. All data were obtained on surface.

The Igneous Complex of the Sudbury Structure consists of noritic, gabbroic, and granophyric rocks that have been intruded along the contact between the Onaping Formation and deformed Superior and Southern Province rocks. The Whitewater Group forms the sedimentary core of the Sudbury Basin. From base to top, the Whitewater Group consists of heterolithic breccias of the Onaping Formation, slates of the Onwatin Formation, and greywackes of the Chelmsford Formation. Contacts within the Whitewater Group are gradational and conformable. For a more thorough description of the major rock units the reader is referred to Dressler (1984), Muir and Peredery (1984), Naldrett and Hewins (1984), and Rousell (1984).

The origin of the Sudbury Structure is still a matter of considerable controversy. Recent estimates of basin shortening (Brocoum and Dalziel 1974; Muir 1984; Clendenen 1986; Clendenen *et al.* 1988) that show the basin to have been originally subcircular have further fueled the debate. However, little is known about the large-scale pattern of total strain upon which all such models are based. As pointed out by Morrison (1984), knowledge of the origin of the Sudbury Structure could change current exploration strategies and thereby assist in the discovery of new ore deposits.

In order to address some of the problems of Sudbury Basin geology, the authors are continuing a long-range project to map the pattern of apparent total strain to reconstruct the kinematics of deformation of the Sudbury Structure. The project should aid in the search for additional ore deposits and perhaps settle the debate over the origin of the Sudbury Structure.

SYNOPSIS OF THE APPARENT TOTAL STRAIN PATTERN

The 1986 and 1987 field seasons were devoted mainly to detailed structural and lithological mapping in the west-central core and southern parts of the Sudbury Structure. After seven and a half months of field mapping and follow-up laboratory research, the following major results were obtained:

1. The Onaping Formation, as well as the Igneous Complex, is virtually unstrained in many areas. However, a major zone of ductile shear, the Fairbank–Whitson Lakes Deformation Zone (FWLDZ) cuts the Onaping Formation and Igneous Complex in the southern Sudbury Structure (Shanks and Schwerdtner 1987).
2. By contrast, the Chelmsford and Onwatin formations are strained pervasively at the Earth's surface, either by buckle folding or other mechanisms of ductile deformation (Shanks and Schwerdtner 1987).
3. All rock types in the Igneous Complex were ductile and deformed severely in places.
4. South of the Sudbury Structure, the enveloping rocks show finite-strain effects only in narrow zones of ductile shear (for example, the Creighton Deformation Zone).
5. Many dislocations shown as faults (or lineaments) on published geological maps coincide with narrow zones of ductile shear.
6. Schistosity dips southeast throughout the FWLDZ and elsewhere in the southern Sudbury Structure. This contrasts with the northerly dip of the major lithological boundaries determined underground.
7. Chelmsford Formation concretions are natural strain gauges that record the entire tectonic deformation as well as an unknown portion of the compaction strain.
8. Standard strain analysis techniques using the shape of deformed markers underestimate the ductile portion of the total strain in rocks that have well developed C-S fabrics. This is revealed by contrasting aspect ratios of markers as determined by the C-S angle method (Ramsay and Huber 1983; Ragan 1985) and standard shape techniques (Robin 1977).
9. The k-values (Flinn 1962) for deformed rocks of the Fairbank–Whitson Lakes Deformation Zone

indicate nearly plane strain conditions (assuming no volume change).

DETAILED STRUCTURAL MAPPING

FAIRBANK–WHITSON LAKES DEFORMATION ZONE (FWLDZ)

This zone is nearly 40 km long and extends from west of Fairbank Lake northeastward to Whitson Lake (Figure 275.1). In map view, the FWLDZ cuts across the principal lithological contacts at a small angle. All rocks are highly strained within this zone, which includes only a small portion of norite. (This explains the fact that almost the entire norite body of the southern Sudbury Structure is unaffected by ductile strain.)

The schistosity dips southeast throughout the entire FWLDZ (Figure 275.1), and the associated stretching lineation is subperpendicular to schistosity strike. The angle of dip of schistosity is lowest near the middle of the zone. This agrees with theoretical models of ductile deformation zones in which the magnitude of shear is largest toward the middle of the zone and the associated schistosity is subparallel to the boundaries. The zone exhibits an overthrust sense of displacement as revealed by the polarity of C-S fabrics (Shanks and Schwerdtner 1987), the asymmetry of small folds in schistosity (Photo 275.1), the rotation sense of competent inclusions, the orientation of shear bands, and the facing of fiber steps (roughness direction) on slickensided slip surfaces. C-S fabrics are not restricted to granophyric rocks, but are also well developed in the lower Onaping Formation.

Southeast of the FWLDZ, ductile shear zones ranging in width from 1 cm to 100 m in map view are common (Photo 275.2). Most of these high-order zones are only a few centimetres thick, some dipping north or northwest. Virtually all small-scale shear zones have a reverse sense of displacement, suggesting that the southern Sudbury Structure was foreshortened in a northwest direction.

ENVELOPING ROCKS SOUTH OF THE SUDBURY STRUCTURE

Our mapping has shown that ductile deformation zones are also common in the enveloping rocks south of the Sudbury Structure. Outside these zones, however, the level of finite strain is generally very low. This rules out an earlier hypothesis advanced by Shanks (1987) that the Sudbury Structure contains the northwestern limit of a regional field of high finite strain.

The Creighton Deformation Zone, one such zone of ductile deformation, is up to 100 m wide in map view and contains the Lockerby segment of the Creighton Fault. Both the schistosity and inferred boundaries of the zone dip north, and are well exposed on Vermilion River. This important shear zone needs to be traced laterally, and its termination studied in detail.

FOLD SYSTEM IN THE SEDIMENTARY CORE OF THE SUDBURY STRUCTURE

A detailed survey was made of the fold system in the western portion of the Chelmsford Formation, and a number of important relationships were established (Shanks and Schwerdtner 1987). The beds of the Chelmsford Formation are deformed into a northeast-trending system of buckle folds, which Shanks has mapped in detail (Figure 275.2 simplified from Figure 10, Shanks 1987). The fold pattern is attributed to northwest-southeast compression, and the double plunge of the folds may not be due to a northeast-southwest shortening component (Shanks and Schwerdtner 1987).

The folds are nearly upright structures with subhorizontal axes. Although only quasi-cylindrical, a northwest-southeast vertical section across the Chelmsford Formation has been constructed using the method of concentric arcs (Busk 1929; Shanks and Schwerdtner 1987). To the southeast in this fold system, axial planes verge north at modest angles compatible with reverse shear in the FWLDZ.

The Busk method uses adjacent bedding readings in pairs and assumes that the fold style is concentric (Figure 275.3). While this assumption is permissible in view of the open folds seen in some roadcuts west of the town of Chelmsford, a more accurate profile could be obtained by the Mertie (1947) method (in progress).

Balanced cross-sections are obtained when either the bed lengths or areas of all beds in the section are the same as measured between points of no interbed slip (i.e. between axial planes of folds, Dahlstrom 1969). Figure 275.3 illustrates that in horizons with cusp shaped hinges the parallel model is not operative and the proposed geometry of these deeper zones may be incorrect (*see* Ragan 1985). Balancing of such horizons is possible, but requires assumptions about the subsurface geology (*see* Ragan 1985, p.230). The many faults shown in the core of the Sudbury Structure on published maps suggest a possible mechanism by which the section could be balanced, but this only enhances the notion of intrabasin faulting without further confirmation. The authors therefore have deferred section balancing until the sedimentary core has been studied in sufficient detail. They therefore present the section only as an approximation to the folded surface and as a preliminary estimate of shortening associated with folding.

Such an estimate of shortening is obtained by using the folded surface passing through the point S on the present erosion plane. For this horizon, measured between the fixed points at X and X′, the shortening is less than 10 percent (*see* Shanks and Schwerdtner 1987 for a description of the technique).

GAUGES OF PALEOSTRAIN

If potential strain gauges prove to be reliable indicators of total paleostrain, a proper estimate of the original northwest-southeast diameter of the Sudbury Basin could be made (Shanks and Schwerdtner 1987). Laboratory work is therefore concerned with testing all potential strain gauges.

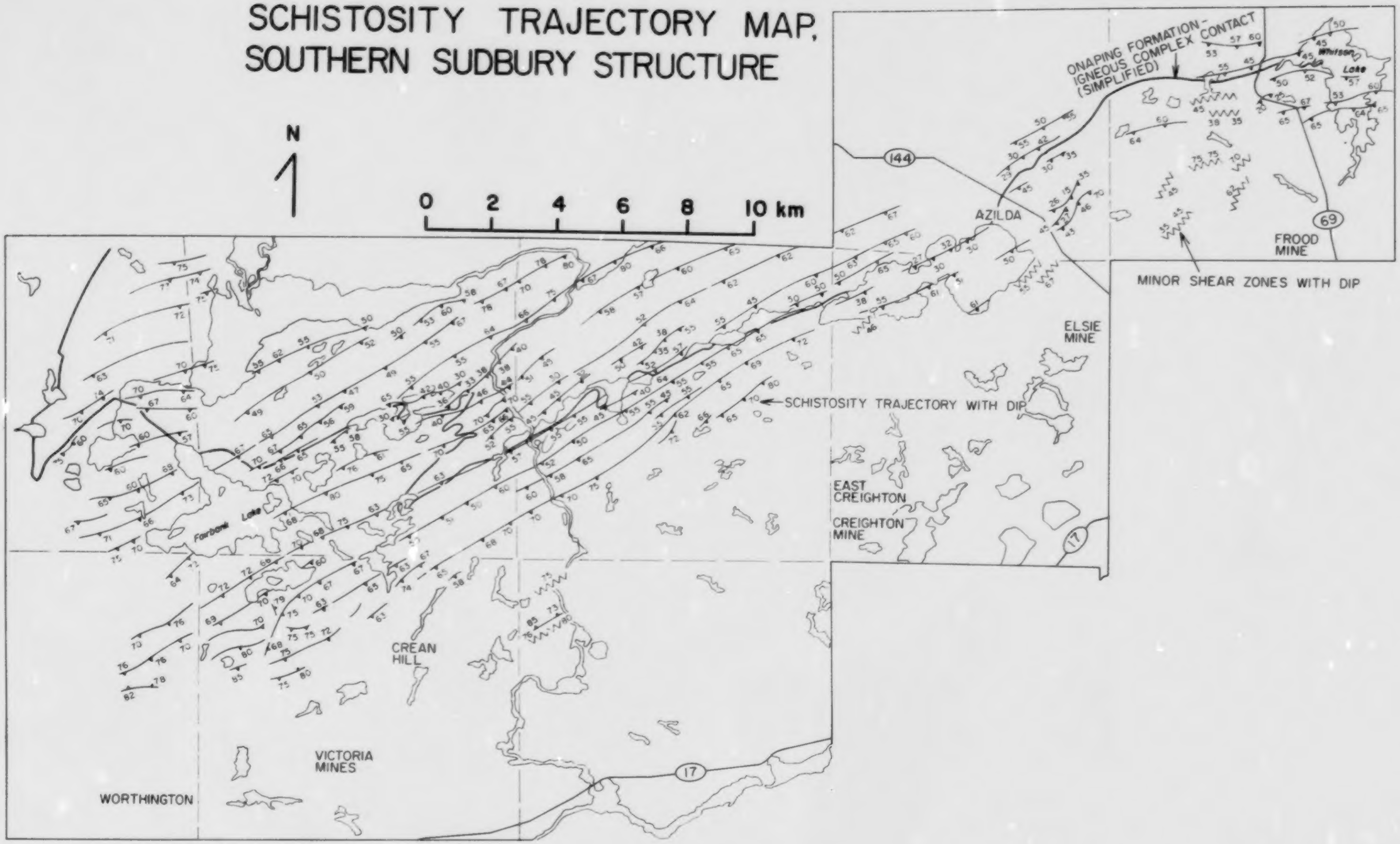
SCHISTOSITY TRAJECTORY MAP,
SOUTHERN SUDBURY STRUCTURE
N
0 2 4 6 8 10 km
ONAPING FORMATION-IGNEOUS COMPLEX CONTACT (SIMPLIFIED)
Whitson Lake
144
69
AZILDA
FROOD MINE
MINOR SHEAR ZONES WITH DIP
ELSIE MINE
SCHISTOSITY TRAJECTORY WITH DIP
EAST CREIGHTON
CREIGHTON MINE
17
Fairbank Lake
CREAN HILL
VICTORIA MINES
WORTHINGTON

Figure 275.1. *The schistosity trajectory map of the FWLDZ shows that the angle of dip is lowest toward the central portion of the zone. In the southwestern Sudbury Structure, the strike of schistosity is subperpendicular to lithological contacts. A simplified geological contact between the Igneous Complex and the overlying Onaping Formation is shown.*

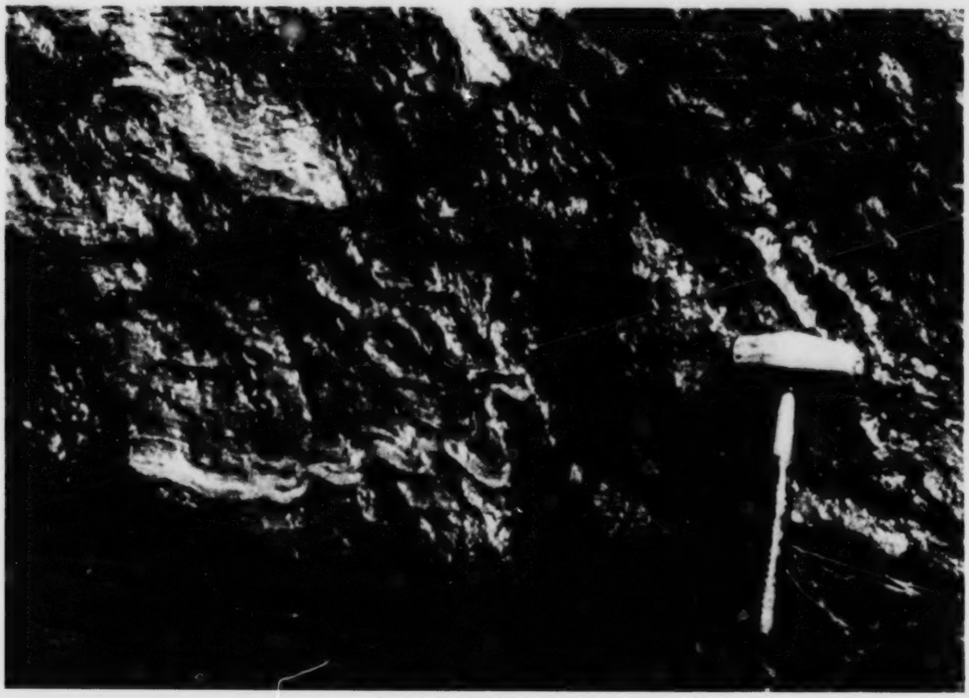

Photo 275.1. *Asymmetric S-folds developed in clasts, and schistosity of the Onaping Formation (left of hammer). Fold asymmetry indicates reverse shear (photo looks east).*

FRAGMENTS

Fabric analysis of unstrained Onaping Formation rocks have been made. Detailed investigation of their fabric showed the following:

1. There is no initial anisotropic fabric present.
2. Felsic fragments tend to have aspect ratios near unity.
3. Chloritic shards have aspect ratios of between two and three, but the distribution of shard long-axes is apparently random.

These findings confirm our earlier results (Shanks and Schwerdtner 1987) and imply that if no competency contrast exists between marker and matrix, then the total ductile strain is determinable (neglecting volume change). This assumes complete lithification prior to the commencement of tectonic deformation.

Similar results of strain analysis between the Robin method (1977) and the Fry method (1979) (Shanks and Schwerdtner 1987) indicate a viscosity contrast near unity and reflect passive deformation of the marker. Because few natural populations approximate a uniform distribution, the Fry method has been difficult to apply; further, ideally passive deformation is difficult to demonstrate in most natural strain markers we have investigated. Earlier results suggestive of passive deformation (Shanks and Schwerdtner 1987) have not been confirmed to date.

The Flinn deformation plot (Figure 275.4) shows that k-values of deformed rocks of the Fairbank–Whitson Lakes Deformation Zone cluster about the k=1 line, suggestive of plane deformation (assuming no volume change).

C-S FABRICS

The angle between C- and S-planes is a potentially useful strain gauge (Ramsay and Huber 1983; Ragan 1985) in determining the variation in shear magnitude across the FWLDZ. In the FWLDZ and elsewhere, the shear magnitude increases with the number of C-planes, at the expense of the S-surfaces (*see also* Berthe *et al.* 1979). The net result of this process is to obscure or destroy S-surfaces.

Predicted values of marker aspect ratios on the profile plane, as calculated by the C-S angle method, are commonly far greater than those determined using the Robin (1977) technique. Therefore simple measurement of the marker aspect ratios in highly sheared rock would significantly underestimate the ductile portion of the strain. Using the C-S angle method is permissible provided one realizes that this furnishes only a minimum displacement magnitude since discontinuous slippage is ignored. Standard shape-based strain analysis techniques can be employed only in rocks lacking C-planes or in rocks in which C-S fabric development is poor.

CONCRETIONS

Working to restore the Sudbury Structure to its predeformational geometry, Brocoum and Dalziel (1974), Clendenen (1986), and Clendenen *et al.* (1988) used the shapes of concretions as gauges of total paleo-a.

b.

Photo 275.2. *(a) Dip-slip ultramylonite zone with overthrust displacement sense developed in coarse-grained granophyre (photo looks east). (b) Reverse shear zone developed at the contact between "remobilized" granite dike and coarse-grained gabbro (photo looks east).*

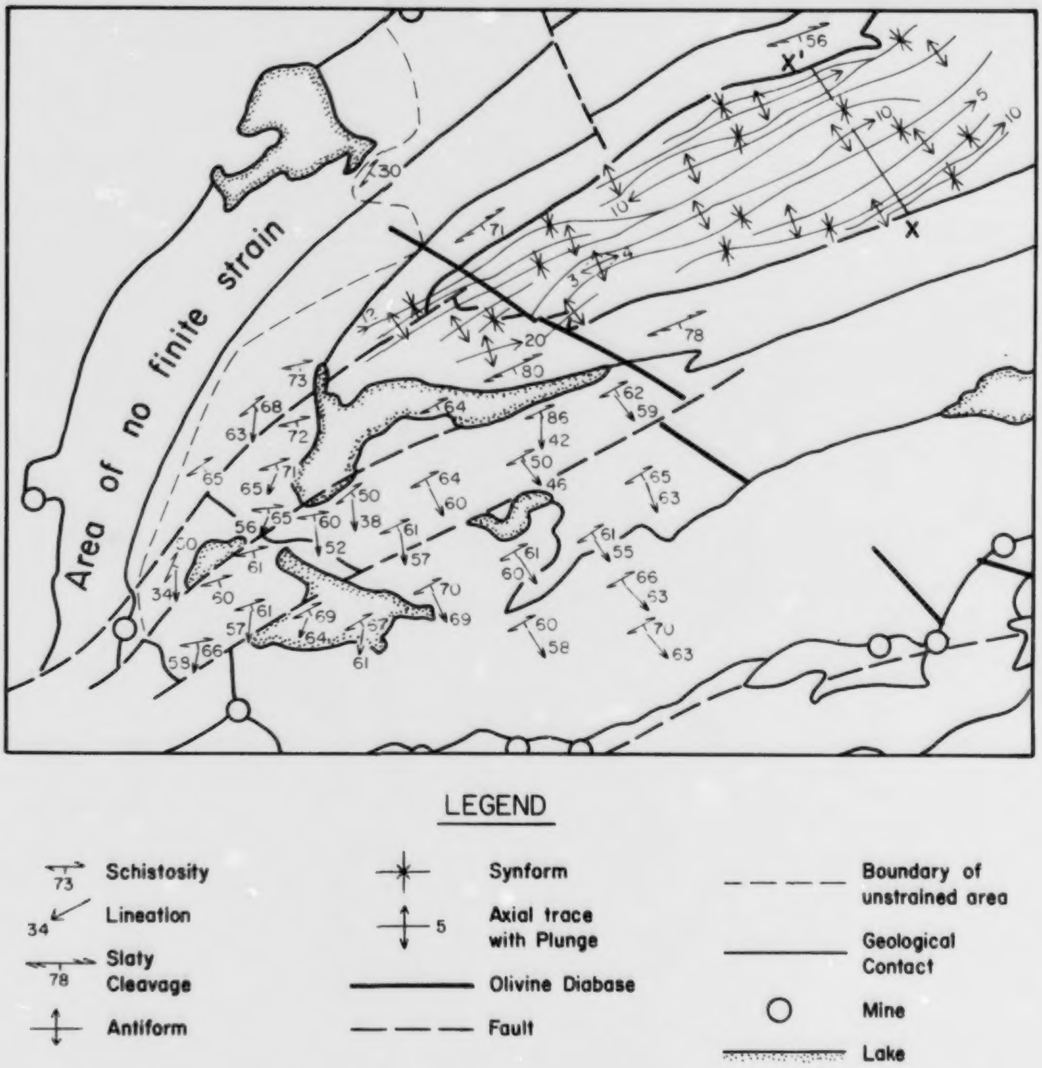
Area of no finite strain
X'
X
LEGEND
73 Schistosity
34 Lineation
78 Slaty Cleavage
Antiform
Synform
5 Axial trace with Plunge
Olivine Diabase
Fault
Boundary of unstrained area
Geological Contact
Mine
Lake

Figure 275.2. *The sinuous and/or bifurcating fold system, developed in the sedimentary core, lacks linear zones of hinge-line depressions thereby precluding significant cross folding. Section line X-X' of Figure 275.3 is also shown.*

strain, and estimated the amount of northwest-southeast shortening across the inner core of the Sudbury Structure. (For a critique of their restoration *see* Shanks 1987 and Shanks and Schwerdtner 1987.) Although Rousell (1972) reported that a concretion is cut by an erosional scour (truncation against an upper impermeable layer?), recent work by Shanks and Schwerdtner (1987) showed that concretions are elongate along the dominant anisotropy plane, being either bedding or a subvertical cleavage (Photo 275.3). (The bedding-cleavage angle is generally greater than 45 degrees.) The apparent anisotropy control of concretion orientation points to several possibilities: a) there are several generations of concretion growth; b) concretions formed over a long period of time; or c) the concretions are post-tectonic.

In an attempt to determine the age of formation of Chelmsford Formation concretions, Shanks and Schwerdtner (in preparation) analyzed three concretions: one from a thickly bedded wacke unit, and two from a well layered sandstone horizon. If the cement content reflects the original porosity of the sediment at the time of concretion formation (*see* Raiswell 1971; Oertel and Curtis 1972), then the high initial porosities preserved within their cores suggest that Chelmsford Formation concretions grew in poorly compacted sediments. Although another concretion remains to be analyzed, available results imply that the shapes of Chelmsford Formation concretions are important natural strain gauges recording the tectonic

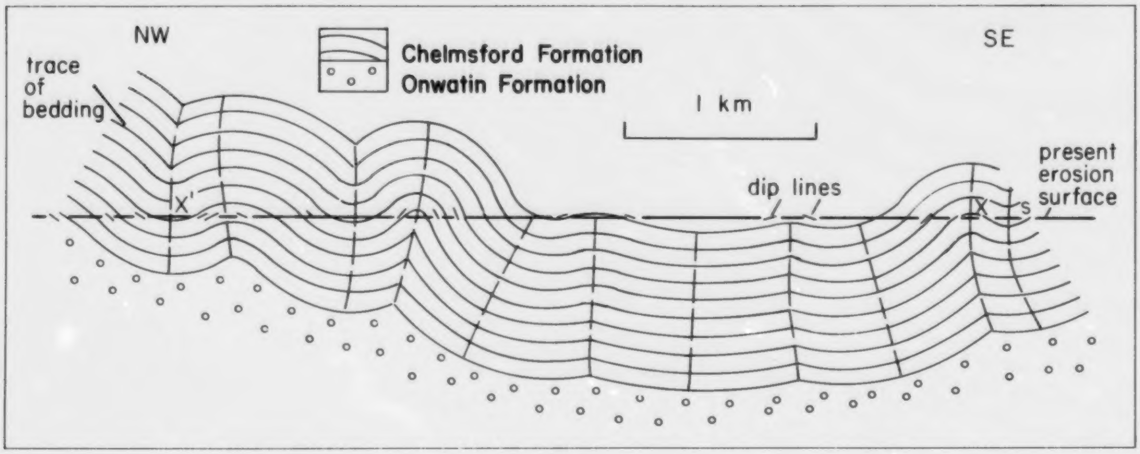

Figure 275.3. *Vertical northwest-southeast section of folds within the sedimentary core of the Sudbury Structure. The section line is located west of the town of Chelmsford (X-X' in Figure 275.2). Assuming flexural slip folding, the shortening associated with folding is less than 10 percent measured between X and X' on surface S (see text for further details).*

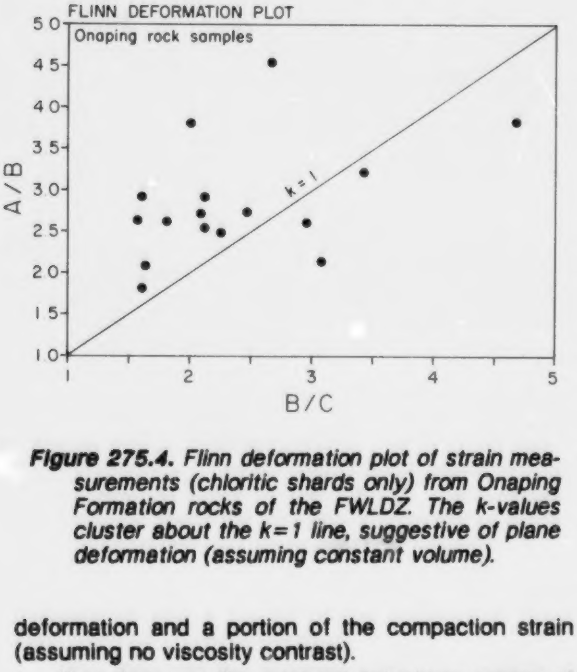

Figure 275.4. *Flinn deformation plot of strain measurements (chloritic shards only) from Onaping Formation rocks of the FWLDZ. The k-values cluster about the k=1 line, suggestive of plane deformation (assuming constant volume).*

deformation and a portion of the compaction strain (assuming no viscosity contrast).

How then can the apparent anisotropy control of concretion orientation be explained? Rf/phi strain analyses (Ramsay 1967; Ramsay and Huber 1983) show that sectional strain ratios are consistently greater than the initial axial ratios of wacke-bed concretions. Consequently, wacke-bed concretions are flattened in the cleavage plane. A similar analysis of concretions in the sandstone beds is not possible owing to the small number of concretions present. However, if the sectional strain ratio is less than the undeformed axial ratios of sandstone-bed concretions, then these concretions should not be flattened in the cleavage.

CONCLUSIONS

The Fairbank–Whitson Lakes Deformation Zone is a large zone of reverse ductile shear that may be a branch of the Murray Fault System. The extent to which reverse shear, in the Fairbank–Whitson Lakes Deformation Zone, has contributed to the present oval map pattern of the Sudbury Structure remains to be determined. A minimum estimate of displacement shall be made using the angle between C- and S-surfaces, assuming a model of simple shear deformation.

Ductile deformation zones are also common in the enveloping rocks south of the Sudbury Structure. The lateral extent and terminations of these zones remain to be studied. Outside these deformation zones, the level of finite strain is low, which rules out an earlier hypothesis that the Sudbury Structure contains the northwestern limit of a regional field of high finite strain.

A vertical section across the inner core of the Sudbury Basin shows a nearly upright fold style. To the southeast in this fold system, axial planes have a northward vergence compatible with reverse-directed shear in the southern part of the Fairbank–Whitson Lakes Deformation Zone. Preliminary estimates of shortening associated with the folding are less than 10 percent, assuming plane strain flexural-slip deformation.

The results of the concretion analyses promise a useful strain gauge. Proper estimates of Sudbury Basin shortening using the shapes of concretions can be compared to estimates of horizontal shortening derived from structural unfolding methods (Busk 1929; Mertie 1947; Shanks and Schwerdtner 1987).

ACKNOWLEDGMENTS

The authors would like to thank P.-Y.F. Robin (Department of Geology, University of Toronto) for discussions on matters of strain determination, and

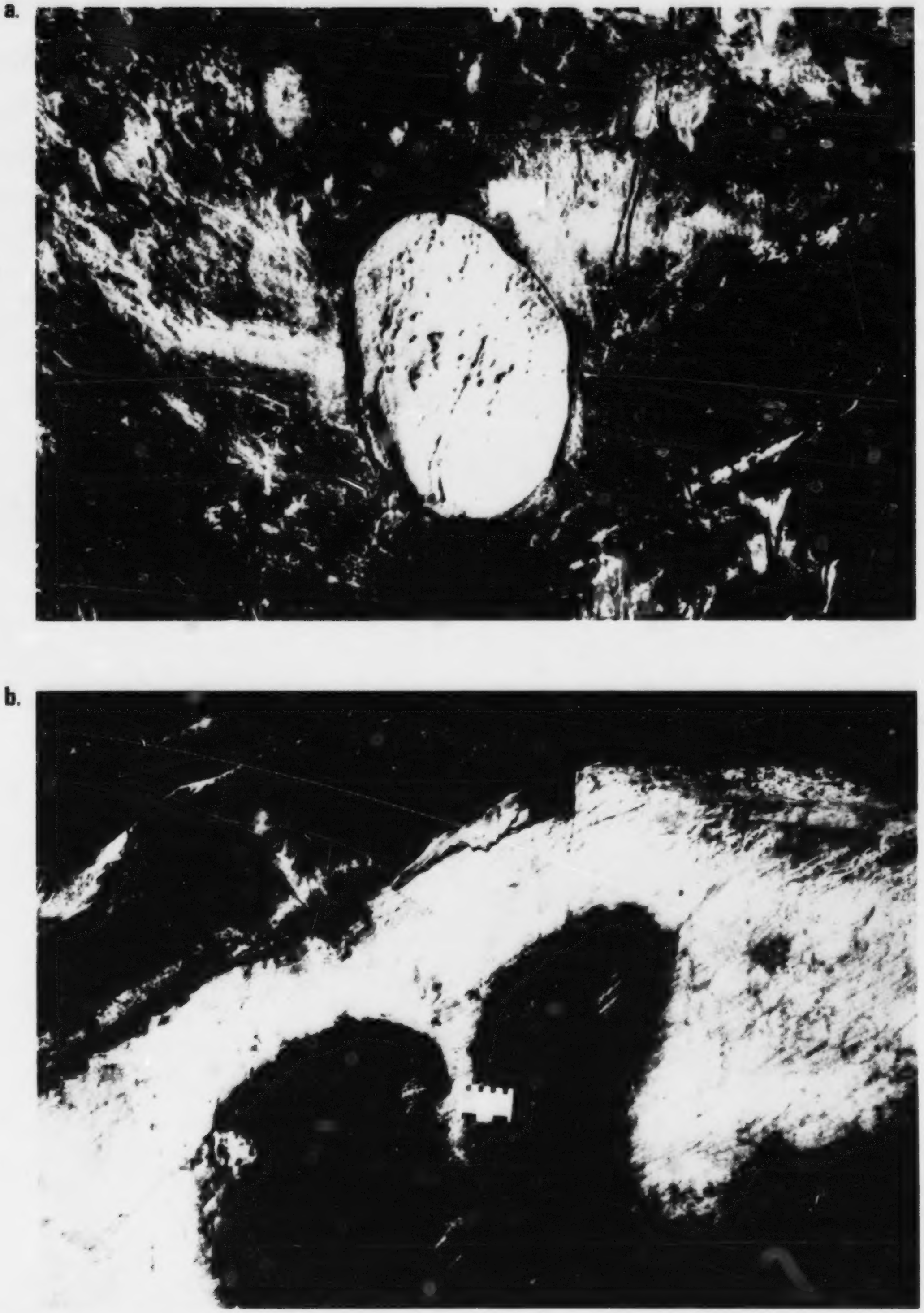

***Photo 275.3.** Small road cut west of Chelmsford in which the orientation of deformed concretions varies between (a) wacke and (b) fine-grained sandstone beds. See text for details.*

Alan Kendall (Department of Geology, University of Toronto) for advice on cathodoluminescence used to analyze concretions. The authors would also like to thank technicians Ifor Davies and Jaroslav Zapletal (Department of Geology, University of Toronto) for repeated repairs to our pack-sack drill.

REFERENCES

Berthe, D., Choukroune, P., and Jegouzo, P.
1979: Orthogneiss, Mylonite and Non Coaxial Deformation of Granites: The Example of the South Armorican Shear Zone; Journal of Structural Geology, Volume 1, Number 1, p.31-42.

Brocoum, S.J., and Dalziel, I.W.D.
1974: The Sudbury Basin, the Southern Province, the Grenville Front, and the Penokean Orogeny; Geological Society of America Bulletin, Volume 85, Number 10, p.1571-1580.

Busk, H.G.
1929: Earth Flexures; Cambridge University Press, London, 106p.

Clendenen, W.S.
1986: Finite Strain Study of the Sudbury Basin, Ontario; Unpublished M.Sc. Thesis, Department of Geological Sciences, University of Colorado, Boulder, Colorado.

Clendenen, W.S., Kligfield, R., Hirt, A.M., and Lowrie, W.
1988: Strain Studies of Cleavage Development in the Chelmsford Formation, Sudbury Basin, Ontario; Tectonophysics, Volume 145, p.191-211.

Dahlstrom, C.D.A.
1969: Balanced Cross Sections; Canadian Journal of Earth Sciences, Volume 6, p.743-757.

Dressler, B.O.
1984: Chapter 4, General Geology of the Sudbury Area; p.57-82 *in* The Geology and Ore Deposits of the Sudbury Structure, edited by E.G. Pye, A.J. Naldrett, and P.E. Giblin, Ontario Geological Survey, Special Volume 1, 603p. Accompanied by Map 2491, at a scale of 1:50 000, Map NL-16/17-AM Sudbury, at a scale of 1:1 000 000, and 3 charts.

Flinn, D.
1962: On Folding During Three-Dimensional Progressive Deformation; Quarterly Journal of the Geological Society of London, Volume 118, p.385-433.

Fry, N.
1979: Random Point Distributions and Strain Measurement in Rocks; Tectonophysics, Volume 60, p.89-105.

Mertie, J.B.
1947: Delineation of Parallel Folds and Measurement of Stratigraphic Dimensions; Geological Society of America Bulletin, Volume 58, Number 8, p.779-802.

Morrison, G.G.
1984: Chapter 23, Morphological Features of the Sudbury Structure in Relation to an Impact Origin; p.513-520 *in* The Geology and Ore Deposits of the Sudbury Structure, edited by E.G. Pye, A.J. Naldrett, and P.E. Giblin, Ontario Geological Survey, Special Volume 1, 603p. Accompanied by Map 2491, at a scale of 1:50 000, Map NL-16/17-AM Sudbury, at a scale of 1:1 000 000, and 3 charts.

Muir, T.L.
1984: Chapter 21, The Sudbury Structure; Considerations and Models for an Endogenic Origin; p.449-489 *in* The Geology and Ore Deposits of the Sudbury Structure, edited by E.G. Pye, A.J. Naldrett, and P.E. Giblin, Ontario Geological Survey, Special Volume 1, 603p. Accompanied by Map 2491, at a scale of 1:50 000, Map NL-16/17-AM Sudbury, at a scale of 1:1 000 000, and 3 charts.

Muir, T.L., and Peredery, W.V.
1984: Chapter 7, The Onaping Formation; p.139-210 *in* The Geology and Ore Deposits of the Sudbury Structure, edited by E.G. Pye, A.J. Naldrett, and P.E. Giblin, Ontario Geological Survey, Special Volume 1, 603p. Accompanied by Map 2491, at a scale of 1:50 000, Map NL-16/17-AM Sudbury, at a scale of 1:1 000 000, and 3 charts.

Naldrett, A.J., and Hewins, R.H.
1984: Chapter 10, The Main Mass of the Sudbury Igneous Complex; p.235-251 *in* The Geology and Ore Deposits of the Sudbury Structure, edited by E.G. Pye, A.J. Naldrett, and P.E. Giblin, Ontario Geological Survey, Special Volume 1, 603p. Accompanied by Map 2491, at a scale of 1:50 000, Map NL-16/17-AM Sudbury, at a scale of 1:1 000 000, and 3 charts.

Oertel, G., and Curtis, C.D.
1972: Clay-Ironstone Concretion Preserving Fabrics Due to Progressive Compaction; Geological Society of America Bulletin, Volume 83, Number 9, p.2597-2606.

Ragan, D.M.
1985: Structural Geology: An Introduction to Geometrical Techniques; Third Edition, Wiley and Sons, New York, New York.

Raiswell, R.
1971: The Growth of Cambrian and Liassic Concretions; Sedimentology, Volume 17, p.147-171.

Ramsay, J.G.
1967: Folding and Fracturing of Rocks; McGraw-Hill Book Company, New York, 568p.

Ramsay, J.G., and Huber, M.I.
1983: The Techniques of Modern Structural Geology Volume 1: Strain Analysis; Academic Press, New York, 307p.

Robin, P.-Y.F.
1977: Determination of Geologic Strain Using Randomly Oriented Strain Markers of Any Shape; Tectonophysics, Volume 42, p.T7-T16.

Rousell, D.H.
1972: The Chelmsford Formation of the Sudbury Basin—A Precambrian Turbidite; p.79-91 *in* New Developments in Sudbury Geology, edited by J.V. Guy-Bray, Geological Association of Canada, Special Paper 10.
1984: Chapter 8, Onwatin and Chelmsford Formations; p.211-218 *in* The Geology and Ore Deposits of the Sudbury Structure, edited by E.G. Pye, A.J. Naldrett, and P.E. Giblin, Ontario Geological Survey, Special Volume 1, 603p. Accompanied by Map 2491, at a scale of 1:50 000, Map NL-16/17-AM Sudbury, at a scale of 1:1 000 000, and 3 charts.

Shanks, W.S.
1987: Deformation of the Sudbury Structure, A Ph.D. Topic Proposal; Unpublished Manuscript, Department of Geology, University of Toronto, Toronto.

Shanks, W.S., and Schwerdtner, W.M.
1987: Deformation of the Sudbury Structure and Its Footwall; Grant 275, p.92-98 *in* Geoscience Research Grant Program, Summary of Research, 1986-1987, edited by V.G. Milne, Ontario Geological Survey, Miscellaneous Paper 136, 241p.
In preparation: The Use of Concretion Shapes as Strain Gauges; An Example from the Sudbury Basin.

Grant 280 Lead Isotope Study of Gold Mineralization in the Dome Mine Quartz-Fuchsite Vein

R.P. Moritz, J.H. Crocket, and A.P. Dickin

Department of Geology, McMaster University, Hamilton

ABSTRACT

The quartz-fuchsite vein environment in the Dome Mine, Timmins area, has been the subject of a lead isotope study. The vein is characterized by a consistent gold-galena association. Both metals are most certainly coeval and were deposited by the same hydrothermal fluid. The present study seeks to recognize possible sources of lead, and perhaps gold, in Archean lode deposits. Isotopic compositions were obtained for eight galena samples from the quartz-fuchsite vein, five porphyry samples, and one slate composite sample. The lead isotope compositions of the majority of the galena samples falls in a tight cluster. This grouping is colinear with the lead isotope composition of the porphyry and the slate composite samples. This pattern, together with the geological setting of the quartz-fuchsite vein and the genetic model proposed for this vein, strongly suggests a genetic relationship between the quartz-fuchsite vein and the porphyries from the Dome Mine environment.

INTRODUCTION

The quartz-fuchsite vein (QFV) at the Dome Mine, Timmins area, has been the subject of a study to evaluate the source of gold in Archean lode deposits. Galena is intimately associated with native gold in the QFV. This relationship is so consistent that it can be assumed that both metals are coeval, and were deposited by the same hydrothermal fluid. This inferred similarity in age has also been documented by earlier studies in the Timmins area (Hurst 1935; Ferguson *et al.* 1968). Any information obtained from the lead isotopic composition of the galena samples may be directly relevant to the origin of the gold. Thus, lead isotopes could prove useful in constraining possible gold sources. In particular, the lead isotope signature may be evaluated in terms of local rock sources, or lower crust and/or upper mantle sources.

The lead isotope study of the QFV is part of a project to characterize the site and the mechanism of ore deposition, the source of gold and of the ore-bearing fluid in Archean lode gold deposits, and the timing of gold mineralization in the geological evolution of the Timmins area (Moritz 1988). Two previous contributions based on preliminary lead isotope results suggested a genetic link between quartz-feldspar porphyries from the Dome Mine area, and the mineralization in the QFV (Moritz *et al.* 1987a, 1987b). This suggestion is in agreement with the geological and geochemical studies carried out in the environment of the QFV by Moritz (1988).

This second geoscience research grant report on the lead isotope study of the QFV still favours the genetic relationship between porphyry stocks and gold mineralization. The main modification and improvement presented herein is that the two-stage lead evolution model developed by Stacey and Kramers (1975), or Thorpe's (1982) local Superior model, probably yields more accurate initial lead isotope compositions for the local quartz-feldspar porphyries than the single-stage model used in more recent contributions (Moritz *et al.* 1987a, 1987b). Moreover, the possibility of the mixing of lead from the QFV and lead derived from a more radiogenic crustal source has been confirmed and explained. The analytical methods are described in a report by Moritz *et al.* (1987a). The methods of model lead-lead age calculations, constants, and symbols used presently can be found in the 1985-1986 geoscience research grant report by Moritz *et al.* (1987a). Since the first report, additional details on the geological setting of the QFV have been gained, and a new genetic model has been suggested for this vein. Thus, the geological setting, the anatomy, and the genesis of the QFV will be briefly reviewed in the light of recent findings, to interpret correctly the lead isotope data.

GEOLOGICAL SETTING

The QFV is located in a zone of carbonatized rocks and altered porphyries in contact with slates (Figure 280.1). Holmes (1968), Davies (1977), Rogers (1982), and Hodgson (1983) have suggested that this zone of altered rocks is the location of the Dome Fault, which is thought to be a branch of the Destor–Porcupine Fault. However, according to Roberts (1981), and Roberts and Reading (1981), there is no evidence for major displacements along this zone; they suggest that the slates, the carbonatized rocks, and the South Greenstones (basalts) are a continuous sequence.

The altered porphyries are schistose, carbonatized, sericitized, and albitized quartz-feldspar porphyries. The porphyry lenses from the altered rock zone are petrographically similar to the Preston porphyry, one of the major porphyry bodies of the Timmins gold mining camp (McAuley 1983). According to McAuley (1983), the porphyry bodies from the Dome Mine environment are cogenetic and predate regional metamorphism. The carbonatized rocks are most probably altered komatiites (Fryer *et al.* 1979; Roberts and Reading 1981; Moritz 1988).

The alteration of the host rocks of the QFV is centred around one of the major porphyry lenses present in the zone of carbonatized rocks, rather than around the gold-bearing vein (Figure 280.1). The intensity of country rock fracturing, quartz veining, and fuchsite and pyrite development in the carbonatized komatiites increases towards the porphyry lens. Most of the major and trace elements introduced into the komatiites during alteration were probably derived from the immediate neighbouring porphyry bodies and, to a lesser extent, from the slates (Moritz 1988).

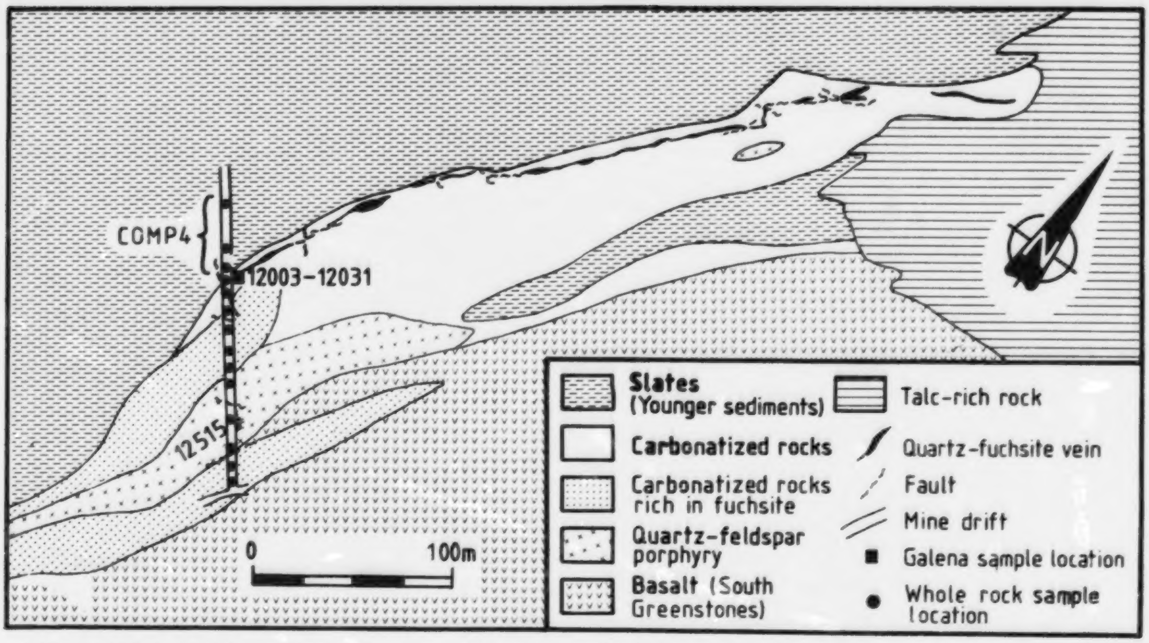

Figure 280.1. *Local geology of the Dome Mine Quartz-Fuchsite vein on the 12th level (adapted from Dome Mine 12th level plan). Locations of underground samples are also shown.*

ANATOMY AND GENESIS OF THE QUARTZ–FUCHSITE VEIN

The QFV is subparallel to the northern contact between the slates and the carbonatized rocks (Figure 280.1). It occurs between the 6th and the 17th levels of the mine. It has a northeastern trend, and commonly dips towards the southeast. Except for the upper 6th and 8th levels, the gold is entirely hosted within the 500 m by 550 m by 3.5 m (average thickness) vein.

The QFV is discontinuous along strike (Figure 280.1). It is composed of two types of quartz material: one which is massive, and consists almost entirely of relatively unstrained quartz, and is usually of low gold grade; and a second type which consists of alternating bands of strained and recrystallized quartz and phyllosilicates (fuchsite and/or chlorite) and/or wall rock, and which contains high gold concentrations.

The regional D1 foliation (Roberts *et al.* 1978; Roberts 1981) in the wall rock is discordant with respect to the orientation of the QFV. A fracture cleavage is occasionally well developed in the vein. It is the refracted counterpart of the wall rock foliation. This fracture cleavage, together with crenulated QFV wall rock contacts, indicate that the formation of the gold-bearing vein preceded the development of foliation, and consequently, the D1 compressional deformation event that affected the Timmins area (Moritz 1988).

Galena and gold are consistently associated in the QFV. Often they are accompanied by variable amounts of melonite and altaite. These minerals are intergrown. Small inclusions of altaite, tellurobismuthite, and hessite are found in galena. No intermineral textures permit a temporal sequence of deposition between minerals to be determined. It is assumed that these opaque minerals are coeval. Such age similarity has also been described for other gold deposits in the Timmins area (Hurst 1935; Ferguson *et al.* 1968). Opaque minerals are usually found only in banded quartz. These minerals occur within fractures in quartz, between quartz grains, and along phyllosilicate bands. The deformation sustained by the QFV precludes any detailed discussion of mineral paragenesis. In particular, it is not possible to decide whether the main opaque minerals—gold, galena, and tellurides—have been deposited contemporaneously with quartz, and then mechanically remobilized into fractures and along grain boundaries during the recrystallization of quartz, or if minerals precipitated in a given sequence. Late stage carbonates are present along fractures in quartz, and also replace quartz. Rutile and tourmaline, when occasionally present, are located within the banding. Pyrite is poorly represented in the QFV. Cubic pyrite is either present between quartz grains or along the banding.

Moritz (1988) has shown that the shear zone model commonly applied to the formation of Archean lode gold deposits (for example, Kerrich and Allison 1978; Robert *et al.* 1983; Colvine *et al.* 1984; Robert and Brown 1986; Groves and Phillips 1987) does not adequately explain the genesis of the Dome Mine QFV. Similarly to the gold deposit of the McIntyre–Hollinger Mine (Mason and Melnik 1986a, 1986b), a genetic model linking the emplacement of porphyries with gold ore development is preferred in the case of the QFV. Moritz (1988) suggested that the carbonate rock-slate contact, and the porphyry lens, are the two fundamental ingredients that created the favourable environment for the development of the gold-bearing QFV. The intrusion of the porphyry lens into the komatiites resulted in intense rock fracturing, and hydrothermal fluid circulation centred around that lens. It also increased pore fluid pressure in the country rock. Pore fluid pressure was increased furthermore at the slate-carbonate rock contact, since fluid migration was hindered by the relatively impermeable sediments. Hydraulic extension failure occurred when fluid pressure was greater than the combined least principal stress and tensile strength of the wall rock. Massive barren quartz precipitated during prolonged episodes of fracture growth, opening, and crystallization. Banded ore-bearing quartz was deposited during repetitive and brief periods of crack-seal vein growth. The consistent association of gold, galena, and tellurides with banded quartz suggests that the opaque minerals and quartz were deposited contemporaneously from a hydrothermal fluid, which may have precipitated them in response to numerous repeated pressure drops caused by the crack-seal veining mechanism.

Thus, the present well established geological context of the QFV, and the intimate gold-galena spatial association, are particularly relevant to the lead isotope systematics to recognize possible sources of gold in Archean lode deposits. Moreover, the genetic model proposed by Moritz (1988) for the QFV may be a valuable constraint in the interpretation of the lead isotope results.

SAMPLING

Eight galena samples were collected in the high grade ore zones of the QFV. All but one come from the banded parts. Galena is typically in grain boundary contact with gold. The one sample not from the banded part of the QFV comes from a quartz vein in the wall rock, but in contact with the QFV (sample number 12003, *see* Figure 280.1).

Whole rock lead isotope compositions were determined on various rocks from the Dome Mine environment, particularly the immediate host rocks of the QFV. Slates, carbonatized rocks, and a porphyry lens from a drift cutting the QFV on the 12th level within the mine were analyzed. The Preston porphyry was sampled on the 12th level, whereas the Paymaster and the Preston West porphyries, and an ultramafic flow, were sampled at the surface south of the Dome Mine.

DATA MANIPULATION AND INTERPRETATION

The treatment and interpretation of lead isotope data follows the procedures described by Faure (1986) and Gulson (1986). The basic approach in a source rock investigation is to determine or infer the lead isotopic composition of the possible source rocks at the time of their formation, and compare these compositions with that of the ore, also at its time of formation.

The measured lead isotope compositions of the galena samples do not need to be corrected for the addition of radiogenic lead since their formation. Because of the far greater abundance of lead over uranium or thorium in galena, there is little concern about modification of the initial lead composition due to radioactive decay since the time of formation. The situation is quite different for the whole rock samples. All the rocks contain some uranium, so that it is necessary to correct the observed lead isotope ratios for the radioactive decay of uranium. Various approaches are used by which the starting lead composition can be defined (Lambert 1985; Gulson 1986). This can be achieved by utilizing potassium-feldspar, which usually has a very low uranium abundance with respect to lead. Unfortunately, no potassium-feldspar can be found in any of the lithologies at the Dome Mine, so this method cannot be applied. A similar procedure to determine the initial ratio is by correcting for the *in situ* decay of uranium in the whole rock. However, studies by Rosholt *et al.* (1973) and Zielinski *et al.* (1981) have shown that uranium is very mobile under near-surface conditions, making it difficult to obtain the initial isotopic composition. A further suggestion is to take the least radiogenic composition from galena, or another lead-rich mineral, as the best approximation to the initial ratios. This procedure is redundant, since we want to determine whether or not a lithology from the Dome Mine had, at the time of its formation, a lead isotope composition similar to that of the lead from galena associated with gold in the QFV. Thus, as a first approach, the only remaining possibility is to obtain the initial ratio in a $^{207}Pb/^{204}Pb$ versus $^{206}Pb/^{204}Pb$ diagram, by fitting a line through the array of whole rock data points of a given lithology ($^{207}Pb/^{206}Pb$ age), and extrapolating that same line until it intersects a model growth curve with a given μ value ($^{238}U/^{204}Pb$ ratio). The μ value is selected to give the same age for the lithology as deduced by other geochronological methods (for example, U-Pb age).

In order to use the latter method, a lead evolution model has to be chosen. Several such models are proposed (for example, Holmes 1946; Houtermans 1946; Cumming and Richards 1975; Stacey and Kramers 1975; Zartman and Doe 1981; Thorpe 1982). In the first geoscience research grant report (1985-1986) on the lead isotope study of the Dome Mine QFV (Moritz *et al.* 1987a), the single-stage Holmes-Houtermans lead evolution model (Faure 1986) was used, whereas in the present study, Stacey and Kramers' model (1975) and Thorpe's local Superior lead evolution model (1982) were opted for. This was done because these models yield lead-lead model ages for sulphides from a massive sulfide deposit (Kidd Creek mine, Timmins area), and for a komatiitic flow (Fred's flow, Munro Township), that are in good agreement with the most likely age of their host rocks (Table 280.1). Calculations with the single-stage model (Faure 1986) are given for comparison purposes.

The lead composition of the galena samples from the Kidd Creek Mine (Franklin *et al.* 1983; Tilton 1983), and the chalcopyrite samples from Fred's Flow (Brevart *et al.* 1986), are also utilized to give an estimate of the μ value of possible source rock reservoirs in the Archean. Galena samples from the Kidd Creek massive sulphide deposit contain lead

TABLE 280.1. COMPARISON BETWEEN LEAD-LEAD MODEL AGES OBTAINED FOR SULPHIDES FROM THE KIDD CREEK MASSIVE SULPHIDE DEPOSIT AND FROM THE LAYERED KOMATIITIC FRED'S FLOW (MUNRO TOWNSHIP) AND AGES OBTAINED BY OTHER MEANS ON THEIR HOST ROCKS.

Locality and Type of Sulphide	Lead Isotope Ratios $\frac{^{206}\mathrm{Pb}}{^{204}\mathrm{Pb}}$	 $\frac{^{207}\mathrm{Pb}}{^{204}\mathrm{Pb}}$	Ref.
Kidd Creek massive sulphide deposit : galenas	13.29	14.46	1
	13.27	14.47	1
	13.28	14.47	2
Munro Township Fred's Flow : chalcopyrites	13.352	14.461	3
	13.268	14.444	3

LEAD-LEAD MODEL AGES (m.y.) and μVALUES

Single-stage (Faure 1986)		Two-stage (Stacey and Kramers 1975)		Superior model (Thorpe 1982)	
Age	μ	**Age**	μ	**Age**	μ
2640	7.67	2709	8.45	2715	8.62
2667	7.72	2757	8.77	2749	8.77
2658	7.71	2743	8.69	2738	8.73
2585	7.60	2627	8.08	2652	8.44
2646	7.65	2707	8.35	2717	8.57

AGES (m.y.) OBTAINED BY OTHER METHODS ON THE HOST ROCKS

Age	Methods	Ref.
2717±4	U-Pb zircon	4
Between 2703±2 and 2710±21	U-Pb zircon	5
2724±20	Lead-Lead	3
2662±120	Sm-Nd	6
2726±93	Re-Os	7

μvalues are also listed for each model.
References: 1 - Franklin *et al.* (1983), 2 - Tilton (1983), 3 - Brevart *et al.* (1986), 4 - Nunes and Pyke (1981), 5 - Nunes and Jensen (1980), 6 - Zindler (1982), 7 - Walker *et al.* (1988).

mainly of crustal origin, whereas chalcopyrite samples from Munro Township komatiites are representative of mantle-type lead.

RESULTS AND DISCUSSION

WHOLE ROCK LEAD ISOTOPE RATIOS

Isotopic ratios were obtained for five porphyry samples and one composite slate sample (Table 280.2). The carbonatized rocks and the ultramafic flow did not yield any reliable lead isotope results. In all probability this was due to low lead concentrations in these samples. Low concentrations of lead are characteristic of unaltered komatiites (Table 2 *in* Brevart *et al.* 1986), and it is suggested that the komatiites of the Dome Mine were not greatly enriched in lead during subsequent alteration and metamorphic processes. It is doubtful that the carbonatized komatiitic wall rocks of the QFV contributed much of the lead now present in the galenas. Thus, the local carbonatized komatiites can be ruled out with great confidence as a major source rock reservoir for lead.

The lead isotope ratios of the three whole rock samples collected underground (Table 280.2, samples COMP4, 12302, and 12515) are colinear (Figure 280.2). In contrast, the surface samples (Table 280.2, samples 608, 609, and 709) fall off this linear array (Figure 280.2). Assuming that all porphyries are cogenetic (McAuley 1983) and that their evolution can be represented by a two-stage model, the crystallization age of the Preston Porphyry, which is 2685±3 Ma (Marmont *in* Masliwec *et al.* 1986), can be used to calculate the slope of their theoretical secondary isochron. The calculated slope is 0.1835. The theoretical secondary isochron fits the lead isotope distribution of the colinear underground samples, which yield a slope of 0.1822±0.0545 (least square fitting method of York (1969)) (Figure 280.2). The intersection of the geochron at 2685 Ma with the secondary porphyry isochron gives the initial lead composition of the porphyries. The position of the 2685 Ma geochron in the lead-lead diagram is a function of the parameters of the chosen model. These parameters are the $^{206}\mathrm{Pb}/^{204}\mathrm{Pb}$ and $^{207}\mathrm{Pb}/^{204}\mathrm{Pb}$ ratios at the initiation of the lead evolution, the starting time of the model, and the variation in μ with time.

There is a good agreement between the initial ratios of the porphyry samples computed from Stacey and Kramers' model (1975), and Thorpe's model (1982), whereas Holmes-Houtermans' single-stage model (Faure 1986) yields lower initial ratios (Figure 280.2; Table 280.3). The isotopic ratios corresponding to the intersection of the 2685 Ma geochron and the secondary porphyry isochron, and the lead isotope composition of the source at the initiation time of the model, permits the computation of the growth curve of the porphyry source reservoir and its μ value. These μ values are listed in Table 280.3. The μ values obtained by both the single-stage model and the two-stage model indicate a source reservoir for the porphyries which is depleted in uranium. The μ value of 8.64 calculated with Stacey and Kramers' model is lower than their terrestrial average μ value of 9.74. The value of 7.79 yielded by the single-stage model agrees well with μ

TABLE 280.2. ISOTOPIC COMPOSITION OF WHOLE ROCKS FROM THE DOME MINE ENVIRONMENT. ALL DATA ARE CORRECTED FOR MASS FRACTIONATION USING SRM NBS 981. Samples 60l, 609, and 709 were collected at the surface. Samples COMP4, 12302, and 12515 were collected on the 12th level (Figure 280.1).

Sample Number	Rock Type and Name of Lithology	$^{206}\mathrm{Pb}$ $^{204}\mathrm{Pb}$	$^{207}\mathrm{Pb}$ $^{204}\mathrm{Pb}$	$^{208}\mathrm{Pb}$ $^{204}\mathrm{Pb}$
COMP4	Composite sample of slates lying north of the carbonate rock zone	18.171	15.381	38.537
608	Paymaster porphyry	19.320	15.547	38.501
609	Paymaster porphyry	18.317 18.283	15.238 15.236	37.073 37.040
709	Preston West porphyry	23.648	16.300	40.352
12302	Preston porphyry	18.822	15.508	37.861
12515	Porphyry lens in the carbonate rock zone	18.024 18.092	15.366 15.384	36.275 36.313

values between 7.4 and 7.9 obtained by independent studies on the Archean mantle (for example, Chauvel *et al.* 1987; Dupré and Arndt 1987; Shirey and Carlson 1987). REE patterns indicate that the slates in the Dome Mine environment are partially derived from local porphyries (Moritz 1988), thus it is not surprising that the slate composite sample falls on the secondary isochron defined for the porphyries (Figure 280.1, sample COMP4).

Several reasons can be suggested to account for three porphyry samples lying off the secondary isochron. The alteration of the U-Pb ratio of the surface samples could be a possible cause. Alternatively, their discordant behavior might be an original feature of the porphyries. Reworking of ancient crust, or isotopic contamination from older crust might be the origin of the data scatter (for example, Moorbath and Taylor 1981). Depending on the proportions of different crustal and mantle material in the melt from which the porphyries crystallized, the source reservoir might have been fairly heterogeneous, yielding highly variable initial ratios (for example, Gariépy and Allègre 1985). These different cases imply the presence of a relatively older crustal reservoir. Indirect evidence of an older sialic reservoir comes from the presence of zircons in detrital sediments from the Pontiac Group, which are at least 2940 Ma old, while some could be as old as 3150 Ma (Gariépy *et al.* 1984).

It is virtually impossible to decide whether one or the other above mentioned scenarios is more likely. As illustrated by the galena samples from the Kidd Creek Mine, which contain mainly crustal lead, and the chalcopyrite samples from Fred's Flow (Munro Township), that have mainly mantle lead (Table 280.1; Figure 280.3), it may well be that in the Archean the various lead source reservoirs did not have significantly different μ values. This could be the result of a small age difference between production of older crustal source material from the mantle, and the subsequent melting of either the crust or both the mantle and the crust to generate the porphyry magma. For instance, if the older crust was generated some 2940 Ma ago (Gariépy *et al.* 1984), then the porphyries crystallized only some 250 Ma later, at about 2685 Ma (Marmont *in* Masliwec *et al.* 1986).

In spite of the nonlinearity of the whole rock data from the porphyries, the lead ratios can still be approximated by a two-stage model. In this case, it would be more accurate to call the secondary isochron a "scatterchron". If all whole rock data are used to compute the initial lead isotope ratio of the porphyries, then the μ values are not drastically affected, and are 7.69, 8.27, and 8.51, instead of 7.79, 8.64, and 8.71 for the single-stage model, Stacey and Kramers' model, and the local Superior model, respectively. However, it adds another degree of uncertainty to the true initial lead isotope composition of the porphyries 2685 Ma ago. The most appropriate lead evolution models to use are Stacey and Kramers' model (1975), and the local Superior model described by Thorpe (1982). The Holmes-Houtermans' single-stage model (Faure 1986) yields lead-lead ages too young for pyrite samples from the Kidd Creek massive sulfide deposit, and chalcopyrite samples from Fred's Flow, in comparison to the age of their host rocks (Table 280.1). The single-stage model probably gives lead compositions for the porphyries that are only a lower estimate of the true initial ratio.

GALENA LEAD ISOTOPE RATIOS

The lead isotopic composition of the most likely reservoirs for galena from the QFV are known approximately. Chalcopyrite samples from Fred's Flow (Munro Township) provide an estimate of the lead isotope composition of the mantle beneath the Abitibi belt, and of a volcanic pile consisting predominantly of rocks derived from the mantle. Galena samples from the Kidd Creek massive sulphide deposit con-

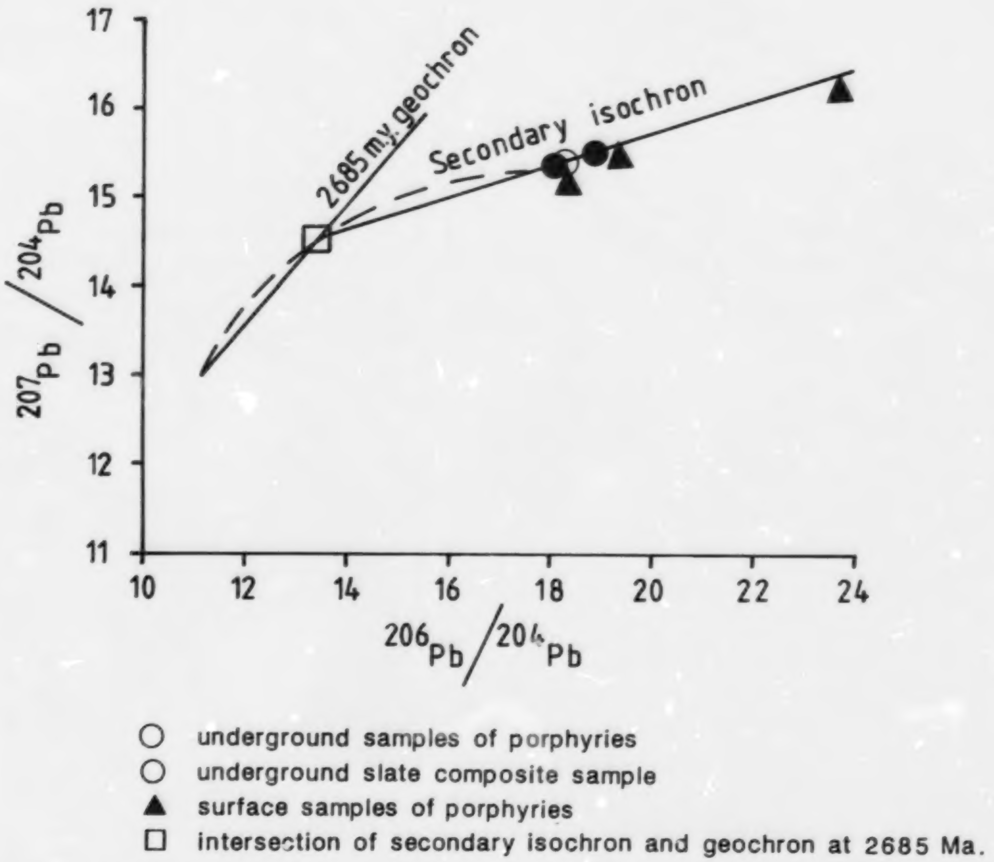

Figure 280.2. *Whole rock lead isotope data of the porphyry and slate samples from the Dome Mine environment. The position of the secondary isochron is constrained by its slope (calculated with the help of the 2685 Ma U-Pb zircon age of the Preston Porphyry; Marmont in Masliwec et al. 1986), and the distribution of the underground samples. The composition of the surface samples off the secondary isochron may be due to alteration, or may be a primary feature (see text for discussion). The intersection of the secondary isochron and the geochron at 2685 Ma yields the initial isotope composition of the porphyries.*

tain lead mainly derived from the crust. The initial lead isotope ratio of the local porphyries has also been established. In addition, local carbonatized komatiites have been ruled out as a major lead source.

The lead isotopic compositions of galena associated with gold are listed in Table 280.4, and shown in Figure 280.3, together with the composition of the major potential lead sources. Within the reproducibility of measurements, six out of eight galena samples cluster tightly near the origin of the secondary isochron of the local porphyries, as determined with the two-stage model (Stacey and Kramers 1975) and the Superior model (Thorpe 1982). The model ages of the galena samples fall within a small range, and μ values indicate a source depleted in uranium relative to the terrestrial average value of 9.74 given by Stacey and Kramers (1975) (Table 280.4). The spread of this grouping is attributed to error in measuring ^{204}Pb, and to mass dependent isotopic fractionation.

The similar lead isotope composition of the galena samples and the initial ratio of the porphyry samples from the Dome Mine environment may be interpreted as evidence of a genetic affiliation between both. Alternatively, this pattern may be fortuitous, with the porphyry bodies and galenas being of the same age, but not from the same source. It was noted above that various source reservoirs may not have developed significantly different μ values, thus rendering it difficult to recognize on the basis of isotopic data alone lead derived from different reservoirs. Possible sources include an upper mantle or a lower crustal reservoir, a fluid generated by metamorphic outgassing of a volcanic pile composed chiefly of basalts and komatiites, or the local intrusives. The fairly uniform lead composition of the six galena samples from the main cluster suggests an

TABLE 280.3. INITIAL LEAD ISOTOPE RATIOS OF THE PORPHYRIES CALCULATED WITH DIFFERENT LEAD EVOLUTION MODELS. THE CORRESPONDING μ VALUES OF THE SOURCE RESERVOIR ARE ALSO GIVEN.

Model	Initial Lead Isotope Ratios of the Porphyries		μ Value of the Source Reservoir
	$\frac{^{206}Pb}{^{204}Pb}$	$\frac{^{207}Pb}{^{204}Pb}$	μ
Single-stage (Faure 1986)	13.271	14.489	7.79
Two-stage (Stacey and Kramers 1975)	13.387	14.512	8.64
Superior model (Thorpe 1982)	13.383	14.510	8.71

isotopically well homogenized source. Moreover, given the close spatial association of gold mineralization and porphyries in the Timmins area (Ferguson *et al.* 1968), and the genetic model proposed for the QFV, the porphyries from the Dome Mine environment are the most likely source of the lead. However, this genetic relationship does not imply that the ultimate source of gold in the QFV are the porphyries from the Dome Mine. It is possible that the felsic stocks from the Timmins mining camp may be the upper visible apophyses of larger magmatic bodies at depth, which may have supplied the ore components of the QFV.

Two galena samples have "anomalous" lead compositions with respect to the main galena cluster. The two "anomalous" samples and the main galena grouping are colinear. This linear array has a slope of 0.33±0.07 (York 1969) (Figure 280.4). The process which generated this line can be approximated by a mixing model, with the main galena cluster as one end member, and a radiogenic crustal component as the other. It is possible to determine approximately when this contamination event occurred by making a few sound assumptions. The closest source for radiogenic lead is the adjacent volcanic and sedimentary rock sequence of the Tisdale and Deloro Groups (Pyke 1982). The Tisdale volcanism lasted about 22 Ma (Nunes and Pyke 1980, 1981). The length of the volcanism which generated the rocks of the Deloro Group is not so well constrained. However, for the sake of argument, let us attribute a comparable duration of approximately 22 Ma to the Deloro volcanism. In this case, deposition of the volcanic pile lasted from about 2750 to 2703 Ma. For convenience of calculation, the beginning of radiogenic lead accumulation is time-averaged at 2725 Ma. Using this reasonable age, and the slope of the linear galena array, the time of addition of radiogenic lead from the adjacent volcanic pile to galena in the QFV can be calculated as 1970 Ma$^{+510}_{-720}$ (Figure 280.4). It is entirely possible that more than one contamination event took place. Independent evidence for a possible alteration of the lead isotopic system in the time span established above is given by Masliwec *et al.* (1986), who recognize in model $^{40}Ar/^{39}Ar$ age spectra of the Dome Mine fuchsites a significant disturbance 2450 Ma ago and a second milder perturbation 1800 Ma ago. Several thermal episodes could have caused the remobilization of lead from nearby volcanic and sedimentary strata, and conceivably the perturbations in the argon age spectra. For instance, the Kenoran and Hudsonian orogenies occurred at 2480 Ma and 1735 Ma, respectively (Stockwell *et al.* 1976). Additionally, diabase dikes intruded this part of the Abitibi belt. Measured or inferred ages range from Early to Late Precambrian (Leech *in* Ferguson *et al.* 1968; Pyke 1982). In a comprehensive study, Franklin *et al.* (1983) found very similar "anomalous" lead isotope patterns in many gold deposits from the Abitibi Greenstone Belt. They attribute the distribution of the "deviant" leads to Kenoran metamorphic events, and possibly to the Nipissing diabase intrusion event, which took place 2170 Ma ago (Krogh and Davis 1974). The above mentioned thermal events might also explain the scatter shown by the porphyry lead ratios.

CONCLUSIONS

1. In the light of a broad geological and geochemical study in the QFV environment (Moritz 1988), the similarity between the lead isotopic composition of galena from the QFV, and the initial lead ratio of the porphyries, suggests a genetic link between the gold mineralization in the QFV and the emplacement of local quartz-feldspar porphyries.
2. Without a good knowledge and understanding of the local geological setting, a lead isotope study alone might be meaningless and not sufficient to define a unique ore source in the case of Archean lode gold deposits. The reason is that various lead source reservoirs in the Archean may not have developed significantly different U-Pb ratios, and as a result, cannot be distinguished by current analytical techniques.
3. After the precipitation of galena in the QFV, one or more contamination events took place broadly between 1250 and 2480 Ma ago, which can be attributed to Kenoran and Hudsonian orogenies, or to the intrusion of diabase dikes in the area. This conclusion is compatible with the disturbances found in the argon age spectra from samples of fuchsite from the Dome Mine (Masliwec *et al.* 1986).
4. The scatter of the porphyry and slate whole rock data is due either to alteration of the U-Pb ratios after their formation, or to primary lead isotopic variations in the source of the porphyries. The second alternative implies the existence of an older sialic reservoir.
5. Despite the nonlinearity of the data, the lead evolution of the porphyries can be approximated by a two-stage model confirming the conclusions reached by McAuley (1983), and Kerrich and Fryer (1979), that the porphyries are cogenetic, and that the slates are genetically related to the porphyries.

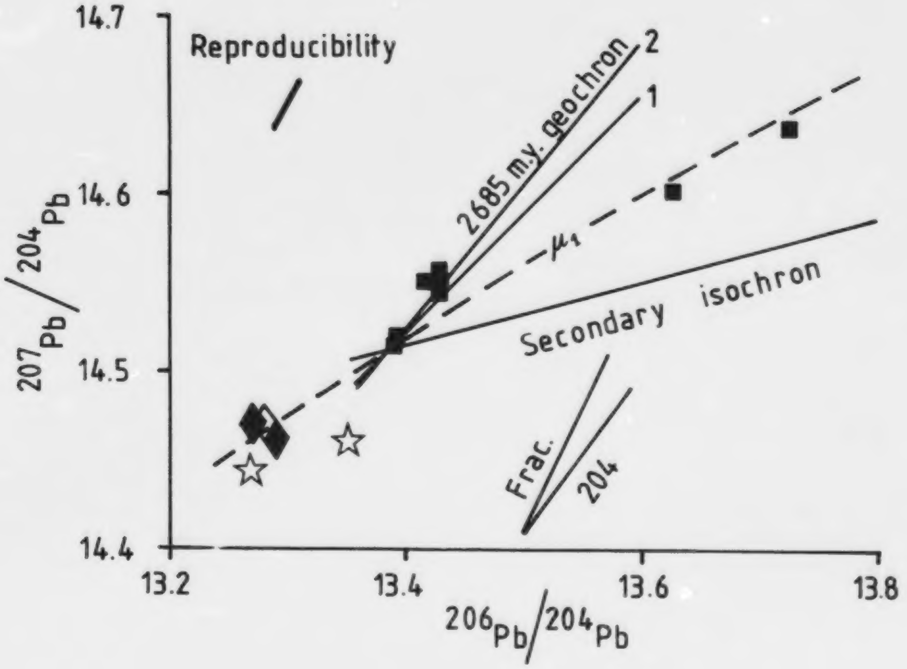

■ galena from the quartz fuchsite vein

☆ chalcopyrite from the layered komatiitic Theo's flow, Munro Township, Ontario (Brevart et al. 1986)

◆ galena from the Kidd Creek massive sulfide deposit, Ontario (Franklin et al. 1983)

◇ galena from the Kidd Creek deposit (Tilton, 1983)

1 geochron at 2685 Ma according to the two-stage model (Stacey and Kramers 1975)

2 geochron at 2685 Ma according to the Superior model (Thorpe 1982)

μ_1 growth curve of the source reservoir of the porphyries, μ_1 = 8.46 and 8.71 according to the two-stage model (Stacey and Kramers 1975), and the Superior model (Thorpe 1982), respectively

Frac. mass dependent isotope fractionation error

204 error of measurement of the ^{204}Pb isotope

Figure 280.3. *Lead isotope composition of the galena samples associated with gold in the Dome Mine quartz-fuchsite vein.*

TABLE 280.4. LEAD ISOTOPE COMPOSITIONS OF GALENAS ASSOCIATED WITH GOLD IN THE DOME MINE QUARTZ-FUCHSITE VEIN. Model ages and μ values are given as well for each sample. Errors are +18/-29 and +14/-19 m.y. for the two-stage model (Stacey and Kramers 1975) and the Superior model (Thorpe 1982), respectively. All data are corrected for mass fractionation using SRM NBS 981.

Sample Number	$^{206}Pb/^{204}Pb$	$^{207}Pb/^{204}Pb$	$^{208}Pb/^{204}Pb$	Lead-Lead Model Ages (m.y.) and μ Two-stage model Age	μ	Superior model Age	μ
8002D	13.725	14.638	33.376	2496	8.51	2502	8.64
8006G	13.611	14.606	33.304	2576	8.66	2575	8.72
	13.612	14.600	33.296	2563	8.57	2566	8.68
8010F	13.398	14.525	33.204	2692	8.74	2685	8.75
	13.389	14.513	33.158	2680	8.61	2679	8.70
10005D	13.400	14.531	33.183	2701	8.82	2691	8.79
	13.383	14.500	33.107	2663	8.46	2669	8.62
10017B	13.440	14.555	33.270	2694	8.92	2680	8.84
	13.418	14.535	33.203	2685	8.76	2677	8.77
12003	13.398	14.518	33.158	2678	8.63	2677	8.70
	13.387	14.518	33.179	2693	8.70	2688	8.74
12031	13.419	14.564	33.290	2739	9.22	2712	8.97
	13.408	14.538	33.234	2704	8.87	2691	8.82
13010	13.429	14.557	33.296	2713	9.03	2694	8.89

6. Low μ values for the sources of the galena and the porphyries indicate that both were derived from an uranium-depleted reservoir.

ACKNOWLEDGMENTS

The authors would like to thank the management of Dome Mines Limited (now Placer Dome) for access to the quartz-fuchsite vein; Dean S. Rogers (Chief Geologist, Dome Mine, South Porcupine, Ontario) for arranging the field work and for helpful guidance and discussions. Field work was partially supported by an NSERC grant to J.H. Crocket.

REFERENCES

Brevart, O., Dupré, B., and Allègre, C.J.
1986: Lead-Lead Age of Komatiitic Lavas and Limitations on the Structure and Evolution of the Precambrian Mantle; Earth and Planetary Science Letters, Volume 77, p.293-302.

Chauvel, C., Dupré, B., Arndt, N.T., and Hofmann, A.W.
1987: Composition of the Archean mantle: Evidence from Pb and Nd Isotopes; p.31 *in* Abstracts with Program, Geological Association of Canada/ Mineralogical Association of Canada, Volume 12, 111p.

Colvine, A.C., Andrews, A.J., Cherry, M.E., Durocher, M.E., Fyon, A.J., Lavigne, M.J., Jr., Macdonald, A.J., Marmont, Soussan, Poulsen, K.H., Springer, J.S., and Troop, D.G.
1984: An Integrated Model for the Origin of Archean Lode Gold Deposits; Ontario Geological Survey, Open File Report 5524, 98p.

Cumming, G.L., and Richards, J.R.
1975: Ore Lead Isotope Ratios in a Continuously Changing Earth; Earth and Planetary Science Letters, Volume 28, p.155-171.

Davies, J.F.
1977: Structural Interpretation of the Timmins Mining Area, Ontario; Canadian Journal of Earth Sciences, Volume 14, p.1046-1053.

Dupré, B., and Arndt, N.T.
1987: Pb Isotopes in Archean Komatiites, Basalts and Sulphides; Terra Cognita, Volume 7, p.272.

Faure, G.
1986: Principles of Isotope Geology; Second Edition, John Wiley and Sons, New York, 589p.

Ferguson, S.A., Buffam, B.S.W., Carter, O.F., Griffis, A.T., Holmes, T.C., Hurst, M.E., Jones, W.A., Lane, H.C., and Longley, C.S.
1968: Geology and Ore Deposits of Tisdale Township, District of Cochrane; Ontario Department of Mines, Geological Report 58, 177p. Accompanied by Map 2075, scale 1:12 000 or 1 inch to 1000 feet.

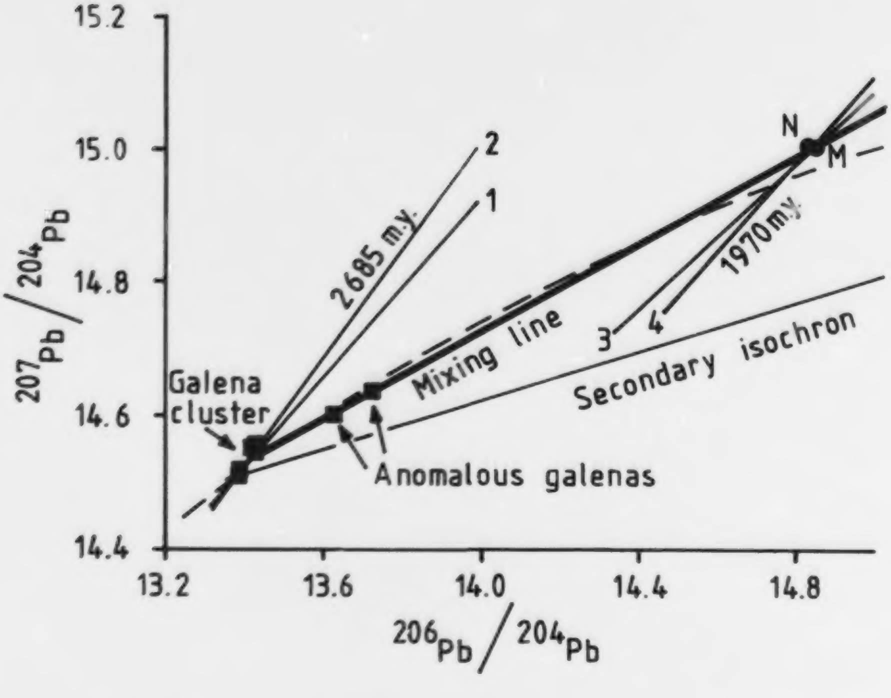

■ galena from the quartz fuchsite vein

— — — growth curve of the source of the porphyries

1 geochron at 2685 Ma in the two-stage model (Stacey and Kramers 1975)

2 geochron at 2685 Ma in the Superior model (Thorpe 1982)

3 geochron at 1970 Ma in the two-stage model

4 geochron at 1970 Ma in the Superior model

M composition of radiogenic lead from the Timmins area volcanic and sedimentary sequences at 1970 Ma, two-stage model

N composition of radiogenic lead from the Timmins area volcanic and sedimentary sequences at 1970 Ma, Superior model

Figure 280.4. *Mixing responsible for the generation of "anomalous" galena samples in the quartz-fuchsite vein. The "anomalous" galena samples are the result of the mixing of lead from the quartz-fuchsite vein galena (main galena cluster), and radiogenic lead from the surrounding rock sequences (points M and N) 1970 Ma ago (time-averaged).*

Franklin, J.M., Roscoe, S.M., Loveridge, W.D., and Sangster, D.F
1983: Lead Isotope Studies in Superior and Southern Provinces; Geological Survey of Canada, Bulletin 351, 60p.

Fryer, B.J., Kerrich, R., Hutchinson, R.W., Peirce, M.G., and Rogers, D.S.
1979: Archean Precious Metal Hydrothermal Systems, Dome Mine, Abitibi Greenstone Belt. 1. Patterns of Alteration and Metal Distribution; Canadian Journal of Earth Sciences, Volume 16, p.421-439.

Gariépy, C., and Allègre, C.J.
1985: The Lead Isotope Geochemistry and Geochronology of Late-Kinematic Intrusives from the Abitibi Greenstone Belt, and the Implication for Late Archaean Crustal Evolution; Geochimica et Cosmochimica Acta, Volume 49, p.2371-2383.

Gariépy, C., Allègre, C.J., and Lajoie, J.
1984: U-Pb Systematics in Single Zircons from the Pontiac Sediments, Abitibi Greenstone Belt; Canadian Journal of Earth Sciences, Volume 21, p.1296-1304.

Groves, D.I., and Phillips, G.N.
1987: The Genesis and Tectonic Control on Archaean Gold Deposits of the Western Australia Shield—A Metamorphic Replacement Model; Ore Geology Reviews, Volume 2, p.287-322.

Gulson, B.L.
1986: Lead Isotopes in Mineral Exploration; Development in Economic Geology, Elsevier, Amsterdam, Volume 23, 245p.

Hodgson, C.J.
1983: The Structure and Geological Development of the Porcupine Camp—A Re-evaluation; p.211-225 *in* The Geology of Gold in Ontario, edited by A.C. Colvine, Ontario Geological Survey, Miscellaneous Paper 110, 278p.

Holmes, A.
1946: An Estimate of the Age of the Earth; Nature, Volume 157, p.680-684.

Holmes, T.C.
1968: Dome Mines Limited; p.82-98 *in* Geology and Ore Deposits of Tisdale Township, by S.A. Ferguson and Associated Geologists, Ontario Department of Mines, Geological Report 58, 177p.

Houtermans, F.G.
1946: Die Isotopenhäufigkeiten in Natürlichen Blei und das Alter des Urans; Naturwissenschaften, Volume 33, p.185-186.

Hurst, M.E.
1935: Vein Formation at Porcupine Ontario; Economic Geology, Volume 30, p.103-127.

Kerrich, R., and Allison, I.
1978: Vein Geometry and Hydrostatics during Yellowknife Mineralization; Canadian Journal of Earth Sciences, Volume 17, p.1653-1660.

Kerrich, R., and Fryer, B.J.
1979: Archean Precious Metal Hydrothermal Systems, Dome Mine, Abitibi Greenstone Belt. II. REE and Oxygen Isotope Relations; Canadian Journal of Earth Sciences, Volume 16, p.440-458.

Krogh, T.E., and Davies, G.L.
1974: The Age of the Sudbury Nickel Irruptive; Geophysical Laboratory, Geochemistry, Radiometric Geochronology, Carnegie Institute, Washington, Yearbook, Volume 73, p.567-569.

Lambert, R., St.J.
1985: Lead Isotopes in Archean Rocks and the Evolution of the Mantle; p.49-53 *in* Evolution of Archean Supracrustal Sequences, edited by L.D. Ayres, P.C. Thurston, K.D. Card, and W. Weber, Geological Association of Canada Special Paper 28, 380p.

Masliwec, A., McMaster, D., and York, D.
1986: The Dating of Ontario's Gold Deposits; Grant 233, p.107-114 *in* Geoscience Research Grant Program, Summary of Research, 1985-1986, edited by V.G. Milne, Ontario Geological Survey, Miscellaneous Paper 130, 235p.

Mason, R., and Melnik, N.
1986a: The McIntyre–Hollinger Investigation, Timmins, Ontario: a Gold Dominated Porphyry Copper System; p.577-583 *in* Current Research, Part B, Geological Survey of Canada, Paper 86-1B, 884p.
1986b: The Anatomy of an Archean Gold System—The McIntyre–Hollinger Complex at Timmins, Ontario, Canada; p.40-55 *in* Proceedings, Gold'86, an International Symposium on the Geology of Gold, Toronto, edited by A.J. Macdonald, 517p.

McAuley, J.B.
1983: A Petrographic and Geochemical Study of the Preston, Preston West and Paymaster Porphyries, Timmins, Ontario; Unpublished M.Sc. Thesis, Laurentian University, Sudbury, 118p.

Moorbath, S., and Taylor, P.N.
1981: Isotopic Evidence for Continental Growth in the Precambrian; p.491-525 *in* Precambrian Plate Tectonics, edited by A. Kröner, Elsevier, Amsterdam, 781p.

Moritz, R.P.
1988: Geological and Geochemical Studies of the Gold-Bearing Quartz-Fuchsite Vein at the Dome Mine, Timmins Area; Unpublished Ph.D. Thesis, McMaster University, Hamilton, 280p.

Moritz, R.P., Crocket, J.H., and Dickin, A.P.
1987a: Lead Isotope Study of Gold Mineralization in the Dome Mine Quartz-Fuchsite Vein; Grant 280, p.115-125 *in* Geoscience Research Grant Program, Summary of Research, 1986-1987, edited by V.G. Milne, Ontario Geological Survey, Miscellaneous Paper 136, 241p.

Moritz, R.P., Crocket, J.H., and Dickin, A.P.
1987b: Lead Isotope Study of the Gold-Bearing Quartz-Fuchsite Vein, Dome Mine, Timmins, Ontario; p.778 *in* Abstracts with Programs, Geological Society of America, Volume 19, 922p.

Nunes, P.D., and Jensen, L.S.
1980: Geochronology of the Abitibi Metavolcanic Belt, Kirkland Lake Area—Progress Report; p.40-45 *in* Summary of Geochronology Studies, 1977-1979, edited by E.G. Pye, Ontario Geological Survey, Miscellaneous Paper 92, 45p.

Nunes, P.D., and Pyke, D.R.

1980: Geochronology of the Abitibi Metavolcanic Belt, Timmins–Matachewan Area—Progress Report; p.34-39 *in* Summary of Geochronology Studies, 1977-1979, edited by E.G. Pye, Ontario Geological Survey, Miscellaneous Paper 92, 45p.

1981: Time-Stratigraphic Correlation of the Kidd Creek Ore Body with Volcanic Rocks South of Timmins, Ontario, as Inferred from Zircon U-Pb ages; Economic Geology, Volume 76, p.944-951.

Pyke, D.R.

1982: Geology of the Timmins Area, District of Cochrane; Ontario Geological Survey, Report 219, 141p. Accompanied by Map 2455, scale 1:50 000.

Robert, F., and Brown, A.C.

1986: Archean Gold-Bearing Quartz-Veins at the Sigma Mine, Abitibi Greenstone Belt, Quebec: Part I. Geologic Relations and Formation of the Vein System; Economic Geology, Volume 81, p.578-592.

Robert, F., Brown, A.C., and Audet, A.J.

1983: Structural Control of Gold Mineralization at the Sigma Mine, Val d'Or, Quebec; Canadian Institute of Mining and Metallurgy Bulletin, Volume 76, p.72-80.

Roberts, R.G.

1981: The Volcanic-Tectonic Setting of Gold Deposits in the Timmins Area, Ontario; p.16-28 *in* Genesis of Archean, Volcanic-Hosted Gold Deposits, Symposium Held at the University of Waterloo, March 7 1980, edited by E.G. Pye and R.G. Roberts, Ontario Geological Survey, Miscellaneous Paper 97, 175p.

Roberts, R.G., and Reading, D.J.

1981: Volcanic-Tectonic Setting of Gold Deposits in the Timmins District—Carbonate-Bearing Rocks at the Dome Mine; Grant 32, p.222-228 *in* Geoscience Research Grant Program, Summary of Research 1980-1981, edited by E.G. Pye, Ontario Geological Survey, Miscellaneous Paper 98, 340p.

Roberts, R.G., Carnevali, J., and Harris J.D.

1978: The Volcanic-Tectonic Setting of Gold-Quartz Vein Systems in the Timmins District, Ontario; p.187-190 *in* Current Research, Part B, Geological Survey of Canada, Paper 78-1B, 22p.

Rogers, D.S.

1982: Diamond Drilling as an Aid in Ore Definition at the Dome Mine; Canadian Institute of Mining and Metallurgy Bulletin, Volume 75, p.98-104.

Rosholt, J.N., Zartman, R.E., and Nkomo I.T.

1973: Lead Isotope Systematics and Uranium Depletion in the Granite Mountains, Wyoming; Bulletin of the Geological Society of America, Volume 84, p.989-1002.

Shirey, S.B., and Carlson, R.W.

1987: Pb and Nd Isotope Evolution of the Archean Crust and Mantle; Terra Cognita, Volume 7, p.272.

Stacey, J.S., and Kramers, J.D.

1975: Approximation of Terrestrial Lead Isotope Evolution by a Two-Stage Model; Earth and Planetary Science Letters, Volume 26, p.207-221.

Stockwell, C.H., McGlynn, J.C., Emslie, R.F., Sanford, B.V., Norris, A.W., Donaldson, J.A., Fahrig, W.F., and Currie, K.L.

1976: Geology of the Canadian Shield, Part A, Economic Geology; p.43-150 *in* Geology and Economic Minerals of Canada, edited by R.J.W. Douglas, Geological Survey of Canada, Department of Energy, Mines and Resources, Report Number 1, 364p.

Thorpe, R.I.

1982: Lead Isotope Evidence Regarding Archean and Proterozoic Metallogeny in Canada; Revista Brasileira de Geociências, Volume 12, p.510-521.

Tilton, G.R.

1983: Evolution of Depleted Mantle: the Lead Perspective; Geochimica et Cosmochimica Acta, Volume 47, p.1191-1197.

Walker, R.J., Shirey, S.B., and Stecher, O.

1988: Comparative Re-Os, Sm-Nd and Rb-Sr Isotope and Trace Element Systematics for Archean Komatiite Flows from Munro Township, Abitibi Belt, Ontario; Earth and Planetary Science Letters, Volume 87, p.1-12.

York, D.

1969: Least-Square Fitting of a Straight Line with Correlated Errors; Earth and Planetary Science Letters, Volume 5, p.320-324.

Zartman, R.E., and Doe, B.R.

1981: Plumbotectonics—The Model; Tectonophysics, Volume 75, p.135-162.

Zielinski, R.A., Peterman, Z.E., Stuckless J.S., Rosholt, J.N., and Nkomo, I.T.

1981: The Chemical and Isotopic Record of Rock-Water Interaction in the Sherman Granite, Wyoming and Colorado; Contribution to Mineralogy and Petrology, Volume 78, p.209-219.

Zindler, A.

1982: Nd and Sr Isotopic Studies of Komatiites and Related Rocks; p.399-420 *in* Komatiites, edited by N.T. Arndt and E.G. Nisbet, Allen and Unwin, London, 526p.

Grant 286 The Geochemistry, Origin, and Economic Potential of Platinum Group Element Bearing Rocks of the Lac des Iles Complex, Northwestern Ontario

J.M. Sweeny and A.D. Edgar

Department of Geology, University of Western Ontario, London

ABSTRACT

Platinum group mineralization occurs within several varieties of cumulate gabbroic rocks of the Lac des Iles Complex, northwestern Ontario. Pyroxenes in these rocks range from fresh to completely altered. Based on analyses of major elements, trace elements, and platinum group elements (PGE) in whole rocks, and analyses of platinum group minerals (PGM), the origin of the Lac des Iles PGE mineralization has been interpreted to be caused, in part, by alteration processes involving late-stage fluids.

This paper reports the results of: 18 new PGE and Au, Cu, and Ni analyses from rocks with varying degrees of alteration; 8 new analyses (including F and Cl) of amphiboles; 4 apatite analyses; and representative analyses of 9 PGM from a total of 144 discrete mineral grains. The distribution and textural relationships of these PGM relative to the origin of the Lac des Iles Complex are discussed.

INTRODUCTION

This paper presents the results of the second year's investigation of the platinum group element (PGE) mineralization in the Lac des Iles Complex, northwestern Ontario. The original objectives of this study were outlined by Sweeny and Edgar (1987), who also described previous work and the regional and local geology. These authors focused their attention on the Roby Zone of the Lac des Iles Complex (Sweeny and Edgar 1987, Figures 286.1 and 286.2) which consists of several varieties of gabbroic rocks distinguished by detailed mapping and petrography. These rocks are cumulate gabbro, gabbronorite, and norite, all of which have variable grain sizes and proportions of minerals. A detailed study of the petrography and rock and mineral chemistry was also done on a 1.3 m channel sample across a pegmatitic gabbro dike intruding norite and leucogabbro.

Based on variations in the whole rock and pyroxene chemistry, the area has been subdivided into a western gabbro, eastern gabbro, and a hybrid zone. The gabbroic rocks range from fresh to those with totally altered pyroxenes. In their previous report, Sweeny and Edgar (1987) presented 24 analyses for all PGE, Au, Cu, Ni, and S. Comparison of the Lac des Iles with other PGE deposits using Cu/(Cu+Ni) versus Pt/(Pt+Pd) plots (Sweeny and Edgar 1987, Figure 286.3), and plots of chondrite normalized average to 100 percent sulphides versus (PGE+Au) (Sweeny and Edgar 1987, Figure 286.4) indicates that alteration played an important role in the genesis of the Lac des Iles PGE mineralization, but that this was not the only factor.

This paper presents electron microprobe analyses of 9 platinum group minerals (PGM); 8 of these species have been previously identified and analyzed by Cabri and Laflamme (1979) and Dunning (1979) for the Lac des Iles Complex. The ninth is a Pt-Fe alloy which has not been previously identified. Analyses have also been made of amphibole and rare apatite grains in the mineralized rocks, to assess the possible role of F and Cl in the alteration of the host rocks. Additional to these mineral analyses, the present report includes a further 18 PGE analyses, which modify the Cu/(Cu+Ni) versus Pt/(Pt+Pd) diagram previously reported by Sweeny and Edgar (1987, Figure 286.3).

These new data are used to corroborate the concept that PGE mineralization at Lac des Iles results from combined magmatic and fluid-dominated processes. The final model for the genesis of this deposit will be presented by Sweeny (in preparation), and eventually will be included in an Open File Report to be published by the Ontario Geological Survey.

ANALYTICAL METHODS

Methods used for the PGE, Cu, Ni, Au, S, and major oxide chemistry, as well as for mineral chemistry, are given by Sweeny and Edgar (1987). The PGM analyses reported here were done on a JEOL 8600 Superprobe at an accelerating voltage of 15 kV and a sample current of 250 μamperes. Pure metals were used as standards for the PGM determinations.

RESULTS

PLATINUM GROUP ELEMENTS

Complete analyses for the PGE, Au, Cu, Ni, and S are presented in Table 286.1. This table also includes the name of each rock analyzed, and a visual estimation from thin section of the percent alteration of pyroxenes. All of the samples, with the exception of 85-RHS-50, are from locations within the hybrid zone. These data, along with previous fire assay and neutron activation analyses, are plotted on the Cu/(Cu+Ni) versus Pt/(Pt+Pd) diagram of Figure 286.1.

MINERAL CHEMISTRY

Electron microprobe data for representative amphibole and apatite grains are presented in Table 286.2. Table 286.3 lists representative analyses for the 9 PGM identified during this study.

DISCUSSION

PLATINUM GROUP MINERALS

A total of 144 discrete PGM grains were identified from 23 polished thin sections using the electron microprobe; 113 were quantitatively analyzed. Table 286.4 shows the number, type, and distribution of PGM in polished sections. The majority of PGM grains identified occur as small ($\leq$150 μm) anhedral

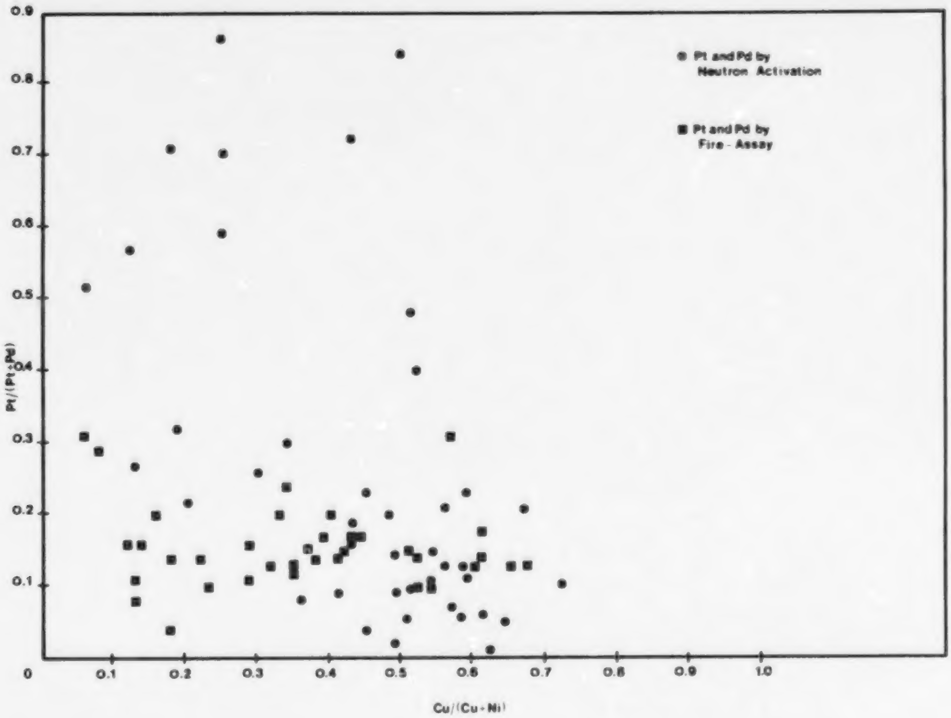

Figure 286.1. *Variation in Pt/(Pt+Pd) with Cu/(Cu+Ni) for the Lac des Iles Complex samples.*

grains which are hosted in sulphides, silicates, within larger PGM grains, or at sulphide-silicate boundaries.

Possible exsolution textures were observed between moncheite and merenskyite (Photos 286.1 and 286.2). The two grains shown in these photos are approximately 100 μm apart in the thin section, and both occur along a sulphide-silicate boundary. In Photo 286.1, merenskyite is exsolved in moncheite as lobes and lamellae. Photo 286.2 shows moncheite exsolved in merenskyite and also contains a small subhedral inclusion of gold. An isolated grain of braggite occurs within the pentlandite host between the two larger PGM grains. Irregular grains of kotulskite are found within the adjacent secondary silicates (not shown).

The most common PGM identified during this study was kotulskite (Table 286.4) followed by merenskyite and the braggite series. Previous workers in the area (Cabri and Laflamme 1979; Dunning 1979; Watkinson and Dunning 1979; Talkington and Watkinson 1984) found the braggite series to be the most common of the PGM, while kotulskite was ranked second in abundance. The Pd-rich nature of the Lac des Iles rocks is reflected in the abundance of palladium over platinum minerals.

A subhedral two-phase grain of kotulskite and moncheite (Photo 286.3) occurs within chalcopyrite in a large sulphide clot from a fresh gabbronorite (Sample 85-RHS-775). This same section also contains subhedral grains of a Pt-Fe alloy in a small chalcopyrite clot situated within silicates (Photo 286.4). This is the first reported occurrence of a Pt-Fe alloy from the Lac des Iles Complex. The idiomorphic habit of the Pt-Fe alloy against the sulphide, as opposed to the irregular contact with the silicates, indicates that the Pt-Fe alloy grew into the sulphide before the sulphide had completely crystallized (Vermaak and Hendriks 1976).

Merenskyite (not shown) and kotulskite are often found as anhedral blebs within secondary silicates (Photo 286.5). This association of palladium bismutotellurides with silicates may be accounted for by postmagmatic mobilization and redistribution of these volatile minerals into the surrounding silicate environment (Vermaak and Hendriks 1976).

Au-Ag alloys containing minor Pt and Pd occur as rounded blebs within chalcopyrite and pentlandite or as blebs and rims attached to chalcopyrite grains within silicates. A further study of the PGM-sulphide-silicate relationships may permit a paragenetic sequence to be determined for the PGE mineralization and alteration.

AMPHIBOLES AND APATITE

Microprobe analyses of amphiboles from mineralized rocks show F and Cl contents that range from 0.0 to 0.13 weight percent, while nonmineralized rocks have no detectable halogen contents. Boudreau *et al.* (1986) have indicated that the high-temperature hydrothermal fluids which affected the lower portions of the Stillwater and Bushveld complexes were Cl rich. This interpretation is based on compositional data from amphiboles, phlogopites, and apatites within the PGE ore zones. Amphiboles from mineralized rocks at

TABLE 286.1. PGE, Au, Cu, NI, AND S VALUES FROM ROCKS OF THE HYBRID ZONE.

				(ppb[1])					(ppm[2])			
Sample #	**Rock**	**Pd**	**Pt**	**Os**	**Ir**	**Ru**	**Rh**	**Au**	**Cu**	**Ni**	**S**	**Mineralization**
85-RHS-50	Gabbro*	31	42	<3	<0.1	10	<2	1	42	315	0.01	-
85-RHS-65[3]	Gabbronorite	5	32	<3	<0.1	13	<4	5	119	355	0.03	trace
86-LDI-2	Gabbronorite	1700	320	<4	3.8	19	19	710	5310	7160	4.75	2-3%
86-LDI-10	Gabbronorite	8600	740	5	0.5	18	8	580	1030	1800	0.20	0.5%
86-LDI-12	Gabbronorite	1300	140	<3	0.1	<10	1	130	630	605	0.21	trace
86-LDI-14	Pegmatitic Leucogabbro*	66	71	<3	<0.1	13	<4	1	20	285	0.01	-
86-LDI-17	Melagabbronorite*	14000	230	<3	0.3	<5	3	250	1075	1100	0.43	<1%
86-LDI-19	Gabbronorite	270	<7	<3	<0.2	<5	1	12	353	219	0.00	trace
86-LDI-24	Pegmatitic Gabbro*	10000	660	<3	0.6	<16	5	750	3010	1950	1.25	2%
86-LDI-28	Gabbronorite	45	<10	<3	<0.1	9	<3	65	2800	1100	0.60	0.5%
86-LDI-34	Gabbronorite	68	46	<3	<0.1	11	<4	16	140	130	0.07	trace
86-LDI-38	Gabbronorite	770	80	<3	0.4	<5	2	130	650	940	0.30	0.5%
86-LDI-57	Gabbro*	7000	730	<3	0.4	<12	7	670	1790	1830	0.44	0.5%
86-LDI-60	Gabbronorite	26	11	<3	<0.1	<5	<1	8	198	375	0.04	-
87-LDI-102	Gabbronorite*	9500	650	<3	0.6	24	6	790	3400	3300	0.64	1-2%
87-LDI-103	Pyroxenite*	9100	630	<3	0.6	15	6	560	3100	2200	0.90	1%
87-LDI-109	Pegmatitic Gabbro*	14000	700	<6	0.8	<5	12	2300	7600	4300	1.12	2%
87-LDI-313	Pegmatitic Gabbro*	20000	910	7	0.9	70	4	2800	5900	7200	1.30	3%

1. Analyses of PGE and Au by neutron activation.
2. Analyses of Cu and Ni by fire assay.
3. Duplicate analysis.

* - The pyroxene in these samples has >95% alteration. Samples without this designation have <50% alteration of pyroxenes.

TABLE 286.2. REPRESENTATIVE MINERAL ANALYSES FROM THE LAC DES ILES COMPLEX.

	Amphibole Analyses							
	1	2	3	4	5	6	7	8
SiO_2	55.12	54.88	51.82	54.29	45.42	54.45	47.49	54.13
TiO_2	0.05	0.01	0.06	0.13	0.96	0.03	1.32	0.19
Al_2O_3	1.03	0.32	4.98	1.95	10.00	1.2 5	7.15	4.30
Cr_2O_3	0.09	0.02	0.01	0.00	0.04	0.14	0.00	0.04
FeO	11.18	21.74	11.86	10.35	15.76	17.31	12.94	7.38
MnO	0.34	0.58	0.21	0.25	0.16	0.48	0.16	0.14
MgO	16.66	19.51	16.66	17.55	11.67	20.43	13.97	18.45
CaO	12.18	0.60	11.08	12.83	11.61	3.33	12.30	12.94
Na_2O	0.11	0.01	0.46	0.29	1.43	0.18	0.89	0.35
K_2O	0.00	0.00	0.00	0.00	0.22	0.00	0.44	0.05
Cl	0.04	0.02	0.05	0.00	0.00	0.08	0.00	0.00
F	0.00	0.09	0.00	0.00	0.13	0.03	0.08	0.04
Sum	96.80	97.78	97.19	97.64	97.40	97.71	96.74	98.01
-0=Cl, F	0.01	0.04	0.01	0.00	0.05	0.03	0.03	0.02
Sum	96.79	97.74	97.18	97.64	97.35	97.68	96.71	97.99
Number of Ions on a basis of 24 (O, OH, F, Cl)								
Si	8.273	8.288	7.781	8.079	7.038	8.141	7.314	7.908
Al^{iv}	0.000	0.000	0.219	0.000	0.962	0.000	0.686	0.092
Al^{vi}	0.182	0.057	0.662	0.342	0.863	0.220	0.611	0.648
Fe	1.403	2.746	1.489	1.288	2.042	2.164	1.667	0.902
Cr	0.011	0.002	0.001	0.000	0.005	0.017	0.000	0.005
Mg	3.727	4.391	3.729	3.893	2.695	4.553	3.267	4.617
Mn	0.043	0.074	0.027	0.032	0.021	0.061	0.021	0.017
Ti	0.006	0.001	0.007	0.015	0.112	0.003	0.153	0.021
Ca	1.959	0.097	1.783	2.046	1.927	0.533	2.030	2.025
Na	0.032	0.003	0.134	0.084	0.430	0.052	0.266	0.099
K	0.000	0.000	0.000	0.000	0.043	0.000	0.086	0.009
Cl	0.010	0.005	0.013	0.000	0.000	0.020	0.000	0.000
F	0.000	0.043	0.000	0.000	0.064	0.014	0.039	0.018

	Apatite Analyses			
	9	10	11	12
CaO	56.80	57.03	57.07	54.79
P_2O_5	40.18	40.76	40.65	40.16
SiO_2	0.02	0.10	0.15	0.17
Al_2O_3	10.00	0.00	0.02	0.04
MnO	0.00	0.02	0.12	0.14
FeO	0.04	0.18	0.16	0.23
MgO	0.03	0.03	0.03	0.06
Cl	1.55	0.54	2.23	1.85
F	0.00	0.30	0.00	0.12
Sum	98.62	98.98	100.42	97.57

1. 86-LDI-017, actinolite after cpx near sulphide clot, melagabbronorite
2. 86-LDI-073, anthophyllite after opx, norite
3. 86-LDI-072, actinolite after cpx, mineralized pegmatitic gabbro
4. 86-LDI-052, actinolite after cpx, altered eastern gabbro
5. 86-LDI-059, primary magnesio-hornblende, oxide-rich gabbro
6. 86-LDI-075, anthophyllite after opx, mineralized gabbro

cpx = clinopyroxene

7. 86-LDI-024, actinolite, mineralized pegmatitic gabbro
8. 87-LDI-102, actinolite, beside kotulskite in altered gabbronorite
9. 87-LDI-102, euhedral apatite, core
10. 87-LDI-102, same grain, between core and rim
11. 87-LDI-102, euhedral apatite, core
12. 87-LDI-102, same grain as 9, 10, rim

opx = orthopyroxene

TABLE 286.3. REPRESENTATIVE ELECTRON MICROPROBE PGM ANALYSIS.

	1 Kotulskite	2 Merenskyite	3 Moncheite	4 Sperrylite	5 Stillwaterite	6 Braggite	7 Vysotskite	8 Pt-Fe Alloy	9 PGE-Au Alloys
Pt	0.11	0.90	39.51	52.24	n.d.	38.86	2.05	84.90	1.31
Pd	42.72	25.48	2.16	0.07	79.56	31.79	66.65	1.00	3.90
Te	49.71	66.83	56.64	0.18	n.d.	0.03	n.d.	n.d.	n.d.
Bi	7.34	4.31	0.65	n.d.	0.01	n.d.	n.d.	n.d.	n.d.
As	0.05	n.d.	n.d.	45.25	19.88	n.d.	n.d.	n.d.	n.d.
Sb	0.12	0.58	0.57	n.d.	.08	n.d.	n.d.	n.d.	n.d.
Ni	n.d.	0.55	0.16	0.03	n.d.	7.06	6.27	0.19	0.14
Fe	0.58	0.34	0.07	1.16	0.86	0.56	1.15	10.15	0.24
S	0.03	0.03	0.05	0.73	0.03	21.07	23.31	0.09	0.05
Au	n.d.	0.31	1.12	0.10	n.d.	0.05	n.d.	0.45	82.07
Ag	n.d.	-	-	0.03	0.40	-	n.d.	n.d.	11.78
TOTAL	100.67	99.34	100.93	99.78	100.82	99.42	99.43	96.78	99.48

n.d. = not detected
- = not analyzed

1. Sample 87-LDI-103, altered pyroxenite, PGM in pyrrhotite
2. Sample 87-LDI-102, altered gabbronorite, PGM in pentlandite
3. Sample 87-LDI-102, altered gabbronorite, PGM in pentlandite
4. Sample 86-LDI-073, fresh norite, PGM in silicate
5. Sample 86-LDI-024, altered pegmatitic gabbro, PGM in silicate
6. Sample 87-LDI-102, altered gabbronorite, PGM in chalcopyrite
7. Sample 87-LDI-103, altered pyroxenite, PGM in pentlandite
8. Sample 85-RHS-775, fresh norite, PGM in chalcopyrite; low total due to presence of Cu, which was not analyzed
9. Sample 87-LDI-109, altered pegmatitic gabbro PGM in chalcopyrite

TABLE 286.4. PGM SPECIES LOCATIONS AND ABUNDANCES.

PGM	Ideal Formula	Sulphides	Silicates	Sulphide-Silicate Boundary	PGM	Total
Kotulskite	PdTe	31*	20	21	1	73
Merenskyite	$PdTe_2$	14	3	3	2	22
Moncheite	$PtTe_2$	2	1	2	2	7
Braggite Series	[(Pd,Pt)S]	6	2	5	0	13
Sperrylite	$PtAs_2$	1	3	1	1	6
Stillwaterite	Pd_8As_2	1	1	1	0	3
Pt-Fe Alloy	-	0	0	2	0	2
PGE-Au Alloys	-	11	3	3	1	18
Total		66	33	38	7	144

*Numbers represent discrete grains identified.

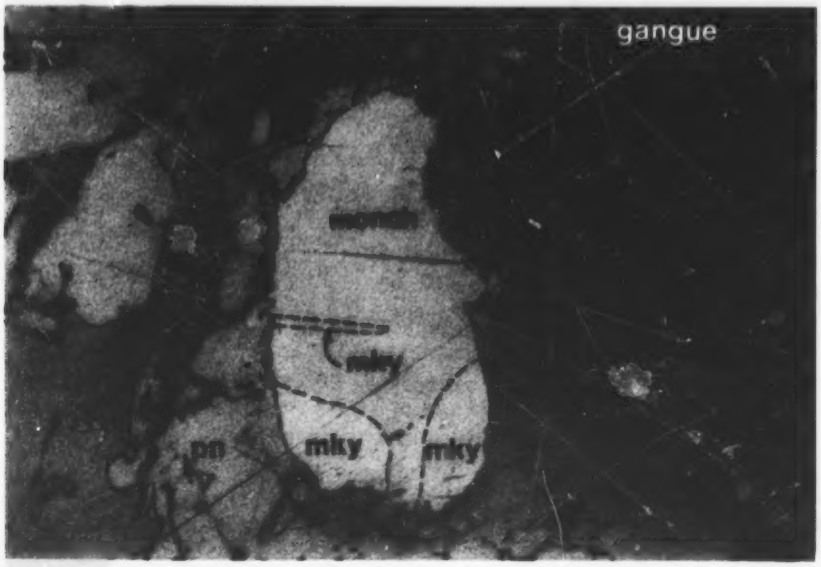

Photo 286.1. Exsolved merenskyite (mky) in moncheite (monch) hosted in pentlandite (pn) and pyrrhotite (po). A braggite (br) grain occurs to the left. The fracture at X joins Photo 286.2 at X. Magnification x400; partly crossed nichols, reflected light.

Lac des Iles show a slight halogen enrichment, although the role of F and Cl in PGE transport has not yet been established.

The amphiboles that occur at Lac des Iles are generally pseudomorphs after primary pyroxenes. Orthopyroxene alters to fibrous masses of anthophyllite and is also associated with talc and chlorite. Clinopyroxene alters to actinolite, a typical mineral in the eastern gabbro. Actinolite is commonly rimmed by hornblende, which is interpreted to be a primary reaction rim on the original clinopyroxene grain (Sutcliffe *et al.*, in preparation). Long bladed actinolite occurs intergrown with sulphides and occasionally may be associated with PGM (Photo 286.6). Actinolite also forms euhedral grains within sulphide clots and around the isolated PGM grains (Photo 286.5) where they are not formed by alteration of a primary pyroxene.

Magnesio-hornblende forms large euhedral to subhedral grains associated with sulphides and may contain as much as 0.13 weight percent F (Analysis 5, Table 286.2). These amphiboles are interpreted to be of primary magmatic origin.

Two euhedral grains of apatite and one euhedral grain of monazite were observed within sulphides in an altered gabbronorite from the hybrid zone (Sample 86-LDI-102, Table 286.1). Microprobe analyses of the apatite give Cl values that are comparable to apatites from the Stillwater and Bushveld complexes (Boudreau *et al.* 1986). The timing of crystallization of the phosphates is not well constrained; however, they may be primary minerals that were incorporated into the sulphide blebs during sulphide remobiliza-

gangue
mky
ch
mky

Photo 286.2. *Exsolved moncheite (monch) in merenskyite (mky) with a gold (Au) inclusion at the top. Host is pentlandite (pn) and pyrrhotite (po). Fracture at X joins Photo 286.1 at X. Magnification x400; partly crossed nicols, reflected light.*

tion. These grains occur near the edges of the sulphide clots and the grain boundaries are slightly corroded.

PLATINUM GROUP ELEMENTS

Figure 286.1 shows two distinct trends. The majority of analyses form a trend of constant Pt/(Pt+Pd) and increasing Cu/(Cu+Ni), while the other trend shows increasing Pt/(Pt+Pd) with increasing Cu/(Cu+Ni). The former trend is typical of most rocks from Lac des Iles and does not appear to be consistent with trends from other PGE deposits (Naldrett *et al.* 1980; Naldrett 1981; Sweeny and Edgar 1987). The second trend includes samples containing PGE abundances that are less than 500 ppb (Pt+Pd) but where Pt is generally greater than Pd. No correlation was observed between lithology and the observed trends, although the alteration of lithologies may be important. Alteration is presently being examined with an emphasis on determining primary magmatic alteration versus secondary hydrothermal or deuteric alteration.

FUTURE PLANS

A further examination of the PGM-sulphide-silicate association will be used to determine a paragenetic sequence for Lac des Iles. This will be combined with a more detailed petrographical study of the amphiboles to correlate PGE and PGM concentrations with amphibole types. A genetic model for the Lac des Iles Deposit will be presented in Sweeny (in preparation).

ACKNOWLEDGMENTS

The authors thank R.L. Barnett and Dave Kingston for their assistance with the electron microprobe analyses. John Forth and Walt Harley made polished probe sections. Drafting was done by Heather Charbonneau. Richard Sutcliffe is thanked for his advice and encouragement.

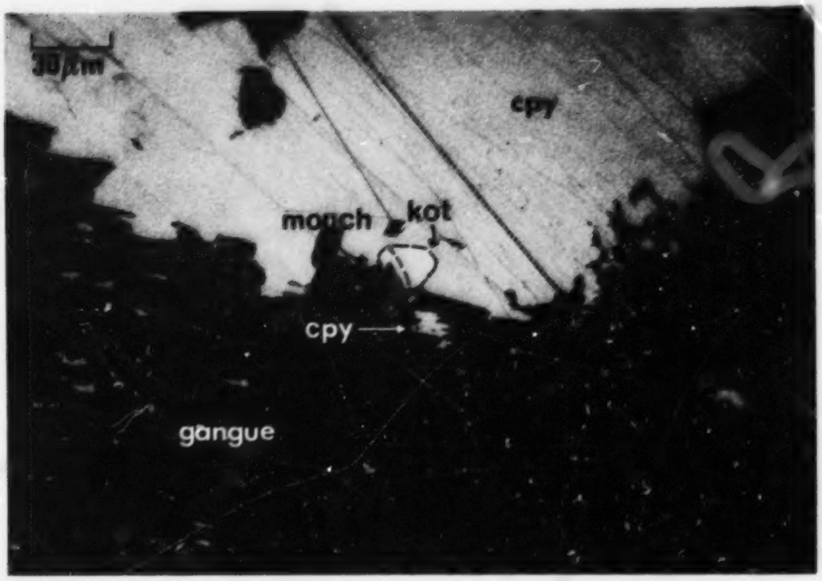
30 μm
cpy
monch
kot
cpy
gangue

Photo 286.3. *Euhedral two-phase kotulskite (kot) and moncheite (monch) grain in chalcopyrite (cpy) at a sulphide-silicate boundary. Magnification x400; plane polarized, reflected light.*

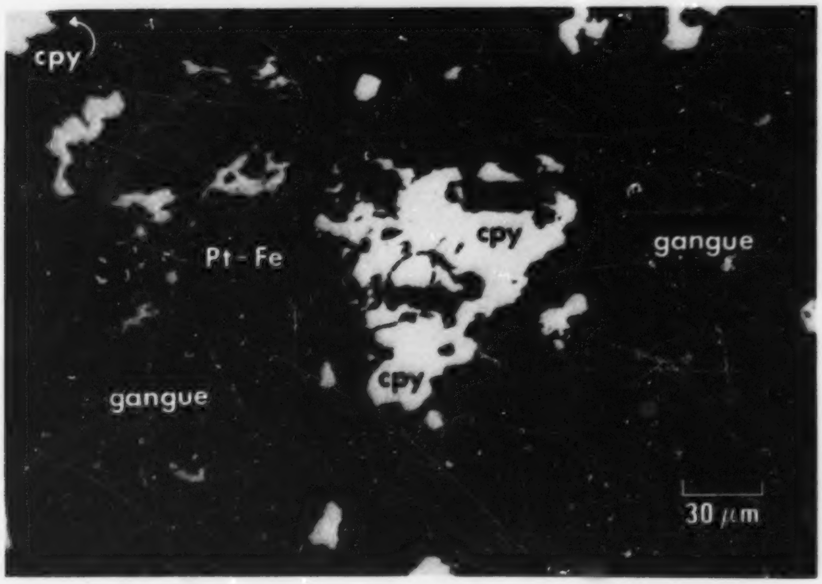
cpy
cpy
Pt-Fe
gangue
gangue
cpy
30 μm

Photo 286.4. *Pt-Fe alloy (Pt-Fe) grains in chalcopyrite (cpy) and silicates. Magnification x400; plane polarized, reflected light.*

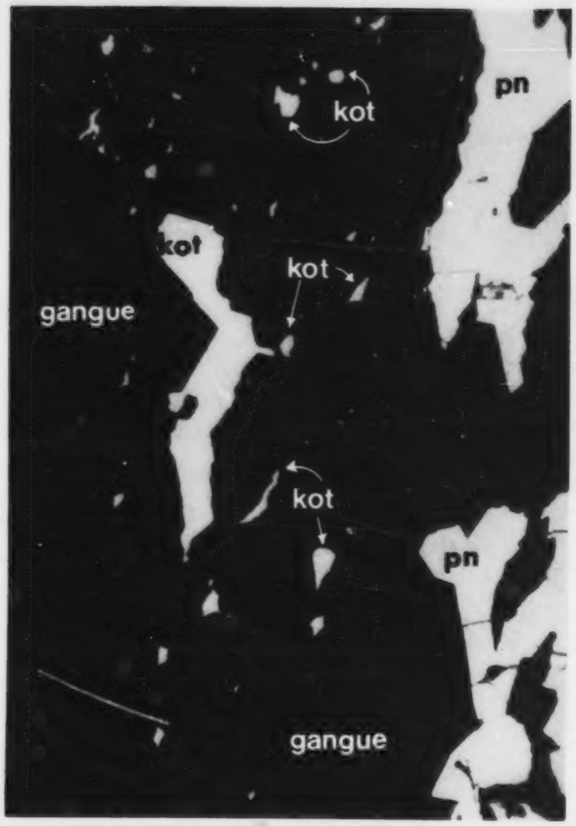
pn
kot
kot
kot
gangue
kot
kot
pn
gangue

Photo 286.5. *Large kotulskite (kot) grain in centre with smaller grains surrounding in gangue. Pentlandite (pn) is to the left. Magnification x400; plane polarized, reflected light.*

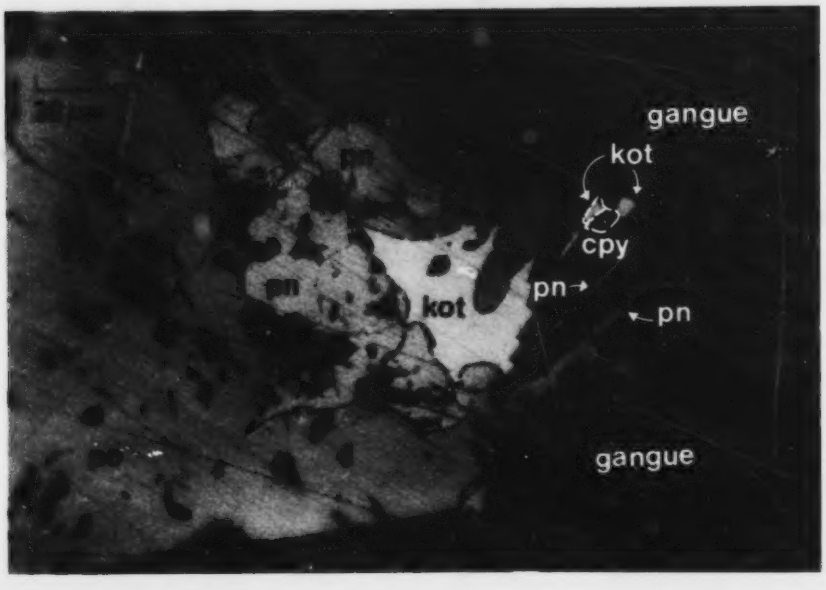
gangue
kot
pn
cpy
pn
pn→
kot
←pn
gangue

Photo 286.6. *Anhedral kotulskite (kot) grain in pentlandite (pn) and pyrrhotite (po). Smaller grains attached to chalcopyrite (cpy) in gangue. Magnification x400; plane polarized, reflected light.*

REFERENCES

Boudreau, A.E., Mathez, E.A., and McCallum, I.S.

1986: Halogen Geochemistry of the Stillwater and Bushveld Complexes: Evidence for Transport of the Platinum-Group Elements by Cl-Rich Fluids; Journal of Petrology, Volume 27, Part 4, p.967-986.

Cabri, L.J., and Laflamme, J.H.G.

1979: Mineralogy of Samples from the Lac des Iles Area, Ontario; CANMET, Energy, Mines and Resources Canada, Report 79-27, 20p.

Dunning, G.R.

1979: The Geology and Platinum Group Mineralization of the Roby Zone, Lac des Iles Complex, N.W. Ontario; Unpublished M.Sc. Thesis, Carleton University, Ottawa, 129p.

Naldrett, A.J.

1981: Platinum-Group Element Deposits; p.199-231 *in* Platinum-Group Elements: Mineralogy, Geology, Recovery, edited by Louis J. Cabri, Canadian Institute of Mining Metallurgy, Special Volume 23, 267p.

Naldrett, A.J., Innes, D.G., and Sowa, J.M.

1980: Platinum Group Element Concentrations in Some Magmatic Ores in Ontario; Grant 17, p.171-178 *in* Geoscience Research Grant Program, Summary of Research, 1979-1980, edited by E.G. Pye, Ontario Geological Survey, Miscellaneous Paper 93, 263p.

Sutcliffe, R.H., Sweeny, J.M., and Edgar, A.D.

In preparation: The Lac des Iles Complex, Ontario; Petrology and PGE Mineralization in an Archean Mafic Intrusion.

Sweeny, J.M.

In preparation: The Geochemistry and Origin of the Roby Zone, Lac des Iles Complex; M.Sc. Thesis, The University of Western Ontario, London.

Sweeny, J.M., and Edgar, A.D.

1987: The Geochemistry, Origin and Economic Potential of Platinum Group Element Bearing Rocks of the Lac des Iles Complex, Northwestern Ontario; Grant 286, p.140-152 *in* Geoscience Research Grant Program, Summary of Research, 1986-1987, edited by V.G. Milne, Ontario Geological Survey, Miscellaneous Paper 136, 241p.

Talkington, R.W., and Watkinson, D.H.

1984: Trends in the Distribution of the Precious Metals in the Lac des Iles Complex, Northwestern Ontario; Canadian Mineralogist, Volume 22, Part 1, p.125-136.

Vermaak, C.F., and Hendriks, L.P.

1976: A Review of the Mineralogy of the Merensky Reef, with Specific Reference to New Data on the Precious Metal Mineralogy; Economic Geology, Volume 71, Number 7, p.1244-1269.

Watkinson, D.H., and Dunning, G.

1979: Geology and Platinum-Group Mineralization, Lac des Iles Complex, Northwestern Ontario; Canadian Mineralogist, Volume 17, p.453-462.

Grant 288 Petrogenesis of Archean Trondhjemite-Tonalite-Granodiorite (TTG) Intrusions and Their Relationships to Gold Mineralization, Renabie and Magino Areas, Wawa

R.A. Jemielita, N.J. Callan, and E.T.C. Spooner

Department of Geology, University of Toronto, Toronto

ABSTRACT

Mineralization at the Renabie mine (5.5 million tonnes at ~6 g/tonne gold and ~2 g/tonne silver) consists of gold-bearing quartz veins occupying brittle/ductile shear zones in Archean gneissose trondhjemite and variably foliated tonalite intrusions of the Wawa Domal Gneiss Terrane (WDGT), outside the confines of a greenstone belt. Mineralization occurred after major plutonic magmatism, peak regional metamorphism and deformation, and is bracketed by geochemically evolved late aplite dikes. Younger intrusions include lamprophyre and diabase dikes. Mineralization at Magino (1.9 million tonnes at ~7 g/t gold; at a depth <152 m) is less well constrained temporally, but is closely associated spatially with composite granodiorite stocks intruding mafic metavolcanics of the Michipicoten Greenstone Belt.

Tonalite, trondhjemite, and granodiorite (TTG) lithologies from Renabie and Highway 651, and Magino granodiorites, define a trondhjemitic calc-alkaline trend characterized by high alumina-type (>15 percent Al_2O_3) trondhjemites, and strong sodium enrichment in the more evolved lithologies. These rocks have geological, mineralogical, and major and rare earth element (REE) characteristics similar to those of other Archean TTG rocks from the WDGT, and other Archean grey gneiss terranes worldwide. Lamprophyres at Renabie and nearby properties consist of calc-alkaline minettes and ultrabasic types.

At Renabie, chondrite normalized rare earth element (REE) distribution patterns vary in geometry sympathetically with the sequence of intrusion, from trondhjemite through tonalite, to aplite and pegmatite. REE fractionation is moderate, with a progressive increase in middle to heavy REE contents from trondhjemite to tonalite, and pronounced negative europium anomalies in aplites and pegmatites. Lamprophyres display typically steep highly fractionated REE patterns, attributed to a volatile enriched mantle source. Granodiorites at Magino exhibit REE patterns similar to those of the TTG lithologies, and increasing ΣREE (where ΣREE = total concentration of all rare earth elements in each sample), indicative of increasing fractionation.

REE data imply that TTG lithologies were generated by progressive and increasing partial melting of a hydrated, garnet-bearing tholeiitic amphibolite/eclogite source rock. Fractional crystallization may have influenced the evolution of the plutonic TTG magmas, but was the dominant mechanism during the evolution of the sodium-rich aplitic and pegmatitic phases (negative europium anomalies are indicative of plagioclase fractionation), and also, possibly, of the gold-bearing hydrothermal fluids as well. Archean gold-quartz lode mineralization is often associated with sodium-rich intrusions and/or metasomatism and, in this instance, may be the product of the strong high level fractionation of TTG magmas.

INTRODUCTION

Mineralization at the Renabie mine (5.5 million tonnes at ~6 g/tonne gold, and ~2 g/tonne silver) consists of gold-bearing quartz veins occupying brittle/ductile shear zones in Archean gneissose trondhjemite and variably foliated tonalite intrusions of the Wawa Domal Gneiss Terrane (WDGT), outside the confines of a greenstone belt (Callan and Spooner 1987). Mineralization at the Magino mine consists of gold-bearing quartz veins in shear zones, within a composite granodiorite stock intruding metavolcanic lithologies of the Michipicoten Greenstone Belt (Bruce 1942). Reserves currently stand at 1.9 million tonnes at ~7 g/t gold to a depth of 152 m, but recent drilling has indicated strong mineralization at depths of ~600 m (The Northern Miner 1988). This paper presents preliminary results of a geochemical study of trondhjemite-tonalite-granodiorite (TTG) lithologies, together with minor intrusions, from: the Renabie gold mine and nearby properties; the western part of the Wawa Domal Gneiss Terrane along Highway 651; and, the granodiorites of the Magino Mine (Figure 288.1). This work complements previous field, structural, and petrographic studies of the Renabie mine area (Callan and Spooner 1987, 1988), and constitutes part of a wider investigation into the relationships between Archean lode gold deposits and intrusions previously confined to the Abitibi Subprovince (Burrows and Spooner 1988). In addition, this work examines the potential genetic connection between TTG lithologies and Archean gold mineralization (Spooner *et al.* 1987).

REGIONAL GEOLOGY

The Renabie gold mine is situated at the western margin of the Wawa Domal Gneiss Terrane (WDGT), near the contact with the Michipicoten Greenstone Belt (Figure 288.1). The study area is accessed via Highway 651 running south from the town of Missanabie for about 40 km. Outcrops along the road consist of mostly gneisses and granitoids of the WDGT, and occasional enclaves composed of Michipicoten Greenstone Belt lithologies (Figure 288.1) (Milne *et al.* 1972; Downes 1983). This part of the WDGT is characterized by amphibolite facies trondhjemite, tonalite, and granodiorite (TTG) gneisses, but these change eastwards over 120 km into granulite-grade paragneiss, mafic gneiss, tonalite, and anorthosite of the Kapuskasing Structural Zone (KSZ) (Percival 1986). The KSZ is bounded to the east by a sharp lithological, structural, and

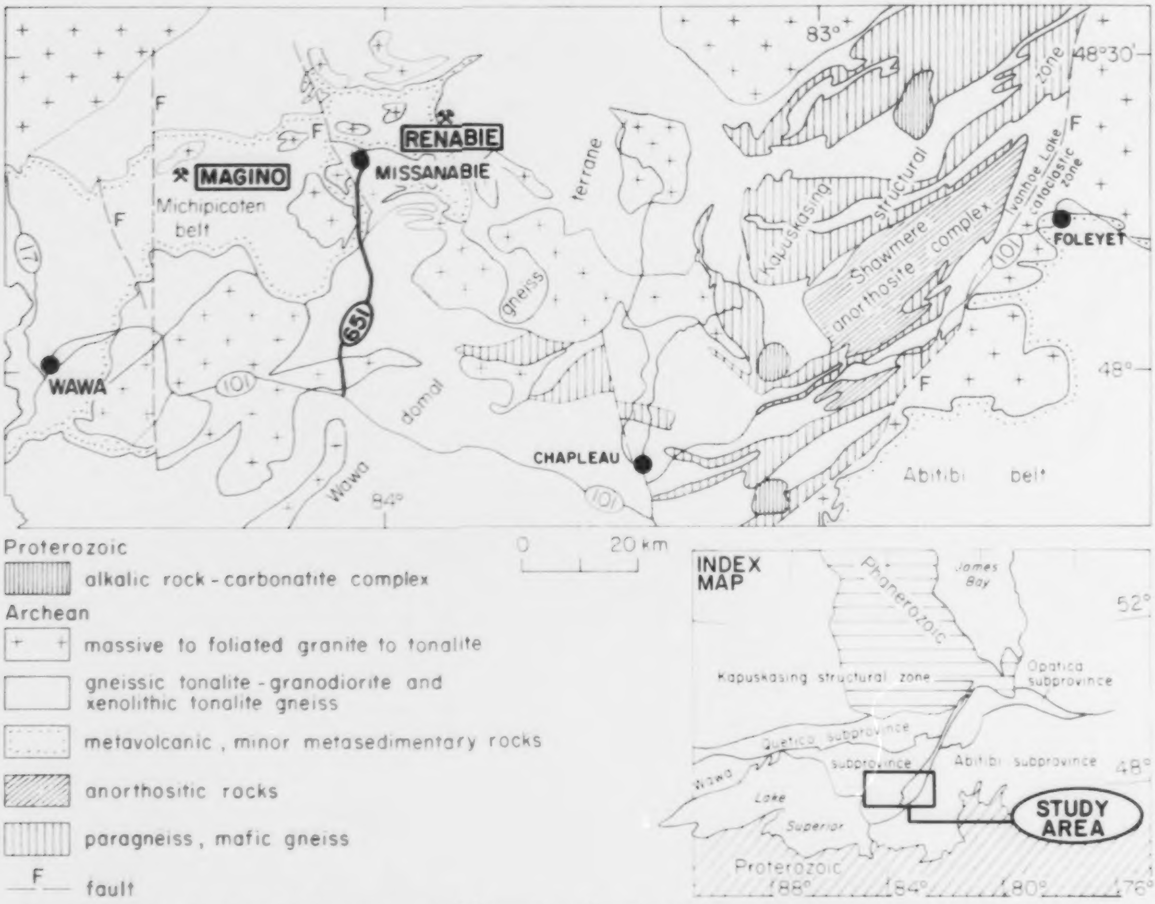
83°
48°30'
48°
84°
F
RENABIE
MAGINO
MISSANABIE
Michipicoten belt
17
651
101
WAWA
CHAPLEAU
FOLEYET
terrane
gneiss
domal
Wawa
Kapuskasing structural zone
Showmere anorthosite complex
Ivanhoe Lake cataclastic zone
Abitibi belt
0 20 km
Proterozoic
alkalic rock - carbonatite complex
Archean
massive to foliated granite to tonalite
gneissic tonalite - granodiorite and xenolithic tonalite gneiss
metavolcanic, minor metasedimentary rocks
anorthositic rocks
paragneiss, mafic gneiss
fault
INDEX MAP
James Bay
Phanerozoic
52°
Kapuskasing structural zone
Opatica subprovince
Quetico subprovince
Wawa subprovince
Abitibi subprovince
48°
Lake Superior
STUDY AREA
Proterozoic
88°
84°
80°
76°

Figure 288.1. *Geology of the Wawa–Abitibi region showing the Renabie, Magino, and Highway 651 study areas (modified after Percival 1986).*

metamorphic discontinuity, the Ivanhoe Lake Cataclastic Zone (ILCZ). The sequence is interpreted to be an oblique Archean crustal cross-section (Percival and Card 1983), corresponding to an approximate vertical thickness of 25 km, which was uplifted along a northwest-dipping reverse fault represented at the surface by the ILCZ. The Renabie area is located within the Missinaibi Lake Batholith (MLB), which consists of a discrete mafic tonalitic intrusive phase of the areally extensive WDGT, and which is thought to represent one of its oldest components (Percival 1981). The Highway 651 samples represent members of the dominant lithologies from the western part of the WDGT (Milne *et al.* 1972; Downes 1983).

The Magino gold mine, located near Goudreau about 40 km northeast of Wawa, occurs within an irregular granodiorite (Webb Lake) stock (~1750 m in length and 75 to 100 m in width) intruding metavolcanic lithologies of the Michipicoten Greenstone Belt (Bruce 1942; Milne *et al.* 1972). Further mineralization has been encountered within the North Zone and Lovell Lake plugs about 1 km to the north and north-west of the main plug, respectively. All of the past producing gold mines in the Goudreau–Lochalsh area are spatially associated with felsic intrusions (Heather and Arias 1987).

INTRUSIVE LITHOLOGIES

RENABIE MINE AND VICINITY

Callan and Spooner (1987) described the geological relationships at the Renabie mine and nearby Nudulama (~1.5 km east of Renabie) and Braminco (~1.8 km southeast of Renabie) properties, and recognized two main intrusive lithologies, Renabie gneissose trondhjemite and variably foliated Renabie "shaft" tonalite. The tonalite contains sheets of a more mafic phase, and is also cut by typically concordant microtonalite dikes. The plutonic lithologies are intruded by aplitic and pegmatitic minor phases, and in places by dikes of lamprophyre and diabase.

In the vicinity of the Renabie mine, gneissose trondhjemite is considered to be the oldest of the TTG lithologies, forming a zone 200 to 350 m wide marginal to the metavolcanic rocks of the Michipicoten Greenstone Belt, and itself intruded by the younger tonalite (Callan and Spooner 1987). The

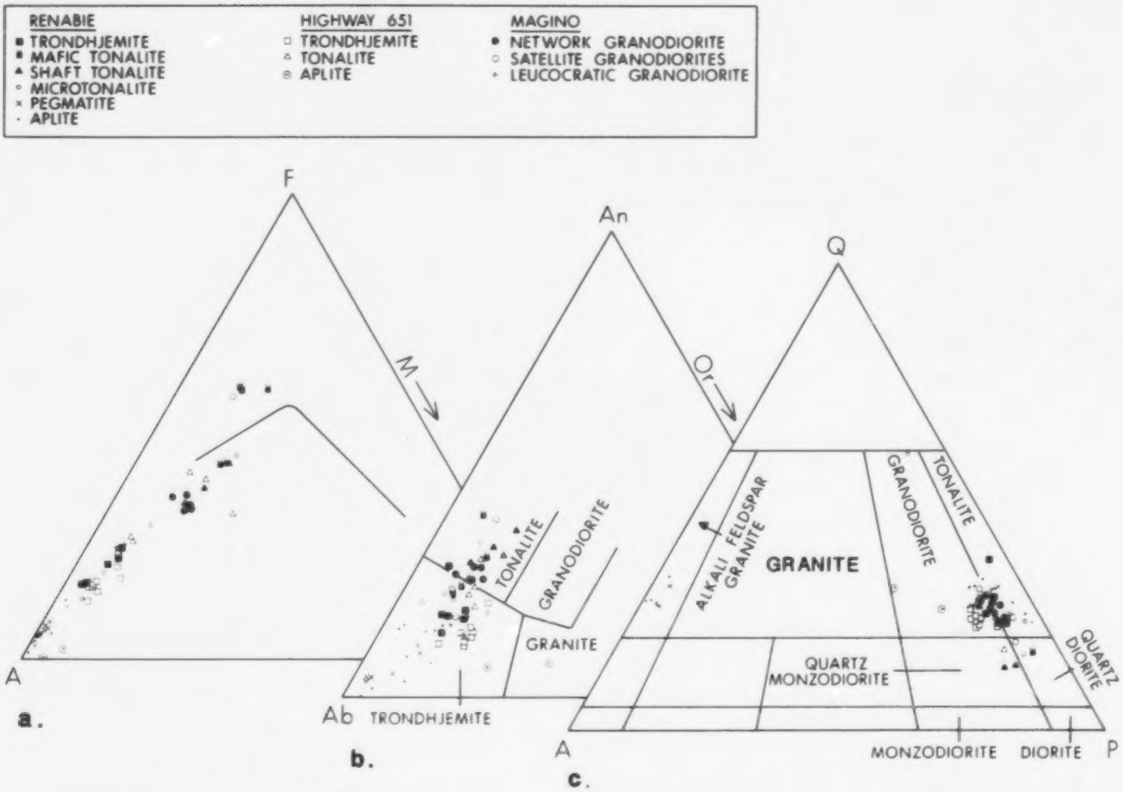

Figure 288.2. Major element analyses of trondhjemite-tonalite-granodiorite (TTG) lithologies from the present study plotted on (left to right): a) AFM diagram (where A = (Na_2O+K_2O), F = ($FeO+Fe_2O_3$ recalculated to FeO), and M = (MgO), quantities are calculated on a molecular (i.e. oxide) basis); b) An-Or-Ab diagram (Barker 1979; modified after O'Connor 1965); and c) QAP diagram (after Streckeisen 1976).

tonalite hosts dikes (10 cm to 1 m wide) of microtonalite oriented subparallel to the foliation.

The plutonic TTG lithologies are cut by concordant and discordant dikes of aplite and pegmatite. Within the gneissose trondhjemite these rocks generally have a well developed fabric, but in the tonalite these minor intrusions are less strained, having been emplaced at a late stage in fabric development. The above rocks are generally cut by the shear zone hosted gold-bearing quartz veins at Renabie, and nearby Nudulama and Braminco properties; however, aplite dikes are sometimes seen to cut gold-bearing quartz veins in the main ore zone at Renabie (N.J. Callan, R.A. Jemielita, personal observation, 3455-foot level, 1987; Phil Olson and Alex Kusik, geologists, Renabie Mine, personal communication, 1988). The mineralization was therefore bracketed by late stage aplite intrusions.

Lamprophyre dikes occur in the Renabie mine where they are sometimes strongly deformed, and at Braminco where they are undeformed. The lamprophyres crosscut the ore zones at both properties. Diabase dikes comprise the youngest intrusive lithology in the area, and are undeformed and discordant. Large diabase dikes in the area (for example, Nudulama property) trend north-northwest, and may be members of the MacKenzie swarm, having a Rb-Sr age of about 1660 Ma (Thurston *et al.* 1977; Bennett 1978; Downes 1983).

HIGHWAY 651 LITHOLOGIES

Samples taken from roadside exposures along Highway 651 consist of gneissose trondhjemites, tonalites, and aplites (field terms). These samples are representative of the massive and gneissose granitoids of the western margin of the WDGT, and are described as granitic, granodioritic, dioritic, and trondhjemitic gneisses (Milne *et al.* 1972; Downes 1983). These rocks were analyzed to provide data from TTG lithologies remote from known gold mineralization (precise sample locations are available from N.J. Callan).

MAGINO GRANODIORITES

A representative suite of samples was collected from the composite Webb Lake granodiorite stock, which hosts the Magino gold mine (Bruce 1942), by N.J. Callan and E.T.C. Spooner in September 1986. The dominant lithology is referred to as "network" granodiorite; it is intruded internally in places by leucocratic granodiorite. Granodiorites from the satellitic North Zone and Lovell Lake stocks, located near the Webb Lake Stock, were also sampled. Sage (1987) described the Webb Lake Stock as a trondhjemite.

IGNEOUS GEOCHEMISTRY

MAJOR ELEMENTS

Major, trace, and rare earth element (REE) analyses were performed on 66 samples. Major element analyses were carried out by X-Ray Assay Labs Ltd., Toronto, who also determined H_2O^+, H_2O^-, and CO_2. REE analyses were made by instrumental neutron activation analysis using the Slowpoke Research Reactor facility at the University of Toronto. This paper examines major element and REE data, together with calculated CIPW normative values for each sample (Table 288.1). Major element data are plotted on standard AFM (Wager and Deer 1939), An-Or-Ab (O'Connor 1965; Barker 1979), and QAP (Streckeisen 1976), triangular diagrams (Figures 288.2a, 288.2b, and 288.2c, respectively).

The major element data reveal strong similarities in geochemistry between the Renabie and Highway 651 TTG lithologies, and the Magino granodiorites (Table 288.1; Figure 288.2). Tonalites, microtonalites, and trondhjemites delineate an evolutionary trend on the An-Or-Ab and QAP diagrams, but a corresponding temporal sequence of intrusive compositions is not supported by field evidence (Callan and Spooner 1987). Trondhjemites from Renabie (SiO_2=69.0 to 72.9 percent), and Highway 651 (SiO_2=69.4 to 71.1 percent) are mostly high alumina-type (Al_2O_3>15 percent; from Table 1, Barker and Arth 1976), but straddle the granodiorite-tonalite field boundary on the QAP diagram (Figure 288.2c); however, these rocks are classed as trondhjemites due to their low normative colour index values ($m<10$; Streckeisen 1976), and plot in the trondhjemite field on the An-Or-Ab diagram (Figure 288.2b). Mafic phases of the Renabie tonalites (SiO_2=55.8 to 67.4 percent), Renabie and Highway 651 normal tonalites (Renabie SiO_2=58.6 to 66.9 percent, Highway 651 SiO_2=63.1 to 69.9 percent; Figures 288.2b, 288.2c), and Renabie microtonalites (SiO_2=59.9 to 69.5 percent) have similar compositions, and mostly group around the granodiorite-tonalite field boundary on the QAP diagram (Figure 288.2c), and in the tonalite field on the An-Or-Ab diagram (Figure 288.2b). One sample of microtonalite from Nudulama has SiO_2=82.3 percent, probably due to silicification. All of the above lithologies are quartz normative. Aplites (SiO_2=64 to 77 percent) and pegmatites (SiO_2=72.3 to 76 percent) from Renabie, adjacent properties, and Highway 651 mostly plot within the tonalite field (Figure 288.2c), reflecting their relatively CaO- and Na_2O-rich compositions (Table 288.1); however, their low normative colour index values ($m<10$) classify these rocks as trondhjemites. Some aplites and pegmatites plot in the alkali feldspar granite field, and tend towards an albititic composition (Figures 288.2b, 288.2c). These samples have normative plagioclase compositions with <5 percent An; soda was therefore calculated as albite (alkali feldspar), according to the classification scheme of Streckeisen (1976), producing an apparently bimodal distribution of aplite and pegmatite compositions. Renabie aplites and pegmatites are the most silica- and alkali-rich lithologies sampled (Na_2O=5.17 to 11.5 percent). These lithologies are dominantly quartz normative; however, small quantities of corundum are sometimes present, and one aplite (sample rnap3) has substantial normative nepheline. Most of the lithologies sampled belong to a calc-alkalic evolutionary trend on the AFM diagram (Figure 288.2a).

Two distinct types of lamprophyre have been recognized during this study. The lamprophyre from the Renabie mine (SiO_2=53.9 and 55.2 percent) is massive to strongly deformed, and cuts the main ore zone. This rock, probably an altered minette, is composed of phlogopite, chlorite, epidote, carbonate, and potassium-feldspar, and belongs to the calc-alkalic lamprophyre group (Streckeisen 1978). At the Braminco property, olivine-phyric ultrabasic lamprophyre dikes (SiO_2=28.1 and 31.4 percent) cut the ore zone almost at right angles. The low silica contents of these rocks reflect their olivine-rich composition. Minor intrusions of this composition have been described in this vicinity (Bennett 1978), and in nearby areas (Downes 1983).

The Magino "network" granodiorites (SiO_2=63.9 to 65.6 percent) and leucocratic granodiorites (SiO_2=69.1 to 69.3 percent) straddle the granodiorite-tonalite field boundary on the QAP diagram (Figure 288.2c), but are classed respectively as tonalite and trondhjemite on the An-Or-Ab diagram (Figure 288.2b). Low normative colour index values ($m<10$, Streckeisen 1976; "network" granodiorites m=8.5 to 10.3, leucocratic granodiorites m=5.3 to 5.9) show that these rocks have trondhjemitic affinities, in agreement with Sage (1987) who classed the Webb Lake Stock as a trondhjemite. The "network" granodiorites are corundum normative, probably due to (sericitic?) hydrothermal alteration. There is an apparent evolutionary trend from network granodiorite to leucocratic granodiorite (Figure 288.2a). The satellite stock granodiorites are obviously different lithologies (SiO_2=54.7 and 69.8 percent), and represent the least (Lovell Lake plug) and most (North Zone plug) evolved intrusive rocks sampled in this area. The most important point about the Magino granodiorites is that they correspond compositionally with the tonalite and trondhjemite (TTG) compositional fields of the Renabie and Highway 651 samples, and all are quartz normative. For example, in the AFM diagram (Figure 288.2a), the Magino "network" granodiorite compositions correspond exactly with the alkali-rich end of the Renabie tonalite field.

RARE EARTH ELEMENTS

Rare earth element data have been normalized (N) to the chondritic values determined by Haskin *et al.* (1968) and Nakamura (1974), as recommended by Rock (1987), and are plotted on REE distribution diagrams (Figures 288.3, 288.4, and 288.5).

Renabie gneissose trondhjemites display a narrow range of fractionated and moderately steep REE patterns (Figure 288.3a), usually with a small negative europium anomaly or none at all (La_N/Yb_N=41.7 to 9, Tb_N/Yb_N=4.5 to 1.6). Middle to heavy REE pat-

TABLE 288.1: MAJOR ELEMENT, CIPW NORMATIVE MINERALOGY, AND CHONDRITE NORMALIZED RARE EARTH ELEMENT DATA FOR SAMPLES ANALYZED DURING THE PRESENT STUDY.

		RENABIE	GNEISSOSE	TRONDHJEMITE				RENABIE	MAFIC	TONALITE	RENABIE	SHAFT	TONALITE		RENABIE MICRO	TONALITES
	rn88-45	rn88-74	rn88-75	rn88-95	rn88-33	br88-8	rn88-81	rn88-82	rn88-93	rn88 -94	rn88-44	rn88-59	rn88-61	nd88-1	rn88-66	rn88-65
SiO2	71.1	72.7	72.3	72.9	69.8	69	63.5	55.8	67.2	67.4	58.8	59.2	65.6	66.9	69.5	59.9
TiO2	0.21	0.2	0.16	0.17	0.24	0.27	0.58	1.13	0.37	0.36	0.55	0.65	0.47	0.34	0.34	0.63
Al2O3	15.1	14.7	14.7	14.3	15.1	15.7	15.8	15.8	16.3	16.1	18.1	17.6	15.8	16	14.7	17
Fe2O3	2	1.51	1.53	1.59	2.32	2.69	5.97	10.9	3.63	3.6	6.48	6.51	4.64	3.78	3.09	6.75
MnO	0.04	0.04	0.04	0.02	0.06	0.05	0.11	0.13	0.06	0.08	0.1	0.1	0.08	0.07	0.05	0.11
MgO	0.5	0.32	0.25	0.41	0.86	0.62	2.1	2.83	1.25	1.23	2.44	2.37	1.78	1.54	0.92	2.48
CaO	2.81	2.59	2.52	3.91	2.88	3.06	5.29	7.27	3.98	3.98	6.19	5.94	4.79	4.66	3.56	6.25
Na2O	5.74	5.68	5.92	4.76	5.61	5.55	4.42	3.88	5.39	5.58	4.15	4.61	4.1	4.82	5.18	4.59
K2O	1.08	1.3	1.29	0.54	1.6	1.57	1.25	0.64	1.17	1.08	1.88	1.37	1.84	1.05	1.07	0.99
P2O5	0.08	0.04	0.05	0.02	0.06	0.07	0.13	0.17	0.1	0.1	0.16	0.16	0.12	0.08	0.09	0.15
Total	98.62	98.96	98.76	98.62	98.2	98.5	99.12	98.53	99.45	99.47	98.43	98.41	98.72	99.13	98.49	98.85
H2O+	0.3	0.2	0.2	0.2	0.4	0.3	0.2	0.6	0.2	0.1	0.7	0.6	0.4	0.4	0.4	0.6
H2O-	0.1	0.1	0.1	0.1	0.1	0.1	0.1	0.1	0.1	0.1	0.1	0.1	0.1	0.1	0.1	0.1
CO2	0.15	0.07	0.55	0.15	0.25	0.19	0.04	0.11	0.03	0.02	0.08	0.17	0.08	0.01	0.08	0.04
Total	99.17	99.33	99.61	99.07	98.95	99.09	99.46	99.34	99.78	99.69	99.31	99.28	99.3	99.64	99.07	99.59
Quartz	27.37	29.63	27.91	35.32	25.19	23.84	19.34	12.45	21.27	20.99	11.44	11.6	23.52	21.62	27.19	13.28
Orthoclase	6.36	7.76	7.72	3.25	9.63	9.42	7.45	3.84	6.95	6.41	10.06	8.23	9.21	6.15	6.42	5.92
Albite	49.25	47.54	50.72	39.66	47.47	47.67	37.73	33.14	45.85	47.46	35.67	39.63	35.14	41.62	44.5	39.29
Anorthite	12.48	11.43	9.85	17.38	11.96	13.5	19.75	24.25	16.92	15.78	26.21	23.38	19.87	19.96	13.91	23.13
Diopside	1.03	1.05	2.06	1.79	1.89	1.26	4.81	9.1	1.84	2.68	3.16	4.43	2.74	2.78	2.73	5.84
Hypersthene	1.61	0.79	0.2	0.97	1.74	1.91	5.32	6.54	3.67	3.13	7.23	6.29	4.91	4.14	2.1	6.02
Magnetite	1.47	1.11	1.13	1.21	1.71	1.91	4.37	5.09	2.65	2.62	4.76	4.8	3.41	2.87	2.28	4.98
Ilmenite	0.4	0.38	0.31	0.33	0.46	0.52	1.11	2.18	0.71	0.69	1.06	1.25	0.9	0.65	0.66	1.21
Apatite	0.14	0.09	0.12	0.05	0.14	0.17	0.31	0.41	0.24	0.24	0.38	0.38	0.29	0.19	0.22	0.36
Sum	99.99	99.99	99.99	99.99	99.99	99.99	99.99	100	99.99	99.99	99.99	100	99.99	99.99	99.99	99.99
LaN	34.7	56.3	68	18.2	30.6	30.3	53.1	41.4	33.7	32.8	29.8	30.3	40	32.2	68.1	36.3
CeN	24.1	38.8	46.6	10.1	24	21.8	48.7	37.2	26.7	25.5	26.6	29.7	31.9	24.6	52.6	33.7
NdN	14.7	17.8	19.7	3.7	12.1	9.4	28.5	23.2	18.6	13.7	28.9	24.2	27.9	16.5	27.1	22.9
SmN	7.2	8.8	9.6	1.7	8.4	7.6	18.8	18.6	8.9	8.6	21.4	17.5	18.5	11.2	13.9	16.8
EuN	4	6.9	7.5	4.9	6.3	6.5	11.5	12.1	7.6	7.6	8.4	11	8.1	7.5	9	12.7
TbN	3.7	4.3	4.7	2	5.4	4.4	8.8	10.2	4.1	2.5	14.7	9.9	9	6.6	3.4	8.5
YbN	0.8	1.8	1.9	1.1	3.4	2.8	7.3	6.2	2.5	2.3	6.2	4.8	6.4	3.9	3.2	6.3
LuN	1.4	2.9	2.8	1.8	4.6	3	7.4	6.5	2.5	3.2	5.5	5.4	6.1	4	3.2	6.7
LaN/YbN	41.7	31.2	35.5	15.1	9	10.7	7.3	6.6	13.4	14.3	4.8	6.3	7.4	8.3	21	5.6
LaN/SmN	4.8	6.4	7.2	9.3	3.6	4	3.2	2.5	3.8	3.8	1.4	1.7	2.4	2.9	4.8	2.3
TbN/YbN	4.5	2.4	2.4	1.9	1.6	1.6	0.9	1.6	1.6	1.1	2.4	2.1	1.7	1.7	1.1	1.3

	RENABIE	MICRO-	TONALITES			HIGHWAY	651		TRONDHJEMITE				HIGHWAY	651	TONALITES	
	nd88-17	nd88-20	nd88-21	mn85-42	mn85-43	mn85-77	mn85-80	mn85-1	mn85-2	mn85-11a	mn85-15	87-A	87-b	87-1	87-g	mn85-52
SiO2	69.8	82.3	69.5	71.1	70.1	69.4	68.7	70	70.6	70	70.8	67.2	64.6	69.9	69.3	63.1
TiO2	0.14	0.11	0.19	0.21	0.24	0.25	0.29	0.27	0.27	0.27	0.23	0.67	0.53	0.34	0.36	0.58
Al2O3	18.8	8.72	16.6	15.6	15.5	15.8	15.9	15.4	15.5	15.5	15.4	14.8	15.8	15.4	16.3	16
Fe2O3	1.18	0.84	1.76	1.39	1.69	2.06	2.07	1.67	1.81	1.96	1.7	5.03	5.01	2.99	2.85	4.86
MnO	0.03	0.02	0.03	0.03	0.03	0.06	0.04	0.04	0.03	0.03	0.03	0.09	0.08	0.05	0.05	0.07
MgO	0.39	0.25	0.53	0.8	0.67	1	0.76	0.53	0.55	0.59	0.52	1.26	1.74	0.75	0.71	3.38
CaO	3.7	1.77	3.67	2.4	2.72	2.66	3.24	2.41	2.34	2.62	2.39	4.17	5.17	3.4	3.26	4.96
Na2O	6.44	2.92	5.87	5.99	5.54	5.6	5.13	5.99	5.68	5.74	6.06	4.67	4.5	5.12	6.21	5.04
K2O	0.55	1.15	0.9	2.14	1.48	1.99	1.97	2.03	2.12	1.92	2.04	1.13	1.19	1.37	1.65	1.48
P2O5	0.05	0.04	0.05	0.07	0.09	0.07	0.09	0.08	0.08	0.07	0.07	0.19	0.14	0.09	0.11	0.19
Total	99.08	98.12	99.1	99.53	98.93	99.07	99.19	98.62	99.18	98.7	99.24	99.21	98.66	99	98.8	99.59
H2O+	0.2	0.6	0.3	0.3	0.2	0.4	0.4	0.3	0.3	0.2	0.1	0.5	0.5	0.4	0.3	0.5
H2O-	0.1	0.1	0.1	0.1	0.1	0.1	0.1	0.1	0.1	0.1	0.1	0.1	0.1	0.1	0.1	0.1
CO2	0.06	0.48	0.03	0.03	0.01	0.08	0.12	0.03	0.01	0.01	0.04	0.08	0.05	0.13	0.03	0.01
Total	99.44	99.3	99.53	99.96	99.24	99.63	99.81	99.05	99.59	99.01	99.48	99.89	99.31	99.63	99.23	100.2
Quartz	22.47	56.09	23.67	21.03	20.87	21.34	24.62	22.21	22.94	23.38	23.16	25.64	21.11	26.89	25.25	14.2
Orthoclase	3.28	6.93	5.37	12.54	8.86	11.67	11.74	12.16	12.63	11.5	10.86	6.73	7.13	8.17	9.87	8.47
Albite	54.99	25.17	50.12	53.27	56.93	49.81	43.75	51.39	50.16	49.2	51.46	39.63	36.59	43.76	44.82	43.06
Anorthite	16.46	7.43	18.43	8.48	6.75	11.2	14.86	9.27	9.72	11	10.55	15.21	19.86	15.16	13.65	18.46
Diopside	2.21	1.01	1.3	2.48	3.43	1.39	0.77	1.67	1.17	1.37	1.23	2.78	4.38	1.1	1.61	5.84
Hypersthene	0.33	0.43	1.34	0.85	0.81	2.5	2.17	1	1.33	1.43	0.97	3.63	4.1	2.19	1.94	7.3
Magnetite	0.86	0.62	1.29	0.1	1.17	1.43	1.62	1.38	1.33	1.44	1.19	3.88	3.69	1.9	2.1	3.47
Ilmenite	0.27	0.21	0.36	0.4	0.48	0.48	0.55	0.52	0.52	0.52	0.4	1.28	1.02	0.65	0.69	1.06
Apatite	0.12	0.09	0.12	0.17	0.21	0.17	0.21	0.19	0.19	0.17	0.17	0.45	0.33	0.19	0.26	0.45
Sum	99.99	99.99	99.99	99.93	99.99	99.99	99.99	99.99	99.99	99.99	99.99	100	100	99.99	99.99	99.99
LaN	14.9	17.4	8.8	30.3	48.3	38.4	46.6	69.6	67	57.8	62.1	74.6	29.6	66	62.8	99.8
CeN	11.5	13.1	6.2	25.2	39.3	28.9	30.8	51.6	48.7	37	38.1	62.5	23.9	40.5	40.6	78.4
NdN	4.2	8	2.8	16.7	21.6	16.2	15.6	23.4	24.9	19.3	19.1	38.6	16.2	20.7	21.9	41.6
SmN	2.9	3.5	2	9.1	11.6	8.7	8.7	11.3	12	7.1	10.8	23.6	12.5	10.9	12.6	19.9
EuN	4.7	3.6	3.9	6.7	8.3	5.6	6.5	7.6	8.3	6.1	8.2	15.6	8.9	6.6	9.9	14.1
TbN	1.3	1.6	0	3.7	6.2	3.8	2.3	2	3.3	1.9	4.1	12	6.1	3.3	7.7	8.7
YbN	0.7	1.2	1	1	1.4	1.9	2.3	1.6	1.8	1.1	2	10.8	4.9	2.2	3.8	4.6
LuN	1	1.2	0.9	1.4	1.4	2.3	2.5	2.4	2.1	1.1	1.4	11.7	6.8	3.2	4.3	4.7
LaN/YbN	21.5	14.2	8.5	31.3	35.6	18.8	20.1	43.4	41	51.3	26.3	6.9	6	25.6	14.7	21.8
LaN/SmN	5.2	5	3.2	3.3	4.2	4.2	5.3	6.2	5.6	8.2	4.8	3.2	2.4	5.2	4.2	5
TbN/YbN	1.8	1.3	0	3.6	3.6	1.9	1	1.2	2	1.7	2.1	1.1	1.2	1.6	2.2	1.9

TABLE 288.1 CONT'D: MAJOR ELEMENT, CIPW NORMATIVE MINERALOGY, AND CHONDRITE NORMALIZED RARE EARTH ELEMENT DATA FOR SAMPLES ANALYZED DURING THE PRESENT STUDY.

	PEGMATITES							APLITES										
	rn86-87	rn86-60	rn86-53	rn86-78	rn86-77	rn86-43	rn86-40	mn85-44	mn85-59	rn86-73	rn86-79	rn86-80	rn86-92	br86-13	br86-14	nd86-16	nd86-23	rnap-1
SiO2	75.1	74.9	75.9	73.7	72.3	76	72.4	73.7	75.7	71.3	75.1	74.8	75.4	77	76	74	72.5	74.1
TiO2	0.06	0.05	0.06	0.08	0.06	0.07	0.08	0.1	0.03	0.19	0.05	0.14	0.04	0.05	0.05	0.06	0.05	0.08
Al2O3	14	14.3	13.3	14.6	15.7	13.6	15.5	14.6	13.9	15.5	13.5	13.7	14.2	13.6	13.8	14.8	16.1	15.2
Fe2O3	0.45	0.49	0.25	0.76	0.57	0.63	0.7	0.7	0.38	1.64	0.53	1.18	0.39	0.45	0.51	0.95	0.32	0.45
MnO	0.02	0.02	0.01	0.03	0.02	0.02	0.03	0.02	0.01	0.04	0.12	0.03	0.03	0.02	0.02	0.03	0.02	0.02
MgO	0.04	0.06	0.08	0.09	0.11	0.08	0.17	0.2	0.03	0.38	0.01	0.18	0.03	0.03	0.06	0.24	0.08	0.2
CaO	1.58	1.58	1.85	1.83	1.94	0.92	2.04	1.32	1.09	2.68	0.58	1.41	1.33	0.49	0.57	1.99	2.85	1.98
Na2O	7.73	7.77	7.15	6.57	6.96	6.96	6.26	5.91	4.67	6.09	5.17	6.2	6.71	6.72	7.73	6.15	6.99	5.78
K2O	0.31	0.28	0.36	1.17	1.04	0.79	2.03	2.89	4.03	1.3	4.37	1.44	0.87	1.1	0.59	0.96	0.46	1.09
P2O5	0.02	0.02	0.01	0.02	0.02	0.01	0.03	0.03	0.01	0.05	0.02	0.04	0.03	0.03	0.03	0.03	0.04	0.03
Total	99.31	99.5	98.97	98.55	98.74	99.1	99.24	99.47	99.85	99.17	99.43	99.1	99.03	99.49	99.46	99.21	99.41	98.89
H2O+	0.1	0.2	0.2	0.1	0.1	0.2	0.2	0.2	0.1	0.2	0.1	0.2	0.1	0.2	0.2	0.2	0.2	0.3
H2O-	0.1	0.1	0.1	1	0.1	0.1	0.1	0.1	0.1	0.1	0.1	0.1	0.1	0.1	0.1	0.1	0.1	0.1
CO2	0.11	0.16	0.54	0.29	0.19	0.24	0.12	0.01	0.01	0.29	0.1	0.6	0.13	0.14	0.1	0.23	0.22	0.19
Total	99.62	99.96	99.81	99.94	99.13	99.64	99.66	99.78	100.06	99.76	99.73	100	99.36	99.93	99.86	99.74	99.93	99.48
Quartz	26.78	26.16	30.47	27.99	24	30.71	26.84	26.59	30.79	26.08	27.53	30.47	30.52	32.78	27.48	30.07	24.64	32.18
Corundum							0.28							0.54		.0.1		1.03
Orthoclase	1.84	1.66	2.16	7.02	6.22	4.71	11.59	17.17	23.85	7.74	25.98	8.59	5.19	6.53	3.45	5.72	2.73	6.51
Albite	66.89	66.05	61.13	56.4	59.64	59.59	50.55	50.27	39.57	51.96	43.99	52.94	57.33	57.16	66.54	52.44	59.49	49.45
Anorthite	2.61	3.33	3.17	6.72	8.64	3.48	9.78	4.6	5.07	11.21	0.73	5.38	6.12	2.24	1.44	9.75	11.26	9.64
Diopside	0.8	0.78	0.49	1.07	0.8	0.88		1.28	0.24	1.52		1.2	0.29		0.36		0.65	
Wollastonite	1.9	1.48	2.26	0.03		0.01					0.43				0.31		0.79	
Hypersthene					0.07		0.56	0.11	0.11	0.61	0.8	0.23	0.1	0.24		1.03		0.86
Magnetite	0.33	0.36	0.19	0.56	0.42	0.47	0.45	0.51	0.28	1.2	0.39	0.86	0.29	0.33	0.28	0.7	0.23	0.34
Ilmenite	0.11	0.11	0.11	0.15	0.15	0.13	0.09	0.19	0.06	0.36	0.09	0.27	0.08	0.09	0.06	0.11	0.09	0.11
Apatite	0.05	0.06	0.02	0.05	0.06	0.02	0.07	0.07	0.02	0.12	0.05	0.09	0.07	0.07	0.07	0.7	0.09	0.07
Sum	99.99	99.99	99.99	99.99	99.99	99.99	99.99	99.99	99.99	99.99	99.99	99.99	99.99	99.99	99.99	99.99	99.99	99.99
LaN	24.8	13.6	3.8	20.7	18.6	20	33.9	3.7	3.6	20.5	23.8	59.3	15.8	9.3	10.9	13.5	2.3	3.6
CeN	20.9	11.4	2.4	16.9	10.4	16.6	27	3 N.D.		19.3	23.4	46.8	13.9	8.2	9.6	10.6	1.3	2.3
NdN	10.7	6.7	0.9	7.1	3.7	8.6	10.7	0.1	0.2	10.3	16.6	21.1	7.1	2.7	4.1	9.1	0.1	0.7
SmN	11.8	10.4	2.4	7.3	4.5	8.7	7.6	0.9	2.2	6.6	18.7	9.9	6.4	5.2	6.1	6.5	1.1	2.8
EuN	4.7	2.1	2.8	6.2	6.9	3.3	7.1	1.6 N.D.		3.4	1.6	5.3	4.4	1.8	2	4.4	1.8	1.2
TbN	6.7	9.4	3.5	4.1	2.4	5.6	2.8	2.1	6.4	6	16.1	3.6	6.2	7.2	6.4	3.6	0.8	4.9
YbN	3.4	10.4	2.7	4.6	1.7	3.9	1.8	0.4	1.6	3.7	19.2	1.3	3.3	9.6	7.5	3.4	0.8	3.1
LuN	6.3	11.7	2.7	6.3	1.9	4.2	2.7	0.4	2.4	6.2	22.1	1.5	3.3	11.1	8.9	4.5	1.1	4
LaN/YbN	7.3	1.3	1.4	4.5	9.8	5.1	18.7	9.5	2.3	5.6	1.2	46.4	4.9	1	1.5	4	2.9	1.1
LaN/SmN	2.1	1.3	1.6	2.9	3.7	2.3	4.5	4	1.7	2.3	1.3	6	1.9	1.8	1.8	2.1	2.1	1.3
TbN/YbN	2	0.9	1.3	0.9	1.4	1.4	1.6	5.6	3.9	1.6	0.8	2.8	1.9	0.8	0.9	1.1	1	1.6

	APLITES	
	rnap2	rnap3
SiO2	71.1	64
TiO2	0.07	0.06
Al2O3	16.2	19.5
Fe2O3	0.46	0.17
MnO	0.01	0.01
MgO	0.23	0.07
CaO	2.86	1.73
Na2O	7.15	11.5
K2O	0.38	0.46
P2O5	0.02	0.16
Total	98.47	97.98
H2O+	0.3	0.2
H2O-	0.1	0.1
CO2	0.32	0.62
Total	99.19	98.8
Quartz	22.6	
Orthoclase	2.26	2.78
Albite	61.44	65.31
Anorthite	11.16	0.24
Nepheline		7.75
Diopside	1.61	0.38
Wollastonite	0.49	2.86
Hematite		0.01
Magnetite	0.34	0.12
Ilmenite	0.13	0.12
Apatite	0.05	0.44
Sum	99.98	100
LaN	1	2.2
CeN	0.9	1.9
NdN	0.1	0
SmN	0.5	2.7
EuN	1.2	1.9
TbN	2.2	3.3
YbN	0.7	1
LuN	1	1.4
LaN/YbN	1.4	2.2
LaN/SmN	2.1	0.8
TbN/YbN	3	3.2

	LAMPROPHYS			
	r11	r11-m	b21-1	b21-2
SiO2	56.2	53.9	31.4	28.1
TiO2	0.85	0.85	3.78	3.69
Al2O3	14.3	14.1	4.28	2.58
Fe2O3	6.66	6.99	14.6	14.8
MnO	0.11	0.12	0.2	0.22
MgO	4.39	4.81	20.5	18.7
CaO	5.41	6.84	10.1	12.9
Na2O	3.33	3.92	0.23	0.38
K2O	3.44	2.12	1.81	1.5
P2O5	0.22	0.22	0.63	0.66
Total	93.91	93.37	87.43	81.51
H2O+	1.7	1.8	3.3	2.5
H2O-	0.1	0.1	0.3	0.6
CO2	3.83	3.82	8.1	14.6
Total	99.54	99.09	99.13	99.21
Quartz	6.87	5.21		
Orthoclase	21.86	13.42		
Albite	30	35.52		
Anorthite	14.82	15.66	6.06	1.04
Leucite			9.59	6.53
Nepheline			1.21	2.14
Diopside	9.73	15.24	16.37	17.59
Hypersthene	9.76	7.67		
Olivine			38.9	31.69
Ca-Orthosilicate			8.15	15.38
Magnetite	6.3	6.42	12.02	13.16
Ilmenite	1.31	1.32	8.21	6.6
Apatite	0.55	0.58	1.44	1.82
Sum	100	100	100.03	100.04
LaN	91.9	86.6	230.4	311.2
CeN	78.6	75	167.7	225.1
NdN	56.9	54.5	98.4	130.7
SmN	33.4	32.2	47.4	61.9
EuN	18.6	18.7	31.1	41.2
TbN	13	14.4	17.1	18.4
YbN	6.5	6	5.2	6.1
LuN	7.6	6.6	4.4	6.1
LaN/YbN	14	14.3	44.7	51.2
LaN/SmN	2.8	2.7	4.9	5
TbN/YbN	2	2.4	3.3	3

		MAGNO	NETWORK	Q-DIORITES			SATELLITE GRANODIORITE		LEUCOCRATIC GRANODIORITE	
	mag86-2	mag86-3	mag86-10	mag86-12	mag86-14	mag86-16	mag86-20	mag86-22	mag86-38	mag86-39
SiO2	64.3	64.6	65.6	64.6	65	63.9	54.7	69.8	69.3	69.1
TiO2	0.44	0.44	0.47	0.46	0.51	0.45	1.04	0.28	0.29	0.27
Al2O3	15.3	15.4	15.7	15.5	15.4	15.5	15.7	14.2	14.3	13.8
Fe2O3	3.77	3.88	4.14	3.84	4.15	3.91	8.62	2.29	2.49	2.47
MnO	0.05	0.05	0.06	0.05	0.06	0.05	0.18	0.03	0.03	0.04
MgO	1.56	1.59	1.15	1.67	1.38	1.59	1.48	0.61	0.67	0.66
CaO	3.89	3.47	3.14	3.33	3.77	4.06	6.78	2.46	2.44	2.69
Na2O	4.61	4.84	5.13	4.48	4.57	5.03	3.73	5.3	5.54	5
K2O	1.25	1.22	0.93	1.28	1.11	0.8	0.93	1.31	1.38	1.63
P2O5	0.1	0.1	0.13	0.1	0.13	0.1	0.34	0.09	0.1	0.09
Total	95.17	95.57	96.44	95.28	96.08	95.39	93.38	96.34	96.42	95.65
H2O+	1.7	1.6	1.3	1.7	1.6	1.5	2.2	0.9	0.7	0.7
H2O-	0.1	0.1	0.1	0.1	0.1	0.1	0.1	0.1	0.1	0.1
CO2	2.37	2.12	1.34	2.05	2.09	2.19	4.52	1.79	1.67	2.66
Total	99.34	99.39	99.18	99.11	99.77	99.18	100.2	99.13	98.89	99.11
Quartz	23.66	22.66	24.35	24.65	24.75	21.65	15.1	28.69	29.96	28.98
Corundum		0.05	0.69	0.92	0.14					
Orthoclase	7.76	7.54	5.7	8.43	6.83	4.95	5.88	8.03	8.33	9.45
Albite	40.09	42.85	45.01	39.61	40.24	44.62	33.8	46.55	48.61	44.23
Anorthite	18.72	17.33	15.27	16.66	18.68	18.19	25.01	11.51	10.51	11.18
Diopside	0.7					1.6	7	0.4	1.11	1.75
Hypersthene	5.07	5.52	4.43	5.49	4.98	4.66	3.03	2.18	1.78	1.77
Magnetite	2.88	2.93	3.11	2.92	3.14	2.98	6.61	1.73	1.88	1.88
Ilmenite	0.88	0.87	0.92	0.9	1.01	0.89	2.11	0.51	0.57	0.54
Apatite	0.26	0.26	0.32	0.26	0.32	0.26	0.86	0.22	0.24	[illegible]
Sum	99.99	99.99	99.99	99.99	99.99	99.99	100	99.99	99.99	99.99
LaN	41	43.9	47.8	42.2	41	46.4	89.4	94.2	130.2	117.8
CeN	33.6	34.4	40.2	2	33.8	34.8	82.3	78.1	111.2	100.8
NdN	17.5	19.1	23.5	19.7	22.7	19.7	57	44.7	67.8	60.1
SmN	11.1	11.8	13	11.4	12.1	11.3	33.1	21.8	30.4	27.6
EuN	8	8.5	9	7.7	8	7.8	21.4	11.7	17.3	15.2
TbN	3.8	7.9	6	6.5	6.4	4.1	16.8	7.3	11.1	9.7
YbN	3.1	3.4	4	3.5	4.2	3.8	14.1	5	7.5	6.6
LuN	4.1	3.2	4.7	3.7	4.9	4	15	6	7.1	6.5
LaN/YbN	13.4	13.1	11.9	12.2	9.7	12.2	6.3	18.8	17.4	17.9
LaN/SmN	3.7	3.7	3.7	3.7	3.4	4.1	2.7	4.3	4.3	4.3
TbN/YbN	1.3	2.3	2	1.9	1.5	1.1	1.2	1.4	1.5	1.5

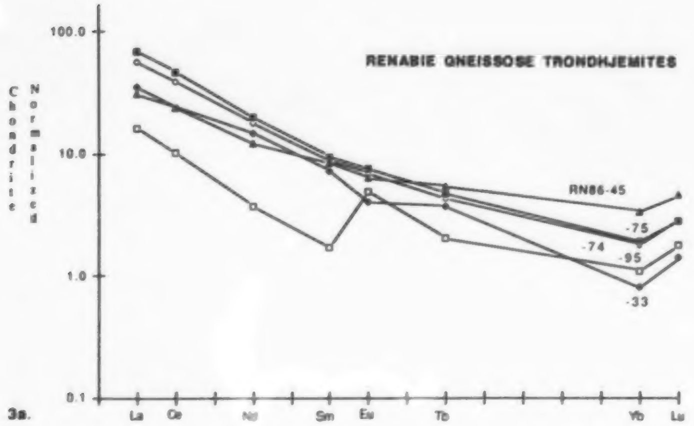

3a.

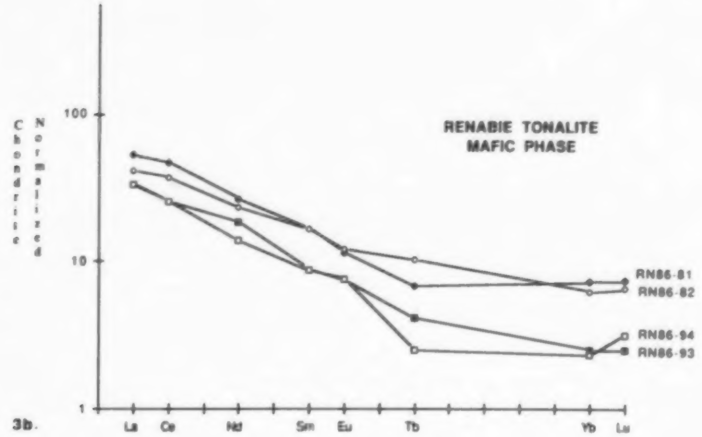

3b.

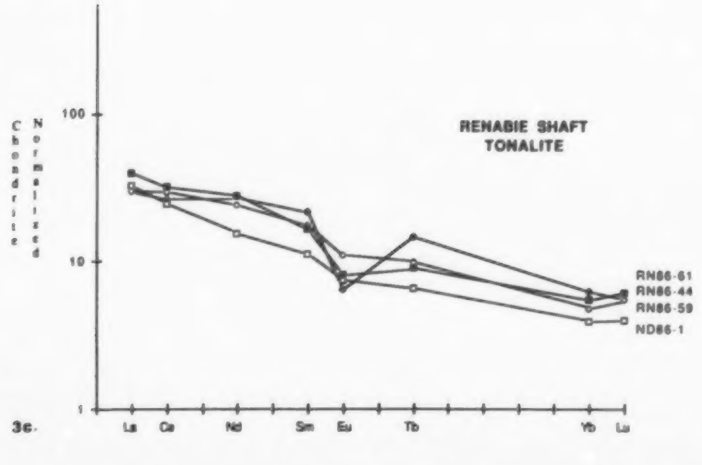

3c.

Figure 288.3. *Chondrite normalized rare earth element (REE) distribution plots for: a) Renabie gneissose trondhjemites; b) Renabie tonalites (mafic phases); c) Renabie "shaft" tonalite.*

Figure 288.3. *Continued.*

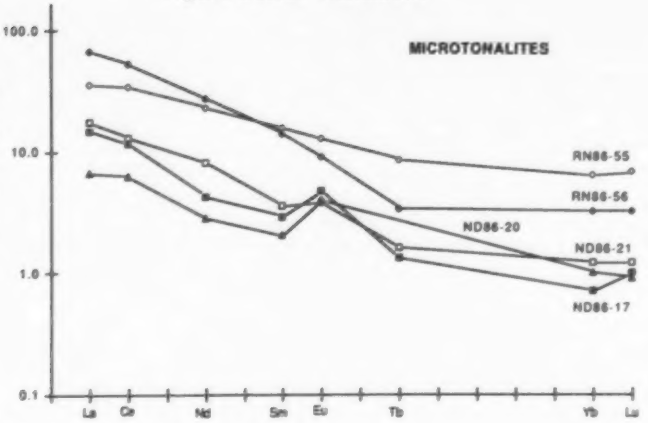

3d.

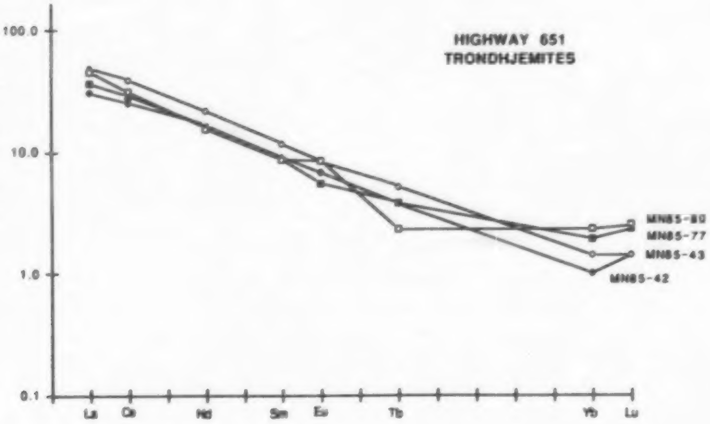

3e.

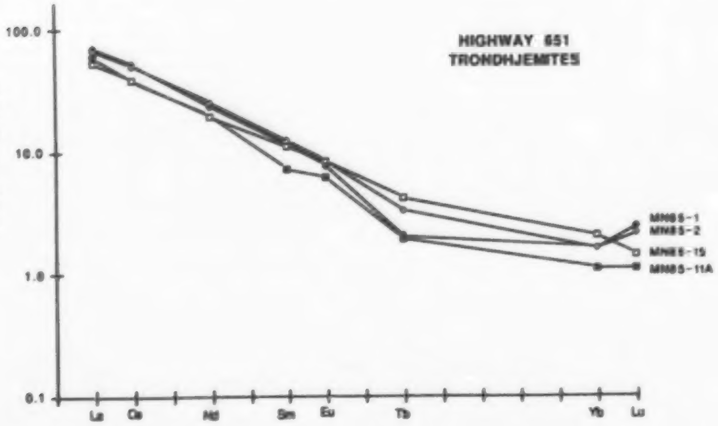

3f.

Figure 288.3. *Chondrite normalized rare earth element (REE) distribution plots for: d) microtonalites; e) Highway 651 trondhjemites; f) Highway 651 trondhjemites.*

Figure 288.3. *Continued.*

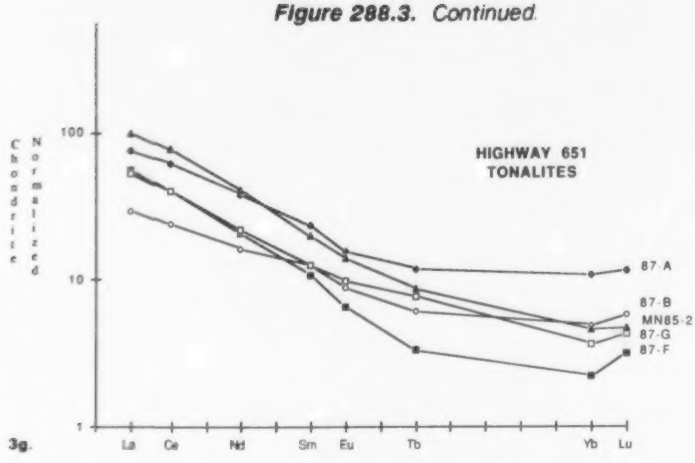

Figure 288.3. *Chondrite normalized rare earth element (REE) distribution plots for: g) Highway 651 tonalites.*

terns range from steep to shallow due to variations in heavy REE contents. Sample rn86-595 has low ΣREE and a strong positive europium anomaly, the latter probably reflecting its plagioclase-rich (cumulate?) mineralogy.

Mafic phase (tonalite) samples have moderately fractionated ΣREE values, with enrichment of light REE, and moderate to strong heavy REE enrichment (La_N/Yb_N=14.3 to 6.6, Tb_N/Yb_N=1.6 to 0.9; Figure 288.3b). Strong europium anomalies are absent. The flat middle to heavy REE patterns probably reflect the more mafic mineralogy of these rocks, and possibly the presence of sphene as a minor phase. The more felsic examples (high SiO_2, low MgO) have lower ΣREE, probably due to an abundance of low REE phases, for example, plagioclase and quartz.

The Renabie "shaft" tonalites exhibit moderately fractionated, shallow-dipping REE patterns (La_N/Yb_N=8.3 to 4.8, Tb_N/Yb_N=2.4 to 1.7; Figure 288.3c), with a flatter geometry, lower light REE, and higher heavy REE values than the gneissose trondhjemites. High heavy REE values suggest the melting of garnet in the source rock, and low light REE may indicate the fractionation of a light REE-bearing phase. Tonalites have moderate to strong negative europium anomalies, indicating plagioclase fractionation as a residual phase in the source rock during partial melting, or during subsequent magmatic differentiation. The convex upward shape of the REE distribution pattern of sample rn86-444 represents middle REE enrichment, possibly in sphene and/or hornblende (Gromet and Silver 1983).

Renabie microtonalites (prefix "rn") have fractionated REE patterns with steep light-middle REE, and flat middle-heavy REE patterns (La_N/Yb_N=21 and 5.6, Tb_N/Yb_N=1.1 and 1.3; Figure 288.3d). Europium anomalies are absent. The Nudulama microtonalites (prefix "nd"), are less fractionated (lower ΣREE, La_N/Yb_N=21.5 to 6.5, Tb_N/Yb_N=1.8 to 1.3), and in addition display strong positive europium anomalies, the latter probably reflecting enrichment in (cumulate) plagioclase (low REE-bearing phase).

Highway 651 trondhjemites display moderately steep REE patterns, with moderate enrichment of light REE, and low heavy REE values (La_N/Yb_N=55.3 to 18.8, TbN/Yb N= 3.8 to 1; Figures 288.3e, 288.3f). A small positive europium anomaly is indicative of enrichment in plagioclase.

Highway 651 tonalites have moderate to highly fractionated (La<100 times, Yb>10 times chondrite), REE patterns (La_N/Yb_N=25.8 to 6, Tb_N/Yb_N=2.2 to 1.1; Figure 288.3g). The patterns are steep from light to middle REE, but flat from middle to heavy REE.

The Highway 651 trondhjemite and tonalite samples display similar REE behaviour to the Renabie samples with respect to progressive increases in heavy REE in the more mafic tonalites. This trend may also be the result of dilution of ΣREE by low REE phases (plagioclase) in the trondhjemites.

Renabie aplites have variable ΣREE contents but mostly flat REE distribution patterns (La_N/Yb_N=46.4 to 1, Tb_N/Yb_N=5.6 to 0.8; Figure 288.4a, 288.4b). Light REE values range from 60 times to chondrite normal, and heavy REE from 22 times to 0.4 times chondrite. The aplites appear to form two groups, one characterized by moderate CaO and tonalitic composition, the other having low CaO and plotting in the alkali granite field (Figure 288.2c). Negative europium anomalies range from strong to moderate in sympathy with low (~0.5 percent) to moderate (~2.0 percent) CaO contents, respectively.

Pegmatites display similar ΣREE patterns to some aplites and have relatively flat patterns (La_N/Yb_N=18.7 to 1.3, Tb_N/Yb_N=2 to 0.9; Figure 288.4c). Europium anomalies vary from strongly negative to positive in sympathy with low (<1.58 percent) and moderate (~2 percent) CaO contents. Pegmatites with flat REE patterns have higher ΣREE, negative europium anomalies, and low CaO. Low ΣREE values and flat REE distribution patterns, characteristic of the aplites and pegmatites, reflect the dominance of REE-poor quartz and feldspars which dominate their mineralogies.

Lamprophyres have characteristically highly fractionated REE patterns (La_N/Yb_N=51.2 to 14, Tb_N/Yb_N=3.3 to 2; Figure 288.4d) (Bachinski and Scott 1979; McNeil and Kerrich 1986). Europium anomalies are weakly negative or nonexistent. Braminco lamprophyres have more fractionated light REE values (La 230 times and 311 times chondrite) compared with Renabie (~90 times chondrite). The Renabie lamprophyre also has a weak negative europium anomaly. The dissimilarities in REE patterns between the Renabie and Braminco lamprophyres is supported by their dissimilar mineralogy and major element geochemistry (Table 288.1).

Magino "network" granodiorites have moderately evolved REE patterns with steep light to middle REE, and flat middle to heavy REE distributions (La_N/Yb_N=13.4 to 9.7, Tb_N/Yb_N=2.3 to 1.1; Figure 288.5a). All samples are closely grouped except for terbium analyses which are variable, probably due to analytical errors. There are no europium anomalies.

Magino satellite stocks have similar REE patterns to the network granodiorites, but are more evolved, displaying higher ΣREE (La_N/Yb_N=18.8 and 6.3, Tb_N/Yb_N=1.4 and 1.2; Figure 288.5b). Differences in ΣREE contents between satellite stocks reflect their compositions; the more mafic Lovell Lake granodiorite has higher middle to heavy REE values (Table 288.1, Figure 288.5b).

Magino leucocratic granodiorites have similar REE patterns to the other Magino samples, but light to middle REE patterns have a convex upward shape, possibly due to enrichment in sphene, and small negative europium anomalies. The heavy REE are more enriched (La_N/Yb_N=17.9 to 17.4, Tb_N/Yb_N=1.5; Figure 288.5c) than in the other samples (except for mag86-20).

The similar shape of the REE distribution patterns for the Magino samples, together with the progressive increase in light REE from network to leuco-granodiorites, is probably due to crystal fractionation and evolution of the magma. The most notable aspect of the Magino REE data, as with the Magino whole rock data, is the close similarity with both the Renabie mine area, and the Highway 651 tonalite data; these lithologies form a geochemically related suite regardless of the presence or absence of gold mineralization.

Variations in ΣREE contents within lithological groups seem to be influenced by mineralogy. Mafic lithologies exhibit higher middle to heavy REE values, but abundant low REE-bearing minerals; quartz and feldspar have a diluting effect on the REE content of felsic rocks. Erratic REE patterns, especially in aplites, may be due to analytical errors exacerbated by the low ΣREE contents of these lithologies.

PETROGENESIS OF THE TTG MAGMAS

The majority of the TTG lithologies analyzed in the present study exhibit relatively high La_N/Yb_N ratios (>5) and low Yb_N values (<11). These rocks plot within the field of Archean TTG lithologies (Figure 6 *in* Martin 1987). Rocks of this composition are attributed to the partial melting of a hydrous tholeiitic source with a hornblende and garnet-bearing residue (Martin 1986, 1987). Both hornblende and garnet concentrate heavy REEs relative to melts. It is also possible that these trends represent crystallization of a heavy REE-bearing phase or phases; however, Gromet and Silver (1983) found that REE-concentrating minerals form during the early stages of magma crystallization, and effectively preserve the REE characteristics of the source region and derivation mechanism. The distribution of values in the present study (Figure 288.6) corresponds closely with the calculated trajectories for progressive partial melting of a tholeiitic garnet-bearing (25 percent) amphibolite or eclogite (Martin 1986) (Figure 288.4). The highest La_N/Yb_N values obtained correspond to about 25 percent and >50 percent partial melting, respectively, of amphibolite or eclogite. Lower La_N/Yb_N and correspondingly higher Yb_N values indicate increasing degrees of partial melting of the source. The Renabie and Highway 651 lithologies can be grouped into a sequence of increasing partial melting of the source, from trondhjemites to tonalites (Figure 288.6). This interpretation is supported by the sequence of intrusion based on field evidence at Renabie (Callan and Spooner 1987, 1988), which indicates that the Renabie trondhjemite (lower degree of partial melting) was emplaced earlier than the Renabie tonalite.

The Magino granodiorites also fall within the field of Archean TTG lithologies, and overlap in composition with the Renabie and Highway 651 tonalites, indicating a derivation by substantial partial melting (>50 percent) of a similar source rock composition.

DISCUSSION

The close spatial and temporal relationships between Archean gold-quartz vein/shear zone mineralization, and aplites related to the TTG lithologies at the Renabie mine support a potential genetic connection. The Renabie TTG lithologies display a trondhjemitic calc-alkalic evolutionary trend characterized by sodium enrichment during magmatic evolution; their major and REE geochemistry is similar to TTG rocks from other parts of the WDGT, and Archean grey gneiss terranes elsewhere in the world (Cullers and Graf 1984; Rudnick and Taylor 1986; Martin 1987). There is no evidence, on the basis of major element or REE analyses, for unusual TTG lithological compositions associated with mineralization. Mineralization is bracketed by late stage sodium-rich aplites, but postdates plutonic TTG magmatism, regional metamorphism, and deformation. On the basis of crosscutting intrusive timing relationships, it seems most probable that gold mineralization at Renabie is related to the late evolved aplites, and/or to concealed comagmatic intrusions. A close spatial relationship between Archean lode gold mineralization and sodium-rich intrusions and metasomatism has been widely recognized, but a genetic relationship is not clear. Burrows and Spooner (1988), however, propose the derivation of gold-enriched magmas by fractionation at high crustal levels, to account for Archean lode gold deposits associated with small stocks in the Abitibi Subprovince (for example, Lamaque Mine, Val D'Or). Late stage aplites at Renabie and leucocratic granodiorites at Magino were probably generated by similar fractional crystall-

Figure 288.4. *Continued.*

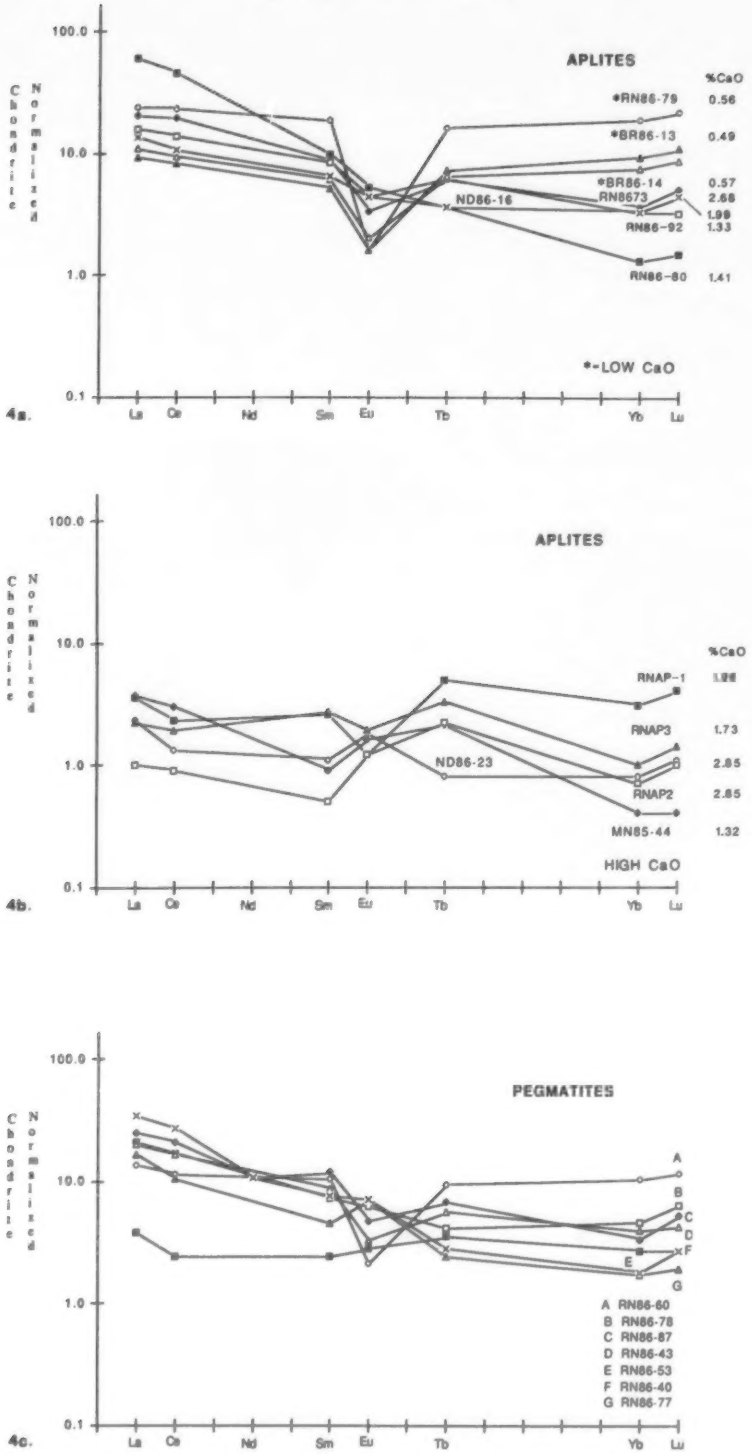

Figure 288.4. Chondrite normalized rare earth element (REE) distribution plots for: a), b) aplites; c) pegmatites.

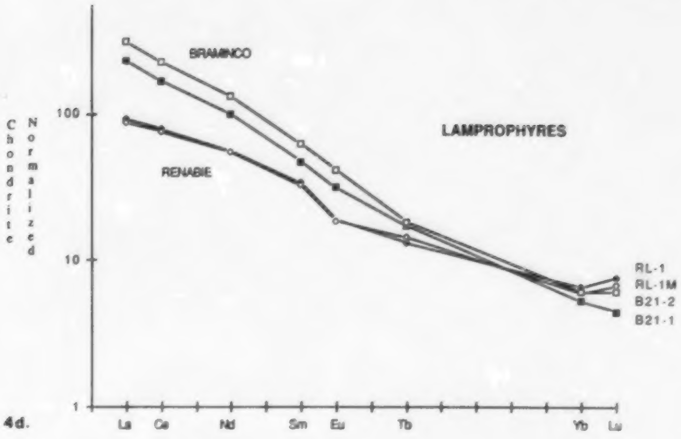

4d.

Figure 288.4. *Chondrite normalized rare earth element (REE) distribution plots for: d) lamprophyres.*

ization at relatively high crustal levels, and are most closely related to gold mineralization temporally.

Mineralization at Magino postdates intrusion, but the granodiorite lithologies display progressive geochemical evolution. Gold veins may, therefore, be genetically related to the youngest and most evolved lithology (leucocratic granodiorite). A similar relationship has been noted at the Lamaque mine in Quebec (Burrows and Spooner 1988).

The lamprophyres in the Renabie mine postdate mineralization, but are sometimes strongly deformed; however, the Braminco lamprophyres are undeformed and probably much younger than mineralization. The lamprophyres are thought to be unrelated to mineralization genetically. REE data for TTG lithologies sampled during the present study are consistent with a genetic model of the partial melting of hydrous tholeiitic garnet-bearing amphibolite or eclogite (Martin 1986, 1987). This interpretation is supported by other workers (Barker and Arth 1976; Rudnick and Taylor 1986). It is probable that the TTG lithologies analyzed during the present study were generated by the progressive partial melting of such a source.

CONCLUSIONS AND FURTHER WORK

1. TTG lithologies analyzed during the present investigation have similar geological, mineralogical, and major and rare earth element characteristics to other Archean TTG rocks from the Wawa Domal Gneiss Terrane, and to Archean grey gneiss terranes worldwide.
2. At the Renabie and Magino mines, gold mineralization is closely related spatially to intrusions with TTG compositions.
3. A major finding is that the major element and REE compositions of the main Magino plug, which intrudes a greenstone belt, and with which gold mineralization is spatially associated, are very similar to the compositions of the Renabie tonalite which hosts gold mineralization outside the Michipicoten Greenstone Belt.
4. At Renabie, mineralization occurred after major plutonic magmatism, peak regional metamorphism, and deformation. However, it is bracketed by evolved aplite dike intrusions, and postdated by lamprophyre and diabase dikes. Mineralization at Magino postdated intrusion of the youngest and most highly evolved (leucocratic) granodiorite.
5. REE data imply that the TTG lithologies in this study were generated by the progressive partial melting of a hydrated garnet-bearing tholeiitic amphibolite or eclogite source.
6. The importance of fractional crystallization during the evolution of the plutonic TTG magmas has not yet been firmly established, but was probably the dominant mechanism responsible for the evolution of the aplitic and pegmatitic minor intrusions.
7. Gold-bearing hydrothermal fluids may have been derived by fractional crystallization of TTG magmas. The two key reasons for this suggestion are: (1) that Renabie mineralization is temporally bracketed by the intrusion of evolved aplites; and (2) that the compositions of these aplites are compatible with fractionation from the Renabie tonalite of TTG composition (for example, AFM diagram, Figure 288.2a). Hence, this work provides support for the hypothesis that Archean gold-quartz vein/shear zone mineralization was derived from TTG components (Spooner *et al.* 1987).

Future studies will involve detailed thin section petrography of the TTG and minor intrusive lithologies discussed above, to quantify their mineralogical compositions, and in particular the presence of potential REE concentrating phases, such as sphene, allanite, zircon, etc. This work is particularly important, as minor phases such as sphene have been shown to dominate the REE distribution patterns in plutonic granitoids (Gromet and Silver 1983). In addition, trace element data will be examined to characterize further the sampled lithologies, their petrogenetic evolution, and their geochemical relatic

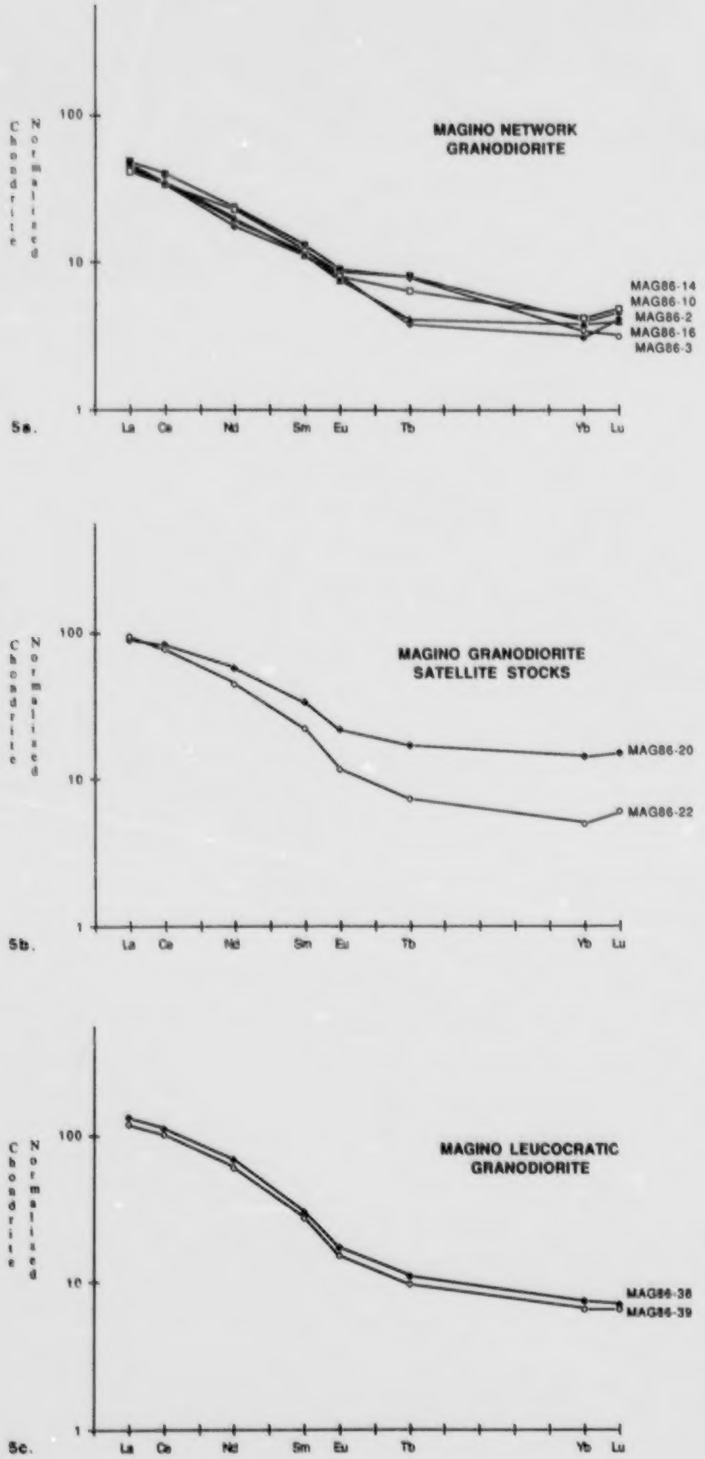

Figure 288.5. *Chondrite normalized rare earth element (REE) distribution plots for: a) Magino (network) granodiorite; b) Magino satellite (granodiorite) stocks; and c) Magino leucocratic granodiorite.*

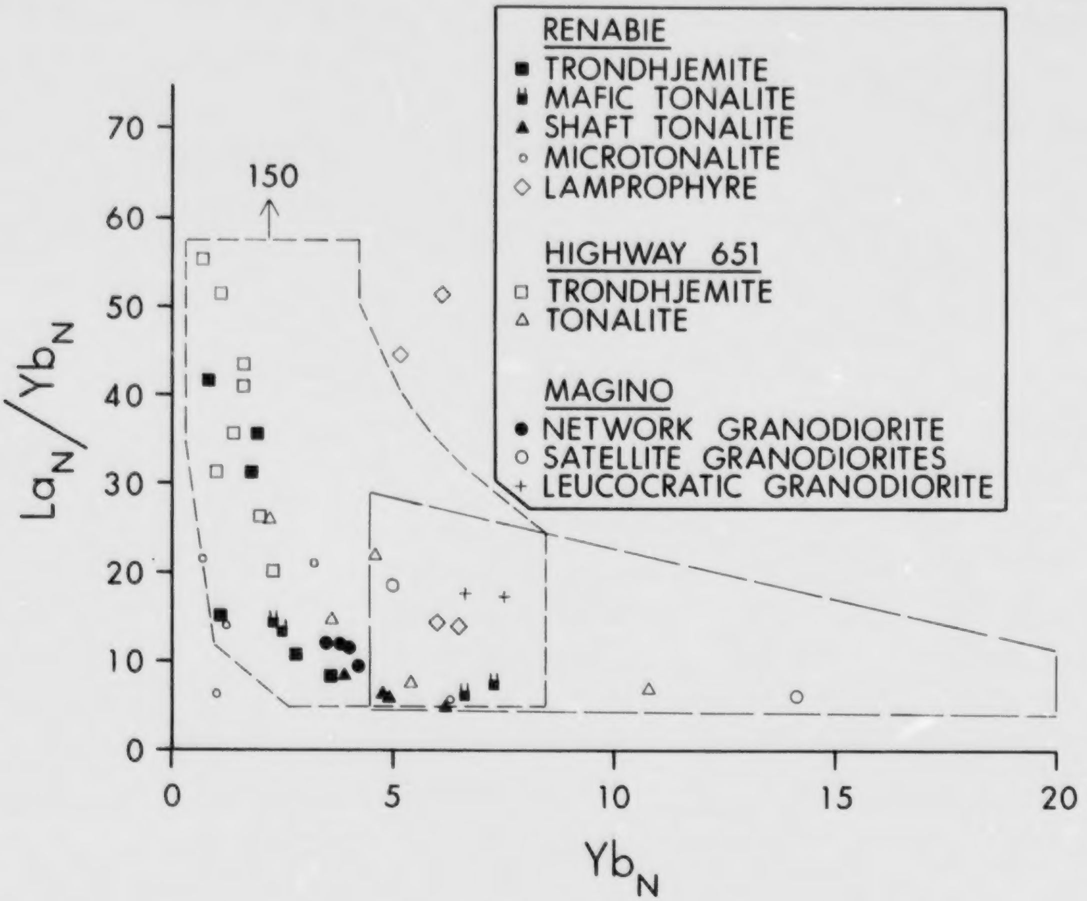

Figure 288.6. *La_N/Yb_N versus Yb_N diagram (after Martin 1987), showing the distribution of samples analyzed during the present study.*

ships to mineralization. Selected samples have been dated by zircon U-Pb geochronology (Jack Satterly Geochronology Laboratory, Royal Ontario Museum, Toronto), and further analyses are planned to provide an absolute time framework for magmatism and mineralization at Renabie.

ACKNOWLEDGMENTS

The authors would like to thank the Royex Gold Mining Corporation very much indeed for permission to work at the Renabie mine, and Phil Olson and Chester Moore (Chief Geologists, Renabie Mine) together with Alex Kusik (Geologist, Renabie Mine) for their consistent support, interest, and discussion. We are also extremely grateful to Muscocho Explorations Limited and McNellen Resources Inc. for permission to visit Magino, and for their hospitality at the project site. Many thanks go to Terry Flanagan, Duncan McPhee, Jim Mallard, and Hans Mathews, for their generous help. Finally, University of Toronto graduate students Dave Burrows, Steve Noble, and John Stix are also thanked for stimulating discussion, and Subhash Shanbhag (University of Toronto) for drafting. Additional financial support for this research has been provided by NSERC Strategic Grant G1862, and Lithoprobe funds awarded to E.T.C. Spooner, which we acknowledge with appreciation.

REFERENCES

Bachinski, S.W., and Scott, R.B.
1979: Rare-Earth and Other Trace Element Contents and the Origin of Minettes (Mica Lamprophyres); Geochimica et Cosmochimica Acta, Volume 43, p.93-100.

Barker, F.
1979: Trondhjemites: Definition, Environment, and Hypotheses of Origin, p.1-12 *in* Trondhjemites, Dacites, and Related Rocks, edited by F. Barker, Elsevier, Amsterdam, 659p.

Barker, F., and Arth, J.G.
1976: Generation of Trondhjemitic-Tonalitic Liquids and Archean Bimodal Trondhjemite-Basalt Suites; Geology, Volume 4, Number 10, p.596-600.

Bennet, G.
1978: Geology of the Crooked Lake Area, District of Sudbury; Ontario Geological Survey, Report 172, 46p. Accompanied by Maps 2380 and 2381, scale 1 inch to 1/2 mile or 1:31 680.

Bruce, E.L.
1942: Geology of the Goudreau–Lochalsh Area, Algoma District; Ontario Department of Mines, Annual Report for 1940, Volume 49, Part 3, 50p. Accompanied by Map 49g, scale 1 inch to 1/2 mile or 1:31 680.

Burrows, D.R., and Spooner, E.T.C.
1988: Relationships Between Archaean Gold-Quartz Vein/Shear Zone Mineralisation and Igneous Intrusions in the Val D'Or and Timmins Areas, Abitibi Sub-Province, Canada: The Geochemical Characteristics of Au Related Magmas; p.302-307 *in* Bicentennial Gold 88, Melbourne, Extended Abstracts, Oral Program, compiled by A.D.T. Good and S.I. Bosma, Geological Society of Australia Inc., Abstracts Number 2, 369p.

Callan, N.C., and Spooner, E.T.C.
1987: Gneissose Trondhjemite/Tonalite Hosted Au-Quartz Vein Mineralization, Renabie Mine Area, Wawa: Geological Characteristics and Shear Zone Control; Grant 288, p.153-175 *in* Geoscience Research Grant Program, Summary of Research, 1986-1987, edited by V.G. Milne, Ontario Geological Survey, Miscellaneous Paper 136, 241p.
1988: TTG (Tonalite-Trondhjemite-Granodiorite) Terrane Hosted Archean Au-Quartz Vein Mineralization, Renabie Mine Area, Wawa, Northern Ontario, Canada; p.60-64 *in* Extended Abstracts, Bicentennial Gold 88 Conference, Melbourne, Australia, Geological Society of Australia Inc., Abstracts Number 23.

Cullers, R.L., and Graf, J.L.
1984: Rare Earth Elements in Igneous Rocks of the Continental Crust: Intermediate and Silicic Rocks—Ore Petrogenesis; p.275-316 *in* Rare Earth Element Geochemistry (Developments in Geochemistry 2), edited by P. Henderson, Elsevier, Amsterdam-Oxford-New York-Tokyo, 510p.

Downes, M.J.
1983: Geology of the Matchinameigus Lake Area, District of Algoma; Ontario Geological Survey Report 233, 40p. Accompanied by Map 2483, scale 1:31 680 or 1 inch to 1/2 mile.

Gromet, L.P., and Silver, L.T.
1983: Rare Earth Element Distributions Among Minerals in a Granodiorite and Their Petrogenetic Implications; Geochimica et Cosmochimica Acta, Volume 47, p.925-939.

Haskin, L.A., Haskin, M.A., Frey, F.A., and Wilderman, T.R.
1968: Relative and Absolute Terrestrial Abundance of the Rare Earths; p.889-912 *in* Origin and Distribution of the Elements, edited by L.H. Ahrens, Pergamon, New York, 1178p.

Heather, K.B., and Arias, Z.J.
1987: Geological Setting of Gold Mineralization in the Goudreau–Lochalsh Area, District of Algoma; p.155-162 *in* Summary of Field Work and Other Activities 1987, by the Ontario Geological Survey, edited by R.B Barlow, M.E. Cherry, A.C. Colvine, Burkhard O. Dressler, and Owen L. White, Ontario Geological Survey, Miscellaneous Paper 137, 429p.

Martin, H.
1986: Effect of Steeper Archean Geothermal Gradient on Geochemistry of Subduction-Zone Magmas; Geology, Volume 14, Number 9, p.753-756.
1987: Petrogenesis of Archaean Trondhjemites, Tonalites and Granodiorites from Eastern Finland: Major and Trace Element Geochemistry; Journal of Petrology, Volume 28, Part 5, p.921-953.

McNeil, A.M., and Kerrich, R.
1986: Archean Lamprophyre Dikes and Gold Mineralization, Matheson, Ontario: The Conjunction of LILE-Enriched Mafic Magmas, Deep Crustal Structures, and Au Concentration; Canadian Journal of Earth Sciences, Volume 23, Number 3, p.324-343.

Milne, V.G., Giblin, P.E., Bennet, G., Thurston, P., Wolfe, W.J., Giguere, J.F., Leahy, E.J., and Rupert, R.J.
1972: Manitouwadge–Wawa Sheet, Algoma, Cochrane, Sudbury, and Thunder Bay Districts; Ontario Division of Mines, Geological Compilation Series, Colour Map 2220, scale 1:253 440 or 1 inch to 4 miles. Compilation 1966-1971.

Nakamura, N.
1974: Determination of REE, Ba, Fe, Mg, Na, and K in Carbonaceous and Ordinary Chondrites; Geochimica et Cosmochimica Acta., Volume 38, p.757-775.

O'Connor, J.T.
1965: A Classification for Quartz-Rich Igneous Rocks Based on Feldspar Ratios; p.B79-B84 *in* Geological Survey Research 1965, U.S. Geological Survey, Professional Paper 525-B, 195p.

Percival, J.A.
1981: Stratigraphic, Structural, and Metamorphic Relations Between the Wawa and Abitibi Subprovinces and the Kapuskasing Structural Zone near Chapleau, Ontario; p.83-90 *in* Current Research, Part A, Geological Survey of Canada, Paper 81-1A, 404p.
1986: The Kapuskasing Uplift: Archean Greenstones and Granulites; *in* Geological Association of Canada, Mineralogical Association of Canada, Canadian Geophysical Union, Joint Annual Meeting, Ottawa '86, Field Trip 16 Guidebook, 37p.

Percival, J.A., and Card, K.D.
1983: Archean Crust as Revealed in the Kapuskasing Uplift, Superior Province, Canada; Geology, Volume 11, p.323-326.

Rock, N.M.S.
1987: The Need for Standardization of Normalized Multi-Element Diagrams in Geochemistry: A Comment; Geochemical Journal, Volume 21, p.75-84.

Rudnick, R.L., and Taylor, S.R.
1986: Geochemical Constraints on the Origin of Archaean Tonalitic-Trondhjemitic Rocks and Implications for Lower Crustal Composition; p179-191 *in* The Nature of the Lower Continental Crust, edited by J.B. Dawson, D.A. Carswell, J. Hall, and K.H. Wedepohl, Geological Society, Special Publication 24.

Sage, R.P.
1987: Geology of Goudreau–Lochalsh and Kabenung Lake Areas, District of Algoma; p.134-137 *in* Summary of Field Work and Other Activities 1987, by the Ontario Geological Survey, edited by R.B. Barlow, M.E. Cherry, A.C. Colvine, Burkhard O. Dressler, and Owen L. White, Ontario Geological Survey, Miscellaneous Paper 137, 429p.

Spooner, E.T.C., Burrows, D.R., Callan, N.J., De Ronde, C.E.J., and Wood, P.C.
1987: TTG Components as Possible Sources for Archean Au Vein Mineralization. Abstract; p.24 *in* Program with Abstracts, GAC-MAC Summer Field Meeting, Yellowknife 1987, Geological Association of Canada.

Streckeisen, A.
1976: To Each Plutonic Rock Its Proper Name; Earth Science Reviews, Volume 12, p.1-33.
1978: Classification and Nomenclature of Volcanic Rocks, Lamprophyres, Carbonatites and Melilitic Rocks. Recommendations and Suggestions; Neues Jahrbuch fur Mineralogie, Abhandlung, Volume 134, p.1-4

The Northern Miner
1988: Muscocho Revises Echo Bay Deal; p.27 *in* The Northern Miner, Volume 74, Number 11, May 23, 1988.

Thurston, P.C., Siragusa, G.M., and Sage, R.P.
1977: Geology of the Chapleau Area, Districts of Algoma, Sudbury, and Cochrane; Ontario Division of Mines, Geoscience Report 157, 293p. Accompanied by Map 2221, scale 1:253 440 or 1 inch to 4 miles, and Map 2351 and 2352, scale 1:250 000.

Wager, L.R., and Deer, W.A.
1939: The Petrology of the Skaergaard Intrusion, Kangerdlugssuag, East Greenland; Meddelelser om Grønland, Volume 105, Number 4, p.1-352.

Grant 290 Maximal Simplicity Gravity Interpretation with Continuous Density Models

R.C. Bailey[1] **and S.W. Reford**[2]

[1]Geology and Physics Departments, University of Toronto, Toronto

[2]Physics Department, University of Toronto, Toronto

ABSTRACT

Maximal simplicity gravity modeling produces a gridded approximation to continuous density distributions within the Earth. In this paper is demonstrated the performance of the method using surface gravity and density measurements from the Kirkland Lake area of Ontario. The choice of inconsistent regional gravity and regional reference density is immediately visible in a model of density across the Round Lake Batholith, as is the correction of the inconsistency. The imaging of structure is observed to become attenuated and blurred with increasing depth.

INTRODUCTION

Deducing something about the density distribution of the Earth from gravity measurements made at the surface is a very non-unique inverse problem. Two methods of handling the ambiguities currently exist: first, the relatively old-fashioned method of forward modeling (choosing the structure of relatively simple models *a priori* and testing them against the data); and second, extremal methods that choose, out of the many possible general density models that fit the data, that one which extremizes (maximizes or minimizes) some overall quantitative attribute of the model. The old-fashioned method generally works best, because the various extremal models selected by different methods have all been somewhat implausible. It is not reasonable, for example, to expect the Earth to have a density distribution which absolutely minimizes the error of fit (to well below the measurement error level), or produces the smallest root-mean-square density variation, or the smoothest density model. Nevertheless, extremal methods can be automated straightforwardly.

Last year we reported on an extremal method which has the advantages of both approaches. Using a linear-inequality-programming algorithm, we minimize a quantitative measure of the model, which in this case is the sum of the magnitudes of the density differences between adjacent cells in a regular finely gridded model. Information about density acquired from surface or drillhole is easily incorporated as constrained cell density values. The essential property of this measure is that, without precluding the existence of a more complex gradational structure, it prefers models with as many cells as possible having the same values as their neighbours, therefore leading to a simple structure.

Having reported last year on the performance of the method on simple synthetic structures, we report here on its application to gravity and surface density data collected by the Ontario Geological Survey (OGS), on profiles in the Timmins–Kirkland Lake area. Two profiles have been selected here to demonstrate some of the characteristics of the method on real data.

THEORETICAL METHODOLOGY

The density distribution to be modeled is, for computational purposes, represented as a regular rectangular grid of rectangular cells of uniform density separated by linear boundaries. Although the method is equally applicable to three dimensions, all models referred to in this report are two-dimensional, with infinite strike length assumed. All sections shown are across strike. The computational problem may be summarized (after Bailey and Reford 1987) as the minimization of a "simplicity norm" (S), given by the sum of the density changes across all the cell boundaries, subject to the following constraints:

1. that the data be fitted within a specified margin of error
2. that any available estimates of cell densities (such as those obtained by sampling on the ground or in boreholes) be respected for those cells which are sampled
3. that our prejudices regarding overall reasonable limits on any density be respected

The models to be shown in this report were obtained by iteratively minimizing S, subject to the above constraints, using the NAG Fortran Library subroutine E04UAF—a general purpose non-linear iterative optimization routine. This routine does not allow models with very many cells to be solved in a short time, but is easy to use.

Previous experience with synthetic data (Bailey and Reford 1987) showed that if no constraints of type 2 above were applied, the density models obtained tended to have smoother density variations than the true models simply because these are simpler in the sense of the simplicity norm above. The application of either surface or borehole density constraints was sufficient, in the synthetic models examined, to recover a good approximation to the synthetic model.

THE DATA

GRAVITY MEASUREMENTS

The gravity data for the two test profiles used here were collected under contract by Paterson, Grant and Watson, Ltd. for the OGS in the Abitibi greenstone belt, as part of the Kirkland Lake, Larder Lake, Matheson, and Cochrane area survey (KLAC). These data were Bouguer corrected and then contoured. Profiles were then selected from the contoured map for analysis. Both of these (labelled 11 and 15, respectively) are shown on Figure 290.1. Density values from sampling in the area were used as a guide for applying density constraints of type 2 above. A regional gravity map was obtained by smoothing the gravity data using a space domain two-dimensional non-linear filter (Naudy and Dreyer 1968). The interpreted anomalous profiles were obtained by subtrac-

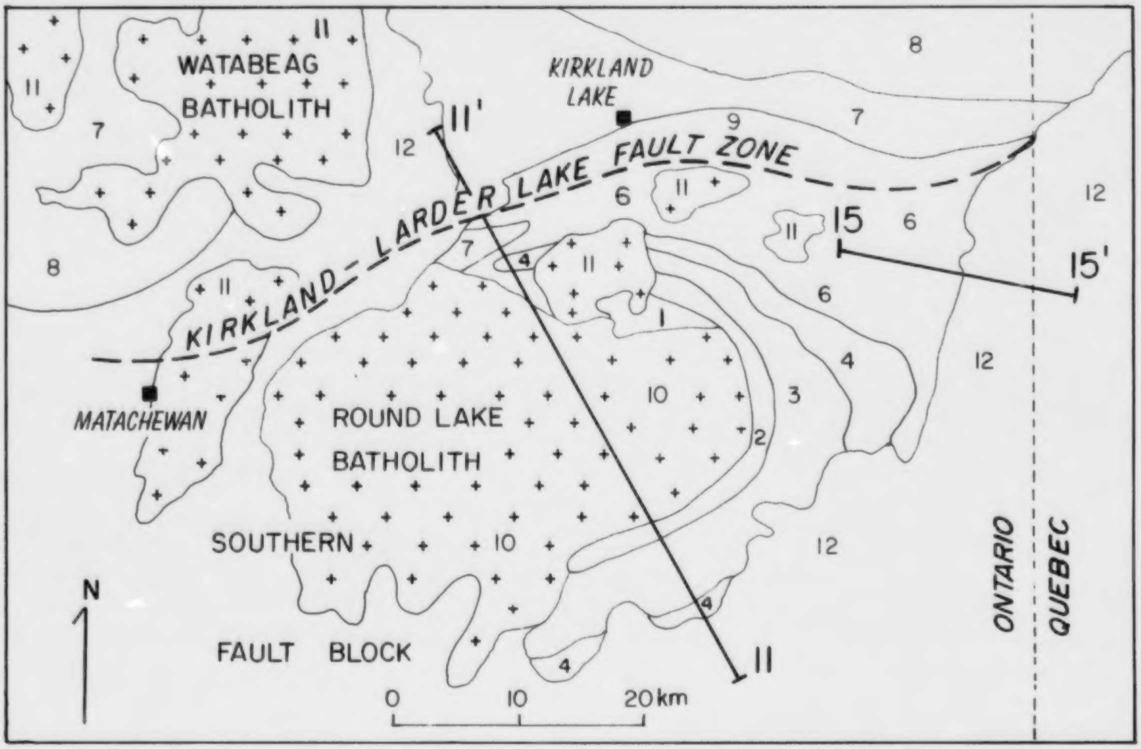
WATABEAG BATHOLITH
KIRKLAND LAKE
KIRKLAND - LARDER LAKE FAULT ZONE
MATACHEWAN
ROUND LAKE BATHOLITH
SOUTHERN FAULT BLOCK
11'
11
15
15'
N
0
10
20km
ONTARIO
QUEBEC
12
11
10
9
8
7
6
4
3
2
1

LEGEND

PROTEROZOIC

12 Cobalt Group

ARCHEAN

– Granitic Rocks

11 Granodiorite, monzonite, quartz monzonite, syenite

10 Massive to gneissic quartz diorite, tonalite, trondhjemite

– Upper Supergroups

9 Timiskaming Group

8 Blake River Group

7 Kinojevis Group

6 Larder Lake Group

– Lower Supergroups

4 Skead Group

3 Catherine Group

2 Wabewawa Group

Figure 290.1. *Generalized geological map of the survey area, taken from Jensen (1985). Two gravity profiles (11 and 15) are shown.*

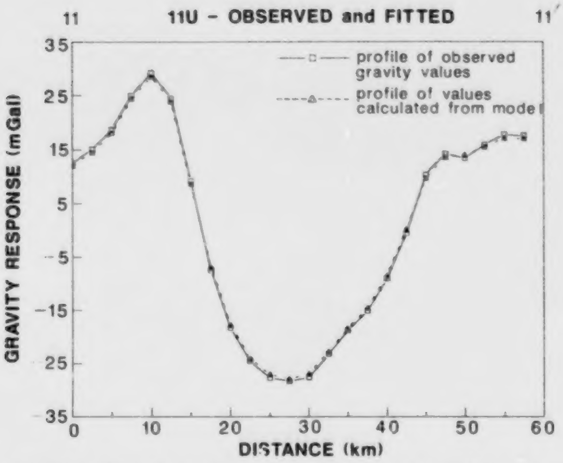

***Figure 290.2.** Model 11U: The fit of gravity observations to the values calculated from the model. South is on the left.*

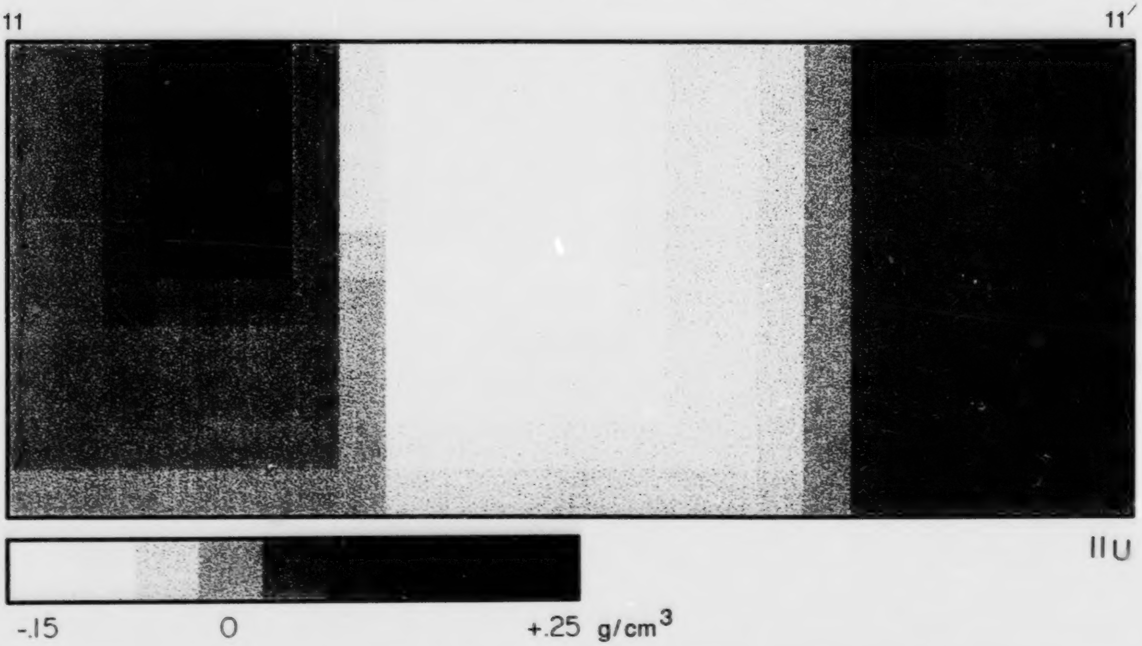

***Figure 290.3.** Model 11U: A grey scale plot of anomalous density under profile 11. No surface density constraints were applied. The legend shows density deviations from the reference density of 2.74 g/cm^3. The Earth's surface is at the top, and south is to the left. Vertical exaggeration is 2.5:1.*

tion of this regional from the original data. These anomalous gravity profiles were used as the input to the present analysis.

DENSITY MEASUREMENTS

As part of the same OGS program, the densities of surface samples taken on the profile were determined. As the gravity data for the profiles interpreted here were abstracted from gravity maps, sampled surface densities do not lie exactly on profiles. They were used as a guide to choosing reasonable density constraints for the density models.

THE CONSISTENCY PROBLEM

In calculating a regional gravity field and subtracting it from the gravity measurements, one is implicitly choosing a regional average density. That is, the density models that fit the residual gravity anomaly necessarily have as values the deviations from some regional average or reference density that is consistent with the regional field. However, in real life, one has no direct estimate of the appropriate regional density. There is no guarantee that the average surface sampled density is a reasonable estimate of this regional average density; not only because the surface is not densely sampled, but also because sampling is not carried out at depth.

The way in which an inconsistent choice of regional gravity and regional average density shows up is by making it difficult to model the observed anomalous field with reasonable density distributions. What counts as "difficult" and "reasonable" is of course often very subjective; in what follows, we shall show in at least one case how such inconsistency is straightforwardly detected in the density models obtained, and how consistency is then achieved.

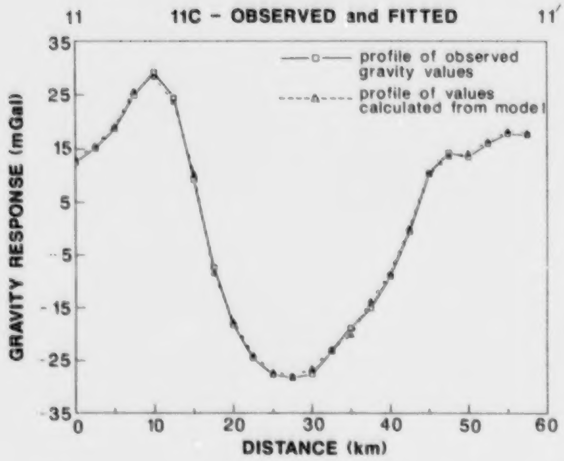

Figure 290.4. *Model 11C: The fit of gravity observations to the values calculated from the model. South is on the left.*

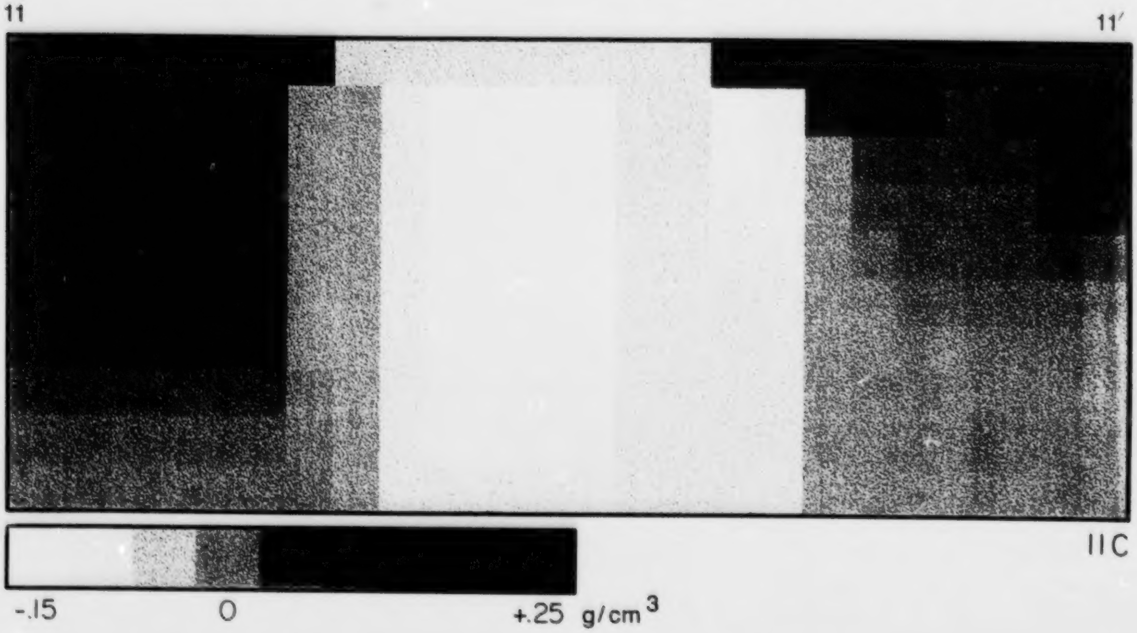

Figure 290.5. *Model 11C: A grey scale plot of anomalous density under profile 11. Surface density constraints were applied. The legend shows density deviations from the reference density of 2.74 g/cm³. The Earth's surface is at the top, and south is to the left. Vertical exaggeration is 2.5:1.*

PROFILE LOCATIONS

Profile 11 is about 58 km in length. The major density contrast seen on the profile is that between the large Round Lake Batholith—occupying the central 25 km of the profile—and the surrounding denser rocks to the north and south. The profile also crosses the Kirkland–Larder Lake Fault Zone near the northern end of the profile at approximately kilometre 49. A more detailed description of the geology along the profile is to found in a report by Jensen (1985).

Profile 15 is about 20 km in length, and is chosen to cross a major step in the gravity data; this step is presumably associated with the transition from metasediments and volcanic rocks on the west to the lighter rocks of the Pontiac Massif on the east. Again, a detailed description of the geology is to be found in a report by Jensen (1985). It is worth noting that Proterozoic sediments are assumed to overlap the western margins of the Pontiac Massif, and that the true contact between these rock types at depth probably lies west of the surface contact (Jensen 1985).

PROFILE 11 MODELS

MODEL STRUCTURE

The density model used for profile 11 was a regular grid of rectangular cells, each 2500 m across by 1000 m deep. The grid is 24 cells across by 10 cells deep, and represents a cross-section of the Earth's crust 60 km across by 10 km deep. Note that the grey scale plots used to display density models for this profile produce square cells, and that there is therefore a vertical exaggeration of 2.5:1 on profile 11 plots. The data are obtained from the anomalous gravity contour map as described previously, at regular intervals of 2.5 km;. there is, therefore, one point per cell along the surface on this profile.

Implicit assumptions are made by the modeling technique. First, the anomalous density below the bottom of the model (here at 10 km) is assumed to

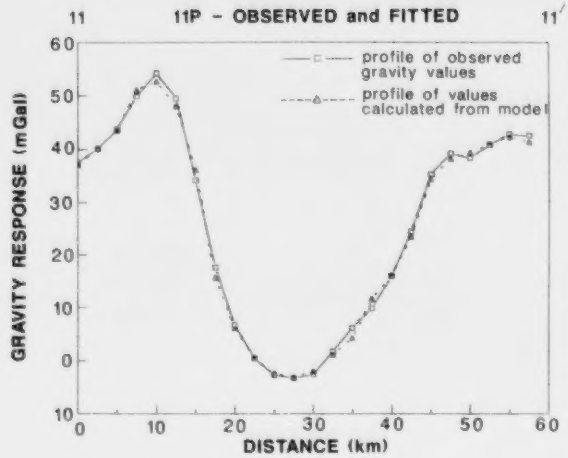

Figure 290.6. Model 11P: The fit of gravity observations to the values calculated from the model. South is on the left.

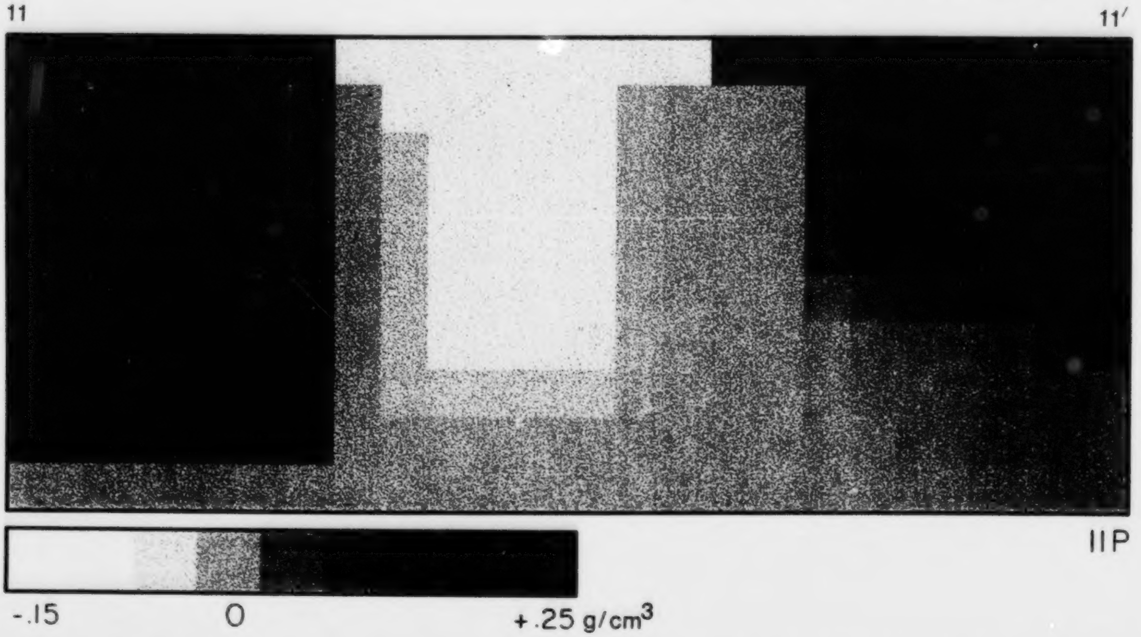

Figure 290.7. Model 11P: A grey scale plot of anomalous density under profile 11 for a regional gravity adjustment of 25 mGal. Surface density constraints were applied. The legend shows density deviations from the reference density of 2.74 g/cm³. The Earth's surface is at the top, and south is to the left. Vertical exaggeration is 2.5:1.

be everywhere zero (lower truncation). This is clearly a source of error in the modeling process. However, computing speed limitations dictated such a lower truncation of the model for practical reasons. In addition, the errors introduced by this are not as large as might first be supposed. Removal of a regional gravity guarantees that most of what is left as anomalous gravity arises from density anomalies in the shallower parts of the crust; very deep anomalies produce very broad features at the surface that will appear mainly in what is computed as a regional field.

The second implicit assumption is that whatever vertical heterogeneity exists at each edge (end) of the model can be assumed to carry on indefinitely off the edges of the model; that is, the Earth off the model edges is assumed to be horizontally stratified with no horizontal density variations. Given that no data is being fitted off the edges, this is a reasonable assumption; all that is needed is an estimate of the effects of the off-model density variations. As the contribution of these decreases rapidly as the inverse square of distance, they need only be correct close to the edges, and the horizontally stratified model is suitable and easy to calculate.

Thirdly, the model is two-dimensional, and has infinite strike length across the profile. Since geological mapping clearly shows that the structures are not two-dimensional, and do not have infinite strike length, a three-dimensional implementation of the method would clearly do better. In the model presented here, one would expect the deeper structures to be interpreted as more shallow than the truth because of this.

MODEL RESULTS

The results of applying the method to the data for profile 11 are shown in two types of figures: first, as plots comparing the observed gravity values

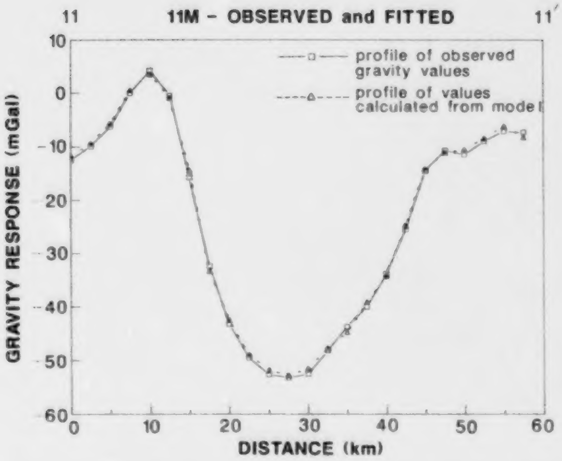

Figure 290.8. *Model 11M: The fit of gravity observations to the values calculated from the model. South is on the left.*

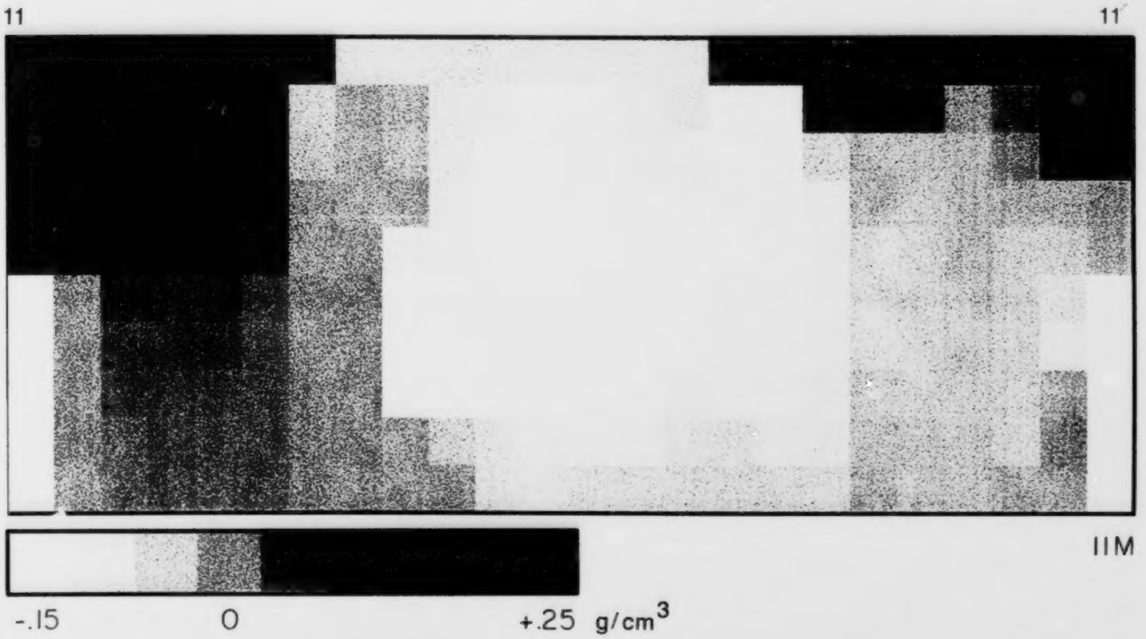

Figure 290.9. *Model 11M: A grey scale plot of anomalous density under profile 11 for a regional gravity adjustment of -10 mGal. Surface density constraints were applied. The legend shows density deviations from the reference density of 2.74 g/cm³. The Earth's surface is at the top, and south is to the left. Vertical exaggeration is 2.5:1.*

(interpolated from the map as described previously) with the calculated gravity values for the density model; and second, as grey scale plots showing the actual density models. The darkness of the scale is proportional to the anomalous density. A legend is shown in each grey scale plot relating anomalous density (in g/cm³) to the grey shading level. The individual cells of the model are clearly visible in these plots, which therefore give some idea of the maximum possible model resolution.

With no density constraints of type 2 applied, the modeling program produced the fit of modelled to observed gravity data shown in Figure 290.2. The iterative fitting procedure was stopped when the average difference between the values was less than 0.5 mGal. This, although larger than the measurement error, was judged acceptable (since the assumption of infinite strike length introduces errors considerably in excess of the measurement errors). The corresponding density model (11U) is shown in Figure 290.3, using a grey scale plot. The darker areas indicate higher anomalous density (reference density = 2.74 g/cm³). A scale is provided on the figure. Note that the dominant feature is a light area corresponding to the Round Lake Batholith, surrounded by denser regions—corresponding to metasediments and metavolcanics—on either side. As no sampled density constraints have been incorporated into the model, it is not surprising that the density contrasts are rather diffuse (even at the surface), and decay away at depth.

It is possible to use the surface density sampling data to constrain the densities in the top layer of cells in the model. Because the cells have a finite depth, the surface contraints applied only extend to a depth of 1 km. The densities of all but the southernmost 7.5 km of the profile were constrained. This southernmost end is thought to have a relatively thin veneer of Proterozoic sediments; surface density

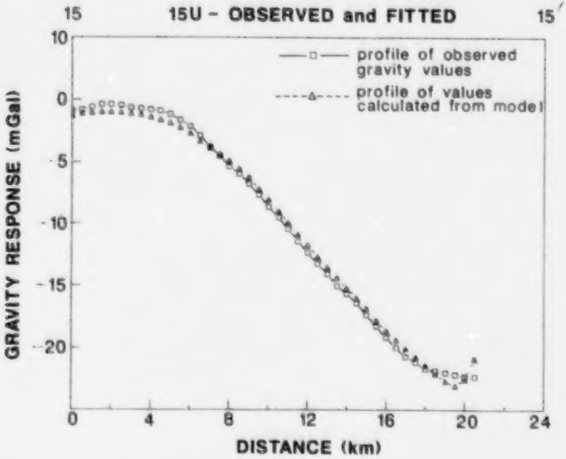

Figure 290.10. *Model 15U: The fit of gravity observations to the values calculated from the model. West is on the left.*

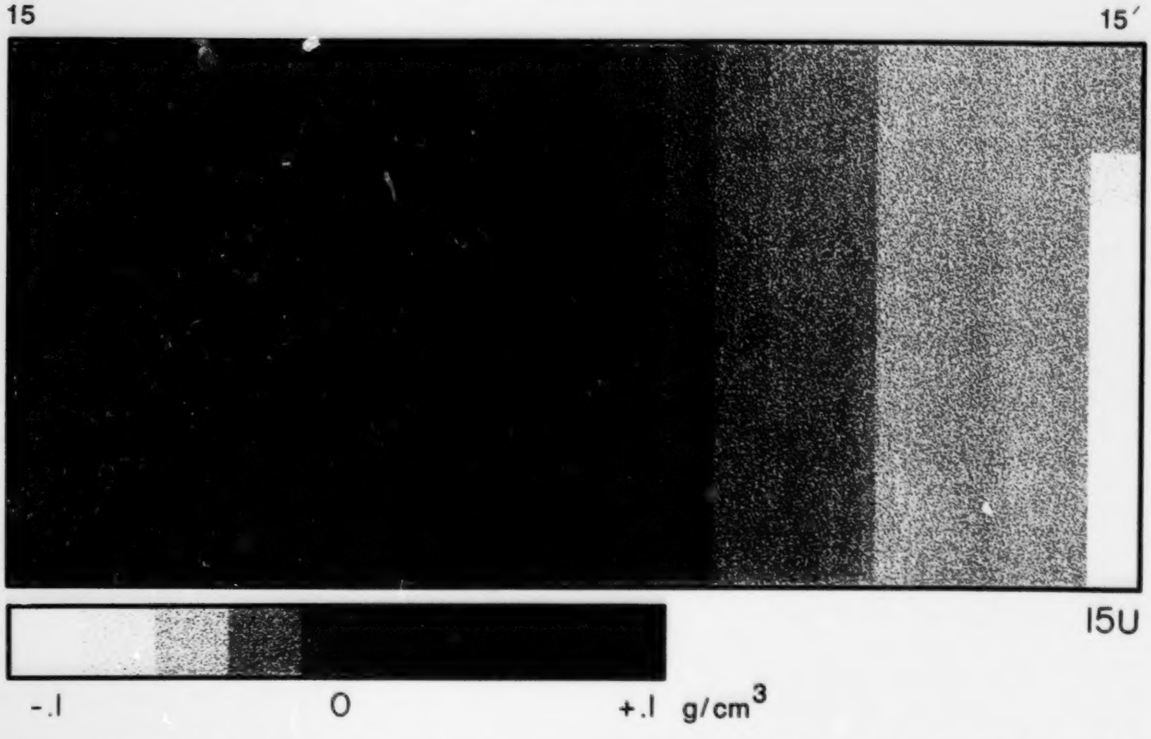

Figure 290.11. *Model 15U: A grey scale plot of anomalous density under profile 15. No surface density constraints were applied. The legend shows density deviations from the reference density of 2.74 g/cm^3. Earth's surface is at the top, and west is to the left. No vertical exaggeration.*

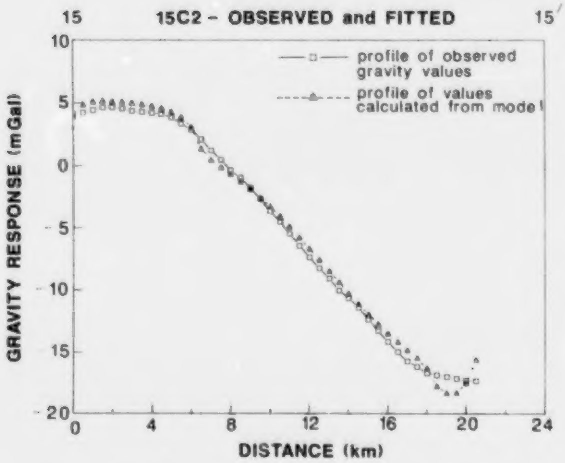

Figure 290.12. *Model 15C2: The fit of gravity observations to the values calculated from the model. West is on the left.*

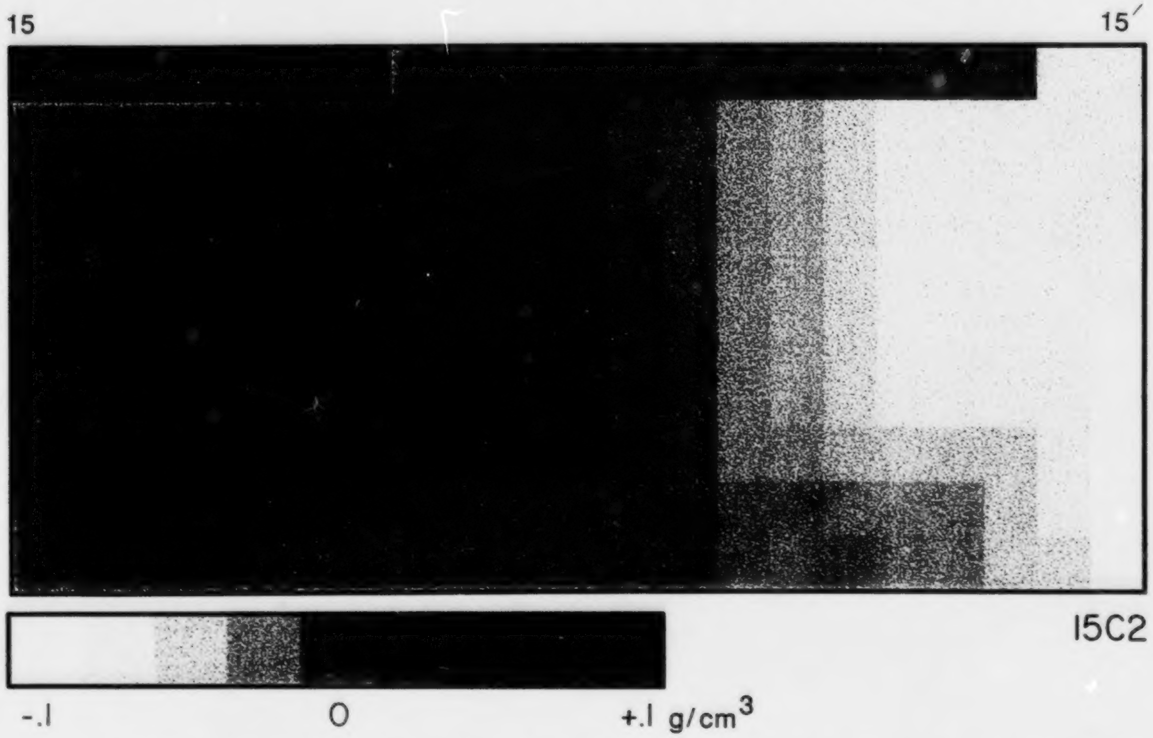

Figure 290.13. *Model 15C2: A grey scale plot of anomalous density under profile 15. Surface density constraints were applied, and the regional gravity field was adjusted. The legend shows density deviations from the reference density of 2.74 g/cm³. The Earth's surface is at the top, and west is to the left. No vertical exaggeration.*

samples are therefore presumed unrepresentative of densities at depth. As shown by the grey scale plot (Figure 290.5) of the resulting model (11C), the constrained densities are (moving northwards): 2.98 g/cm³ over the Catherine Group; 2.68 g/cm³ over the Round Lake Batholith; increasing again over the Kinojevis Group to 2.83 g/cm³; and then to 2.95 g/cm³ north of the Kirkland–Larder Lake Fault Zone.

The fit shown in Figure 290.4 for this model (11C) is virtually as good as that for the unconstrained model (11U) shown in Figure 290.2. The density section (Figure 290.5), however, is quite different, and shows one implausible feature: specifically the "layer" on top of the Round Lake Batholith. The densities of the surface row of cells across the Round Lake Batholith are necessarily correct, as they are constrained. The next layer down shows an abrupt change to a batholithic "core density" which is noticeably lighter. Rather than believing in such vertical heterogeneity, which coincides exactly with the model boundary between constrained and unconstrained cell densities, it seems to us preferable to believe that an incorrect regional gravity has been removed, or more accurately, that the presumed regional gravity and the presumed regional average density have been chosen inconsistently. A striking result of this method, then, is to offer a method for detecting this type of inconsistency in gravity modeling.

For modeling purposes, it does not matter which of either the presumed regional gravity or the presumed regional average density is changed to achieve consistency. We chose to adjust the presumed regional gravity by a constant amount. The adjustment which removed the discrepancy between the surface layer and the deeper layers of cells in the Round Lake Batholith was 25 mGal. The resulting fit to the data, and the density model obtained (11P), are shown in Figures 290.6 and 290.7, respectively. This represents the best that can be done with this method, using only profile data and a two-dimensional model. The downward tapering and attenuation of the roots of the structures is probably caused by a combination of three effects: the approximation of a three-dimensional structure by a two-dimensional model; the removal of part of the gravity effects of deeper structures as part of the regional field; and the designed propensity of the model for producing a simple structure.

The major feature seen is, of course, the contrast of the light material of the Round Lake Batholith against the denser material of the metasediments and metavolcanics to the north and south. The highest densities in the south lie under the Catherine Group basalts; somewhat lighter deep densities are indicated at depth at the location of the Nipissing diabase. It is interesting that lighter material is seen at depth north of the Round Lake Batholith; this may well be because the Otto Stock underlies this part of the profile (Jensen 1987). A vertical density contrast is clearly visible at or near the Kirkland–Larder Lake Fault Zone (the 2.5 km cell size does not permit accurate location).

Finally, for the sake of interest, Figures 290.8 and 290.9 show the fit and the density section (11M), respectively, of the model if the regional gravity is adjusted in the wrong direction by about 10 mGal; the simplest model fitting the data by the method is implausibly complex.

PROFILE 15 RESULTS

The density model used for profile 15 was a regular grid of rectangular cells, each 1000 m across by 1000 m deep. The grid is 21 cells across by 10 cells deep, and represents a cross-section of the Earth's crust 21 km across by 10 km deep. There is no vertical exaggeration on the grey scale plots used to display the density models for this profile. The data are obtained from the anomalous gravity contour map as described previously, at regular intervals of 500 m; there are, therefore, two points per cell along the surface on this profile. All the *caveats* and assumptions that were discussed above for profile 11 are also applicable here.

A fit of model to data with no surface density constraints for profile 15 yielded the fit shown in Figure 290.10, and the extremely bland density model (15U) shown in Figure 290.11. Most of the density contrast is localized on the east side of the model. Constraining the surface densities and adjusting the regional gravity as for profile 11 yielded the fit shown in Figure 290.12, and the more realistic model (15C2) shown in Figure 290.13. The layer of Proterozoic sediments of the Cobalt group is observed to overlap the lighter rocks of the Pontiac Massif, just as predicted.

DISCUSSION

In considering the above results, it is worth noting again that none of this structure has been put in a *priori* except for that known at the surface, in contrast to more conventional methods which, for example, must make assumptions about how many regions of different density exist prior to modelling. It is also worth noting that it is quite possible for Nature to have produced a more complicated model than is recovered here, especially on small scales; the above density models are not meant to be exact models of the Earth's density distributions—no method based on surface gravity measurements can achieve that. They are meant to represent the simplest structures (in a strictly defined sense) that are consistent with the surface data. In particular, very deep structures are not clearly seen, because the information content of the residual gravity maps is reduced with increasing depth, for the reasons discussed above.

REFERENCES

Bailey, R.C., and Reford, S.W.
1987: Improved Computer Interpretation of Gravity and Magnetic Data; p.176-182 *in* Geoscience Research Grant Program, Summary of Research 1986-1987, edited by V.G. Milne, Ontario Geological Survey, Miscellaneous Paper 136, 241p.

Jensen, L.S.
1985: Stratigraphy and Petrogenesis of Archean Metavolcanic Sequences, Southwestern Abitibi Subprovince, Ontario; p.65-87 *in* Evolution of Archean Supracrustal Sequences, edited by L.D. Ayres, P.C. Thurston, K.D. Card, and W. Weber, Geological Association of Canada, Special Paper 28, 380p.

Naudy, H., and Dreyer, H.
1968: Essai de Filtrage Non-lineaire Applique aux Profils Aeromagnetiques; Geophysical Prospecting, Volume 16, Number 2, p.171.

Grant 291 Evaluation of Geobotanical Remote Sensing as an Aid to Mineral Exploration in Northeastern Ontario

A.E. Beswick, P.J. Beckett, G.M. Courtin, and G.O. Tapper

Centre in Mining and Mineral Exploration Research, Laurentian University, Sudbury

ABSTRACT

Bedrock mapping, and sampling of A and B horizon soils and a variety of vascular and nonvascular plant species have been carried out in southern Haultain Township near Gowganda, where silver with cobalt-nickel arsenide mineralization is exposed on surface, and 35 km to the west in Kelvin Township where base metal anomalies have been reported in the overburden. Soil and vegetation samples have been analyzed by AA spectrometry for Fe, Mn, Cu, Ni, Co, Pb, Zn, and As. In both areas, microclimatic data have been obtained at two adjacent sites with differing elevations. Relationships between all data have been statistically evaluated and found to be complex. Airborne MEIS multispectral digital imagery were also acquired for the Kelvin Township site at a spatial resolution of 1.06 m, in five 0.010 μm spectral bands centred at 0.680, 0.713, 0.753, 0.782, and 0.792 μm. At six different locations within the Kelvin site, essentially pure stands of trembling aspen (*Populus tremuloides*) were sampled for leaves, twigs, trunk wood, and roots. The associated A and B horizon soils were also sampled. In addition, more than 200 nonvascular plant samples and underlying humus soils were collected for base metal analysis. The six aspen stands identified in the field were located on colour infrared airphotos and precisely located on a surveyed 10 m grid. Base metal analytical data for soils collected at two of the six locations indicate that they are anomalous, whereas the remainder are not. The ground-based information has been applied to develop a supervised classification of the MEIS digital imagery, using a PCI micro-based image processing system. Preliminary results indicate the ability to identify anomalous reflectance among the aspen vegetation located over base metal soil anomalies.

INTRODUCTION

The potential applications to mineral exploration of digital imagery, obtained from a variety of airborne and spaceborne remote sensor systems, have been investigated by a number of workers for more than a decade. Significant improvements have been realized both in sensor capability, and in the hardware and software used to process the images they obtain. The most successful applications have been developed using imagery obtained from high spectral and spatial resolution airborne systems, especially for mapping rock types, soils, and hydrothermal alteration assemblages in areas where these materials are exposed directly on the earth's surface (for example, Vane and Goetz 1988).

Similar image analysis for heavily vegetated terrains can only reveal useful geological information indirectly via variations in the spectral characteristics of the vegetation cover. Contemporary remote sensors have the ability to distinguish between various plant species and communities present on the imagery. It is well known that certain species and communities have affinities for soils with various geochemical characteristics. These affinities increase the complexity of their spatial distribution. Plant distributions are also strongly influenced by non-geological environmental factors such as topographically induced microclimatic differences or variations in soil moisture content due to physical differences in the underlying soils (Beswick *et al.* 1987). Interpretation and analysis of remotely sensed imagery thus requires a thorough understanding of both the ecology and the geology of the area under investigation. This project is concerned with the development of such an understanding, and has several component objectives that involve both field and laboratory work combined with the analysis of remote sensor data.

OBJECTIVES

The overall objective of this project has been to determine the relationships between spectral reflectance changes in vegetation, and either metal-induced stress or enhanced growth related to metallic mineral occurrences, as detected by remote sensing techniques. The aim is to develop a scientific basis for the use of geobotanical remote sensing techniques as an aid to mineral exploration in areas of glacial and residual overburden having heavy vegetation cover. The primary objectives are to:

1. understand the geochemical and biochemical processes involved in the release and uptake of various metals from rock and overburden into the various species and tissues (roots, trunk or stem, leaves and fruit) of vascular (trees and shrubs), and nonvascular (lichens, mosses and fungi) plants
2. determine the effects of metal-induced stress or enhanced growth on the chemical, structural, and spectral characteristics of vascular and nonvascular plants
3. determine the effects of ecological factors on plant spectral characteristics and to distinguish these, as far as possible, from metal-induced effects
4. characterize spectral responses of a variety of plant species in areas with and without anomalous metal concentrations
5. determine the nature of temporal shifts in vegetation spectral responses in mineralized areas, in order to optimize the use of seasonally acquired, remotely sensed data for mineral exploration in vegetated terrains

With these objectives in mind, a set of closely integrated field and laboratory studies have been carried out over the past two years. It was the original intention to focus all aspects of the field work,

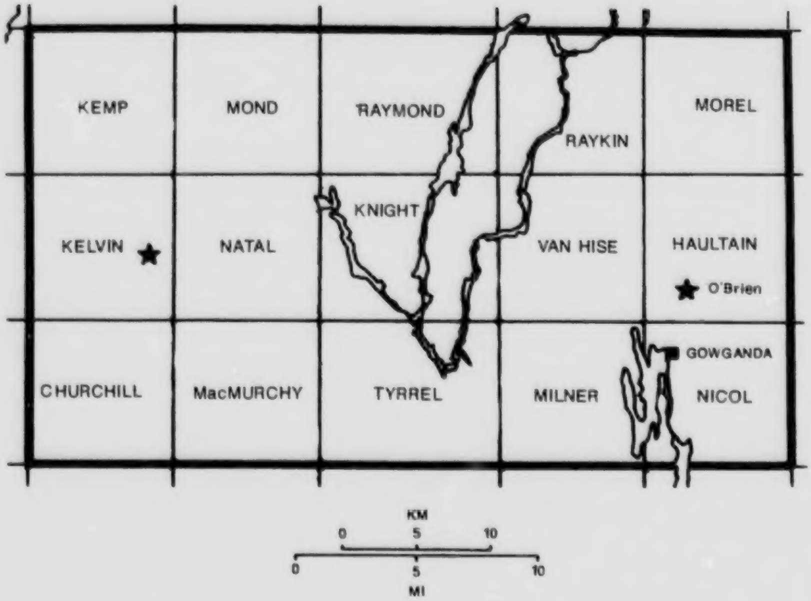

Figure 291.1. *Township map for a portion of northeastern Ontario (Gowganda area) with the geobotanical sites indicated by stars.*

and to acquire remotely sensed multi-spectral and multi-temporal digital imagery in the Gowganda area of northeastern Ontario, on and around the Agnico Eagle silver property, which we refer to as the Kilpatrick Lake site. As indicated by Beswick *et al.* (1987), the Kilpatrick site was adequate to meet some of the initial objectives but proved inadequate for others. This being the case, work over the past year has been focused instead on a site in Kelvin Township some 35 km to the west of the town of Gowganda, here referred to as the Katie Lake site. The two sites have been located on Figure 291.1. A detailed description of the Kilpatrick Lake site was presented by Beswick *et al.* (1987), along with a summary of work carried out and results obtained up to June, 1987. An update of this information is summarized below. A description of the work carried out and the results obtained to date for the Katie Lake site follows.

THE KILPATRICK LAKE SITE

Site Description

This site covers an area of approximately 1 km^2 and is located some 4 km to the northeast of Gowganda, adjacent to the abandoned Capital Mine. The southern half of the site is underlain by Archean mafic volcanics; these are unconformably overlain by greywackes of the Coleman Member of the Gowganda Formation, in the northern half of the site. These greywackes host the Capital Mine silver deposit and several cobalt arsenide veins, which have been exposed by recent trenching near the abandoned mine shaft at the top of the slope. Details of the geology of the area can be found in a report by McIlwain (1978).

Three major plant communities are found within this area: almost pure stands of trembling aspen (*Populus tremuloides*); almost pure stands of black spruce (*Picea mariana*); and mixed wood stands of balsam fir (*Abies balsamea*), white spruce (*Picea glauca*), white birch (*Betula papyrifera*), and trembling aspen, with speckled alder (*Alnus rugosa*) as the main understory shrub. A and B soil horizons are well developed over most of the site.

Field Work and Results

On the site and in the surrounding area 90 A horizon and 130 B horizon soil samples, as well as 1007 vascular plant parts (leaves, needles, twigs, etc.) and 100 nonvascular plant samples were collected. Two weather station masts 14 m in height and 400 m apart, with an elevation difference of 10 m, were established on the site to collect various microclimatic data, from the top of the tree canopy down into the soils.

All soil and vegetation samples have been analyzed by atomic absorption spectrometry (AA) techniques for Cu, Ni, Co, Mn, Pb, Zn, and As. The relationships between metal levels in various plant species, different plant tissues, and the A and B soil horizons have been examined statistically, and the results summarized below.

Vascular Plants

The vascular plant-soil metal relationships have been evaluated for the three major tree canopy species; balsam fir, white birch, and trembling aspen. Metal levels in all plant parts are more strongly correlated with those in the A rather than the B soil horizons, particularly for arsenic in A and B soils, and for nickel and cobalt in A soils. The A horizon soils in

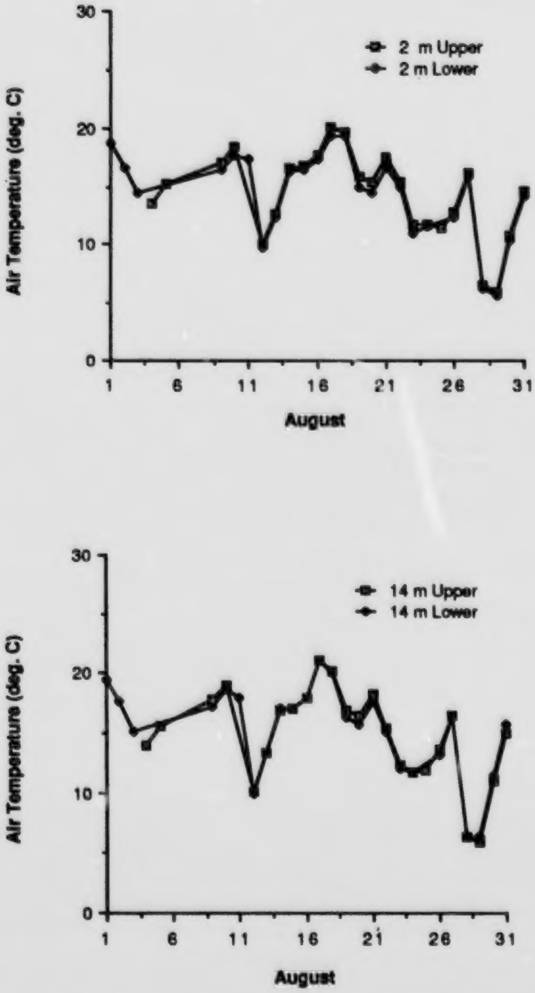

Figure 291.2. Air temperature data for the month of August at two heights within the canopy for both weather stations on the Kilpatrick Lake site.

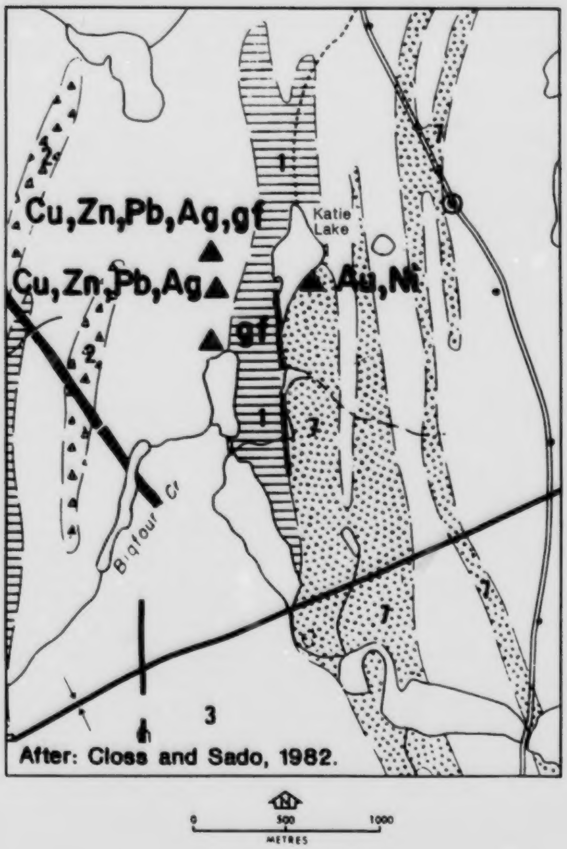

Figure 291.3. Bedrock geology of the Katie Lake site in Kelvin Township, taken from Closs and Sado 1982.

almost every case have higher metal concentrations than the underlying B soils. For all metals except lead, and particularly for arsenic, strong positive correlations exist between levels in roots, and in needles or leaves, in each species.

Nonvascular plants

Fungi growing on the ground and on trees have been sampled and analyzed along with their respective substrates. The results indicate that many metals, particularly cobalt and arsenic, are strongly enriched in mushrooms compared to their substrates but the enrichments are not linear. Overall, the results suggest that mushrooms have the potential to form a useful geobotanical tool. In particular, fungi found on trees may have wider use than ground growing mushrooms because they are present throughout the year and thus may be sampled at any time. The tree substrate often contains much lower metal amounts than the humus layer, but since most arboreal fungi are long lived there is the potential to accumulate relatively large amounts of metal.

Microclimate

Microclimatic data for three summer months have been assembled for the Kilpatrick Lake site from the two weather stations. These data indicate (Figure 291.2) that there is no significant difference between the air temperatures measured at the two stations, either at the top of the canopy (14 m) or at standard screen height (2 m), suggesting that there is little likelihood that microclimatic differences across the site can effect plant metabolism sufficiently to cause detectable differences in vegetation spectral reflectance characteristics. A more detailed investigation of microclimatic effects has been carried out at the Katie Lake site (see discussion following) in order to determine if this conclusion is sustainable.

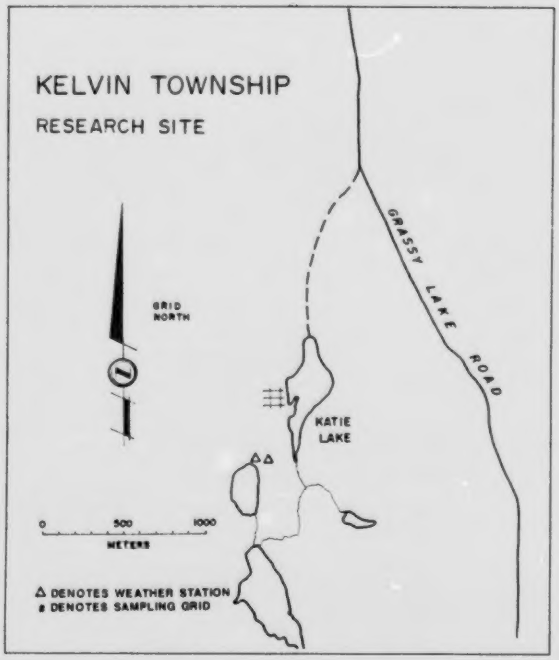
KELVIN TOWNSHIP
RESEARCH SITE
GRID NORTH
GRASSY LAKE ROAD
KATIE LAKE
0
500
1000
METERS
Δ DENOTES WEATHER STATION
# DENOTES SAMPLING GRID

Figure 291.4. Map of Kelvin Township site indicating the position of the intensive sampling grid and two weather stations.

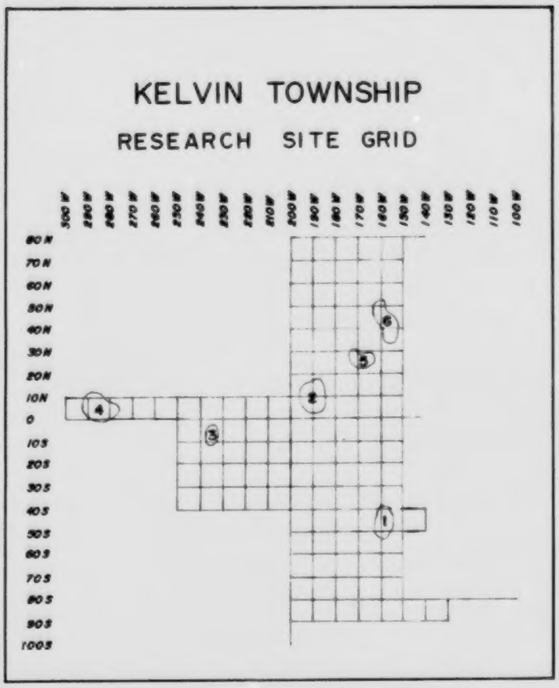
KELVIN TOWNSHIP
RESEARCH SITE GRID
300W
290W
280W
270W
260W
250W
240W
230W
220W
210W
200W
190W
180W
170W
160W
150W
140W
130W
120W
110W
100W
80N
70N
60N
50N
40N
30N
20N
10N
0
10S
20S
30S
40S
50S
60S
70S
80S
90S
100S
1
2
3
4
5
6

Figure 291.5. Ten-metre sampling grid for the Katie Lake site in Kelvin Township.

THE KATIE LAKE SITE

Site Description

The site is located on the west side of a small unnamed lake in Kelvin Township which we have called Katie Lake (Figure 291.3). The site is underlain by ultramafic to felsic metavolcanics associated with minor amounts of intrusive felsic rocks which have been extensively intruded by later diabase dikes. Metal anomalies in the overburden of the area appear to be closely associated with serpentinized komatiites and basaltic komatiites. These contain high nickel and chrome values (~595 ppm and 1550 ppm, respectively), as well as other high base metal concentrations (Sado and Clarke 1974). For details of the bedrock and overburden geology and geochemistry the reader is also referred to Closs and Sado (1982), and Carter (1986).

The vegetation cover over the site is dense and diverse, with different major plant communities being associated with undulating topographic highs and lows, and different moisture regimes. The gentle slopes of the northern section are covered with mixed stands of trembling aspen, white birch, balsam fir, and spruce. The trees are mostly mature, with trembling aspen reaching heights of 30 m. Depressions are filled with swamp species such as speckled alder and white cedar. Prominent rocky ridges, especially at the southern end of the site, are covered by jack pine with an understory of abundant lichens. Mosses and lichens also occur in clearings in the mixed aspen stands.

Field Work

Two field trips, each of two weeks duration, were undertaken in June and August/September of 1987, to collect samples of bedrock, A and B horizon soils, and vascular and nonvascular plants over the site.

At six different locations within the overall site, essentially pure stands of trembling aspen (the most dominant tree species in the area) were identified. Within each of these stands, five such trees were sampled for leaves, twigs, trunk wood, and roots; that is, 120 plant parts (respective A and B horizon soils were also sampled for each tree). In addition, more than 200 nonvascular plant samples and underlying humus soils were collected over the site for base metal analysis.

Two 14 m weather station masts were also established on the site (Figure 291.4) during the summer of 1987; one on a glacial outwash terrace at an elevation of 308 m, and one on an adjacent ridge with a gravelly till overburden and an elevation of 328 m. Both locations are populated with jack pine of the same age (67 yrs.). A variety of microclimatic data have been assembled.

The six aspen stands identified in the field were also located on colour infrared airphotos, and on the Multispectral Electro-Optical Imaging Scanner (MEIS) digital imagery supplied by the Ontario Centre for Remote Sensing. The stands were also precisely located on a surveyed 10 m grid (Figure 291.5).

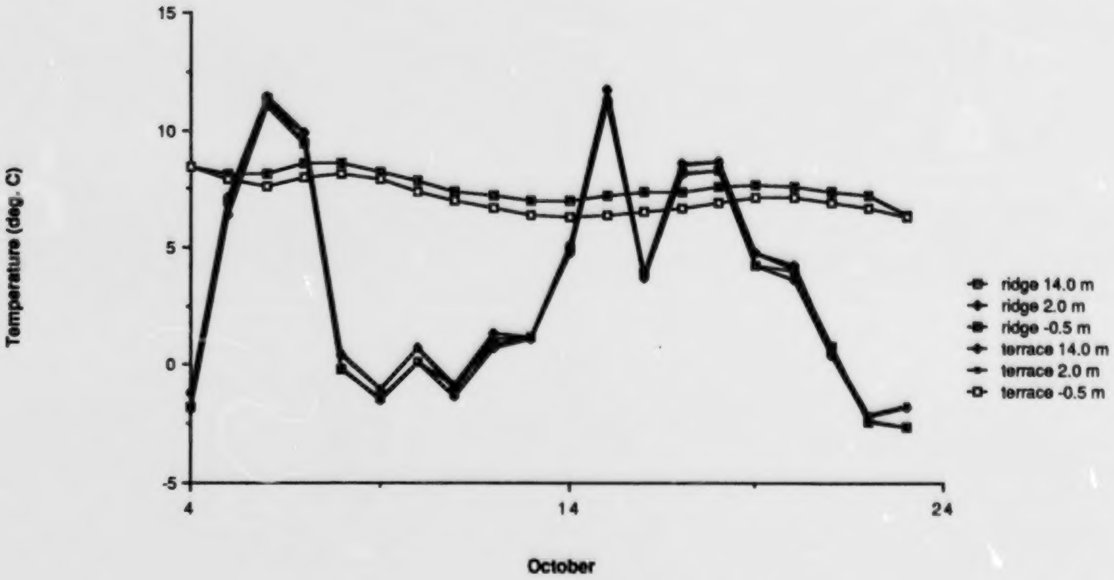

Figure 291.6. *Comparison of air and soil temperature for a gravelly till ridge, and an adjacent outwash terrace for the period October 4 to 24, at Katie Lake.*

TABLE 291.1: TOTAL METAL CONTENT (ppm) OF A_0 SOILS FROM THE SIX TREMBLING ASPEN STANDS AT KATIE LAKE. VALUES REPORTED ARE MEANS OF FIVE REPLICATES AND THE CORRESPONDING PERCENT COEFFICIENT OF VARIATION (CV).

STAND	Cu	CV	Ni	CV	Co	CV	Pb	CV	Zn	CV	Mn	CV	As	CV
1	28	25.4	153	57.7	14	27.8	86	20.5	73	56.8	1477	58.2	3	40.4
2	24	27.8	50	53.0	10	59.3	90	34.4	142	44.8	708	61.9	2	20.4
3	25	10.8	104	13.8	18	34.2	118	22.9	395	38.6	2187	77.2	6	6.8
4	14	23.3	19	22.5	4	38.9	51	37.7	116	40	442	66.3	2	32.5
5	29	7.6	195	29.5	41	15.3	81	28.3	353	17.2	4551	30.3	6	11.0
6	27	29.4	52	51.1	12	70.8	134	29.8	208	73.8	2773	64	3	48.8

RESULTS

Vascular Plants

All of the 120 vegetation samples have been dried and ground in preparation for chemical analysis. The organic A0 horizon soils associated with the trees sampled have been analyzed for Cu, Ni, Co, Mn, Pb, Zn, and As by atomic absorption methods (Table 291.1). These values compliment the preliminary data for some 30 A and B soils collected in June 1987, from two transects run across the site, and centred over the base metal anomaly reported by Closs and Sado (1982).

The analytical results obtained to date have confirmed the selection of two suitable control aspen stands; one with low background values for all metals analyzed, and another stand with anomalously high metal levels (stands 4 and 5, respectively; Figure 291.5). The latter also appears on the MEIS imagery as an anomalous signature (see discussion following).

Nonvascular Plants

One hundred and sixty mushrooms, plus their associated substrates, were collected using the same grid as that for higher vegetation. Mushroom and substrate sample preparation and metals analysis, as well as an evaluation of the results, will be completed prior to April 1989.

Microclimate

Despite the vertical relief separating the two sites, little temperature difference was observed, even at a time when diurnal fluctuations were quite marked. Air temperatures taken at 14 m and 2 m above ground, and soil temperatures taken at a depth of 0.5 m, were recorded for a 20 day period during October, 1987. The results (Figure 291.6) indicate that air temperatures at the two locations were virtually identical, and soil temperatures varied by less than a degree, with the terrace being cooler than the ridge.

The moisture status of the soils varied over the measurement period between a maximum water hold-

TABLE 291.2: MOISTURE STATUS OF JACK PINE SHOOTS, AND OF THE ORGANIC AND MINERAL SOIL HORIZON, FOR A GRAVELLY TILL RIDGE AND AN ADJACENT OUTWASH TERRACE, AT KATIE LAKE, ONTARIO.

			GRAVELLY TILL RIDGE		
	ORGANIC HORIZON VEGETATION		MINERAL HORIZON		
DATE	MOISTURE $g^{H20}/g^{MATERIAL*}$	POTENTIAL (bar)	MOISTURE $g^{H20}/g^{MATERIAL*}$	POTENTIAL (bar)	POTENTIAL (bar)
20 Aug.	0.50	-4.5	0.12	-18.0	
26 Aug.	1.05	>-0.3	0.17	-3.7	-15.4
26 Sept.	0.85	>-0.3	0.15	-4.0	19.6
24 Oct.	2.30	>-0.3	0.18	-2.5	
			OUTWASH TERRACE		
20 Aug.	0.55	-27.0	0.08	-21.0	
26 Aug.	1.14	-0.5	0.08	-21.0	-20.0
26 Sept.	0.89	-5.2	0.10	-14.4	-20.8
24 Oct.	1.85	>-0.3	0.21	-1.5	

* dry weight

ing capacity of >-0.3 bars, and an extreme drought of -27.0 bars, with the terrace soils being generally drier than those on the ridge (Table 291.2).

Tissue water potentials from both sites measured during August and September 1987 ranged from -15.4 to -20.8 bars (Table 291.2). Whereas for most tree species values lower than -15 bars would lead to death from drought, jack pine and many other conifers are capable of withstanding such dry conditions without injury. Thus, these low values are not thought to have produced any limiting stress condition, nor is the range between the two locations expected to result in any physiological differences that could be detected by remote sensors.

Wind speeds on the ridge (~3.1 m/s) were found to be significantly higher than on the terrace (~2.2 m/s). Over a long period of time such differences might be expected to alter the morphology of the tree canopies and effect changes in the spectral reflectance. No measurable differences were observed in needle length or in needle colour between the two sites, however, terrace trees were generally found to be 4 m taller than those on the ridge.

Metal levels in soils and jack pine needles are listed in Table 291.3. The results indicate that for the terrace soils all metals have concentrations less than 100 ppm, whereas the ridge soils have relatively elevated levels for nickel (579 ppm), zinc (474 ppm), and manganese (493 ppm), with cobalt, copper, and lead levels all less than 100 ppm.

Metal levels in jack pine needles at the two locations indicate that the only major difference is in manganese values. Although the terrace needles are manganese enriched by 4 times the level in their soils, the ridge needles still contain 2.5 times the levels in the terrace needles.

In summary, of all the parameters measured for the two locations, the only significant differences appear to be in the manganese levels in the jack pine needles. Any differences which might exist in the MEIS spectral signatures of the jack pine (yet to be evaluated) must therefore be attributable to differences in needle metal levels, and not to one or more microenvironmental factors.

Remote Sensing

In parallel with the above field studies, digital image data for the Katie Lake site was examined using a PCI-IMAVISION (EASI/PACE) system, installed on a microcomputer (IBM-AT). For further information concerning the system the reader is referred to the PCI-IMAVISION EASI/PACE Operator's Manual (PCI Inc. 1987).

The imagery used in this study (Tapper and Dempsey 1988) has a 1.06 m spatial resolution, in five extended, red and near infrared, spectral bands centred at 0.680, 0.713, 0.753, 0.782, and 0.792 μm, each approximately 0.010 μm in width. These data were acquired in mid-1984 by the Canada Centre for Remote Sensing's (CCRS) MEIS II push-broom scanner. These bands sample only the rise portion of the vegetation spectra, between the low point of the spectra at the chlorophyll absorption band located at 0.670 μm, and the peak or "red shoulder" of the spectra at 0.800 μm. This region is important for detection of any so called "red edge" effects between "stressed" and "unstressed" vegetation (Horler *et al.* 1982; Horler *et al.* 1983). The lack of visible wavelength data makes conventional band ratio analysis unusable and unreliable (Curran 1983), therefore, preliminary image analysis to date has consisted of several image enhancement technique sequences to classify the imagery. These were: radiometric enhancements of the data; and, unsupervised and supervised classifications of the data set. Band ratios of the data have been used, however, to determine the clustering accuracy of classification routines.

TABLE 291.3: CONCENTRATION (ppm) OF SIX METALS IN THE MINERAL SOIL AND IN JACK PINE NEEDLES ON A GRAVELLY TILL RIDGE AND AN ADJACENT OUTWASH TERRACE, AT KATIE LAKE, ONTARIO.

	MINERAL SOIL		NEEDLES	
METAL	RIDGE	TERRACE	RIDGE	TERRACE
Cu	37	6	4	4
Ni	579	52	17	59
Co	64	13	1.5	1
Pb	15	5	2	2
Zn	474	14	57	41
Mn	493	60	538	225

The radiometric enhancement of the Katie Lake data did not provide good separation between the spectral signatures of the "background" and "anomalous" aspen sites. The enhancement procedure, however, was successful in separating the overall general aspen signature from the other vegetative cover on-site.

Histograms of pixel radiance (brightness) values for the aspen data in the five spectral bands indicated a tendency to bimodality, suggesting it might be possible to discriminate between background and anomalous signatures via an unsupervised classification of the data set (PCI Inc. 1987). The results of the unsupervised classification for Katie Lake imagery showed that the pixel radiance numbers for the background and anomaly training sites were too similar to be well discriminated by this technique.

On the basis of these results, a supervised classification, which makes full use of all "ground truth" and field data to "train" the computer on designated background and anomalous segments of the imagery, was decided upon as the vegetation cover classification method.

The supervised classification of the Katie Lake MEIS data was successful in delineating "background" aspen on the image, and in identifying potentially "anomalous" aspen signatures. One of these anomalous signatures coincides closely with the area of anomalous soil and vegetation geochemistry obtained to date. Other vegetation cover types (jack pine and areas of mixed swamp species) were also classified and their signatures identified.

The resultant supervised classification is presented in Chart A (*in pocket, inside back cover*). The control category of aspen is displayed as a light green colour; the anomaly aspen as bright red. Other categories of land cover also can be identified: jack pine is dark green; alder-cedar-balsam fir swamp is black; and water is medium blue. Several areas of extremely bright high radiance pixels are displayed as white and were unclassified, that is, their spectral signatures do not fall within the ranges defined by the designated training sites.

To date, preliminary analysis of the digital imagery, in conjunction with overburden geochemical data for the site obtained thus far (and that taken from Sado and Clarke 1974, and Singhroy *et al.* 1985), suggests that several of the aspen stands referred to above are located over base metal soil anomalies, whereas others are located in areas with background base metal levels. Base metal analytical data for soils collected at two of the six locations appear to confirm these suggestions. Further confirmation is expected with analysis of the remainder of a matrix of botanical samples (roots, wood, twigs, and leaves or needles) and soil samples from on-site locations.

EXPERIMENTAL WORK

In addition to the field, analytical, and image processing results reported above, relevant experimental work has been carried out in the laboratory on three fronts. The spectral reflectance effects of nickel and copper toxicity on vascular (white birch) (Courtin *et al.* 1987), and nonvascular plants (caribou lichen) (Beckett and Courtin 1987), have been studied under controlled environmental conditions by comparing the results from plants watered with aqueous metal salt solutions of various concentrations, with the results from those watered with pure water. In addition, these effects have been monitored in the laboratory using two different portable spectrometers in order to evaluate their relative merits for use in taking spectral measurements in the field (McDonald *et al.* 1988). Furthermore, one portable spectrometer has been evaluated in the field in terms of the various ways vegetation spectral measurements might best be made on the ground (Tapper *et al.* 1987). These studies indicate that significant spectral response effects are recognizable, at least in white birch, when nickel levels in their tissues exceed 27 ppm, and in lichens when copper levels reach ~100 ppm.

SUMMARY AND CONCLUSIONS

The work at Kilpatrick Lake amply illustrates the complexity of vascular and nonvascular plant tissue-soil metal relations. Overall, it can be said that for vascular plants readily visible to remote sensors, the metal levels in their soils are best reflected in balsam fir, white birch, and aspen. This is particularly true for arsenic in A and B horizon soils, and for nickel and cobalt in A horizon soils.

It appears that nonvascular plant metal contents may be sensitive indicators of soil metal anomalies, particularly for arsenic, cobalt, and copper; and further, that long lived arboreal fungi are more effective (over the long term) than seasonal ground mushrooms in concentrating metals relative to their substrates.

Microclimatic data for the site suggests that in relatively gently undulating terrains typical of the Canadian Shield, variations in environmental factors such as temperature, soil moisture, plant tissue water potentials, and wind velocity are not sufficient to distinguish appreciable differences in the spectral responses of any particular tree species growing in the range of different microenvironments.

These conclusions are generally supported by work carried out at the Katie Lake site where, in addition, an examination of MEIS digital imagery data suggests that recognizable differences exist between the spectral signatures of aspen trees growing in metal enriched soils, and those with background base metal levels.

Experimental work carried out in the field and in the laboratory suggests that significant spectral response effects are recognizable, at least in white birch, when nickel levels in their tissues exceed 27 ppm, and in lichens when copper levels reach ~100 ppm. The results of such experiments also indicates that significant differences can arise in vegetation spectral reflectance measurements made in the field or in the laboratory, depending on the instrument used and the methodology employed to take the measurements.

In summary and overall, these results support the suggestion that biogeochemistry in combination with spectral geobotany have a valid role to play as mineral exploration tools, provided that the explorationist takes care to be aware of the complexities involved in interpreting the geochemical, ecological, and digital imagery data at hand.

FUTURE WORK

Analytical data for the balance of vegetation samples collected at the Katie Lake site in 1987 is currently (June 1988) being acquired, and will be completed and evaluated before the end of March 1989. Further field sampling of soils and aspen for chemical analysis will be conducted in the summer of 1988 at the Katie Lake site, in locations as yet not sampled but identified as anomalous from the supervised classification of the MEIS imagery. Improvements in the methodology of the image processing techniques applied to the MEIS data will be ongoing as further soil and plant metal analyses are obtained. The improved methodology, based on the integration of all soil and vegetation analytical data with the MEIS spectral characteristics for the six aspen stands at the Katie Lake site, will also be defined prior to March 1989. It is also planned to obtain and evaluate new MEIS imagery for the Katie Lake site, with a wider range of spectral bands, so that temporal effects and additional spectral band data can be evaluated for targeting base metal enriched sites. Finally, an examination of Landsat Thematic Mapper (TM) imagery over the site will be undertaken to evaluate the effects of reduced spatial and spectral resolution.

ADDENDUM

Chart A (Located in back pocket). The photograph depicts the Katie Lake site and represents the "supervised classification" of the MEIS II data. The different colours on the photograph show the distribution of he different cover types. Also shown are the 10 m sampling grid, and the location of the six trembling aspen stands.

REFERENCES

Beckett, P.J., and Courtin, G.M.
1987: Spectral Reflectance From Lichen Treated With Copper; p.661-666 *in* Proceedings, ERIM 5th Thematic Conference on Remote Sensing for Exploration Geology, Environmental Research Institute of Michigan, Reno, Nevada, 1987, 835p.

Beswick, A.E., Beckett, P.J., Courtin, G.M., and, Tapper, G.O.
1987: Remote Sensing and Geobotany as an Aid to Mineral Exploration in Northern Terrains; Grant 291, p.183-199 *in* Geoscience Research Grant Program, Summary of Research 1986-1987, edited by V.G. Milne, Ontario Geological Survey, Miscellaneous Paper 136, 241p.

Carter, M.W.
1986: Geology of Cabot and Kelvin Townships, District of Sudbury; Ontario Geological Survey Report 249, 52p. Accompanied by Map 2470, scale 1:31 680 or 1 inch to 1/2 mile.

Closs, L.G., and Sado, E.V.
1982: Bedrock and Overburden Geochemistry Investigations in the Midlothian Lake and Natal Lake Areas, Districts of Sudbury and Timiskiming; Ontario Geological Survey, Study 24, 68p. Accompanied by five charts.

Courtin, G.M., Beckett, P.J., and Tapper, G.O.
1987:Shift in Spectral Response of Nickel-Loaded and Control Shoots of White Birch (*Betula papyrifera* Marsh); p.441-449 *in* Proceedings, ERIM 5th Thematic Conference on Remote Sensing for Exploration Geology, Environmental Research Institute of Michigan, Reno, Nevada, 835p.

Curran, P.J.
1983: Estimating Green LAI From Multispectral Aerial Photography; PERS, Volume 49, Number 12, p.1709-1720.

Horler, D.H.N., Dockray, M., Barber, J., and Barringer, A.R.
1982: Red Edge Measurements of Remotely Sensed Plant Chlorophyll Content, Report to the Commission on Space Research on Remote Sensing and Mineral Exploration, 10p.

Horler, D.N.H., Dockray, M., and Barber, J.
1983: The Red Edge of Plant Reflectance; International Journal of Remote Sensing, Volume 4, Number 2, p.273-288.

McDonald, M.K., Courtin, G.M., and Beckett, P.J.
1988: A Comparative Investigation of the Spectral Shift in Nickel-Treated White Birch and Copper-Treated Reindeeer Lichen Using the Barringer REFSPEC Spectrometer and the Barringer Hand Held Reflectance Radiometer; *in* Proceedings, ERIM 6th Thematic Conference on Remote Sensing for Exploration Geology, Environmental Research Institute of Michigan, Houston, Texas. In Press.

Mcllwaine, W.H.
1978: Geology of the Gowganda Lake–Miller Lake Silver Area, District of Timiskiming; Ontario Geological Survey Report 175, 161p. Accompanied by Maps 2348 and 2349, scale 1:31 680 or 1 inch to 1/2 mile.

PCI Inc.
1987: PCI-IMAVISION, EASI-PACE User's Manual, Version 3.2, Toronto, 200p.

Sado, E.V., and Clarke, W.A.
1974: Quaternary Geology of Halliday, Midlothian, Kelvin, Natal Townships and Parts of Churchill and MacMurchy Townships, Districts of Sudbury and Timiskiming; Ontario Geological Survey, Preliminary Map 957, Geological Series, scale 1:31 680 or 1 inch to 1/2 mile.

Singhroy, V.H., Sado, E., and Bruce, W.
1985: Spectral Geobotany in Glaciated Environments: Test over a Mineralized Till Site in Northern Ontario; p.701-702 *in* Proceedings, ERIM, 4th Thematic Conference on Remote Sensing for Exploration Geology, Environmental Research Institute of Michigan, Colorado Springs, Colorado, 792p.

Tapper, G.O., Courtin, G.M., and Beckett, P.J.
1987: Surrogate Spectral Reflectances of Vegetation Applied to Geobotanical Remote Sensing; p.545-554 *in* Proceedings, 5th Thematic Conference on Remote Sensing for Exploration Geology, Environmental Research Institute of Michigan, Reno, Nevada, 835p.

Tapper, G.O., and Demsey, D.
In Press: MEIS II and Surface Data Integration For Detection of Geobotanical Anomalies; *in* Proceedings, 6th Thematic Conference on Remote Sensing for Exploration Geology, Environmental Research Institute of Michigan, Houston, Texas.

Vane, G., and Goetz, A.F.H.
1988: Terrestrial Imaging Spectroscopy; Remote Sensing of Environment, Volume 24, Number 5, p.1-29.

Grant 294 Quaternary Geology and Geochemical Exploration in the Matheson Area

M.B. McClenaghan[1], **O.P. Lavin**[1], **I. Nichol**[1], **and J. Shaw**[2]

[1]Department of Geological Sciences, Queen's University, Kingston

[2]Department of Geography, Queen's University, Kingston

ABSTRACT

The Matheson area in northeastern Ontario is of great interest for gold exploration because it is similar geologically to the adjacent Timmins gold camp. Exploration in the area, however, is hampered by extensive and thick glacial overburden. For this reason, till geochemistry has become an important exploration method in the area. The use of till geochemistry is limited by a complex and poorly documented glacial stratigraphy. The primary objective of this study is to identify criteria for distinguishing the various till units in the area to make till geochemistry a more effective exploration method.

The first year of this study focused on the examination of lithological and multielement geochemical data for 24 overburden drillholes from the study area, to determine both local and regional till stratigraphy. Up to three separate till units were identified in the drillholes. The uppermost till unit in most drillholes appears to have an "acidic" geochemical composition, characterized by relatively high concentrations of SiO_2 and low concentrations of Cu and Ni; while underlying till units commonly have a "basic" geochemical composition, characterized by high Cu and Ni concentrations combined with relatively low concentrations of SiO_2.

The second year of this study, the results of which are described in this report, focused on the comparison of mineralogical and pebble lithological abundance patterns with the previously identified geochemical patterns. The compositions of the bedrock sources appear to be a major control on the mineralogical and pebble compositions of the tills, such that tills can be divided into two distinct types: "felsic", containing pebbles of mainly felsic to intermediate composition; and "mafic", containing pebbles of mainly mafic metavolcanic lithologies. The uppermost till unit in the area consistently has a felsic composition, while underlying till units commonly have mafic compositions. The felsic tills were most likely derived from the granitic and gneissic bedrock north of the study area. Mafic tills probably reflect the local greenstone bedrock and, being locally derived, are more reliable sampling media for exploration purposes.

In addition to the stratigraphic patterns observed, west to east changes in some mineral abundances and, more significantly, a decrease in the abundance of Paleozoic carbonate pebbles from west to east was found. This west to east pattern is displayed by all till units and, as a result, cannot be explained using the current models for ice flow patterns across the area.

INTRODUCTION

The primary objective of this study is to identify the stratigraphic relationships and genesis of the till units in the Matheson area using a variety of geochemical and geological characteristics of overburden samples collected by the Ontario Geological Survey (OGS) during the Black River–Matheson (BRIM) overburden drilling project. A better understanding of the regional Quaternary stratigraphy will make till geochemistry a more effective method in the search for gold deposits in the Matheson area.

The study area is located in the west-central portion of the Abitibi Greenstone Belt (Figure 294.1) and is underlain predominantly by mafic metavolcanic rocks. Two major shear zones strike west through the area and are defined by two major fault zones: the Destor–Porcupine, and the Pipestone. In the Matheson area, numerous gold deposits are associated with these two fault zones (Whittaker 1986).

The Quaternary stratigraphy of the Matheson area consists of a complex sequence of multiple till units separated by glaciolacustrine sediment. Two separate till units below the uppermost till have been discovered through the use of overburden drilling (Ontario Geological Survey 1986a, 1986b; Bird and Coker 1987; DiLabio *et al.* 1988), and are informally referred to as the middle till and the lower till to indicate their relative stratigraphic positions. The lower till has been recognized in only a few overburden drillholes, and is identified solely on the basis of its stratigraphic position below the two overlying till units. Glaciolacustrine and/or glaciofluvial sediment separate it from the overlying till units. An ice flow direction of 150° has tentatively been assigned to this lower till unit (Alcock, in preparation). The middle till unit has been observed in overburden drill cores and exploration pits. This till is commonly separated from the uppermost till by intervening glaciolacustrine sediment, informally referred to as the Owl Creek beds (DiLabio *et al.* 1988). Striations in the area indicating ice flowed toward approximately 240° have been tentatively related to the ice sheet that produced this till (Alcock, in preparation; Steele *et al.*, in preparation). The uppermost till unit, the Matheson till, was deposited during the Late Wisconsinan (Hughes 1959). Striations and landforms indicate that ice flowed toward approximately 170° during this time. Throughout most of the area, Matheson till is overlain by lacustrine clay and silt deposited in glacial lakes Barlow and Ojibway.

The effectiveness of till geochemistry in gold exploration in the Matheson area is limited by several factors related to the thick and varied overburden. These are summarized below:

1. The glacial stratigraphy is complex, including multiple till sheets that were probably related to

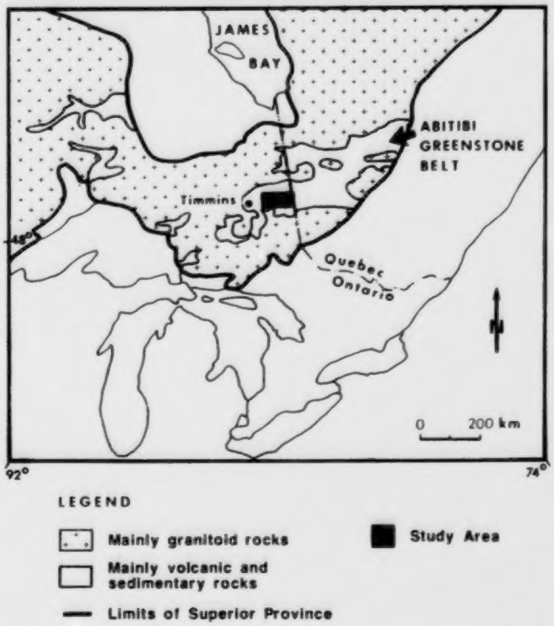
JAMES BAY
ABITIBI GREENSTONE BELT
Timmins
48°
Quebec
Ontario
0 200 km
92°
74°
LEGEND
Mainly granitoid rocks
Mainly volcanic and sedimentary rocks
Limits of Superior Province
Study Area

Figure 294.1. *Location of the study area in northeastern Ontario.*

more than one glacial advance and ice transport direction.

2. Knowledge of the subsurface stratigraphic relationships is severely limited by the thick and areallyextensive glaciolacustrine silt and clay deposits that blanket most of the area, and by the lack of surface exposures of till below this silt and clay cover.
3. Till units below the Matheson till are infrequently preserved, thus limiting examination and documentation of their characteristics.

These limitations are effectively made worse by the nature of reverse circulation drilling, the most commonly used overburden drilling technique in the area. This drilling method produces a chip and mud slurry in which all structures and most textures are destroyed, thus making the identification of separate till units and an interpretation of the stratigraphy extremely difficult or impossible.

The Ontario Geological Survey (OGS) is currently involved in a multidisciplinary multiyear project (BRIM) designed to assist and stimulate exploration in the Matheson area (Baker *et al.* 1985). A major component of the OGS project consists of overburden drilling and till geochemistry. The present study involves the examination of data and analyses of samples from the first two years (1984 and 1985) of the BRIM overburden drilling project in order to address the exploration problems outlined above. The results presented here were obtained during the second year of this study. Results from the first year of the study are presented in McClenaghan *et al.* (1987) and are summarized below.

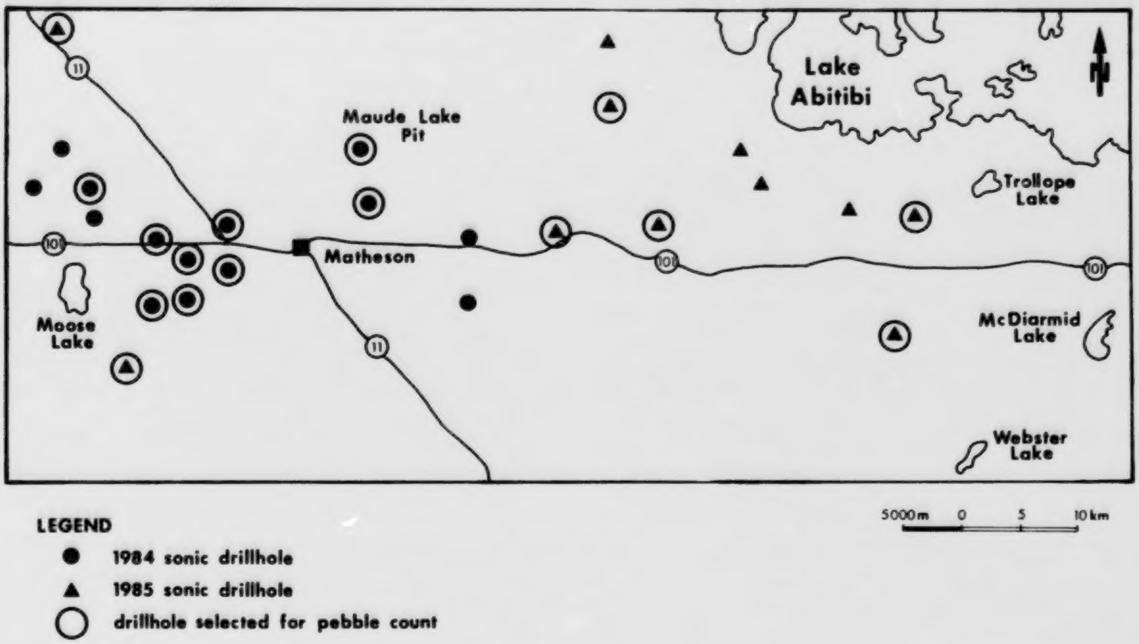
Lake Abitibi
Maude Lake Pit
Trollope Lake
Matheson
101
11
Moose Lake
McDiarmid Lake
Webster Lake
5000m 0 5 10km
LEGEND
1984 sonic drillhole
1985 sonic drillhole
drillhole selected for pebble count

Figure 294.2. *Location of the 24 selected drillholes and the Maude Lake pit.*

PREVIOUS WORK

Twenty-four BRIM overburden drillholes and a stratigraphic section exposed at the Maude Lake pit were selected for detailed examination (Figure 294.2). Data provided by the OGS for 282 till samples from these

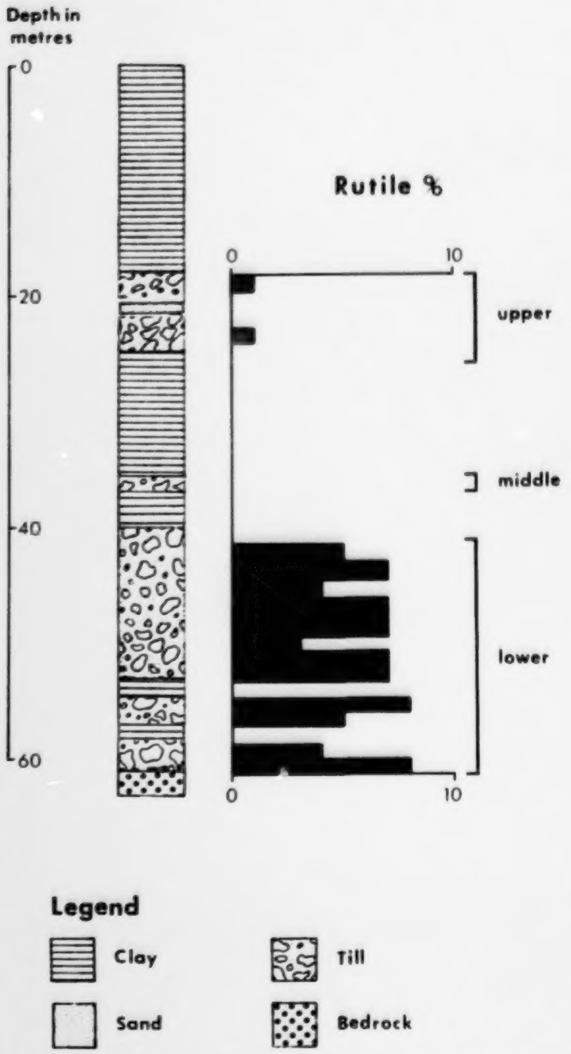

Figure 294.3. *Classification of till samples into till units, and rutile abundance in the till units of drillhole 84-28 (graphic log modified from OGS 1986a).*

drillholes and from the Maude Lake pit included drill logs, mineralogical data, textural data, and multielement geochemical data for three fractions. The three fractions that were analyzed geochemically are: a) the nonmagnetic heavy mineral concentrate, herein referred to as the heavy mineral fraction; b) the <0.063 mm fraction, herein referred to as the fine fraction; and c) the <1.7 mm fraction, herein referred to as the total matrix fraction. The first year of this study focused on till fabric analysis at the Maude Lake pit and the examination of the OGS multielement geochemical data (McClenaghan *et al.* 1987). The results are summarized below.

Beds of till in individual drillholes were grouped into units based primarily on their relative stratigraphic positions in the drillholes. For example, the uppermost till unit encountered in the drillholes was designated as the upper till unit and, where present, underlying till units were designated as middle and lower till units, as demonstrated in Figure 294.3. This method of classification provided the framework for the comparison of the geochemical data for the till units.

Fabric analysis was carried out on the lower till at the Maude Lake pit to determine the ice flow direction for this till unit. Results indicate that it was deposited by ice flowing toward approximately 240°.

Examination of the multielement geochemical data indicates that till samples can be classified into one of two distinctive geochemical groups, and that these two groups generally correspond to the relative stratigraphic position of the samples. Samples from the upper till unit, which are interpreted to be Matheson till based on stratigraphic position, generally have higher concentrations of SiO_2 and lower concentrations of Cu, Ni, and Co in all or most fractions. Tills of this chemical character have been termed "acidic" due to similarities between their relative chemical compositions and bedrock of "acidic" composition. Lower tills commonly have lower concentrations of SiO_2 and higher concentrations of Cu, Ni, and Co, and are referred to as "basic" tills.

The chemical differences observed allow relatively accurate discrimination between till units where the stratigraphy is based on concentrations of numerous elements. Intuitively, it would seem that some combination of the distinctive elements could be used to maximize the discrimination between the two geochemically distinct types of till. Multivariate statistical techniques were applied to test this possibility, both on a regional scale and a local scale. Discriminant function analysis was used with a subset of till samples that can be confidently distinguished based on stratigraphy. This approach provided only limited additional distinction between till samples when compared to selected single element comparisons. Ultimately, Cu in the fine and total matrix fractions and Ni in the heavy mineral fraction were determined to be the most efficient geochemical discriminators between till units. Upper till samples generally have concentrations of less than 30 ppm Cu in the fine fraction and less than 50 ppm Ni in the heavy mineral fraction. Lower till units generally have greater concentrations of Cu and Ni.

The empirical geochemical relationships recognized in these till samples suggest different bedrock sources for the chemically distinct till units. The mineral abundances in the heavy mineral concentrates and the lithological compositions of clasts in the till samples were examined and quantified during the second year of this study in order to compare them with the geochemical differences and assist in identifying potential bedrock source area differences. These results are presented below.

MINERAL ABUNDANCES IN HEAVY MINERAL CONCENTRATES

Mineral abundances in the heavy mineral concentrate were determined for OGS samples by a commercial laboratory (Overburden Drilling Management Limited, Nepean, Ontario). The data provided consist of abun-

TABLE 294.1. SUMMARY STATISTICS FOR DISCRIMINANT ANALYSIS OF THE MINERAL ABUNDANCE DATA.

Variables in Analysis	Step	Variable Added	% Classified Correctly	F-Value**	Degrees of Freedom
Garnet, Epidote,	1	Garnet	67.2	9.4	1,175
Pyroxene_L, Pyrite_L,	2	Pyroxene	65.5	8.0	2,174
Hornblende, Sphene,	3	Hornblende	72.3	8.6	3,173
Ilmenite, Hematite_L,	4	Epidote	71.2	9.0	2,172

L indicates log transformed

** F-Value is a statistical measure of the discrimination. Higher F-values generally indicate a statistically more significant discrimination. Actual significance can be read from standard statistical tables.

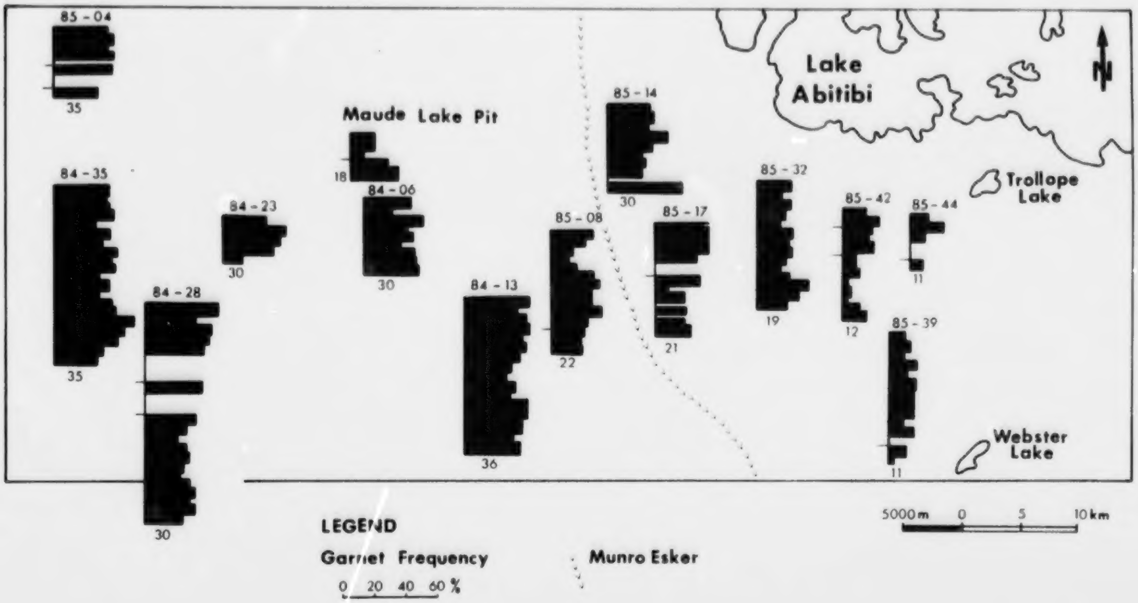

***Figure 294.4.** Abundance of garnet in the heavy mineral concentrate in till samples and average garnet abundance, reported at the bottom of each drillhole, for selected drillholes across the study area. In drillholes that contain multiple till units, the top of each till unit is indicated on the left side of each drillhole.*

dances of various mineral species present in 100 grain portions of the nonmagnetic heavy mineral fractions (specific gravity >3.3 g/cm^3) of individual till samples. Of the 13 mineral species identified in the heavy mineral concentrates, only 8 have been included in this study. Five mineral species have been excluded because their levels of abundance are too low to be of significance. The mineralogical data were examined using a variety of techniques. A description of the methods used and the results obtained are summarized below.

For some individual drillholes, mineral abundance patterns correspond to previously identified geochemical and lithological discontinuities, as shown in Figure 294.3, where rutile abundance in drillhole 84-28 is plotted. Based on the observed stratigraphy and geochemistry, this hole contains three till units. The highest rutile abundance corresponds to the lowermost till unit and, as indicated by the geochemical results, the middle till unit is similar in composition to the upper till unit.

Dramatic differences in mineral abundance often define contacts previously identified between till units (Figure 294.3); however, this is not universally applicable throughout the study area. In some cases, the abundance of individual minerals establishes discontinuities, while in others, the mineral abundance patterns do not correspond to geochemical and/or stratigraphic discontinuities.

Discriminant analysis was performed on the mineralogical data to determine, quantitatively, if there was a "best" combination of minerals for discriminating between till units on a regional scale, as was done with the geochemical data. Explanations of this multivariate statistical method and training group selection procedures are reported in McClenaghan *et*

a) Heavy Mineral Fraction

	Felsic	Mafic$_L$	Volc	Sed$_L$	Ultra$_L$	Paleo$_L$
Felsic						
Mafic$_L$	·					
Volc	-◉	-•				
Sed$_L$	·	·	-•			
Ultra$_L$	·	·	·	•		
Paleo$_L$	·	·	·	·	·	
Au$_L$	-•	·	•	·	·	·
As$_L$	·	·	·	·	·	·
Sb$_L$	·	·	·	·	·	·
Cu$_L$	-•	·	·	·	·	·
Zn$_L$	·	·	·	·	·	·
Co$_L$	·	·	·	·	·	·
Ni$_L$	-•	·	·	·	·	·
U	◉	·	-•	·	·	·
Ti	·	·	·	·	·	·
Zr	•	·	-•	·	·	·
W$_L$	·	·	·	·	·	·

d) Major Oxides

	Felsic	Mafic$_L$	Volc	Sed$_L$	Ultra$_L$	Paleo$_L$
Felsic						
Mafic$_L$	·					
Volc	-◉	-•				
Sed$_L$	·	·	-•			
Ultra$_L$	·	·	·	•		
Paleo$_L$	·	·	·	·	·	
SiO_2	•	•	-•	·	·	·
Al_2O_3	·	·	·	·	·	-◉
MgO_L	-•	·	·	·	·	·
CaO	·	·	·	·	·	•
Na_2O	·	·	·	·	·	·
K_2O	◉	·	-•	·	·	•
TiO_{2L}	-◉	·	•	·	·	-•
P_2O_5	·	·	·	·	·	•
MnO_L	-◉	·	◉	·	·	-•

b) Fine Fraction

	Felsic	Mafic$_L$	Volc	Sed$_L$	Ultra$_L$	Paleo$_L$
Felsic						
Mafic$_L$	·					
Volc	-◉	-•				
Sed$_L$	·	·	-•			
Ultra$_L$	·	·	·	•		
Paleo$_L$	·	·	·	·	·	
Au$_L$	·	·	·	·	·	·
As$_L$	-•	·	•	·	·	·
Cu$_L$	-◉	·	◉	·	·	·
Zn$_L$	-◉	·	•	·	·	·
Co$_L$	-•	·	•	·	·	-•
Ni$_L$	-◉	·	•	·	·	·
U	·	·	·	·	·	·
Ti$_L$	-•	·	•	·	·	·
Zr	•	·	-•	·	·	·

Felsic - Felsic to intermediate intrusives
Mafic - Mafic intrusives
Volc - Volcanics
Sed - Sediments
Ultra - Ultramafics

N = 162
L = log transformed

Correlation coefficients

●	> 0.8
◉	0.6 - 0.8
•	0.4 - 0.6
·	< 0.4
-	negative correlation

c) Total Matrix Fraction

	Felsic	Mafic$_L$	Volc	Sed$_L$	Ultra$_L$	Paleo$_L$
Felsic						
Mafic$_L$	·					
Volc	-◉	-•				
Sed$_L$	·	·	-•			
Ultra$_L$	·	·	·	•		
Paleo$_L$	·	·	·	·	·	
Au$_L$	·	·	•	·	·	·
As$_L$	·	-•	·	·	·	·
Cu$_L$	-◉	-•	◉	·	·	·
Zn$_L$	-◉	·	◉	·	·	·
Co$_L$	-◉	·	•	·	·	·
Ni$_L$	-◉	·	•	·	·	·
U	·	·	·	·	·	·
Ti$_L$	-◉	·	•	·	·	·
Zr	·	·	·	·	·	·

Figure 294.5. *Correlation coefficients for the pebble lithological data and the heavy mineral, fine, and total matrix fraction geochemical data.*

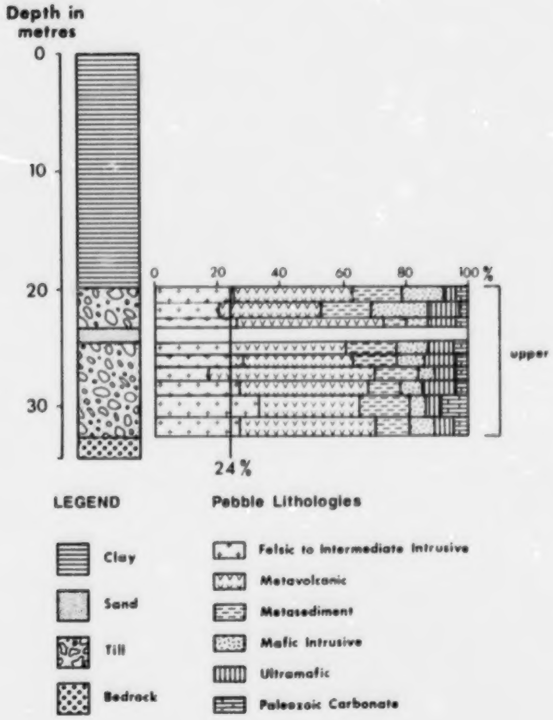

Figure 294.6. *Abundance of the six pebble lithologies in till samples from drillhole 84-06 (graphic log modified from OGS 1986a).*

al. (1987). As shown in Table 294.1, garnet is the most important discriminating mineral but results in only 67 percent of the training group samples being correctly classified into their respective till units. Other minerals add very little to the discrimination. This implies that: a) heavy mineral abundance is not a universally applicable means of discriminating till units; and b) a single mineral approach is only effective for discriminating till units in individual drillholes.

Despite its limited use as a stratigraphic marker, the mineralogical data can provide valuable information concerning the composition of the local bedrock source, which may not be readily apparent from the geochemical data. An example that has particular significance to exploration is discussed below.

Of the 24 drillholes included in the study, only 2 drillholes, which are 6 km apart, contain significant quantities of rutile in the lower till units. Interestingly, both drillholes also contain anomalous concentrations of gold grains in corresponding till samples. This unique combination of anomalous concentrations of rutile and gold in the lower tills of these two holes suggests the till was derived from the same or very similar bedrock source. The rutile is most likely derived from either a pegmatitic intrusion in mafic metavolcanic bedrock or a zone of carbonate alteration in mafic metavolcanic bedrock, as is commonly found associated with gold mineralization (C.J. Hodgson, Professor, Department of Geological Sciences, Queen's University, personal communication, 1988). A more detailed examination of the shape and colour of the rutile grains from these two holes may give an indication of: a) the source of the rutile, if it is indeed the same rock type for both drillholes; b) the composition of the bedrock source; and c) the distance of glacial transport of the rutile as compared to the gold grains.

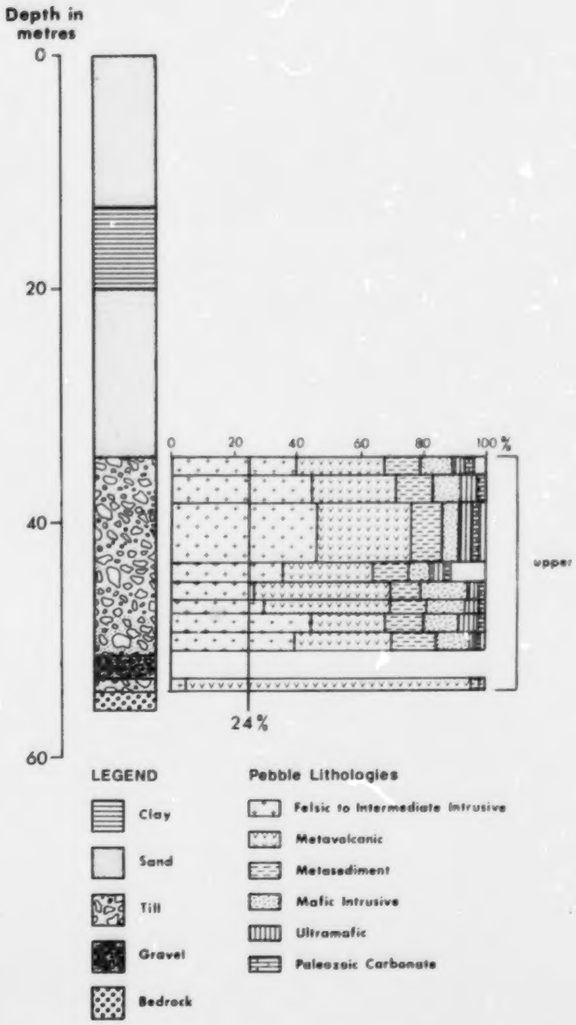

Figure 294.7. *Abundance of the six pebble lithologies in till samples from drillhole 85-14 (graphic log modified from OGS 1986b).*

Although regional stratigraphic relationships are weak in the heavy mineral abundance data, persistent lateral variations are apparent for selected minerals. As can be seen in Figure 294.4, garnet frequency in till samples decreases from west to east. A similar, but reversed, pattern exists for epidote (not illustrated). Initially this pattern may not appear to be conclusive; however, it is more definite than the stratigraphic patterns, remembering that garnet is the most effective mineral for stratigraphic discrimination.

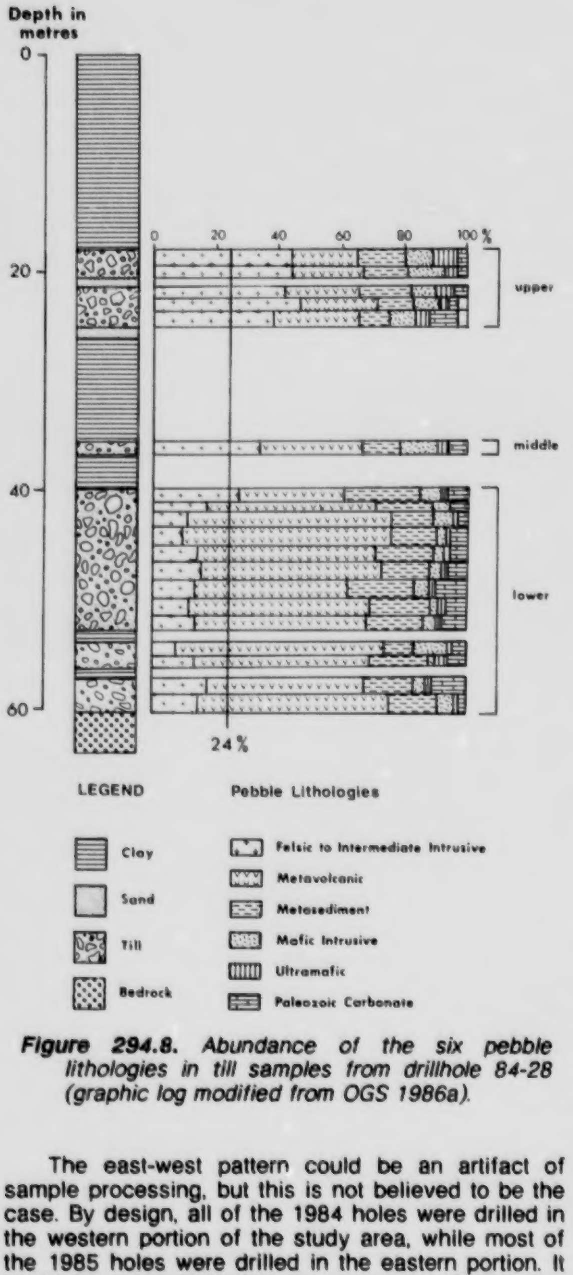

Figure 294.8. *Abundance of the six pebble lithologies in till samples from drillhole 84-28 (graphic log modified from OGS 1986a).*

The east-west pattern could be an artifact of sample processing, but this is not believed to be the case. By design, all of the 1984 holes were drilled in the western portion of the study area, while most of the 1985 holes were drilled in the eastern portion. It could be suggested that the east-west differences represent batch differences introduced by inconsistent mineral identification; however, two 1985 holes drilled in the western portion have mineral abundances similar to those of the surrounding holes drilled in 1984. In addition, similar, but more definite patterns are found for selected pebble lithologies, as is described in the following section. Therefore, these patterns are believed to reflect real differences between the tills in the east and those in the west.

PEBBLE LITHOLOGY ABUNDANCES

The abundance of various pebble lithologies for approximately 300 pebbles in the 4 to 90 mm size fraction of selected OGS till samples were documented for comparison with the geochemical results, to help distinguish between till units and to determine provenance. The size range for "pebbles", according to the Wentworth (1922) classification, is 4 to 64 mm; however, since the limiting diameter of the sonic core barrel is 90 mm, the term pebble is used here, for convenience, to refer to all clasts between 4 and 90 mm. Till samples from 15 drillholes and from a section at the Maude Lake pit, as shown in Figure 294.2, were selected to include a variety of stratigraphic sequences, including holes containing one, two, or three till units. Pebbles were classified into seven lithological categories: a) felsic to intermediate intrusive; b) mafic intrusive; c) metavolcanic; d) ultramafic; e) metasediment; f) Paleozoic carbonate; and g) "other". These lithologies reflect the major bedrock types found within the study area and to the north.

Results of the pebble classification indicate a strong correlation between the frequency of certain pebble lithologies and multielement geochemistry for the same sample intervals (Figure 294.5): Similar correlations are apparent in all three fractions; however, the fine and total matrix fractions have the strongest correlation with pebble abundance. Frequencies of felsic to intermediate intrusive pebbles are negatively correlated with Au, As, Cu, Zn, Co, Ni, Ti, MgO, TiO_2, and MnO, and are positively correlated with Zr, U, SiO_2, and K_2O. Contrastingly, the frequency of metavolcanic pebbles is positively correlated with Au, As, Cu, Zn, Co, Ni, Ti, MgO, TiO_2, and MnO, and are negatively correlated with Zr, U, SiO_2, and K_2O.

For individual drillholes, some pebble lithology frequency patterns correspond to previously identified geochemical and lithological discontinuities. Examples of this feature are shown in Figures 294.6, 294.7, and 294.8. Till units were found to contain surprisingly consistent abundances of the various lithologies; however, in some drillholes there are significant differences in abundance between till units, as demonstrated in Figure 294.8. Also, in two of the drillholes, greater than 80 percent of the pebbles in the lowermost till sample are derived from the local bedrock lithology. An example of this feature is shown in Figure 294.7. In this case, the multielement geochemical data for the bottom till samples are significantly different from those of the overlying till unit. Also, the physical and chemical characteristics of the bottom till sample are significantly different from those of the overlying till unit. This evidence strongly suggests that a large proportion, if not all, of this lowermost sample is actually bedrock, pulverized during drilling and mistakenly identified as till.

Discriminant analysis was performed on the pebble frequency data to determine, quantitatively, the best combination of pebble lithologies for discriminating between till units on a regional scale. Training group selection and application of this multivariate statistical method are similar to those used for the evaluation of the mineral abundance data. As shown in Table 294.2, the abundance of felsic to

TABLE 294.2. SUMMARY STATISTICS FOR DISCRIMINANT ANALYSIS OF THE PEBBLE LITHOLOGY DATA.

Variables in Analysis	Step	Variable Added	% Classified Correctly	F-Value**	Degreees of Freedom
Felsic to intermediate	1	Felsic intrusive	82.2	60.3	1,105
intrusive, Mafic intrusive$_L$,	2	Ultramafic	84.1	36.8	2,104
Metavolcanic, Metasediment$_L$,	3	Metasediment	85.1	26.3	3,103
Ultramafic$_L$, Paleozoic carbonate$_L$	4	Mafic intrusive	85.1	20.2	4,102

L indicates log transformed

** F-Value is a statistical measure of the discrimination. Higher F-values generally indicate a statistically more significant discrimination. Actual significance can be read from standard statistical tables.

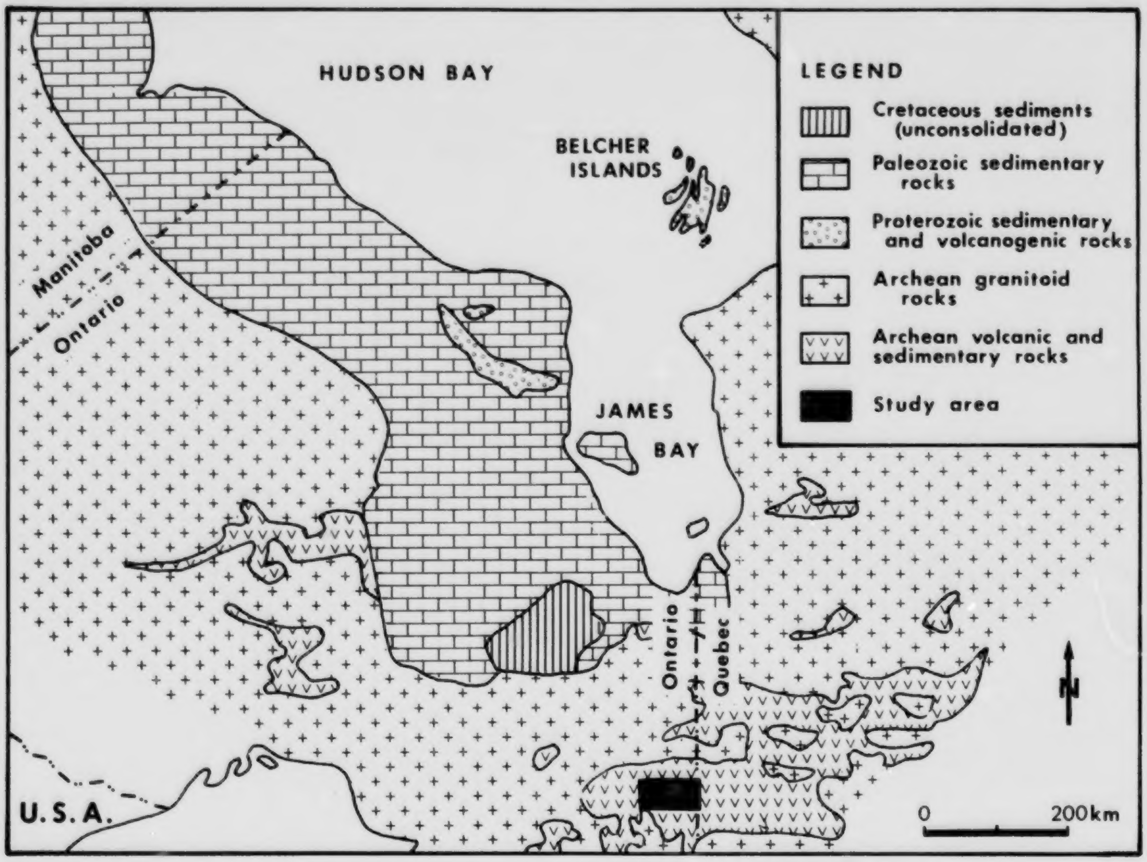
HUDSON BAY
BELCHER ISLANDS
JAMES BAY
Manitoba
Ontario
Ontario
Quebec
U.S.A.
LEGEND
Cretaceous sediments (unconsolidated)
Paleozoic sedimentary rocks
Proterozoic sedimentary and volcanogenic rocks
Archean granitoid rocks
Archean volcanic and sedimentary rocks
Study area
N
0
200km

Figure 294.9. Regional bedrock geology.

intermediate intrusive pebbles is the most important discriminator and results in 82 percent of the training group samples being correctly classified into their respective till units. Pebble lithology variables added subsequently contribute very little to the discrimination. This implies that the abundance of felsic to intermediate intrusive pebbles is an effective means of discriminating between till units across the study area.

As determined by discriminant analysis, a threshold of 24 percent felsic to intermediate pebbles effectively separates upper till units from lower till units for the training group samples. Samples from the upper till unit generally have greater than 24 percent felsic to intermediate intrusive pebbles and samples from lower till units generally have less than 24 percent felsic to intermediate intrusive pebbles and a compensating greater percentage of mafic metavolcanic pebbles. An example of this is shown in Figure 294.8. The frequency and mix of different till unit types based on pebble lithology abundances are

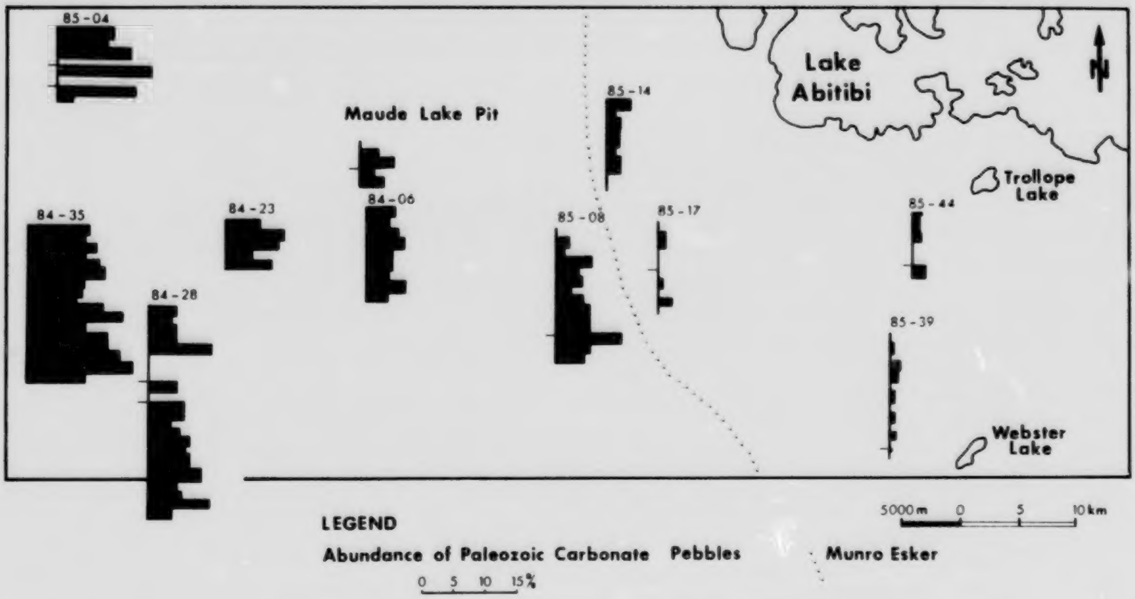

Figure 294.10. *Abundance of Paleozoic carbonate pebbles in selected drillholes across the study area. In drillholes that contain multiple till units, the top of each till unit is indicated on the left side of each drillhole.*

similar to those previously identified by geochemical composition.

In addition to the major lithological types represented in the samples, three bedrock lithologies from unique source areas were identified in some till samples. These include: a) oolitic jasper, derived from Proterozoic rocks of the Belcher Islands (Prest and Nielsen 1987); b) Paleozoic carbonate, derived from the James Bay Lowlands (Shilts 1980); and c) lignite, probably derived from Cretaceous sediments in the James Bay Lowlands. The presence of these unique lithologies in the tills of the Matheson area indicates minimum transport distances of approximately 240 km for the lignite and Paleozoic carbonates and 800 km for the oolitic jasper, based on the present day distribution of possible source rocks (Figure 294.9). The relationship between the presence of unique pebble lithologies and the acidic/basic compositional groups is not obvious. At this point, only the lignite abundance appears to be limited to the uppermost acidic till unit.

While the abundance of Paleozoic carbonate pebbles in the till does not display any obvious stratigraphic patterns, it does display a marked regional east-west pattern, as shown in Figure 294.10. Abundance appears to decrease significantly from 5 to 15 percent in the western part of the study area to 2 percent or less in the eastern part. This carbonate abundance pattern is similar to that reported by Hughes (1965), who found that the abundance of carbonate pebbles in the Matheson till decreased toward the southeast, from 32 percent in the Smooth Rock Falls area (100 km northwest of the study area) to 1 percent or less in the Ramore area on the south-central edge of the study area. However, in this study the decrease in Paleozoic carbonate pebble abundance, as shown in Figure 294.10, was also displayed by till units below the uppermost (Matheson) till unit. The eastward decrease in abundance of Paleozoic carbonate pebbles suggests that farther to the east the abundance becomes zero. Shilts (1980) and Veillette (1986) reported an eastern limit of Paleozoic carbonate clast dispersal just east of the Ontario/Quebec border. No other pebble lithology displays such a striking regional pattern; however, it should be recalled that garnet and epidote frequency also display east-west patterns.

In summary, the frequency of certain pebble lithologies appears to be well correlated with geochemical data from the same samples, not only in a variable-to-variable comparison, but also in the patterns displayed.

DISCUSSION

Pebble lithological data appear to be more useful than heavy mineral abundances in identifying stratigraphic units on a regional scale, although specific, but variable, heavy minerals often clearly distinguish one till unit from another in individual holes. Based on the abundance of felsic to intermediate intrusive pebbles, a threshold of 24 percent felsic to intermediate pebbles can be used effectively to divide till units into one of two groups: a) "felsic" tills; and b) "mafic" tills. Till units that were classified as felsic also display an acidic geochemistry. Till units classified as mafic display a basic geochemistry. An example of this feature is shown in Figure 294.11. The upper and middle till units in this drillhole display acidic/felsic characteristics (greater than 24 percent felsic to intermediate intrusive pebbles, and less than

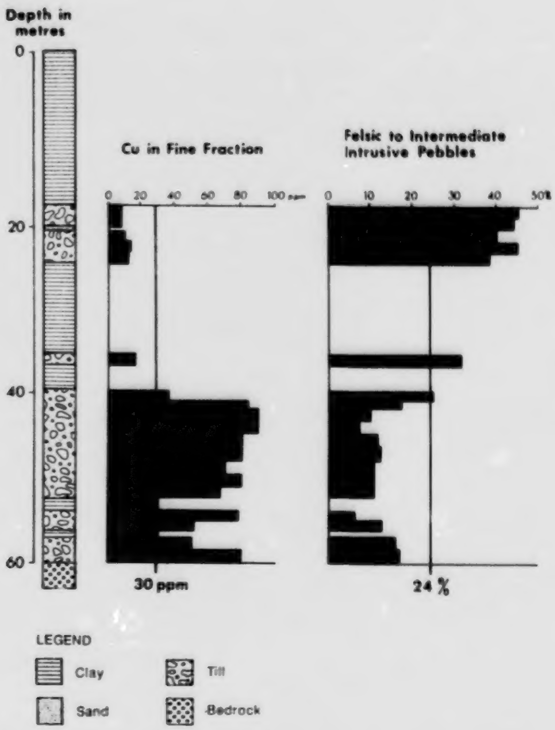

Figure 294.11. Abundances of felsic to intermediate intrusive pebbles and Cu in the fine fraction for drillhole 84-28 (graphic log modified from OGS 1986a).

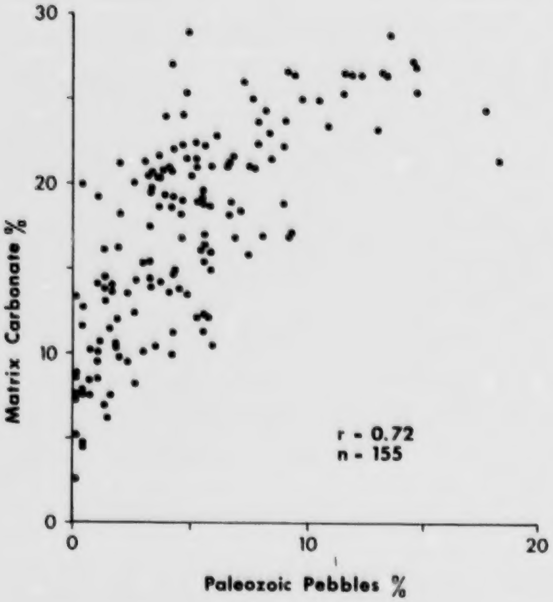

Figure 294.12. Relationship between the abundance of Paleozoic carbonate pebbles and carbonate content in the till matrix. n=number of samples; r=correlation coefficient.

30 ppm Cu) while the lowermost till unit displays basic/mafic characteristics (less than 24 percent felsic to intermediate intrusive pebbles, and greater than 30 ppm Cu).

In general, the pebble fraction appears to indicate bedrock sources that are similar to those indicated by the finer till fractions (heavy mineral concentrate, fine and total matrix fractions). This point is further emphasized by the strong positive correlation between the abundance of Paleozoic carbonate pebbles and the carbonate content in the matrix fraction (<0.063 mm) of the till samples (Figure 294.12).

The felsic/mafic pebble abundance patterns of the till units in the study area are similar to those reported for till units in the Casa Berardi area, 100 km to the northeast. In the Casa Berardi area, Sauerbrei *et al.* (1987) reported two till units separated, in most cases, by glaciolacustrine sediment. At least 80 percent of the cobble-sized clasts in the lower till unit consists of local greenstone bedrock lithologies, while 20 percent or less are foreign intrusive lithologies. In contrast, the upper till unit contains a significantly higher percentage (>30 percent) of intrusive bedrock lithologies. These differences in abundance were used to distinguish between the two till units when they were found in contact with one another.

Certain elements and pebble lithologies display distinct abundance patterns that coincide with major lithological discontinuities and indicate different source areas for the different till units; however, Paleozoic carbonate pebbles, carbonate content in the till matrix, and some heavy minerals show an east to west distribution that crosses the stratigraphic boundaries. If it is assumed that the geochemical and pebble lithological (acidic versus basic) differences between till units within a drillhole are a function of different ice flow directions (150°, followed by 240°, followed by 170°) how can the east-west abundance patterns for the Paleozoic carbonate pebbles and the heavy minerals be explained? Likewise, if it is assumed that the east-west differences are the result of till deposition from a single ice sheet, how can the stratigraphic (or vertical) differences between till units be explained? Also, the presence of organic-rich sediment between the upper till unit and an underlying till unit in two of the 24 drillholes, and in drillholes farther to the west in the Timmins area (DiLabio *et al.* 1988), suggests that if the organic material is *in situ*, there was a considerable period of time between the deposition of each till unit.

The Munro Esker appears to mark a sharp boundary between drillholes that contain high abundances of Paleozoic carbonate pebbles in the western portion of the study area and drillholes that contain considerably lower abundances in the eastern portion (Figure 294.10). The significance of this observation is not yet clear, and may prove to be of little value in explaining the east-west patterns displayed by the till units. Garnet abundance gradually decreases toward the east, as indicated by the average garnet abundance for each drillhole (Figure 294.4); however, in this case, the Munro Esker appears to have little significance in the east-west pattern.

The acidic/basic differences between till units may simply reflect distal versus local derivation of debris and not separate ice flow events. Debris derived from the erosion of bedrock north of the greenstone belt and transported south toward the study area should display an acidic/felsic composition. Where the glacier has eroded local greenstone bedrock, the till will display a basic geochemical composition and contain a larger component of local bedrock clasts.

CONCLUSIONS

1. Relative abundances of various heavy minerals are of little use as regional stratigraphic markers; however, they can provide valuable information about the compositions of local bedrock sources.
2. Pebble lithological abundances correlate well with the geochemistry of the heavy mineral, fine, and total matrix till fractions. "Acidic" tills have higher abundances of felsic to intermediate intrusive pebbles. "Basic" tills have higher abundances of mafic metavolcanic pebbles.
3. The west to east difference in Paleozoic carbonate pebble abundance and the change in mineral abundance across the study area are not surprising. What is puzzling is that these patterns are common to all till units and not just the uppermost till unit, commonly assumed to be Matheson till.

IMPLICATIONS FOR EXPLORATION

The results presented above are important to mineral exploration in the Matheson area because they contribute to the understanding of the complex Quaternary stratigraphy of the area. This understanding in turn improves the effectiveness of till geochemistry as a method of exploration. For example, the contrast between mafic and felsic till compositions can be used to distinguish till units in overburden drill holes. Thus, a geochemical anomaly can be assigned a stratigraphic position, and the till unit it represents a likely ice transport direction. Till units that display a mafic composition are better sampling media than those that display a felsic composition because they are derived from local (greenstone) bedrock sources. Visual examination of pebble lithologies in till samples allows the proper identification of ground up bedrock mistaken for till. This is important if anomalous gold values are found in these samples.

FUTURE WORK

Future work is intended to clarify the genetic reasons for the empirical lithological, mineralogical, and pebble abundance differences between till units identified thus far. A better understanding of the relationships between the stratigraphy and the composition of the till will significantly improve till geochemistry exploration techniques in the Matheson area.

1. Submission of selected heavy mineral concentrate samples from 1984 and 1985 for a second mineralogical grain count will help to determine whether the east-west changes in mineral abundance are related to a bias between sampling years.
2. Examination of the abundance of Paleozoic carbonate pebbles in the >1.7 mm fraction from all remaining till samples and, perhaps, some till samples from the 1987 or 1988 OGS sonic drilling program, will help to confirm the east-west pattern identified thus far.
3. Evaluation of lithology and shape of pebbles should provide useful information as to the genesis and distance of transport of the till units.
4. Comparison of till geochemistry and pebble lithology abundances to bedrock geochemistry and lithology for each drillhole, will indicate if the till is of local derivation and if so, how the various bedrock lithologies influence till geochemistry.
5. Examination of thin sections prepared from oriented drill core may help in establishing ice flow directions for the lower till units in the Matheson area.

ACKNOWLEDGMENTS

The authors would like to thank the Geophysics-Geochemistry Section of the Ontario Geological Survey, Toronto, for making all data and samples used in this study readily available. J.M. Kuska is thanked for typing the manuscript and drafting all figures. Robert Redford and Norman Bowen are thanked for their assistance with the preparation of this manuscript.

REFERENCES

Alcock, P.W.
In preparation: Quaternary Geology of the Timmins Area, Districts of Cochrane, Timiskaming and Sudbury.

Baker, C.L., Steele, K.G., and McClenaghan, M.B.
1985: Reconnaissance Till Sampling Program, Matheson–Lake Abitibi Area, Cochrane District; p.329-333 *in* Summary of Field Work and Other Activities 1985, by the Ontario Geological Survey, edited by John Wood, Owen L. White, R.B. Barlow, and A.C. Colvine, Ontario Geological Survey, Miscellaneous Paper 126, 351p.

Bird, D.J., and Coker, W.B.
1987: Quaternary Stratigraphy and Geochemistry at the Owl Creek Gold Mine, Timmins, Ontario, Canada; *in* Geochemical Exploration 1985, edited by R.G. Garrett; Journal of Geochemical Exploration, Volume 28, p.267-284.

DiLabio, R.N.W., Miller, R.F., Mott, R.J., and Coker, W.B.
1988: The Quaternary Stratigraphy of the Timmins Area, Ontario, as an Aid to Mineral Exploration by Drift Prospecting; p.61-65 *in* Current Research, Part C, Geological Survey of Canada, Paper 88-1C.

Hughes, O.L.
1959: Surficial Geology of the Smooth Rock and Iroquois Falls Map Areas, Cochrane District, Ontario; Unpublished Ph.D. Thesis, University of Kansas, Lawrence, Kansas, 190p.

1965: Surficial Geology of Part of the Cochrane District, Ontario, Canada; p.535-565 *in* International Studies on the Quaternary, edited by H.E. Wright Jr., and David G. Frey; Geological Society of America, Special Paper 84.

McClenaghan, M.B., Lavin, O.P., Nichol, I., and Shaw, J.
1987: Quaternary Geology and Geochemical Exploration in the Matheson Area; Grant 294, p.200-214 *in* Geoscience Research Grant Program, Summary of Research, 1986-1987, edited by V.G. Milne, Ontario Geological Survey, Miscellaneous Paper 136, 241p.

Ontario Geological Survey
1986a: Sonic Drillholes 84-06 and 84-28, Cochrane District; Ontario Geological Survey, Maps 80 766 and 80 760, Geophysical/Geochemical Series, Geology 1984, 1985.
1986b: Sonic Drillhole 85-14, Milligan Township, Cochrane District; Ontario Geological Survey, Map 80 857 Geophysical/Geochemical Series, Geology 1985.

Prest, V.K., and Nielsen, E.
1987: The Laurentide Ice Sheet and Long-Distance Transport; Geological Survey of Finland, Special Paper 3, p.91-101.

Sauerbrei, J.A., Pattison, E.F., and Averill, S.A.
1987: Till Sampling in the Casa–Berardi Gold Area, Quebec: A Case History in Orientation and Discovery; p.297-314 *in* Geochemical Exploration 1985, edited by R.G. Garrett, Journal of Geochemical Exploration, Volume 28.

Shilts, W.W.
1980: Flow Patterns in the Central North American Ice Sheet; Nature, Volume 286, p.213-218.

Steele, K.G., Baker, C.L., and McClenaghan, M.B.
In preparation: Models of Glacial Stratigraphy Determined from Drillcore, Northeastern Ontario, Canada.

Veillette, J.J.
1986: Former Southwesterly Ice Flows in the Abitibi–-Timiskaming Region: Implications for the Configuration of the Late Wisconsinan Ice Sheet; Canadian Journal of Earth Sciences, Volume 23, p.1724-1741.

Wentworth, C.K.
1922: A Scale of Grade and Class Terms for Clastic Sediments; Journal of Geology, Volume 30, Number 5, p.377-392.

Whittaker, P.J.
1986: Gold Metallogenesis Along the Pipestone and Destor–Porcupine Deformation Zones and Associated Structures; p.404-412 *in* Summary of Field Work and Other Activities 1986, by the Ontario Geological Survey, edited by P.C. Thurston, Owen L. White, R.B. Barlow, M.E. Cherry, and A.C. Colvine, Ontario Geological Survey, Miscellaneous Paper 132, 435p.

Grant 295 Karst Episodes and Permeability Development, Silurian Reef Reservoirs, Ontario

Leigh Smith, Douglas J. Grimes, and Steven Charbonneau

Department of Geological Sciences, Queen's University, Kingston

ABSTRACT

The Rosedale pinnacle reef bioherm and the Fletcher platform/bank bioherm, located in the southwestern Ontario subsurface, are part of the Guelph Formation of Middle Silurian age. Development of these reservoirs was governed by cyclical sea level fluctuations. Rising sea levels produced episodes of reef growth; falling sea levels caused episodes of reef exposure and development of paleokarst.

There were seven major episodes of subaerial exposure, so that each pinnacle reef bioherm is a vertical succession of six different biohermal units separated by erosional discontinuities. Some of these erosional episodes caused major changes in depositional facies. These facies varied upward from platform to mud mound to reef complex to karstic and restricted cap facies.

Each episode of exposure also resulted in the creation of laterally extensive leached zones of enhanced permeability and increased porosity in the then upper portion of the reef. Paleosols and crusts were formed, which created a vertical seal. This seal was enhanced by the formation of overlying impermeable limestones during the next sea level rise.

There is abundant evidence of diagenesis in marine, meteoric phreatic, and burial environments, resulting in different types of pore-occluding calcite cements, especially in the lower portion of each bioherm.

Only major karstic episodes could have created reservoir-grade zones of laterally extensive permeability.

INTRODUCTION

Large carbonate bioherms are present in the subsurface Middle Silurian rocks of southwestern Ontario. They occur within a broad area along the southeastern margin of the Michigan Basin. Over 70 percent of those located so far contain hydrocarbon reserves. Some are now used for the seasonal storage of natural gas.

This project is a study of several of these bioherms, to identify the origin and delineate the three-dimensional geometry of their commercially useful porosity and permeability. Figure 295.1 shows the location of the Rosedale Field in Lambton County, and the Fletcher Field in Kent County. The Rosedale reservoir is contained within laterally extensive permeable zones in a limestone pinnacle reef bioherm, and the Fletcher reservoir within a dolomitized platform or bank reef complex. These reefs were chosen for the first part of this study because they represent the two principal types of bioherm, and both are represented by continuous drill core. The Warwick pinnacle reef reservoir is one of those that will be studied in the next project, to aid in the correlation of permeable and karstic zones within different pinnacle reef bioherms.

These bioherms are stratigraphically located within the Guelph Formation (Table 295.1). They rest on the regional carbonate platform of the Lockport Formation, which in turn unconformably overlies the regionally extensive Rochester Formation. These reefal bioherms are sealed, overlain, and laterally surrounded by impermeable carbonate and evaporite units of the Salina Formation. The available drill cores are continuous from the upper portions of the Rochester Formation to the lower units of the Salina Formation.

A slightly more rapid downwarping during the Middle Silurian developed the initial phase of the Michigan Basin, and caused deposition of only a thin unit of the Lockport Formation. A very gentle slope surrounded this shallow basin, causing the localized development of pinnacle reef bioherms (Figure 295.2). The rest of the region developed areally extensive reef-bank platforms (Trevail and Smith 1987). The combined effect of this slightly differential tectonism and the differential bioherm growth that resulted caused the regional thickness variations in the Lockport and Guelph formations shown by Bailey (1986). Sanford *et al.* (1985) suggest that rejuvenation of basement fault blocks controlled both the origin and development of these reservoir units.

OBJECTIVES

The major objective of this study is to delineate the internal nature and three-dimensional geometry of the permeable zones in the Silurian pinnacle and platform/bank reef reservoirs of southwestern Ontario. This work is also testing our concept that there were several subaerial karstic episodes during the development of these bioherms, and that each episode formed a zone of increased permeability and enhanced porosity in each reef. Detailed knowledge of these zones, and of the extent to which they are sealed by karstic crusts and fills, evaporite plugging, or by overlying units, will greatly aid enhanced hydrocarbon recovery, and their use as gas storage reservoirs and fluid waste disposal reservoirs.

METHODS

Detailed sedimentological description of slabs from the Rosedale and Fletcher drill cores have identified the original organic components and depositional features in the bioherms. The erosional (karstic) aspects were then clearly and separately identified. Thin sections, scanning electron microscope (SEM) photographs, and cathodoluminescence techniques were used to identify the growth patterns and zoning of pore-occluding cements. Thin section study and cathodoluminescence techniques revealed grain and cement truncation patterns along pore walls; and showed the succession of erosional and precipitational events which have had effects on rock porosity. Thin section staining and X-ray diffraction

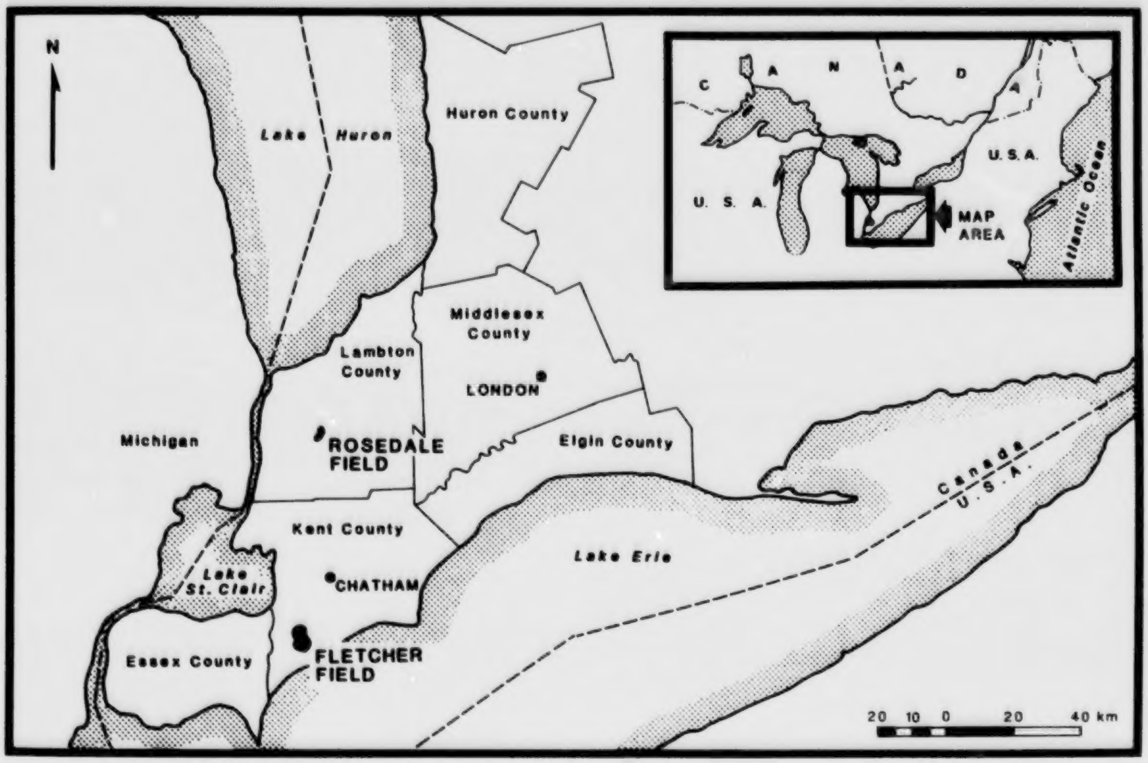

Figure 295.1. *Location of Silurian reef reservoirs in southwestern Ontario.*

analyses identified the carbonate mineral species and variations in iron content. Variations in $\delta^{13}C$ and $\delta^{18}O$ isotope signatures in calcite pore cements allowed the identification of fresh water signatures in crusts, soils, and phreatic cements. Similar evaluations of cores from other pinnacle reefs (for example, the Warwick reef) are in progress.

Well logs have helped to identify the major porous zones, in contrast to those that are substantial in core but may have little lateral extent. Data reports and production information from the files of the Ministry of Natural Resources are being used to delineate permeable zones.

The overall method of study is to understand the succession of depositional, karstic, and diagenetic environments that were responsible through time for the present state of the permeability and associated cements in the Middle Silurian reefal bioherms of southwestern Ontario.

DEPOSITIONAL HISTORY

Not only were the two reefal bioherms investigated in this study formed in different paleogeographical situations (Figure 295.2), but the structure contour map of the Rosedale pinnacle bioherm (Figure 295.3), and the structure maps of the Fletcher platform/bank bioherm show that the Fletcher type is considerably larger and more continuous laterally. In addition, the Rosedale mass consists entirely of limestone, while the Fletcher mass consists of dolostone.

FACIES—ROSEDALE

The first detailed description of the Rosedale bioherm was made by Bainbridge (1973). The present study uses an analysis of our more specific descriptions to subdivide the bioherm into the succession of four discrete depositional facies outlined in Table 295.1 and in Figure 295.4.

The Lockport Formation platform facies consists of sand waves and coalesced mounds of crinoid and brachiopod remains. This wackestone was regionally dolomitized. The Guelph Formation bioherm of the Rosedale reservoir developed on this platform as wackestones and packstones of the bryozoan/coral mud mound facies. The overlying reef mass proper is composed of a complex of reef core facies mudstones and floatstones with corals, bryozoans, and stromatoporoids intermingled with bedded bioclastic floatstones of reef flank facies. This reef mass complex is topped by a unit of subaerially (karstically) altered and brecciated mudstone. Although there are other intervals showing karstic alteration in the Rosedale section, this is the most conspicuous example. Above this discontinuity is the restricted cap facies of leached mudstone and stromatolitic boundstone, overlain by nodular anhydrite. The Warwick pinnacle reef (Pearson 1980) shows a similar succession of facies.

TABLE 295.1: SILURIAN LITHIC UNITS IN ROSEDALE 8-9-IIA WELL

STRATIGRAPHIC UNIT	DEPOSITIONAL FACIES
Salina Formation	Restricted Regional
	Restricted Cap 23 m
Guelph Formation	Karstic Cap 15m
	Reef Mass 54 m
	-complex of Reef Core and Reef Flank facies
	Mud Mound 31 m
Lockport Formation	Platform 27 m
Rochester Formation	Regional Shale

FACIES—FLETCHER

This reefal structure was first described by Chalkley (1983). During the present study it was found that dolomitization had substantially obscured original depositional textures. As a result, only two biohermal facies were recognized above the Lockport Formation platform: reef core wackestone/floatstone with corals and stromatoporoids, and the reef flank beds of bioclastic floatstone (Grimes and Smith 1987).

SUBAERIAL EXPOSURE

Most early workers thought that the Lockport–Guelph Formation carbonate units and the succeeding Salina Formation evaporite units accumulated during one long submarine episode. Mesolella *et al.* (1974) interpreted two episodes caused by sea level fluctuations, but thought a period of subaerial exposure to be only "possible". Sarg (1982) thought that the development of reef porosity was due to salinity variation without exposure. Huh *et al.* (1977), Sears and Lucia (1979), Petta (1980), and Cercone and Lohmann (1986) identified one exposure episode, mainly because of the general duality of off-reef Salina units. Kahle (1974) identified the many karstic features in a reef in northern Ohio. However, the idea that there was only one karstic episode and that it occurred after the growth of the entire bioherm has been a persistent misconception.

Our research into the growth phases of these Silurian bioherms has discovered that a period of major subaerial exposure delineated each phase (Smith 1984). There were seven such episodes of subaerial exposure during the development of the Guelph Formation bioherms (Figure 295.4). Each of these karstic episodes formed a zone of increased permeability and enhanced porosity, laterally interconnected but vertically sealed by subaerial or later submarine cementation. Precipitation of pore-occluding halite also occurred at specific levels within the reefal mass, probably during episodes of extreme sea level lowering.

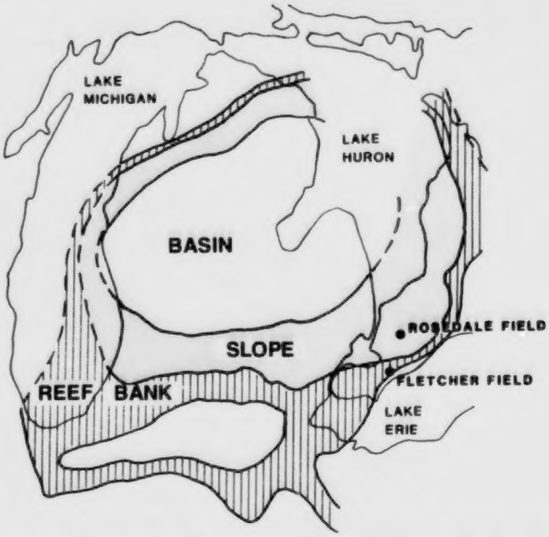

Figure 295.2. *Environments of the Michigan Basin region during the Middle Silurian (after Briggs and Briggs 1974).*

Each of these leached, once vadose zones is complex in internal detail, and is far more extensive laterally than vertically. They are separated vertically from one another by intervals of unaltered and nonporous carbonate, karstic crusts and soils, fills in karstic conduits, and by intervals with precipitated evaporite. They possess, therefore, the best reservoir characteristics in each bioherm. These zones of enhanced porosity and permeability in the Rosedale bioherm have been delineated and described in detail by Grimes (1987). Those in the Fletcher bioherm are less distinct in detail, due to later dolomitization. Equivalent porosity zones in the Warwick reef are now being delineated by Charbonneau.

The Rosedale bioherm is thus very similar to modern reefs such as the Eniwetok Atoll, in the east-central Pacific, where Buddemeier and Oberdorfer (1986) found several "solution unconformities" showing abundant karstic features.

DIAGENETIC HISTORY

Considerable physical and chemical alteration of the original sediments in the bioherms was caused by submarine diagenesis, and by changes during and just after subaerial exposure. Petrographical and chemical studies show that there were stages in the development of these diagenetic changes which were caused by variations in the chemistry of the pore fluids. Data on carbon and oxygen stable isotopes is being used to evaluate conclusions derived from the petrographical and chemical data.

The results of each diagenetic stage are unevenly distributed throughout the bioherms. This re-

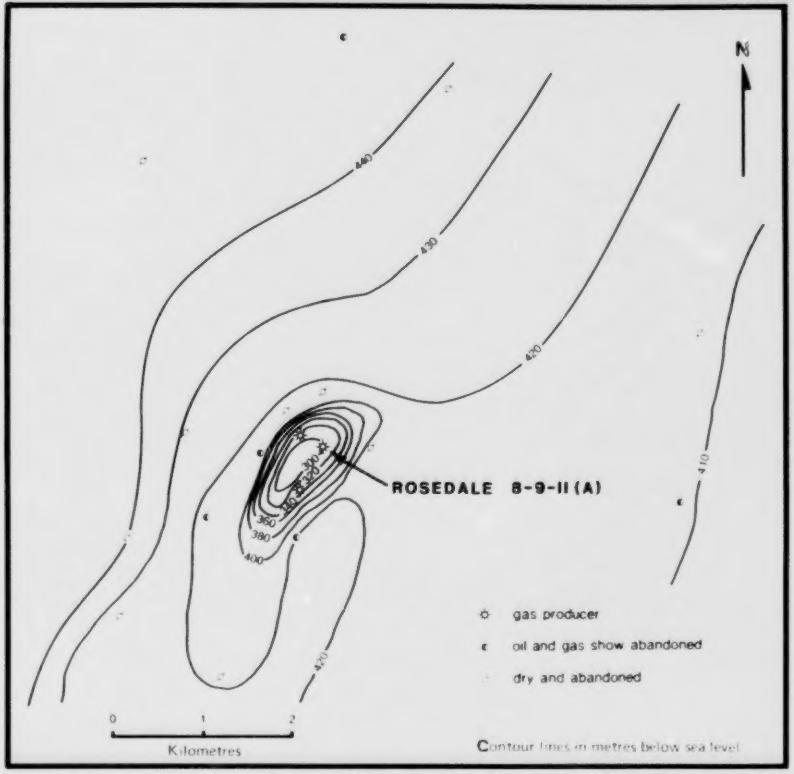

Figure 295.3. *Structure contours for the top of the Guelph Formation, Rosedale Field (see Figure 295.1 for location).*

sults from variations in the original carbonate sediment and its primary depositional porosity, from a variability in karstic porosity enhancement, and from the variable residence times of pore fluids. Original shelter porosities have survived in some places within the lower and middle portions of the bioherms, associated with bryozoans and stromatoporoids. Karstically enhanced vuggy porosities are more important in the upper portions, including fenestral porosities in the cap facies.

ROSEDALE

The Rosedale reservoir underwent early marine, meteoric-phreatic, and burial diagenetic stages. Early marine cement in the form of isopachous pore-lining fibrous calcite is mainly restricted to the mud mound wackestone facies. It lines primary shelter porosity, initially associated with fenestrate bryozoan fragments but later enhanced by vadose solution. Marine and/or vadose silt deposition gave each pore the characteristic flat base below a very irregular top surface. A solution event interrupted the precipitation of fibrous calcite, truncated the crystals, and left a pyrite concentration on the lower surface of the pore. Return of marine waters caused precipitation of a second fibrous calcite layer on the truncation surface.

Many of these pores were not filled with isopachous calcite but were infilled later by blocky calcite of probable meteoric phreatic origin. This produced one of the characteristic types of stromatactis structure, and caused the loss of porosity in the lower portions of the bioherm.

Burial cementation is not volumetrically significant in the Rosedale reservoir. Pore-lining euhedral white dolomite and euhedral calcite are found in a few vugs and fractures. Cercone and Lohmann (1986) found hydrocarbon-bearing inclusions in both the dolomite and calcite spar in a northern Michigan bioherm, which emphasizes their burial environment genesis. Simo and Lehmann (1988), however, found that hydrocarbon migration postdated such cements in central Indiana.

FLETCHER

The Fletcher bioherm also contains much isopachous pore-lining cement, but this cement has been thoroughly dolomitized along with the surrounding rocks. These cements also occur in karstically altered zones, as in the Rosedale, partially or fully occluding the enhanced porosity. A burial phase of pore-lining euhedral white dolomite postdates the complete dolomitization of the bioherm.

The original structural background, shown in Figure 295.2, appears to have predetermined the lack of pervasive dolomitization in isolated pinnacle bioherms, while platform/bank bioherms were thoroughly dolomitized. The regionally extensive Lockport Formation platform was also well dolomitized. At those times when the marine waters of the region were sufficiently enriched in magnesium to dolomitize the bioherms, the more widespread plat-

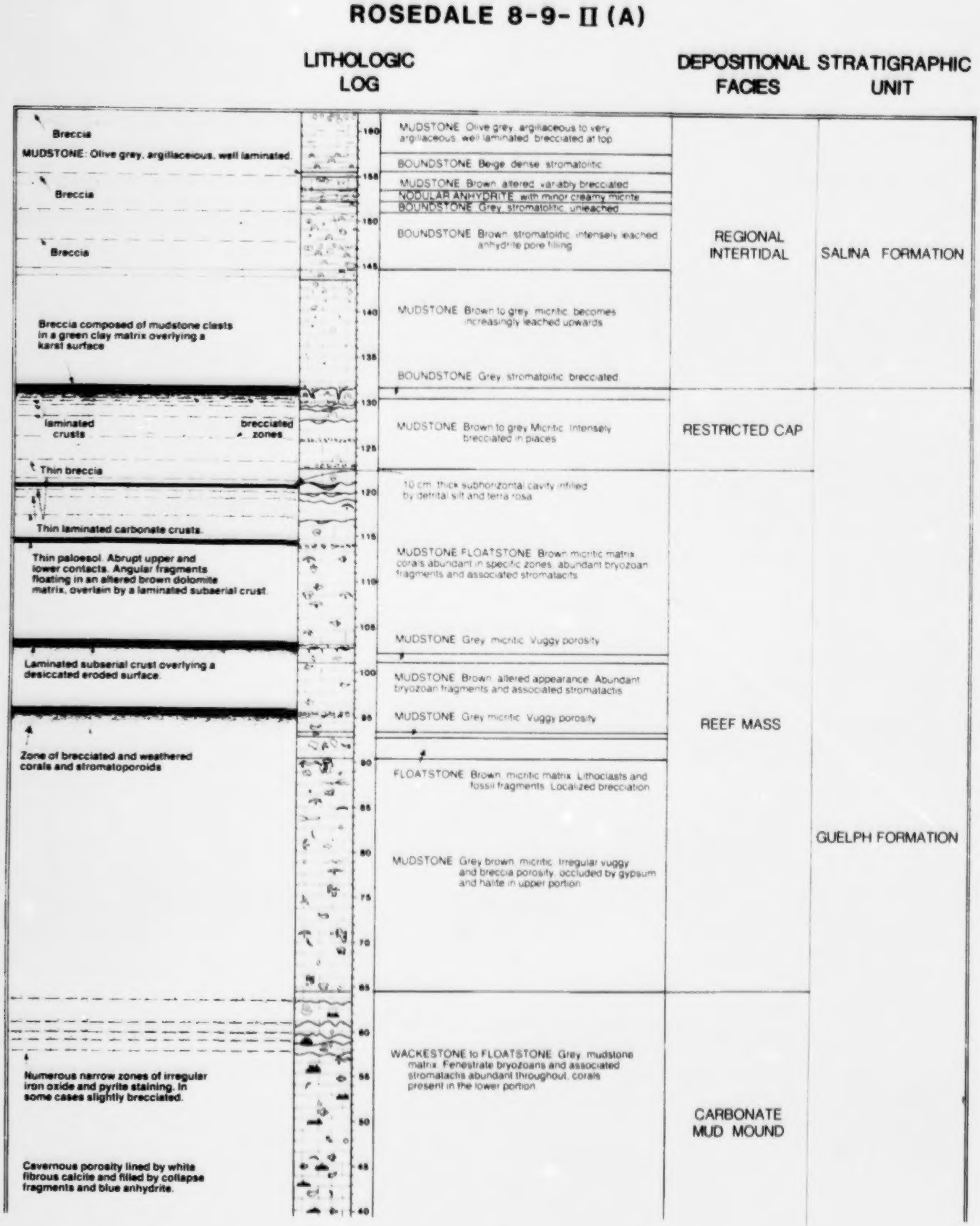
ROSEDALE 8-9-II (A)
LITHOLOGIC LOG
DEPOSITIONAL FACIES
STRATIGRAPHIC UNIT
Breccia
MUDSTONE: Olive grey, argillaceious, well laminated.
Breccia
Breccia
Breccia composed of mudstone clasts in a green clay matrix overlying a karst surface
laminated crusts
brecciated zones
Thin breccia
Thin laminated carbonate crusts.
Thin paloesol. Abrupt upper and lower contacts. Angular fragments floating in an altered brown dolomite matrix, overlain by a laminated subaerial crust.
Laminated subaerial crust overlying a desiccated eroded surface.
Zone of brecciated and weathered corals and stromatoporoids
Numerous narrow zones of irregular iron oxide and pyrite staining. In some cases slightly brecciated.
Cavernous porosity lined by white fibrous calcite and filled by collapse fragments and blue anhydrite.
160
155
150
145
140
135
130
125
120
115
110
105
100
95
90
85
80
75
70
65
60
55
50
45
40
MUDSTONE Olive grey, argillaceous to very argillaceous, well laminated, brecciated at top
BOUNDSTONE Beige dense stromatolitic
MUDSTONE Brown altered variably brecciated
NODULAR ANHYDRITE with minor creamy micrite
BOUNDSTONE Grey stromatolitic unleached
BOUNDSTONE Brown stromatolitic intensely leached anhydrite pore filling
MUDSTONE Brown to grey micritic becomes increasingly leached upwards
BOUNDSTONE Grey stromatolitic brecciated
MUDSTONE Brown to grey Micritic Intensely brecciated in places
10 cm thick subhorizontal cavity infilled by detrital silt and terra rosa
MUDSTONE FLOATSTONE Brown micritic matrix corals abundant in specific zones abundant bryozoan fragments and associated stromatacits
MUDSTONE Grey micritic Vuggy porosity
MUDSTONE Brown altered appearance Abundant bryozoan fragments and associated stromatactis
MUDSTONE Grey micritic Vuggy porosity
FLOATSTONE Brown micritic matrix Lithoclasts and fossil fragments Localized brecciation
MUDSTONE Grey brown micritic Irregular vuggy and breccia porosity occluded by gypsum and halite in upper portion
WACKESTONE to FLOATSTONE Grey mudstone matrix Fenestrate bryozoans and associated stromatactis abundant throughout, corals present in the lower portion
REGIONAL INTERTIDAL
RESTRICTED CAP
REEF MASS
CARBONATE MUD MOUND
SALINA FORMATION
GUELPH FORMATION

Figure 295.4. *Stratigraphic section of the Rosedale core showing depositional and karstic features (from Grimes 1987).*

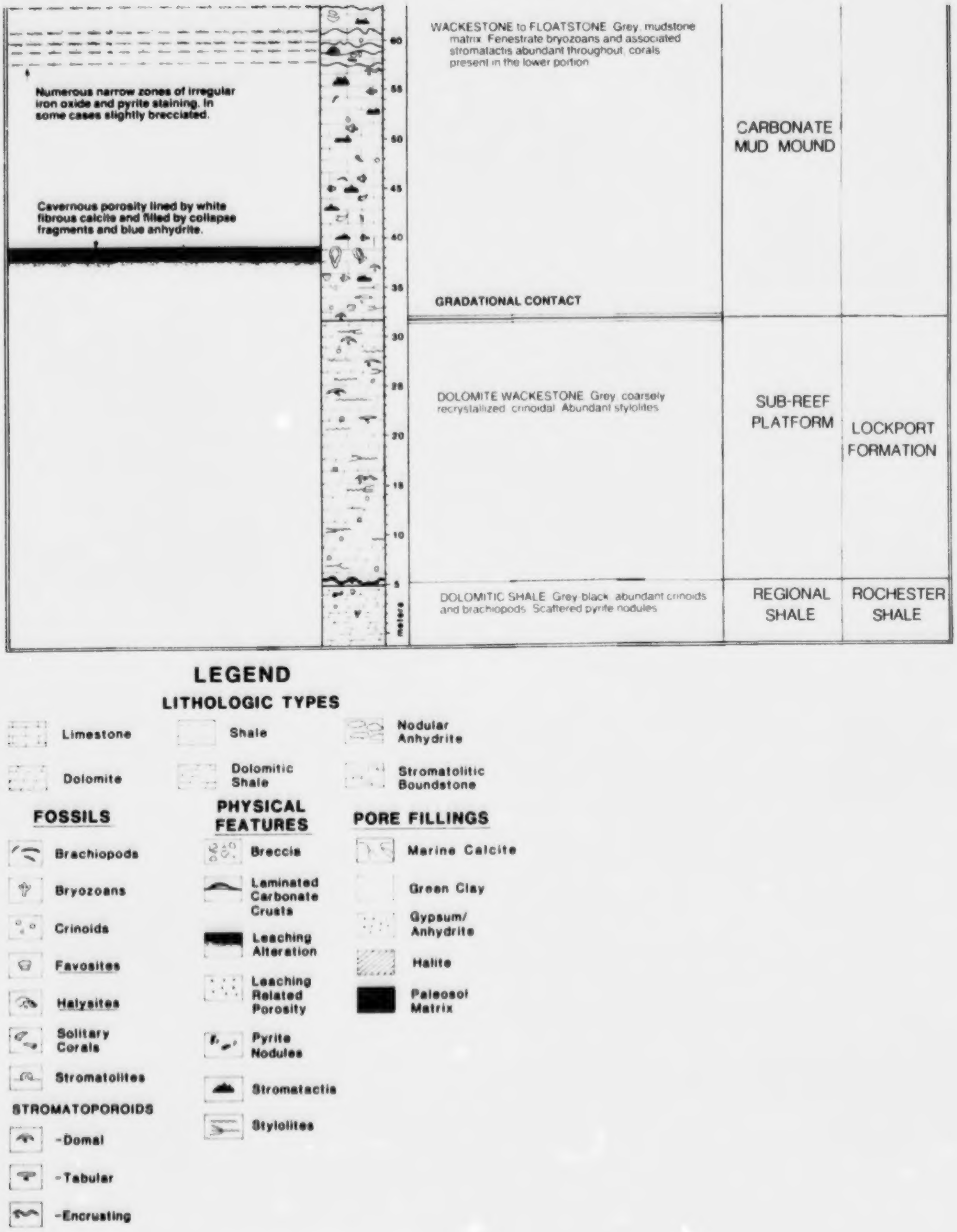
Numerous narrow zones of irregular iron oxide and pyrite staining. In some cases slightly brecciated.
Cavernous porosity lined by white fibrous calcite and filled by collapse fragments and blue anhydrite.
60
55
50
45
40
35
30
25
20
15
10
5
meters
WACKESTONE to FLOATSTONE Grey, mudstone matrix. Fenestrate bryozoans and associated stromatactis abundant throughout, corals present in the lower portion
GRADATIONAL CONTACT
DOLOMITE WACKESTONE Grey coarsely recrystallized crinoidal. Abundant stylolites
DOLOMITIC SHALE Grey-black abundant crinoids and brachiopods. Scattered pyrite nodules
CARBONATE MUD MOUND
SUB-REEF PLATFORM
LOCKPORT FORMATION
REGIONAL SHALE
ROCHESTER SHALE
LEGEND
LITHOLOGIC TYPES
Limestone
Dolomite
Shale
Dolomitic Shale
Nodular Anhydrite
Stromatolitic Boundstone
FOSSILS
Brachiopods
Bryozoans
Crinoids
Favosites
Halysites
Solitary Corals
Stromatolites
STROMATOPOROIDS
-Domal
-Tabular
-Encrusting
PHYSICAL FEATURES
Breccia
Laminated Carbonate Crusts
Leaching Alteration
Leaching Related Porosity
Pyrite Nodules
Stromatactis
Stylolites
PORE FILLINGS
Marine Calcite
Green Clay
Gypsum/ Anhydrite
Halite
Paleosol Matrix

Figure 295.4 continued. *Stratigraphic section of the Rosedale core showing depositional and karstic features (from Grimes 1987).*

ISOTOPE RESULTS: THE ROSEDALE REEF

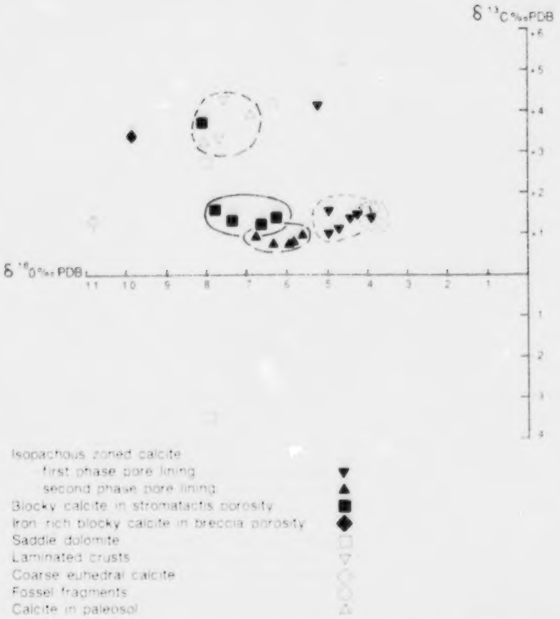

__Figure 295.5.__ Occurrence of $\delta^{13}C$ and $\delta^{18}O$ in typical fossils and diagenetic carbonate minerals (after Grimes 1987) from the Rosedale 8-9-IIA drill core.

form masses constricted sea water flow. This forced the magnesium-rich marine waters through the pores of the bioherm, especially if these had just been karstically enhanced. The less constrained water currents in the slope environment flowed around the relatively small pinnacles, leaving them undolomitized.

Mixed water dolomitization, if it occurs at all, cannot be called upon to produce this pervasive dolomitization. It may have operated locally during a few of the exposure episodes, as it seems to have done at two levels in the Fletcher bioherm and at one level in the Warwick bioherm. The Rosedale bioherm was not affected at those times, even though it was also exposed.

ISOTOPE ANALYSIS

The results of analysis for the stable isotope ratios of $\delta^{18}O$ and $\delta^{13}C$ are listed in Table 295.2. The basic assumption behind this analysis is that the composition of the oxygen and carbon isotopes in the cements will reflect the composition of the pore fluids from which they precipitated and/or with which they later reacted. However, oxygen isotopic composition varies with temperature, salinity, and biological activity, while carbon isotopic composition varies with organic matter content and the sediment/rock source of the bicarbonate ion. Because there is little agreement in the literature on absolute values relative to particular ancient environments, we have used the isotope values primarily to separate the cement

TABLE 295.2: STABLE ISOTOPE ANALYSES

	PDB $\delta^{18}O$ ‰	PDB $\delta^{13}C$ ‰
Rosedale 8-9-IIA		
Bioclastic Calcite		
-type 1	-3.95	+1.41
	-3.99	+1.49
	-3.86	+1.44
-type 2	-6.32	+4.31
	-3.45	+4.03
	-4.73	+5.28
Isopachous zoned Calcite		
-first phase, pore lining	-6.43	+0.95
	-5.67	+0.76
	-5.94	+0.88
	-6.83	+1.03
	-5.63	+1.03
-second phase, pore lining	-4.74	+1.21
	-5.00	+1.64
	-3.91	+1.34
	-5.02	+1.14
	-4.23	+1.47
Marine Calcite in solution joint	-4.01	+1.53
Blocky Calcite in "stromatactis" structure		
-iron rich	-7.41	+1.48
	-7.80	+1.76
	-6.38	+1.49
	-6.71	+1.42
Calcite in Paleosols	-6.75	+3.21
	-8.02	+3.83
	-8.02	+3.40
	-6.89	+3.97
Laminated-Crust Calcite	-7.50	+4.22
	-7.66	+3.38
Coarse euhedral Calcite	-10.82	+1.38
Fletcher 2-4-IX		
"Bioclastic" Dolomite	-5.81	+0.82
	-5.60	+0.84
	-6.92	+3.61
Isopachous zoned Dolomite (after Calcite)	-5.22	+1.24
	-5.33	+1.14
	-5.44	+1.07
	-5.22	+0.96
	-4.97	+1.10
	-4.53	+1.09
Matrix Dolomite	-4.85	+0.70
Saddle Dolomite	-5.96	+1.47

phases in the pores of the bioherms (Figure 295.5), and to delineate the sequence of events in their history (as done, for example, by Dickson and Coleman 1980).

It appears that the "Bioclastic Calcite—Type 1" signatures from the Rosedale bioherm (Table 295.2) give a close indication of normal sea water composition during Middle Silurian time. If so, it only emphasizes how much the pore waters varied in other environments. The signature shift from the first phase isopachous cement (slightly mixed waters?) to the second phase (closer to normal sea water), to the blocky cement (meteoric phreatic?), shows that these different cements were precipitated from different pore waters. This is significant, as the three cement types in each case were sampled from the same pore.

Differing signatures from calcites in laminated crusts and paleosols are important indicators of the more variable subaerial environments. The signatures from the coarse euhedral calcites clearly show a burial environment.

The signatures from the Fletcher core appear to show strongly the homogenizing effects of pervasive dolomitization (Table 295.2).

HYDROCARBON/STORAGE RESERVOIRS

Our research has shown the presence of seven major subaerial karstic episodes during development of the Rosedale bioherm. Each episode formed a laterally extensive zone of increased permeability and vuggy or leached porosity. This permeability is laterally connected, but vertically restricted beneath a zone of subaerial cementation or evaporite plugging and between sections of marine-cemented rock which were not affected by karstic processes. Some other zones of enhanced permeability were formed, especially lower in the bioherm, but were later sealed by marine and phreatic cementation. Each bioherm is enclosed by the impermeable carbonates and evaporites of the Salina Formation.

The persistent concept that there was only one karst episode at the end of bioherm construction has lead to the assumption that the major permeability interconnections in the Guelph reefal bioherms are vertical. Our demonstration that there are laterally extensive and separate zones of enhanced permeability within these bioherms should have a major impact on exploration procedures, formation testing, well completions, enhanced recovery techniques, gas storage and retrieval methods, and techniques of subsurface waste disposal.

CONCLUSIONS

1. Development of the subsurface Silurian bioherm reservoirs in southwestern Ontario was governed by cyclical sea level fluctuations.
2. The succession of growth stages and depositional facies were identified in the Rosedale pinnacle bioherm and the Fletcher platform/bank bioherm.
3. There were seven major episodes of subaerial exposure during development of the Rosedale pinnacle bioherm.
4. Each karst episode produced a zone of laterally extensive and vertically restricted enhanced porosity and permeability.
5. Marine, meteoric phreatic, and burial diagenesis created pore-occluding cements, especially in the lower portions of each bioherm.
6. Only major karstic episodes, probably followed by relatively rapid sea level rise, seemed able to create lasting zones of enhanced permeability.

FUTURE OBJECTIVES

We plan to:

1. study other reefs in southwestern Ontario to further delineate reservoir zones and study their specific features in detail
2. correlate karstic features between reefs so that lithofacies and eustatic sea level patterns can be identified and compared, and their effects on off-reef sedimentation identified
3. test the idea that each depositional stage and each karstic episode produced characteristic sediment in the off-reef area (this sediment should give evidence of reef locations)
4. test the ideas of Sanford *et al.* (1985) using the above studies, to see if basement-block movement occurred during formation of these Middle Silurian reservoirs
5. make a preliminary evaluation of the Attawapiskat reefs of the Moose River Basin, northeastern Ontario, as potential reservoirs

ACKNOWLEDGMENTS

The Rosedale cores were given by Union Gas Limited, through the assistance of Thomas Bainbridge. The Fletcher cores, and cuttings from Lake Erie, were given by Consumers Gas Limited. We thank Steven Colquhoun for initiating the Fletcher study. The cores were slabbed by the Petroleum Resources Laboratory of the Ministry of Natural Resources. Other cores are made available at the Core Library Facility of this laboratory. We wish to thank P.A. Palonen, Rae Booth-Horst, and especially R.A. Trevail for their considerable assistance to the project.

We thank Canterra Energy Limited for supplying thin sections, and K.C. Lohmann and his laboratory for the stable isotope analyses. Field study of quarries in Ohio, Indiana, and Illinois was funded by the Advisory Research Committee of Queen's University. Eric Gosselin assisted with the SEM analysis. Ela Rusak was reponsible for the drafting and photography, and Dorinda Hannah typed the manuscript.

REFERENCES

Bailey, S.M.B.
1986: A New Look at the Development, Configuration and Trapping Mechanisms of the Silurian Guelph Reefs of Southwestern Ontario; Ontario Petroleum Institute, Twenty-Fifth Annual Conference, Paper Number 14, 28p.

Bainbridge, T.W.
1973: The Sedimentology of a Silurian Pinnacle Reef in the Michigan Basin; Unpublished B.Sc. Thesis, Queen's University, 62p.

Briggs, L.I., and Briggs, D.
1974: Niagara–Salina Relationships in the Michigan Basin; p.1-30 *in* Silurian Reef–Evaporite Relationships, edited by R.V. Kesling, Michigan Basin Geological Society, Field Conference, 111p.

Buddemeier, R.W., and Oberdorfer, J.A.
1986: Internal Hydrology and Geochemistry of Coral Reefs and Atoll Islands: Key to Diagenetic Variations; p.94-111 *in* Reef Diagenesis, edited by J.H. Schroeder and B.H. Purser, Springer, Berlin, 455p.

Cercone, K.R., and Lohmann, K.C.
1986: Diagenetic History of the Union 8 Pinnacle Reef (Middle Silurian), Northern Michigan, U.S.A.; p.381-398 *in* Reef Diagenesis, edited by J.H. Schroeder and B.H. Purser, Springer, Berlin.

Chalkley, P.
1983: The Sedimentologic Correlation and History of the Fletcher Silurian Pinnacle Reef, Eastern Michigan Basin; Unpublished B.Sc. Thesis, Queen's University, 54p.

Dickson, J.A.D., and Coleman, M.L.
1980: Changes in Carbon and Oxygen Isotope Composition During Limestone Diagenesis; Sedimentology, Volume 27, Number 1, p.107-118.

Grimes, D.J.
1987: Depositional Models, Subaerial Facies, and Diagenetic Histories of the Rosedale and Fletcher Reefs, Southwestern Ontario; Unpublished M.Sc. Thesis, Queen's University, 120p.

Grimes, D.J., and Smith, L.
1987: Depositional and Diagenetic History of the Fletcher Reservoir, a Platform Reef in Southwestern Ontario; p.86 *in* Reef Research Symposium, Canadian Society of Petroleum Geologists, Banff, Abstracts Volume, 111p.

Huh, J.M., Briggs, L.I., and Gill, D.
1977: Depositional Environments of Pinnacle Reefs, Niagara and Salina Groups, Northern Shelf, Michigan Basin; p.1-21 *in* Reefs and Evaporites, edited by J.H. Fisher, American Association of Petroleum Geologists, Studies in Geology 5, 196p.

Kahle, C.F.
1974: Nature and Significance of Silurian Rocks at Maumee Quarry, Ohio; p.31-54 *in* Silurian Reef–Evaporite Relationships, edited by R.V. Kesling, Michigan Basin Geological Society.

Mesolella, K.J., Robinson, J.D., McCormick, L.M., and Ormiston, A.R.
1974: Cyclic Deposition of Silurian Carbonates and Evaporites in Michigan Basin; American Association of Petroleum Geologists Bulletin, Volume 58, Number 1, p.34-62.

Pearson, E.M.
1980: Sedimentology and Diagenesis of the Warwick Reef (Silurian), Lambton County, Southwestern Ontario; Unpublished M.Sc. Thesis, University of Waterloo, 250p.

Petta, T.J.
1980: Silurian Pinnacle Reef Diagenesis—Northern Michigan: Effects of Evaporites on Pore Space Distribution; p.32-42 *in* Carbonate Reservoir Rocks, Society of Economic Paleontologists and Mineralogists, Core Workshop No. 1, 183p.

Sanford, B.V., Thompson, F.J., and McFall, G.H.
1985: Plate Tectonics—A Possible Controlling Mechanism in the Development of Hydrocarbon Traps in Southwestern Ontario; Canadian Petroleum Geology Bulletin, Volume 33, Number 1, p.52-71.

Sarg, J.F.
1982: Off-Reef Salina Deposition (Silurian), Southern Michigan Basin—Implications for Reef Genesis; p.354-384 *in* Deposition and Diagenetic Spectra of Evaporites, Society of Economic Paleontologists and Mineralogists, Core Workshop No. 3, 395p.

Sears, S.O., and Lucia, F.J.
1979: Reef Growth Model for Silurian Pinnacle Reefs, Northern Michigan Reef Trend; Geology, Volume 7, Number 6, p.299-302.

Simo, A., and Lehmann, P.
1988: Deposition and Diagenesis of a Cratonic Silurian Platform Reef, Pipe Creek Jr., Indiana (Abstract); American Association of Petroleum Geologists Bulletin, Volume 72, Number 2, p.248-249.

Smith, L.
1984: The Guelph–Lower Salina in Southwestern Ontario: Subaerial Exposure and Episodic Reef Growth in a Syn-Erosional Basin; Geological Association of Canada, Abstracts, Volume 9, p.107.

Trevail, R.A., and Smith, L.
1987: Cratonic Tectonism as Control of Spatial Distribution and Form of Silurian Pinnacle and Platform Reefs, Southwestern Ontario; Reef Research Symposium, Banff, Abstracts Volume, p.61.

Grant 298 The Geological Setting of Gold Deposits in the Porcupine Mining Camp

R. Mason, D.I. Brisbin, and S. Aitken

Department of Geological Sciences, Queen's University, Kingston

ABSTRACT

Field-based studies in the Porcupine gold camp of northeastern Ontario have elucidated the sequence of geological events in the camp, and the place of gold mineralization within this sequence. The recognition of two major angular unconformities within the volcanic-sedimentary sequence north of the Destor–Porcupine Fault Zone is indicative of multiple tilting and/or folding episodes. Porphyritic felsic intrusions and associated heterolithic breccia bodies postdate the deposition of the youngest sedimentary rocks in the area, the tectonism which resulted in the unconformities, and the subsequent folding.

Hydrothermal alteration and mineralization overprint, and thus postdate, the porphyries. Alteration and mineralization are zoned about porphyry centres, and productive mineralized structures are located adjacent to porphyries, thus indicating a localization of mineralization about intrusive centres. Outside of major mineralized centres, there is a strong lithological control of style and intensity of alteration and mineralization. Fracture-controlled alteration is widespread, occurring throughout both Tisdale and northern Deloro townships. The presence of heterolithic breccia bodies, the dominance of the fracture-controlled alteration style, and the utilization of primary permeability in rocks such as pillow breccias by hydrothermal fluids all indicate that alteration occurred (mineralization was emplaced) at shallow levels in the crust.

Regional cleavage and linear fabrics transect axial planes of folds in the camp. In addition, the cleavage and linear fabrics deform, and thus postdate, mineralized structures. The style and intensity of cleavage development were controlled by primary lithological heterogeneities, the style of hydrothermal alteration, and the mineralogy of altered rocks. In particular, flattened fracture stockworks now appear as spaced cleavages.

INTRODUCTION

This report follows two previously published reports by Mason and Brisbin (1987), and Brisbin *et al.* (1987), and is a description of progress on a field based study in the Porcupine Camp, due to be completed in 1989. It can be regarded as a continuation of, and companion to, the 1987 report by Mason and Brisbin which outlines the stratigraphy of the Tisdale Group. The research project involves the detailed geological mapping of Tisdale Township and the northern portion of Deloro Township, at a scale of 1:6000 (Figure 298.1), and a reappraisal of the timing and location of gold mineralization at Timmins with respect to the geological evolution of the area. To complement the field mapping, diamond-drill core and reverse circulation drill chip samples provided by two exploration companies, and diamond-drill core stored at the Ministry of Northern Development and Mines core library facility in Timmins, have been logged. The compilation of available mine records and plans, along with assessment work records filed at the Resident Geologist's Office in Timmins, is continuing and will be completed by the end of 1988.

During the 1987 field season, mapping was concentrated in eastern Tisdale Township, from the border with Deloro Township in the south, to the border with Murphy Township in the north. An area northeast of Number 8 shaft at the Dome Mine, stripped to bedrock by Placer Dome Incorporated, was mapped at a scale of 1:1200 and has been described by Aitken (1988). The main emphasis of the present report is on hydrothermal alteration, mineralized structures, and deformation.

STRUCTURE

UNCONFORMITIES

The relationship of sedimentary formations to Tisdale Group volcanic rocks at Timmins has been variously interpreted. Burrows (1911) included all sedimentary rocks in the camp in the Timiskaming "Series", interpreting them to unconformably overlie the volcanic rocks. Hurst (1939) placed the Timiskaming unconformity within the sedimentary sequence, so that the sedimentary rocks below the Timiskaming unconformity were included with the Keewatin volcanic sequence and were considered to overlie the volcanic rocks conformably. This interpretation was supported by Ferguson *et al.* (1968). Moore (1953) placed the Timiskaming unconformity at the base of the Krist felsic pyroclastic rocks (for discussion of stratigraphic terminology *see* Mason and Brisbin 1987). Pyke (1982) suggested that sedimentary rocks of the Timmins area are time equivalent to volcanic rocks of the upper Deloro Group and Tisdale Group, and proposed the Porcupine Group to include all the sedimentary rocks in the area.

The sedimentary rocks preserved in the Porcupine Syncline (Figure 298.1) consist of two distinct sequences separated by a well defined unconformity. The upper sedimentary sequence contains polymictic conglomerates. The unconformity is exposed in the "greenstone nose" at Dome (Holmes 1968), and is also exposed in outcrops opposite the entrance to the South Porcupine Hospital, and to the north of South Porcupine, where conglomerates overlie a sequence of thinly bedded wacke-argillite units with angular discordance.

The sedimentary sequence in the Porcupine Syncline and the Kayorum Syncline (Figure 298.1) consists of a basal argillite unit overlain by Krist fragmental felsic volcanic rocks, which are in turn overlain by a wacke-argillite sequence. At the Moneta Mine, Buffam (1948) shows the truncation of Tisdale mafic flows by the Krist fragmental unit, with a marked discordance of strike. Moore (1953) reported on sections across the contact of the basal argillite, along the north limb of the Porcupine Syncline, and showed that this sequence overlies a sharply trun-

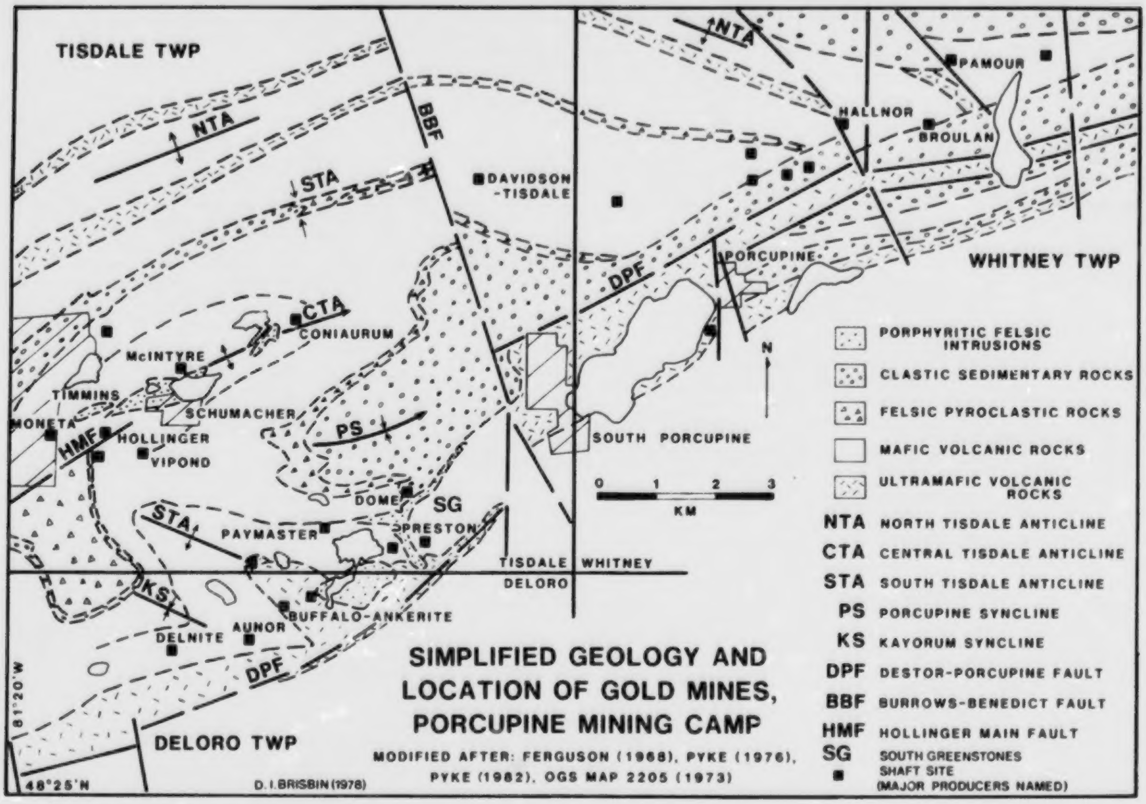
TISDALE TWP
NTA
STA
BBF
DAVIDSON -TISDALE
CTA
CONIAURUM
McINTYRE
TIMMINS
SCHUMACHER
MONETA
HMF
HOLLINGER
VIPOND
PS
DOME
SG
PAYMASTER
PRESTON
STA
KS
BUFFALO-ANKERITE
AUNOR
DELNITE
DPF
TISDALE
WHITNEY
DELORO
DELORO TWP
81°20'W
48°25'N
D.I.BRISBIN (1978)
PAMOUR
HALLNOR
BROULAN
PORCUPINE
DPF
WHITNEY TWP
N
SOUTH PORCUPINE
0 1 2 3
KM
SIMPLIFIED GEOLOGY AND LOCATION OF GOLD MINES, PORCUPINE MINING CAMP
MODIFIED AFTER: FERGUSON (1968), PYKE (1976), PYKE (1982), OGS MAP 2205 (1973)
PORPHYRITIC FELSIC INTRUSIONS
CLASTIC SEDIMENTARY ROCKS
FELSIC PYROCLASTIC ROCKS
MAFIC VOLCANIC ROCKS
ULTRAMAFIC VOLCANIC ROCKS
NTA NORTH TISDALE ANTICLINE
CTA CENTRAL TISDALE ANTICLINE
STA SOUTH TISDALE ANTICLINE
PS PORCUPINE SYNCLINE
KS KAYORUM SYNCLINE
DPF DESTOR-PORCUPINE FAULT
BBF BURROWS-BENEDICT FAULT
HMF HOLLINGER MAIN FAULT
SG SOUTH GREENSTONES
■ SHAFT SITE (MAJOR PRODUCERS NAMED)

Figure 298.1. *Simplified geology and location of gold mines in the Porcupine Mining Camp.*

cated surface of Tisdale mafic flows. The inspection of mapped relationships shows a marked variation in the thickness of the Gold Centre Formation across the Porcupine Syncline (Mason and Brisbin 1987), and shows that this formation is completely absent on the east limb of the Kayorum Syncline. Thus, the field evidence points to an unconformity separating the lower sedimentary sequence from the Tisdale Group.

Another problematic area, the North Tisdale Syncline (Figure 298.1), may thus simply represent an erosional remnant of the lower sedimentary sequence unconformably overlying a south-facing sequence of mafic flows.

Sedimentary units interlayered with Tisdale Group mafic flows are exposed in a road cut east of the Dome Extension townsite (Figures 298.2 and 298.3). The recognition of this relationship in outcrop (described further below) confirms the time equivalence of some of the sedimentary and volcanic rocks in the area, as suggested by Pyke (1982).

FOLDING

The Tisdale sequence was at least tilted, if not folded, prior to the deposition of the sedimentary sequences which overlie the Tisdale rocks, but the major folds in the study area appear to affect both Tisdale and Timiskaming sequences alike. The porphyry intrusions in the camp all appear to postdate this major folding event. Another significant feature of the folding is the lack of planar fabrics associated with the folds (Roberts 1981; this study). The overall distribution of stratigraphic units in southern Tisdale Township, together with bedding attitudes and facing directions mapped in Porcupine Group sedimentary rocks, confirm the position and shape of the Porcupine Syncline as shown by Ferguson *et al.* (1968) on ODM Map 2075.

On the northern flank of the Porcupine Syncline (Figure 298.1), the Central Tisdale Anticline is an east-north-east plunging fold. The variolitic pillowed flows of the Vipond Formation have been traced in outcrop and in diamond-drill core east-northeast from the west side of the Coniaurum Mine tailings (northwest of the Coniaurum Closure) to the Burrows–Benedict Fault. In this area, northeast of the Coniaurum Mine, a south facing sequence of Tisdale Group rocks has been confirmed from mapping, and the examination of available diamond-drill core. The tight anticline shown on ODM Map 2075 (Ferguson *et al.* 1968) is not present. The exact location of the northern limb of the Central Tisdale Anticline, in northeastern Tisdale Township, is uncertain.

Two second-order anticlinal folds have been mapped on surface on the southeastern limb of the Central Tisdale Anticline. The closure of the easternmost fold occurs along the eastern boundary of the

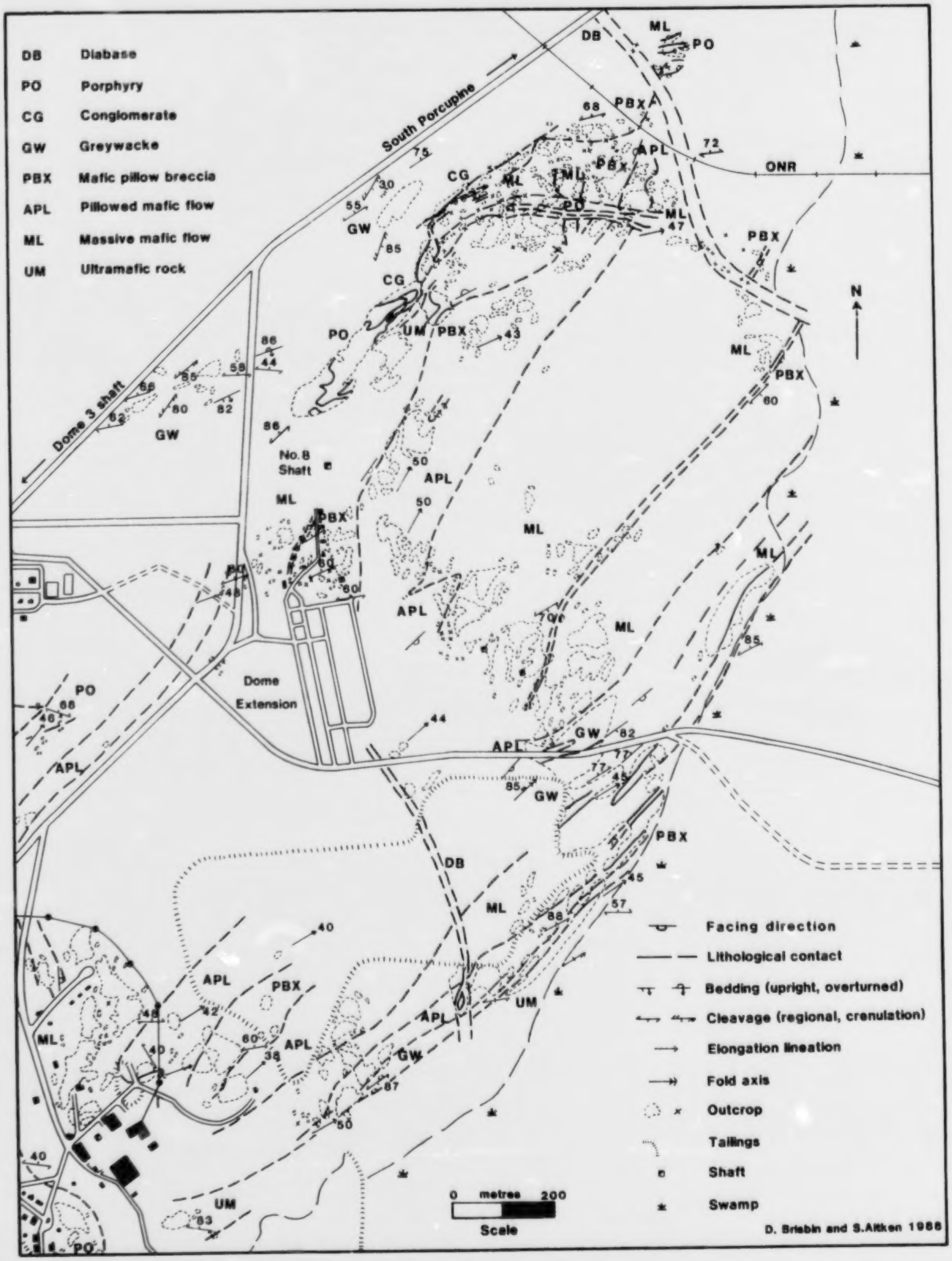
DB Diabase
PO Porphyry
CG Conglomerate
GW Greywacke
PBX Mafic pillow breccia
APL Pillowed mafic flow
ML Massive mafic flow
UM Ultramafic rock
South Porcupine
Dome 3 shaft
No.8 Shaft
Dome Extension
ONR
N
Facing direction
Lithological contact
Bedding (upright, overturned)
Cleavage (regional, crenulation)
Elongation lineation
Fold axis
Outcrop
Tailings
Shaft
Swamp
0 metres 200
Scale
D. Brisbin and S.Aitken 1988

Figure 298.2. Geology of southeastern Tisdale Township.

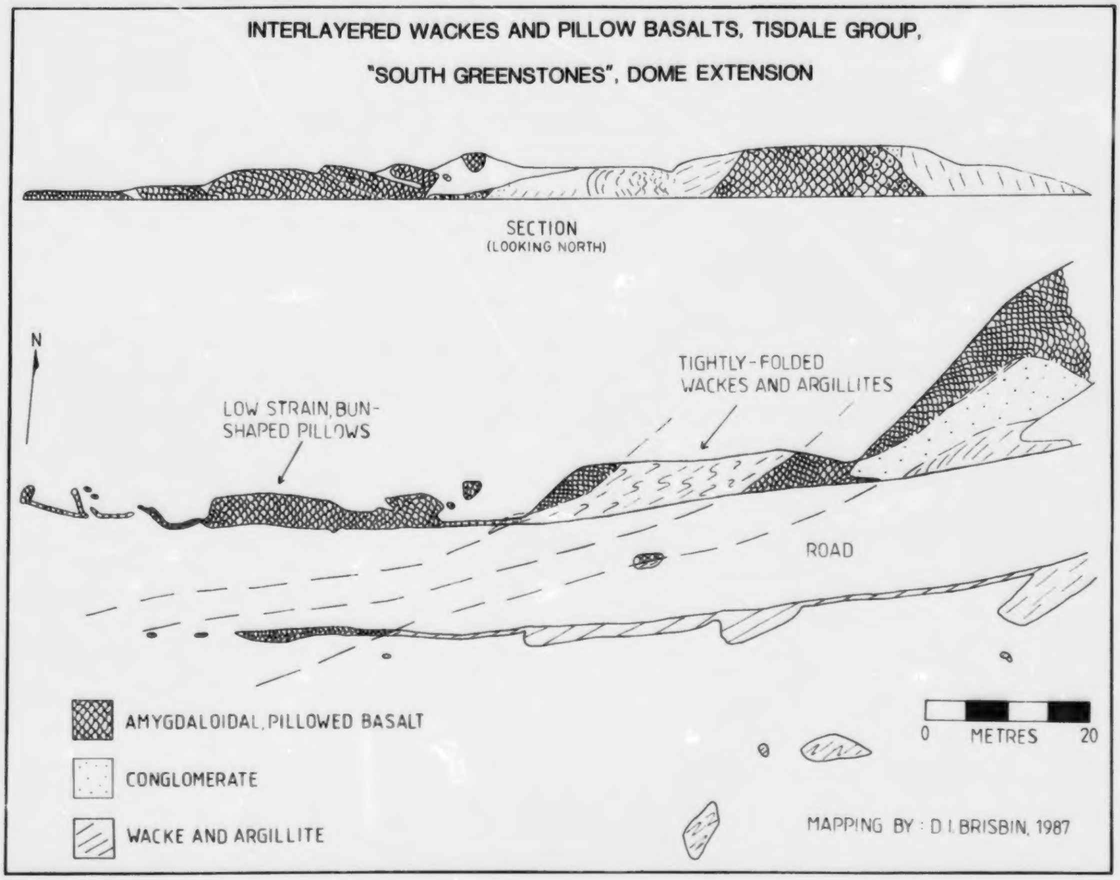
INTERLAYERED WACKES AND PILLOW BASALTS, TISDALE GROUP,
"SOUTH GREENSTONES", DOME EXTENSION
SECTION
(LOOKING NORTH)
N
LOW STRAIN, BUN-SHAPED PILLOWS
TIGHTLY-FOLDED WACKES AND ARGILLITES
ROAD
AMYGDALOIDAL, PILLOWED BASALT
CONGLOMERATE
WACKE AND ARGILLITE
0
METRES
20
MAPPING BY : D.I. BRISBIN, 1987

***Figure 298.3.** Detailed geology of road cut exposure east of the Dome Extension townsite.*

Coniaurum property. The second closure is just east of the town of Schumacher. Both folds are defined by the outcrop distribution of the V10B flow unit, which is not as irregular along the fold closures as shown by Ferguson *et al.* (1968). The closure near Schumacher was mapped down plunge on the Coniaurum Mine 1000-foot level by Ferguson *et al.* (1968). The authors gained access to the 1000-foot level in 1986, and confirmed the existence of the fold shown by Ferguson *et al.*

The western closure of the Central Tisdale Anticline on the Moneta Property plunges steeply (±80°) east-northeast as described previously by Ferguson *et al.* (1968).

The outcrop patterns shown by Ferguson *et al.* (1968) on Map 2075 for the V10B flow unit, from the Vipond Mine east to Gold Centre, have been confirmed. It is difficult or impossible to measure dips in outcrops of the Vipond units in the absence of good contacts and three dimensional exposures. However, the irregular distribution of this unit is suggestive of interference folding, or the influence of topography on gently dipping strata. Shallow dips are suggested in this area by the presence of only two lithologies: a brecciated variolitic pillowed flow unit (V10B); and a moderately to strongly carbonatized and fractured massive flow unit (V10A or V11). The exposure of such a limited portion of Tisdale Group stratigraphy, over such a large area relative to sections exposed north, northeast, and southeast, is also suggestive of shallow dips. The area east of the Vipond Mine appears to be an arch between the east-plunging Porcupine Syncline to the east, and the west-plunging Kayorum Syncline to the southwest (Figure 298.4).

A portion of southeastern Tisdale Township is underlain by a series of mafic volcanic flows which are isolated from Tisdale Group mafic volcanic rocks exposed elsewhere in the township. These flows are known as the "South Greenstones" (Figure 298.1) at the Dome Mine (Holmes 1968). The mafic volcanic rocks are bounded to the east by the Burrows–Benedict Fault, to the southeast by the Destor–Porcupine Fault, to the southwest by the Preston Porphyry, and to the north and northwest by sedimentary rocks of the Timiskaming Group (Figure 298.4).

Previous workers (Holmes 1968; Roberts 1981) had interpreted the "South Greenstones" as a south-facing sequence of flows, separated from the Vipond flows to the north by the Preston Porphyry. The map of Ferguson *et al.* (1968) shows the "South Greenstones" as tightly folded along east-west axes, with a

Photo 298.1. *Tourmalinized heterolithic breccia dike, northeast of Number 8 shaft, Dome Mine. Viewed in plan.*

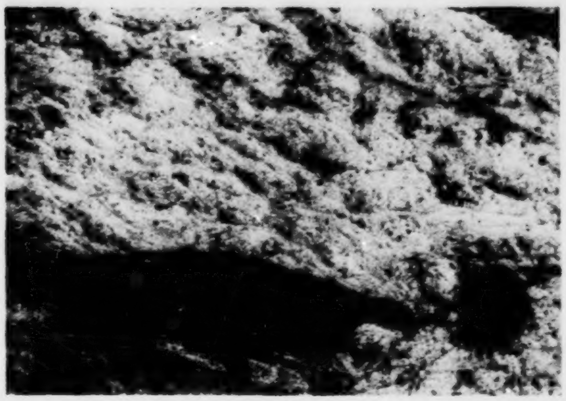

Photo 298.2. *Xenolith of argillite in porphyry, northeast of Number 8 shaft, Dome Mine. Viewed in plan.*

major anticline, the Simpson Lake Anticline (South Tisdale Anticline on Figure 298.1) extending through the Preston Porphyry, and to the west of the Dome Mine.

Holmes (1968) stated that the attitude of narrow but persistent flow breccias defines a northeast strike and subvertical dip to the south, and he interpreted grain size variations in massive portions of the flows to indicate south facings. Ferguson *et al.* (1968) interpreted south facing directions on ODM Map 2075, based upon shapes of pillows in the mafic flows. Holmes (1968) indicated that the south-dipping and facing "South Greenstones" could not be correlated with mafic flows to the west of the Preston Porphyry, which dip and face north.

Recent detailed mapping (Aitken 1988) confirms subvertical dips of flow contacts in the "South Greenstones", but has revealed good evidence of north facing directions in the flows northeast of Dome Number 8 shaft (Figure 298.2). The interpretation of north facings is based upon the recognition of flow contacts. In one flow, a gradation upwards and to the north, from pillows to pillow breccia, and the sharp contact of the pillow breccia with the massive base of the overlying flow were observed (Photo 298.3).

South facing directions are indicated by pillows in mafic flows, and graded bedding in intercalated clastic sedimentary rocks, on the southeastern side of the "South Greenstones" in a road cut on a gravel road located 500 m southeast of the Dome Extension townsite. The geological relationships exposed at this outcrop are illustrated in Figure 298.3. Two sedimentary units are conformably interbedded with amygdaloidal pillowed flows. The flows exhibit good examples of pedunculate pillows (i.e. pillows with convex smooth upper surfaces and basal protuberances) which show no planar fabric but have been elongated. A thin basal conglomeratic grit is developed in both sedimentary units. The clasts are oligomictic and consist of mafic volcanic clasts in a wacke matrix. Cyclically interbedded wackes and argillites overlie the conglomerates.

Exposures of the interbedded wackes and argillites show intense folding of the bedding with well developed axial planar cleavage. Hurst (1939) shows a fault contact between the sedimentary rocks and underlying amygdaloidal pillow flows to the north on ODM Map 47A. Ferguson *et al.* (1968) assigns the sedimentary rocks to the Timiskaming Group and adjacent flows to the Keewatin Group on ODM Map 2075, thus implying an unconformable contact. Neither Hurst nor Ferguson *et al.* recognized that there are in fact two units of sedimentary rocks separated by a conformable pillowed mafic flow. Although the contact between the northern sedimentary unit and underlying mafic flows to the northwest is badly broken on this outcrop, there is neither evidence of a fault, nor is there evidence of an unconformity. Facing directions in both the flows and sedimentary rocks are to the southeast, and the oligomictic lithology of the basal conglomerates is out of character with the typical Timiskaming-type polymictic conglomerates. The juxtaposition of mafic flows showing low strain with highly deformed interbedded wacke and argillite, is due to the heterogeneous strain distribution between rocks of differing competencies.

The opposition of north and south facing directions on the north and south sides, respectively, of the "South Greenstones" is interpreted as defining an anticline with a northeast-striking axis. This anticline may be the extension of the South Tisdale Anticline (Figure 298.4) east of the Preston Porphyry. Both the Vipond Formation and the Gold Centre Formation are absent east of the Preston Porphyry. These units have been removed along the south side of the anticline by movement along the Destor–Porcupine Fault. They are not exposed at surface along the north side of the anticline, where Timiskaming sedimentary rocks and Central Formation flows are in unconformable or faulted contact, but they have been traced underground at the Dome Mine.

Holmes (1968) pointed out that the "South Greenstones" do not resemble the flows of the Vipond Formation exposed in the Dome Mine, but that they are similar to flows of the Central and Northern formations exposed elsewhere in Tisdale Township (Ferguson 1968; Mason and Brisbin 1987). These

Photo 298.3. *Flow top breccia in contact with the massive base of an overlying flow. Facing direction is north (right). Northeast of Number 8 shaft, Dome Mine. Viewed looking west.*

Photo 298.4. *Interbedded greywacke and argillite, the Timiskaming Group. A crenulation cleavage cuts an earlier continuous cleavage in the argillite layers. Outcrop west of the hospital in South Porcupine. Viewed in plan.*

formations conformably underlie the Vipond Formation, and are exposed on surface immediately south of the Dome Mine Property, on the Paymaster and Preston mine properties. Both the South Greenstone sequence, and the Central and Northern formations, are typified by: very fine- to fine-grained massive mafic flows with mesoscopic leucoxene; mafic pillowed flows, with selvages less than 10 mm wide defining sparsely to densely amygdaloidal pillows (amygdules ± 1 mm in diameter), which are generally less than 150 by 50 cm^2 in plan view; and, mafic pillow breccias with irregularly shaped pillow fragments generally less than 15 cm in size.

Davies and Whitehead (1980) interpret the "South Greenstones" as belonging to the Northern Formation, based upon the comparison of their immobile trace element Zr, Y, and TiO_2 contents with those of known Northern Formation rocks elsewhere in Tisdale Township. However, because the "South Greenstones" can be traced stratigraphically upwards without discordance into the Vipond Sequence, they should logically be correlated with the Central Formation.

PORPHYRIES AND HETEROLITHIC BRECCIAS

The study area is characterized by a suite of felsic porphyry intrusions which postdate folding but predate gold mineralization. Heterolithic breccias are commonly associated with the porphyry intrusions and occur as pebble dikes, as mantles around porphyry contacts, and as irregular pipe-like bodies. Albitite dikes occur in the Hollinger–McIntyre Complex and at Dome Mines, and appear to represent the last rock forming event prior to the emplacement of the gold mineralization. Marmont and Corfu (1988) have shown that albitite dikes at McIntyre (Figure 298.1) postdate the Pearl Lake Porphyry by at least 12 Ma. The intrusive nature of the porphyries can be demonstrated in nearly all cases by the occurrence of xenoliths of volcanic and sedimentary country rocks within the porphyry bodies, and the discordant nature of porphyry contacts with respect to volcanic and sedimentary units. The more massive (less schistose) porphyries exhibit good igneous textures with well preserved phenocrysts of quartz and/or feldspar.

In spite of the fact that gold mineralization postdates the albitite dikes, which themselves postdate the porphyry intrusions, there is still a remarkable spatial association of intense hydrothermal alteration and mineralized structures with porphyry contacts, a relationship which is particularly well illustrated in both the Hollinger–McIntyre–Coniaurum Complex, and at the Dome, Preston, and Paymaster mines. This suggests that the sites for subsequent emplacement of hydrothermal fluids and gold mineralization were prepared at the time of porphyry emplacement. The mineralizing event appears to have been related to hydrothermal activity associated with the emplacement of the albitite dikes.

The Paymaster, Preston, and West Preston porphyries include quartz, quartz-feldspar, and feldspar porphyritic varieties. Mapping has revealed intense stockwork fracturing in these porphyries and adjacent country rocks, and a fracture-controlled style of alteration (Photo 298.5) similar to that documented by Mason and Melnik (1986) in the Pearl Lake and associated porphyries. A gradation from sericite ± pyrite in fractures close to mineralization, to chlorite in fractures cutting the porphyry further removed from mineralization, is present in the Preston and West Preston porphyries. An increase in alteration intensity (i.e. increasing amounts of sericite, ankerite, and pyrite) and quartz vein density occurs, from south to north, in both the Preston and West Preston porphyries.

Xenoliths of argillite are present in porphyry cropping out northeast of Dome Number 8 shaft (Photo 298.2), near the contact of the porphyry with conglomerate, greywacke, and argillite of the Timiskaming Group. This observation supports Holmes' (1944) description of the porphyry bodies exposed underground in the Dome Mine intruding, and thus postdating, the Timiskaming sedimentary rocks.

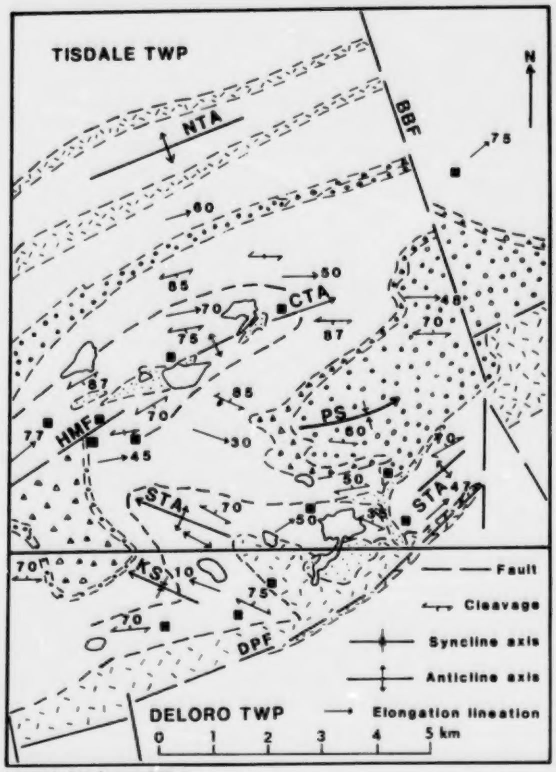

Legend: See figure 298.1

Figure 298.4. Average orientation of cleavage and linear elongation fabrics in the Porcupine Mining Camp.

Anhydrite was identified, along with quartz and dravite, in a vein cutting amygdaloidal pillowed flows east of Number 8 shaft, at the Preston Mine. Anhydrite is common in veins associated with the copper zone at the McIntyre Mine (Langford and Hancox 1936; Davies and Luhta 1978; Mason and Melnik 1986), but it has not previously been documented elsewhere in the camp.

Heterolithic breccias were first described in the Porcupine Camp by Whitman (1915). These breccias have been documented on the Coniaurum (Piroscho 1985), McIntyre (Mason and Melnik 1986), and Hollinger (Mason and Melnik 1986) properties (Davies 1988), where they show a close spatial association with quartz-feldspar porphyry bodies. Additional occurrences of heterolithic breccia have been mapped by the authors in and adjacent to the Crown, Preston, and Paymaster porphyries. The heterolithic breccias occur as dikes and pipes, cutting both the porphyry bodies and surrounding volcanic country rocks, and as irregular bodies mantling the margins of porphyry bodies (for example, the Crown Porphyry). They are composed of rounded to angular fragments of quartz-feldspar porphyry and mafic volcanic rock in variable proportions. The porphyry fragments are light grey and weather white. The volcanic fragments are chloritic and green on both fresh and weathered surfaces. The microcrystalline ("rock flour") groundmass is composed of variable amounts of quartz, carbonate, plagioclase, sericite, chlorite, and leucoxene (Davies 1988). Tourmaline is abundant in the groundmass of a heterolithic breccia dike exposed northeast of Number 8 shaft on the Dome Property (Photo 298.1). A spectacular exposure of the north margin of the Crown Porphyry occurs on a hydro line just north of the Crown Shaft on the Hollinger Property. Massive porphyry grades outward into a marginal zone of inclusion-rich porphyry which, in turn, grades out into a heterolithic breccia. This outcrop clearly illustrates the process of brecciation of the porphyry and surrounding country rocks by explosive hydrothermal activity, and the development of heterolithic breccias as an end product of this process.

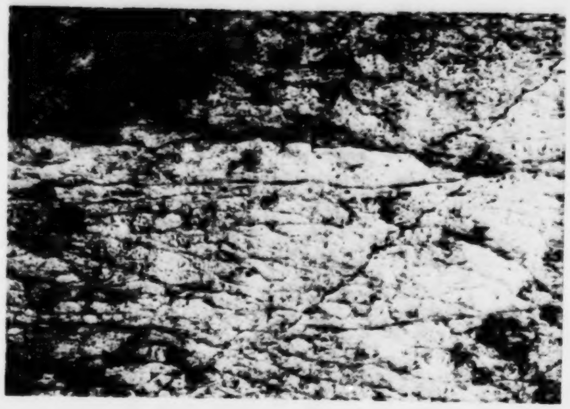

Photo 298.5. *Anastomosing sericite-filled fracture stockwork in the Paymaster Porphyry, Paymaster Property. Viewed in plan.*

As noted above, heterolithic breccia dikes and pipes cut the porphyries, and the breccia dikes contain fragments of porphyry. Where quartz veins and heterolithic breccias are present in the same exposure, the veins cut the breccias, and the breccias are hydrothermally altered. Cleavage and linear fabrics are developed in the porphyries, heterolithic breccias, and veins. The development of heterolithic breccias appears to have immediately followed, and been synchronous with, the intrusion of the quartz-feldspar porphyries. Mineralized quartz veins postdated the emplacement of porphyries and heterolithic breccias. Finally, the deformation that resulted in the development of regional cleavage and linear fabrics overprinted porphyries, heterolithic breccias, and veins.

ALTERATION

Since Burrows (1911) recognized the extensive carbonatization of rocks in the Porcupine Camp, and the iron carbonate enrichment of wall rocks adjacent to quartz veins in particular, much has been written on wall rock alteration in the camp. Hore (1913), Bain (1933), and Graton and McKinstry (1933) described the carbonatization, sericitization, pyritization, and silicification which typically occur adjacent to auriferous quartz veins. Bain (1933) noted the decrease in abundance of these alteration minerals away from the vein. In addition, Graton and McKinstry (1933) noted the presence of a zonation in vein and wall rock alteration mineralogy on the Hollinger property.

Fyon and Crocket (1979, 1980, 1983), Davies *et al.* (1982), Whitehead *et al.* (1980), and Fryer *et al.* (1979) have confirmed and elaborated on the zonation of alteration minerals described by Bain (1933), and Graton and McKinstry (1933).

The detailed mapping of Tisdale and northern Deloro townships has shown that the entire area has been affected to some extent by stockwork fracturing and related hydrothermal alteration. Mason and Melnik (1986) first pointed out the primary and secondary permeability controls on hydrothermal alteration at the McIntyre Mine, and this study has demonstrated for the first time the dominance of stockwork fracturing as a secondary type of control on alteration throughout the area mapped. We regard this as of major significance in interpreting the genesis of the gold deposits in the Timmins Camp. The hydrothermal alteration consists of pervasive, selective, and fracture-controlled carbonatization, and fracture-controlled sericitic and chloritic alteration. Cross-cutting relationships between fractures filled with different minerals indicates that the alteration/mineralization history was not simple, and either occurred in a number of episodes, or as a continuous process with the evolution of hydrothermal fluid chemistry over time. The stockwork-type fracturing created large volumes of permeable rock and thus allowed access to hydrothermal fluids. It was subsequently shortened during regional deformation, and metamorphic recrystallization under greenschist facies conditions accompanied this deformation. These relationships can be clearly seen both in outcrops and in thin sections.

Mineralized centres are characterized by proximal sericitic/ferroan dolomite-ankerite alteration, and distal chlorite/calcite alteration. Most of the intensely hydrothermally altered zones and mineralized structures are associated with porphyry intrusions, breccia pipes and dikes, and albitite dikes. The volume of fractured and altered rocks around the mineralized centres is far greater than the centres themselves, and indicates catastrophic energy release related to retrograde boiling during the development of the hydrothermal systems involved (Burnham and Ohmoto 1980). A similar area of fracturing and alteration has been recently described around the Sierrita–Esperanza Porphyry Copper Complex in Arizona by Titley *et al.* (1986). Gold mineralization occurred late in the evolution of the hydrothermal systems (Keys 1938, 1940; Armstrong 1960) in the Porcupine Camp, and is much more restricted in extent than the early barren hydrothermal alteration (Graton and McKinstry 1933).

The comparison of the distribution of alteration assemblages and lithostratigraphic units on 1:6000 scale maps in preparation reveals that, outside of major mineralized areas, there is a strong measure of lithological control on the location and style of alteration. Massive flows such as the 99 Flow unit and the V10A flow unit appear to have acted as barriers that confined hydrothermal fluids, whereas rocks with primary permeability, such as pillow breccias, have acted as conduits.

The role of the massive flows in having constrained hydrothermal fluids is best illustrated on the Hollinger and Coniaurum properties. The densely veined and mineralized Central Ore Zone at Hollinger is contained within the Central Formation, and is bounded to the south by the 99 Flow, a massive flow at the base of the Vipond Formation. Outside of the Central Ore Zone, in the overlying Vipond Formation, alteration is selective, occurring only immediately adjacent to widely spaced veins. The 99 Flow unit itself is pervasively carbonatized and intensely fractured, with sericitic alteration along the fractures. The V8 flow unit which immediately overlies it is relatively unaltered. A similar situation is present on the Coniaurum Property, where the C15 flow unit of the Central Formation and the overlying 99 Flow unit are both moderately to strongly carbonatized. Discontinuous auriferous quartz veins occur within the 99 Flow unit, and in interflow sedimentary units adjacent to it; some of these were mined as ore at the Coniaurum Mine. The overlying V8 flow unit is again relatively unaltered. Thus, on both the Hollinger and Coniaurum properties, hydrothermal fluids have penetrated the relatively permeable amygdaloidal pillowed flows and pillow breccias of the Central Formation, but were restrained by the massive 99 Flow unit.

Where hydrothermal fluids penetrated into the Vipond Formation, the V10A, another massive flow unit, has acted as a barrier in a similar fashion to that described above. The V10A flow unit occurs between the distinctive variolitic V8 and V10B flow units in the Vipond Formation. Wherever it crops out around the Porcupine Syncline (Figure 298.1) in southern Tisdale Township, it is moderately to strongly fractured and carbonatized (Photo 298.7). The fractures are filled with one or more of sericite, chlorite, carbonate, quartz, or tourmaline. Again the V10B flow unit, which immediately overlies the V10A flow unit, is relatively unaltered.

Evidence of hydrothermal fluids preferentially utilizing lithologies of high primary permeability is widespread, a factor emphasized by Mason and Melnik (1986) at the Hollinger and McIntyre mines. Pillow breccias, flow top breccias, and pillow selvages (Photo 298.8) have often undergone one or more of carbonatization, chloritization, and sericitization with or without pyritization. Carbonaceous argillites occur at interflow horizons throughout the Tisdale Group. Although these thin interflow sedimentary sequences, which vary in thickness from a few centimetres to tens of metres, are rarely exposed at surface, they are commonly intersected by mine workings and diamond-drill holes. Significant amounts of gold were, and in some cases still are, produced by the mining of single vein structures and vein systems located within these interflow sedimentary units at the Moneta, Hollinger, Vipond, McIntyre, Coniaurum, Dome, Paymaster, and Buffalo–Ankerite mines. Thus, the interflow contacts and sedimentary units provided favourable loci for fluid movement and subsequent quartz-gold deposition.

The demonstrated affinity of hydrothermal fluids for rocks with high primary permeability (for example,

Photo 298.6. *Shortened sericite-filled fracture stockwork defines a spaced anastomosing cleavage in the Pearl Lake porphyry, 85 pit, Hollinger Mine. Viewed looking northeast.*

pillow breccias) necessitates this permeability being available to the fluids at the time of mineralization. As such, metamorphism and ductile deformation (cleavage and lineation development) could not have preceded or been synchronous with mineralization, because primary pore spaces would be sealed and unavailable to hydrothermal fluids. The timing relationships between mineralized structures, related alteration, and subsequent metamorphic recrystallization related to penetrative fabric development support the above observation.

The new recognition of the dominance and areal extent of fracture-controlled alteration places severe constraints on the depth of emplacement of these systems (Burnham and Ohmoto 1980). It underscores the incompatibility of typically brittle structures associated with near-surface epithermal-mesothermal hydrothermal systems, with the contemporaneous development of linear elongation fabrics, cleavage, and greenschist facies metamorphism associated with penetrative fabric development at greater depths.

MINERALIZED STRUCTURES

The disposition of gold orebodies and hydrothermal alteration, in and around porphyry intrusions within the study area, has invoked discussion on possible genetic links between the two throughout the history of the Timmins camp. We have suggested previously in this report that the porphyries were responsible for the preparation of mineralized sites, but Marmont and Corfu (1988) have demonstrated a large enough time gap between porphyries and albitite dikes (which also predate the mineralization) to preclude the porphyries as sources for mineralizing fluids. Thus there is a genetic link between the porphyries and gold mineralization only in the sense of ground preparation of subsequently mineralized sites.

Many of the major orebodies in the Porcupine camp were developed in favourable lithostructural sites (flow tops, permeable units, brittle units, and contacts in general) adjacent to porphyry contacts, and most of the large vein systems at McIntyre dip northwards off the contact of the Pearl Lake Porphyry. The major vein swarm which constituted the Central Ore Zone at the Hollinger Mine was closely associated with porphyry contacts. We have noted a decline in the intensity of hydrothermal alteration associated with several major mineralized structures with increasing distance from porphyry contacts, suggesting a proximal-distal relationship with respect to the source of the mineralizing fluids. This has been observed downdip along mineralized structures at the McIntyre and Dome mines, suggesting that in these cases fluids travelled downdip into downward-propagated cracks off the porphyry contacts.

Our recognition of widespread stockwork fracturing and hydrothermal alteration, controlled by a combination of the secondary permeability induced by the fracturing, and primary permeability along contacts, and in porous units such as breccias, clearly indicates a near-surface low stress environment (Burnham and Ohmoto 1980) at the time of alteration and subsequent mineralization. The porphyry intrusions and associated heterolithic (hydrothermal) breccias indicate the same near-surface environment prior to alteration and mineralization. All these features are common to Cenozoic hydrothermal systems, which develop mesothermal to epithermal stockwork mineralization of porphyry type. The interpretation of the Hollinger–McIntyre Complex as a gold-dominated porphyry system (Mason and Melnik 1986) is not only supported by this study, but the now known extent of fracture-controlled alteration in the study area implies clearly that the mineralization throughout the study area is related to normal porphyry-type hydrothermal systems, developed in association with near-surface felsic intrusions.

The restricted distribution of high strain zones to areas of sericitic alteration, and the evidence for the dominant shortening and elongation of mineralized structures and all pre-mineralized rock units associated with pure shear mechanisms (rather than simple shear), are all factors which point to the penetrative deformation in the study area having occurred as a separate episode after the mineralization, and at or below the brittle-ductile transition zone within the crust. The penetrative deformation is incompatible

Photo 298.7. *Fracture-controlled ankerite alteration in the V10A (massive mafic flow), Coniaurum Property. Viewed in plan.*

with the widespread stockwork fracturing and the hydrothermal breccias in the area, and thus these phenomena could not have been synchronous. Variations in strain states of mineralized structures, and their environments, are clearly related to the nature of the lithotypes involved, the degree and nature of hydrothermal alteration, and the presence or absence of pre-existing planar anisotropies. These variations in strain state do not reflect temporal variations in stress.

CLEAVAGE AND LINEAR ELONGATION FABRICS

Roberts (1981) has demonstrated that the regional cleavage and linear elongation fabrics in the Timmins Camp are not related to, and postdate, the major folds mapped in the camp. Mason and Melnik (1986) have shown that these same fabrics all postdate mineralized structures and hydrothermal alteration, which themselves postdate the porphyry and albitite bodies. The present study has confirmed these findings, and there is indeed no evidence of penetrative fabrics which predate hydrothermal alteration and mineralized structures.

The dominant cleavage in the south half of Tisdale Township strikes between 090 and 120° and occurs only locally, that is, in the Hollinger–McIntyre area, and in the area to the south and east of Dome Number 8 shaft (Figure 298.4). It is not clear whether this localized 060 to 070° orientation is a variation in the 090 to 120° strike, or whether it is a separate, more localized cleavage. Frequently, traces of two cleavages (conjugate sets?) can be observed in outcrop, but it is not possible to establish any difference in timing between these. The only area in which two cleavages have been mapped together that show a consistent timing relationship is in the core of the Porcupine Syncline, where greywackes and argillites respectively show spaced and continuous cleavages at 110°, and a later discontinuous crenulation cleavage at 040° (Photo 298.4). These two cleavages in the sedimentary rocks were also described by Roberts (1981).

Subhorizontal and, less commonly, subvertical intersection lineations are developed where regional cleavage surfaces are strongly developed. The traces of these crenulation cleavages are not observed when viewed parallel to the regional cleavage surfaces. The subhorizontal crenulation cleavage is particularly well developed in open pit exposures in the Central Ore Zone on the Hollinger Mine Property, in strongly sericitized schistose wallrocks adjacent to subvertical quartz-ankerite veins.

The trend of linear elongation fabrics is generally east-northeast over the map area. The plunge varies from 25 to 30°E to 80°E, with an average of 45°E (Figure 298.4). Varioles and pillows within the V8 flow unit are elongated at 10°W, in outcrops southwest of Aunor Lake in northern Deloro Township (Figure 298.4), and it appears that there is a domain of west-plunging elongation fabrics close to the Destor–Porcupine Fault Zone.

The intensity of cleavage development shows a direct relationship to primary lithology and texture (for example, massive, pillowed, brecciated, etc.), and to the presence or absence of sericite-or-chlorite filled fractures resulting from hydrothermal activity. Rennie (1988) has recently described and illustrated the effects of alteration mineralogy and lithological heterogeneity on the style and intensity of cleavage development within rocks of the Hollinger–McIntyre–Coniaurum Complex. In mafic volcanic flows, uniformly textured flows and pillow interiors are less susceptible to cleavage development than pillow selvages, pillow breccias, and flow top breccias. The same is true of greywackes and conglomerates relative to argillites in sedimentary units. The intensity of strain is thus not only a function of the stress applied, but also of the nature of the lithologies involved.

On the Chisholm (McIntyre) Property northwest of Aunor Lake in southern Tisdale Township, massive uniformly textured flows occur interlayered with amygdaloidal pillowed flows of the Central Formation. The massive flows show low to moderate strain (weak cleavage development), whereas the amygdaloidal pillowed flows show high strain (strong shortening and elongation of pillows, combined with cleavage development throughout the pillows). On the Dome and Preston properties in southeastern Tisdale Township, sedimentary rocks occur interbedded with amygdaloidal pillowed flows (Figure 298.2). The sedimentary rocks are tightly folded, and have a well developed cleavage. The mafic flows immediately adjacent to them are much less deformed; they lack cleavage and exhibit well preserved pillows from which facing direction determinations can be made.

Alteration fabrics and mineralogy also have a strong influence on the type and intensity of cleavage developed, particularly in massive (uniformly textured) rocks such as porphyries and massive mafic flows. In these rocks, there is an absence of control by primary features, and where cleavage is developed in these rocks it appears to be related to the development of fracture-controlled sericitic alteration. Even in strongly sericitic rocks, such as those of the Central Ore Zone of the Hollinger Mine, closely spaced sericitic fractures can be

Photo 298.8. *Chloritization of selvages in pillowed mafic flow of the Central Formation, Davidson-Tisdale Property. Viewed in plan.*

resolved (Photo 298.6). During deformation, sericitic fracture stockworks become flattened parallel to cleavage, and elongated parallel to the linear elongation fabrics. A continuous cleavage develops within each fracture due to the alignment of sericite. Viewed in hand specimen or outcrop scale, the cleavage is anastomosing and spaced, and the uniform rock of the microlithons between the fractures is relatively undeformed. This cleavage was thus generated by the shortening of a pre-existing sericitized fracture stockwork.

The intensity of cleavage development is thus not only a function of stress applied and lithology, but also depends on the development and density of sericite-filled fractures. Hence, more intensely sericitized rocks are generally more intensely cleaved. This is the reason why high strain zones (see below) are commonly developed in altered and mineralized rocks, and intensely developed cleavages are only developed in sericitized rocks. Those rocks which have undergone only carbonate and (or) chlorite facies alteration show moderate cleavage intensity at best. Fractures filled with carbonate minerals or quartz usually show offset, boudinage, or folding in response to stress, and they do not readily develop a cleavage.

Zones of intense cleavage are termed "high strain zones" rather than "shear zones". In fact, over most of the study area, the high strain zones appear to be zones of intense shortening and elongation, resulting from dominantly pure shear stress. The boundaries to these zones tend to be gradational, and the zones do not usually show any evidence of typical shear zone fabrics (S-type and C-type fabrics). Furthermore, kinematic indicators show conflicting senses of movement, even at outcrop scale. High strain zones may be confined to one lithology or may transgress lithological contacts. They are typically lensoidal, both along strike, and downdip. The high strain zone associated with sericitic alteration in and around the Pearl Lake porphyry is much wider at the surface than at depth. This relationship is not compatible with the usual geometric profile of a shear zone, which typically grades from narrow brittle features close to the surface, into wider ductile shear zones at depth.

CONCLUSIONS

New insight into the Porcupine Mining Camp has resulted from a detailed study of outcrops and geological relationships in Tisdale Township. The gold deposits are closely related to felsic intrusive centres; the hydrothermal systems related to these centres were very large near-surface phenomena, with features resembling modern hydrothermal systems associated with felsic intrusions.

The fold structures in the camp appear to have formed without developing penetrative fabrics. The felsic intrusions occurred after folding. Hydrothermal activity, together with gold mineralization, appears to have occurred during the terminal phases of felsic intrusion in brittle structures typical of near-surface environments.

Minerals formed as a result of hydrothermal alteration were subsequently recrystallized and moulded by a regional deformation event, which resulted in the development of a penetrative cleavage and linear elongation fabric. Sericitic alteration close to mineralized structures appears to have localized high strain zones, with penetrative fabrics cutting across alteration and mineralized structures alike. The high strain zones appear to have resulted from pure shear, and are characterized by intensely developed planar and linear fabrics.

ACKNOWLEDGMENTS

This research project is being funded by the Ontario Geological Survey through Ontario Geoscience Research Grant 298.

The authors are grateful to Giant Yellowknife Mines Limited, Pamourex Limited, Placer Dome Limited, and Moneta Porcupine Mines Limited for access to their properties and geological records. In addition, we would like to thank Bill MacRae, Pam Sangster, and Chris Hamblin for their help.

Nadia Melnik, Collette Rennie, and Jim Davies have all made significant contributions to understanding the breccias, mineralization, alteration, and fabric development in the Hollinger–McIntyre–Coniaurum Complex, and have provided much useful discussion and information during the past year.

The authors would also like to thank Karen Brisbin for her help with illustrations, and Sheila McPherson for preparation of the manuscript.

REFERENCES

Aitken, S.
1988: Surface Geology Adjacent to the No. 8 Shaft, Dome Mines Ltd., Tisdale Township, Ontario; Unpublished B.Sc. Thesis, Queen's University, Kingston, 39p.

Armstrong, C.M.
1960: Metallic Mineralization at the Hollinger Mine, Ontario; Unpublished B.Sc. Thesis, Queen's University, Kingston, 86p.

Bain, G.W.
1933: Wall-Rock Mineralization Along Ontario Gold Deposits; Economic Geology, Volume 28, Number 8, p.705-743.

Brisbin, D.I., Speidel, F., and Mason, R.
1987: Geology of the North Zone of the Delnite Mine at Timmins, Ontario; Grant 298B, p.224-229 *in* Geoscience Research Grant Program, Summary of Research, 1986-1987, edited by V.G. Milne, Ontario Geological Survey, Miscellaneous Paper 136, 241p.

Buffam, B.S.W.
1948: Moneta Porcupine Mine; p.457-464 *in* Structural Geology of Canadian Ore Deposits, Canadian Institute of Mining and Metallurgy, Montreal, Volume 1, 948p.

Burnham, C.W., and Ohmoto, H.
1980: Late-Stage Processes of Felsic Magmatism; Mining Geology, Special Issue Number 8, p.1-11.

Burrows, A.G.
1911: The Porcupine Gold Area; Ontario Bureau of Mines, Annual Report for 1911, Volume 20, Part 2, 33p. Accompanied by Map 20e, scale 1:63 360 or 1 inch to 1 mile, and Map 20f, scale 1:126 720 or 1 inch to 2 miles.

Davies, J.F., and Luhta, L.E.
1978: An Archean "Porphyry-Type" Disseminated Copper Deposit, Timmins, Ontario; Economic Geology, Volume 73, p.383-396.

Davies, J.F., and Whitehead, R.E.S.
1980: Further Immobile Element Data from Altered Volcanic Rocks, Timmins Mining Area, Ontario; Canadian Journal of Earth Sciences, Volume 17, p.419-423.

Davies, J.F., Whitehead, R.E.S., Cameron, R.A., and Duff, D.
1982: Regional and Local Patterns of CO_2-K-Rb-As Alteration: A Guide to Gold in the Timmins Area; p.130-143 *in* Geology of Canadian Gold Deposits, edited by R.W. Hodder and William Petruk, Canadian Institute of Mining and Metallurgy, Special Volume 24, 286p.

Davies, J.P.E.
1988: Hydrothermal Breccias at the Hollinger–McIntyre–Coniaurum Complex, Timmins, Ontario; Unpublished M.Sc. Thesis, Queen's University, Kingston.

Ferguson, S.A., Buffam, B.S.W., Carter, O.F., Griffis, A.T., Holmes, T.C., Hurst, M.E., Jones, W.A., Lane, H.C., and Longley, C.S.
1968: Geology and Ore Deposits of Tisdale Township, District of Cochrane; Ontario Department of Mines, Geological Report 58, 177p. Accompanied by Colour Map 2075 and 12 charts.

Fryer, B.J., Kerrich, R., Hutchinson, R.W., Pierce, M.G., and Rogers, D.S.
1979: Archaean Precious Metal Hydrothermal Systems, Dome Mine, Abitibi Greenstone Belt. 1. - Patterns of Alterations and Metal Distribution; Canadian Journal of Earth Sciences, Volume 16, p.421-439.

Fyon, J.A., and Crocket, J.H.
1979: Geological and Geochemical Guide to Gold Mineralization of the Porcupine Camp, Timmins Area; p.192-198 *in* Summary of Field Work, 1979, by the Ontario Geological Survey, edited by V.G. Milne, O.L. White, R.B. Barlow, and C.R. Kustra, Ontario Geological Survey, Miscellaneous Paper 90, 245p.
1980: Gold Exploration in the Timmins District Using Field and Lithogeochemical Characteristics of Carbonate Alteration Zones; p.113-129 *in* Geology of Canadian Gold Deposits; edited by R.W. Hodder and William Petruk, Canadian Institute of Mining and Metallurgy, Special Volume 24, 286p.
1983: Gold Exploration in the Timmins Area; Ontario Geological Survey, Study 26, 56p. Accompanied by 2 charts and 2 maps.

Graton, L.C., and McKinstry, H.E.
1933: Outstanding Features of Hollinger Geology; Canadian Institute of Mining and Metallurgy, Transactions, Volume 36, p.1-20.

Holmes, T.C.
1944: Some Porphyry-Sediment Contacts at the Dome Mine, Ontario; Economic Geology, Volume 39, Number 2, p.133-141.
1968: Dome Mines Limited; p.82-98 *in* Geology and Ore Deposits of Tisdale Township, by S.A. Ferguson *et al.*; Ontario Department of Mines, Geological Report 58, 177p.

Hore, R.E.
1913: On the Origin of the Porcupine Gold Deposits; Canadian Mining Journal, Volume 34, p.548-551.

Hurst, M.E.
1939: Porcupine Area, District of Cochrane, Ontario; Ontario Department of Mines, Map 47A, scale 2000 feet to 1 inch or 1:24 000.

Keys, M.R.
1938: Comparative Study of the Mineralogy of the Auriferous Quartz Veins Encountered in the Hollinger Mine, Porcupine District; Unpublished M.Sc. Thesis, Queen's University, Kingston, 47p.
1940: Paragenesis in the Hollinger Veins; Economic Geology, Volume 35, Number 5, p.611-628.

Langford, G.B., and Hancox, E.G.
1936: Hypogene Anhydrite from McIntyre Mine, Porcupine District, Ontario; Economic Geology, Volume 31, Number 6 p.600-610.

Marmont, S., and Corfu, F.
1988: Timing of Gold Introduction in the Late Archean Tectonic Framework of the Canadian Shield: Evidence for U-Pb Zircon Geochronology of the Abitibi Belt; p.45-51 *in* Bicentennial Gold '88, Melbourne, Extended Abstracts, Oral Programme, compiled by A.D.T. Good and L.I. Bosma, Geological Society of Australia Inc., Abstracts Number 2, 369p.

Mason, R., and Brisbin, D.I.
1987: The Geological Setting of Gold Deposits in the Porcupine Mining Camp; Grant 298A, p.215-223 *in* Geoscience Research Grant Program, Summary of Research, 1986-1987, edited by V.G. Milne, Ontario Geological Survey, Miscellaneous Paper 136, 241p.

Mason, R., and Melnik, N.
1986: The Anatomy of an Archean Gold System—The McIntyre–Hollinger Complex at Timmins, Ontario, Canada; p.40-55 *in* Proceedings of Gold '86, An International Symposium on the Geology of Gold Deposits, edited by A.J. Macdonald, Toronto, 1986, 517p.

Moore, E.S.
1953: The Structural History of the Porcupine Gold Area, Ontario; Royal Society of Canada, Transactions, Third Series, Volume 47, Section 4, p.39-53.

Piroshco, D.W.
1985: Relationship of Hydrothermal Alteration to Structure and Stratigraphy at the Coniaurum and Davidson Tisdale Gold Deposits, Tisdale Township, Northeastern Ontario; Unpublished M.Sc. Thesis, Queen's University, Kingston, 102p.

Pyke, D.R.
1982: Geology of the Timmins Area, District of Cochrane; Ontario Geological Survey, Geological Report 219, 141p. Accompanied by Colour Map 2455, scale 1:50 000, 3 charts, and 1 sheet microfiche.

Rennie, C.T.
1988: The Significance of Style of Deformation and Alteration in the McIntyre–Hollinger–Coniaurum Complex, Timmins, Ontario; Unpublished M.Sc. Thesis, Queen's University, Kingston.

Roberts, R.G.
1981: The Volcanic-Tectonic Setting of Gold Deposits in the Timmins Area, Ontario; p.16-28 *in* Genesis of Archean, Volcanic Hosted Gold Deposits, Symposium Held at the University of Waterloo, March 7, 1980, edited by E.G. Pye and R.G. Roberts, Ontario Geological Survey, Miscellaneous Paper 97, 175p.

Titley, S.R., Thompson, R.C., Haynes, F.M., Manske, S.L., Robinson, L.S., and White, J.L.
1986: Evolution of Fractures and Alteration in the Sierrita–Esperanza Hydrothermal System, Pima County, Arizona; Economic Geology, Volume 81, p.343-370.

Whitehead, R.E.S., Davies, J.F., and Cameron, R.A.
1980: Carbonate and Alkali Alteration Patterns in the Timmins Gold-Mining Area; Grant 30, p.244-256 *in* Geoscience Research Grant Program, Summary of Research, 1979-1980, edited by E.G. Pye, Ontario Geological Survey, Miscellaneous Paper 93, 263p.

Whitman, A.R.
1915: Rocks of the Porcupine District; Canadian Mining Institute, Transactions, Volume 18, p.256-276.

Grant 300 The Genesis of Silver Vein Deposits in the Thunder Bay Area, Northwestern Ontario

S.A. Kissin and T.C. McCuaig

Department of Geology, Lakehead University, Thunder Bay

ABSTRACT

Five vein-type mineral occurrences in the Schreiber–Terrace Bay area were investigated by fluid inclusion and sulphur isotope techniques, as well as by field and mineralogical methods. The Deadhorse Creek North and South and Morley High Grade occurrences appear to be genetically related galena-sphalerite-freibergite-calcite veins, formed at moderate (160° to 175°C) to high (355°C) temperatures, respectively, based on fluid inclusion homogenization temperatures. Sulphur isotopic compositions of paired sphalerite-galena samples yielded values in the range $\delta^{34}S = +1$ to $+6$. Calculated equilibration temperatures from sulphur isotope partitioning were approximately 100°C higher than those obtained from fluid inclusions for the Deadhorse Creek North and South veins, suggesting a pressure of trapping of 105 MPa, equivalent to a depth of 3.8 km. Higher pressures are indicated for the Morley High Grade Occurrence. The Mogotherium Occurrence contains an unusual silver-copper-bismuth-tellurium assemblage and may be genetically related to the Terrace Bay Batholith. The Harkness–Hays and Gold Range occurrences are typical Archean gold veins. The Terrace Bay Greenstone Belt appears to contain lead-zinc-silver veins of inferred Proterozoic age throughout its length, supporting a genetic link to Keweenawan rifting.

INTRODUCTION

The work on silver vein deposits completed in the past year deals with a group of occurrences occurring approximately 250 km east of Thunder Bay in the Schreiber–Terrace Bay–Marathon area (Figure 300.1). Franklin *et al.* (1986) demonstrated that a group of veins near Deadhorse Creek at the western edge of the Port Coldwell Alkaline Complex are of Proterozoic age. These veins, which Franklin *et al.* (1986) referred to as Port Coldwell veins, appear to be genetically related to veins in the Thunder Bay area, as discussed in last year's report (Kissin and Jennings 1987). The veins were described briefly by Walker (1967) and more recently by Patterson *et al.* (1984, 1985), who designated them as Type 2a (Zinc-Lead-Silver Veins-Metavolcanic Type) base metal deposits. They include the Deadhorse Creek North, Deadhorse Creek South, McKellar Creek, and possibly, the Morley High Grade occurrences. The latter lies some 40 km west of the Deadhorse Creek area (Figure 300.1), and Patterson *et al.* (1984) originally designated it as a Type 3 (Metavolcanic-Heated-Dilatent Zone Type) gold occurrence, based on reported low gold values and its proximity to the Terrace Bay Batholith.

The occurrences consist of narrow veins of galena, sphalerite, and minor pyrite with quartz and carbonate gangue. A deposit of about 36 000 tons containing 7.28 percent zinc, 1.45 percent lead, and 8.27 ounces silver per ton (Patterson *et al.* 1984), based on bulk sampling, has been identified on the Deadhorse Creek North Property. Grab samples have yielded higher values, up to 56.40 ounces silver per ton. At the Deadhorse Creek South Property, 35 000 tons have been outlined, grading 27.65 ounces silver per ton, 19.87 percent lead, and 9.08 percent zinc (Patterson *et al.* 1985). The Morley High Grade Occurrence is comparable with 0.196 ounces gold per ton, 41.57 ounces silver per ton, 25.85 percent zinc, 7.06 percent lead, and 0.185 percent copper from 30 samples (Patterson *et al.* 1984). In spite of the relatively high silver values, none of the previous reports have determined the silver carrier in these occurrences.

Some recent discoveries in the vicinity of the Terrace Bay Batholith were briefly described by Patterson *et al.* (1987) and include the Ferguson and Mogotherium occurrences. The Mogotherium samples were found to contain silver, copper, bismuth, and tellurium, as well as minor gold values. The occurrences were designated as Type 1 (Terrace Bay Batholith-Contact Zone Type) gold occurrences, although the unusual elemental content merits further investigation. In contrast, the Harkness–Hays and Gold Range properties, which are adjoining properties near Schreiber, are typical of gold occurrences of the area and have been described as Type 1 gold occurrences by Patterson *et al.* (1986; 1987).

These occurrences of differing vein-type ores within a relatively small area were considered to be worthy of study in that the silver-bearing base metal veins (Type 2a) may be more extensive than previously believed, as they seem to be related to regional factors (Franklin *et al.* 1986) rather than intrusions (for example, the Coldwell Complex or Terrace Bay Batholith). From an exploration standpoint, it seems desirable to determine whether properties such as the Morley High Grade and Mogotherium should be viewed as gold prospects or silver occurrences. To these ends, the mineralogy, fluid inclusions, sulphur isotopes, as well as features of the field geology of the Deadhorse Creek North and South, Morley High Grade, Mogotherium, and, for comparison, Harkness–Hays and Gold Range occurrences were investigated.

GEOLOGICAL BACKGROUND

The eastern portion of the study area was described in detail by Walker (1967) and the western portion by Harcourt and Bartley (1938), while a recent summary of geology with emphasis on the Terrace Bay Batholith has been made by Marmont (1984). Based on the preceding sources, the geology of the area may be summarized as follows (Figure 300.1). The oldest rocks of the area are Archean metavolcanics and associated metasedimentary rocks of the Abitibi–Wawa Subprovince forming a segment called the Terrace Bay Greenstone Belt. Iron-rich tholeiites and calc-alkaline felsic metavolcanics are inter-

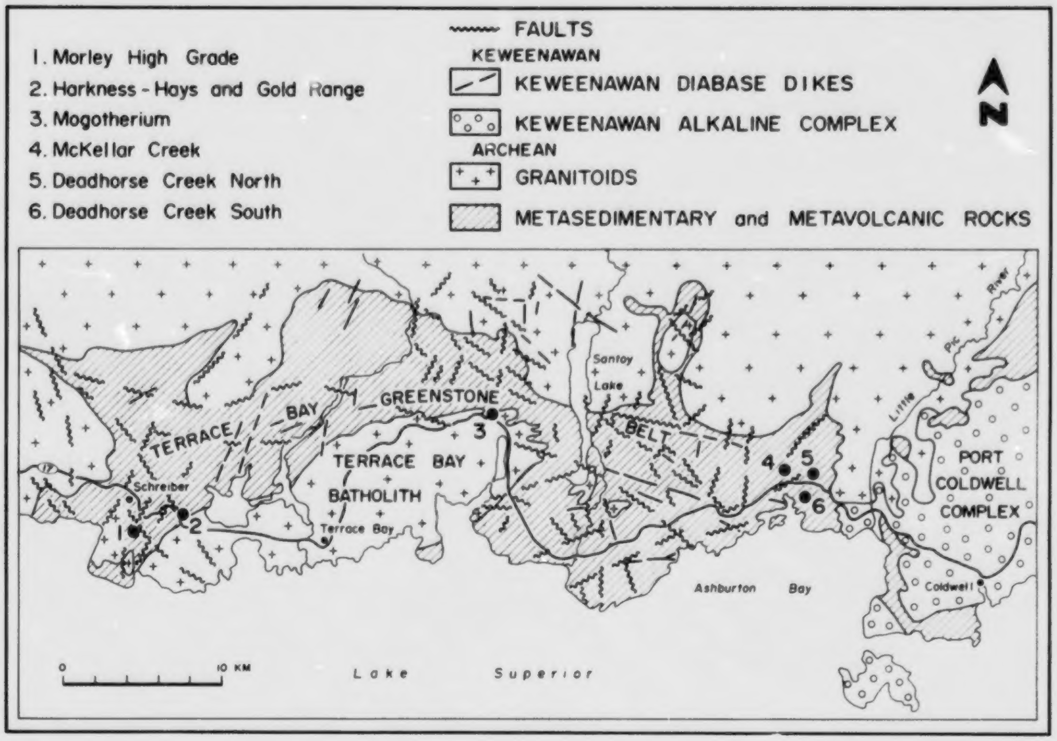
FAULTS
KEWEENAWAN
KEWEENAWAN DIABASE DIKES
KEWEENAWAN ALKALINE COMPLEX
ARCHEAN
GRANITOIDS
METASEDIMENTARY and METAVOLCANIC ROCKS
1. Morley High Grade
2. Harkness - Hays and Gold Range
3. Mogotherium
4. McKellar Creek
5. Deadhorse Creek North
6. Deadhorse Creek South
N
TERRACE BAY GREENSTONE BELT
TERRACE BAY BATHOLITH
PORT COLDWELL COMPLEX
Schreiber
Terrace Bay
Santoy Lake
Little Pic River
Ashburton Bay
Coldwell
Lake Superior
0
10 KM
1
2
3
4
5
6

Figure 300.1. Location map for deposits studied and generalized geology of the Schreiber–Terrace Bay area.

bedded with greywackes and argillites, with minor iron formation and conglomerate. Minor dikes and sills of gabbro and diorite intrude the metavolcanic and metasedimentary rocks. Metamorphic grades range from greenschist to near granulite facies within the area. Intruding all of the above is the later Terrace Bay Batholith, in outcrop approximately 25 km by 8 km, near the centre of the study area. The batholith consists predominantly of granodiorite with minor diorite, quartz monzonite, tonalite, and biotite-hornblende granite. A metamorphic aureole extending approximately 0.5 km into the country rocks surrounds the batholith.

Proterozoic rocks associated with Keweenawan events include the Port Coldwell Alkaline Complex, which occurs on the eastern edge of the study area, and diabase dikes and sills. A well defined contact aureole extends approximately 1 km beyond the margin of the Port Coldwell Complex. Diabasic hypabyssal intrusions are minor features and occur on a scattered basis. They frequently occupy faults, which occur in an east- to northeast-striking set and a transcurrent north-striking set. Although some older structures are present, most vertical displacement appears to have been related to Keweenawan events.

METHODOLOGY

Fluid inclusion studies were carried out using an SGE Fluid Inclusion Research System mounted on a specially adapted Leitz SM-POL polarizing microscope. The system was calibrated using standards of known melting and freezing points. As all calibration errors were ±1°C or less, no corrections were employed.

Analyses of selected sulphide minerals were carried out using a Hitachi 570 scanning electron microscope equipped with a Tracor Northern TN2000 energy dispersive analyzer (SEM-EDA). The standardless software routine SQ from Tracor Northern program 5502 was utilized in obtaining analyses, which were automatically normalized to near 100 percent.

Sulphur isotopic analyses were conducted by standard techniques by Geochron Laboratories Division, Kreuger Enterprises Incorporated, Cambridge, Massachusetts.

RESULTS

MINERALOGY

Deadhorse Creek North and South

The Deadhorse Creek North (DHN) and South (DHS) occurrences are outwardly very similar, consisting of growth-banded calcite, sphalerite, and galena with minor chalcopyrite, pyrite, and quartz. Both are rather narrow veins with narrow low-grade alteration zones extending about 1 to 2 m on either side. The DHS vein has an attitude of 290/60 and a width of 1 to 10 cm, while the DHN vein has an attitude of 280/80 and a width of <5 cm to 1.5 m. The DHS vein does not appear to be brecciated, and appears to have been deposited in a single pulse, an observation

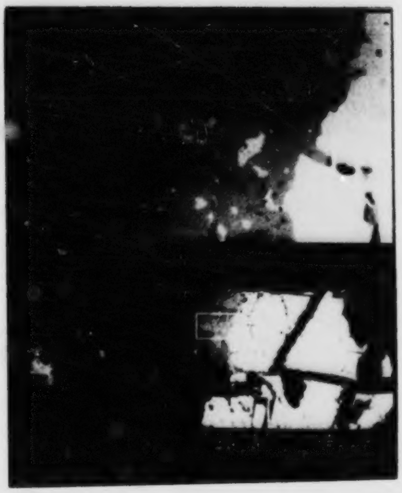

Photo 300.1. *Electron microscope photograph of mineralization from Deadhorse Creek South (DHS 13) showing (a) the association of freibergite with sphalerite (grey, left) and galena (white, right). The inset (b) shows the intimate intergrowth of freibergite and sphalerite, and numerous inclusions of chalcopyrite (white) in freibergite.*

supported by fluid inclusion studies. The DHN vein has clearly experienced at least one episode of brecciation in which fragments of earlier vein material were cemented by later-deposited material. The DHS vein is hosted in metasediments, while the DHN vein is hosted in metavolcanics near the contact of an Archean metagabbro intrusion. Both veins cut across earlier structures and fabrics including the contact aureole of the Port Coldwell Alkaline Complex. A north-striking fault following Deadhorse Creek appears to offset the veins for some metres laterally.

No silver-carrying mineral is evident in hand specimens from the veins; however, in polished section a mineral resembling tetrahedrite is present in considerable amounts in association with galena (Photo 300.1). SEM-EDA analysis revealed that the mineral is freibergite, the silver analogue of tetrahedrite (Table 300.1). Based on its abundance and tenor of silver, this mineral clearly accounts for the silver values in the Deadhorse Creek veins.

In the DHS vein the paragenetic sequence is rather simple, and the vein is symmetrically banded. From the vein wall to the centre of the vein, the sequence is as follows: a) hydrothermal pyrite in wall rock adjacent to the vein; b) calcite + pyrite adjacent to the wall rock; c) growth-banded sphalerite with minor amounts of galena, calcite, and chalcopyrite; d) large euhedral galena crystals associated with sphalerite, chalcopyrite, and freibergite; and e) barren coarse-grained calcite in the vein centre.

The paragenetic sequence of the DHN vein is more difficult to decipher owing to one or more episodes of brecciation followed by additional mineralization. However, according to McCuaig (1988), an early phase of calcite was followed by cockade-textured galena and sphalerite. As well as galena and sphalerite, the vein contains noticeably more pyrite and chalcopyrite, with minor quartz. Freibergite is associated with galena and chalcopyrite and a small amount of a chalcocite-digenite intergrowth is present. As the latter represents the breakdown products of a high-temperature digenite-chalcocite solid solution (Barton 1973), hypogene origin of the intergrowth is likely.

Morley High Grade

The Morley High Grade (MHG) vein has an attitude of 185/60, and in its 7 m of exposure its width is approximately 20 cm. The paragenetic sequence is fairly well preserved, although an episode of brecciation and recementation has occurred. Although the felsic metavolcanic host rocks lie near the thermal aureole of the Terrace Bay Batholith and are of higher metamorphic grade than those hosting the Deadhorse Creek North and South occurrences, the MHG vein is clearly not metamorphosed. The mineralogy consists of fine-grained sphalerite + calcite ± pyrite near the vein walls and wall rock inclusions grading to fine-grained sphalerite + galena + chalcopyrite + pyrite + freibergite. The carbonate content is low, and no gold mineralization is visible, although gold values have been reported (Patterson *et al.* 1987).

The three occurrences (DHS, DHN, and MHG) are thus quite similar in terms of their mineralogy. All are lead-zinc-silver veins with freibergite as the silver carrier. The paragenetic sequence is broadly similar with early calcite + sphalerite ± pyrite followed by sphalerite + galena ± chalcopyrite ± freibergite, with freibergite and chalcopyrite later than galena.

Mogotherium

The Mogotherium (MOG) Occurrence, as observed in this study, consists of an anastomosing quartz vein in high-grade metavolcanics within 100 m of the contact of the Terrace Bay Batholith. No mineralization was observed in the present study; however, a sample of mineralized vein was obtained from B.R. Schnieders (Geologist, Ministry of Northern Development and Mines, Thunder Bay). The mineralization is unusual (Photo 300.2). Most of the mineralization is an unidentified opaque copper-bismuth-lead sulphide. Its composition (Table 300.2) does not correspond to that of any known mineral within the Cu_2S-Bi_2S_3-PbS composition plane, according to a summary by Makovicky (1981). Further study is needed, however, before this conclusion can be taken as definite. Also present are irregular to subhedral inclusions of hessite (Ag_2Te), vermicular inclusions of native bismuth, and an intergrowth consisting of hessite, chalcopyrite, and native bismuth, which are evidently decomposition products of a high-temperature phase. Small amounts of argentite rim grains of the copper-bismuth-lead-sulphur mineral, evidently as late-stage products.

Harkness–Hays and Gold Range

The Harkness–Hays and Gold Range (GR) properties contain four *en echelon* quartz veins striking from 200° to 270° and dipping 60°N. The veins occur within well defined alteration zones in metavolcanics within the contact aureole of the Terrace Bay Batholith. The veins vary from 1 cm to 1 m in thickness, but are generally less than 5 cm thick and consist of quartz with minor calcite. Abundant disseminated pyrite is present in the altered wall rock but is absent in unaltered country rock. Gold with accessory chalcopyrite, sphalerite, galena, molybdenite, and tellurides have been reported (Patterson *et al.* 1987), but were not observed in the present study.

FLUID INCLUSION STUDIES

Fluid inclusions were found in sphalerite (sp), calcite (calc), and quartz (q) from all of the five occurrences, although the size and quality of inclusions was considerably less than was hoped. Inclusions were first frozen in order to determine eutectic temperatures ($T_{eut.}$) and final melting temperatures ($T_{f.m.}$), which yield information on the solution composition and salinity, respectively. Inclusions were then heated in order to obtain homogenization temperatures ($T_{hom.}$). The latter are uncorrected for pressure and therefore represent minimum filling temperatures for the inclusions.

Table 300.3 lists the data obtained from DHS, GR, and MHG samples. Notable at the outset is the lack of evidence for boiling in the veins, with homogenization to vapour noted only in DHS-17-1. The DHS vein yielded the most extensive results and, due to the simple paragenesis, the most reliably interpretable results. A histogram of homogenization temperatures for all data is given in Figure 300.2. The temperatures are strongly clustered about a mean of 160° to 170°C, and considering sphalerite data alone (Figure 300.3), it is apparent that this range of temperature is that of ore deposition. The tails of the distribution for all data represent early low-temperature and late high-temperature barren calcite.

The eutectic temperatures for DHS seem to be representative of the NaCl-H_2O at -20.8°C, or its metastable eutectic at -28°C. A few values in the <-30°C range in early high-temperature calcite may be representative of $MgCl_2$-H_2O (-33.6°C) or NaCl-$MgCl_2$-H_2O (-35°C), according to data given by Crawford (1981). The salinities, calculated from final melting temperatures by Potter *et al.* (1978, Equation 2), are moderate to low and are reasonably closely grouped except for some metastable positive values obtained for DHS-8-4 calcites, as well as lower salinities from other inclusions in this sample. These values are probably due to the low salinity and small size of the inclusions.

The DHN fluid inclusion data (Table 300.4) are more difficult to interpret due to the two episodes of crystallization interrupted by brecciation. The sphalerite $T_{hom.}$ are tightly grouped about 175°C; however, calcite seems to fall into two populations of $T_{hom.}$, one at 160°C and one at 215°C. However, the high-temperature calcites yielded $T_{eut.}$ of -31.0, -31.7, and -55.1°C, quite different from those of the other inclusions, which fall in the realm of NaCl-H_2O or its metastable eutectic. As well, the high-temperature calcites have markedly lower salinities than the other inclusions. The -31°C eutectics probably represent $MgCl_2$-H_2O, while the -55°C value is close to the NaCl-$CaCl_2$-H_2O eutectic of -52.0°C.

TABLE 300.1: SEM-EDA ANALYSIS OF FREIBERGITE (DHS-13)

ELEMENT	LINE	wt.%	*PROPORTIONS	
Cu	K	17.92	5.22	
				►9.90
Ag	L	27.30	4.68	
Fe	K	5.70	1.89	
				►2.50
Zn	K	2.10	0.61	
Sb	L	24.66		3.75
S	K	22.27		12.85
Total		99.95		

*based on 29 atoms in $(Cu,Ag)_{10}(Fe,Zn)_2Sb_4S_{13}$

The calcite with $T_{hom.}$ close to 165°C and the sphalerite with $T_{hom.}$ close to 175°C appear to represent the first phase of mineralization, while the high-temperature calcite cements the brecciated early ore. The latter is mostly barren and was precipitated from a less saline solution of variable composition. The quartz present in the vein is evidently a late mineral, crystallized after the high-temperature calcite.

The MHG inclusions (Table 300.3) yielded much higher homogenization temperatures than those obtained from the Deadhorse Creek veins. Sphalerite has a mean $T_{hom.}$ of approximately 355°C, while calcite has a cluster around 320°C with a tail to much lower temperatures. Salinities are fairly uniformly low, and $T_{eut.}$ in the -28 to -30°C range probably represent the metastable NaCl-H_2O eutectic.

The few determinations from the GR veins show a wide variation of $T_{hom.}$ in quartz, with a high of 428°C (Table 300.3). The eutectic temperatures represent the NaCl-H_2O system. The sole salinity determination is moderate.

The inclusion data from MOG (Table 300.5) show a range of $T_{hom.}$ from 140° to 299°C, although half of the data lie between 170° and 200°C. As these were all obtained from a specimen of 4 cm^2, some caution is needed in interpreting these results. The eutectic temperatures reflect the metastable NaCl-H_2O eutectic, while salinities show some variation.

SULPHUR ISOTOPIC STUDIES

Sulphur isotopic ratios were determined on paired galena and sphalerite specimens from the sulphide-rich Deadhorse Creek and Morley High Grade occurrences. The specimens were selected from grains in mutual contact, and the sphalerites had yielded fluid inclusion data. The results are given in Table 300.6, together with the Δsphalerite-galena equilibration temperatures calculated from an equation by Rye and Ohmoto (1979) using Δ, the difference in $\delta^{34}S$ between sphalerite and galena, and $T_{hom.}$ from sphalerite. While all values are within the range +1 to +6 per mil, there are significant differences among the pairs. The related Deadhorse Creek deposits yield nearly identical Δsphalerite-galena $T_{eq.}$ and $T_{hom.}$

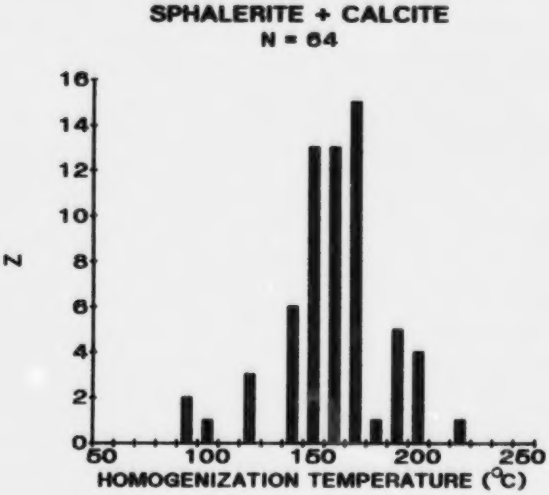

Figure 300.2. *Fluid inclusion homogenization temperatures from all Deadhorse Creek South specimens.*

TABLE 300.2: SEM-EDA ANALYSIS OF UNKNOWN Cu-Bi-Pb-S MINERAL FROM MOGOTHERIUM

ELEMENT	LINE	wt.%	at.%
Cu	K	11.19	18.35
Pb	M	47.84	24.05
Bi	M	27.45	13.69
S	K	13.51	43.91
Total		99.99	

values; however, the values of $\delta^{34}S$ themselves are quite different. This can be explained by supposing that the source of the sulphur in the two occurrences is different or that the galena and sphalerite are not in isotopic equilibrium.

In MHG, the data from two pairs are in close agreement, although that of the third, MHG-b-2, is significantly different. Since $T_{hom.}$ in sphalerite is the same for all three pairs, it seems unlikely that MHG-b-2 is in isotopic equilibrium with the other two samples.

There is a marked discrepancy between $T_{eq.}$ and $T_{hom.}$ in all the pairs, but, except for MHG-b-2, in which $T_{eq.} < T_{hom.}$, the difference in temperatures may yield useful information if the sulphide pairs are in isotopic equilibrium. The agreement in DHS-X and DHN-8 amounting to 105°C and 100°C, respectively, is suggestive of equilibrium, while MHG-b-1 and MHG-c show discrepancies of 182°C and 148°C, respectively. These temperature discrepancies could be equivalent to the temperature correction in °C. Reference to the data of Potter (1977) could then provide a means of determining the pressure of trapping of the inclusion, if $T_{eq.}$ = temperature of trapping. This approach must be employed with caution, however, as it is dependent not only on the accuracy of the $\delta^{34}S$ determinations but on the sulphide pairs retaining high-temperature isotopic equilibrium. As well, $T_{eq.}$ is not a linear function of Δ and is increasingly imprecise with increasing temperature.

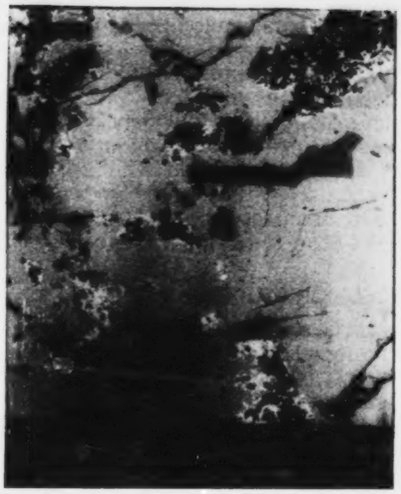

Photo 300.2. *Electron microscope photograph of mineralization from Mogotherium (MOG 1) showing hessite (AGTE), vermicular native bismuth (BI), and a complex intergrowth within a matrix of a copper-bismuth-lead-sulphur mineral.*

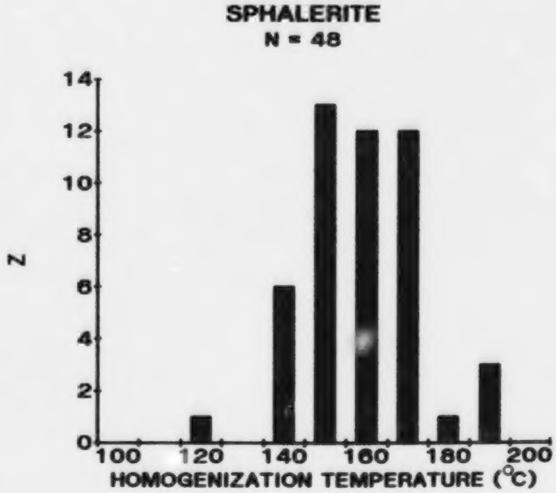

Figure 300.3. *Fluid inclusion homogenization temperatures from Deadhorse Creek South sphalerite.*

If DHN and DHS are assumed (based on fluid inclusion measurements) to have a salinity of 15 weight percent NaCl, the Potter (1977) data yield a pressure of trapping of 105 MPa for a temperature correction of 100°C and a homogenization temperature of 175°C. This pressure corresponds to a depth of 3.8 km, probably not a completely unreasonable figure, assuming an average density of 2750 kg/m^{-3}

for the country rocks. The pressure of trapping estimated on the same basis for MHG, would be on the order of 200 MPa. However, it is a much less precise figure due to the poorer agreement in the magnitude of the temperature correction.

The low positive $\delta^{34}S$ values for all sulphides may be suggestive of the source of the sulphur. On the one hand, the values are within the range of those of volcanogenic sulphide deposits (Rye and Ohmoto 1979) suggesting possible derivation of sulphur, without fractionation, from volcanogenic sulphides, perhaps in the metavolcanic wall rocks. On the other hand, Robinson and Ohmoto (1973) suggested that Proterozoic seawater sulphate may have a composition of $\delta^{34}S = +25$ per mil. If a pressure-corrected temperature of 275°C is accurate for the deposition of the Deadhorse Creek sulphides, the equilibrium fractionation between SO_4^{2-} and HS^- is approximately 23 per mil (Rye and Ohmoto 1979), yielding sulphides with low positive $\delta^{34}S$.

DISCUSSION

The studies on mineralogy, fluid inclusions, and sulphur isotopes reported do not provide definitive answers as to the affinities of the five occurrences investigated, but do provide support for some inferences. Firstly, on the basis of similarities in mineralogy, paragenesis, sulphur isotopes, and fluid inclusion temperatures, the DHS, DHN, and MHG occurrences seem to be of the same type. While this inference does not place great demands on credulity for the closely spaced DHN and DHS occurrences, the extension of the type some 40 km westward to the Schreiber area greatly extends this silver district.

Franklin *et al.* (1986) indicated, mostly on the basis of lead isotopic studies, that the Deadhorse Creek veins are of Proterozoic age and related to silver deposits in the vicinity of Thunder Bay. The evidence that this type of deposit occurs across the length of the Terrace Bay Greenstone Belt is in accord with implications by Franklin *et al.* (1986) and specific suggestions by Kissin (1988) that the genesis of these deposits is related to processes accompanying Keweenawan rifting, and therefore are to be expected to occur over wide areas related to regional tectonics, rather than localized geological factors.

The DHN, DHS, and MHG differ, however, in some significant ways from the deposits in the Thunder Bay area. The former are sulphide-rich and have grades of lead, zinc, and silver that are of economic interest. Silver occurs only in freibergite. In contrast, the sulphide content is low in deposits in the Thunder Bay area. Minor amounts of copper were produced from a few of the Island Belt deposits. Silver occurs almost exclusively as native silver and argentite (Franklin *et al.* 1986) in this area. Kissin and Jennings (1987), as well as Franklin *et al.* (1986), noted the frequent occurrence of boiling in the Thunder Bay veins, while those in the present study show scant evidence of boiling. The Thunder Bay area veins have close spatial relationships with Proterozoic hypabyssal intrusions, while those in the present study area display no consistent relationship to igneous rocks. Finally, the tentative calculations made here show the DHN, DHS, and MHG veins to have formed at significant depths, whereas the data of Jennings (1987) indicate considerable variation in depth in various deposits in the Thunder Bay area.

The MOG and GR occurrences are clearly quite different in mineralogy if not in their fluid inclusion characteristics. The GR was selected as typical of Archean gold occurrences, and it clearly differs from the MOG occurrence. The unusual mineral assemblage in MOG may indicate, as was suggested earlier (Patterson *et al.* 1987), that it is related to the Terrace Bay Batholith, suggesting that this area may be a fertile one for exploration.

CONCLUSIONS

The past year's work in the Schreiber–Terrace Bay–Marathon area leads us to the following conclusions:

1. On the basis of similarities in mineralogy, fluid inclusions, paragenesis, and sulphur isotope data, the Deadhorse Creek North and South and Morley High Grade occurrences are genetically related. The MHG was deposited at higher temperatures and pressures, but the mineral assemblage galena + sphalerite + freibergite ± pyrite ± chalcopyrite in carbonate gangue is identical to that of the DHN and DHS.
2. Isotopic studies reveal a low positive range of $\delta^{34}S$ from +1 to +6 per mil. The source sulphur may be either of volcanogenic origin or may have formed by equilibrium fraction of reduced seawater sulphate.
3. The unusual silver-bismuth-copper-tellurium assemblage of the Mogotherium Occurrence may reflect a relationship to the Terrace Bay Batholith.

ACKNOWLEDGMENTS

The following people from the Department of Geology, Lakehead University, provided assistance in this work: A.L. Hammond and R.L. Viitala, thin- and polished-section preparation; S.T. Spivak, drafting; R.L. Sherlock, data processing; and W.C. Bons, typing. A.J. Mackenzie of the Instrumentation Laboratory provided assistance in the operation of the analytical scanning electron microscope. B.R. Schnieders and A.A. Speed of the Ministry of Northern Development and Mines, Thunder Bay Office, graciously introduced us to the field area and supplied some important specimens.

REFERENCES

Barton, P.B., Jr.
1973: Solid Solutions in the System Cu-Fe-S. Part I: The Cu-S and CuFe-S Joins; Economic Geology, Volume 68, p.455-465.

Crawford, M.L.
1981: Phase Equilibria in Aqueous Fluid Inclusions; p.75-100 *in* Short Course in Fluid Inclusions: Applications to Petrology, edited by L.S. Hollister and M.L. Crawford, Mineralogical Association of Canada, 304p.

TABLE 300.3: FLUID INCLUSION DATA FROM THE DEADHORSE CREEK SOUTH (DHS), HARKNESS-HAYS AND GOLD RANGE (GR), AND MORLEY HIGH GRADE (MHG) OCCURRENCES.

Sample No.	Host	$T_{hom.}$(°C)[1]	$T_{eut.}$(°C)	$T_{f.m.}$(°C)	Salinity[2]
DHS-17-1	sp	190.0	-31.2	-8.0	14.2
DHS-17-1	sp	165.0	-29.8	-8.0	14.2
DHS-17-1	sp		-24.8	-8.0	14.2
DHS-17-1	sp	183.0	-24.0	-8.0	14.2
DHS-17-1	sp		-23.8		
DHS-17-1	sp	171.5 (v)			
DHS-17-1-2	sp	199.3	-22.5	-7.5	13.3
DHS-17-1-2	sp	190.4			
DHS-4-1	sp	156.5	-22.7		
DHS-4-1	sp	157.0			
DHS-4-1	sp	171.3		-12.2	21.9
DHS-4-1	sp	159.4	-21.7	-12.0	21.5
DHS-4-1	sp	169.3	-23.8		
DHS-4-1	sp	155.0			
DHS-4-1	sp	176.9		-9.8	17.4
DHS-4-1	sp	169.8			
DHS-4-1	sp	170.5		-5.0	8.8
DHS-4-2	sp	158.5			
DHS-4-2	sp	150.1			
DHS-4-2	sp	148.0			
DHS-4-2	sp	147.0		-10.6	18.9
DHS-4-2	sp	160.3			
DHS-4-2	sp		-25.3	-10.0	17.8
DHS-4-3	sp	158.1		-9.4	16.7
DHS-4-3	sp	166.5			
DHS-4-3	sp	165.6	-23.7		
DHS-4-3	sp	151.5			
DHS-4-3	sp	163.0	-24.4		
DHS-4-3	sp	160.0	-24.4		
DHS-4-3	sp			-7.6	13.4
DHS-4-4	sp	157.9			
DHS-4-4	sp	157.2			
DHS-4-4	sp	150.6			
DHS-4-4	sp	140.0			
DHS-5-1	sp	178.2			
DHS-5-1	sp	169.3			
DHS-5-1	sp	156.0			
DHS-5-1	sp	168.7			
DHS-5-1	sp	175.0			
DHS-5-1	sp	175.3			
DHS-5-1	sp	178.2			
DHS-5-1	sp	178.0			
DHS-5-2	sp	175.6	-32.0	-9.0	16.0
DHS-5-2	sp	148.9	-27.3	-11.7	21.0
DHS-5-2	sp	128.0	-27.3	-11.7	21.0
DHS-5-2	sp	149.0	-23.0	-3.5	6.2
DHS-5-2	sp	174.8	-23.5	-11.0	19.7
DHS-5-2	sp	162.5			
DHS-5-2	sp	145.9			

1. (v) indicates homogenization to vapour.
2. Equivalent weight percent NaCl from equation 2 of Potter *et al.* (1978).

sp = sphalerite
calc = calcite
q = quartz

TABLE 300.3 (CONT.): FLUID INCLUSION DATA FROM DHS, GR AND MHG.

Sample No.	Host	$T_{hom.}$(°C)	$T_{eut.}$(°C)	$T_{i.m.}$(°C)	Salinity[1]
DHS-6-1	calc	95.0			
DHS-6-2	calc	219.0			
DHS-6-3	calc	197.2	-32.1	-5.4	9.5
DHS-8-1	calc	209.4	-34.5		
DHS-8-1	calc	175.6	-38.7		
DHS-8-1	calc	200.1			
DHS-8-1	calc	198.0			
DHS-8-1	calc			-5.8	10.2
DHS-8-2	sp		-30.1	-4.4	7.7
DHS-8-2	sp	169.5	-25.4	-4.4	7.7
DHS-8-2	sp	155.3	-24.3		
DHS-8-2	sp	170.6	-23.0		
DHS-8-3	calc	179.1	-22.5	-5.9	10.4
DHS-8-3	calc	208.8	-22.8	-5.5	9.7
DHS-8-3	calc	172.3	-25.3		
DHS-8-3	calc	205.2	-23.0	-5.3	9.3
DHS-8-4	calc		-27.4		
DHS-8-4	calc	120.0	-22.3	3.0	
DHS-8-4	calc	96.6	-22.4	2.5	
DHS-8-4	calc	341.1	-23.0	-5.9	10.4
DHS-8-4	calc	105.2		-3.0	5.3
DHS-8-4	calc	123.6		-2.9	5.1
DHS-8-4	calc			-4.5	7.9
DHS-8-4	calc	168.4			
GR-3-2	q	280.0	-23.1		
GR-3-2	q	255.0			
GR-3-2	q	185.0			
GR-3-2	q	428.0		-6.6	11.6
GR-3-2	q	346.7	-28.3		
GR-3-2	q	351.4			
GR-3-2	q	335.0			
MHG-B-3	sp	356.0	-28.9		
MHG-B-3	sp		-30.6		
MHG-B-3	sp		-31.4		
MHG-C-3-1	calc	224.6		-1.0	1.8
MHG-C-3-1	calc	328.6		-4.0	7.0
MHG-C-3-1	calc	327.1		-4.0	7.0
MHG-C-3-1	calc	326.1			
MHG-C-3-1	calc	203.5			
MHG-C-3-1	calc	308.6			
MHG-C-3-1	calc	318.5			
MHG-C-3-1	calc	324.2			
MHG-C-3-2	sp	350.6	-29.8	-5.4	9.5
MHG-C-3-2	sp		-30.6	-4.0	7.0
MHG-C-3-2	sp	356.8			

1. Equivalent weight percent NaCl from equation 2 of Potter *et al.* (1978).

TABLE 300.4: FLUID INCLUSION DATA FROM THE DEADHORSE CREEK NORTH (DHN) OCCURRENCE.

Sample No.	Host	$T_{hom.}$(°C)	$T_{eut.}$(°C)	$T_{f.m.}$(°C)	Salinity[1]
DHN-13-A-1	q		-23.4	-2.1	3.7
DHN-13-A-1	q	156.1	-7.8	-3.1	5.5
DHN-13-A-2	q	147.0			
DHN-13-A-2	q	260.0	-31.0	0.0	
DHN-13-D	calc	230.1			
DHN-13-D	calc	205.6			
DHN-13-D	calc	211.3		-4.5	7.9
DHN-13-D	calc	201.6			
DHN-14-K-1	calc	214.5	-55.1	-2.7	4.8
DHN-14-K-1	calc	227.4	-31.7	-2.1	3.7
DHN-14-L-2	calc	132.3			
DHN-14-L-2	calc	161.7	-23.8		
DHN-14-L-2	calc	166.3			
DHN-14-L-2	calc	175.3	-25.6	-2.2	3.9
DHN-2-B	sp	161.3	-33.6	-8.6	15.2
DHN-5-A-2	sp	150.4		-3.0	5.3
DHN-5-A-2	sp	156.8		-3.0	5.3
DHN-5-B	calc	170.0	-27.4		
DHN-6-A	calc		-27.3	-4.5	7.9
DHN-6-A	calc			-5.2	9.2
DHN-7-C	calc	350.6	-28.5	-5.6	9.9
DHN-8-A	calc	217.0			
DHN-8-A-1	sp	202.4		-8.2	14.5
DHN-8-A-1	sp	198.3			
DHN-8-A-2	calc	217.0		-3.0	5.3
DHN-8-A-3	sp	163.0			
DHN-8-A-3	sp	165.0			
DHN-9-B	sp	175.4	-25.0	-5.9	10.4
DHN-9-B	sp	177.5		-5.5	9.7
DHN-9-B	sp	180.4	-20.0	-6.7	11.8

1. Equivalent weight percent NaCl from equation 2 of Potter *et al.* (1978).
s = sphalerite
calc = calcite
q = quartz

Franklin, J.M., Kissin, S.A., Smyk, M.C., and Scott, S.D.
1986: Silver Deposits Associated with the Proterozoic Rocks of the Thunder Bay District, Ontario; Canadian Journal of Earth Sciences, Volume 23, p.1576-1591.

Harcourt, G.A., and Bartley, M.W.
1938: Schreiber Area, Thunder Bay District; Ontario Department of Mines, Map 47J, scale 1:31 360 or 1 inch to 1/2 mile.

Jennings, E.A.
1987: A Survey of the Mainland and Island Belts, Thunder Bay Silver District, Ontario: Fluid Inclusions, Mineralogy and Sulphur Isotopes; Unpublished M.Sc. Thesis, Lakehead University, 159p.

Kissin, S.A.
1988: Nickel-Cobalt-Native Silver (Five-Element) Veins: A Rift-Related Ore Type; p.268-279 *in* Proceedings Volume, North American Conference on the Tectonic Control of Ore Deposits and the Vertical and Horizontal Extent of Ore Systems, edited by G. Kisvarsanyi and S.K. Grant, University of Missouri–Rolla, 567p.

Kissin, S.A., and Jennings, E.A.
1987: The Genesis of Silver Vein Deposits in the Thunder Bay Area, Northwestern Ontario; Grant 300, p.230-241 *in* Geoscience Research Grant Program, Summary of Research, 1986-1987, edited by V.G. Milne, Ontario Geological Survey, Miscellaneous Paper 136, 241p.

Makovicky, E.
1981: The Building Principles and Classification of Bismuth-Lead Sulphosalts and Related Compounds; Fortschritte der Mineralogie, Volume 59, p.137-190.

Marmont, S.
1984: The Terrace Bay Batholith and Associated Mineralization; Ontario Geological Survey, Open File Report 5514, 95p. Accompanied by 10 photos, 7 figures, 4 tables, and 1 map in back pocket.

McCuaig, T.C.
1988: The Deadhorse Creek Zn-Pb-Ag Veins and Their Relationship to Other Vein Deposits of the Schreiber–Terrace Bay–Marathon Region; Unpublished H.B.Sc. Thesis, Lakehead University, Thunder Bay, 59p.

TABLE 300.5: FLUID INCLUSION DATA FROM THE MOGOTHERIUM (MDG) OCCURRENCE.

Sample No.	Host	$T_{hom.}$(°C)	$T_{eu.}$(°C)	$T_{f.m.}$(°C)	Salinity[1]
MOG-1-A	q		-28.0	-9.9	17.6
MOG-1-A	q		-27.4		
MOG-1-A	q	183.0			
MOG-1-B	q	218.0			
MOG-1-B	q	175.0		-4.0	7.0
MOG-1-B	q	180.0			
MOG-1-B	q	189.3			
MOG-1-B	q	225.0			
MOG-1-C	q	190.3	-28.7	-6.4	11.3
MOG-1-C	q	145.0	-24.8	-4.3	7.6
MOG-1-C	q	140.5			
MOG-1-C	q	253.9		-7.3	12.9
MOG-1-C	q	138.9			
MOG-1-C	q	299.6			
MOG-1-C	q	244.5			

1. Equivalent weight percent NaCl from equation 2 of Potter *et al.* (1978).
q = quartz

TABLE 300.6: SULPHUR ISOTOPIC DATA FROM THE DEADHORSE CREEK NORTH AND SOUTH (DHN, DHS) AND MORLEY HIGH GRADE (MHG) VEINS.

SAMPLE NO.		$\delta^{34}S$	$\Delta_{sp\text{-}gn}$[1]	T_{eq}(°C)[2]	$T_{hom.}$(°C)[3]
DHS-X	Galena	+1.9	2.5	265	160
	Sphalerite	+4.4			
DHN-8	Galena	+3.4	2.6	275	175
	Sphalerite	+6.0			
MHG-b-1	Galena	+2.0	1.1	537	355
	Sphalerite	+3.1			
MHG-b-2	Galena	+1.0	2.4	275	355
	Sphalerite	+3.4			
MHG-c	Galena	+1.8	1.2	503	355
	Sphalerite	+3.0			

[1] Difference in $\delta^{34}S$ between sphalerite and galena.
[2] Equilibration temperature from the equation of Rye and Ohmoto (1979).
[3] Fluid inclusion homogenization temperature.
sp = sphalerite
gn = galena

Patterson, G.S., Mason, J.K., and Schnieders, B.R.
1984: Report of Activities 1983, Thunder Bay Resident Geologist Area, North Central Region; p.47-106 *in* Report of Activities 1983, Regional and Resident Geologists, edited by C.R. Kustra, Ontario Geological Survey, Miscellaneous Paper 117, 275p.
1985: Thunder Bay Resident Geologist Area, North Central Region; p.56-133 *in* Report of Activities 1984, Regional and Resident Geologists, edited by C.R. Kustra, Ontario Geological Survey, Miscellaneous Paper 122, 297p.
1986: Thunder Bay Resident Geologist Area, North Central Region; p.70-135 *in* Report of Activities 1985, Regional and Resident Geologists, edited by C.R. Kustra, Ontario Geological Survey, Miscellaneous Paper 128, 340p.

Patterson, G.C., Scott, J.F., Mason, J.K., Schnieders, B.R., MacTavish, A.D., Dutka, R.J.A., Kennedy, M.C., White, G.A., and Hinz, P.
1987: Thunder Bay Resident Geologist Area, North Central Region; p.27-127 *in* Report of Activities 1986, Regional and Resident Geologists, edited by C.R. Kustra, Ontario Geological Survey, Miscellaneous Paper 134, 322p.

Potter, R.W., II
1977: Pressure Corrections for Fluid Inclusion Homogenization Temperatures Based on the Volumetric Properties of the System NaCl-H_2O; Journal of Research, United States Geological Survey, Volume 5, p.603-607.

Potter, R.W., II, Clynne, M.A., and Brown, D.L.
1978: Freezing Point Depression of Aqueous Sodium Chlorite Solutions; Economic Geology, Volume 73, p.284-285.

Robinson, B.W., and Ohmoto, H.
1973: Mineralogy, Fluid Inclusions and Stable Isotopes of the Echo Bay U-Ni-Ag-Cu Deposits, Northwest Territories, Canada; Economic Geology, Volume 68, p.635-656.

Rye, R.G., and Ohmoto, H.
1979: Isotopes of Sulfur and Carbon; p.509-567 *in* Geochemistry of Hydrothermal Ore Deposits, 2nd edition, edited by H.L. Barnes, John Wiley and Sons, Toronto, 798p.

Walker, J.W.R.
1967: Geology of the Jackfish–Middleton Area, District of Thunder Bay; Ontario Department of Mines, Geological Report 50, 41p. Accompanied by Maps 2107 and 2112, scale 1 inch to 1/2 mile.

Grant 301 Computer Software for Micro-PIXE Analysis of Mineralogical Specimens

J.L. Campbell, J.A. Maxwell, and W.J. Teesdale

Department of Physics, University of Guelph, Guelph

ABSTRACT

The proton microprobe facility at the University of Guelph has recently started operation and is being used primarily in the micro-PIXE analysis of mineralogical specimens, especially Canadian sulphide minerals. In order to provide rapid and accurate conversions of the X-ray spectra to elemental concentrations, an extensive suite of computer software has been developed. These software programs fit the spectrum by nonlinear least squares methodology and then convert the X-ray intensities into elemental concentrations using a calibration based upon synthetic standards. The speed of the programs is such that concentration results are computed within minutes of completion of the measurement. Various unique aspects of the programs that are particularly relevant to the mineralogical context are described.

INTRODUCTION

In the last few years, proton-induced X-ray emission using micron-diameter beams (micro-PIXE or μ-PIXE) has emerged as a complementary technique to the electron microprobe for the elemental analysis of mineralogical specimens. Both techniques provide spatial resolutions of about 1μ in X-ray analysis, but μ-PIXE can offer significantly better detection limits. The application of μ-PIXE to sulphide mineral studies has been pioneered by L.J. Cabri and his colleagues at CANMET using proton microprobes at Heidelberg, Germany, and Los Alamos, U.S.A. A recent review (Cabri 1988) provides an overall summary of this area, and an extensive study (Remond *et al.* 1987) of sulphide minerals using both electron and proton microprobes demonstrates the claim made above regarding detection limits. For the specific case of sphalerite, μ-PIXE afforded improvement factors of up to 30 relative to the electron microprobe for elements such as silver.

Our role in recent CANMET analyses of sulphide minerals has been the computer processing of the raw X-ray spectra recorded at remote proton microprobes, and the subsequent derivation of elemental concentrations. With the recent installation at the University of Guelph of a Canadian proton microprobe designed specifically for mineralogical applications, it became necessary to expand our software capability to provide rapid and accurate processing of large numbers of X-ray spectra. It is especially important to have the option of deriving preliminary concentration data before the spectrum accumulation is complete in order that effective decisions be taken as the analysis proceeds.

The software developed by us prior to this project was of a rather general nature (Maxwell *et al.* 1984). This software had, however, been tested successfully in an international intercomparison of five PIXE programs, which were deployed upon a representative set of X-ray spectra from biological, environmental, and geological specimens (Campbell *et al.* 1987). The version developed here with mineralogical analysis in mind contains several new features including a calibration based upon synthetic sulphide standards.

MICRO–PIXE

In the μ-PIXE analysis of mineral specimens, the specimens are usually thick enough to stop the proton beam, as shown schematically in Figure 301.1. Hence the theoretical yield Y (Z) of characteristic X-rays from an element Z of weight concentration C_Z and atomic mass A_Z is given by (Campbell and Cookson 1984):

(1)

$$Y(Z) = NC_Z \frac{N_{av}\omega_Z b_Z \epsilon_Z}{A_Z} \int_{E_0}^{0} \frac{\sigma_Z(E)\ T_Z(E)\ dE}{S(E)}$$

This assumes a homogeneous specimen, so that the yield distribution along the proton track (typically 50μ long) is governed by the proton stopping power S(E) and the ionization cross-section $\sigma_Z(E)$. The quantity $T_Z(E)$ represents the X-ray attentuation from successive depths within the specimen and depends upon the attenuation coefficient μ/ρ of the X-ray concerned in the matrix. N_{av} is Avogadro's number, ω_Z the K (or L) fluorescence yield, b_Z the fraction of K (or L) X-rays falling in the principal $K\alpha$ (or $L\alpha$) line, N the number of incident protons (energy E), and ϵ_Z is the absolute efficiency of the Si(Li) X-ray detector. E_0 is typically 2 to 4 MeV.

The expression (1) is very similar to its counterpart in electron probe microanalysis (EPMA). However in the proton case, because of the straight path of the proton, the theoretical yield can be evaluated directly from well established literature data. In contrast, electrons scatter within the specimen and complex Monte Carlo techniques are needed to compute the expected yield for EPMA.

The spectrum of characteristic X-rays of the trace, minor, and major elements is superimposed on a continuous bremsstrahlung background (*see* Johansson and Campbell, in press) as shown in Figure 301.2. This is a secondary bremsstrahlung from electrons ejected from atoms by proton impact and is therefore much less intense than the primary bremsstrahlung in EPMA. However, the X-ray production cross-sections are of similar magnitude. The outcome is that an energy-dispersive spectrum taken with a Si(Li) detector exhibits higher peak-to-background ratios, and it is this difference that results in μ-PIXE's superior detection limits.

The Guelph μ-PIXE facility provides typically 5 nA of beam current in a 5 x 5 μm^2 spot. Mineralogical work is generally done with 2 nA to avoid specimen damage. The smallest spot size attained to date is 2 x 2 μm^2 with 1 nA of current. Any larger spot size may be chosen. The specimen chamber is equipped

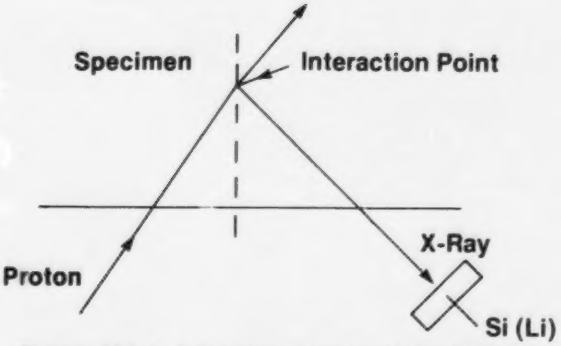

Figure 301.1. *Schematic diagram of the PIXE analysis of a specimen thick enough to stop the proton beam.*

with a Tyoda viewing microscope removed from an ETEC electron probe. This permits viewing of the specimen during analysis at magnifications of 94, 160, or 300. The pressure in the specimen chamber is about 10^{-6} torr. The duration of one analysis varies from 10 to 40 minutes. The specimen holder also contains synthetic sphalerite and pyrrhotite standards, which provide calibration as described below.

The bremsstrahlung background and the characteristic X-ray peaks of the matrix elements contribute a very large fraction of the recorded intensity. Absorbers, typically aluminum of a few hundred microns thickness, are therefore interposed to suppress these contributions in favour of the X-rays of trace elements that have higher atomic numbers than the matrix.

SPECTRUM FITTING

Following standard practice in PIXE (*see* Johansson and Campbell, in press), we extract the characteristic peak intensities from the X-ray spectrum by constructing a numerical model of the spectrum and then varying its parameters to achieve a best fit to the measured spectrum; the matching is done by nonlinear least-squares fitting, using the chi-squared test as a criterion of fit. The programs are written in Fortran.

Construction of the model requires a data base of the energies and intensities of the K and L X-rays for all possible elements of interest. The model spectrum for each element is then built by constructing Gaussian peaks in the appropriate intensity ratios at the appropriate spectral positions. The peak centroids are linearly related to the X-ray energies, as are the squares of the peak widths; the four parameters of these two linear relationships are taken as variables to be determined by the fit. The other unknowns are the heights of the principal peaks for each element. Thus, if n elements contribute to the X-ray spectrum, the fitting program has to cope with n+4 variable parameters. In essence, the least-squares fitting routine adjusts the positions, widths, and intensities (heights) of the peaks under the constraints of the linear calibrations and the intrinsic intensity ratios, to achieve the best match to the data.

Because of X-ray attenuation, the relative intensities for a given element are matrix dependent. Before the least-squares fit commences, the data base values have to be corrected for this effect using equation (1); these values must be corrected for the effects of any X-ray absorbers (such as the detector window) between the specimen and detector. This requires that the data base also contain the ionization cross-sections, fluorescence yields, proton stopping powers, and X-ray attenuation coefficients used by equation (1).

A major portion of this project was the generation of empirical expressions for ionization cross-sections and of tables of relative X-ray intensities. Details of that work are published elsewhere (Campbell 1988). The proton stopping powers used are the recent ones of Ziegler *et al.* (1985). X-ray attenuation coefficients pose something of a problem. There exist several convenient semi-empirical schemes, but since these are intended for EPMA use they usually cover an energy range that is not as wide as that employed in μ-PIXE. This forces us to adopt quite an old scheme (Leroux and Thinh 1977) which is the only such scheme to cover the 1 to 40 keV X-ray energy range. We are in the process of devising a replacement for this.

In modelling the spectrum we differ in four specific aspects from the approach generally taken. Firstly, our X-ray library contains weak "satellite" lines, which if not explicitly accounted for, could masquerade as low concentrations of elements not actually present. Secondly, our peaks are not pure Gaussian, but have low-energy tails; the parameters of these tails have been determined by the authors using a characterization technique described elsewhere (Campbell *et al.* 1987). Inclusion of these tails in the model spectrum is of particular importance for sulphide minerals where the matrix peaks are very intense. Thirdly, we provide the option of defining any element to be a surface film rather than a bulk constituent, again a useful option for mineralogy. Finally, instead of using an analytical model to describe the bremsstrahlung background, we remove the background from the data by a mathematical filtering operation, and apply the same operation to the model spectrum prior to performing the least-squares fit. The effect of the "top-hat" filter that we use is illustrated in Figure 301.3. This method, widely used in EPMA (Schamber 1977) has not yet found widespread acceptance in PIXE. We prefer it because it obviates the need for additional variable parameters and avoids any assumptions regarding the background shape.

The chi-squared values from these fits are usually close to 1.0. An example of a pyrrhotite containing Se and Pd is in Figure 301.4. In addition to providing the X-ray peak intensities, the fitting software also computes three measures of the error in these. The first is derived from the error matrix of the fit and represents the uncertainty of the fitting procedure with regard to its final set of parameter changes. The second is a simplistic statistical counting error viz. $(P + 2B)^{1/2}$ where P is the peak area and B the underlying "background" count (Clayton 1986); B is computed as the difference in summed intensity between the data and the computed spectrum. In a third

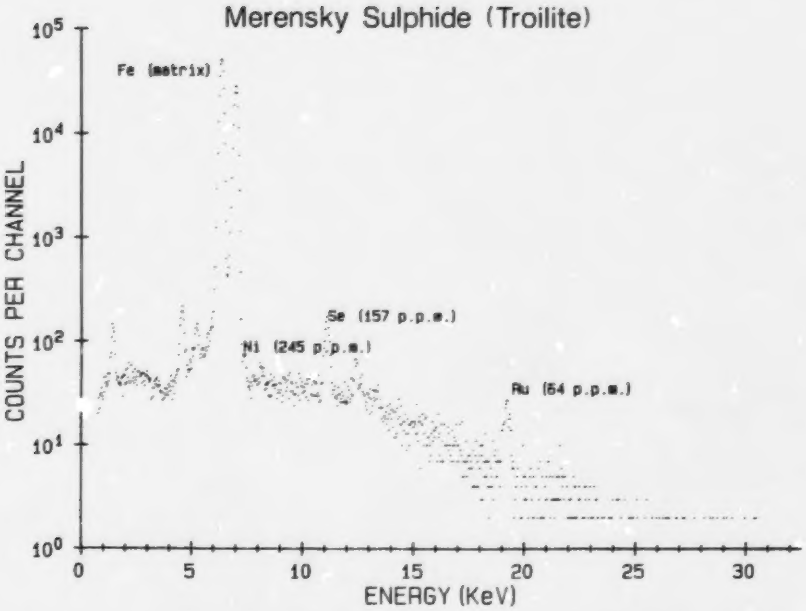

Figure 301.2. *PIXE spectrum of a Merensky sulphide (troilite) measured with 4 MeV protons. Intensity (counts per channel) is recorded versus X-ray energy (in keV units).*

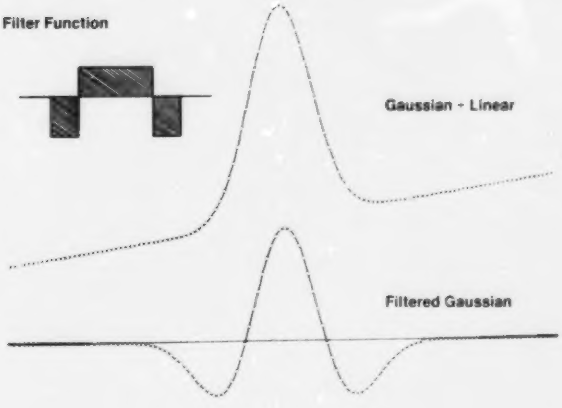

Figure 301.3. *Top-hat filter and its effect when convoluted with a Gaussian peak superimposed on a linear background.*

estimate, 1 percent of the area of any overlapping peaks is incorporated in the second error estimate to reflect uncertainties in the Kβ/Kα intensity ratios stored in the atomic physics data base.

The output also provides for each element the depth within the specimen above which 90 percent of the detected X-rays originate. This quantity depends on the atomic numbers of the trace and matrix elements. Table 301.1 illustrates this point for the K X-rays of Se, Mo, and Ag in various sulphide minerals; in the calculations, the proton beam entered the specimen at 45° to the normal, corresponding to the arrangement in our specimen chamber. It is important to note that a given analysis probes a different specimen volume for each element, a point which underlines the importance of the assumption of homogeneity.

STANDARDIZATION

μ-PIXE analyses can be approached in several ways. For example, one can use pure single-element standards or dispense with standards and conduct absolute analyses. Our preference is to use synthetic standards having a general resemblance to the specimens at hand. Several synthetic base metal sulphide standards have been made available to us by CANMET.

Equation (1) can be rewritten as:

$$Y(Z) = HC_Z Y_1(Z,M) \quad \in_Z^i \exp(-\mu x) \qquad (2)$$

Here, $Y_1(Z, M)$ is the theoretical X-ray yield for unit concentration of element Z per unit solid angle, for a predefined proton charge. Our work on the atomic physics data base suggests that $Y_1(Z,M)$ can be computed with accuracy to ±5 percent. ϵ_Z' is the detector's intrinsic or relative efficiency (=1 between 7 and 15 keV). The exponential term is the transmission through any additional absorbers present; sometimes thin aluminum foils (thickness x, attenuation coefficient μ) are interposed to suppress a low-energy bremsstrahlung background. The quantity H incorporates experimental parameters such as the detector solid angle and the calibration constant of whatever device is used to measure beam charge. H is then measured by determining the Kα (or Lα) X-ray yield from the various trace elements in the synthetic standards. Table 301.2 shows some preliminary results (which remain to be verified) from cur-

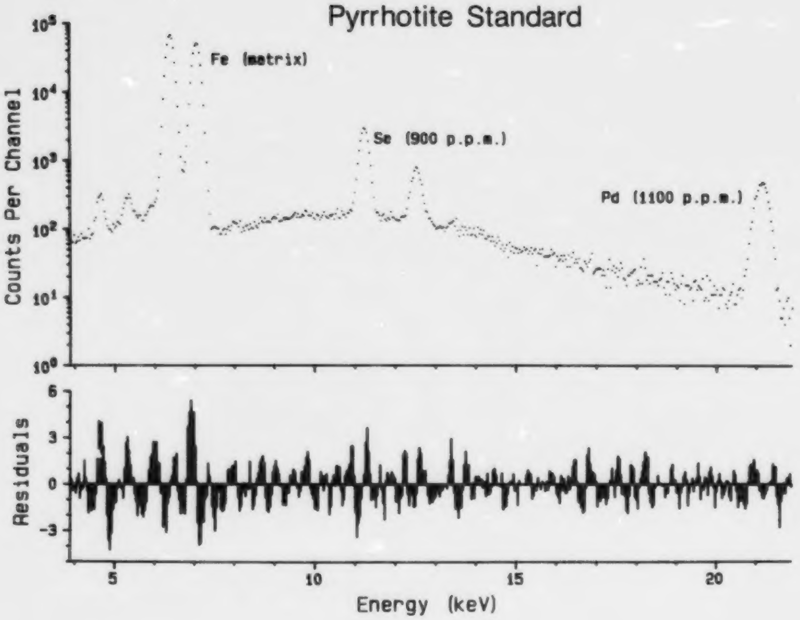

Figure 301.4. *Results of fit to the PIXE spectrum of a synthetic pyrrhotite standard. The residuals are in units of one standard deviation.*

TABLE 301.1. COMPUTED DEPTHS FOR 90% X-RAY YIELDS USING 3 MeV PROTONS ENTERING SPECIMEN AT 45° TO SURFACE.

Matrix	Composition	Density	Depth (Micrometres)		
			Se	Mo	Ag
Sphalerite	ZnS	4.0	17.9	23.4	24.4
Chalcopyrite	$CuFeS_2$	4.2	18.2	22.2	22.8
Pyrrhotite	FeS	4.8	16.5	19.3	19.6
Pyrite	FeS_2	5.0	16.1	18.1	18.2
Galena	PbS	7.5	14.6	12.7	15.9

TABLE 301.2. PRELIMINARY VALUES FOR THE CALIBRATION PARAMETER H MEASURED USING SYNTHETIC STANDARDS CONTAINING TRACE ELEMENTS AT ABOUT 0.1% CONCENTRATION.

Matrix	Trace Element	H
Pyrrhotite A	Se	0.0407
	Pd	0.0414
Pyrrhotite B	Cu	0.0389
	Pd	0.0459
Sphalerite	Ag	0.0415
	In	0.0444

rent work at Guelph. The agreement among the different standards is quite good; we attribute the discrepancies to uncertainties in the absorber transmission due in turn to uncertainties in X-ray attenuation coefficients.

Once it has computed peak intensities, the spectrum fitting software converts these, using the determined H value, to concentrations expressed in parts per million by weight. The software also converts error estimates and detection limits to ppm units.

The option also exists of standardizing using the known concentration of a major matrix element (for example, Zn in sphalerite). We have compared these two approaches elsewhere (Campbell *et al.* 1987) and tend to prefer the H-value method; it is a little less sensitive to uncertainties in X-ray transmission in the absorber interposed to suppress the intense matrix peaks.

OTHER ASPECTS OF THE SOFTWARE

Most of our work to date has been on specimens thick enough to stop the proton beam completely. However, the software also handles specimens thin enough to transmit the beam at a reduced energy. Either the exit energy or the thickness of the specimen must be specified. This permits us to handle thin sections.

All PIXE codes use the most intense X-ray line (Kα or Lα) as the measure of characteristic X-ray intensity. If a trace element Kα line overlaps with the matrix Kβ line, as is the case for germanium (Ge) in a

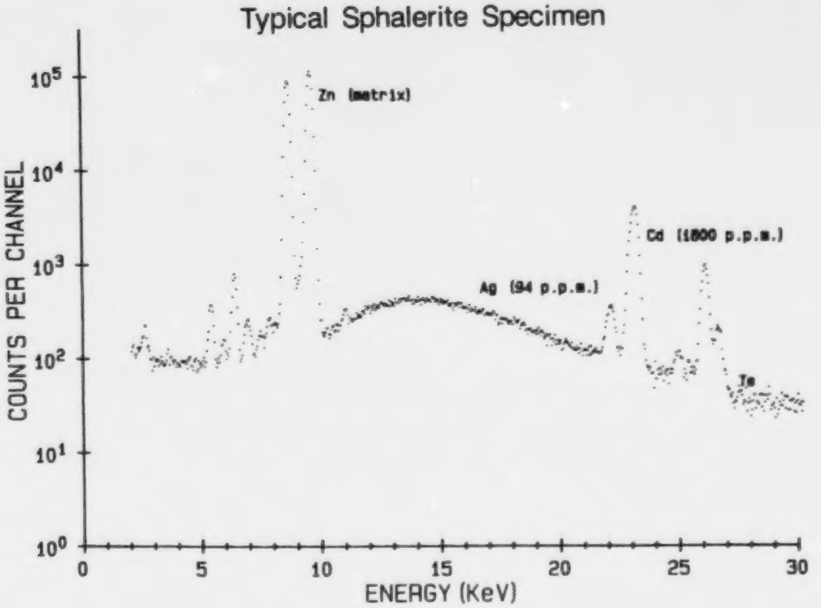

Figure 301.5. *PIXE spectrum of a Nanisivik sphalerite (ZnS) containing about 200 ppm of germanium. The Ge Kα peak overlaps the Zn Kα matrix peak. The Ge Kβ peak is just visible, to the right of the Zn matrix peaks.*

sphalerite (ZnS) matrix, the detection limit is very poor (about 300 ppm in our example). In this case (shown in Figure 301.5) the Ge Kβ line, although weak, is clearly separate (the small peak seen just to the right of the Zn Kβ line) and interference free. Our software therefore allows the user to designate the Kβ temporarily as the principal line. In our example, the manoeuvre improves the detection limit to 50 ppm under our typical measurement conditions.

Presently the software does not determine matrix element concentrations; these are part of the input and are assumed known from stoichiometry or prior EPMA analysis. We plan to extend the software to provide full analysis of major and minor elements, which will require an iterative methodology since the concentration of each partly determines (via matrix attenuation) the X-ray yields of the others. Preliminary tests have been successful.

COMPUTER HARDWARE

The PIXE analysis computer program described here, entitled GUPIX.V2A, was developed on a DEC MINC 11/23. It handles spectral regions of lengths of up to 512 channels, containing X-rays of 32 elements. An IBM PC/XT compatible version was derived during this project, and it handles 1024 channel spectra.

In addition to the numerical output, graphics are provided. The user can plot the measured spectrum, the fit, the difference (i.e. the continuum background), and the residues of the fit; the latter are the weighted channel-by-channel differences expressed in units of one standard deviation. Figure 301.4 displays a typical graphics output. Presently the graphics packages are in the process of completion. The version written for DEC computers uses the REGIS package, which is available on DEC terminals from the VT125 model upward. Currently a driver is being written for the IBM XT computer's graphics. Fits on these two computers require several minutes. A micro-VAX version of the software is being produced in the interests of greater speed. This will provide concentration data within one minute of spectrum accumulation, ensuring that data processing is never a limiting factor on analysis time.

SUMMARY AND FUTURE OBJECTIVES

An extensive suite of software has been developed to assist in μ-PIXE analysis on the proton microprobe facility at the University of Guelph. The software includes various special features which render it especially suitable for the mineralogical applications for which that instrument is primarily designed. Provided the matrix constitution is known, the concentration of any trace or minor element that contributes to the X-ray spectrum can be derived using a procedure based upon synthetic standards. The software developed in this project will be a principal tool in collaborative mineralogical research using this state-of-the-art facility.

In addition to exploiting the present facility, we are contemplating adding a wavelength-dispersive X-ray spectrometer to facilitate the determination of the major elements composing the matrix. This would relieve us of the need for prior EPMA analysis, eliminate assumptions regarding stoichiometry, and provide with ease information on matrix substitution (for example, iron for zinc in sphalerite). Figure 301.6 provides an effective illustration of the dependence of trace element X-ray yield upon matrix composition,

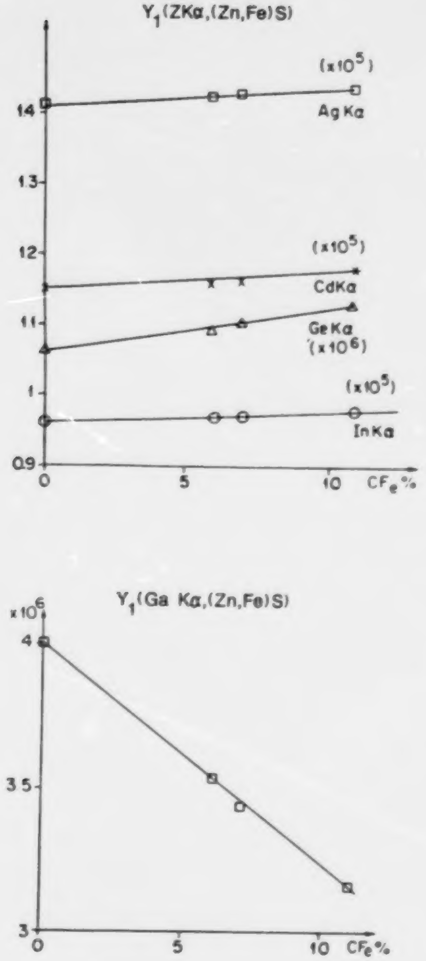

***Figure 301.6.** The X-ray yield Y_1 (Z, M) as defined in the text for trace elements Z (Ga, Ge, Ag, Cd, In), computed as a function of the Fe weight fraction in a sphalerite matrix. The sensitivity to Fe content is small, except for Ga, which shows a sharp decrease with substitution of Fe for Zn in sphalerite. From Remond et al. (1987), with the permission of the authors and publisher.*

showing the quantity Y_1 (Z, M) for a sphalerite matrix as a function of the percentage substitution of iron for zinc. The sensitivity to iron content is small, except in the case of gallium (Ga). In the latter case, the Ga Kα energy is just below the Zn K absorption edge, and so Ga Kα X-rays are only weakly attenuated by the matrix. They are, however, strongly attenuated by iron, since they lie above its K edge. Therefore substitution of Zn by Fe leads to a steep decrease in the Ga K X-ray yield per unit Ga concentration. In view of current interest in Ga in sphalerites, accurate μ-PIXE measurements of the matrix in such specimens is desirable.

All of our work to date has centred upon sulphide minerals; it is hoped in the near future to explore the usefulness of μ-PIXE in a wider range of mineral types.

ACKNOWLEDGMENTS

We are most grateful to Dr. L.J. Cabri of CANMET for his collaboration and stimulation.

REFERENCES

Cabri, L.J.
1988: Applications of Proton and Nuclear Microprobes in Ore Deposit Mineralogy and Metallurgy; Nuclear Instruments and Methods in Physics Research, Volume B30, p.459-465.

Campbell, J.L.
1988: Assessment of a Self-Consistent Theoretical Data Base for L X-Ray Relative Intensities in PIXE; Nuclear Instruments and Methods in Physics Research, Volume B31, p.518-524.

Campbell, J.L., Cabri, L.J., Rogers, P.S.Z., Traxel, K., and Benjamin, T.M.
1987: Calibration of Micro-PIXE Analysis of Sulphide Minerals; Nuclear Instruments and Methods in Physics Research, Volume B22, p.437-441.

Campbell, J.L., and Cookson, J.A.
1984: PIXE Analysis of Thick Targets; Nuclear Instruments and Methods in Physics Research, Volume B3, p.185-197.

Campbell, J.L., Maenhaut, W., Bombelka, E., Clayton, E., Malmquist, K., Maxwell, J.A., Pallon, J., and Vandenhaute, J.
1986: An Inter-Comparison of Spectral Data Processing Techniques in PIXE; Nuclear Instruments and Methods in Physics Research, Volume B14, p.204-220.

Campbell, J.L., Perujo, A., and Millman, B.M.
1987: Analytic Description of Si(Li) Spectral Lineshapes Due to Monoenergetic Photons; X-Ray Spectrometry, Volume 16, p.195-201.

Clayton, E.J.
1986: PIXAN: The Lucas Heights PIXE Analysis Computer Package, Australian Atomic Energy Commission Report AAEC/M113.

Johansson, S.A.E., and Campbell, J.L.
In press: PIXE: A Novel Technique for Elemental Analysis; John Wiley and Sons Limited, to be published in September 1988.

Leroux, J., and Thinh, T.P.
1977: Revised Tables of X-Ray Mass Attenuation Coefficients; Corporation Scientifique Claisse Incorporé, Quebec.

Maxwell, J.A., Leigh, R.G., Campbell, J.L., and Paul, H.
1984: Least-Squares Fitting of PIXE Spectra with a Digital Filter Treatment of the Continuum; Nuclear Instruments and Methods in Physics Research, Volume B3, p.301-304.

Remond, G., Cesbron, F., Traxel, K., Campbell, J.L., and Cabri, L.J.
1987: Electron Microprobe Analysis and Proton-Induced X-Ray Spectrometry Applied to Trace Element Analysis in Sulphides: Problems and Prospects; Scanning Microscopy, Volume 1, p.1017-1037.

Schamber, F.H.
1977: A Modification of the Linear Least-Squares Fitting Method Which Provides Continuum Suppression; p.241-258 *in* X-Ray Fluorescence Analysis of Environmental Samples, edited by T.G. Dzubay, Ann Arbor Science Publishers.

Ziegler, J.F., Biersack, J.P., and Littmark, U.
1985: The Stopping and Range of Ions in Solids; Pergamon Press, New York.

Grant 305 Metamorphic Petrology of the White River Gold Prospect, Hemlo Area, Ontario

Y. Pan and M.E. Fleet

Department of Geology, University of Western Ontario, London

ABSTRACT

The White River Property of Lac Minerals Limited is 5 to 10 km east, along stratigraphic strike, of the Hemlo gold deposit. The overall stratigraphy, representation of characteristic rock units, and nature of the gold mineralization are very similar to that of the Hemlo area, but with less deformation and pervasive alteration. However, the zone of anomalous gold values at the White River Property is parallel to the margin of the Cedar Lake Pluton, but stratigraphically away from the zone of highest metamorphic grade, and is not stratigraphically associated with the Hemlo Shear Zone. Trace elements at White River correlate with lithology, not with gold mineralization. Peak metamorphic conditions are similar to those at Hemlo (kyanite-sillimanite zone). However, the style of metamorphism at White River is more akin to the Barrovian type (medium pressure). A detailed study of the mineral chemistry shows that the compositional variations in the amphiboles and plagioclase are in good correlation with metamorphic grade. A lower grade calc-silicate-like alteration to chlorite + actinolite + epidote + calcite + sphene is pervasive, and (significantly) mafic rocks of units 2, 4, and 9 exhibit a characteristic prehnite + epidote + calcite alteration. Emplacement of the Cedar Lake Pluton postdates deposition of the supracrustal rocks, and most likely postdates their deformation and metamorphism.

INTRODUCTION

Since the discovery of the Hemlo gold deposit in 1982, active geological mapping and exploration for additional deposits has taken place within the Hemlo–Heron Bay Greenstone Belt, in the Hemlo area and its vicinities. The present project is a systematic study of the petrography, mineral chemistry, geochemistry, and metamorphic petrology of the Hemlo–Heron Bay Greenstone Belt, at the White River Property of Lac Minerals Limited. It is based on drill core material made available by Lac Minerals Limited and surface samples. The study area is 5 to 10 km east, along stratigraphic strike, of the Hemlo gold deposit (Figure 305.1). The overall stratigraphy, representation of characteristic rock units, and nature of the gold mineralization is very similar to that of the Hemlo area, but with less deformation and pervasive alteration. The original aim of the study is to document the variation in gold mineralization, and metamorphic grade and pressure-temperature conditions with proximity to the Cedar Lake Pluton (a possible heat source). It is also anticipated to further the understanding of the relative roles of hydrothermal and metamorphic processes in either forming, or modifying, Hemlo-type gold deposits.

GEOLOGY OF THE WHITE RIVER PROPERTY OF LAC MINERALS LIMITED

The study area and the Hemlo gold deposit are contained within the Hemlo–Heron Bay Greenstone Belt (Figure 305.1) (Muir 1985; Patterson 1985), which is part of the Shebandowan–Wawa Subprovince of the Superior Province of Ontario. In the White River Property, the supracrustal rocks consist of the Playter Harbour Group (tholeiitic flows interbedded with thin tuffaceous and clastic metasedimentary rocks) and the overlying Heron Bay Group (intermediate to felsic metavolcanics which interdigitate and grade into clastic-dominated metasediments eastward). These supracrustal rocks are restricted to a narrow belt up to 4 km wide by the Pukaskwa Gneissic Complex to the south, and the Cedar Lake Pluton to the north (Figure 305.1).

LITHOLOGICAL UNITS

The supracrustal rocks strike approximately 110°, and dip 60°NNE in the western part of the study area, but gradually change to a strike of 095°, and a dip of 45°N in the central and eastern parts. We have divided the supracrustal rocks into nine units on the basis of stratigraphic, lithological, compositional, and textural criteria (Figure 305.2). These are arranged in a north to south (top to bottom) sequence below:

9. metagreywacke with mafic metavolcanics
8. metapelite
7. upper intermediate to felsic metavolcanics
6. quartz-biotite schist
5. biotite-rich greywacke
4. middle mafic metavolcanics
3. lower intermediate to felsic metavolcanics
2. metasediments
1. mafic metavolcanics.

Unit 1 corresponds to the Playter Harbour Group, and units 2 to 9 to the Heron Bay Group.

Unit 1: This lowest unit of mafic metavolcanics structurally overlies the Pukaskwa Gneissic Complex. It consists of mainly massive and variolitic varieties of high-iron tholeiitic flows and pillowed basalts of the Playter Harbour Group (Muir 1985).

Unit 2: Overlying the Playter Harbour Group mafic metavolcanics of unit 1 is a very thick (400 to 700 m) metasedimentary unit with a typical Archean metagreywacke bulk-chemical composition (Condie 1981, Table 4-4). This unit consists of strongly foliated grey-white quartz-feldspar-mica schists. Locally, garnet poikiloblasts are present. Several lenticular fragments of felsic metavolcanics are present in the middle and upper portions of the unit. A band (30 m thick) of dark green amphibolite can be traced subparallel to the foliation in the upper portion. A few wedge-shaped fragments of chromium-rich skarn-like calc-silicate rock (diopside-hedenbergite + epidote + (end-member) albite + (end-member) microcline + (K,Na)-mica + uvarovite ± grossular ± actinolite ± chlorite, with significant quantities of molybdenite, pyrite, and pyrrhotite) occur within the amphibolite

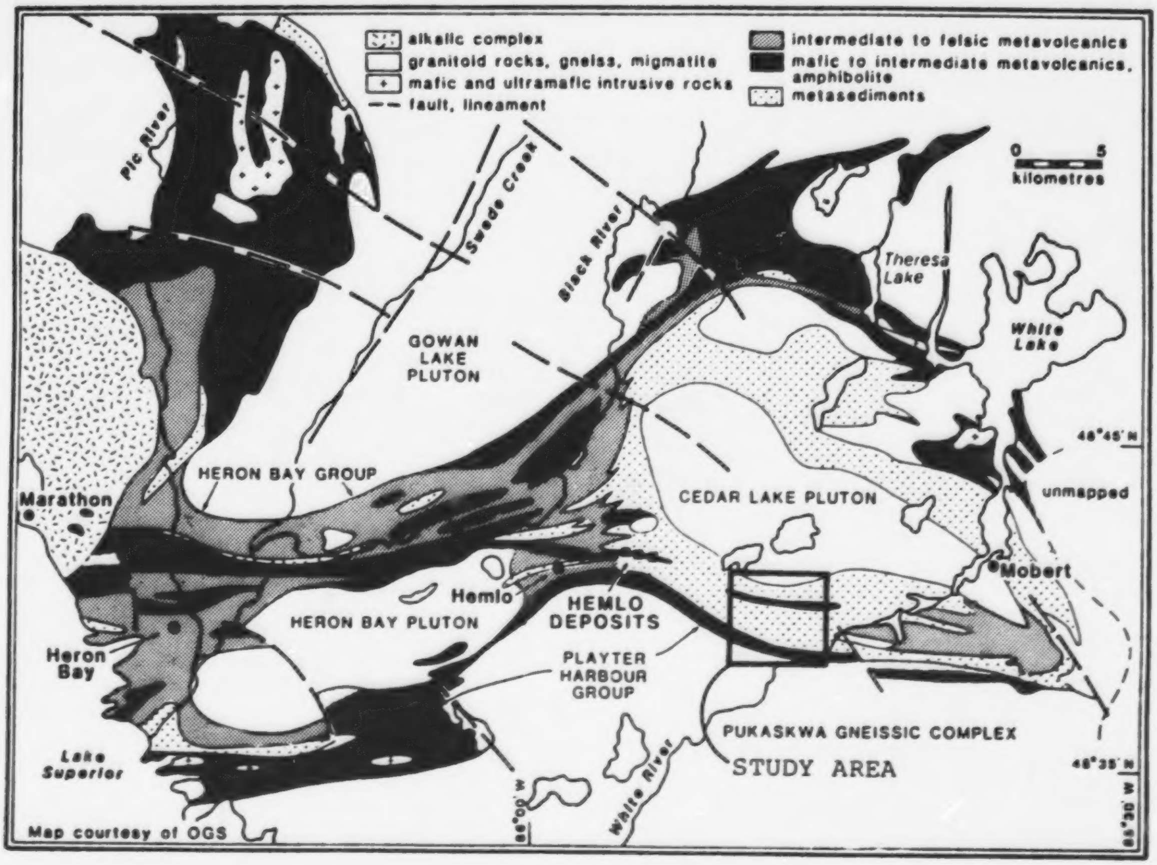
alkalic complex
granitoid rocks, gneiss, migmatite
mafic and ultramafic intrusive rocks
fault, lineament
intermediate to felsic metavolcanics
mafic to intermediate metavolcanics, amphibolite
metasediments
0 5 kilometres
Pic River
Swede Creek
Black River
Theresa Lake
White Lake
GOWAN LAKE PLUTON
HERON BAY GROUP
Marathon
CEDAR LAKE PLUTON
48°45'N
unmapped
Mobert
Hemlo
HERON BAY PLUTON
HEMLO DEPOSITS
PLAYTER HARBOUR GROUP
Heron Bay
PUKASKWA GNEISSIC COMPLEX
Lake Superior
STUDY AREA
48°35'N
86°00'W
White River
85°30'W
Map courtesy of OGS

Figure 305.1. Location map of the White River Property of Lac Minerals Limited, Hemlo, Ontario (from Muir 1985).

band or adjacent to it (this is referred to as the "Cadi zone" by Lac Minerals Limited field geologists).

Unit 3: This unit is composed of a sequence with a variable thickness (550 to 750 m) of intermediate to felsic metavolcanics separated by a thick band (200 m) of metasedimentary rocks. These intermediate metavolcanics are massive locally weakly-foliated fine-grained grey-white rocks containing muscovite, hornblende, biotite, quartz, plagioclase, microcline, epidote, and minor amounts of zircon, tourmaline, magnetite, pyrite, sphene, and apatite. Most of the metavolcanics, particularly in the upper portion, contain quartz and plagioclase phenocrysts (2 mm diameter); the latter are well zoned and extensively replaced by sericite. Locally, the upper portion is relatively enriched in BaO: relict microcline grains have up to 3 weight percent BaO. A wedge-shaped body of felsic metavolcanics is present within the metasedimentary rocks of this unit, near the western limit of the study area.

Unit 4: The middle sequence of mafic metavolcanics attains a maximum thickness of 140 m, and structurally overlies the intermediate metavolcanics of unit 3. This unit is composed of strongly foliated dark green amphibolite (hornblende + biotite + plagioclase + microcline) with pillow structures locally present. A thin (1 to 3 m) layer of actinolite-chlorite schist can be traced along the lower portion. This schist has been interpreted to represent the Hemlo Fault, and is thought to be a regional structure (Patterson 1985). The present whole rock chemistry is consistent with a precursor layer of komatiite and komatiitic basalt. Interestingly, the actinolite-chlorite schist contains an unusual feldspar assemblage (andesine + bytownite-anorthite) (cf. Grove *et al.* 1983). Microveins of prehnite + epidote + calcite + potassic feldspar are extensively developed within the lower portion of the unit, adjacent to the actinolite-chlorite schist.

Unit 5: The middle metasedimentary sequence of supracrustal rocks consists of units 5 and 6, and is approximately 250 m thick in the western part of the study area, and up to 800 m thick in the eastern part. Unit 5 is characterized by a group of foliated medium- to fine-grained quartz-feldspar-biotite schists typical of Archean metagreywacke bulk-chemical composition, and is referred to as a biotite-rich greywacke.

An elongate dike (1000 m long) of altered quartz-feldspar porphyry is subparallel to the foliation in the

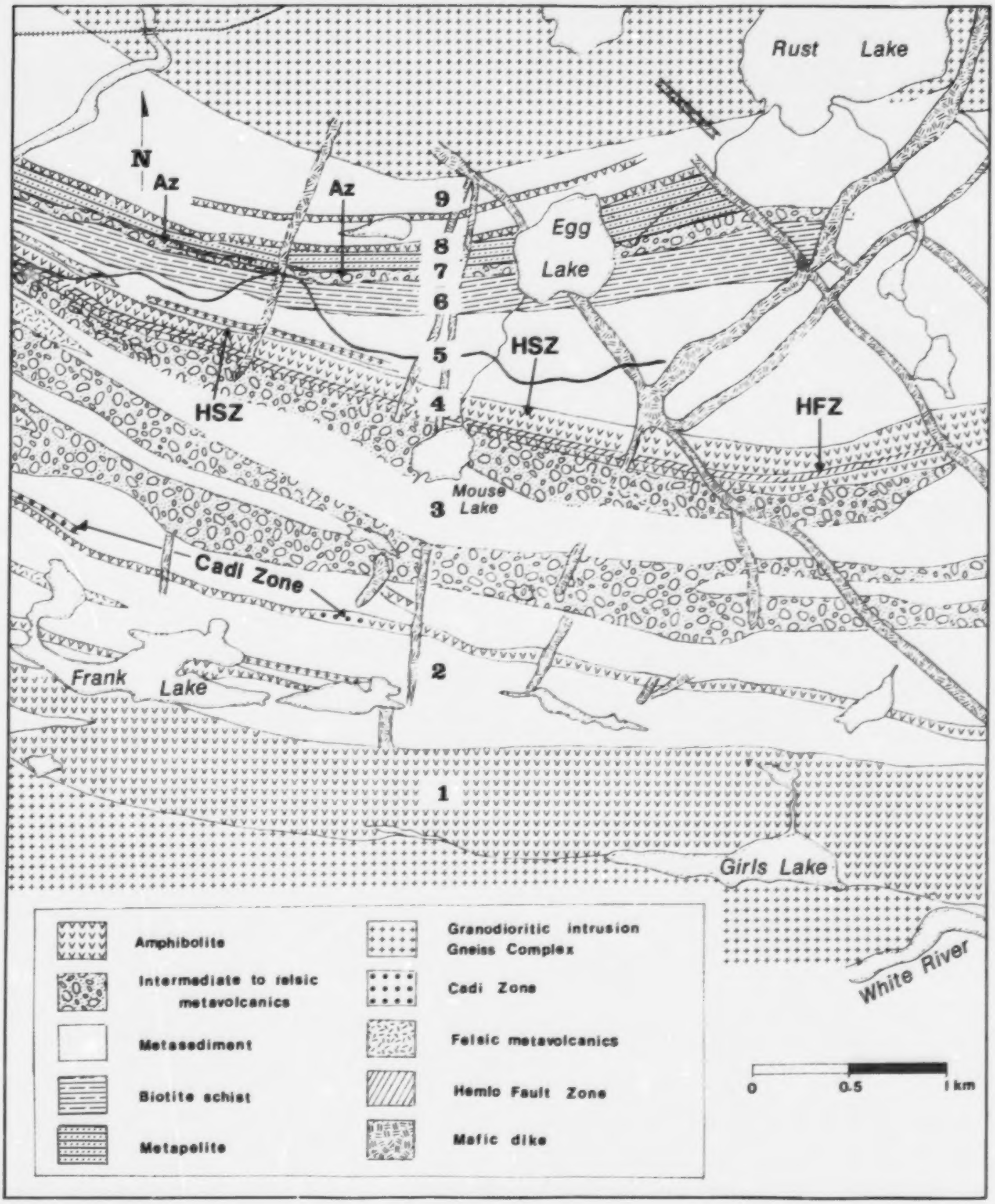
Rust Lake
N
Az
Az
9
8
7
6
5
4
3
2
1
Egg Lake
HSZ
HSZ
HFZ
Mouse Lake
Cadi Zone
Frank Lake
Girls Lake
White River
Amphibolite
Intermediate to felsic metavolcanics
Metasediment
Biotite schist
Metapelite
Granodioritic intrusion Gneiss Complex
Cadi Zone
Felsic metavolcanics
Hemlo Fault Zone
Mafic dike
0
0.5
1 km

Figure 305.2. *Geological map of the White River Gold Prospect of Lac Minerals Limited, Hemlo area (modified from unpublished map by R.A. Campbell of Lac Minerals Limited, 1985).*

lower portion of this unit, and a lenticular fragment of felsic metavolcanics (which is possibly correlatable with the crystal tuff of the Hemlo deposit) is present in the lower portion, at the western limit of the property.

Unit 6: This unit is typified by a group of very strongly foliated medium- to coarse-grained yellowish or brownish grey quartz-biotite schists. Staurolite-quartz-biotite schists, which commonly contain garnet and abundant tourmaline, occur as thin layers (10 cm to 5 m). Staurolite and garnet are poikiloblastic. A second generation of garnet occurs as smaller porphyroblastic grains that may exhibit an "augen" texture.

Sillimanite-quartz-biotite schists, commonly containing garnet and staurolite poikiloblasts, occur as thin bands (2 to 3 cm) in the upper portion. These bands are characterized by fibrolitic sillimanite, poikiloblastic cordierite, and locally developed medium-grained kyanite (partly replaced by muscovite).

Anthophyllite-quartz-biotite schists typically contain (Mg, Fe)-anthophyllite + (minor) gedrite + cummingtonite, and minor amounts of poikiloblastic staurolite and garnet. Anthophyllite is partly replaced by chlorite.

There is a regional banded iron formation (up to 5 m thick) in the lower portion of this unit. Thin magnetite-dominated layers are interbanded with brown hornblende and quartz-rich layers. Very locally, poikiloblastic garnet is replaced by dark green hornblende and chlorite, together with a later finer grained generation of porphyroblastic garnet.

Unit 7: The upper intermediate to felsic metavolcanic unit is approximately 100 m thick, and is in gradational contact with the quartz-biotite schists of unit 6. It is distinguished from the metasedimentary rocks by a massive, or locally weakly foliated, fine- to medium-grained texture. It is composed of quartz, plagioclase, microcline, hornblende, epidote, disseminated and veined calcite; minor quantities of magnetite, sphene, apatite, tourmaline, and disseminated pyrite. A few microcline grains have up to 4 weight percent BaO.

Unit 8: The metapelite is approximately 30 m thick, and is in gradational contact with the upper intermediate to felsic metavolcanic sequence of unit 7. It is strongly foliated, containing medium- to coarse-grained quartz, biotite, untwinned plagioclase, chlorite, sphene, apatite, tourmaline, and disseminated calcite.

At the boundary of unit 7 (intermediate to felsic metavolcanics) and unit 8 (metapelite), there is a zone with anomalous gold values ranging from 37 to 610 ppb. It occurs roughly parallel to the margin of the Cedar Lake Pluton and dips to the north. In contrast to the Hemlo gold deposit, the anomalous zone is associated with both metapelite and intermediate to felsic metavolcanics, rather than felsic metavolcanics, and is not spatially associated with the zone of peak metamorphism (units 4, 5, and 6).

Unit 9: The metagreywacke varies in thickness from 350 to 600 m. It is characterized by strongly foliated yellowish grey fine-grained to very fine-grained quartz-feldspar schists, which consist mainly of quartz, plagioclase, biotite, chlorite, sericite, muscovite, and locally, garnet porphyroblasts and minor amounts of sphene, magnetite, and apatite. Prehnite and epidote microveins are present adjacent to mafic flow layers.

Unit 9 contains two laterally extensive bands of mafic metavolcanics which are 10 m thick, and in sharp contact with the enclosing metasedimentary rocks. They are strongly foliated, fine- to medium-grained dark green amphibolites (actinolitic hornblende to hornblende + biotite + plagioclase + microcline), with local abundances of tourmaline grains. Garnet porphyroblasts are present locally in the metagreywacke adjacent to the contact with the Cedar Lake Pluton. Prehnite, epidote, and calcite are present locally within microveins, and in the groundmass.

INTRUSIVE ROCKS

Besides the altered quartz-feldspar porphyry dikes present in the lower portions of unit 5, which are subparallel to the penetrative foliation, early dark green altered mafic dikes are also locally recognized in the study area (cf. Burk *et al.* 1986). They occur parallel to the penetrative foliation of supracrustal rocks and are mainly composed of biotite + plagioclase + pyroxene + hornblende + actinolite + chlorite, where the actinolite and chlorite appear to be hydrothermal alteration (or retrograde) products.

The Cedar Lake Pluton is a porphyritic granodioritic body (quartz + plagioclase + microcline + biotite, with accessory sphene, zircon, and apatite). Toward the contact with the metagreywacke of unit 9, it becomes more pegmatitic. Magmatic textures and features (microcline twinning, etc.) are well preserved, and there are a few isolated xenoliths with mineral assemblages and textures similar to the metagreywacke of unit 9.

Later Proterozoic (Muir 1982) mafic dikes (lamprophyre and diabase) are well developed in the study area. They are steeply dipping and strike perpendicular or nearly perpendicular to the foliation of supracrustal rocks. The lamprophyre is composed mainly of zoned titanium-rich pyroxene, deep-brown biotite, and plagioclase, with some chlorite. Most of these pyroxene phenocrysts are extensively serpentinized. However, the diabase dikes are generally fresh looking and consist mainly of pyroxene and plagioclase; only a few grains of plagioclase have been weakly altered to very fine-grained sericite.

STRUCTURAL GEOLOGY

The large-scale structure of the Hemlo–Heron Bay Greenstone Belt has been described as a broad synform with granitic-granodioritic intrusions (the Heron Bay Pluton and Cedar Lake Pluton) occurring along its fold axis (Patterson 1985). Brittle and ductile deformation (faulting and shearing) commonly occur along the contacts of metavolcanic and metasedimentary rocks subparallel to bedding. At least four distinct generations of events have been recognized by Kuhns *et al.* (1986): a) pre-peak metamorphic F1 folds; b) post-peak metamorphic F2 folds

TABLE 305.1: MAJOR ELEMENT COMPOSITIONS OF SELECTED ROCK UNITS.

UNIT	1	2	2	2	2	3	3
SAMPLE	Amph	Gryw	Clcs	Clcs	ActSc	Flsv	Flsv
SiO_2 (wt%)	48.30	63.30	47.90	53.10	50.20	57.30	66.80
Al_2O_3	15.00	15.70	3.92	8.86	4.88	14.60	15.70
CaO	10.90	4.93	14.30	16.90	21.20	7.64	3.15
MgO	7.81	2.64	17.50	7.38	10.60	3.89	1.39
Na_2O	2.82	4.62	1.05	1.99	1.10	5.52	5.42
K_2O	0.67	1.58	0.14	1.74	0.12	1.31	2.36
Fe_2O_3	12.90	4.79	9.13	8.74	9.73	7.34	3.15
MnO	0.20	0.08	0.21	0.39	0.29	0.19	0.05
TiO_2	0.73	0.47	0.19	0.09	0.32	0.64	0.52
P_2O_5	0.07	0.14	0.03	0.21	0.03	0.20	0.22
LOI	0.90	0.70	3.60	0.70	0.50	1.00	0.90
Total	100.00	98.90	98.00	100.30	99.00	99.60	100.00

UNIT	4	4	5	5	5	5	6
SAMPLE	ActSc	Amph	Porph	LIF	Flsv	BISc	BIF
SiO_2 (wt%)	48.00	49.80	68.60	63.10	71.50	62.00	60.60
Al_2O_3	7.17	13.50	15.50	9.90	14.50	16.40	7.13
CaO	8.41	14.30	2.64	3.50	3.45	2.73	4.23
MgO	19.40	4.96	1.01	2.82	0.54	3.22	3.04
Na_2O	0.55	1.22	5.13	0.61	5.11	4.23	1.41
K_2O	2.16	0.52	2.12	0.68	1.29	2.50	0.95
Fe_2O_3	9.48	12.00	2.61	16.90	2.13	6.17	21.70
MnO	0.19	0.24	0.04	0.13	0.07	0.08	0.08
TiO_2	0.31	1.21	0.36	0.33	0.35	0.65	0.24
P_2O_5	0.01	0.11	0.14	0.15	0.08	0.18	0.51
LOI	2.70	2.10	1.00	0.50	1.00	1.10	0.50
Total	98.70	98.70	99.10	98.30	100.20	99.50	100.10

UNIT	6	6	7	8	9	9	9
SAMPLE	GnBISc	GnBISc	Flsv	Mplt	Amph	Gryw	Amph
SiO_2 (wt%)	63.10	64.20	64.20	65.30	54.60	62.20	48.70
Al_2O_3	17.10	18.50	13.60	15.30	15.40	17.10	13.40
CaO	1.62	1.83	6.11	1.84	8.97	3.49	8.60
MgO	2.76	2.14	2.65	2.99	5.00	2.97	8.98
Na_2O	2.14	3.09	4.92	5.52	3.90	4.46	2.64
K_2O	3.32	2.16	2.35	2.26	2.08	2.22	2.29
Fe_2O_3	6.60	4.70	3.96	4.27	8.09	5.79	11.70
MnO	0.06	0.06	0.06	0.06	0.15	0.08	0.19
TiO_2	0.63	0.74	0.45	0.48	0.65	0.61	0.89
P_2O_5	0.15	0.15	0.18	0.21	0.27	0.19	0.22
LOI	1.80	2.10	0.90	1.10	0.80	0.90	1.10
Total	99.50	99.70	99.80	99.70	100.20	100.30	99.00

(these are the major megascopic structures in this greenstone belt; c) ductile-brittle T1 faulting; and d) brittle T2 faulting.

Two major fracture zones have been identified in the study area. The first fracture zone, which is characterized by the 1 to 3 m thick actinolite-chlorite schist of unit 4, occurs parallel or subparallel to the foliation plane of the amphibolite of unit 4, at the southern margin of the zone of highest metamorphic grade in the centre of the study area (units 4, 5, and 6). It is generally interpreted as the extension of the regional fracture zone (Hemlo Fault Zone) at Hemlo. The Cadi fracture zone lies within mafic metavolcanic rocks or adjacent to the contact between metasedimentary and mafic metavolcanic rocks in the southwestern part of the study area, and is delineated from the surrounding rocks as a magnetic anomaly. Very low frequency (VLF) and ionization potential (IP) electromagnetic surveys also delineate it distinctly. Within the Cadi zone, Z-shaped drag folds related to ductile shearing are locally present.

In the study area, all rocks between the Cedar Lake Pluton and Pukaskwa Gneissic Complex have undergone ductile deformation. The most intense ductile deformation occurs in a narrow zone adjacent to the contact between mafic metavolcanic rocks of unit 4, and metasedimentary rocks of unit 5, and is generally interpreted as the extension of the Hemlo Shear Zone.

TABLE 305.1: CONTINUED

UNIT SAMPLE	9 Gryw	PKSKW Gnss	CDLKP Grndt	CDLKP Pgmt	Dike Lmpp	Dike Dibs
SiO_2 (wt%)	66.10	70.70	63.00	74.70	44.40	49.20
Al_2O_3	16.50	14.80	17.10	13.90	11.00	14.40
CaO	2.90	2.03	3.52	0.85	7.11	12.40
MgO	1.91	0.71	1.23	0.07	14.90	8.74
Na_2O	4.55	5.43	5.80	5.13	1.09	1.68
K_2O	3.40	2.61	2.72	4.04	3.81	0.72
Fe_2O_3	2.69	1.93	3.57	0.50	12.60	10.80
MnO	0.04	0.04	0.04	0.02	0.18	0.18
TiO_2	0.34	0.26	0.56	0.07	0.64	0.71
P_2O_5	0.14	0.08	0.23	0.02	0.03	0.07
LOI	0.50	0.50	0.50	0.50	1.90	1.10
Total	99.30	99.20	98.40	99.50	97.60	100.00

Abbreviations:

Amph-	amphibolite	GnBiSc-	garnet-biotite schist
Gryw-	metagreywacke	Mplt-	metapelite
Clcs-	calc-silicates	Gnss-	gneiss
ActSc-	actinolite schist	Grndt-	granodiorite
Flsv-	intermediate-felsic metavolcanics	Pgmt-	pegmatite
LIF-	local iron formation	Lmpp-	lamprophyre
Porph-	quartz porphyry	PKSKW-	Pukaskwa Complex
BiSc-	biotite schist	CDLKP-	Cedar Lake Pluton
BIF-	banded iron formation	Dibs-	diabase

TABLE 305.2: MAJOR ELEMENT COMPOSITIONS OF SAMPLES WITH ANOMALOUS GOLD VALUES

UNIT	AZ	AZ	AZ	5	3	2
SiO_2 (wt%)	60.10	59.30	67.40	62.30	64.70	53.50
Al_2O_3	12.90	19.20	13.10	15.80	15.201	11.00
CaO	8.67	4.05	3.94	3.14	3.74	5.96
MgO	2.03	2.81	2.04	3.35	2.17	1.26
Na_2O	4.63	1.10	7.63	3.38	3.19	2.21
K_2O	2.31	4.42	0.12	2.58	2.10	0.92
Fe_2O_3	3.51	4.96	4.08	6.35	6.93	17.33
MnO	0.12	0.08	0.05	0.09	0.16	0.08
TiO_2	0.39	0.54	0.48	0.60	0.58	0.43
P_2O_5	0.24	0.22	0.20	0.17	0.13	0.12
LOI	2.50	1.80	0.80	1.00	0.80	7.70
Total	97.50	98.70	100.00	99.20	99.90	100.50
Au(ppb)	42	37	610	56	21	54

Abbreviation:
AZ- anomalous zone (Au zone)

WHOLE ROCK GEOCHEMISTRY

The whole-rock compositions of 111 samples were determined by X-ray fluorescence, neutron activation analysis, and directly coupled plasma (DCP) methods, by Neutron Activation Services Limited, Hamilton. Representative data are reported in Table 305.1.

Some generalities about the compositions of the rock types can be stated. The actinolite-chlorite schists of unit 4 are of extremely high MgO content, with elevated chromium and TiO_2 contents, and are similar in composition to a komatiite or komatiitic basalt. The foliated amphibolite throughout the study area is compositionally similar to average oceanic pillowed basalts (cf. Hyndman 1985): indeed, pillowed structures have been observed locally in the study area. The metagreywacke of the study area is of typical Archean greywacke composition (cf. Condie 1981). The metapelite and the garnet-biotite schists (cordierite-bearing, kyanite-sillimanite-bearing) are similar in composition to Archean shales (cf. McLennan *et al.* 1983), except for the iron enrichment of the latter.

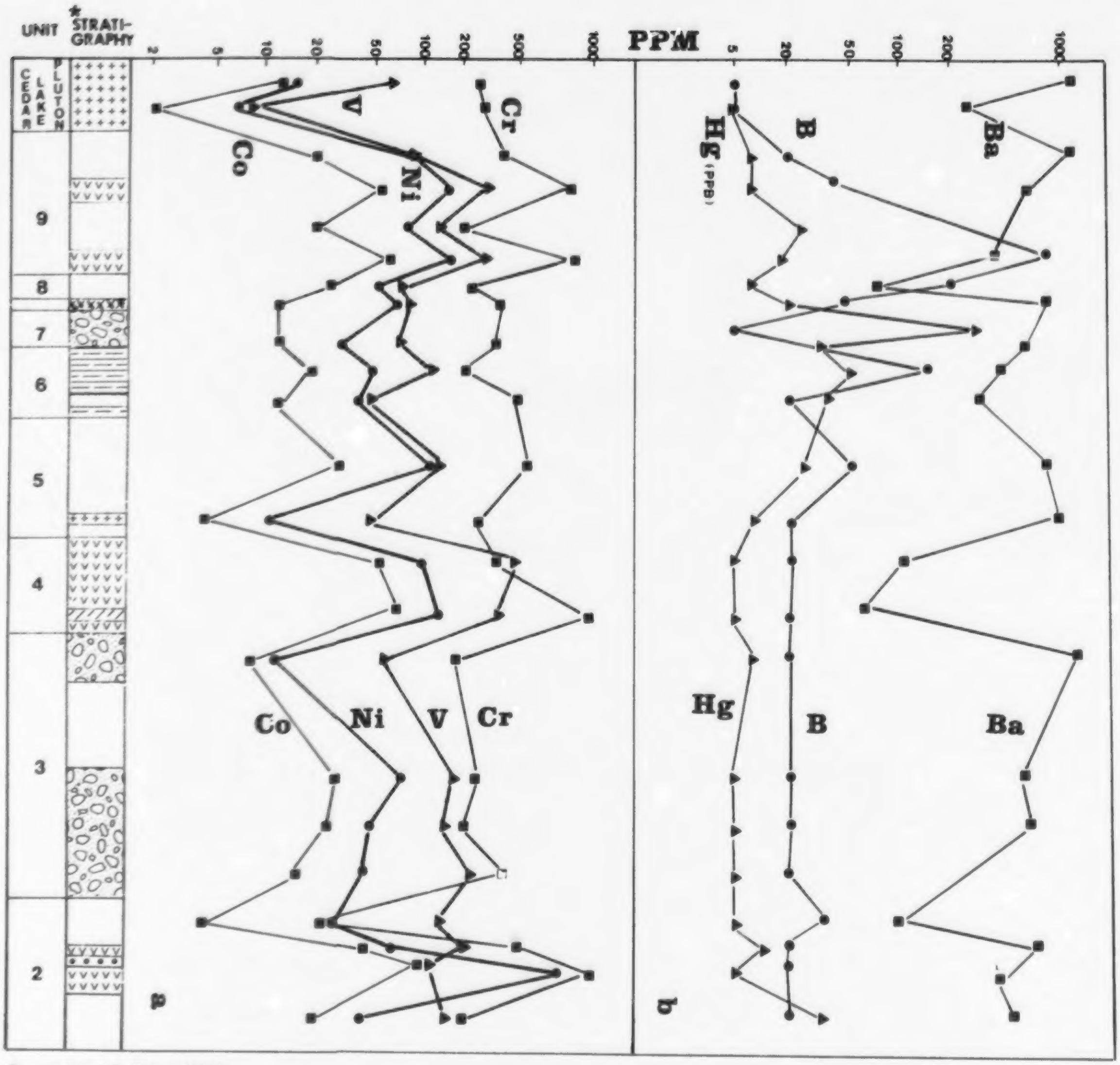

* see legend, Figure 305.2

Figure 305.3. Trace element variation profiles across the greenstone belt at the White River Property: (a) Co, Cr, Ni, and V; (b) possible pathfinder elements B, Ba, and Hg.

The rocks within the zone of anomalous gold values are aluminous and alkalic in nature (Table 305.2); however, individual alkali contents are characteristically quite variable. Gold values within the zone range from 37 to 610 ppb. A few anomalous gold values (up to 56 ppb) have been recorded in other units of the study area.

Preliminary review of the trace element data shows that the gold anomaly is not associated with anomalously high Mo-Ba-Sb-Hg-As-V contents as in the Hemlo gold deposit (Harris 1986). Figure 305.3 shows that Cr, Co, Ni, B, Hg, Ba, and V in the study area correlate with lithology, not with the gold anomaly.

The chondrite-normalized rare earth element (REE) distribution patterns of some selected rocks in the study area are presented in Figure 305.4. Actinolite-chlorite schists occur sporadically in the study area; their REE patterns show no significant fractionation, and are characterized by a high positive cerium anomaly. The basic rocks (mafic flows metamorphosed to amphibolite) are one of the most abundant lithologies in the study area; their REE patterns, except for those from unit 9, are nearly flat, are generally similar to those of the actinolite-chlorite schist, and have positive cerium anomalies and negative europium anomalies. The slight REE fractionation in unit 9 is expressed by $(La/Yb)_N$ ratios of about 5. Metasediments and intermediate to felsic metavolcanics, the most predominant lithologies in the study area, have similar REE patterns. All REE patterns of these rocks show significant fractionation

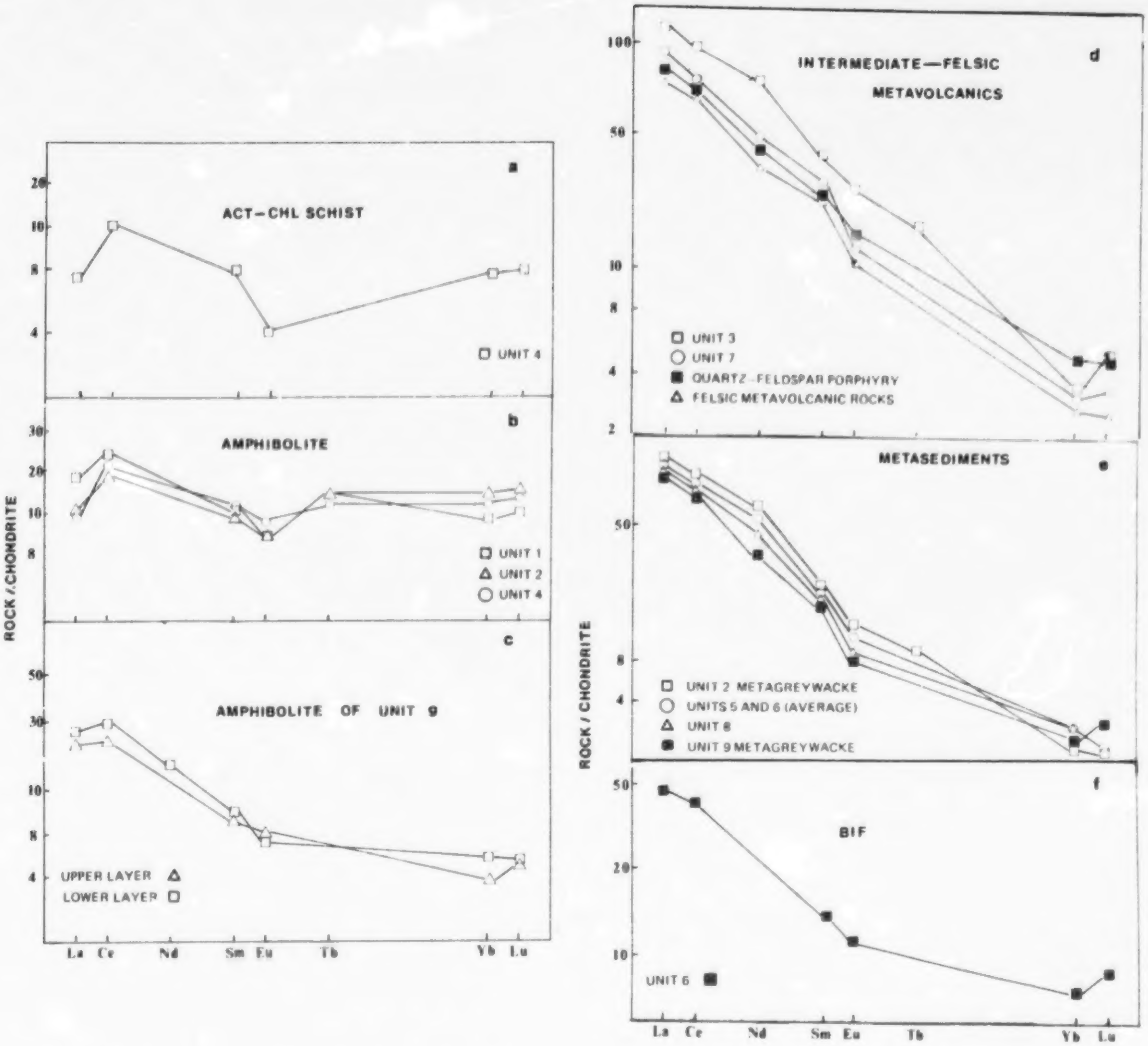

***Figure 305.4** Chondrite-normalized rare earth element (REE) abundances in representative rock lithologies of the White River Property: (a) actinolite-chlorite schist of unit 4; (b) basic rocks (mafic flows metamorphosed to amphibolite); (c) amphibolites of unit 9; (d) intermediate to felsic metavolcanic rocks; (e) metasedimentary rocks; (f) banded iron formation.*

with light REE (LREE) enrichment, and a maximum $(La/Yb)_N$ ratio of about 75 (N refers to chondrite normalized data). In contrast to most of the Archean banded iron formations studied by Fryer (1977), which are low in REE abundancies (2 to 10 times chondrites) and possess positive europium anomalies, the regional banded iron formation of the study area exhibits a strong fractionation trend without a positive europium anomaly.

METAMORPHISM

The White River area has been subjected to low to medium grade regional metamorphism. The local peak metamorphic conditions were similar to those at Hemlo (kyanite-sillimanite zone, Burk *et al.* 1986). However, it appears that peak metamorphism was realized in the footwall (units 4, 5, and 6) to the anomalous zone at the boundary of units 7 and 8, rather than in the hanging wall metapelites of unit 8. A typical peak metamorphic assemblage is quartz + plagioclase ± hornblende ± garnet ± biotite ± sillimanite + potassic feldspar ± kyanite ± cordierite ± anthophyllite ± staurolite. Textural relationships show that peak metamorphism predates, or is synchronous with, peak ductile deformation. Fibrous sillimanite (fibrolite) aggregates and long axes of anthophyllite in the garnet-biotite schists of unit 6, and the long axes of hornblende grains in the amphibolite of unit 4 are aligned parallel to the foliation plane, which is parallel to the zone of highest metamorphic grade. While the staurolite and kyanite porphyroblasts are helicitic, their internal fabrics are discordant to the foliation plane. These observations are similar to those made at Hemlo (Burk *et al.* 1986), where these features are attributed to polymetamorphism in the Hemlo Shear Zone.

To the south and north of the zone of highest metamorphic grade (units 4, 5, and 6), the metamorphic grade can be described as being at or near the greenschist-amphibolite facies transition (cf. Fleet *et al.* 1987), and is characterized by the assemblage actinolitic hornblende + oligoclase + epidote + biotite + chlorite + quartz + sphene + muscovite, with carbonate and tourmaline occurring locally (cf. Laird and Albee 1981).

A detailed investigation of mineral chemistry is one of the major tools of this study. Preliminary electron microprobe analyses for calcic amphiboles and plagioclase are presented here so that the correlation between mineral chemistry and metamorphic grade (cf. Fleet *et al.* 1987; Spear 1980) may be discussed. The proportion of ferric and ferrous iron in calcic amphiboles is calculated by the procedure of Papike *et al.* (1974); the amphibole classification follows Leake (1978). The variation in composition of calcic amphibole and of plagioclase in all rock types throughout the study area shows good correlation with the metamorphic grade (Figure 305.5). In the kyanite-sillimanite zone rocks (units 4, 5, and 6), calcic amphiboles are exclusively brown hornblende, and the anorthite (An) contents of plagioclase grains range from 28 to 42. Elsewhere in other units, the presence of coexisting actinolitic hornblende and oligoclase is consistent with the presence of abundant epidote and chlorite, indicating a metamorphic grade at the greenschist-amphibolite facies transition. In the metagreywacke of unit 9, near the Cedar Lake Pluton, the slightly higher anorthite content of plagioclase (up to An_{27}), together with the presence of almandine porphyroblasts, could be the effect of the contact halo. Actinolite and albite are observed in the study area as late stage hydrothermal alteration products in veins and veinlets, and in the two major fracture zones of the study area, the Cadi zone and the actinolite-chlorite schist of the Hemlo Fault Zone.

Figure 305.6 reports the compositional variation of calcic amphibole with a plot of total iron content (Fe^{2+} + Fe^{3+}) versus aluminum (^{IV}Al) (cf. Fleet *et al.* 1987) for all analyzed calcic amphiboles in the study area. A well defined trend of progressive increase in ^{IV}Al content with metamorphic grade (which peaks in units 4, 5, and 6) is evident and equivalent to that in Sudbury metabasites (Fleet *et al.* 1987): note that the actinolite-chlorite schist of unit 4 is a late-stage alteration assemblage. The mineralogical significance of the slope is not clear at the present time.

ALTERATION

A lower grade calc-silicate-like alteration to chlorite + epidote + actinolite + calcite + microcline + sphene is pervasive throughout the study area; in mafic rocks of units 2, 4, and 9, this alteration is characterized by the assemblage prehnite + epidote + calcite + microcline. Microveins of prehnite and/or epidote are present within, or adjacent to, the mafic flow units; locally, hornblende or actinolitic hornblende are extensively replaced by actinolite and/or prehnite.

The anomalous zone may be enriched in potassium and sodium, as evidenced by the replacement of original "clear" plagioclase by "cloudy" plagioclase and fine-grained microcline; this enrichment has yet to be demonstrated statistically. The intensity of alkali alteration is certainly lower than that in the mineralized zone at Hemlo (cf. Walford *et al.* 1986). In the hanging wall metapelites of unit 8, there is a layer of sericite schist 3 to 8 m in thickness. Microcline is a major component, but white mica is the most abundant mineral. Two generations of white mica are present. The first generation is coarse grained and is oriented parallel to the principle foliation plane. The second generation is fine grained and randomly oriented. A pyritic layer is present in the footwall, stratigraphically below the anomalous zone. Future work will attempt to investigate if the sericite schist, the anomalous zone, and the pyritic layer are genetically related to each other, and to the contact of unit 9 with the Cedar Lake Pluton.

Carbonatization is not a characteristic phenomenon in the study area and has not been examined in detail. However, carbonate-rich veins up to 10 cm thick, and predominantly composed of calcite, are locally well developed in the mafic units, particularly in those of unit 4, adjacent to the actinolite-chlorite schists (one of the major fracture zones in the study area).

The textural relationships (crosscutting nature and irregular distribution) show that these lower grade alterations in the study area are a result of post-peak metamorphism.

INTERIM CONCLUSIONS

At the present time, this study has confirmed the local geology of the White River Property, as detailed by Lac Minerals Limited. The authors have further characterized, and in a few cases modified, the interpretation of some important rock units. Some general conclusions can be made at this time:

1. There are some stratigraphic and lithological similarities between the anomalous gold zone at the top of unit 7 at the White River Property, and the Hemlo gold deposit 5 to 10 km to the west, but there are also some marked differences (points 2, 3, 4, and 5 below).
2. The anomalous zone occurs roughly parallel to the margin of the Cedar Lake Pluton, but stratigraphically away from the zone of highest metamorphic grade (units 4, 5, and 6), and is associated with both metapelites and intermediate to felsic metavolcanic rocks rather than felsic metavolcanic rocks.
3. The anomalous zone is not associated with the Hemlo Shear Zone, which lies in a narrow zone adjacent to the contact between metasedimentary rocks of unit 5 and mafic metavolcanic rocks of unit 4 in the centre of the zone of highest metamorphic grade.
4. The anomalous zone is not associated with extensive hydrothermal alteration (cf. Hemlo, Walford *et al.* 1986). There is some evidence of alkali alteration and sericitization in the hanging

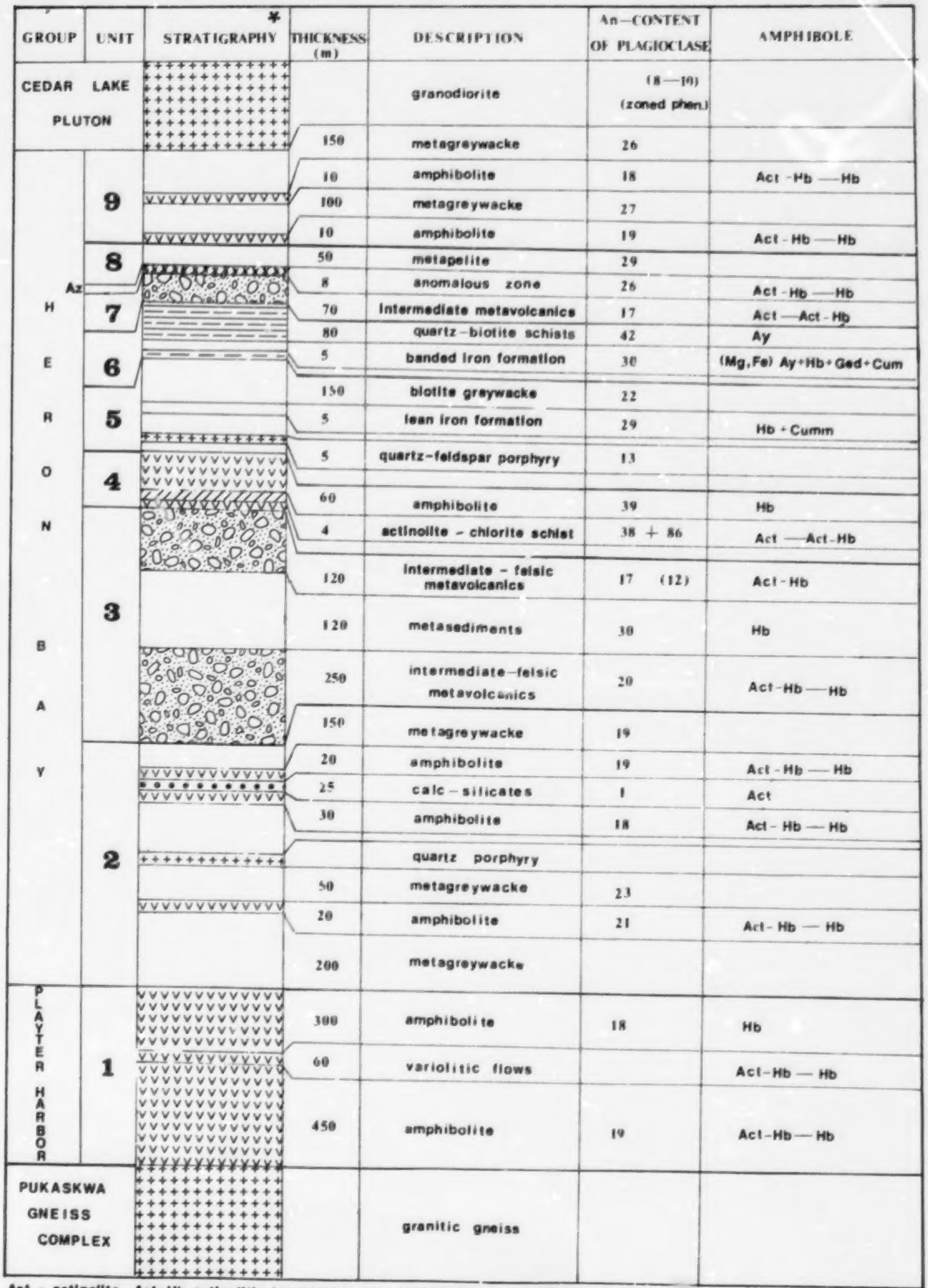

GROUP	UNIT	STRATIGRAPHY *	THICKNESS (m)	DESCRIPTION	An—CONTENT OF PLAGIOCLASE	AMPHIBOLE
CEDAR LAKE PLUTON				granodiorite	(8—10) (zoned phen.)	
HERON BAY	9		150	metagreywacke	26	
			10	amphibolite	18	Act -Hb —Hb
			100	metagreywacke	27	
			10	amphibolite	19	Act - Hb —Hb
	8		50	metapelite	29	
	Az		8	anomalous zone	26	Act - Hb —Hb
	7		70	intermediate metavolcanics	17	Act —Act - Hb
			80	quartz - biotite schists	42	Ay
	6		5	banded iron formation	30	(Mg,Fe) Ay+Hb+Ged+Cum
	5		150	biotite greywacke	22	
			5	lean iron formation	29	Hb + Cumm
			5	quartz-feldspar porphyry	13	
	4		60	amphibolite	39	Hb
	3		4	actinolite - chlorite schist	38 + 86	Act —Act-Hb
			120	intermediate - felsic metavolcanics	17 (12)	Act-Hb
			120	metasediments	30	Hb
			250	intermediate—felsic metavolcanics	20	Act-Hb —Hb
			150	metagreywacke	19	
	2		20	amphibolite	19	Act - Hb — Hb
			25	calc - silicates	1	Act
			30	amphibolite	18	Act - Hb — Hb
				quartz porphyry		
			50	metagreywacke	23	
			20	amphibolite	21	Act- Hb — Hb
			200	metagreywacke		
PLAYTER HARBOR	1		300	amphibolite	18	Hb
			60	variolitic flows		Act-Hb — Hb
			450	amphibolite	19	Act-Hb — Hb
PUKASKWA GNEISS COMPLEX				granitic gneiss		

Act - actinolite Act-Hb actinolitic hornblende Hb - hornblende Ay - anthophyllite Ged - gedrite Cum - cummingtonite
*see legend, Figure 302.2

Figure 305.5. Stratigraphic section of the Hemlo—Heron Bay Greenstone Belt at the White River Property, with compositional variations in amphiboles and plagioclase.

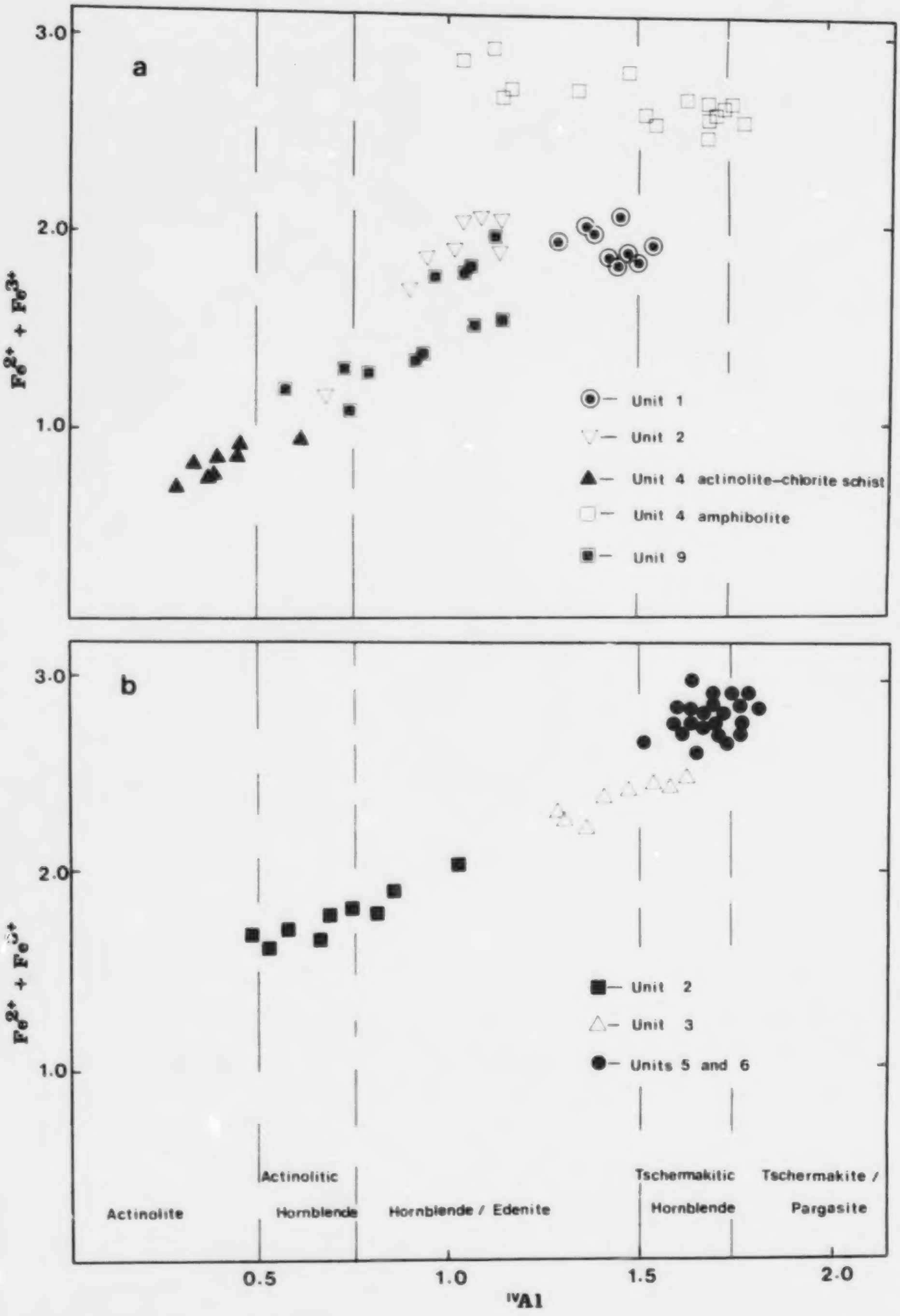

Figure 305.6 Composition of calcic amphiboles from the White River property in: a) mafic metavolcanic rocks; b) metasedimentary rocks (cf. Fleet et al. 1987).

wall, which appears to be a result of post-peak metamorphism.

5. A preliminary review of the trace element data shows that gold enrichment is not associated with anomalously high Mo-Ba-Sb-Hg-As-V contents (cf. Hemlo, Harris 1986). Trace elements at White River correlate with lithology, not with gold mineralization.
6. Peak metamorphic conditions were similar to those at Hemlo (kyanite-sillimanite zone, Burk *et al.* 1986). However, the style of metamorphism at White River is more of a Barrovian type (medium pressure). Moreover, it appears that peak metamorphic conditions were realized in the footwall rocks of the anomalous zone (units 4, 5, and 6), rather than in the hanging wall metapelites (unit 8).
7. Detailed study of the mineral chemistry shows that the compositional variation in the amphiboles and plagioclase are in good correlation with metamorphic grade.
8. A lower grade calc-silicate-like alteration to chlorite + actinolite + epidote + calcite + sphene is pervasive, and significantly, mafic rocks of units 2, 4, and 9 exhibit a characteristic prehnite + epidote + calcite alteration.
9. Emplacement of the Cedar Lake Pluton postdates deposition of the supracrustal rocks, and most likely postdates their deformation and metamorphism.
10. The lithological characteristics of the actinolite-chlorite schist of unit 4 are controlled very largely by a unique bulk chemistry, which caused it to behave as an incompetent unit, rather than by pronounced ductile deformation within the Hemlo Fault Zone.

ACKNOWLEDGMENTS

We thank Lac Minerals Limited for the provision of drill core material, access to the White River Property, and mapping information, and especially thank R.A. Campbell, W.E. Stone, and P.J. Maclean of Lac Minerals Limited for their contribution to the field work. We also thank J.A. Forth for polished thin section preparation, and D.M. Kingston and R.L. Barnett for assistance with microprobe analyses. The study is supported by an Ontario Geological Survey Research Grant No. 305 to M.E. Fleet.

REFERENCES

Burk, R., Hodgson, C.J., and Quartermain, R.A.
1986: The Geological Setting of the Teck–Corona Au-Mo-Ba Deposit, Hemlo, Ontario, Canada; p.311-326 *in* Proceedings of Gold '86, An International Symposium on the Geology of Gold Deposits: Toronto, 1986, edited by A.J. Macdonald, 517p.

Condie, K.C.
1981: Archean Greenstone Belts, Developments in Precambrian Geology, Volume 3; Elsevier Scientific Publishing Company, Amsterdam, 434p.

Fleet, M.E., Barnett, R.L., and Morris, W.A.
1987: Prograde Metamorphism of the Sudbury Igneous Complex; Canadian Mineralogist, Volume 25, Part 3, p.499-514.

Fryer, B.J.
1977: Rare Earth Evidence in Iron Formations for Changing Precambrian Oxidation States; Geochimica et Cosmochimica Acta, Volume 41, p.361-367.

Grove, T.L., Ferry, J.M., and Spear, F.S.
1983: Phase Transitions and Decomposition Relations in Calcic Plagioclase; The American Mineralogist, Volume 68, p.41-59.

Harris, D.C.
1986: Mineralogy and Geochemistry of the Main Hemlo Gold Deposit, Hemlo, Ontario, Canada; p.297-310 *in* Proceedings of Gold '86, An International Symposium on the Geology of Gold Deposits: Toronto, 1986, edited by A.J. Macdonald, 517p.

Hugon, H.
1984: The Hemlo Deposit: Gold Mineralization Within a Dextral Shear Zone; p.212-216 *in* Summary of Field Work and Other Activities, by the Ontario Geological Survey, edited by John Wood, Owen L. White, R.B. Barlow, and A.C. Colvine, Ontario Geological Survey Miscellaneous Paper 119, 309p.

Hyndman, D.W.
1985: Petrology of Igneous and Metamorphic Rocks (2nd Edition); McGraw-Hill Book Company, New York, 786p.

Kuhns, R.J., Kennedy, P., Cooper, P., Brown, P., Mackie, B., Kusins, R., and Friesen, R.
1986: Geology and Mineralization Associated with the Golden Giant Deposit, Hemlo, Ontario, Canada; p.327-339 *in* Proceedings of Gold '86, an International Symposium on the Geology of Gold Deposits: Toronto, 1986, edited by A.J. Macdonald, 517p.

Laird, J., and Albee, A.L.
1981: Pressure, Temperature, and Time Indicators in Mafic Schist; Their Application to Reconstructing the Polymetamorphic History of Vermont; American Journal of Science, Volume 281, Number 2, p.127-175.

Leake, B.E.
1978: Nomenclature of Amphiboles; Canadian Mineralogist, Volume 16, Part 4, p.501-520.

McLennan, S.M., Taylor, S.R., and Eriksson, K.A.
1983: Geochemistry of Archean Shales from the Pilbara Supergroup, Western Australia; Geochimica et Cosmochimica Acta, Volume 47, p.1211-1222.

Muir, T.L.
1982: Geology of the Hemlo Area, District of Thunder Bay; Ontario Geological Survey, Geological Report 217, 65p. Accompanied by Colour Map 2452, scale 1:31 680 or 1 inch to 1/2 mile.

1985: Geology of the Hemlo–Heron Bay Area; p.30-38 *in* Gold and Copper-Zinc Metallogeny within Metamorphosed Greenstone Terrain: Hemlo–Manitouwadge–Winston Lake, Ontario, Canada, A Compendium, edited by R.H. McMillan and D.J. Robinson, Geological Association of Canada and Canadian Institute of Mining and Metallurgy, 91p.

Papike, J.J., Cameron, K.L., and Baldwin, K.
1974: Amphiboles and Pyroxenes: Characterization of Other Than Quadrilateral Components and Estimates of Ferric Iron from Microprobe Data; Geological Society of America, Abstracts with Programs, Volume 6, Number 7, p.1053-1054.

Patterson, G.C.
1985: Exploration History and Field Stop Descriptions of the Hemlo Area; p.66-86 *in* Gold and Copper-Zinc Metallogeny, Hemlo–Manitouwadge–-Winston Lake, Ontario, Canada, A Compendium, edited by R.H. McMillan and D.J. Robinson, Geological Association of Canada and the Canadian Institute of Mining and Metallurgy, 91p.

Spear, F.S.
1980: NaSi-CaAl Exchange Equilibrium Between Plagioclase and Amphibole; Contributions to Mineralogy and Petrology, Volume 281, p.33-41.

Walford, P., Stephens, J., Skrecky, G., and Barnett, R.
1986: The Geology of the "A" Zone, Page–Williams Mine, Hemlo, Ontario, Canada; P.362-378 *in* Proceedings of Gold '86, An International Symposium on the Geology of Gold Deposits: Toronto, 1986, edited by A.J. Macdonald, 517p.

Grant 307 Light Minerals and Specialty Sand in Southern Ontario

James W. Butler and Stephen R. Hicock

Department of Geology, University of Western Ontario, London

ABSTRACT

Silica sand is an important raw material for a wide range of industries in Ontario. High-purity bedrock occurrences of sandstone or quartzite are excellent sources of silica, but are not abundant in Ontario, and are expensive to develop. Much of the silica sand used in Ontario is currently imported from the United States. It would be advantageous to locate and develop unconsolidated deposits of sand in Ontario which have been sorted and enriched in silica by natural geological processes.

This industrial minerals project has identified two main target areas (Huron East and Georgian Bay–Lake Simcoe) of high-quality silica sand potential (up to 79 weight percent SiO_2 and 46 modal percent quartz), based on the limited data available. Both deposits were probably glacially derived, at least in part, from the Lorrain quartzites north of Georgian Bay, and were subsequently reworked. It remains to be determined how these deposits formed, where they came from, if and where there are older buried deposits formed by the same processes, and how this knowledge can be used to find additional high-quality reserves.

Quartz, which is resistant to weathering and may have been concentrated by multiple cycles of transport and reworking, can raise the silica content of a sediment above that of the parent bedrock. Glacial dispersal and facies modeling could therefore be applied to establish a strategy of exploration for silica sand reserves. This type of study has never been attempted in the province and would be timely in view of the increasing demand for this industrial resource, used presently in the automotive (foundry/moulding), fibreglass, glass, ceramic, and related industries of southern Ontario. A better understanding of sediment facies relationships and glacial pathways, dynamics, and depositional environments in southern Ontario could also be realized.

INTRODUCTION

In accordance with the selection committee's recommendations, the initial year of this project was only partially funded, and was spent searching the literature and available unpublished data files to determine the best target areas in southern Ontario to study for silica sand potential. X-ray fluorescence analyses and quartz counts were also performed on donated sand samples from one of the target areas. Funding for the project was terminated after the first year.

SCOPE

Silica sand is an important raw material for a wide range of industries in Ontario. In the past, much emphasis has been placed on high-purity bedrock occurrences of sandstone or quartzite as a source of silica, mainly for glass manufacture and the steel foundry industry. Energy is required to grind and sort this material, adding to the expense of production, which has a significant effect on the profit margin of commercial operations. The cost of production is further increased as finer particle sizes or narrow ranges of particle sizes are required. Another important consideration is the high cost of transporting bulk quantities of silica from distant bedrock sources to industries in southwestern Ontario. Due to the high demand for silica, and the limited occurrence of bedrock sources in Ontario and the high cost of their development, much of the silica sand used in Ontario is imported from the United States.

Since silica sand is required in fine particle sizes or limited particle size ranges, but is expensive to produce, it would be advantageous to locate and develop unconsolidated deposits of sand which have been sorted and enriched in silica by natural geological processes. The investigation of unconsolidated silica sand in southwestern Ontario has been limited; only preliminary reconnaissance studies have been initiated (Springer 1983; Feenstra *et al.* 1985; Trevail *et al.* 1986). These preliminary studies have indicated that the sands of southwestern Ontario are of insufficient quality in terms of silica content for use in glass manufacturing and in steel foundries. However, a detailed investigation of the most promising deposits could be important to the growing number of smaller markets which require silica-rich sand with less rigorous specifications. Silica-based sands of lesser quality are used in iron foundries/mouldings, concrete, extrusion roofing tile, asphalt and asphalt tile, porcelain frit, silica-lime brick, masonry binders, abrasives, autoclaved concrete blocks, cleansing and scouring powders, fertilizer fillers, paint extenders, insecticides, and as traction sand. In addition, sand deposits containing a mixture of quartz and feldspar are used in the manufacture of stoneware, glazes, enamels, and other ceramic products.

Geologists in Michigan and Indiana have made extensive investigations of silica sand deposits. This is a resource that is important to the automotive engine casting industry, and therefore has been important to the American economy as a whole for over 100 years. The demand for silica sand in southern Ontario is increasing; however, sedimentological and geochemical studies applied to finding reserves have not been seriously attempted in this province.

PREVIOUS WORK

The status of silica as an industrial mineral in Canada was summarized long ago by Cole (1923), who described types,. occurrences, and possible commercial uses of silica throughout Canada. A subsequent study by Hewitt (1951, 1963) provided a more detailed account of Precambrian and Paleozoic occurrences of silica in Ontario. A supplement to Hewitt's work was later produced by Vos (1981), who investigated Precambrian quartzites north of Georgian Bay, and Cretaceous silica sands in the James Bay

TABLE 307.1: SAND CHEMICAL ANALYSES FROM THE HURON EAST AND CARADOC TARGET AREAS

SAMPLE AREA	NO. OF SAMPLE	SiO_2 %	Al_2O_3 %	Fe_2O_3 %	TiO_2 %	MnO %	Na_2O+K_2O %	CaO+MgO %	REFERENCE
Owen Sound and Wingham Districts	4	58.7	5.9	1.17	0.16	0.03	2.44	7.34	Feenstra *et al.* (1985) and Feenstra files
Lambton County;	11	51.7	5.6	1.69	0.17	0.06	2.17	20.6	" "
Chatham District	13	37.0	4.5	1.50	0.12	0.05	1.74	29.1	" "
Bosanquet Township (Pinery dunes)	1	79.1	5.09	1.24	0.23	0.03	1.9	7.34	" "
Hay, Bosanquet, Plympton (glacial Lake Warren)	3	71.9	4.29	0.89	0.13	0.02	1.55	11.39	" "
Eastnor Township (glacial Lake Algonquin)	1	60.3	10.5	2.73	0.34	0.06	4.12	11.74	" "
Caradoc Township (donated by T. Hagerty)	5	59.7	7.8	1.81	0.29	0.06	3.11	15.41	this paper

Lowlands. However, studies of Quaternary silica sand produced by the erosion of bedrock have been lacking. The earliest work on sand in Ontario was done by Dell (1959, 1963), who completed reconnaissance studies of the mineralogical compositions of sands in southern and northern Ontario. A detailed study of Quaternary sand for industrial mineral applications has yet to be done.

Sand-sized materials are widespread in southern Ontario; numerous sand plains are shown on the 1:600 000 scale physiographic map by Chapman and Putnam (1984). Specific sand occurrences are shown in the Quaternary map series of the Ontario Geological Survey (OGS). Sand as an aggregate in southern Ontario has been documented and discussed by Hewitt and Karrow (1963). The Aggregate Resource Inventory series of reports by the OGS has also provided valuable information on sand and gravel deposits in many townships. A number of other reports on glacial geology and Quaternary sediments have been published which are useful in interpreting silica sand provenance and origin (Dreimanis 1977, 1981; Karrow 1984; Fulton *et al.* 1986). However, these reports lack detailed information on the mineralogical and geochemical compositions of the sand deposits; information which is vital in determining the suitability of these deposits for specific industrial applications. Unpublished data files on terrestrial silica sand geochemistry and mineralogy are held at the Southwestern District Office of the Ministry of Northern Development and Mines, London.

PROGRESS REPORT

Very little data exists on the silica, quartz, and feldspar contents of southern Ontario sands. So far, two large target areas have been identified as having the best silica potential. One comprises two north-trending ribbons of sand deposits closely hugging the eastern shore of Lake Huron (Chapman and Putnam 1984), and is probably the result of sediment reworked by wind and wave activity since the end of the last glaciation. Silica values as high as 79 weight percent SiO_2, and up to 42 modal percent quartz, occur in the dunes of Bosanquet Township (dunes of the Pinery) (Tables 307.1 and 307.2). The second target is the sand plain between Georgian Bay and Lake Simcoe, which includes fossil beach and wind deposits, probably derived from the Huronian quartzites north of Georgian Bay. In this area, values of up to 31 and 32 modal percent quartz were obtained from samples taken near Midland, and in King County, respectively (Table 307.2); weight percent SiO_2 was not determined for these samples. Dell (1959) found that Huron lobe sands were generally richer in quartz and feldspar than those deposited by the Georgian Bay lobe.

A smaller third target, southwest of London in Caradoc Township, includes fossil deltaic and wind deposits. Samples from this area have silica contents of up to 72 weight percent, and up to 46 modal percent quartz (B.H. Feenstra, Resident Geologist, Ministry of Northern Development and Mines, London, personal communication, 1987). However, five sandy C horizon samples from Caradoc Township, provided by T.P. Hagerty (Ontario Institute of Pedology, Min-

TABLE 307.2: SAND MINERALOGY FROM THE TARGET AREAS

SAMPLE AREA	NUMBER OF SAMPLE	% QUARTZ	% FELDSPAR	% ROCK FRAGMENTS AND CARBONATES	SIZE FRACTION	ORIGIN	REFERENCE
Owen Sound and Wingham Districts	4	31	22	41	0.1-0.7mm	eolian	Feenstra*et al.* (1985) and Feenstra files
Lambton County	11	27	15.5	51	0.1-0.7mm	littoral	
Chatham District	13	25	11	59	0.1-0.7mm	fluvial	" "
Bosanquet Township	1	42	20	28	0.1-0.7mm	eolian (Pinery dunes)	" "
Hay, Bosanquet, and Plymptom Townships	3	40	16.5	41	0.1-0.7mm	littoral (glacial Lake Warren)	" "
EastnorTownship	1	22	37	38	0.1-0.7mm	littoral (glacial Algonquin)	" "
Gananoque area (west of Kingston)	68	31	18	49.5	0.3-0.6mm	littoral; fluvial	Hewitt and Karrow (1963)
Lake Erie sand off Pelee Island	1	21.5	19.5	57.5	0.3-0.6mm	lake sand	" "
Niagara bar sand	1	60	22	15	0.3-0.6mm	fluvial	Hewitt (1963)
Prince Edward County	?	50-56	21-29	18-21	0.3-0.6mm	eolian (Picton dunes)	" "
Caradoc Township	?	33	26	32	fine sand	till; undiff. sands	Dell (1959)
King County	?	32	31	24	fine sand	" "	" "
Penetanguishine	?	31	50	6	fine sand	" "	" "
Lake Ontario shore	?	50	29	21	fine sand	eolian	Hewitt and Karrow (1963), after Woodward, 1949)
Cardoc Township (donated by T. Hagerty)	5	27			fine sand	uncertain sandy C horizon)	this paper

istry of Agriculture and Food, Guelph), were analyzed by X-ray fluorescence (XRF) at the University of Western Ontario and averaged only 60 weight percent silica and about 25 modal percent quartz (Tables 307.1 and 307.2).

SPECULATION ON THE ORIGIN OF TARGET SANDS

The relatively high silica content of these deposits is believed to be the result of multiple cycles of reworking by a number of geological processes. The origin of the silica in the Lake Huron area is likely from quartz within granites and gneisses of the Precambrian Grenville Province, and in the Georgian Bay–Lake Simcoe area, especially from Huronian Lorrain quartzites north of Georgian Bay. Glacial erosion and transport of these bedrock materials resulted in quartz enrichment of the sand-sized fraction of these deposits, while the silt- and clay-sized fractions were enriched in less resistant minerals (mica and feldspar) by glacial crushing and abrasion (Haldorsen 1983). The finer material was selectively removed during glacier melting by subglacial meltwater erosion and transport. The resulting sediment was therefore enriched in silica, even above the concentration of silica in the parent bedrock. Silica content was further increased by subsequent reworking by wind and water along the Lake Huron and Georgian Bay shorelines, as well as along the ancient shorelines of glacial lakes Algonquin and Whittelsey.

In general, the more the sediments have been reworked, the greater the silica content and the narrower the sand size range. Thus it is important to recognize depositional environments and the history of transport of the sediments studied. For example, within the Huron East target area, outwash sand averages 37 weight percent silica and 25 modal percent quartz (13 samples); beach sand averages 51 weight percent silica and 27 modal percent quartz (11 samples); and windblown sand averages 48 weight percent silica and 31 modal percent quartz (4 samples) (Tables 307.1 and 307.2). Reconstructing depositional models for the target areas would give a better understanding of the formation of silica sand deposits, and would therefore help predict where other, perhaps richer, deposits may occur.

BEDROCK SOURCES

A brief investigation of bedrock formations containing silica is important for determining the source and transport paths of quartz found in the target sands. In Ontario, there are six Paleozoic units containing high-silica sandstones: Sylvania, Springvale, Oriskany, Cataract (previously Medina), Clinton, and Potsdam. The Sylvania is quarried in Michigan, and provides some of the purest silica sand found in North America; however, it does not outcrop in Ontario and has been encountered only in drillholes near Amherstburg (Dyer 1930; Reavely and Winder 1961). Bedrock surface exposures of the Springvale and Oriskany sandstones in Haldimand County are very small (less than two square kilometres each). They have been commercially quarried (Hewitt 1951, 1963), but their limited extent make them unlikely sources for significant Quaternary sand deposits. The Cataract and Clinton sandstones (Whirlpool, Grimsby, and Thorold Formations) (Bolton 1957) are also unlikely sources because they occur as thin units exposed only in the Niagara Escarpment, and would not have provided much silica sand through glacial erosion and reworking. The Potsdam occurs in eastern Ontario (Baker 1923; Keith 1949; Powell and Klugman 1979; Klugman and Yen 1980), but glacial advances through that area would have carried debris and concentrated silica sand across the St. Lawrence River into New York State.

The most likely bedrock sources contributing to Quaternary silica sand formation are therefore the Precambrian rocks of the Grenville and Southern provinces of the Canadian Shield. Lorrain quartzite, north of Lake Huron, is quarried by Indusmin Limited (Coltas 1983), and would make an excellent parent for silica sand. Glacial erosion and transport of material from this rock could be in part responsible for silica-rich sand in the two target areas. It has been studied by Collins (1925), Thomson (1962), and Card *et al.* (1977).

CONCLUSIONS

According to the available data, almost all of the known sand deposits of southern Ontario appear to be unsuitable for applications requiring high-quality silica sand. However, some sand samples from the target areas could be suitable for uses which do not have such stringent requirements. By applying glacial dispersal and facies models to sand deposits in the target areas, an exploration strategy could be developed for finding other, perhaps richer, deposits. Field and laboratory investigations of the target sands could determine the processes that led to their formation, and help to better understand glacial behaviour and facies deposition in the Lake Huron and Georgian Bay basins. This could lead to the discovery of new silica reserves. An improved knowledge of glacier pathways over parts of southern Ontario during the last glaciation, and new insights into the nature of glacial comminution and sorting processes could also be realized.

ACKNOWLEDGMENTS

B.H. Feenstra (Resident Geologist, Ministry of Northern Development and Mines, London) suggested the project, and generously provided advice and access to voluminous unpublished data files. E.V. Sado (Ministry of Northern Development and Mines, Toronto) also contributed valuable advice and support. T.P. Hagerty (Ontario Institute of Pedology, Ministry of Agriculture and Food, Guelph) provided samples from Caradoc Township which J.A. Potter (Department of Geology, University of Western Ontario) analyzed for silica and quartz. Research was funded by the Ontario Geoscience Research Grant Program.

REFERENCES

Baker, M.B.
1923: Geology and Minerals of the County of Leeds; Ontario Department of Mines, Annual Report for 1922, Volume 31, Part 6, p.1-26. Accompanied by Map 31c, scale 1:126 720 or 1 inch to 2 miles.

Bolton, T.E.
1957: Silurian Stratigraphy and Paleontology of the Niagara Escarpment in Ontario; Geological Survey of Canada, Memoir 289, 145p.

Card, K.D., Innes, D.G., and Debicki, R.L.
1977: Stratigraphy, Sedimentology, and Petrology of the Huronian Supergroup in the Sudbury–Espanola Area; Ontario Division of Mines, Geoscience Study 16, 99p.

Chapman, L.J., and Putnam, D.F.
1984: The Physiography of Southern Ontario; Ontario Geological Survey, Special Volume 2, 270p. Accompanied by Map P.2715 (coloured), scale 1:600 000.

Cole, L.H.
1923: Silica in Canada, Its Occurrence, Exploitation, and Uses, Part 1–Eastern Canada; Canada Department of Mines, Mines Branch, Report 555, 126p.

Collins, W.H.
1925: North Shore of Lake Huron; Geological Survey of Canada, Memoir 143, 160p.

Coltas, W.H.
1983: The Quebec and Ontario Silica Operations of Indusmin Limited; p.118-121 *in* 19th Forum on the Geology of Industrial Minerals, Proceedings, edited by S.E. Yundt, Ontario Geological Survey, Miscellaneous Paper 114, 216p.

Dell, C.I.
1959: A Study of the Mineralogical Composition of Sand in Southern Ontario; Canadian Journal of Soil Science, Volume 39, Number 2, p.185-196.
1963: A Study of the Mineralogical Composition of Sand in Northern Ontario; Canadian Journal of Soil Science, Volume 43, Number 2, p.189-200.

Dreimanis, A.
1977: Correlation of Wisconsin Glacial Events Between the Eastern Great Lakes and the St. Lawrence Lowlands; Geographie Physique et Quaternaire, Volume 31, p.37-51.

1981: Middle Wisconsin Substage in Its Type Region, The Eastern Great Lakes and Ohio River Basin, North America; Quaternary Studies in Poland, Volume 3, p.21-28.

Dyer, W.S.
1930: Sylvania Sandstone Deposit at Amherstburg; Ontario Department of Mines, Annual Report for 1929, Volume 38, Part 4, p.41-46.

Feenstra, B.H., Trevail, R.A., and Parker, D.K.
1985: Southwestern Regional Geologist Area, Southwestern Region; p.289-297 *in* Report of Activities 1984, Regional and Resident Geologists, edited by C.R. Kustra, Ontario Geological Survey, Miscellaneous Paper 122, 297p.

Fulton, R.J., Karrow, P.F., Lasalle, P., and Grant, D.R.
1986: Summary of Quaternary Stratigraphy and History, Eastern Canada; Quaternary Science Reviews, Volume 5, p.211-228.

Haldorsen, S.
1983: The Enrichment of Quartz in Tills; p.141-150 *in* Tills and Related Deposits, edited by E.B. Evenson, Ch. Schluchter, and J. Rabassa, A.A. Balkema, Rotterdam, 454p.

Hewitt, D.F.
1951: Silica in Ontario; Ontario Department of Mines, Industrial Mineral Circular 2, 16p.
1963: Silica in Ontario; Ontario Department of Mines, Industrial Mineral Report 9, 36p.

Hewitt, D.F., and Karrow, P.F.
1963: Sand and Gravel in Southern Ontario; Ontario Department of Mines, Industrial Mineral Report 11, 151p. Accompanied by Maps 2038, 2039, 2040, 2041, and 2042, scale 1 inch to 16 miles.

Karrow, P.F.
1984: Quaternary Stratigraphy and History, Great Lakes–St. Lawrence Region; p.137-153 *in* Geological Survey of Canada, Paper 84-10, 210p.

Keith, M.L.
1949: Sandstone as a Source of Silica Sand in Southeastern Ontario; Ontario Department of Mines, Annual Report for 1946, Volume 55, Part 5, 36p. Accompanied by Map 1946-9.

Klugman, M.A., and Yen, W.T.
1980: Silica Sand Potential in Eastern Ontario, Preliminary Report II–Beneficiation; Ontario Geological Survey, Open File Report 5305, 39p., 28 tables, 1 map.

Powell, R.D., and Klugman, M.A.
1979: Silica Sand Potential in Eastern Ontario, Preliminary Report I; Ontario Geological Survey, Open File Report 5265, 100p., 2 tables, 2 maps.

Reavely, G.H., and Winder, C.G.
1961: The Sylvania Sandstone in Southwestern Ontario; Transactions of the Canadian Institute of Mining and Metallurgy, Volume 64, p.109-112.

Springer, J.S.
1983: Naturally Sorted Materials of Sand Size from Southwestern Ontario; p.292-296 *in* Summary of Field Work 1983, by the Ontario Geological Survey, edited by John Wood, Owen L. White, R.B. Barlow, and A.C. Colvine, Ontario Geological Survey, Miscellaneous Paper 116, 313p.

Thomson, J.E.
1962: Extent of the Huronian System Between Lake Timagami and Blind River, Ontario; p.76-89 *in* The Tectonics of the Canadian Shield, edited by John S. Stevenson, Royal Society of Canada Special Publication 4, University of Toronto Press, 180p.

Trevail, R., Feenstra, B.H., Pakvis, P., and Sando, J.
1986: Southwestern Regional Geologist Area, Southwestern Region; p.323-340 *in* Report of Activities 1985, Regional and Resident Geologists, edited by C.R. Kustra, Ontario Geological Survey, Miscellaneous Paper 128, 340p.

Vos, M.A.
1981: Silica in Ontario, Industrial Minerals Supplement; Ontario Geological Survey, Miscellaneous Paper 85, 36p.

Woodward, H.W.
1949: Dune Sands of the Sandbanks, Prince Edward County, Ontario; Unpublished B.Sc. Thesis, Queen's University, Kingston.

Grant 310 Application of Surface Radar Sounding Techniques in Peatland Inventories, Southern Ontario: Preliminary Results

B.G. Warner and D.C. Nobes

Department of Earth Sciences and Quaternary Sciences Institute, University of Waterloo, Waterloo

ABSTRACT

Previous studies on the utility of ground penetrating radar (GPR) for peat inventories have met with mixed results. We have embarked on a study of the correlation of the stratigraphy and physical properties of peat with the GPR response. The site selected for study was Ellice Swamp, near Stratford, Ontario. A suite of 17 cores were obtained at a spacing of approximately 100 m. Each core was analyzed for stratigraphy, wet bulk density, water content, organic matter content, and humification at 10 cm intervals. Cross-section profiles were compiled for each of these parameters for comparison with the GPR record. The GPR data were taken at 1 m intervals across the same transect in Ellice Swamp. Preliminary processing of the GPR data reveals some important insights on the utility of GPR in peatland inventories. The base of the peat yields a strong clear reflection event. The character of the event is simpler where there is a lack of limnic peat and gyttja above the basal silty clay. Where limnic peat and gyttja are present, the event is more complex. The surface aerobic zone has a number of small events that are sometimes obscured by the multiples (banded "events" across the GPR section) from the thin snow and ice cover. There is a marked transition in the GPR response between the surface aerobic and the underlying anaerobic zones. The anaerobic peat layers contain relatively few internal reflectors, and appear to be relatively homogeneous and transparent to GPR.

INTRODUCTION

Peatlands are common in northern latitudes, and constitute a potentially important economic resource. Canada has the second largest peat reserves in the world (Zoltai and Pollett 1983). Ontario alone ranks third, with an estimated 26 million hectares of peatlands (Korpijaakko 1981). Peatland inventories currently are normally conducted by extensive mapping and coring programs that are time consuming. A simple and relatively fast method for mapping peat stratigraphy and estimating peat volumes will aid in peatland inventories. We have begun a systematic study to test the utility of ground penetrating radar (GPR) in mapping the areal and stratigraphic extent of peatlands, with the goal of establishing GPR as a simple and effective tool for peat inventories.

Previous studies on the correlation of the GPR response with the physical properties of peat have been inconclusive. Some studies have found a strong correlation between the permittivity (the dielectric coefficient), and the volume and energy content of the

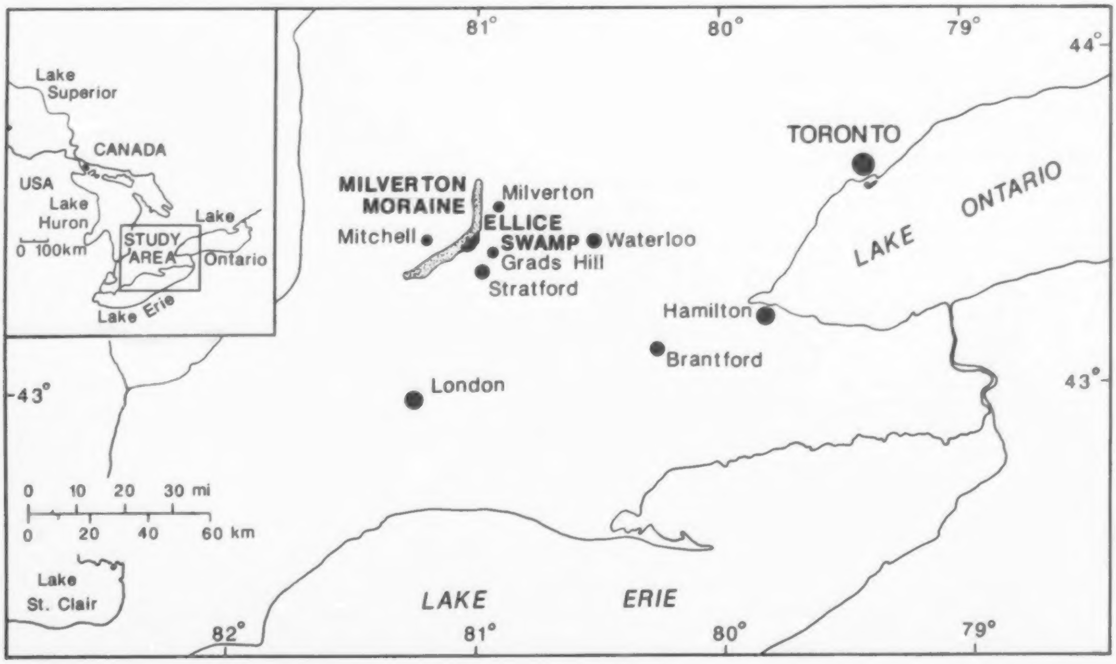

Figure 310.1. Location of Ellice Swamp, near Stratford, Ontario.

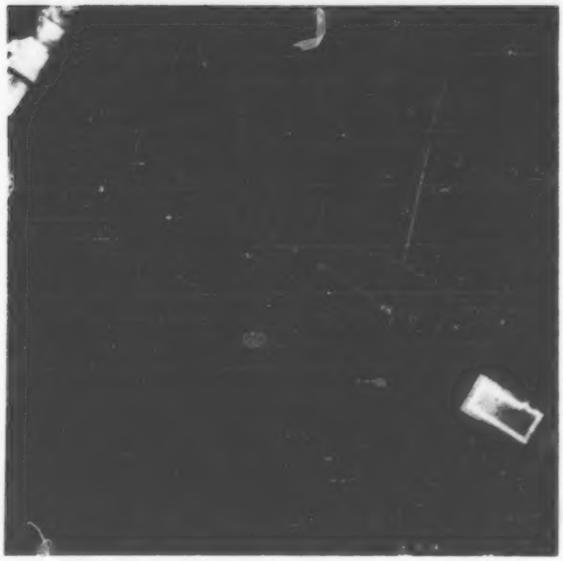

Photo 310.1. *Aerial photograph of the Ellice Swamp. The position of the cut line used for the core and GPR profiles is marked.*

peat (Tolonen *et al.* 1982; Tiuri *et al.* 1983; Tiuri *et al.* 1984). On the other hand, Ulriksen (1982) did not find any correlation between the permittivity and the energy content. All researchers noted a correlation of permittivity with bulk density, which is strongly dependent on the water content. Since the GPR responds to changes in the permittivity, then the peat properties could, in principle, be mapped using GPR.

The purpose of our study was to conduct an intensive field program to compare the GPR response with the results of detailed physical analyses of peat cores. Work on the raw GPR field data study is not yet complete, but preliminary results are most encouraging. The GPR section accurately reflects peat stratigraphy; in particular, the transition from the surface aerobic to the underlying anaerobic zone, and the basal peat-mineral transition is readily apparent. Further analysis is required in order that this work may be extended to other sites and peatland types in the future.

SITE DESCRIPTION AND STUDY METHODOLOGY

The initial site selected for the study was Ellice Swamp, near Stratford in southern Ontario (Figure 310.1). The bog is developed on the eastern flank of the Milverton Moraine (Karrow 1971). Shortly after deglaciation, drainage was impeded which led to local ponding and deposition of lacustrine silts and clays. Silty gyttja, gyttja, and limnic peat represent open-water deposits prior to the onset of peatland development. Moss peat with abundant *Scorpidium scorpioides* and sedge remains form the main body of the peat. A distinct near-surface layer, represented by a well-decomposed amorphous black detrital peat with abundant wood, in turn overlies the peatland. Finally, the modern *Sphagnum* peat is a thin layer about 30 to 50 cm thick at the surface.

The bog is situated on a height of land between the north branch of the Thames and Nith rivers. Black Creek flows through the bog and drains northward into the Nith River. Two man-made drainage ditches are present along its western and eastern boundaries. The vegetation of the modern bog is much disturbed by artificial drainage, frequent fires, peat mining activities, recreational sports trails, and tree plantations. A Canadian National Rail line runs north-south through the bog. There is a narrow belt of alder and willow swamp between the peatland proper and the rail line to the east. Most of the peatland is a *Sphagnum* bog with black spruce and tamarack. Red pine has been planted by the local Conservation Authority. Heath shrubs and a variety of herbs characterize the vegetation understory along the cut line where the coring and radar profiling were conducted. *Sphagnum* moss is the main peat-forming plant today.

The core and GPR profiles were taken along a cut line running northwest-southeast through Ellice Swamp (Photo 310.1). Cores were taken at 100 m intervals, and additional cores were taken concurrently with the GPR profile. The stratigraphy of the peat cores was recorded. Subsamples were taken every 10 cm along each of the 17 cores and analyzed for wet bulk density, water content, degree of humification, and organic matter content. Cross-sections were compiled for each of these physical parameters.

The GPR data was gathered at 1 m intervals across the bog, using a common offset technique. The GPR transmitter and receiver antennae were maintained at a constant separation of 40 cm, as the system was stepped across the bog. To date, only preliminary filtering of the raw radar records has been done to remove some of the response due to the snow and ice that covered the bog at the time of the GPR survey. The 20 to 30 cm thick ice layer caused the GPR signal to reflect numerous times within the ice layer, giving rise to a number of multiples. These multiples appear as banded "events" across the GPR section, at times obscuring the reflected arrivals from the peat. An overall GPR section was constructed by averaging five GPR records to yield an average record every 5 m for the length of the bog. The net presentation thus consists of almost 300 records, rather than almost 1500 raw GPR records.

RESULTS AND DISCUSSION

The cross-sections for water content, humification, organic matter content, and wet bulk density, are shown in Figures 310.2 through 310.5. There is some correlation between the individual parameters, especially humification and organic matter content, and bulk density and stratigraphy (Figure 310.6a). The most direct correlation between the preliminary GPR section and the peat properties can be made with the peat stratigraphy and the peat bulk density. The GPR appears to be responding primarily to density changes associated with stratigraphic variations. The GPR section and stratigraphy are shown for comparison in Figures 310.6b and 310.6a, respectively. A number of important features can be identified in the GPR section (Figure 310.6b).

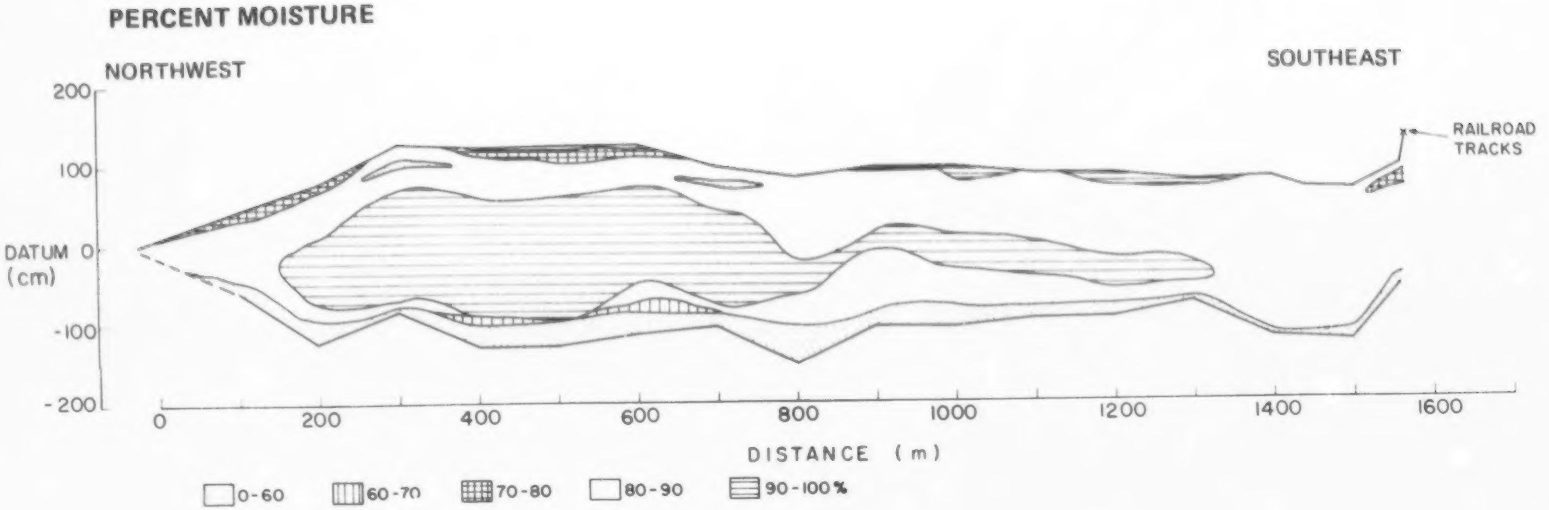

Figure 310.2. *Percent moisture content cross-section from core analyses.*

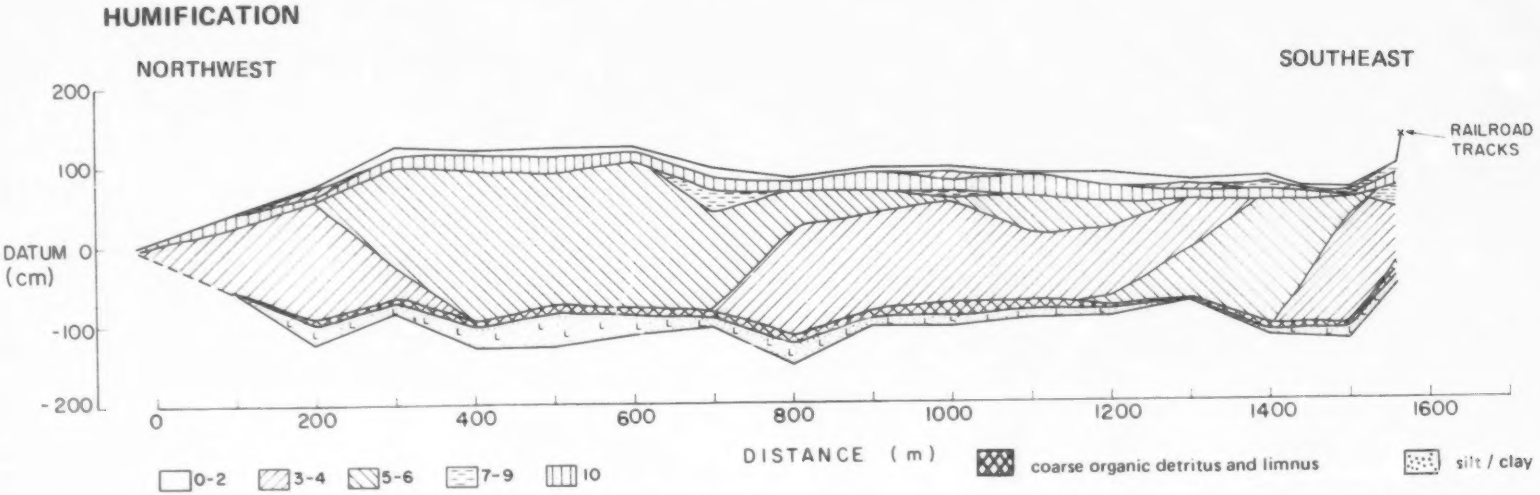

Figure 310.3. *Degree of humification cross-section from core analyses.*

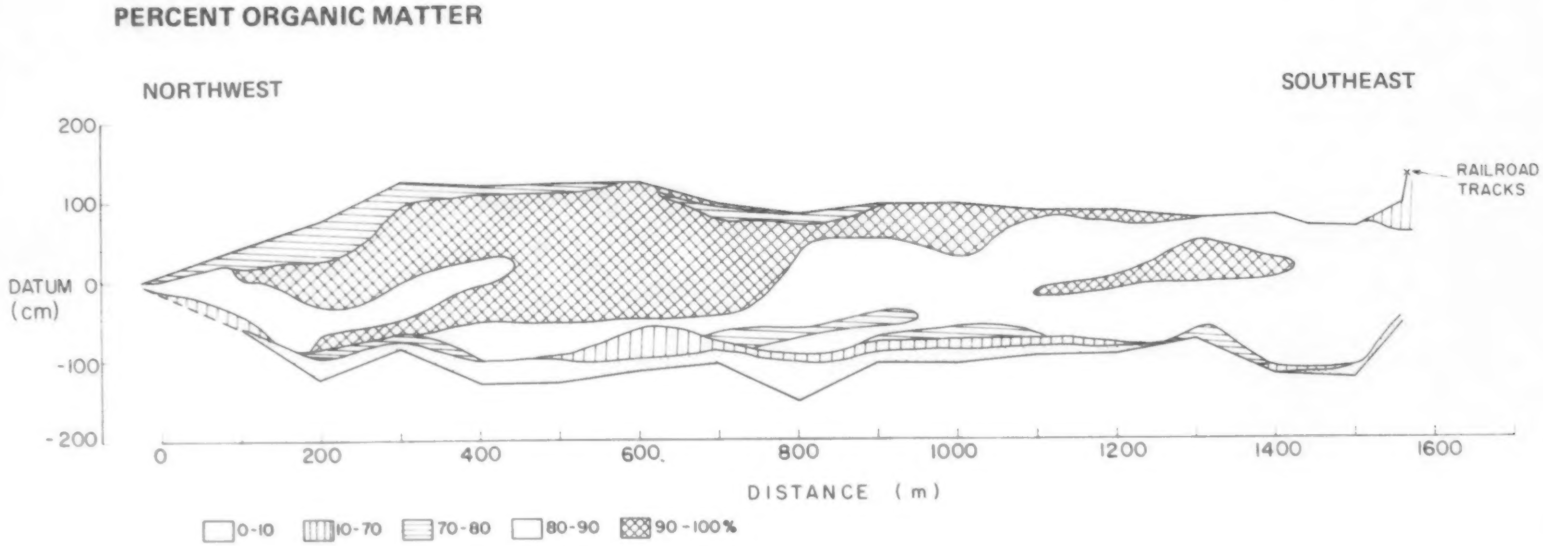

Figure 310.4. *Percent organic matter content cross-section from core analyses.*

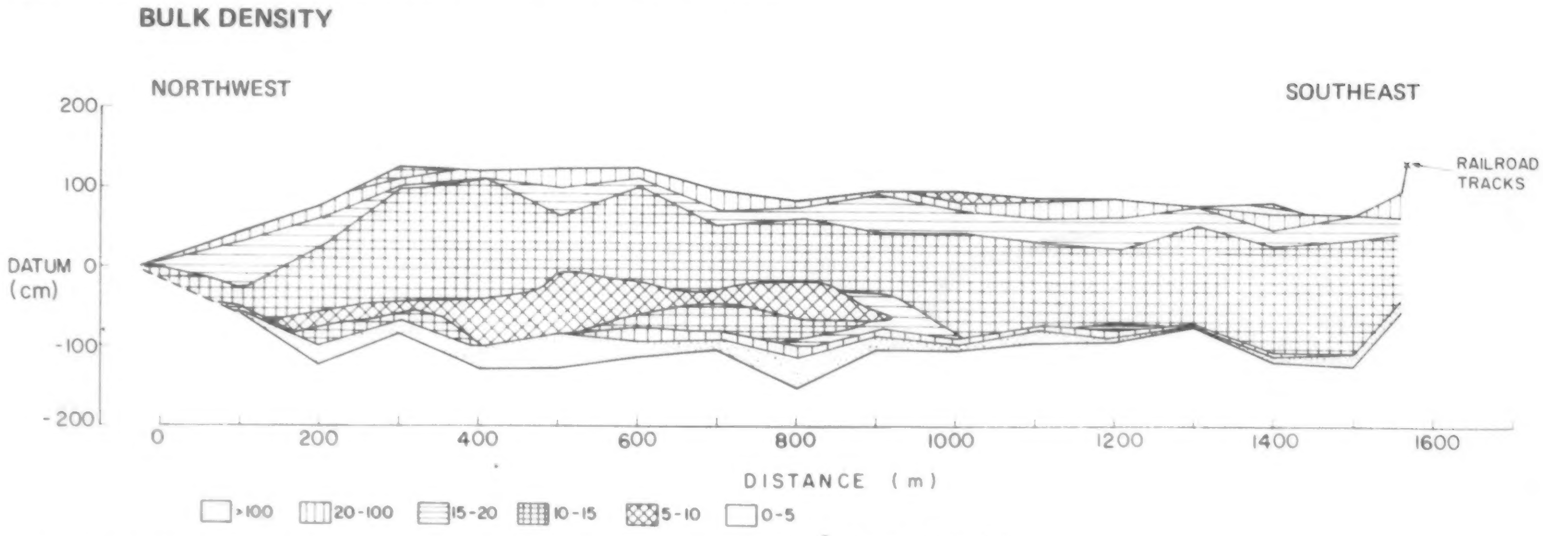

Figure 310.5. *Wet bulk density cross-section from core analyses.*

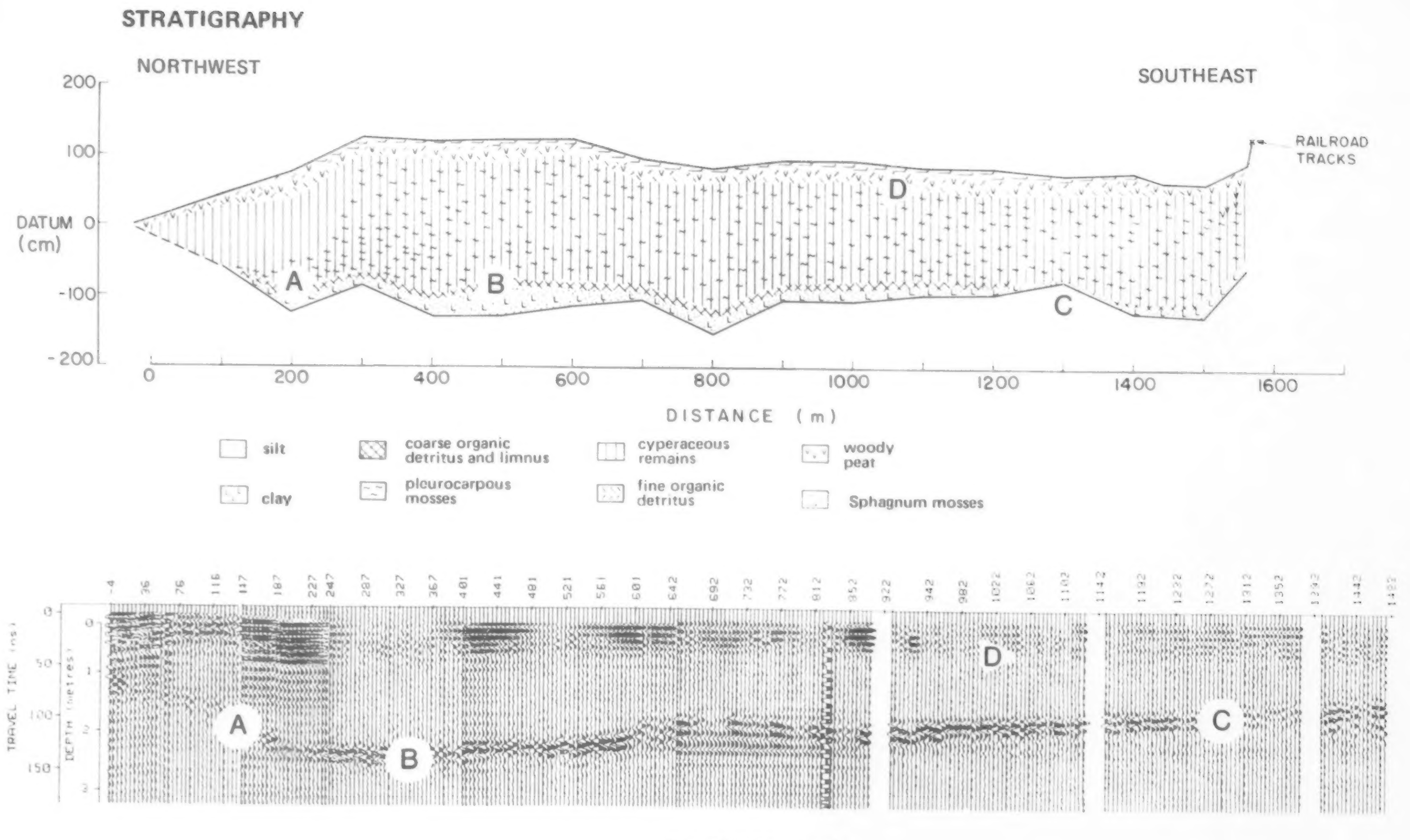

Figure 310.6. *Comparison of the stratigraphy (a) and the GPR response (b) along the Ellice Swamp cut line. The major features are noted as: A: the transition from the peat to the underlying silty clay; B: the more complex reflection which occurs where limnic peat and gyttja are present; C: the simpler event where the limnic detritus is absent; and D: the transition from the surface aerobic to the underlying anaerobic zone.*

The basal silty clay gives rise to a strong clear reflective event on the GPR record (event A, Figure 310.6b). The silty clay is often overlain by a thin layer of limnic detritus, limnic peat, and gyttja. Where the layer of detritus is present, the reflection from the basal clay is more complex (event B); where the detritus is absent, the basal reflection is simpler in character (event C). Finally, the transition from the aerobic to the anaerobic zone is well delineated (event D). The aerobic zone contains a number of small events. The underlying anaerobic zone appears to be relatively transparent to GPR signals, and we have not noted any events within the anaerobic zone.

CONCLUSIONS

This study represents one of the first serious attempts to compare the physical properties of peat with GPR response by compiling cross-sections for each parameter for a single site in southern Ontario. We believe that it would be premature to speculate on wide-ranging applications of the technique. Our tests to date demonstrate great promise for GPR as a tool in assessing both the spatial and vertical extent of peat. However, the real applicability of GPR in peatland inventories must await further testing on a much larger suite of peatland types throughout Ontario.

It is important to note that peatlands are complex ecosystems that vary stratigraphically and areally. Peat has numerous characteristics which depend upon the botanical composition and state of decomposition. These factors in turn can control a variety of other peat parameters. Hence, it would be shortsighted to assume that GPR will be a viable tool in all peatland types, since a whole spectrum of topographically, hydrologically, and morphologically different peat-forming systems exist. Our continuing efforts to apply GPR to other sites will provide an important comparison for the Ellice Swamp site.

ACKNOWLEDGMENTS

Our thanks go to Roland Balloch, John Easton, David Gorling, Richard Greenly, Karen Hanf, Helen Kubiw, and George Schneider for field and laboratory assistance. Drafting was done by Nadia Bahar.

REFERENCES

Karrow, P.F.
1971: Quaternary Geology of the Stratford–Conestogo Area, Ontario; Geological Survey of Canada, Paper 70-34, 11p.

Korpijaakko, E.
1981: A Preliminary Estimate of Ontario's Peat Resources; p.321-330 *in* Proceedings of Symposium on Peat, Thunder Bay, Ontario, Canada International Committee, International Peat Society, 426p.

Tiuri, M., Toikka, M., Marttilla, I., and Tolonen, K.
1983: The Use of Radio Wave Probe and Subsurface Interface Radar in Peat Resource Inventory; p.131-143 *in* Proceedings, Symposium on Remote Sensing in Peat and Terrain Resource Surveys, International Peat Society, Aberdeen, Scotland, 183p.

Tiuri, M., Toikka, M., Tolonen, K., and Rummukainen, A.
1984: Capability of New Radiowave Moisture Probe in Peat Resource Inventory; p.517-525 *in* Proceedings of the 7th International Peat Congress, Volume 1, International Peat Society, Dublin, Ireland, 525p.

Tolonen, K., Tiuri, M., Toikka, M., and Saarilahti, M.
1982: Radiowave Probe in Assessing the Yield of Peat and Energy in Peat Deposits in Finland; Suo, Volume 33, Number 4-5, p.105-112.

Ulriksen, C.P.F.
1982: Application of Impulse Radar to Civil Engineering; Unpublished Ph.D. Thesis, Lund University of Technology, Lund, Sweden, 175p.

Zoltai, S.C., and Pollett, F.C.
1983: Wetlands in Canada: Their Classification, Distribution, and Use; p.245-268 *in* Ecosystems of the World, Volume 4B, Mires: Swamp, Bog, Fen, and Moor, edited by A.J.P. Grove, Elsevier Publishing Company, Amsterdam, 749p.

Grant 312 Subsurface Quaternary Stratigraphy Using Borehole Geophysics

P.F. Karrow[1], **J.P. Greenhouse**[1], **and M.B. Dusseault**[2]

[1]Department of Earth Sciences and Quaternary Sciences Institute, University of Waterloo, Waterloo

[2]Department of Earth Sciences and Civil Engineering, University of Waterloo, Waterloo

ABSTRACT

Under this project, three rotary holes have been drilled and geophysically logged. At one of these sites (at Mannheim), a cored hole was made, from which samples have been taken and analyzed for grain size and carbonate content. The Catfish Creek Till is traceable across the area, and a better understanding of pre-Catfish Creek stratigraphy is being achieved.

INTRODUCTION

This project forms an extension of the work done under Ontario Geoscience Research Grant 128, previously reported by Farvolden *et al.* 1987. Under that grant, funding was provided which allowed the completion of holes and logging along one and part of a second leg of a proposed three-legged (north, west, and east) array in the Kitchener–Waterloo area (Figure 312.1). Under the present grant, two rotary holes and one cored hole were drilled on the west leg, and one rotary hole was drilled on the north leg. All rotary holes were geophysically logged.

LOCAL STRATIGRAPHY

The Quaternary sequence of the Kitchener–Waterloo area as it is presently known is shown in Figure 312.2. The upper half (or less) of the sequence is known from surface mapping (Karrow 1986, 1987), and has been studied in exposures along the Grand River valley. This part of the sequence has proven most readily traceable in the subsurface. The contact between the clay-rich Maryhill Till and the underlying sandy Catfish Creek Till forms a particularly prominent stratigraphic marker across the area.

The lower part of the sequence, below the Catfish Creek Till, is much less well known. Sequences of several tills predominate, with water-laid sediments occurring less frequently. These older deposits require much further study.

The base of the Quaternary sequence rests on the Silurian Salina Formation, which consists of interbedded greenish gray shale and dolostone. Quaternary deposits are 60 m or more in thickness.

MANNHEIM CORED HOLE

The cored hole at Mannheim started in glaciofluvial sediments stratigraphically located below the Maryhill Till. Approximately the upper half of the hole passes through clean sand, with minor amounts of gravel (part of the Waterloo moraine), which then rests on the Catfish Creek Till. Three thin older tills, and intervening sand and gravel, complete the sequence to bedrock at 61 m. Grain size analysis has been performed on 28 samples from this hole; as well, 20 of these samples were analyzed for carbonate content, to aid in correlation.

WEST TO EAST CROSS–SECTION

Based on the two new holes funded by this project on the west leg, and on holes funded by Grant 128, a west to east cross-section has been constructed, extending 10 km from Mannheim through the Greenbrook well field to the Grand River (Figure 312.3). The Catfish Creek Till marker bed, and the Catfish Creek Till–Maryhill Till contact are traceable and approximately define a paleosurface which slopes gently eastward to the Grand Valley. The bedrock surface, on the other hand, slopes eastward down toward the Greenbrook well field, then rises again toward the Grand River, defining a gentle depression which may represent a former course of the Grand River, displaced westward from the present course. Evidently, the displacement eastward took place before Late Wisconsinan time.

GEOPHYSICS

The two projects have provided nine test boreholes throughout the region. Each is cased with 7.5 cm (internal diameter) PVC, filled with water, and available for borehole log development and calibration. These holes are routinely logged with resistivity, caliper (both of these before casing), natural gamma, neutron, and density sondes. The sondes are carefully checked for consistent calibration between holes, so that all logs are recorded in a standard environment. Downhole seismic surveys, including Vertical Seismic Profiling (VSP), have also been conducted in most of the holes, in connection with surface seismic reflection surveys being carried out in the region.

In 1987, the boreholes were also used for testing purposes by: the Geological Survey of Canada (spectral gamma, magnetic susceptibility); Morris Magnetics (magnetic susceptibility); and Geonics Ltd. (induction/conductivity).

The recorded logs are processed and displayed with the PC-based editor VIEWLOG, written by Kassenaar and Dusseault. The objectives are an identification of lithological and stratigraphic units, from the amplitudes and patterns of suites of log responses. Visual analysis is still probably the best available tool but we are actively working on a computerized "expert system" approach to summarize the experience of the human interpreter. Of particular interest is the identification and correlation from hole to hole of pre-Catfish Creek till sequences. In this we believe that good progress is being made. A catalogue of all wells geophysically logged by us in the past 10 years is being published.

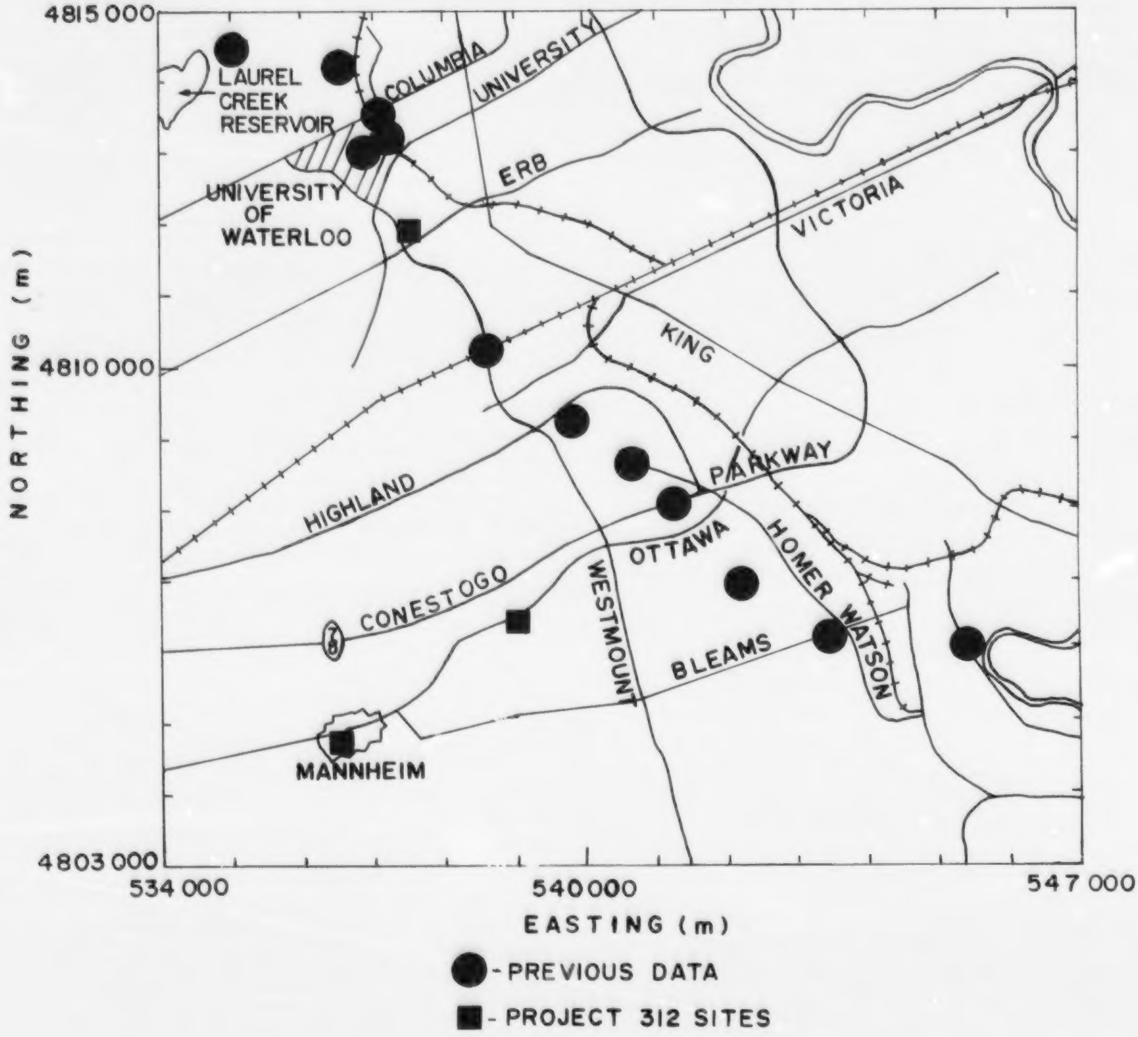
4815 000
4810 000
4803 000
534 000
540000
547 000
NORTHING (m)
EASTING (m)
LAUREL CREEK RESERVOIR
UNIVERSITY OF WATERLOO
COLUMBIA
UNIVERSITY
ERB
VICTORIA
KING
PARKWAY
HIGHLAND
OTTAWA
HOMER WATSON
CONESTOGO
WESTMOUNT
BLEAMS
MANNHEIM
● - PREVIOUS DATA
■ - PROJECT 312 SITES

Figure 312.1. *Map of study area showing previous and new (Grant 312) drilling sites.*

AGE OF TILLS
KITCHENER-WATERLOO AREA

LATE WISCONSINAN	PORT BRUCE STADIAL	PORT STANLEY TILL	13500 BP.
		TAVISTOCK TILL	
		MARYHILL TILL	14500 BP.
	ERIE INTERSTADIAL		15500 BP.
	NISSOURI STADIAL	CATFISH CREEK TILL	22000 BP.
MIDDLE WISCONSINAN	PORT TALBOT INTERSTADIAL	WATERLOO SEDIMENTS	40000 BP.
	?	OLDER TILLS	

Figure 312.2. *Quaternary sequence in the Kitchener–Waterloo area.*

ACKNOWLEDGMENTS

We thank Morris Magnetics and Geonics Ltd. for their contributions to this project. Carol Ann Griffith, an NSERC summer student from Memorial University, St. John's, Newfoundland, assisted in the field work. D. Wagner prepared the diagrams for this report.

REFERENCES

Farvolden, R.N., Greenhouse, J.P., Karrow, P.F, Pehme, P.E., and Ross, L.C.
1987: Ontario Geoscience Research Grant Program, Grant No. 128, Subsurface Quaternary Stratigraphy of the Kitchener–Waterloo Area Using Borehole Geophysics; Ontario Geological Survey, Open File Report 5623, 76p., 18 figures, 9 tables, and 1 appendix.

Karrow, P.F.
1986: Quaternary Geology of the Stratford–Conestogo Area, Ontario; Ontario Geological Survey, Open File Report 5605, 271p., 7 tables, 19 figures, 31 photos, 9 charts (back pocket), and 2 maps (back pocket).
1987: Quaternary Geology of the Hamilton–Cambridge Area, Southern Ontario; Ontario Geological Survey Report 255, 94p. Accompanied by Maps 2508 and 2509, scale 1:50 000, and 4 charts.

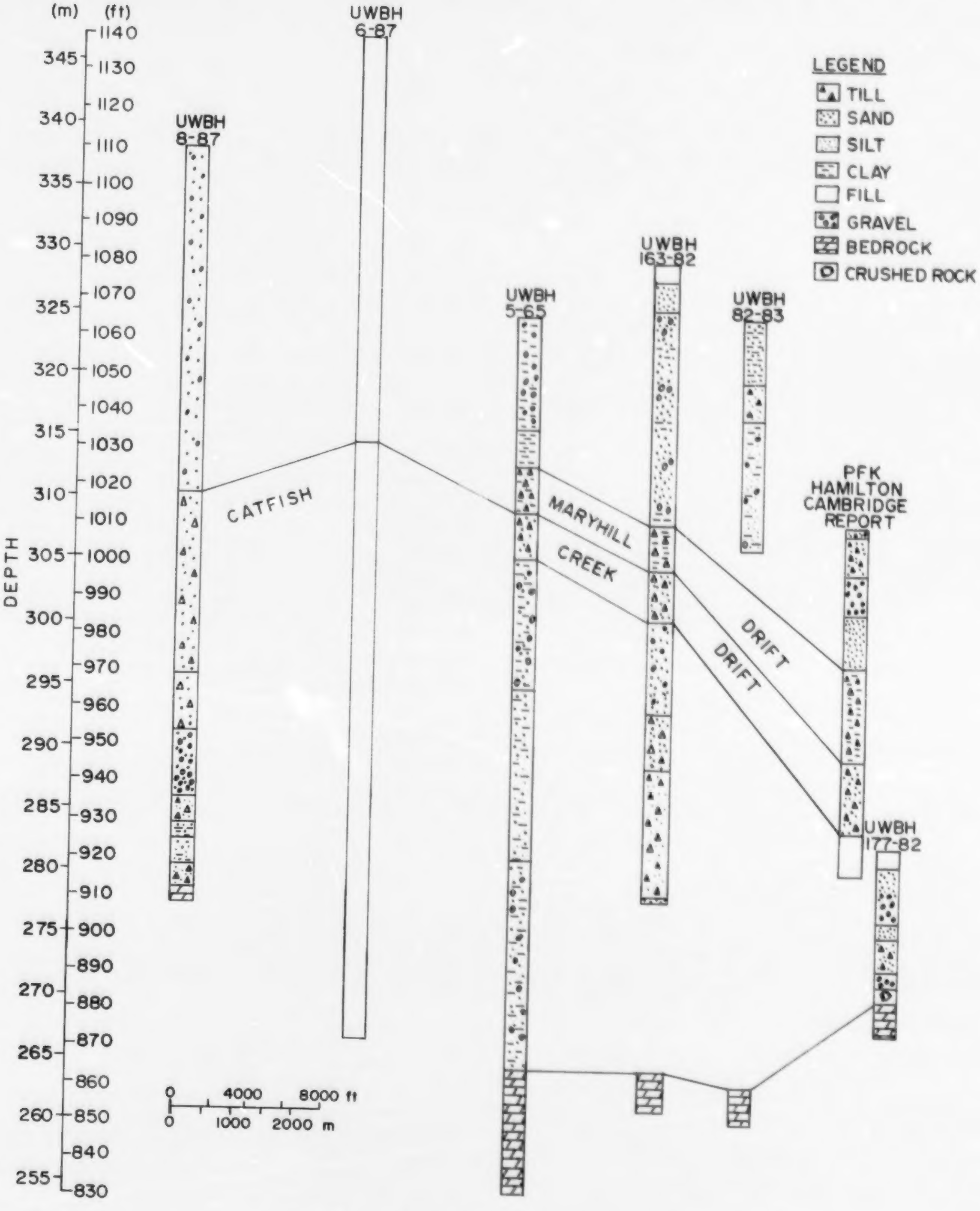
(m)
(ft)
DEPTH
345
340
335
330
325
320
315
310
305
300
295
290
285
280
275
270
265
260
255
1140
1130
1120
1110
1100
1090
1080
1070
1060
1050
1040
1030
1020
1010
1000
990
980
970
960
950
940
930
920
910
900
890
880
870
860
850
840
830
UWBH 8-87
UWBH 6-87
UWBH 5-65
UWBH 163-82
UWBH 82-83
PFK HAMILTON CAMBRIDGE REPORT
UWBH 177-82
CATFISH
MARYHILL
CREEK
DRIFT
DRIFT
LEGEND
TILL
SAND
SILT
CLAY
FILL
GRAVEL
BEDROCK
CRUSHED ROCK
0
4000
8000 ft
0
1000
2000 m

Figure 312.3. Cross-section along west and east legs of a drillhole array in southern Kitchener.

Grant 313 Magmatic-Hydrothermal and Wall Rock Alteration Petrology at the Lake Shore Gold Deposit, Kirkland Lake, Ontario

Kevin D. Hicks and Keiko Hattori

Ottawa–Carleton Geoscience Centre, Department of Geology, University of Ottawa, Ottawa

ABSTRACT

The Lake Shore gold deposit lies in the Kirkland Lake gold camp, the second largest Archean camp in North America. It is hosted in an alkaline intrusive complex composed of augite syenite, syenite, and porphyry. The porphyry unit is the latest intrusion and it hosts over two-thirds of the gold in the Kirkland Lake Camp. Detailed petrography establishes that the porphyry unit is a quartz monzodiorite. The mineralogy of this unit consists of plagioclase, orthoclase, biotite, and hornblende, with accessory magnetite, apatite, titanite, monazite, and zircon. Miarolitic cavities within the porphyry suggests a shallow emplacement and an H_2O-rich nature of the magma.

The porphyry unit displays four successive facies of alterations. The alteration facies (1) is characterized by magnesium-rich secondary biotite (less than 45 mole percent annite) replacing or overgrowing primary biotite and hornblende. It is accompanied by minor titanitization and hematitization of primary magnetite, and by minor sulphate formation. This alteration assemblage indicates that oxidized magmatic-hydrothermal activity took place during the intrusive event of the alkaline complex.

The chlorite facies (2) is characterized by the replacement of all ferromagnesian minerals by chlorite. It is accompanied by minor sericitization and carbonatization.

The phlogopite-hematite facies (3) is characterized by the replacement of chlorite by phlogopite, hematitization of primary and secondary magnetite, and the occurrence of disseminated fine-grained hematite in the groundmass.

Adjacent to the gold veins, fuchsite and pyrite (facies 4) replace phlogopite and hematite, respectively. Increased amounts of carbonate and sericite accompany this alteration.

Spatial distribution of the latter two, and possibly three, alteration facies suggests that they are directly related to gold mineralization.

INTRODUCTION

The Kirkland Lake gold camp is located along the Kirkland Lake Break, a splay structure of the major Kirkland Lake–Larder Lake Fault Zone. The camp is the second largest Archean gold camp in North America, with production of more than 910 000 kg of gold (Ploeger and Crocket 1982). The Lake Shore Deposit, located in the centre of the camp (Figure 313.1), is the largest producer, and so far has yielded more than 264 000 kg of gold between 1918 and 1965 (Ploeger and Crocket 1982). From 1983 to 1987 the mine was reopened and operated by Lac Minerals Ltd. and the crown, and several boundary pillars were removed. During this time, more than 2240 kg of gold were recovered (Frank R. Ploeger, Chief Mine Geologist, Lake Shore Division, Lac Minerals Ltd., Kirkland Lake, personal communication, 1987).

Hydrothermal wall rock alteration associated with Archean lode gold deposits has been well documented in the Archean (for example, Robert and Brown 1986). However, relatively little work has been carried out concerning the temporal change in the alteration. In much younger Phanerozoic deposits, it is well demonstrated that the nature of hydrothermal fluids change with time and space, and that the mineralizaion took place in a specific time of the fluid evolution (for example, Reynolds and Beane 1985). Because gold in the Archean lode deposits was introduced in the late stages of hydrothermal activity, information on the paragenesis of alteration mineralogy may provide a better understanding of the nature of auriferous hydrothermal fluids.

This project was, therefore, initiated to examine the temporal and spatial variations of hydrothermal alteration in the Kirkland Lake gold camp through petrological and geochemical studies.

PREVIOUS INVESTIGATIONS

Previous geological investigations have been carried out in the Kirkland Lake area intermittently since gold was first discovered in the area in 1911. The earliest geological studies of the Kirkland Lake area were carried out by Burrows and Hopkins (1914, 1925), Tyrrell and Hore (1926), and Todd (1928). The earliest major studies of the Kirkland Lake area, including the main ore zone, were by Thomson (1950), and Thomson *et al.* (1950), with a follow-up study of the deeper levels by Charlewood (1964).

Other investigations in the Kirkland Lake area include studies of the Timiskaming Group by Hewitt (1963), Cooke and Moorhouse (1969), and Hyde (1980); regional reconnaissance studies are summarized in Jensen and Langford (1985); studies of gold mineralization by Ploeger and Crocket (1982); and isotope studies at the Macassa deposit by Kerrich and Watson (1985). Hodgson *et al.* (in press) discussed the tectonic setting of the Kirkland Lake gold camp.

Recent investigations at the Lake Shore Deposit on the mineralogy of the ore veins and the wall rock alteration have been carried out by McInnes (1985) and Theriault (1988). A fluid inclusion study has been undertaken by Gallimore (1988).

REGIONAL GEOLOGY

The volcanic rocks of the area north of Kirkland Lake form part of a large east-plunging synclinorium that lies between the Abitibi and Round Lake batholiths (Jensen and Langford 1985). The Destor–Porcupine and Kirkland Lake–Larder Lake fault zones cut the

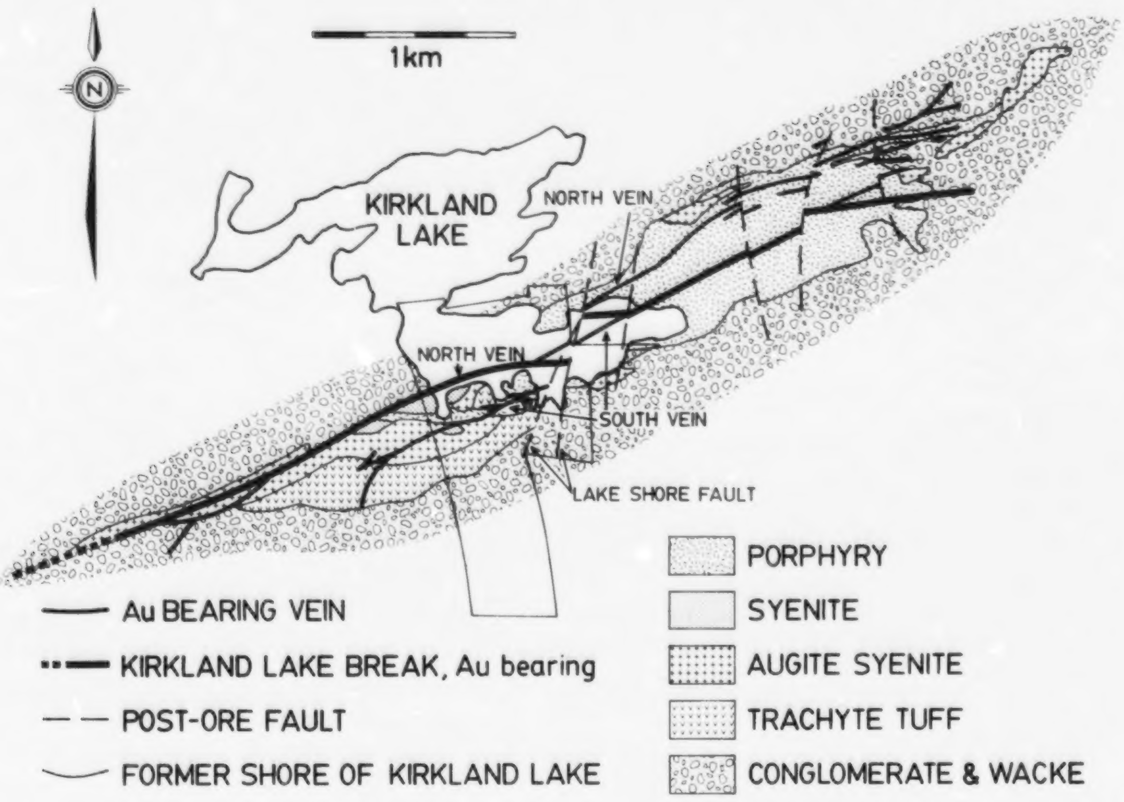

Figure 313.1. *Geology of the Kirkland Lake gold camp (modified after Ploeger and Crocket 1982). The location of the main shaft of the Lake Shore Mine is indicated by the symbol* ★

north and south limbs of the synclinorium, respectively. Two cycles of volcanism are recognized in the area, constituting the Upper and Lower supergroups (Jensen and Langford 1985).

Each of the cycles is composed of a basal komatiitic unit followed by tholeiitic and calc-alkalic units, and contains associated sedimentary and intrusive rocks. The Upper Supergroup is unconformably overlain by metasedimentary and alkalic igneous rocks of the Timiskaming Group.

The Timiskaming Group forms a narrow east-trending belt, 0.5 to 5 km wide, along the Kirkland Lake–Larder Lake Break. It is dominantly composed of sedimentary and volcanic rocks including conglomerate, sandstone, siltstone, argillite, greywacke, chert, iron formation, trachytic flows, agglomerates, and trachyte tuffs (Hyde 1980). Sedimentation of the Timiskaming Group was influenced by fault activity along the Kirkland Lake–Larder Lake Break (Hodgson 1983).

In the Kirkland Lake area, the Timiskaming Group has been intruded by a composite elongated alkalic intrusion consisting of augite syenite, syenite, and porphyry (Figure 313.1). The long axis of the intrusion strikes 060 to 080°, roughly parallel to the strike of the sedimentary and volcanic rocks of the Timiskaming Group. The complex is slightly wedge-shaped, and widens to the east (Figure 313.1). The southern contact of the intrusive complex has a flatter dip than the northern contact; thus the intrusion widens with depth.

The Kirkland Lake–Larder Lake Break is the prominent structural feature of the area. It extends from as far west as Matachewan, eastward past Val d'Or to the Grenville Front (Roberts 1987).

The intrusive complex of the Kirkland Lake Camp hosts most of the main ore zone. The porphyry is the latest phase of the intrusion and hosts approximately two thirds of the gold mineralization.

All three phases, as well as the ore veins, are cut by a north-trending diabase dike at the western end of the property.

Within the conglomerates of the Timiskaming Group, the clasts contain mineral assemblages indicative of prehnite-pumpellyite facies metamorphism, whereas the matrix is unmetamorphosed; this suggests that sedimentation of the Timiskaming Group postdated regional metamorphism (Jolly 1974). This further suggests that the intrusive rocks in Kirkland Lake have undergone only minor regional metamorphism.

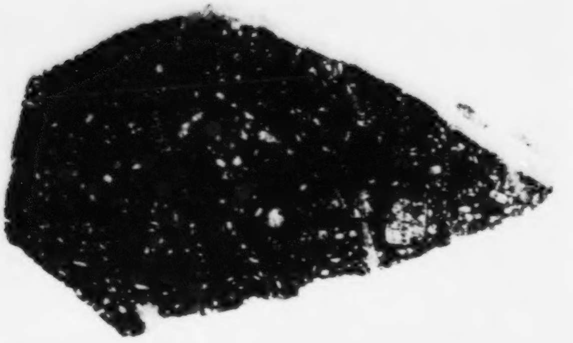

Photo 313.1. *Relatively unaltered porphyry showing the bimodal size distribution of smaller plagioclase (Pl) phenocrysts and larger orthoclase (Or) phenocrysts.*

MINE GEOLOGY

Nearly all of the mineralization lies within the intrusive complex; however, sediments and tuffs of the Timiskaming Group are in fault contact with the North Vein, on the north side of the vein (Figure 313.1), to a depth of about 250 m.

All three phases of the intrusive complex are present within the Lake Shore Deposit. East of the main shaft (Figure 313.1), and at depth, all of the mine workings lie within the porphyry.

AUGITE SYENITE

Augite syenite is the earliest phase of the intrusive complex. In hand specimen, the rock is typically dark grey to olive black and is medium grained with a hypidiomorphic granular texture. The rock is composed dominantly of augite (25 to 45 percent by volume), potassium feldspar (40 to 60 percent by volume), with minor amounts of albite (up to 10 percent by volume), titaniferous magnetite (up to 10 percent by volume), biotite (less than 5 percent by volume), hornblende (less than 3 percent by volume), apatite (less than 2 percent by volume), and titanite (less than 1 percent by volume).

Augite is generally euhedral to subhedral, averages 3 to 5 mm in length, and commonly contains inclusions of apatite. Augite commonly shows moderate alteration to actinolite, chlorite, magnetite, and carbonate.

Albite and orthoclase appear to be primary feldspars and some large grains display perthitic and antiperthitic textures. With alteration, rims of feldspar are commonly replaced by aggregates of fine-grained mosaic orthoclase. Grains are commonly subhedral, varying in size from 1 to 3 mm. Sericite and carbonate alteration of the feldspars is ubiquitous. Biotite is rich in TiO_2 (up to 6.5 weight percent), and it occurs as fine elongated grains up to 1 mm in length within the feldspars. Magnetite displays variable degrees of hematite and titanite alteration along grain edges and fractures.

SYENITE

Syenite is the least abundant intrusive phase. In drill core, and underground, the contact between the augite syenite and the syenite is observed to be transitional, although well defined intrusive contacts are also common. In hand specimen, the rock has a pinkish to orange colour and is medium grained, with a hypidiomorphic granular texture.

The mineralogy of this rock consists mainly of orthoclase with lesser amounts of intergrown oligoclase. Accessory minerals include magnetite and apatite. Secondary minerals include chlorite, carbonate, leucoxene, and sericite.

PORPHYRY

This unit hosts the majority of the gold mineralization at the Lake Shore Property. The porphyry unit predominates in the central part of the intrusive complex and extends to its eastern limit (Figure 313.1). At the west end of the camp it occurs as dikes and small irregularly shaped bodies (Thomson 1950). Well defined contacts between the various intrusive bodies of the porphyry unit are commonly observed in the mine workings and in drill core.

In hand specimen, relatively unaltered porphyry varies in colour from dark grey to olive black. The rock has a distinct porphyritic texture, with lighter coloured phenocrysts of plagioclase and/or orthoclase contrasting with a darker fine-grained groundmass (Photo 313.1). Phenocrysts vary in long axis up to 15 mm, and average 3 mm in size. Angular to subrounded xenoliths of mafic rock up to 5 cm in diameter are common in the porphyry. They are typically darker in colour than the porphyry and are generally composed of hornblende, actinolite, chlorite, and carbonate.

The porphyritic intrusions are divided into four phases based on the mineralogy of the phenocrysts for the least altered rock. These are, in decreasing order of abundance: a) plagioclase-biotite porphyry; b) plagioclase-orthoclase ± biotite porphyry; c) plagioclase-hornblende-biotite porphyry; and, d) quartz-plagioclase ± orthoclase, hornblende, and biotite porphyry (quartz-feldspar porphyry). Well defined intrusive contacts, as well as gradational contacts, are observed between these phases. One phase intruded other phases in one place, and then the latter intruded the former in other places. The intrusive relationship suggests the existence of a common magma reservoir for all phases, and they likely represent different degrees of fractionation of a single parent magma. This is supported by linear variations in the contents of major oxides with the change in SiO_2 contents. Their distribution throughout the complex appears to be random.

Plagioclase is the dominant phenocryst among all phases of the porphyry. The plagioclase exhibits compositional variation from oligoclase ($Ab_{81}An_{13}Or_6$) to albite ($Ab_{87}An_5Or_6$). Well developed albite twins are common, with lesser Carlsbad and pericline twins. The grains are dominantly euhedral. Orthoclase phenocrysts in the orthoclase-bearing phases of the porphyry account for less than 10 modal percent of the rock. They range in size up to 15 mm and are generally subhedral to anhedral. Orthoclase is generally much larger than plagioclase; a bimodal size distribution of feldspars is thus displayed (Photo 313.1). Inclusions of plagioclase are common in the orthoclase.

The replacement of plagioclase by orthoclase is common. However, secondary orthoclase occurs on the rims of plagioclase phenocrysts as fine-grained aggregates in the least altered rock samples. Large single crystals of orthoclase are, therefore, considered to be primary. Significant amounts of calcium and sodium in the orthoclase crystals, detected by energy dispersive spectrometry in electron microprobe study, support their crystallization from a silicate magma.

Biotite is the most common ferromagnesian mineral in the porphyry. It occurs primarily as phenocrysts up to 2 mm in length, with an average size of about 1 mm. Primary biotite is pleochroic from deep reddish brown to dark medium greenish brown. Quartz phenocrysts are relatively rare in the porphyry, never exceeding 5 percent by volume. When present, they occur as partially resorbed oval to rounded grains averaging about 1 mm in size.

Hornblende constitutes less than 7 percent by volume of the porphyry unit. Grains are generally small (less than 1 mm) and have well developed euhedral shapes.

The groundmass of the porphyry is composed primarily of plagioclase and quartz with variable amounts of orthoclase. Accessory minerals include magnetite, apatite, rutile, titanite, monazite, and zircon.

Miarolitic cavities are locally observed in the porphyry (Photo 313.2). These cavities vary from 1 to 4 mm in diameter, averaging about 1.5 mm, and reflect the release of a fluid phase from the cooling magma (Jahns and Burnham 1969). The cavities are generally confined to the biotite-bearing porphyry phases that do not contain hornblende. They are most often zoned, with biotite lining the cavity walls, followed by magnetite/hematite (Photo 313.2). The cores are filled with varying assemblages of quartz, biotite, orthoclase, apatite, and sulphate. The biotite in the cavities has similar optical properties and chemical compositions as the secondary biotite in the rock matrix.

The compositions of the various phases of the least altered porphyry, along with the corresponding CIPW norm calculations, are given in Table 313.1. Normative values for quartz, orthoclase, albite, and anorthite have been recalculated to modal percent and plotted on a Streckeisen diagram (Streckeisen 1973) (Figure 313.2). All values lie within the quartz monzodiorite field, with the exception of one sample that lies within the quartz monzonite field. The large amounts of plagioclase phenocrysts and the relatively minor amounts of primary potassium feldspar recognized in hand specimen substantiates these findings.

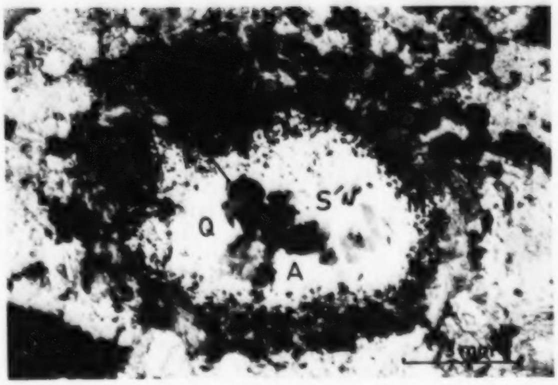

Photo 313.2. *Photomicrograph of a typical miarolitic cavity in the porphyry. The cavities display a zoned nature with secondary biotite (B) lining the cavity walls, followed by magnetite/hematite (M). The interiors are filled with quartz (Q), biotite (B), apatite (A), and sulphate (S). Plane polarized light.*

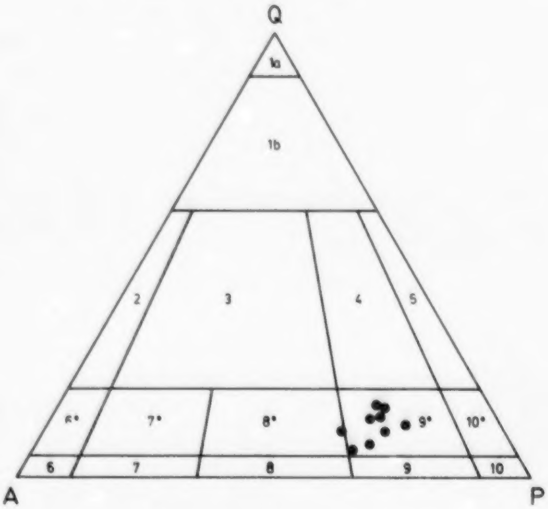

Figure 313.2. *Ternary plot of quartz (Q), alkali feldspar (A), and plagioclase (P) norms (converted to percent by volume) for the porphyry unit. Because plagioclase has an actual composition of oligoclase and albite (>5 percent An), norms of An and Ab are combined to form plagioclase. The classification of the igneous rocks according to Streckeisen (1973) is indicated on the diagram as follows: 1a = quartzolite; 1b = quartz-rich granitoids; 2 = alkali-feldspar granite; 3 = granite; 4 = granodiorite; 5 = tonalite;* 6^{*} *= alkali-feldspar quartz syenite;* 7^{*} *= quartz syenite;* 8^{*} *= quartz monzonite;* 9^{*} *= quartz monzodiorite;* 10^{*} *= quartz diorite; 6 = alkali-feldspar syenite; 7 = syenite; 8 = monzonite; 9 = monzodiorite; 10 = diorite. Note that most samples lie within the quartz monzodiorite field.*

TABLE 313.1: WHOLE ROCK ANALYSES AND CIPW NORMS FOR LEAST ALTERED PORPHYRY

SAMPLE #	018	119	134	137	017	019	135	139	014
SiO_2 wt%	62.03	67.13	64.48	64.22	59.83	61.61	62.50	61.34	65.38
TiO_2	0.39	0.21	0.33	0.33	0.42	0.48	0.40	0.39	0.42
Al_2O_3	14.16	15.31	14.78	14.54	13.86	14.44	14.75	14.22	14.57
Fe_2O_3	1.52	1.13	0.82	1.20	1.60	2.00	1.95	1.77	2.02
FeO *	2.29	1.11	2.54	2.05	2.24	2.54	1.94	2.13	1.79
MnO	0.07	0.04	0.05	0.05	0.08	0.08	0.07	0.07	0.05
MgO	3.11	1.34	1.83	1.95	3.01	2.59	2.16	3.60	2.03
CaO	3.39	1.94	2.67	2.82	4.26	3.67	3.26	3.74	2.08
Na_2O	4.76	6.07	5.61	5.56	5.08	5.45	5.95	5.35	5.53
K_2O	4.12	3.08	3.18	3.42	3.94	3.06	2.52	3.54	3.13
F_2O_5	0.29	0.08	0.22	0.27	0.43	0.32	0.31	0.38	0.21
Ba ppm	2409	2475	2042	2270	2647	1984	3634	2152	1996
Cr	177	90	99	119	186	136	102	196	87
Zr	196	194	180	178	211	182	320	205	163
Sr	1738	4291	1365	1521	1511	1168	5791	1286	747
Rb	126	77	74	84	124	78	68	140	62
Y	19	10	21	15	60	25	14	17	19
Nb	nd	nd	nd	nd	nd	nd	nd	nd	nd
Zn	60	31	50	56	67	66	61	70	72
Ni	62	16	21	26	60	38	21	86	68
V	66	41	49	48	71	59	50	59	44
Total	96.58	98.12	96.95	96.77	95.16	96.56	96.79	96.87	97.49
CIPW norms									
Ap	0.64	0.18	0.48	0.59	0.95	0.70	0.68	0.84	0.46
Il	0.74	0.40	0.63	0.63	0.80	0.91	0.76	0.74	0.80
Mt	2.21	1.64	1.19	1.74	2.33	2.91	2.83	2.57	2.94
Or	24.34	18.19	18.79	20.21	23.28	18.08	14.89	20.92	18.49
Ab	40.29	51.36	47.48	47.05	43.00	46.12	50.35	45.28	46.80
An	5.10	5.43	5.76	4.62	3.38	5.90	6.10	4.33	5.69
Di	7.88	2.93	4.99	6.17	11.98	8.23	6.44	9.35	2.59
Hy	6.41	2.77	5.84	4.20	4.03	4.87	3.74	6.46	4.84
Q	8.52	14.54	11.47	11.20	5.01	8.52	10.02	6.03	14.60

nd = not detected
* determined by titration technique using metavanadate

STRUCTURE

Faults within the mine workings may be divided into two groups: pre-ore and post-ore. The Kirkland Lake Main Break is the predominant pre-ore fault, striking roughly 067°, and paralleling the composite intrusive complex and the regional trend of the Timiskaming Group. Numerous parallel and branching structures lie both north and south of the break. The main break provided a conduit for the intrusion of the host igneous complex and hydrothermal fluid from depth. It was also active long after the cessation of main hydrothermal activity, as evidenced by the occurrence of cataclastic fault gouges along the vein margins.

Post-ore faults generally crosscut the ore veins at high angles. The Lake Shore Fault is the dominant structure of this type, striking 020°and dipping steeply to the east. On surface, the separation of the North Vein across the Lake Shore Fault suggests a horizontal displacement of 190 m, while the vertical component is roughly 100 m (Thomson 1950).

VEINING AND MINERALIZATION

Veins at the Lake Shore Deposit may be divided into three groups: a) hematite and quartz-hematite veins; b) auriferous veins; and c) post-ore veins.

Hematite and Quartz-Hematite Veins

Hematite and quartz-hematite stringers and veinlets are confined within the intrusions. They are abundant in areas proximal to the auriferous veins (less than 15 m); however, they are absent in the rocks immediately adjacent to the auriferous veins, where the sulphidization of iron phases occurs. They are also not observed in auriferous veins. Their exact time of emplacement is uncertain, as crosscutting relationships with other veins are not observed.

Auriferous Veins

Two prominent gold-bearing veins occur in the Lake Shore property: the North Vein, in the Kirkland Lake Main Break; and the South Vein, which lies parallel to and south of the Break (Figure 313.1). Minor, but significant auriferous mineralization occurs parallel to

Photo 313.3. *Typical single fissure vein with molybdenite/graphite lined fracture surfaces and inclusions of wall rock fragments (wf). Sample represents the whole width of the North Vein.*

and north of the Main Break, in the Narrows Break Vein. Numerous diagonal vein fractures lie between these two major auriferous veins, forming diamond-shaped patterns throughout the mine workings (Thomson 1950). The South Vein dips more steeply to the south than the North Vein, and as a result the two structures combine at depth.

Auriferous veins are hosted by all rock types, with the exception of the diabase dikes. The ore veins may be classified into single fissure veins, vein breccias, stockworks, and sheeted veins (Thomson *et al.* 1950).

The single fissure veins are the most common (Photo 313.3). These veins vary in width from 3 cm up to 1.5 m, and are commonly separated from the wall rock on one or both sides by a seam of chloritic gouge up to 2 cm in width. The chloritic gouge is a cataclastic mixture of fine-grained chlorite, quartz, pyrite, and rock fragments. The apparent lack of recrystallization suggests that they were formed by the flouring movement of rocks along the margin of veins long after the main stage of auriferous hydrothermal activity. Vein fillings are composed of quartz, and minor amounts of angular to rounded to brecciated inclusions of altered wall rock (Photo 313.3). Narrower veins are commonly filled only with quartz. Breccia veins (Photo 313.4) are commonly formed where large amounts of wall rock have been incorporated into the veins.

Quartz stockworks are less common. They generally lie adjacent to the main fracture system, forming ore zones up to 20 m in width.

Vein quartz varies from dark greasy grey to white glassy varieties in the main ore zones. Petrographic study by Theriault (1988) suggested that multiple stages of hydrothermal activity took place synchronously with ductile-brittle deformation. Undulatory extinction, sawtooth-like grain boundaries, and displacement of coarse-grained quartz due to pressure solution are very common in the earlier formed greasy grey quartz. Brittle failure of the coarse recrystallized quartz produced extensive fracturing, and the subsequent lining of black seams ("moly-slip") (Photo 313.3). The black material was identified by X-ray photography as a mixture of varying proportions of extremely fine-grained molybdenite, chlorite, sericite, graphite, and quartz (Theriault 1988). Further fracturing of quartz and rock fragments introduced sulphides, together with gold and tellurides, in the late stages of hydrothermal activity.

Pyrite is the most abundant metallic mineral in the veins, averaging 2 to 3 percent by volume. Other sulphide minerals include chalcopyrite, galena, and sphalerite. Gold occurs along fractures in the vein quartz and in the altered wall rocks, and is associated with pyrite and with tellurides. The tellurides present include calaverite, altaite, and coloradoite.

Post-Ore Veins

Several types of post-ore veins are recognized. Late stage fractures within altered wall rocks are commonly filled with carbonate and varying amounts of barite, chlorite, sericite, and chalcopyrite. Post-ore veinlets of quartz and carbonate are also found within the auriferous veins themselves. Small carbonate stringers (less than 1 cm in width) cutting the ore veins at right angles are common (Photo 313.4). Late carbonate stringers and veins are also associated with the Lake Shore Fault. The carbonate in the post-ore veins is strain-free coarse crystalline calcite.

The filling temperatures of fluid inclusions in quartz cutting the auriferous zones are 320 to 330°C; these are similar to those for the auriferous zones (330 to 350°C). However, filling temperatures in calcite are low, ranging from 270 to 280°C, which indicates that the formation of carbonate veins took place later (Gallimore 1988).

ALTERATION OF THE PORPHYRY

Hydrothermal alteration studies carried out on the porphyry from the eastern portion of the mine reveal four distinct alteration facies. These facies include, from least to most altered: a) facies 1—secondary biotite facies; b) facies 2—chlorite facies; c) facies 3—phlogopite-hematite facies; and d) facies 4—fuchsite-sericite-pyrite facies.

The spatial distribution of the latter two facies, and possibly the latter three, suggests that they are

***Photo 313.4.** Photo displaying the typical highly fractured nature of the breccia veins. Note late-stage carbonate (Ca) veins crosscutting the quartz (Q) fracture fillings. Sample is lined on both sides by chlorite gouge and represents the whole width of the North Vein.*

directly related to the mineralization event. These facies form concentric zones about the auriferous veins. The distribution and mineralogical assemblage of the first facies suggests that it is not related to the gold mineralization, but rather to the intrusive activity. The chlorite facies is always found between the phlogopite-hematite facies and either unaltered porphyry or rocks of the secondary biotite facies. This indicates that the chlorite facies is unrelated to the secondary biotite facies, and strongly suggests its association with facies 3 and 4.

SECONDARY BIOTITE FACIES

The secondary biotite facies (facies 1) constitutes the least altered porphyry at the Lake Shore property. The rocks of this facies are generally found at distances greater than 20 m from the auriferous veins; while their distribution at mine scale is not understood at present, almost all rocks without visible alteration display this type of cryptic alteration. In hand specimen, these rocks are indistinguishable from unaltered rocks. This facies is characterized by the replacement and/or overgrowth of the ferromagnesian minerals by secondary biotite, and by the development of fine-grained biotite in the groundmass. Secondary biotite may be differentiated from primary magmatic biotite by its lighter colours, as well as by replacement and overgrowth textures (Photo 313.5). Two generations of secondary biotite may be distinguished by their differing pleochroism and overgrowth textures (Photo 313.6). The earlier formed secondary biotite is pleochroic, from light green to colourless, while later secondary biotite is pleochroic from medium greenish brown to medium green. These two generations are often separated

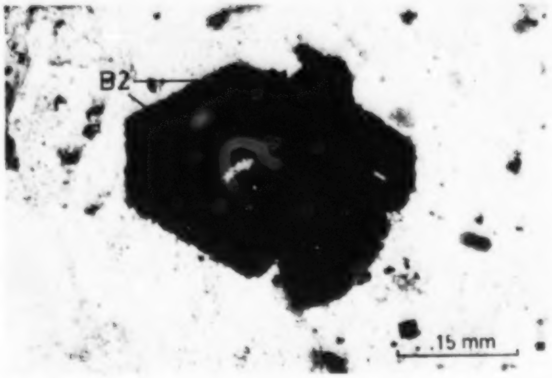

Photo 313.5. *Photomicrograph of secondary biotite (B2) overgrowing primary biotite (B) in the secondary biotite facies. Plane polarized light.*

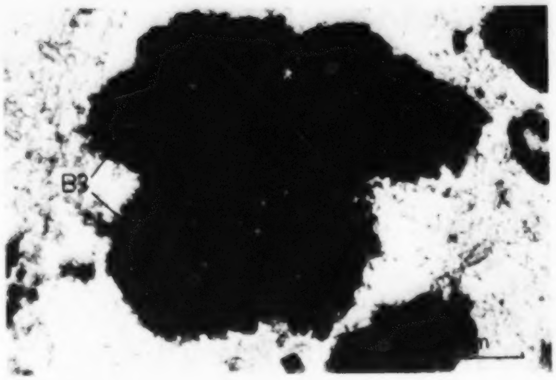

Photo 313.6. *Photomicrograph of late secondary biotite (B3) overgrowing earlier secondary biotite (B2) in the secondary biotite facies. Note the trails of fluid inclusions (FI) separating the two generations of biotite. Plane polarized light.*

from each other in overgrowths by a line of fluid inclusions (Photo 313.6).

The distinction between primary biotite formed from melt and secondary biotite formed from hydrothermal fluid was made based on textures (overgrowth, replacement of hornblende) and chemical compositions. As shown in Figure 313.3, secondary biotite is exceptionally low in TiO_2 and FeO, compared with biotite in normal igneous rocks. Because it is highly unlikely that differing compositions of biotite were formed from a melt at the same time in one place, the biotite with low FeO and TiO_2 contents was identified as secondary biotite.

Where primary biotite is replaced by secondary biotite, small acicular inclusions of rutile commonly form star-shaped asters (sagenite texture) in the secondary biotite because of the excess titanium (Ti) released from the primary biotite. The replacement of hornblende by secondary biotite is indicated by the formation of biotite pseudomorphs after hornblende.

In addition to colour and textural differences, the primary and secondary biotites may be differentiated on the basis of mineral chemistry (Table 313.2, Figure 313.3). The secondary biotites are characterized by higher MgO/FeO ratios and lower TiO_2 contents.

Plagioclase displays variable alteration on the rims of individual grains to albite and orthoclase (Photo 313.7). This alteration forms a fine-grained mosaic which is easily observed upon staining. Analysis of the alteration products using an energy dispersion spectrometer (electron microsopy) indicates near end member compositions, suggesting a hydrothermal origin.

Fine grains of sulphate are commonly developed in this facies. They are typically small (less than 10 microns), occurring disseminated in the groundmass, as inclusions in the secondary biotite, or as inclusions in altered feldspar rims (Photo 313.7). Microprobe analyses (Table 313.3) show the bulk compositions of the sulphate barite-celestine, suggesting that they are of high temperature origin, because there is an immiscibility gap in the series of barite-celestine at low temperatures. Hydrothermal apatite within the sulphate generally shows elevated SO_4^{2-} abundances compared to magmatic apatite (Table 313.3).

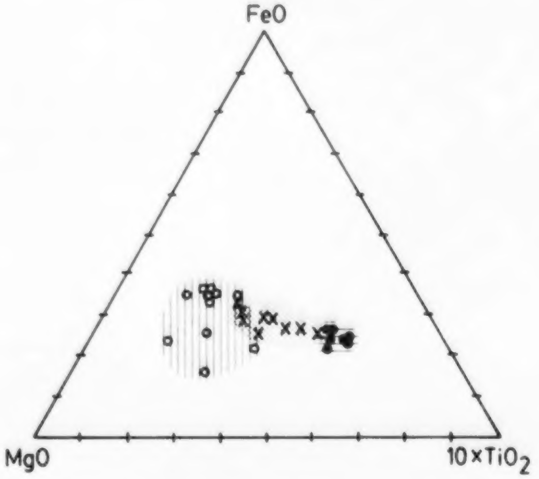

Figure 313.3. *FeO-MgO-TiO_2 (times AO) ternary variation diagram displaying variations in the chemical compositions of the three generations of biotite. Primary biotite = filled circles; early secondary biotite = open circles; late secondary biotite = crosses.*

Magnetite within this facies displays weak hematite and titanite alteration (Photo 313.8). Both of these replacements occur along grain margins and fractures. Mild sericite and carbonate alteration of plagioclase and the groundmass occurs throughout the facies.

TABLE 313.2: COMPOSITIONAL VARIATIONS IN BIOTITES

	1	2	3	4	5	6
SiO_2	40.3	38.68	38.97	39.33	38.78	38.72
TiO_2	0.55	0.7	1.05	1.89	2.39	3.67
Al_2O_3	13.88	13.72	13.26	12.89	13.4	13.34
Cr_2O_3	1.57	1.23	0.52	0.55	0.04	0
FeO	4.46	14.38	14.19	14.48	15.51	15.72
MnO	0.06	0.13	0.09	0	0.12	0.11
MgO	25.47	18.49	18.68	17.3	17.81	14.78
CaO	0.03	0.03	0.03	0	0.03	0
Na_2O	0.07	0.01	0.08	0	0.08	0
K_2O	9.89	9.31	9.55	8.99	8.99	9.3
Cl	0	0	0	na	0	na
F	1.13	0.78	0.73	na	0.9	na
Total	97.4	97.39	97.19	95.43	98.09	95.64

1 Very light green hydrothermal biotite (early hydrothermal)
2 Light green hydrothermal biotite (early hydrothermal)
3 Medium green hydrothermal biotite (late hydrothermal)
4 Dark medium green hydrothermal biotite (late hydrothermal)
5 Dark greenish brown magmatic biotite
6 Deep reddish brown magmatic biotite
na = not analyzed

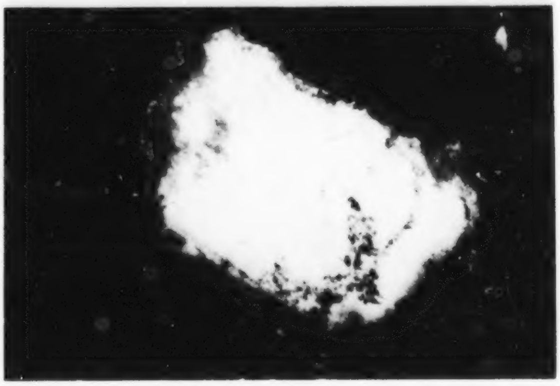

Photo 313.7. *Photomicrograph of altered plagioclase rims in the secondary biotite facies. These rims are composed of a fine-grained mosaic of albite, orthoclase, and sulphate. Plane polarized light.*

TABLE 313.3: MICROROPROBE ANALYSES OF SULPHATE AND APATITE

	84	84-1	135	135-1
CaO	0.08	0.3	55.91	55.54
BaO	15.13	6.82	na	na
P_2O_5	na	na	41.61	41.15
SrO	44.64	54.08	na	na
SO_3	40.22	39.13	0.75	0.38
Total	100.07	100.33	98.27	97.07

84 Sulphate (semi-quantitative)
84-1 Sulphate (semi-quantitative)
136 Hydrothermal apatite in sulphate
136-1 Magmatic apatite
na = not analyzed

CHLORITE FACIES

The rocks of the chlorite facies (facies 2) are similar in colour and texture to the unaltered and secondary biotite facies rocks. These rocks are generally found at distances greater than 15 m, and less than 20 m, from the auriferous veins. Toward the ore veins, these rocks grade into rocks of the phlogopite-hematite facies. Away from the auriferous veins, they are in contact with either the unaltered porphyry, or rocks of the secondary biotite facies.

The chlorite facies is characterized by the replacement of all ferromagnesian minerals by chlorite. The alteration of biotite, either primary or secondary, takes place along grain margins and the 001 cleavage plane (Photo 313.9). The amount of sagenite (rutile) within the chloritized biotite increases with increasing amounts of chlorite. Small grains of secondary magnetite and potassic feldspar are also developed along the cleavage planes; these are formed due to the inability of chlorite to incorporate, respectively, all of the iron (Fe) and potassium (K) released during the breakdown of biotite.

Increased sericitization and carbonatization of the plagioclase and groundmass accompany this alteration. Primary magnetite shows increased alteration to hematite, and titanite coronas become abundant. Siderite alteration is frequently associated with the magnetite/hematite assemblages.

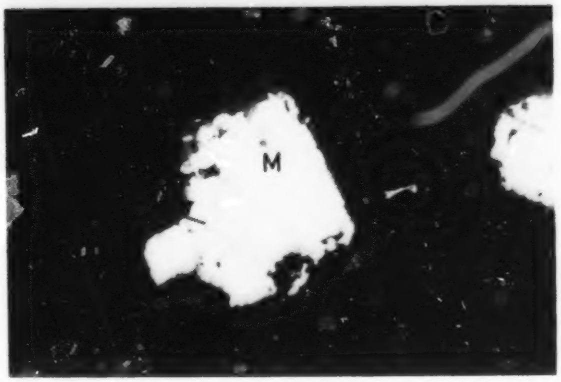

Photo 313.8. *Photomicrograph showing the alteration of primary magnetite (M) to titanite (Ti) along grain margins and fractures in the secondary biotite facies. Reflected light.*

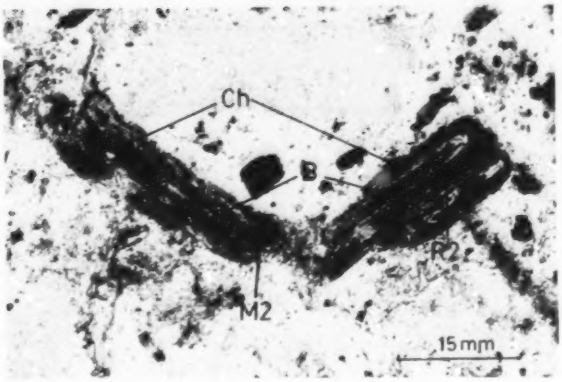

Photo 313.9. *Photomicrograph showing the alteration of biotite (B) to chlorite (Ch) in the chlorite facies. Replacement occurs along grain boundaries and the 001 cleavage. Secondary magnetite (M2) and rutile (R2) are formed due to excess Fe and Ti. Plane polarized light.*

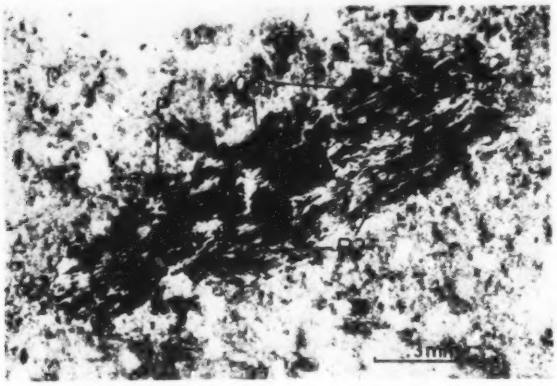

Photo 313.10. *Photomicrograph of phlogopite (P) replacing chlorite (Ch) in the phlogopite-hematite facies. Replacement occurs along grain boundaries and the 001 cleavage. Note secondary magnetite (M2) and rutile (R2) retained from the chlorite facies. Plane polarized light.*

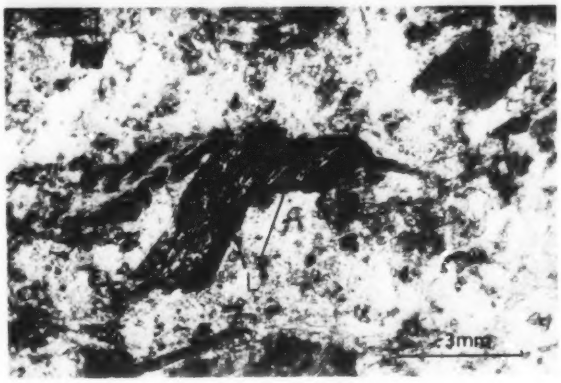

Photo 313.11. *Photomicrograph showing the early stages of deformation in the fuchsite-sericite-pyrite facies. Photomicrograph shows fuchsite (F) being realigned parallel to the foliation planes by gliding along cleavages of mica due to shear deformation. All secondary magnetite and rutile has been replaced by leucoxene (L). Plane polarized light.*

PHLOGOPITE-HEMATITE FACIES

The phlogopite-hematite facies (facies 3) extends from 1 to 2 m away from the auriferous veins, to distances of up to 10 m. This facies is characterized by the replacement of chlorite (after biotite and hornblende) by phlogopite, the hematitization of primary magnetite, and the development of fine-grained hematite in the groundmass. As a result of hematite alteration, the rocks in this facies vary from pinkish red to brick red in colour; however, they still retain the porphyritic texture. In the more altered samples, the plagioclase phenocrysts take on a mild red colouration. Small hematite and quartz-hematite stringers are commonly observed in these rocks. The rocks are highly fractured as evidenced by the numerous chlorite slips.

The replacement of chlorite by phlogopite occurs along grain boundaries and the 001 cleavage (Photo 313.10). Rutile and magnetite inclusions within the grains increase in abundance with alteration, as iron and titanium are released during the breakdown of chlorite. In the most altered samples in this facies, the acicular rutile grains within the phlogopite show hydration to leucoxene.

Primary and secondary magnetite is variably replaced by hematite along grain boundaries and fractures. Small rounded grains of hematite are developed in the groundmass, imparting the red colour to the rocks. Inclusions lined with dark material, likely hematite, in the plagioclase become more apparent with increasing alteration. The breakdown of titanite to rutile and carbonate is commonly observed. Increased sericitization and carbonatization of the plagioclase and groundmass also accompany this alteration.

FUCHSITE-SERICITE-PYRITE FACIES

This facies (facies 4) constitutes the immediate wall rocks of the auriferous veins, extending outward 1 to 2 m from them. The rocks of this facies vary in colour with increasing alteration, from orangey pink to olive green. These rocks are highly fractured and moderately sheared, particularly the footwall rocks, which are more intensely deformed and generally more altered than the hanging wall rocks. The correlation between the intensity of the alteration and the deformation is interpreted as the result of the increase in permeability in rocks during shear deformation. More fluid access to the rocks was provided in the more deformed rocks. In some areas, deformation and alteration is so intense that the porphyritic texture of the rock is obliterated, and only a fine foliation is observed. Apparently, the alteration of feldspars to sericite near the auriferous veins promoted further deformation by weakening the response to the strain.

The fuchsite-sericite-pyrite facies is characterized by the replacement of phlogopite (after chlorite) by fuchsite, pervasive sericitization of the feldspars and the groundmass, and the replacement of hematite and magnetite by pyrite. Fuchsite replacement of phlogopite is identified by the change from colourless phlogopite to pale blue-green fuchsite, and has been confirmed by electron microprobe analyses. Rutile asters formed in the chlorite and phlogopite-hematite facies are completely replaced by leucoxene in this facies. In the more deformed footwall rocks, a foliation is developed with increased shearing. Fuchsite is realigned parallel to the strike of the foliation plane (Photo 313.11). It becomes stretched thin by grinding along cleavage planes in more deformed rocks, and in the most deformed rocks almost all of the fuchsite has been destroyed by shearing, leaving thin dark seams of leucoxene.

Pyrite is formed in this facies at the expense of hematite and magnetite. It occurs up to distances of about 1 m from the ore veins, often extending farther into the more deformed footwall rocks. Again, the increase in permeability due to deformation appeared to have provided greater interaction of fluids with the rocks in the footwall side. In the less deformed rocks of this facies, pyrite inclusions in the fuchsite are common, replacing secondary magnetite.

Carbonate alteration is more prevalent in the less deformed rocks of this facies. Minor silicification and the development of secondary potassic feldspar (microcline?) also accompany this alteration. Primary and secondary titanite and rutile are absent from this facies, having been completely replaced by leucoxene.

POST-ORE ALTERATION

Small fracture fillings of quartz-calcite are common throughout all alteration facies of the porphyry, including the highly altered wall rocks. These veinlets cut variably sericitized plagioclase phenocrysts, indicating that the formation of these veinlets occurred after the alteration associated with gold mineralization; the fracture filling is generally clear optically continuous plagioclase. Increased amounts of carbonate in the groundmass are associated with these late veins, forming halos up to 15 cm from the veins.

DISCUSSION AND CONCLUSIONS

Detailed petrological studies of the hydrothermal alteration at the Lake Shore Property has outlined two distinct superimposed hydrothermal alteration events. The first event was a high-temperature event associated with magmatism. The second event is related to gold mineralization, and overprints the first event in areas proximal to the auriferous veins.

The occurrence of secondary biotite in miarolitic cavities suggests that the secondary biotite facies was a direct result of the alteration caused by the high-temperature magmatic-hydrothermal fluids released during the cooling of the intrusions, or other igneous rocks below the intrusive complex. Because the area has undergone sub-greenschist facies regional metamorphism (Jolly 1974), biotite is not a product of regional metamorphism. Biotite is a common alteration mineral around Archean deposits in high grade metamorphic terrain, such as the Red Lake gold camp (Andrews and Hugon 1985). However, textural evidence presented in this paper clearly indicates that the biotite was formed before the gold mineralization. The only likely event which provided the heat and fluid for biotite formation, is the intrusion of the alkaline complex, or possibly a different magma reservoir beneath the complex. The high magnesium contents in secondary biotite, the SO_4^{2-} in apatite, the formation of hematite and titanite after magnetite, and the presence of sulphates in the cavities as well as throughout this facies indicates a highly oxidized nature for these fluids.

The spatial relationships of alteration facies 3 and 4 as concentric zones about the auriferous veins suggest that the alteration is directly related to the main stage veining and mineralization. The origin of the chlorite facies is somewhat uncertain. This facies is always observed at a greater distance from the auriferous veins than the phlogopite-hematite facies. Considering the fact that phlogopite always replaces chlorite, the chlorite facies may also be an essential part of the wall rock alteration related to the auriferous mineralization. If it is considered a product of the main stage veining, then the three concentric alteration zones about the ore veins may have originated in two ways. One possible origin is that each zone represents different distances to which chemically different hydrothermal fluids penetrated the host rocks. If this was the case, then the inner alteration zones (facies 3 and 4) should be observed encroaching on the unaltered rocks, or on facies 1. This feature is never observed. The second possible origin is that the three zones are the result of the spatial evolution of a single fluid, as the fluid passed through the host rocks and reacted with them. The successive change developed in the micas through the facies, along with the increasing degrees of carbonate, sericite, and hematite alteration toward the auriferous veins, may support the latter hypothesis.

The fluid evolution process would also explain the confinement of the hematite and quartz-hematite stringers and veinlets to the phlogopite-hematite facies. As the fluid permeated the first few metres of the wall rocks, sulphur would be removed from the fluid by the formation of pyrite in facies 4, thus leaving oxidized fluids to permeate the rocks of facies 3, and to a lesser extent facies 2. Pyrite is a stable mineral in a highly oxidized environment, if the partial pressure of sulphur is high (Cameron and Hattori 1987). Alternatively, the confinement of pyrite to facies 4 may be due to a temporal evolution of fluids, and a late introduction of sulphur.

If the spatial fluid evolution hypothesis is correct, the changing chemistry of the fluids can be deduced based on the changes in mineralogy. These changes include a decrease in the amount of CO_2, K, and S, and an increase in Mg and Na in the fluids with depth of percolation into the wall rocks, and occur as a result of the reaction of the fluid with the wall rocks. The prominent hematite alteration in facies 3 indicates a highly oxidized nature for the ore-forming fluids.

ACKNOWLEDGMENTS

The authors wish to thank Frank R. Ploeger and Jim Gray of Lac Minerals Ltd., Lake Shore Division, and Len Cunningham of L.J. Cunningham and Associates for assistance during sampling.

Thanks are also extended to Scott Ercit (National Museum of Natural Sciences, Ottawa) and Dave Kempson (Queen's University, Kingston) for assistance with the electron microprobe analyses. Comments by François Robert (Geological Survey of Canada, Ottawa) helped improve the manuscript.

REFERENCES

Andrews, A.J., and Hugon, H.
1985: Alteration, Metamorphism, and Structure Associated with Archean Volcanic-Hosted Gold Deposits, Red Lake District: Studies in the Campbell and A.W. White Mines; p.193-200 *in* Summary of Field Work and Other Activities 1985, by the Ontario Geological Survey, edited by J. Wood, O.L. White, R.B. Barlow, and A.C. Colvine, Ontario Geological Survey Miscellaneous Paper 126, 351p.

Burrows, A.G., and Hopkins, P.E.
1914: The Kirkland Lake and Swastika Gold Areas; Ontario Bureau of Mines, Annual Report for 1914, Volume 23, Part 2, p.1-39.
1925: Kirkland Lake Gold Area (Revised Edition); Ontario Department of Mines, Annual Report for 1923, Volume 32, Part 4, p.1-52.

Cameron, E.M., and Hattori, K.
1987: Archean Gold Mineralization and Oxidized Hydrothermal Fluids; Economic Geology, Volume 82, Number 5, p.1177-1191.

Charlewood, G.H. (compiled by)
1964: Geology of Deep Developments on the Main Ore Zone at Kirkland Lake; Ontario Department of Mines, Geological Circular 11, 49p.

Cooke, D.L., and Moorhouse, W.W.
1969: Timiskaming Volcanism in the Kirkland Lake Area, Ontario, Canada; Canadian Journal of Earth Sciences, Volume 6, p.117-132.

Gallimore, N.
1988: Fluid Inclusion Geochemistry of Hydrothermal Solutions Responsible for the Kirkland Lake Gold Deposits; Unpublished B.Sc. Thesis, University of Ottawa, Ottawa, 79p.

Hewitt, D.F.
1963: The Timiskaming Series of the Kirkland Lake Area; Canadian Mineralogist, Volume 7, Part 3, p.497-523.

Hodgson, C.J.
1983: Preliminary Report on the Timmins–Kirkland Lake Area; Ontario Geological Survey, Open File Report 5467, 197p.

Hodgson, C.J., Hamilton, J.V., and Guimond, R.P.
In press: Final Report, Grant 227 Relationship Between Gold Deposits and the Tectonic Framework of the Abitibi Greenstone Belt in the Kirkland Lake–Larder Lake Area; Ontario Geological Survey Open File Report.

Hyde, R.S.
1980: Sedimentary Facies in the Archean Timiskaming Group and Their Tectonic Implications, Abitibi Greenstone Belt, Northeastern Ontario, Canada; Precambrian Research, Volume 12, p.161-195.

Jahns, R.H., and Burnham, W.C.
1969: Experimental Studies of Pegmatite Genesis: I. A Model for the Derivation and Crystallization of Granitic Pegmatites; Economic Geology, Volume 64, Number 8, p.843-864.

Jensen, L.S., and Langford, F.F.
1985: Geology and Petrogenesis of the Archean Abitibi Belt in the Kirkland Lake Area, Ontario; Ontario Geological Survey, Miscellaneous Paper 123, 130p. Accompanied by Maps P.2434 and P.2435, scale 1:63 360 or 1 inch to 1 mile, and microfiche sheet.

Jolly, W.T.
1974: Regional Metamorphic Zonation as an Aid in the Study of Archean Terrains; Abitibi Region, Ontario; Canadian Mineralogist, Volume 12, Part 7, p.499-508.

Kerrich, R., and Watson, G.P.
1985: The Macassa Mine Archean Lode Gold Deposit, Kirkland Lake, Ontario: Geology, Patterns of Alteration, and Hydrothermal Regimes; Economic Geology, Volume 79, Number 5, p.1104-1130.

McInnes, B.I.
1985: Ore Petrology and Wallrock Alteration Studies at the Lake Shore Gold Mine, Kirkland Lake, Ontario; Unpublished B.Sc. Thesis, McMaster University, Hamilton, 131p.

Ploeger, F.R., and Crocket, J.H.
1982: Relationship of Gold to Syenitic Intrusive Rocks in Kirkland Lake; p.69-72 *in* Geology of Canadian Gold Deposits, Proceedings of the CIM Gold Symposium, September 1980, edited by R.W. Hodder and William Petruk, Canadian Institute of Mining and Metallurgy, Special Volume 24, 286p.

Reynolds, T.J., and Beane, R.E.
1985: Evolution of Hydrothermal Fluid Characteristics at the Santa Rita, New Mexico, Porphyry-Type Copper Deposit; Economic Geology, Volume 80, p.1328-1347.

Robert, F., and Brown, A.C.
1986: Archean Gold-Bearing Quartz Veins at the Sigma Mine, Abitibi Greenstone Belt, Quebec: Part II. Vein Paragenesis and Hydrothermal Alteration; Economic Geology, Volume 81, Number 3, p.593-616.

Roberts, R.G.
1987: Ore Deposit Models #11: Archean Lode Gold Deposits; Geoscience Canada, Volume 14, Number 4, p.37-52.

Streckeisen, A.
1973: Plutonic Rocks: Classification and Nomenclature Recommended by the IUGS Subcommision on the Systematics of Igneous Rocks; Geotimes, Volume 18, Number 10, p.26-30.

Theriault, R.
1988: A Study of Gold Mineralization at the Lake Shore Gold Mine, Kirkland Lake, Ontario; Unpublished B.Sc. Thesis, University of Ottawa, Ottawa, 83p.

Thomson, J.E.
1950: Geology of Teck Township and Kenogami Lake Area, Kirkland Lake Gold Belt; Ontario Department of Mines, Annual Report for 1948, Volume 57, Part 5, p.1-53.

Thomson, J.E., Charlewood, G.H., Griffin, K., Hawley, J.E., Hopkins, H., MacIntosh, C.G., Ogrizlo, S.P., Perry, O.S., and Ward, W.
1950: Geology of the Main Ore Zone at Kirkland Lake; Ontario Department of Mines, Annual Report for 1948, Volume 57, Part 5, p.54-196.

Todd, E.W.
1928: Kirkland Lake Gold Area; Ontario Department of Mines, Annual Report for 1928, Volume 37, Part 2, p.1-176.

Tyrrell, J.B., and Hore, R.E.
1926: The Kirkland Lake Fault; Transactions, Royal Society of Canada, 3rd Series, Volume 20, Part 1, Section 4, p.51-63.

Grant 316 Placer Formation in Braided River Systems

John P. Burton and Philip W. Fralick

Department of Geology, Lakehead University, Thunder Bay

ABSTRACT

Processes controlling the deposition of heavy minerals in coarse-grained longitudinal gravel bars were studied in braided sections of the North Saskatchewan River, located in Banff National Park, Alberta; and in three rivers north of Lake Superior, Ontario: the Jackpine, Mississagi, and Agawa rivers. Flume tank experimentation was also used to simulate conditions operating in natural braided river systems over longitudinal bars.

Preliminary data indicates that flow velocity during maximum discharge events controls the amount of heavy minerals and clast sizes being deposited in gravel bars. In order for this process to operate, both heavy minerals and clasts must be in transport and subsequently deposited at the same time.

The formation of placer deposits in longitudinal bars appears to be dependent upon the separation of heavy minerals from light minerals during transport. Heavy minerals which accumulate due to depositional rather than erosional processes are found to preferentially concentrate in finer gravels and in matrix sediments that are coarse and poorly sorted. This indicates deposition during high flow events where highly turbulent conditions in lower energy areas of the gravel bar develop. As a result, the downstream sections of the bars sampled were found to contain significantly higher concentrations of magnetite than the upstream head of the bar.

INTRODUCTION

PURPOSE AND OBJECTIVES

Alluvial placer deposits are formed by the preferential accumulation of heavy minerals by a variety of hydraulic processes operating within a fluvial environment. The primary objective of this study is to identify the fundamental conditions present in braided gravel-dominated river systems that maximize the concentration of economic heavy minerals in longitudinal gravel bars.

Traditionally, most research concerning placer development in coarse-grained bars has centred on the Witwatersrand paleoplacer deposits of South Africa. These placer deposits are significant as they alone account for over half the gold mined by man—some 1.4 billion Troy ounces—in a little over one hundred years of exploitation (Pretorius 1981, p.118).

Considering the obvious economic importance of placer deposits, it is surprising that such occurrences have not been the subject of more sedimentological research. As one recent paper stated, "...the physical processes responsible for concentrating heavy minerals have attracted little attention and are poorly understood. The mechanisms of sediment sorting in rough mobile beds under turbulent flows are complex, and present transport theory provides useful but only limited assistance to the problem" (Smith and Beukes 1983, p.1342). These constraints have led most researchers to concentrate on less turbulent sandy systems, or the formation of placer lag deposits as opposed to the depositional accumulation of heavy minerals in coarse longitudinal bars. Coarse-grained gravel bars are areas of high turbulence—a condition that should not be favourable for heavy mineral concentration—yet there are numerous examples of placer deposits that have formed under these conditions (*see* Pretorius 1981, Table 1).

The first direct experiments on the processes involved in heavy mineral deposition in a gravel bed were conducted by Minter and Toens (1970). Magnetite was used in the flume study to simulate the behaviour of detrital gold in a fluvial system. A different size of pebbles was used to construct a simulated gravel bar in each of three runs. Results from these experiments indicate that significant heavy mineral enrichment will not occur under the flow conditions studied.

METHODS

Modern natural braided river systems were examined and sampled to determine the distribution and concentration of heavy minerals in longitudinal gravel bars.

The first area studied was the North Saskatchewan River located in Banff National Park, Alberta (Figure 316.1). It was theorized that glaciofluvial systems developed in unvegetated large braided outwash plains (Photo 316.1a) would have conditions similar to those present during the formation of Proterozoic paleoplacers, such as the deposits at Elliot Lake. Differences in source terrain would, however, affect the supply of heavy minerals in the sediments of the North Saskatchewan River as compared to the relatively plentiful supply from the exposed granitic plutons to the north of Elliot Lake. Sampling in the study area took place on six randomly selected longitudinal gravel bars beginning at the river's source, namely the Saskatchewan Glacier, and continuing downstream approximately 50 km.

The second area the study focused on was north of Lake Superior (Figure 316.1). Three rivers were selected from this area: a) the Jackpine River (Photo 316.1b); b) the Mississagi River (Photo 316.1c); and c) the Agawa River (Photo 316.1d). Each of these rivers exhibits classic braided sections that contain longitudinal gravel bars; these bars were subsequently sampled.

A third aspect of the study involved the simulation of natural braided river systems by means of flume tank experimentation. This was conducted to determine the conditions necessary to maximize heavy mineral accumulations in gravel bars. Both magnetite and lead grains were added to the sand used in the flume to simulate the behaviour of uraninite and gold. The controlled (independent) variables included bed roughness (gravel size), bed shear stress, and sand grain size. The uncontrolled (dependent) variable was the magnetite and lead concentration in the matrix of the gravel. A series of 27 flume runs using various combinations of con-

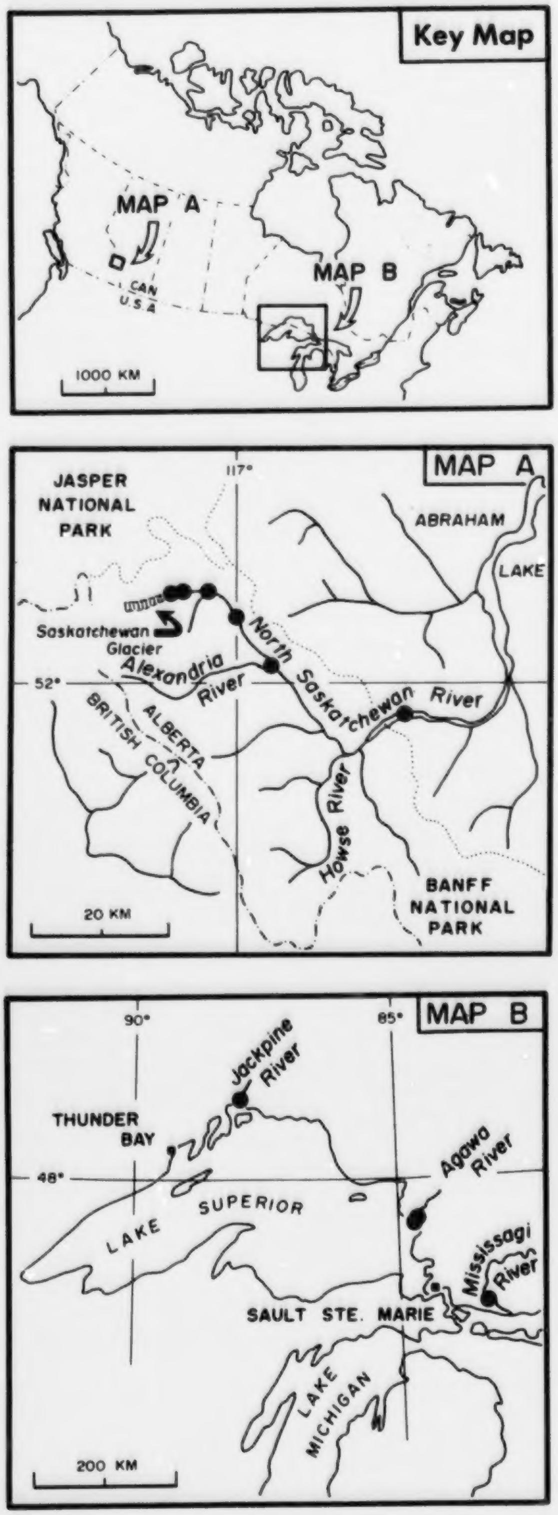
Key Map
MAP A
MAP B
CAN
U.S.A.
1000 KM
MAP A
JASPER
NATIONAL
PARK
117°
ABRAHAM
LAKE
Saskatchewan
Glacier
Alexandria
River
North
Saskatchewan
River
52°
BRITISH
COLUMBIA
ALBERTA
Howse River
BANFF
NATIONAL
PARK
20 KM
MAP B
90°
85°
Jackpine
River
THUNDER
BAY
48°
Agawa
River
LAKE
SUPERIOR
Mississagi
River
SAULT STE. MARIE
LAKE
MICHIGAN
200 KM

Figure 316.1. Location maps of areas studied.

trolled variables were conducted in order to determine which particular combination created the most significant accumulation of heavy minerals.

STATUS OF RESEARCH

To date, all field and laboratory work on samples from the North Saskatchewan River and the three rivers north of Lake Superior has been completed. Due to the large number of scatter diagrams the field studies have generated, only results from the Jackpine River are presented in this report. This selected data set is representative of the other river studies. Flume tank experimentation has been completed and the samples are at present being analyzed. Thus, only preliminary data on magnetite concentrations is presented.

FIELD STUDIES

DESCRIPTION OF BRAIDED RIVER SYSTEMS

Braided rivers are complex natural systems that form in response to conditions such as: large fluctuations of discharge both diurnally and seasonally; a substantial supply of coarse sediments; an increase in slope; and predominantly unconsolidated and unstable river banks due to a pronounced lack of vegetation.

Braided rivers tend to have multiple channels with high width to depth ratios. Such channel shapes move large quantities of coarse detrital sediments more efficiently. In this type of system, channel morphology is very complex; larger sized cobbles, easily transported during maximum discharge events, are deposited as river discharge drops off. This results in the formation of obstacles within the river channel which in turn force the river to diverge. The formation of lower energy areas downstream from these obstacles causes sediment to accumulate, and eventually this process results in the formation of gravel bars within the river channel. Longitudinal gravel bars are typically diamond shaped and form parallel to the dominant direction of flow (Photo 316.1a). The bars are submerged during maximum flow events, during which time they are modified under extremely turbulent conditions. Such conditions typically result in coarse sediments being deposited at the head of a gravel bar, as this is the area of maximum velocity. A significant decrease in velocity over the length of the bar results in a decrease in clast size. The surfaces of many longitudinal bars not only exhibit a decrease in clast size from head to tail, but are also intersected by many chute channels which cut across the bar during decreasing discharge (Photo 316.1a). With continued reduction in discharge, pebbles or sand travelling through chute channels are often deposited, producing finer grained lenses embedded in bar successions. Ripples or dunes migrate along chute channels, often forming chute channel deltas where the chute rejoins the main channel (Photo 316.1e).

Along the sides and at the tail of gravel bars, accumulations of sand known as bar edge sand wedges develop (Photo 316.1f) Such wedges form in response to a reduction in energy at these sites.

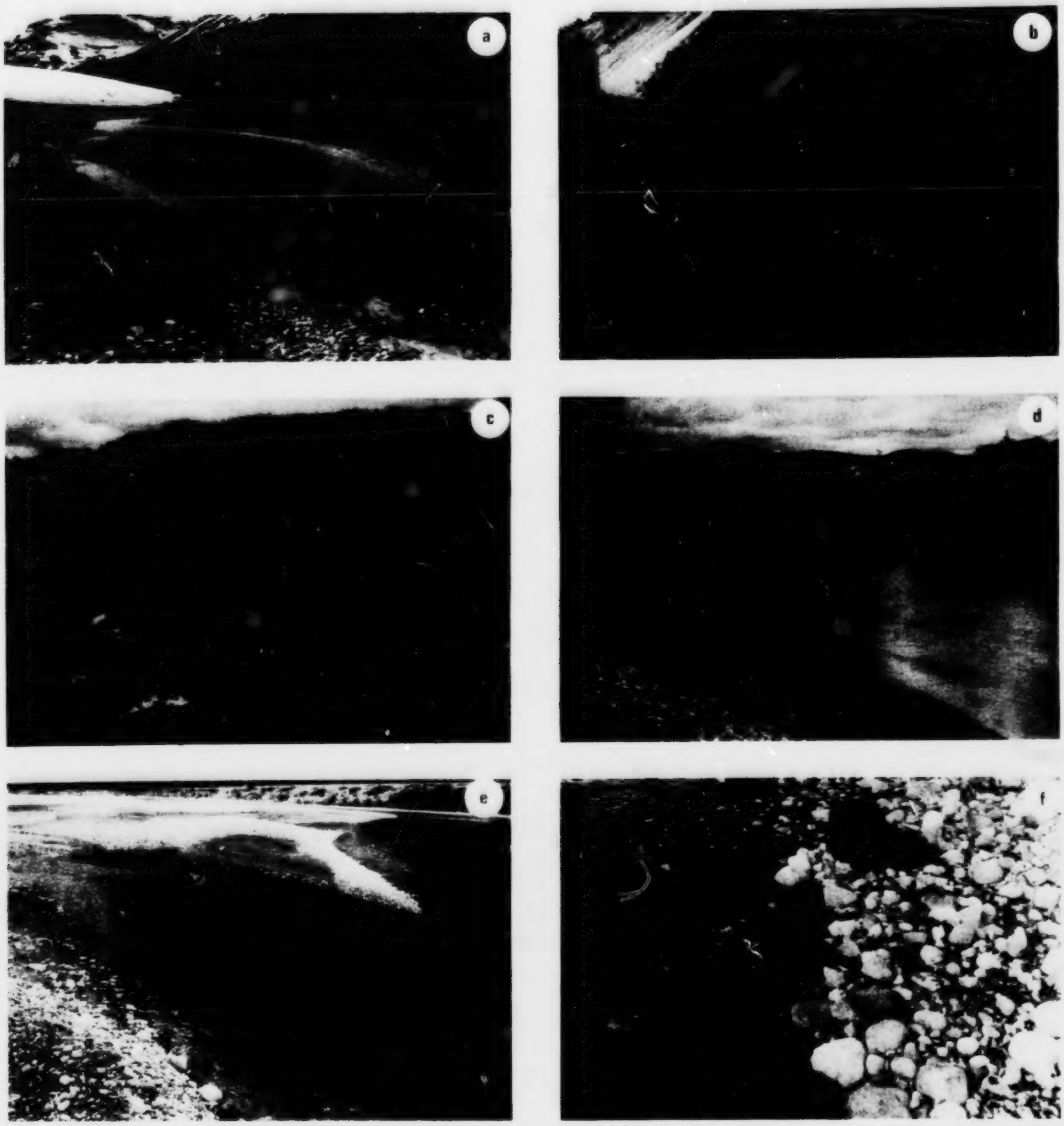

Photo 316.1. *Selected photographs from field studies.* ***a.*** *Longitudinal bar studied on the North Saskatchewan River, Banff National Park, Alberta, proximal to the Saskatchewan Glacier (flow from left to right).* ***b.*** *Longitudinal bar studied on the Jackpine River, north of Lake Superior, Ontario (flow from right to left).* ***c.*** *Longitudinal bar studied on the Mississagi River, north of Lake Superior, Ontario (flow from right to left);* ***d.*** *Longitudinal bar studied on the Agawa River, north of Lake Superior, Ontario (flow from left to right).* ***e.*** *Abandoned chute channel and finer grained sandy lens deposited on longitudinal bar tail, North Saskatchewan River (flow from left to right).* ***f.*** *Bar edge sand wedge formed on side of longitudinal bar, Agawa River (flow direction toward top of photograph).*

SAMPLING PROCEDURE

Due to the complex nature of braided river systems, field sampling concentrated on well developed longitudinal gravel bars. Once selected, the bar was photographed, measured, and sketched. At each sample site, the ten largest clasts in a one metre square area were measured. This was done in order to determine the variation in clast size over the length of the bar. Following the clast measurement, sediment was collected from the matrix. This procedure was repeated at various locations over the bar. Samples were also obtained from bar edge sand wedges, chute channels, and chute delta sands, where present. In all cases, 250 ml of sediment was collected per sample.

INTERPRETATION OF SCATTER DIAGRAMS

Data from the Jackpine River has been analyzed and the results are presented in the form of eleven scatter diagrams which show the relationships between specific variables (Figures 316.2 and 316.3). On each scatter diagram, a best fitting regression line and equation have been calculated, along with the correlation of the line. A combination of linear and exponential regression lines have been fitted to the various graphs.

The first series of six graphs (Figure 316.2) depicts the interaction of several variables of the matrix of the gravel bar. Figure 316.2a plots the mean grain size of quartz sand against the mean grain size of magnetite. This data set displays a significant positive trend indicating that in any given site of the bar, coarse magnetite grains will be deposited with coarse quartz grains. A similar positive trend occurs in Figure 316.2b; where magnetite grains are poorly sorted, quartz grains are similarly poorly sorted. Figures 316.2c and 316.2d indicate that higher percentages of magnetite are found in samples containing coarse magnetite and quartz sand, respectively. Similarly, Figures 316.2e and 316.2f show that magnetite content is higher in poorly sorted matrix material. As sorting improves, the percentage of magnetite in the matrix is significantly reduced.

The second set of graphs (Figure 316.3) is concerned with how cobble size over the surface of a gravel bar is related to average grain size, sorting, and magnetite content of the matrix. Figures 316.3a and 316.3b, respectively, suggest that as cobble size increases, quartz and magnetite sediments present in the matrix become finer grained. Larger cobbles are present in the head of the bar indicating that the matrix in this area is finer grained than the matrix in the bar tail. Figures 316.3c and 316.3d, respectively, suggest that with an increase in cobble size, magnetite and quartz grains become better sorted. Figure 316.3e shows that larger cobbles are associated with lower percentages of magnetite present in the matrix. This suggests that the downstream portion of the bar, which contains smaller cobbles, would have the highest percentage of magnetite.

An interpretation of all of the graphs (Figures 316.2 and 316.3) indicates that the highest percentage of magnetite accumulates in coarse and poorly sorted matrix deposited in areas of the bar where smaller cobbles tend to concentrate. In the bar studied, this results in magnetite content increasing toward the tail of the bar. Bar edge sand wedges, found along the sides and tail of gravel bars (Photo 316.1f), are generally well sorted and contain finer sediments. As a result, according to the results presented, they will not contain a high percentage of heavy minerals.

FLUME EXPERIMENTATION

DESCRIPTION OF EQUIPMENT

A sediment-water recirculating flume at the Department of Geology, Lakehead University, was used to simulate natural gravel bar systems. The flume is of a heavy aluminum construction supporting Plexiglass sides along one section, allowing visual observation of fluvial and sediment interactions (Photo 316.2a). It is about 5 m long, 45 cm wide, and 40 cm deep in the Plexiglass portion, and somewhat narrower in all other sections. Water velocity is regulated by means of a belt and pulley system connecting an electric motor to a paddle wheel. The slope of the flume was fixed. The flume was modified for this project by installing five pressure taps which were used to measure the slope of the hydraulic gradient. Water velocity within the flume was determined by means of an Ott propeller-type current meter. The propeller was positioned in the centre of the flume at 0.4 of the flow depth.

MATERIALS USED

Three sizes of quartz sand (density 2.65 g/cm^3) were used in the flume: fine (2.6 Phi, 0.16 mm); medium (1.9 Phi, 0.28 mm); and coarse (1.1 Phi, 0.48 mm). Well rounded cobbles and pebbles (Photos 316.2a and 316.2b) were sorted into large cobbles (82 cm^2, long axis times short axis), medium cobbles (32 cm^2), and pebbles (11 cm^2). These clasts were used to construct openwork gravel bars in the flume (Photo 316.2a). Magnetite (density 5.5 g/cm^3; average grain size 2.1 Phi, 0.23 mm) was added to each of the three sizes of sand in order to obtain a concentration of 10 percent. In addition, lead (density 11.2 g/cm^3; average grain size 2.3 Phi, 0.20 mm) was added to each of the three sand fractions. The lead to sand ratio was also 1:10.

PROCEDURE

A total of 27 flume runs were systematically conducted with one variable changed following the completion of each run. Variables altered were: a) water velocity; b) sand grain size; and c) clast size of the gravel bar. Each run began with all of the sand positioned upstream of the gravel bar. The bar was completely free of sediment before each run (Photo 316.2a), so that any sediment present after the run had been completed would be directly attributable to a given set of conditions (Photos 316.2b and 316.2c). The thickness of the gravel bars ranged from two clasts for large cobbles, to about six clasts for pebbles. Following bar construction, the flume was filled with water to a depth of 20 cm. The duration of the flume runs ranged from ten minutes for high and medium flow velocities, to five hours for low velocity runs.

During a run, velocity measurements were recorded at six selected sites. Depth of flow from the water's surface to the sediment interface was recorded at the same locations as the velocity measurements. The slope of the energy gradient line was recorded by measuring the difference in hydrostatic head of the water between the five pressure taps. Sediment movement was described and recorded during each run.

After each run was completed, the water was drained and the gravel bar described and photographed. Two sites were sampled, one near the bar head, the other near the tail. At each site, two matrix samples were collected, one from near the base of the bar, the other from surficial sediment. Following the sampling, the flume was set up for the next run with a change in one variable.

INTERPRETATION OF SCATTER DIAGRAMS

Preliminary data obtained from flume runs allows variables such as velocity, percentage of magnetite, and cobble size, to be plotted against one another to identify any significant trends (Figures 316.4 and 316.5). Data was divided by sample site into four separate data sets. Of these, Sites A and B are presented in this report.

The data presented were obtained from the sample location at the head of the gravel bar. Samples were collected from surface sediments that were deposited by avalanche face progradation, and from within the bar where the predominant mode of deposition is that of suspension rain out. This difference in depositional process is reflected in the scatter diagrams presented.

Figures 316.4a and 316.4c (Site A), which plot the percentage of magnetite against water velocity in the experiments using fine and medium sand, respectively, show that magnetite content in the bar increases with increasing velocity. Figure 316.4e, however, indicates that there is no significant trend between magnetite percentage and velocity in the coarse sand. Figure 316.4b (Site B) shows that the percentage of magnetite in fine sand decreases rather than increases with increasing velocity. Figures 316.4d and 316.4f show very little relationship between the amount of magnetite deposited in medium and coarse sands with changing water velocity.

The percentage of magnetite was also plotted against clast size in the flume (Figure 316.5). It is evident that there is very little correlation between these two variables.

A more complete report will be published once final results are obtained following heavy mineral separations and grain size analysis.

DISCUSSION

Three syngenetic models for paleoplacer formation in conglomerates at Elliot Lake were suggested by Fralick and Miall (1981, 1982). These are: 1) the uraninite and quartz pebbles both came from the same source material, and thus the uraniferous conglomerate packages represent the erosion of small sources and the local deposition of the material (mineralization and pebbles genetically linked); 2) the uraninite was deposited in the pores of an openwork gravel due to special hydraulic conditions that were created by the gravel bed (mineralization caused by the pebbles); and 3) both pebbles and uraninite represent heavy material that only extended down gradient and into the basin area during times of intense flow velocity (mineralization and pebbles causatively linked).

We favour the third mechanism, as this agrees with Pretorius' (1981) views that an increase in gradient was an important factor in the formation of some conglomeratic Witwatersrand paleoplacers, and with Fralick and Miall's (1987) contention that Elliot Lake paleoplacers were created by excessive flood events carrying coarse detritus into the basin.

Fralick and Miall (1987) used Zr/Hf ratios in samples from uraniferous conglomerates and nonmineralized sandstones of the Matinenda Formation to show that the sediments had been well mixed prior to sedimentation, and that processes operating in the area of conglomeratic deposition resulted in the formation of paleoplacers. Thus, the conditions outlined in hypothesis 1 did not occur.

Hypothesis 2 attributes the deposition of uraninite in an openwork gravel to hydraulic conditions created over the gravel bar. In order for this hypothesis to be correct, clast size should control the hydraulic conditions generated over a gravel bar and thus control the percentage of magnetite deposited therein. Examination of data obtained from the flume reveals that this is not occurring. The percentage of magnetite accumulating in the gravel bar shows little correlation with clast size (*see* Figure 316.5). Therefore, based on flume experimentation, hypothesis 2 can be rejected. However, cobble size and the percentage of magnetite are in fact related in the gravel bar sampled in the Jackpine River (*see* Figure 316.3). This is at variance with our flume data results and must be further explained.

In our opinion, clast size and the percentage of magnetite show a correlation in natural systems because they are both related to a third variable, namely velocity. This hypothesis is supported by flume data which show that flow velocity has controlled the amount of magnetite deposited in the bar (Figure 316.4). In a natural system, it is therefore logical to assume that flow velocity controls the amount of magnetite being deposited, and also controls the size of the clasts being sedimented at the same site. Thus, flow velocity influences both of these variables and leads to a correlation between them. In order for this to occur the clasts must have been in transport and subsequently deposited at the same time as the heavy minerals were accumulating. Thus hypothesis 2 can be rejected, and we are therefore left with hypothesis 3 as the most probable process operating in the formation of the Witwatersrand and Elliot Lake paleoplacers.

In the natural systems studied, it was observed that the matrix material associated with finer grained gravels contains a higher percentage of magnetite (Figure 316.3). This matrix material is also coarser grained and more poorly sorted than that of the matrix associated with larger clasts at the bar head. Larger cobbles deposited at the upstream portion of

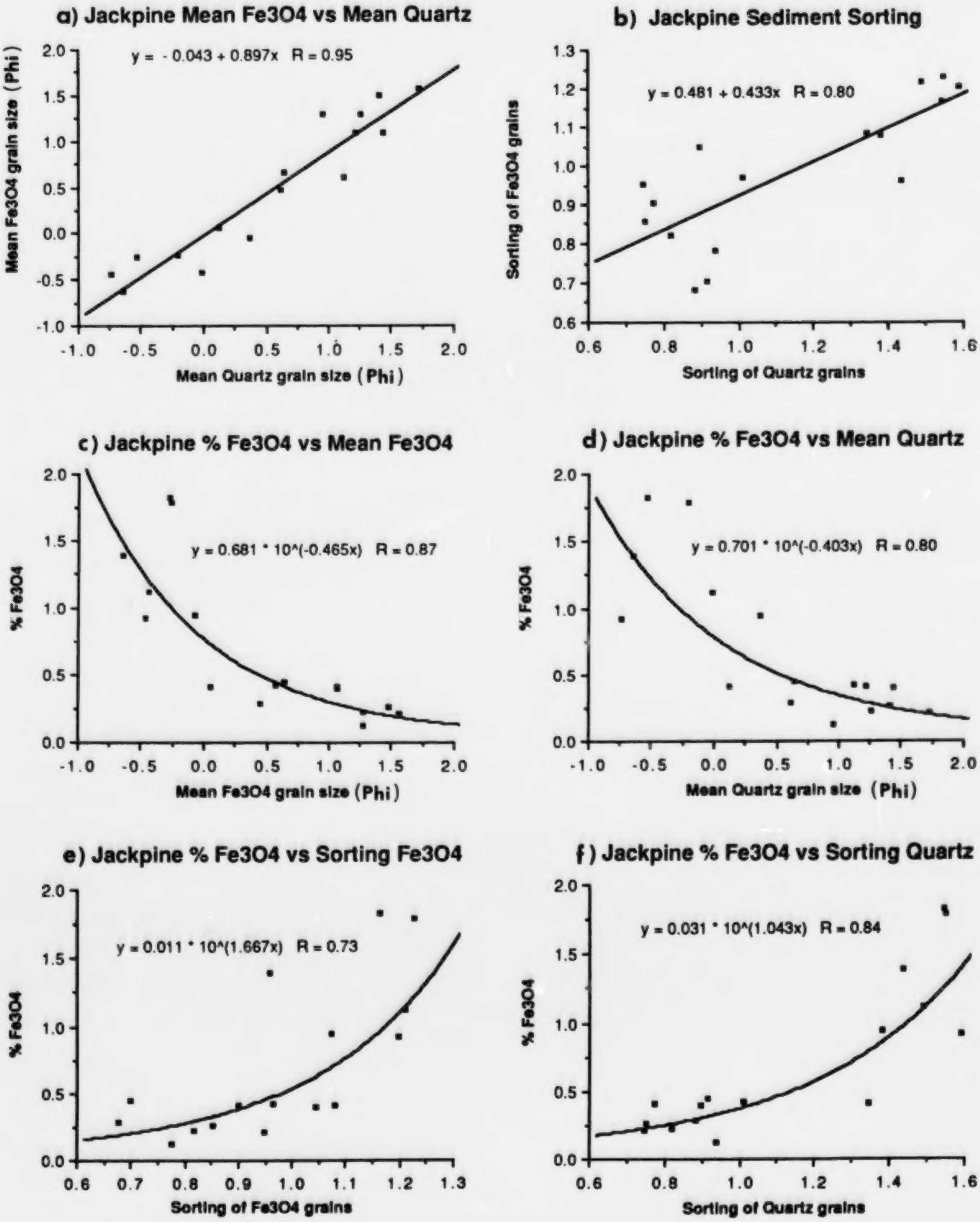

Figure 316.2. *Scatter diagrams of variables measured on matrix material sampled from a longitudinal bar; Jackpine River, north of Lake Superior, Ontario.*

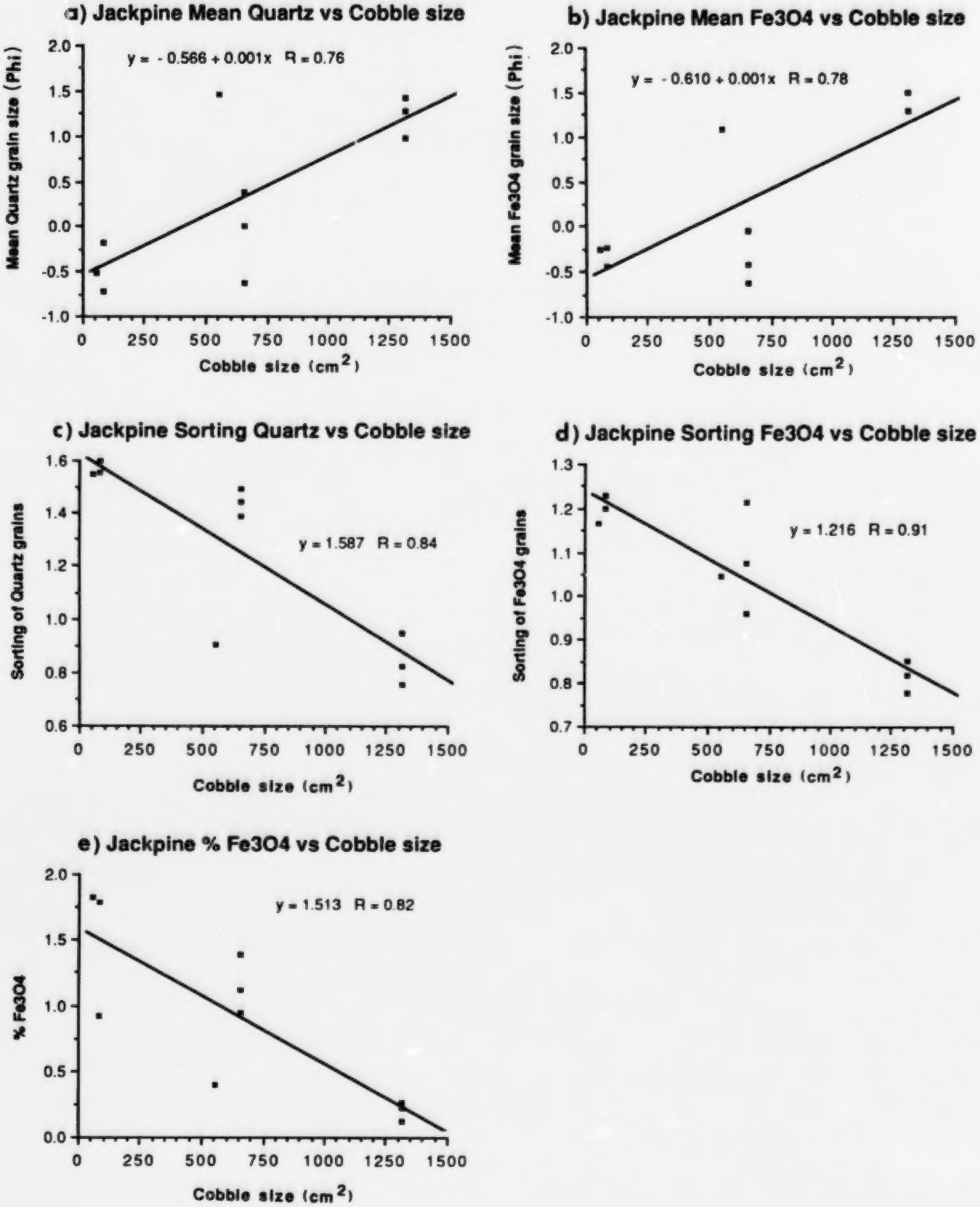

a) Jackpine Mean Quartz vs Cobble size

b) Jackpine Mean Fe3O4 vs Cobble size

c) Jackpine Sorting Quartz vs Cobble size

d) Jackpine Sorting Fe3O4 vs Cobble size

e) Jackpine % Fe3O4 vs Cobble size

__Figure 316.3.__ Scatter diagrams of variables measured on matrix material in relation to cobble size; Jackpine River, north of Lake Superior, Ontario.

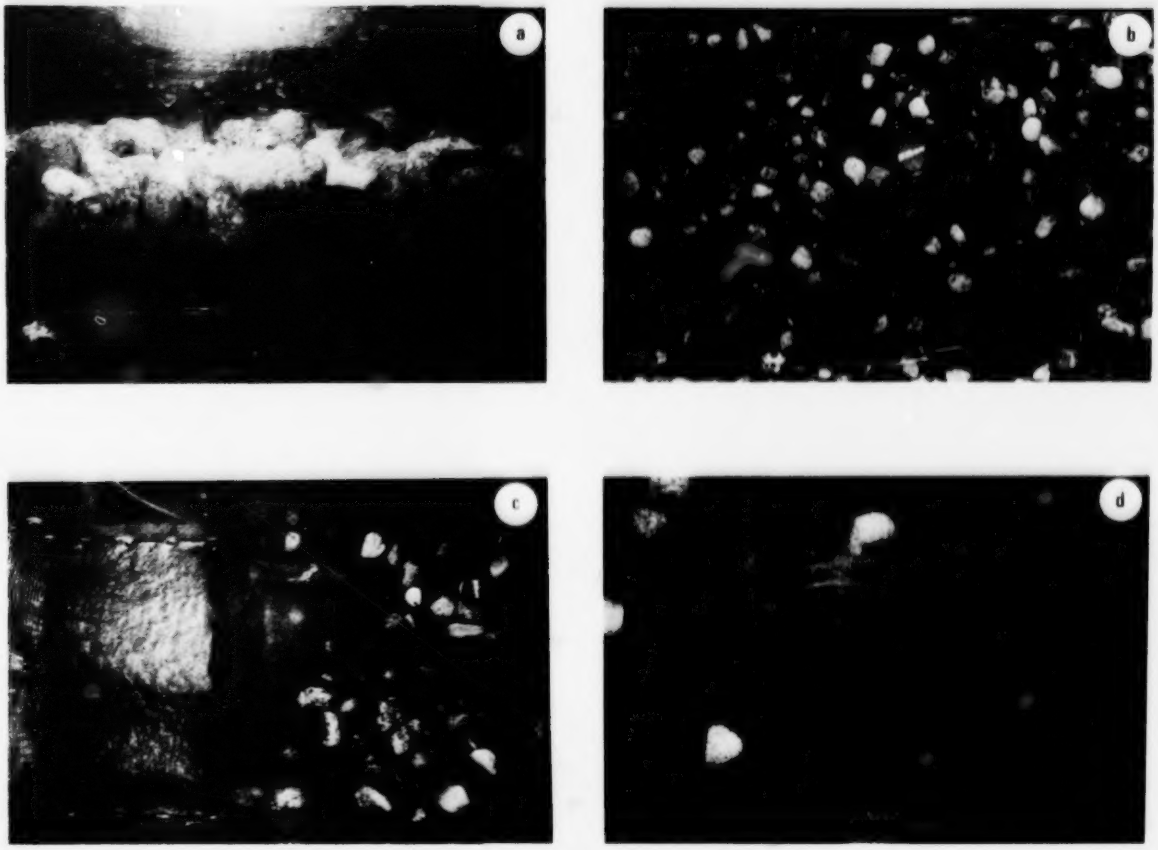

Photo 316.2. *Selected photographs from flume tank experimentation (flow directions from right to left).* ***a.*** *Photograph of openwork, medium-sized cobbles in the flume prior to an experiment.* ***b.*** *Photograph shows pebbly bar with matrix material present following a flume run.* ***c.*** *Photograph of tail section of bar showing sandy bed form prograding over previously sedimented suspension rain out deposit.* ***d.*** *Photograph of heavy mineral concentration developed on the stoss side of lunate and linguoid dunes.*

the gravel bar reflect deposition from high velocity and highly turbulent flow conditions that kept all finer grained sediment in transport. During these high discharge events, both light and heavy sediment remained in suspension, and because of the highly turbulent flow conditions acting on the bar head, this sediment was not deposited at this location. However, with the development of lower energy conditions downstream, heavy minerals were able to accumulate in finer gravels as the gravel bed was being deposited. With a reduction in river discharge and therefore energy throughout the system, finer and less dense sediments being transported by the river were then able to infiltrate the larger cobbles at the bar head. This process resulted in the accumulation of fine and better sorted sediments in the openwork cobbles. The scenario outlined above best explains the results obtained from the Jackpine River study. Data collected from the North Saskatchewan River in Alberta also supports the above proposed sequence of events. In the North Saskatchewan, the bar head generally contained openwork cobbles and matrix; where present, the matrix often showed grading in the upper few centimetres of sediment indicating deposition during waning flows.

Sand in the flume was deposited by one of two mechanisms: a) from suspension rain out (Site A); and b) from avalanche face progradation (Site B) (Photo 316.2c). Sediment deposited by avalanche face progradation has a higher percentage of magnetite than that deposited by suspension rain out. This is related to the processes that are occurring at the site where sediment is being eroded. During early erosive stripping of the medium- and coarse-grained sands, the magnetite grains formed an erosive lag on the bottom of the flume as individual grains settled into interstitial spaces between the larger quartz grains. This process results in a high pivot angle for these grains (Middleton and Southard 1984). Thus, the sand in transport was quartz rich, and when deposited in the gravel bed from suspension rain out, this deposit contained a low percentage of magnetite. As time progressed, most quartz sand grains at the surface were winnowed away, leaving a magnetite-rich lag deposit. At this time, there were no longer sufficient quartz grains to shield the magnetite and it then began to move (Photo 316.2d). The magnetite was subsequently deposited in the avalanche bed form, causing it to contain a higher percentage of magnetite than the previously formed suspension rain out deposits it advanced over (Photo 316.2c).

The fine and medium sands deposited from suspension rain out at Site A shows a positive correlation between the percentage of magnetite and velocity (Figures 316.4a and 316.4c), whereas the coarse sand shows no correlation at all (Figure 316.4e). We believe that this is caused by the magnetite moving in bed load and near-bed suspension load, while the quartz sand moves in suspension load at moderate to high velocities. Obviously there is a velocity that will result in an optimal separation of the two populations. Our curves indicate that this optimal velocity is higher than we could obtain during the flume runs. The lack of correlation in the coarse sand indicates that the quartz and magnetite components behaved similarly at the velocities used. This is an expected result, for at these flow velocities, grain sizes, and densities, neither the coarse sand nor the magnetite should have had a sizeable component moving in suspension transport.

Thus, placer formation by deposition in longitudinal gravel bars appears to be dependent upon the separation of heavy minerals from light minerals (Slingerland 1984). This results from heavy minerals being transported close to the bed while light minerals are kept mostly in suspension higher above the bed. If the light fraction contains a sizeable component in the granule size range, it is very likely that these grains will behave hydraulically similar to that of the relatively finer grained heavier minerals. Such a condition makes the formation of economic placer deposits very unlikely. Extremely high flow velocities also make placer formation difficult, as preferential deposition of heavy minerals is not likely to occur. The majority of grains in both the heavy and light fractions will travel in suspension and thus not be separated. Moreover, lower flow velocities, such as those obtained during flume experimentation, will also not result in the preferential deposition of heavy minerals. During low flows, the critical velocity required to keep light grains in suspension transport is not available, therefore, the given conditions are unable to separate the heavy fraction from the light fraction in transport. This results in an uneconomic deposit where heavy minerals, although present, have not experienced the hydraulic conditions necessary to maximize placer formation.

RELEVANCE TO EXPLORATION

The formation of placer deposits in coarse-grained longitudinal gravel bars is dependent on having the right flow velocities to cause heavy minerals to be transported near the bed while lighter minerals are kept in suspension. Thus, to be able to evaluate the velocity required to form a heavy mineral deposit, one must determine the size and density of both the heavy and light fractions in transport, and calculate the velocities at which the heavy minerals and light minerals separate. However, light sediment with a large granule-sized fraction will generally behave in a similar manner to that of the heavy minerals in transport. This process will result in the mixing of heavy minerals with granule-sized lighter sediments making the formation of a rich placer deposit unlikely.

Heavy mineral lag deposits formed during flume experimentation are representative models of many Pleistocene placer deposits formed throughout the world. Such deposits represent relatively source-proximal occurrences of heavy mineral accumulations. Much larger systems, such as those that operated to form the Witwatersrand and Elliot Lake paleoplacer deposits, must be able to transport heavy minerals over large distances, and also segregate light sediments from finer grained heavy minerals by way of depositional processes rather than erosional.

ACKNOWLEDGMENTS

Financial support for this study was provided by the Ontario Geoscience Research Grant Program 1987-88, Ministry of Northern Development and Mines. Special thanks are extended to Environment

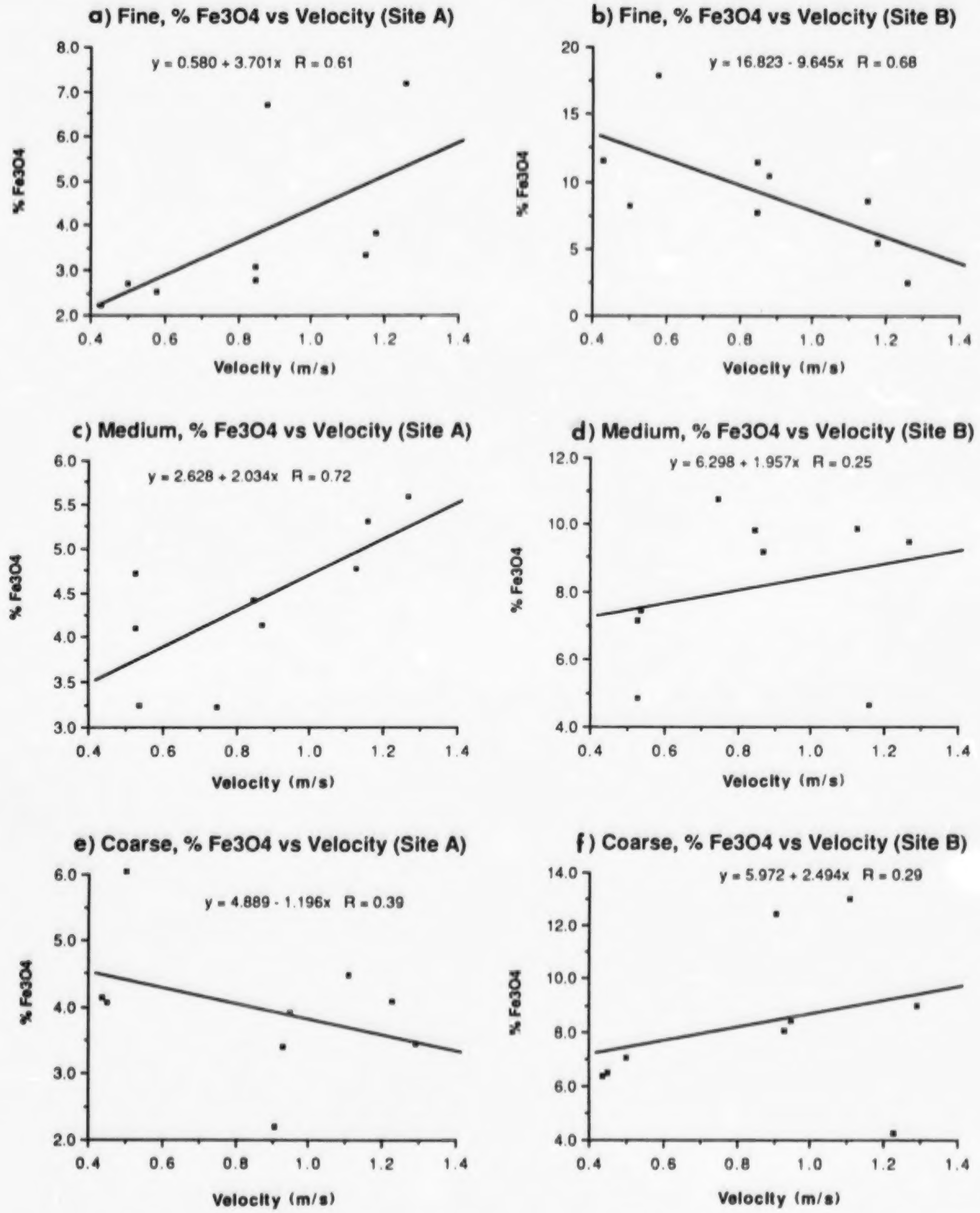

***Figure 316.4.** Scatter diagrams of the percentage of magnetite against water velocity, at two sites in the flume using three different grain sizes.*

a) Fine, % Fe3O4 vs Clast size (Site A)

b) Fine, % Fe3O4 vs Clast size (Site B)

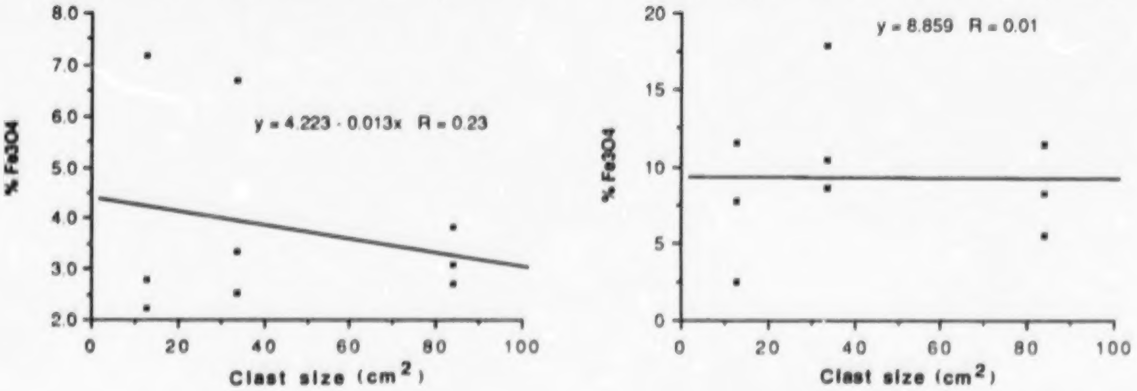

c) Medium, % Fe3O4 vs Clast size (Site A)

d) Medium, % Fe3O4 vs Clast size (Site B)

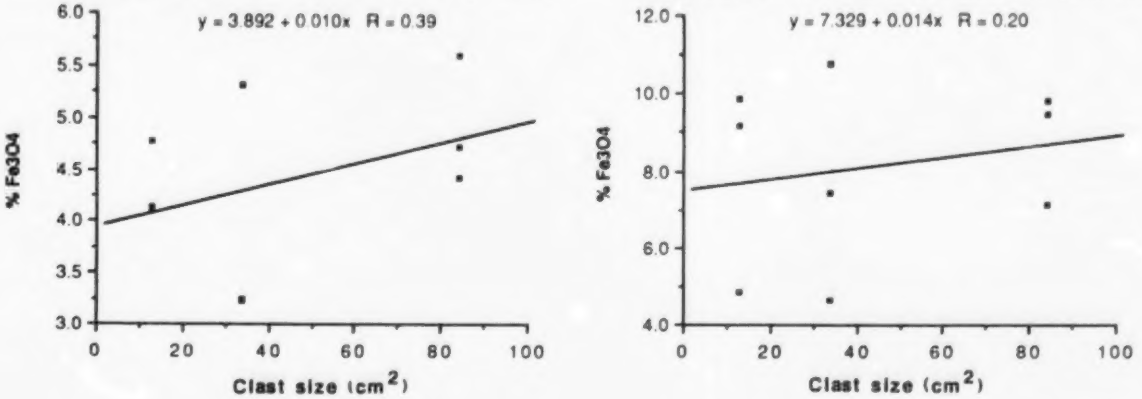

e) Coarse, % Fe3O4 vs Clast size (Site A)

f) Coarse, % Fe3O4 vs Clast size (Site B)

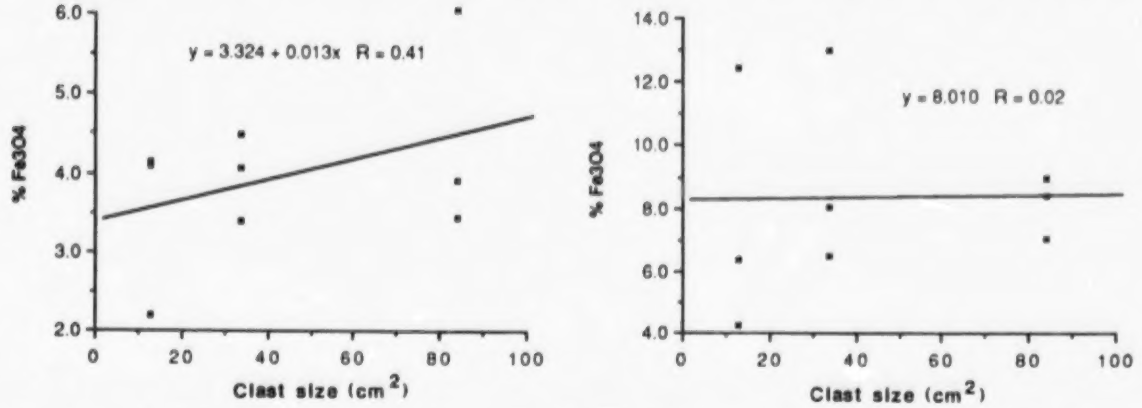

Figure 316.5. *Scatter diagrams of the percentage of magnetite in relation to clast size, in matrix sampled from suspension rain out deposits (Site A) and avalanche face progradation deposits (Site B).*

Canada, Parks, Western Region, for providing a field permit to collect samples in Banff National Park. Thanks are also extended to Sam Spivak who drafted the location maps.

REFERENCES

Fralick, P.W., and Miall, A.D.
1981: Sedimentology of the Matinenda Formation; Grant 84, p.80-89 *in* Geoscience Research Grant Program, Summary of Research 1980-81, edited by E.G. Pye, Ontario Geological Survey, Miscellaneous Paper 98, 340p.
1982: Sedimentology of Huronian Deposits, Including Uranium Bearing Rocks; Ontario Geological Survey, Open File Report 5375, 35p., 18 figures, 1 map.
1987: Glacial Outwash Uranium Placers? Evidence from the Lower Huronian Supergroup, Ontario, Canada; p.133-154 *in* Uranium Deposits in Proterozoic Quartz-Pebble Conglomerates, edited by D. Pretorius, International Atomic Energy Agency Technical Document 427, Vienna, 459p.

Middleton, G.V., and Southard, J.B.
1984: Mechanics of Sediment Movement; Society of Economic Paleontologists and Mineralogists, Short Course Number 3, 2nd Edition, Tulsa, 401p.

Minter, W.E.L., and Toens, P.D.
1970: Experimental Simulation of Gold Deposition in Gravel Beds; Transactions of the Geological Society of South Africa, Volume 73, p.89-98.

Pretorius, D.A.
1981: Gold and Uranium in Quartz-Pebble Conglomerates; p.117-138 *in* Economic Geology, 75th Anniversary Volume, edited by Brian J. Skinner, The Economic Geology Publishing Company, El Paso, Texas, 964p.

Slingerland, R.L.
1984: Role of Hydraulic Sorting in the Origin of Fluvial Placers; Journal of Sedimentary Petrology, Volume 54, Number 1, p.137-150.

Smith, N.D., and Beukes, N.J.
1983: Bar to Bank Flow Convergence Zones: A Contribution to the Origin of Alluvial Placers; Economic Geology, Volume 78, p.1342-1349.

Grant 319 Gypsum Deposits of Southern Ontario

S.J. Haynes, R. Boland, and J. Hughes-Pearl

Department of Geological Sciences, Brock University, St. Catharines

ABSTRACT

Underground mapping, at 1:10 vertical scale, of mines 2 and 3 at the Domtar Construction Materials Ltd. property, Caledonia, reveals that a wide range of facies and textures are present in the mined Main Gypsum Bed. The predominant texture is laminar in Mine 2, but alternating nodular to laminar in Mine 3. Massive, nodular, wisp, and enterolithic textures are locally present in each mine. Hassock texture occurs only in Mine 3, and chickenwire mosaic texture in Mine 2.

Stratigraphic correlation, from 1:10 scale logging of drill cores, indicates that the Main Gypsum Bed is the Salina B-Anhydrite Unit. This unit is overlain by shales and gypsiferous rocks of the Salina B Unit; and is underlain by shales, dolostone, dolomitic shales, and gypsum of the Salina A-2 Unit; dolomitic shales of the Salina A-1 Unit; and dolostones of the Guelph Formation.

Although primary evaporite textures have been modified by contraction/expansion and displacement during the dehydration of gypsum to anhydrite upon burial, and the later rehydration of anhydrite by post-Pleistocene near-surface groundwaters, they are consistent with a subaqueous coastal salina or lagoonal environment of deposition. At the Domtar property, the A and B units of the Salina Formation consist of five distinct dolomitic shale to gypsum cycles—increasing upward in gypsum content—similar to the present day coastal lagoon/estuarine environment of northern Egypt.

INTRODUCTION

All the mined gypsum deposits of southern Ontario and western New York State are hosted by the Upper Silurian Salina Group. In Ontario (Figure 319.1), gypsum mines are situated in the Niagara Peninsula on the eastern flank of the Algonquin Arch; this arch formed a positive area during the Upper Silurian, between the Michigan and Appalachian (Allegheny) basins (Sanford 1969). Commencing in the early 1800s, gypsum mining in Ontario was confined to the Grand River Valley (*see* past producers, Figure 319.1). Most of these operations were small, and the majority had closed by 1900 (Guillet 1964). Today three deposits are in active operation: Domtar Construction Materials Ltd. (Domtar), at Caledonia; Canada Gypsum, at Hagersville; and Westroc Industries, at Drumbo (Figure 319.1).

The aim of this project is to determine the geological factors controlling the distribution of economic gypsum by investigation of the following:

1. the relationship of gypsum to stratigraphy and facies variations in the Salina Formation
2. the depositional environment of the gypsum, from the detailed analysis of lithologies and sedimentary structures in the gypsum beds and their enclosing host rocks
3. the existence of major structures (folds, warps, and collapse structures)
4. the effects of post-depositional hydration/dehydration on the localization of gypsum and anhydrite, from the analysis of minor structures (veins, flow, and expansion/contraction structures), and displacement textures (nodule, mosaic, hassock, and enterolithic)

This report presents results obtained from underground mapping and core logging at the Domtar deposit.

The Domtar property contains three mines: Mine 1, now abandoned; Mine 2, the current producer; and Mine 3, under development (Figure 319.2). Core logging, at 1:10 scale, of holes drilled in 1985-86 between mines 1 and 3, (Figures 319.2, 319.3), indicates that two major gypsum beds ("Main Gypsum Bed" and "Baby Mine Bed", local usage) are present. These are underlain by a laterally semi-continuous sequence of shales, dolostones, and gypsiferous rocks overlying the Guelph Formation, and can be correlated with the A-1 and A-2 units of the Salina Formation (Figure 319.3). The Main Gypsum Bed is the only mined bed in all three mines. It is located about 183 m above sea level, 19 m above the Guelph–Salina Formation contact, and correlates with the B-Anhydrite Unit. The thickness of the Main Gypsum Bed varies from 1.8 to 2.44 m; this variation results from local changes of gypsum grade. The grade of the Main Gypsum Bed varies eastwards from 74 percent gypsum in Mine 2, to 85 percent in Mine 3.

Mine 2 employs conventional "room-and-pillar" mining techniques. Ore is subjected to primary crushing underground, and is transported to the surface by a conveyor belt system, via an incline. After preliminary examination of the underground workings within the Main Gypsum Bed, five underground vertical sections (2-1 to 2-5; Figure 319.2) were selected and mapped at 1:10 vertical scale, to determine along strike (east-west) and downdip (north-south) variations in lithology and texture. Mine 3 consisted, in 1987, of an incline and two small development drifts near the entrance. Mining is carried out by a modified Marietta cutter, resulting in a smooth curved face which is ideal for textural mapping but difficult to sample with conventional hammer and chisel. Ten sections (3-0 to 3-9; Figure 319.2) were mapped at 1:10 vertical scale.

REGIONAL GEOLOGICAL SETTING

During the Upper Silurian, the Algonquin Arch of southwestern Ontario formed a northeast-trending hingeline between the elongate Appalachian Basin of New York, Pennsylvania, and Ohio to the east and southeast, and the circular intracratonic Michigan Basin to the west (Sanford 1969). In the Michigan Basin, a carbonate/evaporite sequence was deposited throughout the Silurian (Sanford 1969; Mesolella *et al.* 1974; Gill 1977a, 1977b; Huh *et al.* 1977; Nurmi and Friedman 1977; Sears and Lucia 1980; Leonard 1983), whereas in the Appalachian Basin considerable clastic sediments and carbonates were depos-

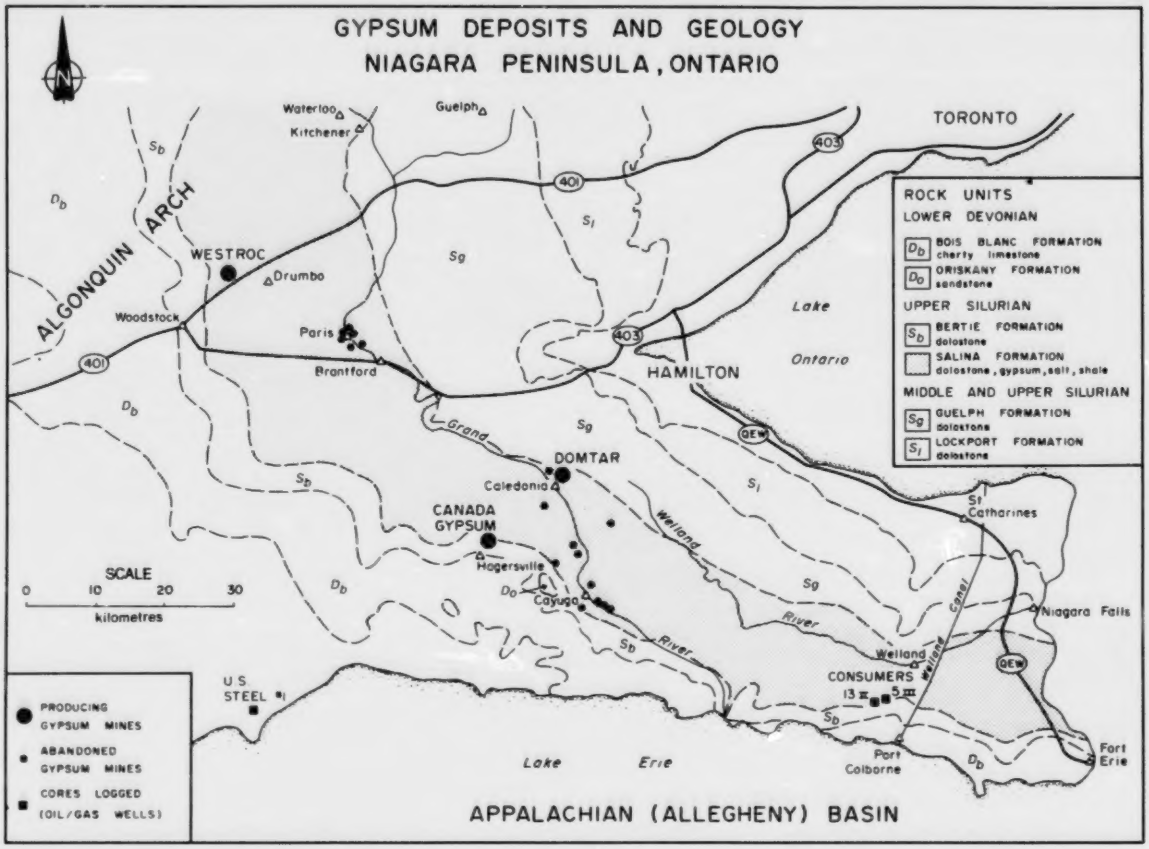
GYPSUM DEPOSITS AND GEOLOGY
NIAGARA PENINSULA, ONTARIO
N
TORONTO
Waterloo
Kitchener
Guelph
ALGONQUIN ARCH
WESTROC
Drumbo
Woodstock
Paris
Brantford
HAMILTON
Lake Ontario
401
403
QEW
Grand
DOMTAR
Caledonia
CANADA GYPSUM
Hagersville
Cayuga
Welland River
Welland Canal
St Catharines
Niagara Falls
Welland
CONSUMERS
13 II
5 III
Port Colborne
Fort Erie
U.S. STEEL #1
Lake Erie
APPALACHIAN (ALLEGHENY) BASIN
Sb
Db
Do
Sg
Sl
SCALE
0
10
20
30
kilometres
ROCK UNITS
LOWER DEVONIAN
Db BOIS BLANC FORMATION cherty limestone
Do ORISKANY FORMATION sandstone
UPPER SILURIAN
Sb BERTIE FORMATION dolostone
SALINA FORMATION dolostone, gypsum, salt, shale
MIDDLE AND UPPER SILURIAN
Sg GUELPH FORMATION dolostone
Sl LOCKPORT FORMATION dolostone
PRODUCING GYPSUM MINES
ABANDONED GYPSUM MINES
CORES LOGGED (OIL/GAS WELLS)

Figure 319.1. *Regional geology and location of gypsum deposits, Niagara Peninsula.*

ited, which thickened toward a provenance to the southeast (Alling and Briggs 1961; Sanford 1969; Treesh and Friedman 1974; Mesolella 1978). The Silurian units of both the Michigan and Appalachian basins thin over the Algonquin Arch (Sanford 1969). Consequently, the area of the Niagara Peninsula, located on the eastern flank of the Algonquin Arch (Figure 319.1), contains mixed Upper Silurian facies of both the Michigan and Appalachian basins. This has led to considerable complexity in stratigraphic correlation, notwithstanding differences in unit nomenclature between the basins, and even international differences in stratigraphic terminology across the Canada–United States border.

This is further complicated by the controversies over facies relationships and diachroneity in the Upper Silurian strata of both basins. Although a discussion of these controversies is beyond the scope of this paper, they result mainly from the lack of reliable stratigraphic time lines (due to a paucity of index fossils), easily recognized regional disconformities, and a lack of surface exposures (most of the data are derived from drillholes).

In recent years, stratigraphic subsurface correlations by the petroleum industry has relied mainly on geophysical logs. Of the different methods employed, gamma-ray logs have proven most successful in correlating the Upper Silurian units across the Michigan and Appalachian basins (Rickard 1969; Mesolella 1978; Carter, in press).

The Late Silurian rocks of the Michigan and Appalachian basins have been divided into Middle to Upper Silurian Niagaran, and overlying Upper Silurian Cayugan. In Ontario these are termed "series" (Sanford 1969), but in the United States they are referred to as "groups" (Alling and Briggs 1961). The Niagaran Series includes carbonates of the Lockport and overlying Guelph formations in the Michigan Basin, and carbonates of the Lockport Formation in the Appalachian Basin. In the Niagara Peninsula, the Guelph and Lockport formations are underlain by argillaceous dolostones of the Decew Formation (Sanford 1969). The Cayugan Series includes evaporite sequences of the Salina ("Formation" in Ontario, "Group" in the United States) that are overlain by dolostones of the Bass Island Formation in the Michigan Basin; or Bertie Formation in the Appalachian Basin, including the Niagara Peninsula (Alling and Briggs 1961; Sanford 1969). The term Salina was first applied by Dana in 1863 to outcrops of the Appalachian Basin in New York, and was subsequently subdivided, in ascending order, into the Vernon Shale, Syracuse Salt, and Camillus Shale by Clark in 1903 (Alling and Briggs 1961). Landes

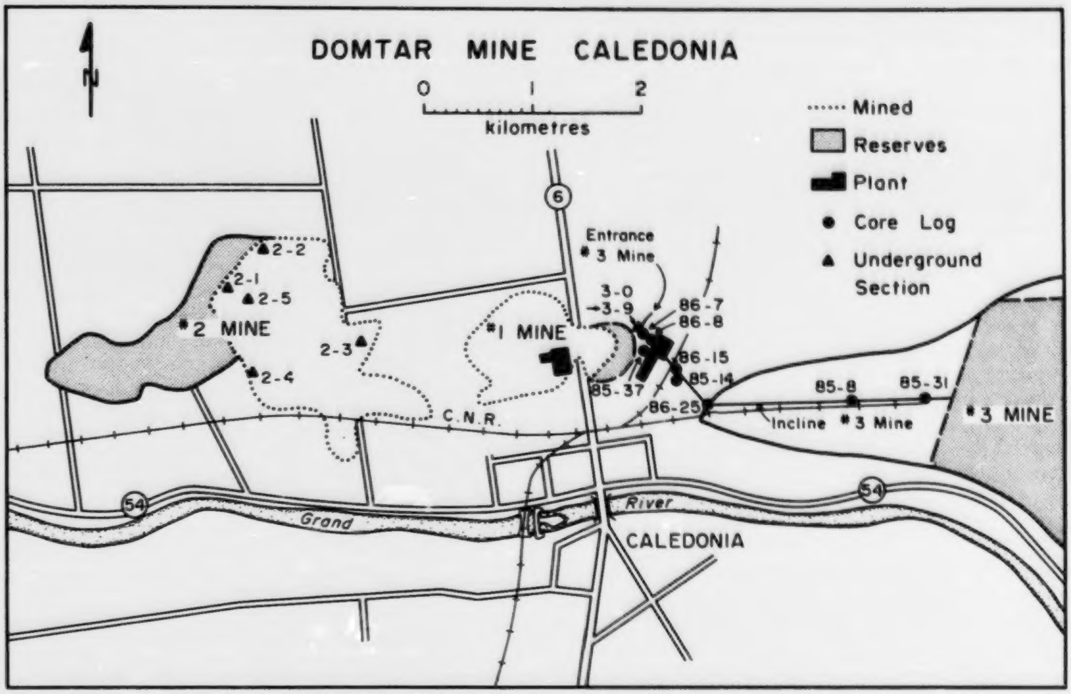
DOMTAR MINE CALEDONIA
N
0
1
2
kilometres
Mined
Reserves
Plant
Core Log
Underground Section
6
Entrance #3 Mine
2-2
2-1
2-5
#2 MINE
2-3
2-4
#1 MINE
3-0
3-9
86-7
86-8
86-15
85-14
85-37
86-25
85-8
85-31
Incline #3 Mine
#3 MINE
C.N.R.
54
Grand
River
CALEDONIA

Figure 319.2. Plan of Domtar Construction Materials Ltd. property, Caledonia, showing position of drillholes and underground sections.

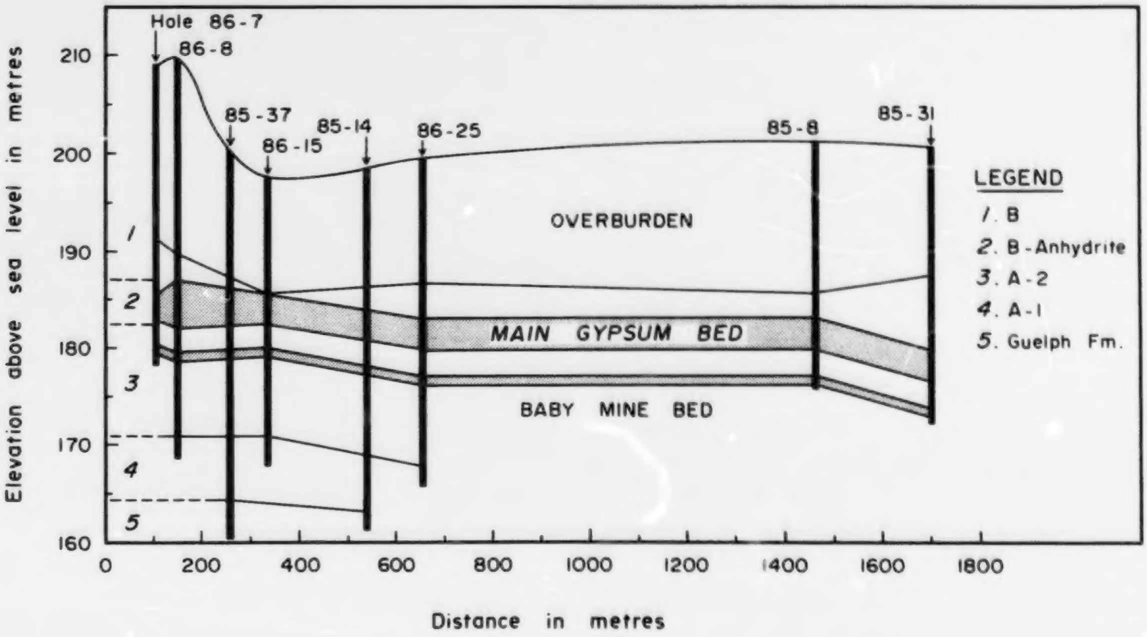
Hole 86-7
86-8
85-37
86-15
85-14
86-25
85-8
85-31
OVERBURDEN
MAIN GYPSUM BED
BABY MINE BED
1
2
3
4
5
LEGEND
1. B
2. B-Anhydrite
3. A-2
4. A-1
5. Guelph Fm.
Elevation above sea level in metres
210
200
190
180
170
160
0
200
400
600
800
1000
1200
1400
1600
1800
Distance in metres

Figure 319.3. Stratigraphic section of Domtar property.

(1945) divided the Salina Group of the Michigan Basin into eight units, A to H in ascending order. However, the G Unit is now regarded as the uppermost Salina Formation, the H Unit being equivalent to the Bass Island and Bertie formations (Alling and Briggs 1961). Evans (1950) subdivided the Salina A Unit into the A-1 evaporite, A-1 carbonate, A-2 evaporite, and A-2 carbonate. The Vernon Formation can be correlated with the Salina A, B, and C units; the Syracuse Formation with Salina D, E, and F units; and the Camillus Formation with the Salina G Unit (Alling and Briggs 1961; Rickard 1969). Mesolella (1978) demonstrated that the C, E, and G units are shales that can be correlated with gamma-ray logs over most of the area covered by the Appalachian and Michigan basins in the United States. However, recent studies by Carter (in press) have shown that all of the Salina units can be correlated by gamma-ray logs across the Algonquin Arch and Niagara Peninsula, from Ontario to New York (Figure 319.4).

The Guelph Formation marks the period of major reef growth at the close of the Niagaran and the beginning of the Cayugan times, with a fringing barrier reef (now dolomite) encircling the Michigan Basin. In Ontario, this barrier reef (marginal bank complex) developed on the western flank of the Algonquin Arch, while shallow lagoonal dolomite facies were deposited over the Niagara Peninsula to the east (Sanford 1969). Toward the centre of the Michigan Basin, pinnacle reefs and interreef facies sediments were deposited (Sanford 1969; Briggs and Briggs 1974; Nurmi 1974). The pinnacle reefs include algal, stromatoporoidal, and stromatolitic zones, while algal facies fringe the front of the barrier reef (Huh *et al.* 1977; Nurmi and Friedman 1977). Although Salina A-1 units generally overlie Niagaran strata, there is considerable dispute over the stratigraphic facies relationship between the Niagaran reefs and the Salina A-1 evaporites. Sears and Lucia (1980) consider that the Guelph marginal bank complex had formed before the deposition of the Salina A-1 evaporites. But, Sloss (1969), and Droste and Shaver (1977), consider that the Guelph reefs of the Michigan Basin, and Mesolella (1978) that the Lockport reefs of the Appalachian Basin, grew contemporaneously with the Salina A-1. However, Mesolella *et al.* (1974) consider that the A-1 evaporites overgrew the reefs in the Michigan Basin, but that the reefs were rejuvenated during later A-1 carbonate time.

SALINA FORMATION, NIAGARA PENINSULA

The marginal facies of the Salina Formation in the Niagara Peninsula, and adjacent parts of the Michigan and Appalachian basins, are presented in Figure 319.4. The anhydrite beds represent the common occurrence of calcium sulphate in the subsurface. However, within about a hundred metres from the present bedrock surface in the Niagara Peninsula, they are usually hydrated to gypsum.

The basal Salina A Unit of the Niagara Peninsula can be divided into separate A-1 and A-2 subunits that correlate with the stratigraphy of the Michigan Basin. From west to east, the halite, limestone, and anhydrite of the A-1 and A-2 subunits in the Michigan Basin change progressively to dolostone, dolomitic shales, and anhydrite in the Niagara Peninsula, with an abrupt change to shale and anhydrite in the Appalachian Basin (Figure 319.4). Over the Algonquin Arch, the basal A-2 anhydrite constitutes the mined gypsum bed of the Westroc Industries mine at Drumbo.

In contrast, the Salina B Unit in the Niagara Peninsula consists of dolomitic shales that can be correlated from the Appalachian Basin westward to the Algonquin Arch. West of the Algonquin Arch, the B Unit changes rapidly to halite in the Michigan Basin. Throughout southeastern Ontario, the base of the B Unit is characterized by an extensive anhydrite unit termed the B-Anhydrite by petroleum industry geologists (T. Carter, Chief Geologist, Petroleum Resources Section, Ontario Ministry of Natural Resources, London, personal communication, 1988). This unit constitutes the Main Gypsum Bed at the Domtar deposit.

The C Unit is present as a consistent shale horizon throughout the Salina of eastern North America.

The D Unit is absent in the Niagara Peninsula. It is characterized by halite in both the Michigan and Appalachian basins.

The E Unit consists of dolostone and shaly dolostone, with local anhydrite beds over most of southwestern Ontario. These change to more shaly facies in both the Appalachian and Michigan basins (Figure 319.4). Correlation of units between Caledonia and drillhole U.S. Steel No. 1, near the northern shore of Lake Erie, (Figure 319.1) suggests that the Canada Gypsum mine is located in the E Unit.

The lower part of the F Unit consists of a thick sequence of halite, dolomitic shales, and thin anhydrite beds in the Appalachian Basin, with a considerably thinner sequence of halite and dolostone in the Michigan Basin. These lower units are absent over the Niagara Peninsula and Algonquin Arch. The upper F Unit consists of dolostone overlain by shale, with thin anhydrite beds that can be correlated from the Appalachian Basin, across the Niagara Peninsula, to the Algonquin Arch (Figure 319.4). Westward, this changes to shale in the Michigan Basin.

The G Unit represents a progressive change from shaly dolostone with anhydrite in the Michigan Basin, to dolostone in the Appalachian Basin (Figure 319.4).

GEOLOGY OF THE DOMTAR DEPOSIT

MINE STRATIGRAPHY AND HOST ROCK LITHOLOGIES

The stratigraphic setting was determined from 1:10 scale core logging of the eight holes drilled between mines 1 and 3 (Figures 319.2, 319.3). A summary of the different lithologies, their stratigraphic positions, and postulated depositional environments is presented in Figure 319.5.

In keeping with the current mining terminology employed at the Domtar property, "gypsite" is defined in this study as a rock containing between 40 and 70 percent gypsum. This classification is based on the 70 percent cut off grade of the ore, and the 40 percent value used in the standard classification of carbonates (for example, gypsiferous dolostone

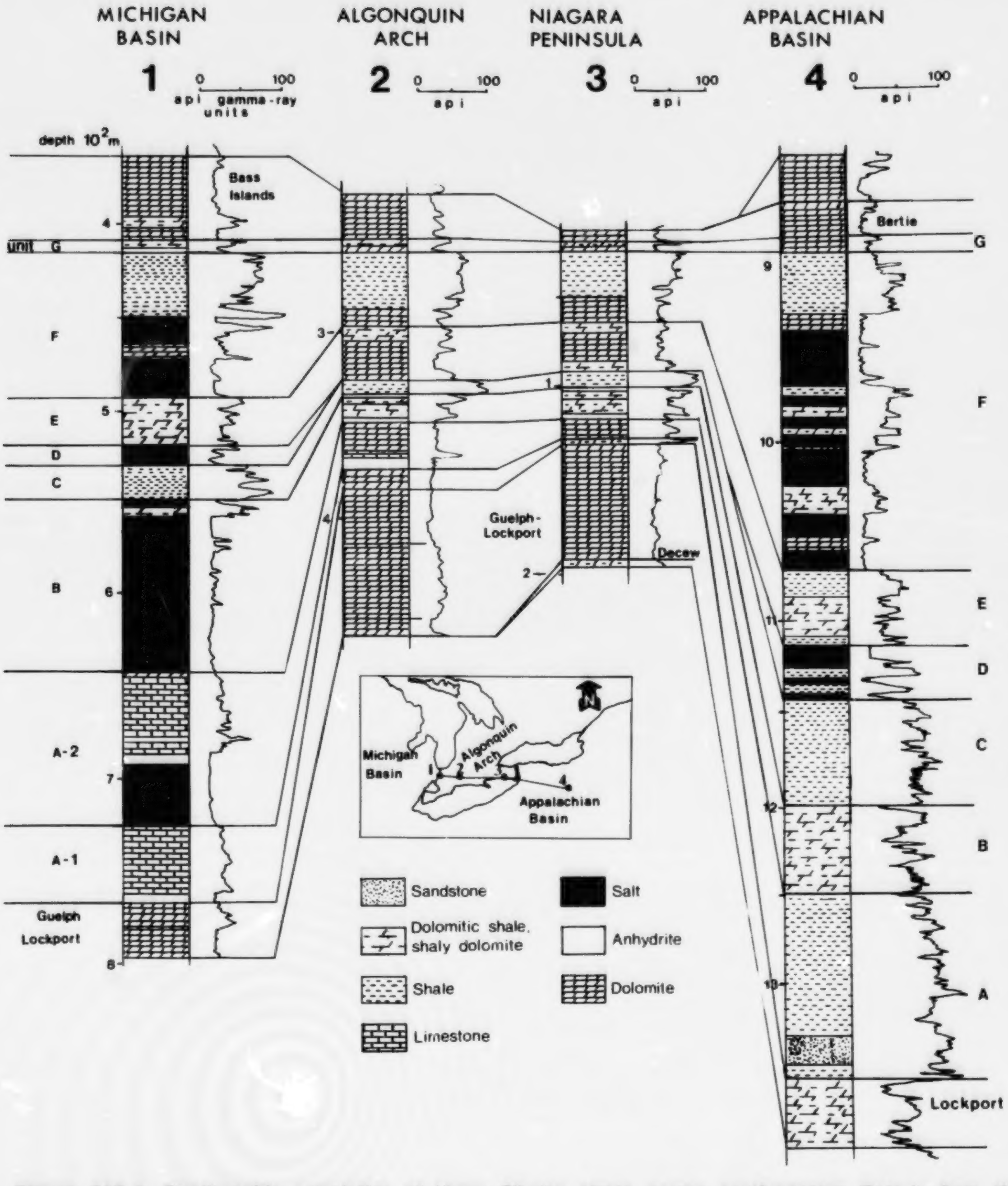
MICHIGAN BASIN
ALGONQUIN ARCH
NIAGARA PENINSULA
APPALACHIAN BASIN
1
2
3
4
0 100 api gamma-ray units
0 100 api
depth 10²m
Bass Islands
unit G
F
E
D
C
B
A-2
A-1
Guelph Lockport
Guelph-Lockport
Decew
Bertie
Lockport
A
Michigan Basin
Algonquin Arch
Appalachian Basin
N
Sandstone
Salt
Dolomitic shale, shaly dolomite
Anhydrite
Shale
Dolomite
Limestone

Figure 319.4. Stratigraphic correlation of Upper Silurian strata across southwestern Ontario from the Michigan Basin to the Appalachian Basin (modified from Carter, in press).

contains less than 40 percent gypsum). Field lithological classifications were cross-checked in the laboratory after the slabbing, polishing, and staining of samples. Although thin sections were examined, it was found that they could give misleading classifications due to their small size.

The Guelph Formation and Salina A-1 Unit were intersected in drillholes 85-14 and 85-37 (Figure 319.3). The A-1 contains 5.7 to 7.2 m of banded dolomitic shale (Figure 319.4 and 319.5). At the base of this dolomitic shale, 2 cm of green shale (only present in drillhole 85-37) underlies about 1 m of fine-grained thinly laminated grey dolostone with rip-up clasts and stringers of mudstone.

This is overlain by about 0.6 m of blue-grey gypsiferous dolostone containing nodules of gypsum. The top of the A-1 Unit consists of about 5 m of fine-grained thinly laminated dolomitic mudstones and

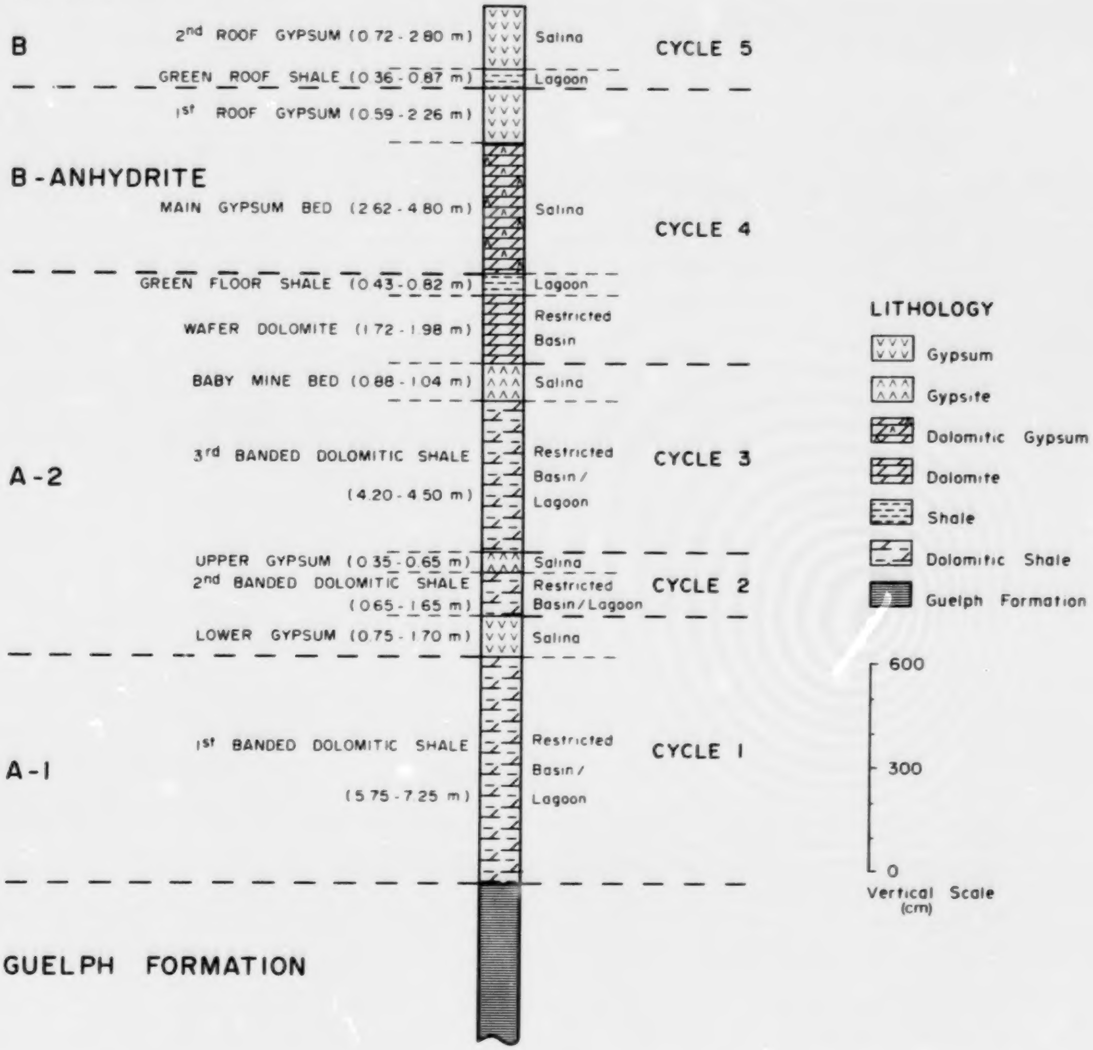
B
2nd ROOF GYPSUM (0.72 - 2.80 m)
Salina
CYCLE 5
GREEN ROOF SHALE (0.36 - 0.87 m)
Lagoon
1st ROOF GYPSUM (0.59 - 2.26 m)
B - ANHYDRITE
MAIN GYPSUM BED (2.62 - 4.80 m)
Salina
CYCLE 4
GREEN FLOOR SHALE (0.43 - 0.82 m)
Lagoon
WAFER DOLOMITE (1.72 - 1.98 m)
Restricted Basin
BABY MINE BED (0.88 - 1.04 m)
Salina
A - 2
3rd BANDED DOLOMITIC SHALE (4.20 - 4.50 m)
Restricted Basin / Lagoon
CYCLE 3
UPPER GYPSUM (0.35 - 0.65 m)
Salina
2nd BANDED DOLOMITIC SHALE (0.65 - 1.65 m)
Restricted Basin / Lagoon
CYCLE 2
LOWER GYPSUM (0.75 - 1.70 m)
Salina
A - 1
1st BANDED DOLOMITIC SHALE (5.75 - 7.25 m)
Restricted Basin / Lagoon
CYCLE 1
GUELPH FORMATION
LITHOLOGY
Gypsum
Gypsite
Dolomitic Gypsum
Dolomite
Shale
Dolomitic Shale
Guelph Formation
600
300
0
Vertical Scale (cm)

Figure 319.5. *Compilation of lithologies and their probable depositional environments, Domtar property.*

shales, with nodular patches of gypsum displacing the laminations. Small scale dewatering structures and millimetre scale displacements along microfractures are common throughout the A-1 sequence and, in places, the basal dolostone is highly contorted. Locally, fine-grained organic debris is present.

The A-2 Unit includes a lower sequence of two successions of gypsum, which are overlain by a dolomitic shale and an upper sequence of gypsum (Baby Mine Bed), dolostone ("Wafer Dolomite", local usage), and shale ("Green Floor Shale", local usage). The lower two gypsum units ("Lower Gypsum" and "Upper Gypsum", local usage; Figure 319.5) generally exhibit nodular textures with local development of laminated layers. Both of these gypsum beds vary in thickness (0.75 to 1.70 m for the Lower Gypsum, 0.35 to 0.65 m for the Upper Gypsum), have sharp upper and lower contacts, and exhibit irregular facies changes along strike from gypsum to gypsiferous dolostone. The two dolomitic shale units overlying the Lower and Upper Gypsum beds consist of repeated green to brown laminated sequences of shales, dolomitic shales, and dolomitic mudstones, with thin gypsum laminates and occasional organic-rich marl laminae. Small scale dewatering structures and microfractures are common.

The Baby Mine Bed (Figure 319.5) is remarkably consistent in thickness (0.88 to 1.04 m), and in lithology (gypsum), throughout the property (1700 m along strike; Ed Koopman, Domtar Mine Engineer, personal communication, 1988). The gypsum is white to buff in colour, and nodular to massive in texture. Brown dolomitic shale constitutes the matrix between the nodules. This is overlain by the 1.72 to 1.98 m thick Wafer Dolomite, which is predominantly dolostone with patches of dolomitic mudstone. Both dolostone and mudstone are thinly laminated, and grading is locally present. The Wafer Dolomite differs from the underlying dolomitic sequences by its high content of gypsum laminae, dissolution pits and vugs (locally infilled with gypsum), and general absence of organic material. Both upper and lower contacts are sharp. The overlying Green Floor Shale is a fissile greenish-grey shale, highly broken in core. Small nodules of gypsum are present locally. Both contacts are sharp.

The B-Anhydrite Unit is represented by the Main Gypsum Bed and the First Roof Gypsum (local usage) (Figure 319.5). Details of the Main Gypsum Bed are presented below. The base of the First Roof Gypsum often consists of shaly dolostone grading upward to gypsite and gypsum. From engineering considerations, the basal shaly dolostone is utilized as the ceiling of the mined bed, the gypsite forming a competent roof unit (0.59 to 2.26 m thick) below the incompetent Green Roof Shale (local usage).

Only the basal sequence of the B Unit is present in drill core. The lowermost unit, the Green Roof Shale, is a 0.36 to 0.87 m thick green-grey shale, in places grading laterally to thinly laminated brown dolostone. Nodular gypsum bands are present in the middle of this unit. The overlying Second Roof Gypsum (local usage) consists of 0.72 to 2.80 m of white nodular to banded gypsite with a matrix of brown dolomitic mudstone. In drillhole 85-31, this is overlain by 0.54 m of green shale, 0.66 m of white nodular and laminated gypsite, followed by 0.96 m of laminated dolomitic mudstone containing a 6 mm band of laminated and nodular gypsum.

MAIN GYPSUM BED

Underground mapping (1:10 vertical scale) was conducted at five stations at Mine 2, spread over an area of approximately 1 km^2 (Figure 319.2). At Mine 3, underground mapping was limited by current development to an area within 50 m of the base of the decline.

A compilation of the differences in lithology and textures between mines 2 and 3 is presented in Table 319.1, and graphically in Figure 319.6. The mined bed at Mine 2 is 2.39 to 4.06 m thick, and is dominated by laminated dolomitic gypsite to gypsum, containing an approximately 0.5 m thick layer of nodular to enterolithic gypsum about two-thirds up from the base. In contrast, the mined bed at Mine 3 consists of 2.62 to 4.80 m of dolomitic gypsum to gypsum, characterized by alternating nodular and laminated textures. The upper third of the mined bed contains several enterolithic layers, and a layer of massive gypsum overlain by hassocks. In both mines, a wide variety of textures are locally developed (Table 319.1; Figure 319.6), but hassock texture is absent from Mine 2, and chickenwire mosaic from Mine 3.

Variations across strike and downdip of the mined bed at Mine 2 are presented as fence diagrams in Figure 319.7 and 319.8. The greatest difference is at station 2-1, in the northwest. Here, the mined bed is predominantly laminated gypsite, with a 40 cm layer of massive gypsum not seen at other stations in the mine. Elsewhere, individual beds in the northern (station 2-2), north-central (station 2-5), southern (station 2-4), and eastern (station 2-3) parts of Mine 2 can be generally correlated downdip and across strike. At these stations, the basal and upper parts of the mined bed are mainly laminated gypsite, but the central section is variable with enterolithic textures predominant in the north, laminated with dolomite wisps predominant in the south, laminated chickenwire mosaic and enterolithic in the north-central, and nodular to laminated in the east.

The laminated textures appear to be primary sedimentary features. Nodules displace the laminations and are interpreted as secondary diagenetic features, formed either by the burial dehydration of gypsum to anhydrite, in the manner proposed by Shearman (1978, 1983), or by the hydration of anhydrite to gypsum by Holocene near-surface groundwaters after postglacial uplift. As Shearman (1978, 1983) has pointed out, the growth of anhydrite nodules can lead to mosaic textures. As calcium is removed from diagenetic brines during the growth of anhydrite nodules, the Mg:Ca ratio of the brines will increase, allowing the conversion of aragonite to dolomite. Dolomite in the laminations and nodule matrix at the Domtar property is micritic in thin section. Therefore, it could have formed penecontemporaneously (for example, in a sabkha), or diagenetically from subaqueous aragonite. The dolomite wisps may have formed originally as discontinuous thin layers of dolomite or aragonite that were later displaced as nodules grew and coalesced. In thin section, broken laths of gypsum are present in many nodules. This is indicative of displacement growth (Shearman 1978, 1983).

The hassocks, found only in Mine 3, may have formed by lateral growth of nodules or, alternatively, during soft-sediment deformation of primary subaqueous gypsum. Similarly, the enteroliths may have formed during either primary subaqueous growth (Brantley *et al.* 1984), penecontemporaneously during supratidal subaerial growth (Warren and Kendall 1985), or diagenetically upon burial transformation to anhydrite (Dean *et al.* 1975). Postglacial hydration of anhydrite to gypsum may have produced at least some of the enterolithic displacement textures.

DEPOSITIONAL ENVIRONMENT, DOMTAR DEPOSIT

Although numerous papers have discussed the depositional environment of the evaporites of the Michigan and Appalachian basins, previous models for the sedimentary environment of gypsum/anhydrite precipitation can be divided into three main groups:

1. subaqueous deposition of gypsum within, or at the margins of, a large barred basin (for example, Dellwig and Evans 1969; Matthews and Egleson 1974; Sonnenfeld 1985)
2. intratidal to supratidal deposition of gypsum and/or anhydrite on marine sabkha flats (for example, Treesh and Friedman 1974; Nurmi and Friedman 1977; Gill 1977b)
3. deposition of the A-1 Carbonate of the Michigan Basin in nonmarine ephemeral (playa) lakes (Leonard 1983; Straw 1985)

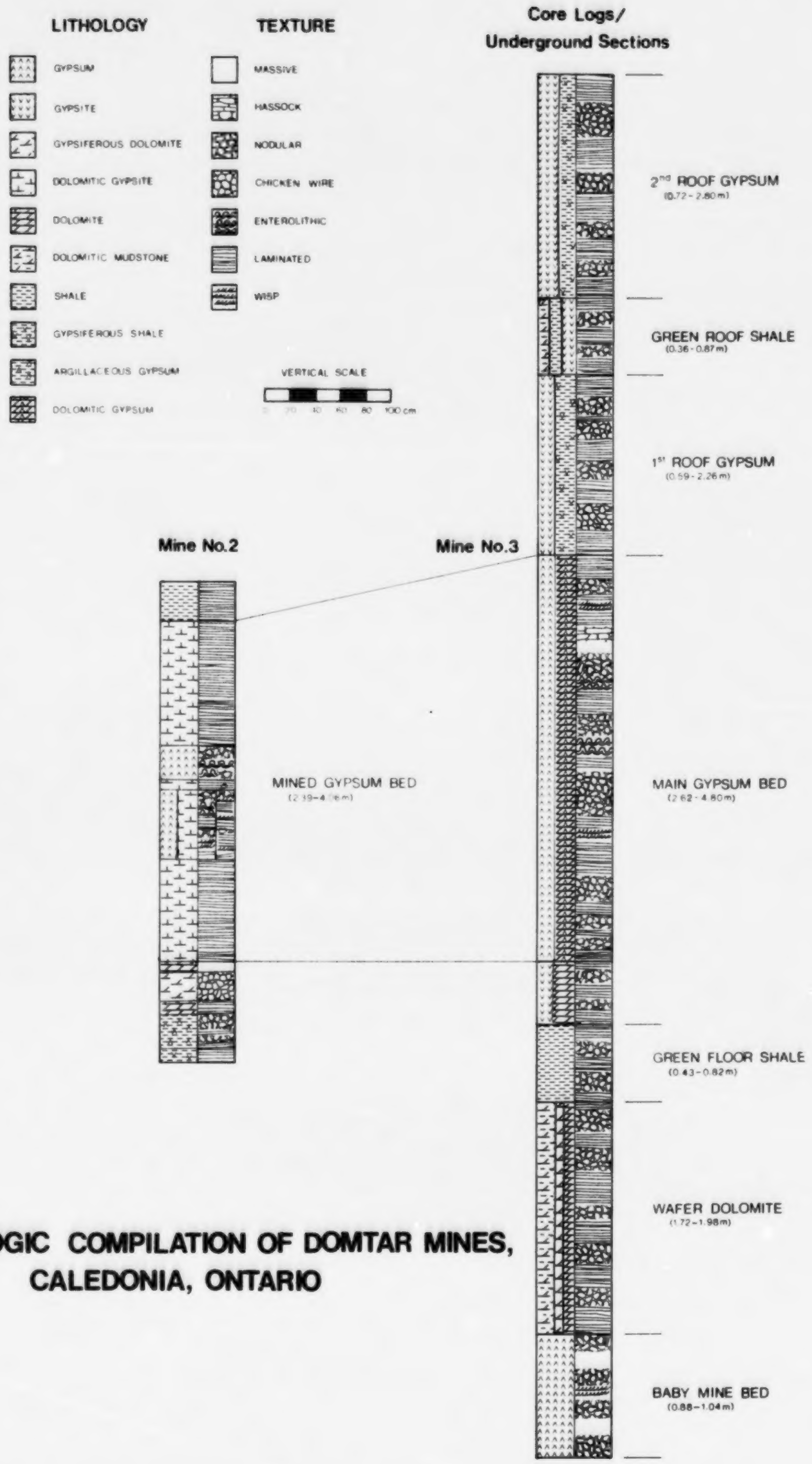
LITHOLOGY
GYPSUM
GYPSITE
GYPSIFEROUS DOLOMITE
DOLOMITIC GYPSITE
DOLOMITE
DOLOMITIC MUDSTONE
SHALE
GYPSIFEROUS SHALE
ARGILLACEOUS GYPSUM
DOLOMITIC GYPSUM
TEXTURE
MASSIVE
HASSOCK
NODULAR
CHICKEN WIRE
ENTEROLITHIC
LAMINATED
WISP
VERTICAL SCALE
0 20 40 60 80 100 cm
Core Logs/
Underground Sections
2nd ROOF GYPSUM
(0.72 - 2.80 m)
GREEN ROOF SHALE
(0.36 - 0.87 m)
1st ROOF GYPSUM
(0.59 - 2.26 m)
Mine No.2
Mine No.3
MINED GYPSUM BED
(2.39–4.06 m)
MAIN GYPSUM BED
(2.62 - 4.80m)
GREEN FLOOR SHALE
(0.43–0.82m)
WAFER DOLOMITE
(1.72–1.98m)
GEOLOGIC COMPILATION OF DOMTAR MINES,
CALEDONIA, ONTARIO
BABY MINE BED
(0.88–1.04m)

Figure 319.6. *Compilation of lithologies and textures in the Main Gypsum Bed and enclosing host rocks at mines 2 and 3, Domtar property.*

TABLE 319.1: COMPARISON OF MAIN GYPSUM BED AT MINES 2 AND 3 DOMTAR CONSTRUCTION MATERIALS LTD., CALEDONIA

	MINE #2	MINE #3 ACCESS
Ore Grade	74% gypsum	80-85% gypsum
Lithologies	gypsum, gypsite, dolomitic gypsite, dolomitic gypsum	gypsum, dolomitic gypsum
Facies Changes	highly variable vertically and horizontally	generally consistent vertically and horizontally
Predominant Texture	laminated	nodular
Textures Present	massive, nodular, enterolithic, chicken-wire, laminated, wisps	massive, nodular, enterolithic, wisps, laminated, hassock
Textures Absent	hassock; massive rare	chicken-wire mosaic
Textural Variation	rapid changes within and between sub-units	generally consistent within and between sub-units
Nodular Texture	mainly restricted to middle part of Main Gypsum Bed	distributed throughout Main Gypsum Bed
Nodule Orientation	elongated in several directions	horizontal elongation
Laminated Texture	only minor small nodules present	laminations follow nodule outlines between nodular sub-units
Contacts between Sub-Units	usually undulation and not easily traced laterally	usually horizontal and easily traced laterally, sharp
Structure	sub-units laterally pinch and swell	sub-units planar
Selenite Partings	common and regular	absent
Dark Brown Mud Bands (Markers)	minor, 0.5 cm thick	common and distinctive, 1.0 cm thick

Evidence used to support these different models is based largely on textures observed in "selected" drill cores. However, this study clearly demonstrates the wide variation of textures seen underground at Domtar Mine 2, and that textures deduced from cores drilled at Mine 3 were discovered to be erroneous when the development drifts were driven. Furthermore, several textures considered as definitive of the supratidal sabkha deposition of anhydrite (for example, laminations, nodules, and enteroliths) can in fact result from the subaqueous deposition of gypsum in hypersaline marine basins, intratidal flats, and even desert playas (Dean *et al.* 1975), the gypsum converting to anhydrite upon burial.

Although specific textures and lithologies of the Main Gypsum Bed, and adjacent units, can apply to all three previous models, none are particularly satisfactory. A large barred basin would likely deposit laterally extensive units of consistent lithology and texture over several kilometres (for example, Figure 1 and 2 *in* Dean *et al.* 1975). This is inconsistent with the rapid variation in facies and textures observed in most of the units at the Domtar property.

The concept of large barred basins can be criticized on the grounds that no modern analogues are presently forming. However, gypsum is presently precipitating in the upper reaches of a long estuarine inlet (Bocana de Virrila) in Peru (Morris and Dickey 1957; Brantley *et al.* 1984). This is evidence for gypsum precipitation in shallow restricted marine basins up to about 20 km from the coast, in an area of continental playas and desert dunes. The Domtar property deposit could have formed in a similar environment. In the modern bocana, the interlocking prismatic growth of gypsum is actively deforming the subaqueous gypsum layers into buckles, and even small isoclinal folds (Brantley *et al.* 1984). Thus, enterolithic gypsum layers are not definitive evidence for subaerial sabkha deposition, as advocated by many workers (for example, Warren and Kendall 1985).

A sabkha model would require evidence of subaerial deflation surfaces, porous host rocks beneath the gypsum beds (upward transpiration of marine "groundwater"), and predominantly brown coloured host rocks similar to those present in the oxidizing environment existing in the middle and upper sabkhas of the Persian Gulf. Although brown coloured units are present at the Domtar property (and sabkhas may have existed), most units are grey to green; the Main Gypsum Bed is directly underlain by the Green Floor Shale which has the attributes of an anaerobic lagoonal or bocana mud. Sabkha models are currently popular, possibly due to the large number of worldwide studies of modern sabkhas. However, none of these studies have reported laterally consistent beds of high grade gypsum/anhydrite as thick as the Main Gypsum Bed (up to 4.80 m).

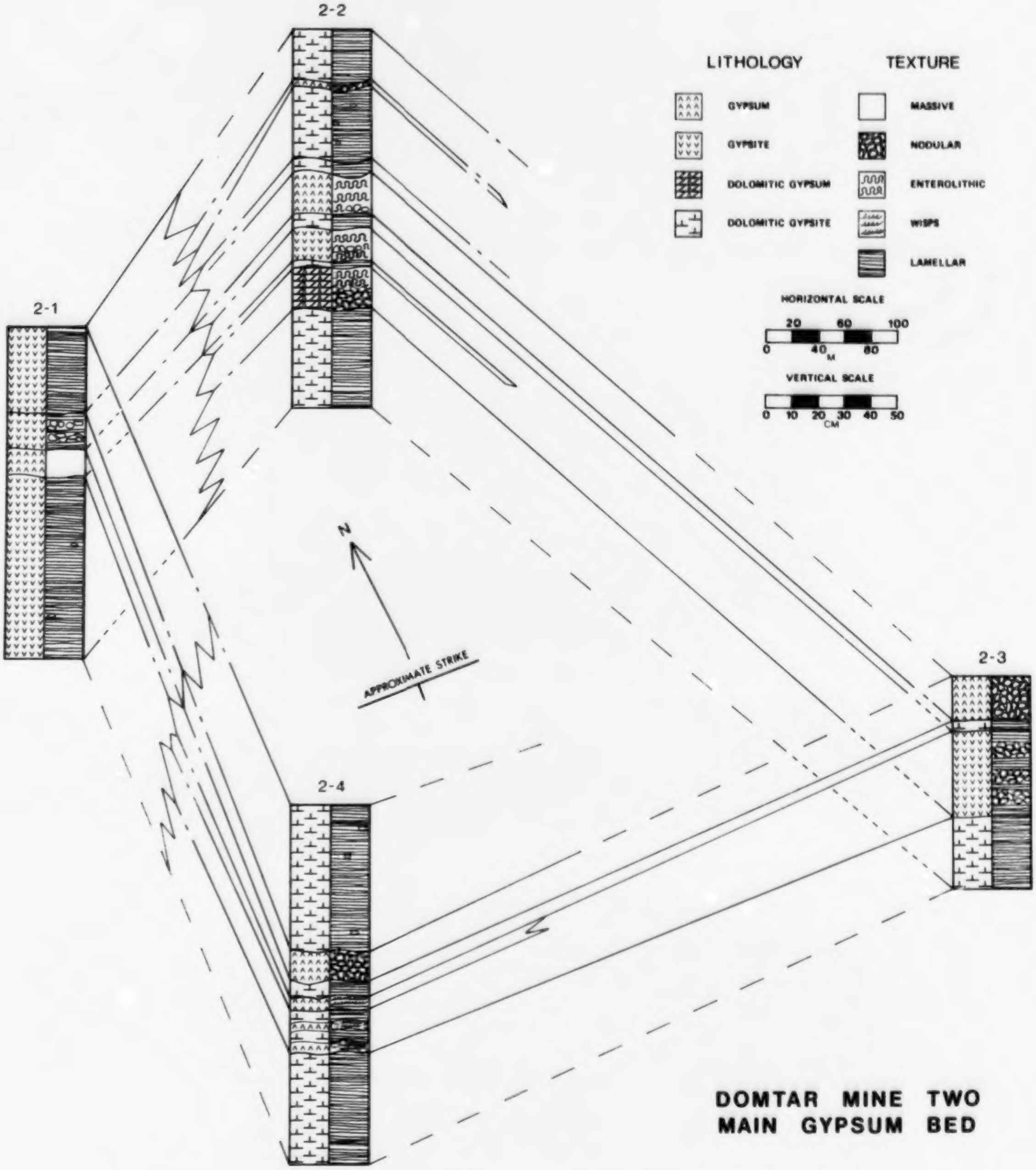
2-2
2-1
2-3
2-4
LITHOLOGY
TEXTURE
GYPSUM
GYPSITE
DOLOMITIC GYPSUM
DOLOMITIC GYPSITE
MASSIVE
NODULAR
ENTEROLITHIC
WISPS
LAMELLAR
HORIZONTAL SCALE
20 60 100
0 40 80
M
VERTICAL SCALE
0 10 20 30 40 50
CM
N
APPROXIMATE STRIKE
DOMTAR MINE TWO
MAIN GYPSUM BED

Figure 319.7. *Fence diagram of lithological and textural variations within the Main Gypsum Bed at Mine 2, illustrating variations along and across strike. Locations of underground sections are given in Figure 319.2.*

A continental playa model should exhibit evidence of desiccation (mud cracks and breccias), although these features could be dissolved during annual rainy seasons. Warren (1982a, 1983a) describes currently mined gypsum (>95 percent pure) in both continental playas, and adjacent wind blown lunettes (about 2 m thick), in an area of eolian carbonate dunes and calcretes within 200 km of the coast of South Australia. The grain size of carbonate and gypsum sediments ranges from silt to sand size. Lunettes and dunes display steep slopes and a variety of dune bedding features. Dune features (cross-bedding, adhesion ripples, etc.) were not observed in the sequences at the Domtar property.

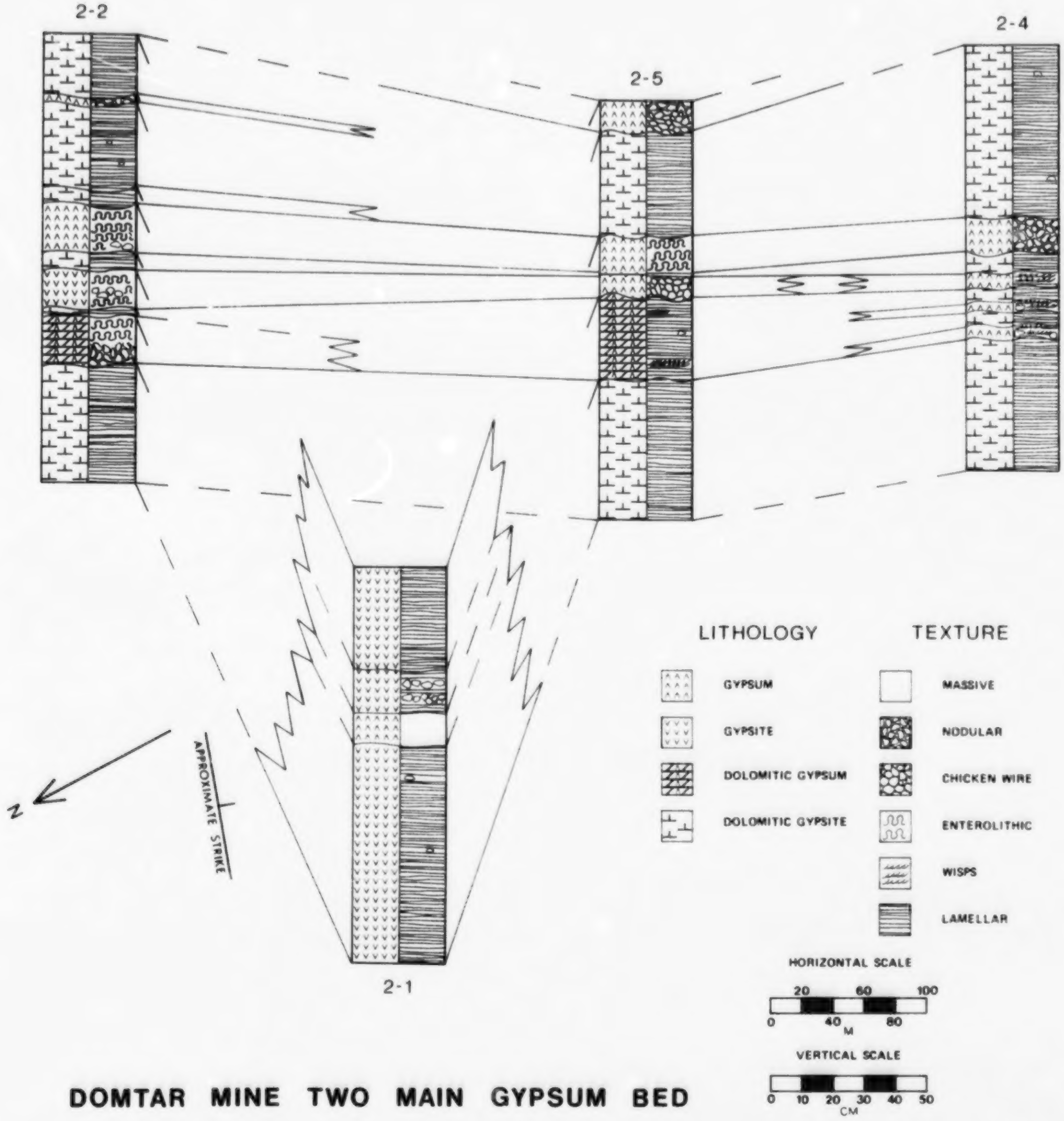
2-2
2-5
2-4
2-1
N
APPROXIMATE STRIKE
LITHOLOGY
GYPSUM
GYPSITE
DOLOMITIC GYPSUM
DOLOMITIC GYPSITE
TEXTURE
MASSIVE
NODULAR
CHICKEN WIRE
ENTEROLITHIC
WISPS
LAMELLAR
HORIZONTAL SCALE
0 20 40 60 80 100
M
VERTICAL SCALE
0 10 20 30 40 50
CM
DOMTAR MINE TWO MAIN GYPSUM BED

Figure 319.8. *Fence diagram of lithological and textural variations within the Main Gypsum Bed at Mine 2, illustrating downdip (north-south) continuity, and across strike discontinuity of lithologies. Locations of underground sections are given in Figure 319.2.*

A more viable model for the succession at the Domtar property is initial deposition of the dolomitic shale units in restricted coastal basins or lagoons. Infilling of the basins, and isolation from the sea by eolian carbonate dunes, or marine bars, created coastal salinas similar to Holocene coastal salinas (mined for gypsum) in South Australia (Warren 1982a, 1982b, 1983b, 1986); brine ponds of the southern Sinai, Red Sea (Gavish 1980); and hypersaline lagoons of northeastern Egypt (West *et al.* 1983). These modern coastal salinas are replenished by marine waters passing through the seaward subsurface barrier, due to the hydrological head created when water levels in the salina are lowered by evaporation. Massive gypsum is precipitated when hypersaline conditions are reached. As the salinas become infilled, the amount of marine water inflow diminishes with the resultant decrease in hydrological head. Eventually a critical point is reached when fresh water, during rainy seasons, dilutes the salina enough for aragonite to precipitate. Rapid vertical movement of the salina halocline from wet to dry periods leads to the formation of laminated gypsarenite. Thus, textures between individual salinas vary from massive to laminated to nodular, depending on the amount of freshwater dilution. Also, massive gypsum layers can form above laminated gypsum sequences during periods of extended drought. If the salinas dry out completely, tepee structures, mud cracks, and desiccation breccias form. However, these can dissolve during rainy periods or marine transgressions. On the flanks of South Australian salinas, carbonate boxworks develop, and stromatolites can proliferate along freshwater channelways. Warren and Kendall (1985) emphasize that salinas and sabkhas are not mutually exclusive. However, salinas form elliptical bull's-eyes of gypsum ringed by carbonate, whereas sabkhas form planar patterns along strike. Salinas, hypersaline lagoons, and bocanas are situated adjacent to both sabkha tidal flats, and continental sabkhas and salinas in South Australia, northern Egypt, the southern Sinai, and Peru, where they pass upward into sabkhas on infilling or marine regression. Thus, primary aragonite formed in subaqueous salinas can be dolomitized by later transpiring groundwaters.

Some gypsiferous lagoons are dominated by clastics. In the Bardawill Lagoon of northern Egypt, gypsum is underlain and flanked by clay and silt sized sediments (Levy 1980), a situation similar to that of the green shale underlying the Main Gypsum Bed at the Domtar property.

The dimensions and sequence of facies changes in the Salina Formation A and B units, across the Algonquin Arch from the Michigan to Appalachian basins, is analagous to the modern evaporites bordering the Sinai block between the Mediterranean and Red seas. The Algonquin Arch and Sinai Block are both positive areas underlain by Precambrian rocks, and flanked by evaporitic basins. In the northern Sinai (West *et al.* 1983), estuarine muds of the Nile delta are flanked by inland sabkhas (playas) depositing halite (for example, the Great Bitter Lake); coastal salinas depositing gypsum (for example, Lake Manzala), or halite (for example, Lake Maryut); and coastal lagoons depositing gypsum (for example, El-Alamein Lagoon), or gypsum and halite (for example, Bardawill Lagoon).

Sakbhas depositing gypsum nodules lie inland of the coastal salinas, and along the intervening stretches of coast. Southward from the Mediterranean, modern sedimentation is characterized by muds of the Nile Valley, and flanking eolian sediments and playas. Along the Red Sea, brine pools and sabkhas (Gavish 1980) are the coastal equivalents of offshore marine carbonates and clastics. Thus, it is tempting to consider the Mediterranean Basin as the modern equivalent of the Appalachian Basin (both foreland basins to orogenic belts), the Sinai an equivalent of southwestern Ontario (both as positive areas), and the Red Sea as an equivalent of the Michigan Basin (both areas of cratonic tectonism). However, this is conjectural. The importance of the comparison of the Michigan and Appalachian basins with the northern and southern Sinai, is that this modern environment clearly illustrates the likelihood that Upper Silurian lagoons, salinas, sabkhas, estuaries, and continental playas were all active within relatively short distances of each other, in both the Michigan and Appalachian basins. Also, changes of sea level, and/or differential vertical movement, would have caused the oscillation of the ancient shorelines back and forth across the Algonquin Arch, resulting in successive vertical changes of facies from subaqueous to subaerial. This comparison reconciles many of the controversies concerning the depositional environments of the Michigan and Appalachian basins.

On burial of the Domtar property sequence, gypsum converted to anhydrite. This may have resulted in the generation, of at least part, of the nodular gypsum textures present in the sequence. Post-Pleistocene uplift allowed the rehydration to gypsum by near-surface groundwaters. The approximately 30 percent volume gain probably created the further growth of nodular textures in the laminated layers of the Main Gypsum Bed. This resulted in displacement textures, hassocks, and dolomite wisps.

The Salina Formation sequence at the Domtar property appears to consist of five dolomitic shale to gypsum cycles of restricted lagoonal basins infilling to salinas, with each cycle becoming progressively enriched in gypsum (Figure 319.5).

CONCLUSIONS

Barred basin, continental playa lake, and supratidal models of primary gypsum/anhydrite deposition for the Domtar property sequence cannot be entirely discounted. However, a subaqueous coastal salina/lagoonal model is preferred for the following reasons:

1. The host dolostones, dolomitic shales/mudstones, and shales exhibit subaqueous features (dewatering structures), and generally green to grey colours indicative of relatively anaerobic environments of deposition.
2. The thickness and predominance of laminated layers, alternating with nodular to massive layers, and the relative paucity of enteroliths in the Main Gypsum Bed, is closer to textures of modern coastal salinas and lagoons than to those of sabkhas.
3. Deflation surfaces and desiccation structures are not obvious.
4. Gypsum nodules are present in many of the shales, indicating mesosaline to hypersaline basinal deposition.
5. Individual rock units display variations in lithology and texture across the Domtar property deposit consistent with an original depositional environment of small lagoons or bocanas. Five cycles of lagoonal/restricted basin sedimentation are present in the A and B units of the Salina Formation, each culminating in the deposition of gypsum.
6. Although displacement textures may have resulted from the hydration of anhydrite to gypsum by Holocene groundwaters, they could be primary subaqueous textures, similar to those presently forming in the Bocana de Virrila in Peru.

It is suggested that a modern analogue for the Upper Silurian strata across the positive high between the Michigan and Appalachian basins (Algonquin Arch) is the Sinai Peninsula, where sedimentation in coastal salinas and lagoons, sabkhas, continental playas, and an estuarine delta are all active within 100 km of each other. This comparison explains the apparently contradictory evidence put forward by previous authors, for subaqueous, supratidal, and subaerial environments during Salina A Unit time.

ACKNOWLEDGMENTS

We particularly wish to thank Ray Hartviksen (Exploration Manager) and Ed Koopman (Mine Engineer), of Domtar Construction Materials Ltd., without whose help and encouragement this project would not have been possible. Penny Kent typed the manuscript. Diagrams were drafted by Peter Brown, Steve Leonard, and J. Hughes-Pearl.

REFERENCES

Alling, H.L., and Briggs, L.I.
1961: Stratigraphy of Upper Silurian Cayugan Evaporites; American Association of Petroleum Geologists, Bulletin, Volume 45, Number 4, p.515-547.

Brantley, S.L., Crerar, D.A., Moller, N.E., and Weare, J.H.
1984: Geochemistry of a Modern Marine Evaporite: Bocana de Virrilá, Peru; Journal of Sedimentary Petrology, Volume 54, Number 2, p.447-462.

Briggs, L.I., and Briggs, D.Z.
1974: Niagara-Salina Relationships in the Michigan Basin; p.1-23 *in* Silurian Reef-Evaporite Relationships, edited by R.V. Kesling, Michigan Basin Geological Society Field Conference, 111p.

Carter, T.
In Press: A Comparison of the Middle Proterozoic Balmat Evaporite Sequence with Niagaran and Cayugan Strata in the Michigan-Appalachian Basin; Proceedings of the Ontario Petroleum Institute, Twenty Sixth Annual Conference.

Dean, W.E., Davies, G.R., and Anderson, R.Y.
1975: Sedimentological Significance of Nodular and Laminated Anhydrite; Geology, Volume 3, Number 7, p.365-372.

Dellwig, L.F., and Evans, R.
1969: Depositional Processes in Salina Salt of Michigan, Ohio, and New York; American Association of Petroleum Geologists, Bulletin, Volume 53, Number 4, p.949-956.

Droste, J.A., and Shaver, R.H.
1977: Synchronization of Deposition: Silurian Reef-Bearing Rocks on Wabash Platform with Cyclic Evaporites of Michigan Basin; p.93-109 *in* Reefs and Evaporites—Concepts and Depositional Models, edited by J.H. Fisher, American Association of Petroleum Geologists, Studies in Geology, Number 5, 196p.

Evans, C.S.
1950: Underground Hunting in the Silurian of Southwestern Ontario; Proceedings of the Geological Association of Canada, Volume 3, p.55-85.

Gavish, E.
1980: Recent Sabkhas Marginal to the Southern Coasts of Sinai, Red Sea; p.233-251 *in* Hypersaline Brines and Evaporitic Environments, Elsevier, New York.

Gill, D.
1977a: The Belle River Mills Gas Field: Productive Niagaran Reefs encased by Sabkha Deposits, Michigan Basin; Michigan Basin Geological Society, Special Paper Number 2, 187p.
1977b: Salina A-1 Sabkha Cycles and the Late Silurian Paleogeography of the Michigan Basin; Journal of Sedimentary Petrology, Volume 47, Number 3, p.979-1017.

Guillet, G.R.
1964: Gypsum in Ontario; Ontario Department of Mines, Industrial Mineral Report Number 18, 126p.

Huh, J.M., Briggs, L.I., and Gill, D.
1977: Depositional Environments of Pinnacle Reefs, Niagara and Salina Groups, Northern Shelf, Michigan Basin; p.1-21 *in* Reefs and Evaporites—Concepts and Depositional Models, edited by J.H. Fisher, American Association of Petroleum Geologists, Studies in Geology, Number 5, 196p.

Landes, K.K.
1945: The Salina and Bass Island Rocks in the Michigan Basin; United States Geological Survey Oil and Gas Inventories, Preliminary Map 40, scale 1 inch to 23 miles.

Leonard, B.J.
1983: Environment of Deposition of the A-1 Carbonate, Salina Group, Michigan Basin; Unpublished M.Sc. Thesis, Western Michigan University, Kalamazoo, Michigan, 83p.

Levy, Y.
1980: Evaporitic Environments in Northern Sinai; p.131-143 *in* Hypersaline Brines and Evaporitic Environments, Elsevier, New York.

Matthews, R.D., and Egleson, G.C.
1974: Origin and Implications of a Mid-Basin Potash Facies in the Salina Salt of Michigan; p.15-35 *in* General Geology of Salt and Other Deposits, edited by A.H. Coogan, Fourth Symposium on Salt, Northern Ohio Geological Society, Volume 1, 530p.

Mesolella, K.J.
1978: Paleogeography of Some Silurian and Devonian Reef Trends, Central Appalachian Basin; American Association of Petroleum Geologists, Bulletin, Volume 62, Number 9, p.1607-1644.

Mesolella, K.J., Robinson, J.D., McCormick, L.M., and Ormiston, A.R.
1974: Cyclic Deposition of Silurian Carbonates and Evaporites in Michigan Basin; American Association of Petroleum Geologists, Bulletin, Volume 58, Number 1, p.34-62.

Morris, R.C., and Dickey, P.A.
1957: Modern Evaporite Deposition in Peru; American Association of Petroleum Geologists, Bulletin, Volume 41, Number 11, p.2467-2474.

Nurmi, R.D.

1974: The Lower Salina (Upper Silurian) Stratigraphy in a Desiccated, Deep Michigan Basin; Proceedings of the Ontario Petroleum Institute, Thirteenth Annual Conference, p.1-25.

Nurmi, R.D., and Friedman, G.M.

1977: Sedimentology and Depositional Environments of Basin-Centre Evaporites, Lower Salina Group (Upper Silurian), Michigan Basin; p.23-52 *in* Reefs and Evaporites—Concepts and Depositional Models, edited by J.H. Fisher, American Association of Petroleum Geologists, Studies in Geology, Number 5, 196p.

Rickard, L.V.

1969: Stratigraphy of the Upper Silurian Salina Group, New York, Pennsylvania, Ohio, Ontario; New York State Museum and Science Service, Map and Chart Series Number 12, 57p.

Sanford, B.V.

1969: Silurian of Southwestern Ontario; Proceedings of the Ontario Petroleum Institute, Eighth Annual Conference, Paper 5, 44p.

Sears, S.O., and Lucia, F.J.

1980: Dolomitization of Northern Michigan Niagaran Reefs by Brine Refluxion and Freshwater/Seawater Mixing; p.215-235 *in* Concepts and Models of Dolomitization, edited by D.H. Zenger, J.B. Dunham, and R.L. Ethington, Society of Economic Paleontologists and Mineralogists, Special Publication Number 28, 320p.

Shearman, D.J.

1978: Evaporites of Coastal Sabkhas; p.6-42 *in* Marine Evaporites, edited by W.E. Dean and B.C. Schreiber, Society of Economic Paleontologists and Mineralogists, Short Course Number 4, 188p.

1983: Syndepositional and Lake Diagenetic Alteration of Primary Gypsum to Anhydrite; Sixth Symposium on Salt, Northern Ohio Geological Society, Volume 1, p.41-50

Sloss, L.L.

1969: Evaporite Deposition from Layered Solutions; American Association of Petroleum Geologists, Bulletin, Volume 53, Number 4, p.776-789.

Sonnenfeld, P.

1985: Flow Regimes in the Silurian of the Michigan Basin; p.157-171 *in* Ordovician and Silurian Rocks of the Michigan Basin and its Margins, edited by K.R. Cercone, J.M. Budai, and J.L. Wilson, Michigan Basin Geological Society, Special Paper 4, 196p.

Straw, W.T.

1985: Facies and Depositional Setting of the A-1 Carbonate (Silurian) in the Michigan Basin; p.143-156 *in* Ordovician and Silurian Rocks of the Michigan Basin and its Margins, edited by K.R. Cercone, J.M. Budai, and J.L. Wilson, Michigan Basin Geological Society, Special Paper 4, 196p.

Treesh, M.I., and Friedman, G.M.

1974: Sabkha Deposition of the Salina Group (Upper Silurian) of New York State; p.35-46 *in* General Geology of Salt and Other Deposits, edited by A.H. Coogan, Fourth Symposium on Salt, Northern Ohio Geological Society, Volume 1, 530p.

Warren, J.K.

1982a: The Hydrological Setting, Occurrence and Significance of Gypsum in Late Quaternary Salt Lakes in South Australia; Sedimentology, Volume 29, p.609-637.

1982b: The Hydrological Significance of Holocene Tepees, Stromatolites, and Boxwork Limestones in Coastal Salinas in South Australia; Journal of Sedimentary Petrology, Volume 52, Number 4, p.1171-1201.

1983a: Pedogenic Calcrete as it Occurs in Quaternary Calcareous Dunes in Coastal South Australia; Journal of Sedimentary Petrology, Volume 53, Number 3, p.787-796.

1983b: On the Significance of Evaporite Lamination; Sixth Symposium on Salt; Northern Ohio Geological Society, Volume 1, p.161-170.

1986: Shallow-Water Evaporitic Environments and Their Source Rock Potential; Journal of Sedimentary Petrology, Volume 56, Number 3, p.442-454.

Warren, J.K., and Kendall, C.G.St.C.

1985: Comparison of Sequences Formed in Marine Sabkha (Subaerial) and Salina (Subaqueous) Settings—Modern and Ancient; American Association of Petroleum Geologists, Bulletin, Volume 69, Number 6, p.1013-1023.

West, I., Ali, Y.A., and Hilmy, M.E.

1983: Facies Associated with Primary Gypsum Nodules of Northern Egyptian Sabkhas; Sixth Symposium on Salt, Northern Ohio Geological Society, Volume 1, p.171-183.

Grant 322 Physical and Chemical Processes of Archean Subaqueous Pyroclastic Rocks

John Stix and Michael P. Gorton

Department of Geology, University of Toronto, Toronto

ABSTRACT

The subaqueous volcaniclastic rocks of the Lost Bay area of northwestern Ontario show abundant evidence of rapid deposition after eruption, without large amounts of post-eruptive geochemical and/or physical modification. As a result, the deposits can be considered as relatively primary pyroclastic rocks. Lithofacies codes have been developed to record descriptive information during mapping, in order to aid in making paleoenvironmental interpretations, as well as to determine the nature of the eruptive and depositional environments. The results of geochemical analyses performed on bulk samples of these pyroclastic rocks show that such samples are not representative of the initial magma composition, but rather represent mixtures of juvenile fragments erupted at different times.

INTRODUCTION

Explosive subaqueous volcanism of intermediate to silicic composition has been studied inadequately in modern environments because of its concealed occurrence. This lack of understanding is particularly striking when contrasted with the extensive body of data on subaerial explosive volcanism. Some workers have extrapolated observations made from subaerial explosive environments to subaqueous environments (for example, Fiske and Matsuda 1964). However, further study is warranted considering the large amounts of debris contributed to the marine sedimentary record by underwater explosive eruptions and volcaniclastic flows. This is especially true in the case of Archean supracrustal sequences where vast thicknesses (kilometres to tens of kilometres) of subaqueous volcaniclastic deposits are preserved on all continents. The effect of water is to (1) add load pressure to control an eruption, and (2) act as an efficient sorting mechanism, due to a viscosity two orders of magnitude greater than that of air. Hence, subaqueous volcaniclastic flow deposits are certain to differ in several important respects from their subaerial counterparts. Furthermore, in the light of recent recognition of the importance of seafloor environments for massive sulphide deposition (Franklin *et al.* 1981), it is clear that the distinction between subaerial and subaqueous eruptive and depositional environments may have new significance for mineral exploration.

The objectives of our research are three-fold: (1) to understand how the eruptions originate and how the subaqueous volcaniclastic flows move and are emplaced; (2) to develop lithofacies codes to aid in the mapping of such deposits; and (3) to investigate how post-eruptive physical fractionation mechanisms (i.e., mechanical mixing and differential sorting of grains) obscure the primary magmatic chemistry of the rocks. In this preliminary report, we discuss aspects of these three objectives. Detailed sedimentary and geochemical work will be published separately.

STUDY AREA

We are investigating Archean-age intermediate to felsic subaqueous volcaniclastic rocks at Confederation Lake, Uchi Subprovince, northwestern Ontario (Figure 322.1). The metamorphosed supracrustal package located in the Confederation Lake area provides evidence of extremely varied cyclical volcanism (Thurston 1985). The abundance of pumice, distinctive grading, and the monolithic nature of many of the deposits signify that they are superb examples of subaqueous products from explosive eruptions, and require detailed volcanological/sedimentological study.

We are examining in the field and laboratory those characteristics of subaqueous volcaniclastic deposits which will help us to interpret (1) the nature of the eruption; (2) the post-eruptive modification of the debris; and (3) the type of volcaniclastic flow generated from the eruption.

VOLCANIC GEOLOGY OF LOST BAY

Our mapping has confirmed Thurston's (1985) contention that Lost Bay is underlain by a sequence of subaqueous volcaniclastic rocks. These rocks have suffered relatively minor physical modification (for example, reworking and resedimentation) subsequent to eruption. Because the rocks contain abundant sedimentological evidence for turbidite deposition but lack sedimentary structures indicative of subaerial or nearshore environments, the rocks appear to have been deposited below wave base as low- or high-concentration turbidity flows. The volcaniclastic package is composed of many individual flow deposits, each of which is generally less than 3 m thick. The deposits are stratified; in general, the coarser the material, the cruder the stratification. The beds strike north to north-northeast and display grading relations suitable for tops determinations. We have made approximately 20 determinations indicating, without exception, that tops lie to the west to northwest. Because the beds dip steeply to the southeast, the beds are overturned.

We have also measured several sections (for example, Figure 322.2). Our purpose is to examine the details of individual deposits. By looking at these sections, we can discern patterns, such as systematic vertical facies variations, that are repeated from one section to the next. This will provide information concerning the nature of the transport and depositional processes that affected the pyroclastic material. We discuss below specific aspects of the Lost Bay volcanic geology.

CLAST COMPOSITION

The Lost Bay deposits are highly pumiceous. The pumice is recognizable because of its vesicularity; the vesicles are now filled with secondary quartz. The pumice has a variable vesicle content, which

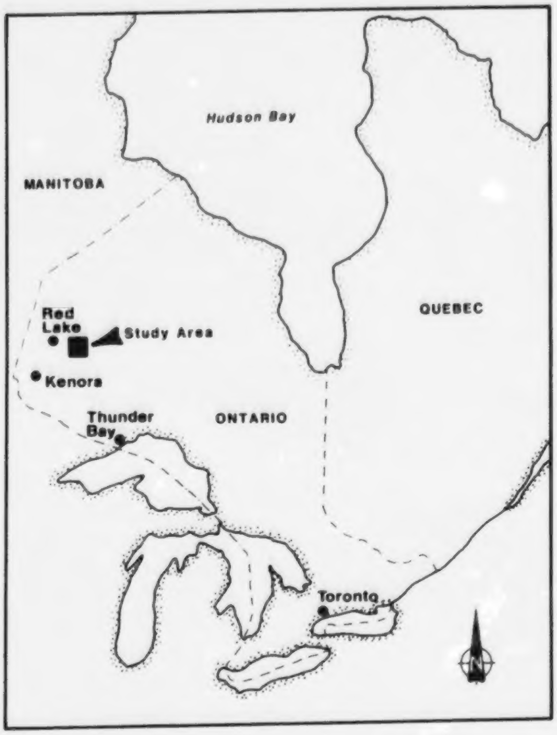

***Figure 322.1.** Location of study area.*

however never exceeds 50 percent, suggesting that highly vesicular pumice was lost due to flotation after the eruption. Many deposits also contain white juvenile clasts that (1) lack vesicles, and (2) were clearly denser than the pumice fragments at the time of eruption. These may have been derived from domes that were fragmented. We have observed that pumice and these dense fragments are end members with respect to vesicles; many fragments have vesicularities intermediate between pumice and dense fragments, and may be part of a continuum. We have observed quartz-feldspar porphyry fragments in deposits in the middle of Lost Bay, but not at the southern end.

MIXING WITH WATER

Because the majority of deposits in Lost Bay are stratified, we believe that the pyroclastic material was mixed with water subsequent to eruption. This mixing most likely occurred (1) in the eruption column, and (2) during movement of the flow. The presence of fine-grained ash that overlies coarser grained pyroclastics may be the result of (1) turbidite deposition and/or (2) co-ignimbrite ash deposition. The ash may have remained suspended in the eruption column or above the coarser grained flow, and was then sedimented subsequent to the emplacement of the coarse-grained material.

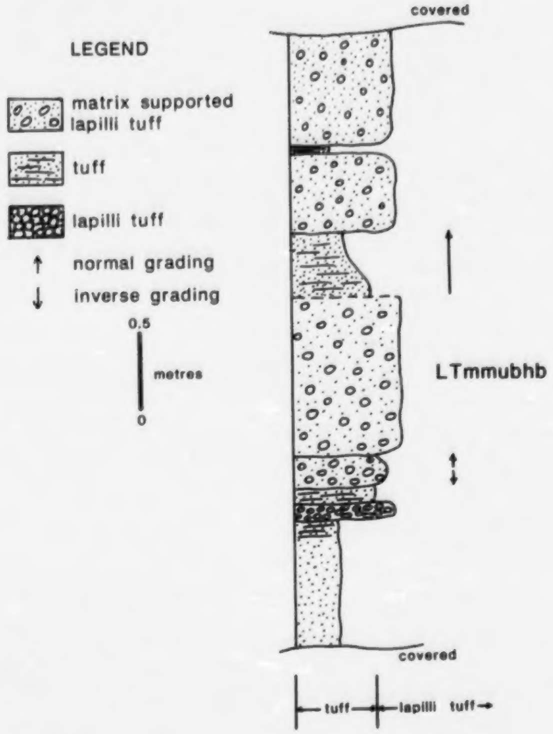

***Figure 322.2.** Stratigraphic section of volcaniclastic rocks, located on the eastern shore of Lost Bay, with sample lithostratigraphic code. The section is composed of tuffs and matrix-supported lapilli tuffs, and one lapilli tuff unit which is framework supported and may be a fallout deposit. The lapilli tuff unit labelled with a lithofacies code is massive, matrix supported, and is most likely not a primary pyroclastic deposit because it is heterolithic and contains both rounded and angular clasts.*

RETENTION OF HEAT

We have not recognized any deposits that were emplaced in a hot state. This is consistent with the fact that the flows were mixed substantially with water. In our terminology, these units would be properly called subaqueous pyroclastic debris flow deposits, rather than true pyroclastic flow deposits.

REWORKING OF PYROCLASTIC MATERIAL

Much of the Lost Bay section has not been significantly reworked. The monolithic nature of the debris, presence of abundant pumice, and lack of rounding indicate contemporaneous explosive volcanism and sedimentation. The north shore of Lost Bay, however, is underlain by fine-grained tuffs and epiclastic sediments. Some of the deposits contain extremely high amounts of detrital quartz; the quartz may have been concentrated by physical processes after eruption.

SORTING

Because the deposits are, in general, poorly sorted, it appears that the flows were emplaced by mass flow processes. This is perhaps the most efficient way by which large thicknesses of pyroclastic and epiclastic material accumulate in the subaqueous environment.

GRADING

Many of the deposits are clearly density graded, that is, dense fragments are normally size graded and pumice fragments are inversely size graded. In certain units, large (>20 cm in diameter) fragments of pumice are concentrated at the top of the volcaniclastic flow, indicating that the pumice was buoyant and less dense than the flow itself. If one is able to recognize pumice, its inversely graded nature in some deposits may provide an indication of topping directions. We have found one deposit that is doubly graded (cf. Fiske and Matsuda 1964).

LITHOFACIES CODES

One way to study subaqueous volcaniclastic rocks is to examine and interpret the various lithofacies of the rocks. This method is a comparatively rapid technique with which to characterize individual deposits and packages of rocks in a purely descriptive way, yet is one which is suitable for environmental interpretation. This approach has been applied successfully to fluvial facies (Miall 1977, 1978) and to glaciogenic sequences (Eyles and Eyles 1983; Eyles *et al.* 1983), but is long overdue for subaqueous volcaniclastic facies.

We are developing a set of lithofacies codes to map volcaniclastic and pyroclastic rocks in Lost Bay and elsewhere. The lithofacies code presented here (Table 322.1) serves as a means for characterizing both primary and secondary pyroclastic flow deposits. The code may be used to log section or to map lithologically. The code looks formidable, but it is simple. Once familiar with the code, a geologist can use it rapidly to study pyroclastic debris because the code provides a thorough nongenetic description of subaqueous pyroclastic deposits. The code can be simplified (or expanded) to any level desired.

Below we discuss the general nature of the different categories. Our forthcoming geological map of Lost Bay will show the practical application of the lithofacies codes.

The eight categories, discussed below, can be grouped in a systematic fashion. Category 1 provides information on the size of constituent material, whereas categories 2 to 4 describe the nature of emplacement of the debris. Categories 5, 6, and 8 characterize post-eruptive processes that occurred prior to final emplacement, and category 7 describes the eruptive source.

1. GRAIN SIZE

The grain size of a deposit describes the size range of constituent fragments. For subaerial pyroclastic fallout material from an explosive eruption, the grain size of both juvenile material and of lithic fragments decreases away from the source (Walker 1971). In the subaqueous environment however, coarse-grained fallout deposits generally are not preserved because pumice often floats. Thus, distal fine-grained ashes are preserved preferentially because the shards sink due to the lack of whole vesicles. The discussion of this lithofacies code, therefore, concerns mainly subaqueous volcaniclastic flows and their deposits.

For subaqueous volcaniclastic flows, the grain size of the subsequent deposits does not necessarily reflect the distance from source, but may instead indicate the competence and capacity of the flow to transport a certain size of material.

2. FABRIC

Massive flows may indicate rapid emplacement by mass flow processes. The concentration of debris in the flow may have been high enough to prevent the segregation of material within the flow. Furthermore, the flow may have incorporated very little water. In contrast, stratified flow deposits indicate a greater degree of sediment-water interaction, such as sediment-water mixing, and the consequent dilution of the flow. Crude stratification is characteristic of the Lost Bay pyroclastic deposits.

Flow deposits often show a vertical and lateral progression of facies from massive to stratified (Walker 1975; Tassé *et al.* 1978). Within vertical sections at Lost Bay, lithofacies commonly grade from a massive base to a stratified top. This may indicate increased mixing of water and dilution of the flow upward, and/or the deposition of suspended fine-grained material, by flow or fallout, after the emplacement of the main part of the flow.

3. SUPPORT MECHANISM

Most massive pyroclastic flow deposits in Lost Bay tend to be matrix-supported, implying a high concentration mass flow. Particle support may be provided by a variety of means such as matrix strength, buoyancy, dispersive pressure, turbulence, and fluidization. Certain deposits may be framework-supported (cf. Walker 1975, for nonvolcanic deposits), indicating a possible depletion of fine-grained material such as vitric ash.

4. COARSE-TAIL GRADING

Grading relations of the coarsest fragments within a flow deposit provide further information regarding support mechanisms, but only for the final stages of emplacement. Normal size grading may indicate turbulence and/or decreased competence of the flow upward. Inverse size grading suggests the presence of dispersive pressure, kinetic sieving (Middleton 1970), and/or decreased competence of the flow at the base due to shear (Naylor 1980). When normal and inverse size grading are found together, the deposit invariably is inversely graded at the base

TABLE 322.1: LITHOFACIES CODE FOR SUBAQUEOUS VOLCANICLASTIC ROCKS

CATEGORY	FACIES CODE	LITHOFACIES
1. grain size	LT------(-)	lapilli-tuff
	L------(-)	lapillistone
	TB------(-)	tuff breccia
	B------(-)	breccia
2. fabric	-m-----(-)	massive
	-s-----(-)	stratified
	-w-----(-)	welded
	-c-----(-)	columnar-jointed
3. support mechanism	--m----(-)	matrix-supported
	--f----(-)	framework-supported
4. coarse-tail grading	---n---(-)	normally size-graded
	---i---(-)	inversely size-graded
	---b---(-)	normally and inversely size-graded
	---d---(-)	density-graded
	---f---(-)	doubly graded
	---u---(-)	ungraded
5. reworking	----r--(-)	rounded and subrounded clasts
	----a--(-)	angular and subangualar clasts
	----b--(-)	rounded to angular clasts
6. composition	-----m-(-)	monolithic
	-----h-(-)	heterolithic
7. juvenile material	------p(-)	pumiceous low-density (<1.6 g/cm ^{3}) clasts
	------d(-)	dense (>1.6 g/cm ^{3}) clasts
	------b(-)	both low-density and high-density clasts
8. lithic material	------(fps,14)	compositions of lithic fragments, if present, listed in order of decreasing abundance; numeral indicates average maximum diameter in cm of the five largest clasts in the unit

lithic fragment symbols:

u	ultramafic-mafic volcanic
i	intermediate volcanic
f	felsic volcanic
p	plutonic
s	sedimentary
m	metamorphic

and normally graded at the top, so that the largest fragments are found in the middle of the unit.

Density grading reflects the importance of the different densities of felsic pyroclastic materials; this type of grading is common in Lost Bay. Relatively dense material may include crystal and lithic fragments ($\rho > 2.5$ g/cm^3, where ρ = density), whereas silicic glass and pumice are less dense ($\rho < 2.2$ g/cm^3). Double grading represents a combination of normal size grading and density grading and was found at one location in Lost Bay. Laminae in a bedded pyroclastic sequence become progressively finer grained upward, whereas individual laminae are density graded (Fiske and Matsuda 1964). The presence of double grading has been elsewhere used (Fiske and Matsuda 1964) as evidence to suggest that subaqueous pyroclastic deposits are direct products of explosive subaqueous eruptions.

5. REWORKING

Commonly, subaqueously emplaced flows contain well-rounded clasts. This may have four main implications: (1) reworking of material has occurred in a subaerial and/or shallow subaqueous environment (Ayres 1982); (2) this material was subsequently resedimented into a deeper subaqueous setting; (3) there existed a hiatus between the time of eruption and final emplacement of the debris; and, (4) the source or sources were at least partly subaerial. Pumice fragments found in deposits on Lost Bay are rounded; because pumice is soft and friable, the pumice may have been rounded during or just after explosive eruption.

The presence of abundant angular debris may indicate a lack of significant reworking, and little or no hiatus between the times of eruption and emplacement. However, the angularity does not necessarily provide any information concerning source environments. Lack of rounding may imply a subaqueous source or rapid emplacement; however, such negative evidence is not diagnostic.

6. COMPOSITION

This characteristic may be used in conjunction with categories 5, 7, and 8. Monolithic debris within a flow deposit implies the derivation of the material from one source, with little or no mixing of material from other sources. Obviously, this does not hold if the sources themselves are of similar composition. Heterolithic deposits suggest derivation from multiple vents and/or mechanical mixing of different materials in a subaerial or shallow subaqueous setting before final emplacement of the debris. The presence of heterolithic material suggests that the flows were secondary and epiclastic.

7. JUVENILE MATERIAL

The nature of juvenile material in a subaqueously emplaced pyroclastic deposit provides information concerning the nature of the eruption. The abundance of pumice indicates that the eruption was caused by the explosive fragmentation of vesiculating magma. Abundant juvenile clasts that lack vesicles (and are therefore denser than pumice) in a deposit suggest collapse and/or fragmentation of domes, spines, and lavas. A mixture of pumice and relatively dense juvenile material (common in Lost Bay deposits) may indicate that pre-existing domes and lavas were fragmented by explosive disruption of vesiculating magma (for example, Fiske and Matsuda 1964). Alternatively, a post-eruptive mixing event may have taken place, whereby the fragmentation of vesiculating magma on the one hand, and the disruption of domes and lavas on the other, may have occurred at separate times, or simultaneously at different locations. The fragmental material was then mechanically mixed and deposited.

8. LITHIC MATERIAL

This category documents post-eruptive mixing of volcanic and nonvolcanic debris, and may be used with categories 5 and 6. Fragment diversity is a direct result of the mixing and modification of originally pyroclastic material. The Lost Bay deposits do not have a great degree of fragment diversity, probably because the debris was deposited relatively rapidly after eruption. The types of sedimentary clasts, if any, may provide constraints upon source environments.

SUMMARY

The lithofacies code outlined above and in Table 322.1 is essentially complete. The elements of the code, when considered together, may be used to interpret the eruptive, transport, and depositional history of coarse-grained subaqueous pyroclastic rocks. We are continuing work on a similar code for fine-grained subaqueous pyroclastic rocks (Table 322.2), and will produce a map of Lost Bay that incorporates the codes.

GEOCHEMISTRY OF LOST BAY PYROCLASTIC ROCKS

We are investigating the geochemistry of the Lost Bay volcaniclastic rocks to examine the effects of post-eruptive fractionation processes which may be unrelated to magmatic differentiation, and to begin to re-evaluate geochemical analyses of volcaniclastic and pyroclastic deposits that supposedly represent magmatic compositions. It is a common practice in Archean greenstone terranes to sample and analyze pyroclastic units with varied crystal contents for major and trace element composition, and then use these results for petrogenetic interpretations. These methods may not be valid because of unrecognized syn- and post-eruptive fractionation and alteration processes.

We have sampled in detail for thin section and geochemical work. We were able to sample individual pumice fragments from an outcrop, as well as take bulk specimens and samples of overlying fine-grained material. This sampling scheme is essential for making geochemical interpretations concerning magmatic compositions and post-eruptive fractionation processes.

Using zirconium and yttrium (two relatively immobile trace elements), determined for individual clasts, we have recognized that the clasts within pyroclastic rocks in Lost Bay are composed of two geochemically distinctive groups (Figure 322.3), in spite of the fact that the fragments appear indistinguishable in outcrop or thin section. The first group of clasts has relatively low concentrations of highly charged elements (Y: 4.0 to 52 ppm; Zr: 123 to 187 ppm; Nb: 2.5 to 12 ppm), a relatively high strontium concentration (138 to 573 ppm), and high Zr/Y ratios that vary systematically (2.4 to 35) (Figure 322.3). This variation in Zr/Y ratios has three implications: (1) the rocks range from geochemically primitive (high Sr and Zr/Y) to evolved compositions (low Sr and Zr/Y); (2) rare earth patterns should be generally steep, with low absolute abundances; and (3) the decreasing Zr/Y ratio with increasing yttrium concentration suggests crystallization and removal of zircon from the magma(s) (the usual situation in the evolution of felsic magmas).

The second group of clasts has much higher concentrations of highly charged trace elements (Y: 63 to 165 ppm; Zr: 318 to 649 ppm; Nb: 17 to 34 ppm), lower and more restricted strontium concentrations (107 to 363 ppm), and lower and almost constant Zr/Y ratios (3.8 to 5.4) (Figure 322.3). In contrast with Group 1 above, these data suggest that Group 2 clasts have high rare earth element (REE) concentrations and flat patterns. Because of the low concentrations of strontium present, the REE patterns also may have substantial negative europium anomalies. The high zirconium concentrations in Group 2

TABLE 322.2: LITHOFACIES CODE FOR FINE-GRAINED SUBAQUEOUS VOLCANICLASTIC ROCKS

CATEGORY	FACIES CODE	LITHOFACIES
1. lithology	T------(-)	tuff
2. grain size	Tf-----(-)	fine-grained, <1/4 mm
	Tm-----(-)	medium-grained, 1/4 - 1/2 mm
	Tc-----(-)	coarse-grained, 1/2 - 2 mm
3. constituents	T-v----(-)	vitric
	T-c----(-)	crystal
	T-l----(-)	lithic
	T-w----(-)	vitric-crystal
	T-x----(-)	crystal-lithic
	T-y----(-)	vitric-lithic
	T-z----(-)	vitric-crystal-lithic
4. composition of vitric material	T--u---(-)	ultramafic-mafic
	T--i---(-)	intermediate
	T--f---(-)	felsic
5. morphology of glass shards	T---v--(-)	vesiculated bubble wall, Y-shaped, spiny, cuspate shards; channelled columns
	T---n--(-)	blocky, platy, angular non-vesicular shards; conchoidal, smooth fracture surfaces
	T---b--(-)	both types of shards present
	T---p--(-)	pumice shards: small grains of pumice <2 mm in diameter
6. fabric	T----m-(-)	massive
	T----s-(-)	stratified
	T----p-(-)	parallel bedding
	T----x(-)	cross-laminating
	T----c-(-)	convolute bedding
7. grading	T-----n(-)	normally size-graded
	T-----i(-)	inversely size-graded
	T-----b(-)	normally and inversely size-graded
	T-----d(-)	density-graded
	T-----f(-)	doubly graded
	T-----u(-)	ungraded
8. crystal content	T------(qab)	crystal phases, if present, listed in order of decreasing abundance

crystal symbols:

q	quartz
p	plagioclase
a	alkali feldspar
b	diotite
h	hornblende
x	pyroxene
o	olivine

clasts indicate that during fractionation zircon did not crystallize, in contrast to Group 1.

Although clasts in Group 2 may appear to form a continuum with those of Group 1 with respect to Zr/Y ratios (Figure 322.3), this is not the case on other variation diagrams. When the two trends appear to meet in Figure 322.3, Group 1 rocks have 126 ppm zirconium, whereas Group 2 rocks have 318 ppm zirconium.

MECHANICAL MIXING IN BULK SAMPLES OF PYROCLASTIC ROCKS

We believe that the bulk sample compositions and the results of the analyses of these pyroclastic clasts are not representative of the composition of the magma. Post-eruptive processes in the subaqueous environment discussed above, such as mixing and differential settling and sorting of crystals, lithic fragments, and glass shards in water, cause a physical fractionation of the particles and obscure the mag-

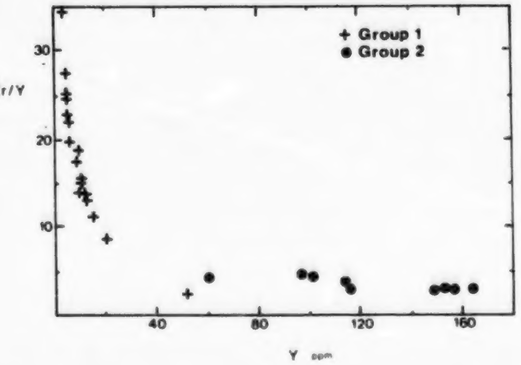

Figure 322.3. *Zr/Y versus Y for clasts from pyroclastic rocks of the eastern shore of Lost Bay. Groups are subdivided on the basis of geochemical trends and Zr concentrations.*

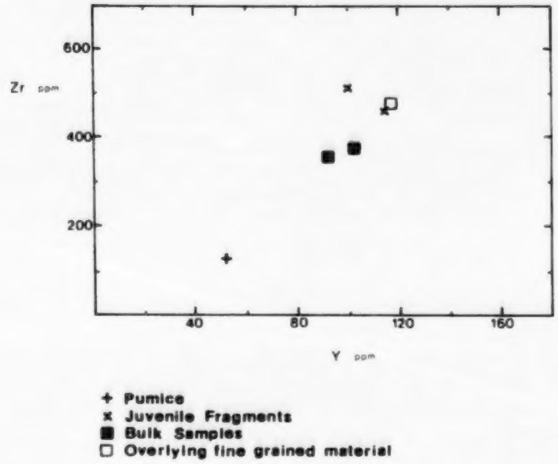

Figure 322.4. *Zr versus Y for various components of a lapilli tuff deposit from one outcrop.*

matic chemistry. This is strikingly illustrated in Lost Bay. In Figure 322.4 we have plotted the compositions of one pumice fragment, two juvenile fragments that lack vesicles, and two bulk rock samples of a single lapilli tuff outcrop, as well as a fine-grained cap of volcaniclastic sediment that overlies the lapilli tuff. We have chosen this outcrop for study because it is a well exposed, easily sampled, and most importantly, is typical of the deposits in Lost Bay. The three fragment compositions reflect the two groups of juvenile material. However, the bulk samples appear to lie on a mixing line between the three fragments and thus do not represent magmatic compositions. To understand magmatic evolution in these rocks, therefore, one must sample individual fragments that represent quenched magma (for example, juvenile fragments), not the bulk sample.

Furthermore, we suggest that the two dense fragments, rather than the pumice, represent the magma that was erupted in this case because (1) the composition of the bulk samples lies closer to that of the dense fragments than to that of the pumice, and (2) the dense fragments have very similar compositions to that of the overlying fine-grained cap. This cap may thus be composed of vitric ash that settled out of suspension after the bulk of the coarser grained, more concentrated flow was deposited. The pumice shown in Figure 322.4 may simply be an accidental fragment in the pyroclastic flow.

CONCLUDING REMARKS

The Lost Bay area is exceptional in that it has preserved a thick sequence of relatively primary pyroclastic and volcaniclastic debris that has not suffered large amounts of post-eruptive reworking and resedimentation. The debris was not deposited hot, however, and has mixed sufficiently with water during eruption and deposition to produce bedded deposits.

The lithofacies codes developed here provide (1) a new approach to mapping subaqueous pyroclastic debris; (2) a means for recording the essential characteristics of individual sections or outcrops in a uniform manner; and (3) an easily manipulated data set that is suitable for interpreting eruptive and depositional environments.

Lastly, we have recognized that bulk samples of pyroclastic and volcaniclastic debris do not represent magmatic compositions. Instead, they appear to fall on a mixing line between juvenile fragments with different major and trace element compositions.

ACKNOWLEDGMENTS

We thank Phil Thurston for encouragement and support, and Moe Lavigne for advice and logistical help.

REFERENCES

Ayres, L.D.
1982: Pyroclastic Rocks in the Geologic Record; p.1-17 *in* Pyroclastic Volcanism and Deposits of Cenozoic Intermediate to Felsic Volcanic Islands with Implications for Precambrian Greenstone Belt Volcanoes, edited by L.D. Ayers, Geological Association of Canada Short Course Notes, Volume 2, 365p.

Eyles, C.H., and Eyles, N.
1983: Sedimentation in a Large Lake: A Reinterpretation of the Late Pleistocene Stratigraphy at Scarborough Bluffs, Ontario, Canada; Geology, Volume 11, Number 3, p.146-152.

Eyles, N., Eyles, C.H., and Miall, A.D.
1983: Lithofacies Types and Vertical Profile Models; An Alternative Approach to the Description and Environmental Interpretation of Glacial Diamict and Diamictite Sequences; Sedimentology, Volume 30, p.393-410.

Fiske, R.S., and Matsuda, T.
1964: Submarine Equivalents of Ash Flows in the Tokiwa Formation, Japan; American Journal of Science, Volume 262, Number 1, p.76-106.

Franklin, M.M., Sangster, D.M., and Lydon, J.W.
1981: Volcanic-Associated Massive Sulphide Deposits; Economic Geology, 75th Anniversary Volume, p.485-627.

Miall, A.D.
1977: A Review of the Braided River Depositional Environment; Earth Science Reviews, Volume 13, p.1-62.
1978: Lithofacies Types and Vertical Profile Models in Braided River Deposits: A Summary; p.597-604 *in* Fluvial Sedimentology, edited by A.D. Miall, Canadian Society of Petroleum Geologists, Memoir 5, 859p.

Middleton, G.V.
1970: Experimental Studies Related to Problems of Flysch Sedimentation; p.253-272 *in* Flysch Sedimentology in North America, edited by Jean Lajoie, Geological Association of Canada Special Paper Number 7, 272p.

Naylor, M.A.
1980: The Origin of Inverse Grading in Muddy Debris Flow Deposits—A Review; Journal of Sedimentary Petrology, Volume 50, p.1111-1116.

Tassé, N., Lajoie, J., and Dimroth, E.
1978: The Anatomy and Interpretation of an Archean Volcaniclastic Sequence, Noranda Region, Quebec; Canadian Journal of Earth Sciences, Volume 15, p.874-888.

Thurston, P.C.
1985: Physical Volcanology and Stratigraphy of the Confederation Lake Area, District of Kenora (Patricia Portion); Ontario Geological Survey, Report 236, 117p. Accompanied by Map 2498, scale 1:50 000.

Walker, G.P.L.
1971: Grain-Size Characteristics of Pyroclastic Deposits; Journal of Geology, Volume 79, p.696-714.

Walker, R.G.
1975: Generalized Facies Models for Resedimented Conglomerates of Turbidite Association; Geological Society of America Bulletin, Volume 86, Number 6, p.737-748.

Grant 323 Lithogeochemistry and Light Stable Isotope (Carbon, Oxygen, and Sulphur) Geochemistry of Hydrothermal Alteration and Breccia Veins from the Cameron Lake Gold Deposit, Northwestern Ontario

D.R. Melling, R.P. Taylor, and D.H. Watkinson

Department of Earth Sciences and Ottawa–Carleton Geoscience Centre, Carleton University, Ottawa

ABSTRACT

The Cameron Lake gold deposit is an Archean vein-type deposit which occurs in deformed basaltic rocks of the Cameron Lake Shear Zone. The fluid activity that accompanied the development of the shear zone introduced massive amounts of CO_2, K, S, and Au, and resulted in hydrothermal carbonatization, sericitization, and sulphidation of the wall rocks adjacent to the breccia veins—the loci of gold mineralization in the deposit.

The fluid-rock interaction is characterized by the development of extensive zones of pervasive host rock alteration characterized by the mineral assemblage quartz + albite + ankerite + siderite + sericite + pyrite + rutile. Analysis of the chemical gains and losses that accompanied host rock alteration indicates that: (1) the lithogeochemical data define a best-fit isocon with Ti, Fe, and Si remaining constant; (2) major additions of CO_2, K, Rb, Ba, Ca, Sr, B, W, S, Au, and Ag were associated with carbonatization, sericitization, and sulphidization; (3) there was an overall loss of Li, Na, Zn, Mg, Al, Cu, and Sb; and (4) a mass increase of approximately 14 percent, most likely related to the conversion of iron-silicates/oxides to pyrite during sulphidization, occurred.

Sulphur isotopic analyses of pyrite samples from auriferous zones at Cameron Lake range from $\delta^{34}S=3.7$ to 0.1 per mil, and yield mean values of 2.9 ± 0.6 per mil for the breccia veins (n=7), and 1.2 ± 0.6 per mil for the pervasively altered rocks (n=5). Changes in $\delta^{34}S$ of pyrite are consistent with the oxidation of the hydrothermal fluid during pyrite deposition, as a consequence of the carbonatization of host rock magnetite; and given the intimate textural relationship between pyrite and gold in the deposit, they suggest that oxidation might well have contributed to gold deposition.

Carbon and oxygen isotopic analyses of ankerite from the deposit yield mean values of $\delta^{13}C=-1.9\pm1.1$ per mil and $\delta^{18}O=11.8\pm0.7$ per mil for the breccia veins (n=7), and $\delta^{13}C=-3.0\pm1.3$ per mil and $\delta^{18}O=11.7\pm0.3$ per mil for the enveloping pervasively altered rocks. The mean $\delta^{13}C$ value for all of the ankerites (n=13) is -2.7 per mil, which suggests a carbon isotopic signature for Cameron Lake that is distinct from other Archean gold deposits in the Superior Province. However, Rayleigh fractionation or mixing with host rock calcite during fluid-rock interaction may well have produced ^{13}C-enriched carbonates, and consequently the initial $\delta^{13}C$ of the hydrothermal fluid was likely to have been lighter than -3 per mil. Such values are consistent with fluid derivation from a magmatic mantle reservoir.

INTRODUCTION

The Cameron Lake gold deposit is located in the Kenora Mining District about 80 km southeast of Kenora (49°17'N, 94°44'W). Since the discovery of significant quantities of gold on the property in 1983 by Nuinsco Resources Limited, research on the deposit has evolved concurrently through the exploration and development stages. The emphasis of previous field-based research at Cameron Lake was directed towards providing an overview of the deposit which included aspects of structural control, deposit geometry, vein paragenesis, alteration mineralogy, and their relationships to gold distribution (Melling 1986; Melling *et al.* 1986; Melling 1987; Melling *et al.* 1988). As a result of completed research on the deposit, as well as other regional studies in the Cameron–Rowan Lakes area (Buck 1986; Chivers 1986; Johns 1986; Melling 1986, 1988), a comprehensive geological database is now available.

The purpose of this current two-year project is to build on, and supplement, previous studies by defining the isotopic signature (^{13}C, ^{18}O, ^{34}S) of various hydrothermal alteration minerals, and to determine the conditions under which gold precipitation occurred through combined isotopic and fluid inclusion studies. In so doing, it will increase the information available on Archean gold deposits in Ontario, and thus contribute to continuing efforts to constrain the possible sources of the fluids involved in their genesis; however, more importantly, this study is designed to provide information concerning the effects of vein formation on the evolution of hydrothermal fluids and gold precipitation.

The purpose of this paper is to integrate the results of isotopic work completed during our first year of study with observations and data on the mineralogy and whole rock geochemistry of the alteration assemblages at Cameron Lake. Documentation of the various types of fluid inclusions is in progress, and this, together with the results of experimental work on them, will be presented in a future paper.

GEOLOGICAL SETTING OF THE CAMERON LAKE PROPERTY

The deposit is situated about 500 m from the north shore of Cameron Lake (Figure 323.1). The property is underlain by mafic volcanic rocks and interbedded intermediate to felsic volcanic rocks—all of the Cameron Lake Volcanic succession (Melling and Watkinson 1986). Subconcordant mafic sills intrude the volcanic rocks, and are interpreted as subvolcanic intrusions. A large concordant felsic porphyry sill is also present. All rocks have been metamorphosed to greenschist facies mineral assemblages.

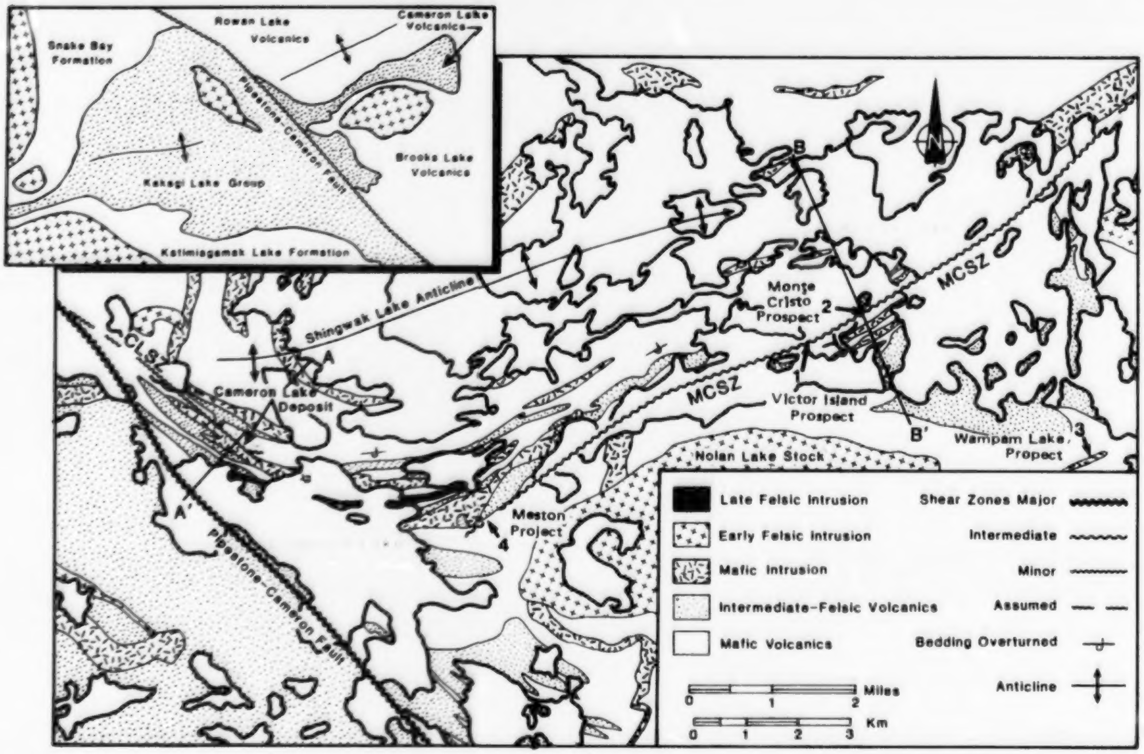
Snake Bay Formation
Rowan Lake Volcanics
Cameron Lake Volcanics
Pipestone-Cameron Fault
Brooks Lake Volcanics
Kakagi Lake Group
Kalimiagamak Lake Formation
Shingwak Lake Anticline
CLSZ
A
Cameron Lake Deposit
A'
B
B'
Monte Cristo Prospect
2
MCSZ
1
Victor Island Prospect
Wampam Lake Propect
3
Nolan Lake Stock
Meston Project
4
Pipestone-Cameron Fault
Late Felsic Intrusion
Early Felsic Intrusion
Mafic Intrusion
Intermediate-Felsic Volcanics
Mafic Volcanics
Shear Zones Major
Intermediate
Minor
Assumed
Bedding Overturned
Anticline
Miles
0
1
2
Km
0
1
2
3

Figure 323.1. *Geology of the Cameron-Rowan Lakes area and the location of the Cameron Lake gold deposit, and the Victor Island (1), Monte Cristo (2), Wampum Lake (3), and Meston (4) gold prospects. CLSZ = Cameron Lake Shear Zone, MCSZ = Monte Cristo Shear Zone. A-A' and B-B' refer to stratigraphic sections discussed by Melling et al.* (1988).

The deposit occurs within deformed basaltic rocks of the Cameron Lake Shear Zone (CLSZ), adjacent to their contact with one of the mafic intrusions (Figure 323.1). The basaltic rocks consist of roughly equal proportions of massive and pillowed flows with less than 10 percent pillow breccia. Thin discordant quartz-feldspar porphyry dikes, several hundred metres long and 1 cm to 3 m thick, have intruded the volcanic succession. Locally, they occur within zones of shearing and are fractured, displaying a complex internal quartz-carbonate vein network. For more comprehensive discussions of the regional geology of the Cameron Lake and surrounding areas, the reader is referred to work by Melling and Watkinson (1986), Melling (1988), and Melling *et al.* (1988).

GEOLOGY OF THE CAMERON LAKE DEPOSIT

The CLSZ has been traced by exploration diamond drilling and property-scale surface mapping for more than 1000 m (Figure 232.1) (Melling *et al.* 1986). Based on these data, an average strike and dip of 315° and 70°N, and a width of between 11 and 60 m has been determined. In detail, however, the CLSZ consists of both anastomosing and *en echelon* shear zones whose orientations are in part controlled by host rock anisotropies. The mafic intrusive rocks in the structural footwall to the deposit exert the greatest control on both the location and the orientation of the shear zone in the vicinity of the deposit (Melling *et al.* 1988). The entire contact between these rocks and the mafic volcanic host rocks to the deposit is sheared.

The mineralogy of the alteration assemblages that characterize the basaltic rocks was studied in diamond-drill hole NC-29, and provides a complete unweathered cross-section of the deposit. Thin section examination, X-ray diffraction studies, and electron microprobe analyses have permitted the recognition of four symmetrical zones of hydrothermal alteration which envelop the deposit. These assemblages, in order of proximity to the deposit are:

1. quartz + albite + chlorite + calcite + ankerite + epidote + actinolite + magnetite
2. quartz + albite + ankerite + sericite + chlorite + calcite + rutile
3. quartz + albite + ankerite + sericite + siderite + chlorite + pyrite + rutile
4. quartz + albite + ankerite + sericite + siderite + pyrite + rutile

Their distribution with respect to gold concentrations and the shear zone are illustrated in Figure 323.2

The first assemblage is recognized in the "least deformed, least altered" basaltic rocks in the hanging wall to the deposit, and is considered, in part, to be the result of regional greenschist facies metamorphism. The rocks are chlorite rich and contain no carbonate porphyroblasts or sericite.

Alteration assemblage 2 is restricted to most chloritic, basaltic, and gabbroic rocks outside of but adjacent to the CLSZ, and is equivalent to the carbonate rhomb alteration mapped on the surface (Melling *et al.* 1987). It is characterized by lower contents of chlorite and calcite, more ankerite, and by the appearance of sericite. Ankerite occurs as euhedra as large as 2 mm, which increase in abundance with proximity to the CLSZ. Ankerite porphyroblasts are generally more abundant in the medium-grained basaltic rocks, and are locally associated with flow contacts. Assemblage 2 forms envelopes up to 10 m wide in the rocks adjacent to wide foliated gold zones, but occurs over narrower widths near the smaller gold shoots. In drillhole NC-29, this type of alteration is about 8 m wide in the hanging wall but is more extensive in the footwall to the deposit, where it occurs in a lozenge of undeformed basaltic rocks in sheared contact with the gabbroic sill (Figure 323.2).

Alteration assemblage 3 occurs in both sheared basaltic rocks on the fringes of the CLSZ, and the sheared gabbroic rocks in the footwall to the deposit (Figure 323.2). It is characterized, in the basaltic rocks, by the absence of calcite, minor amounts of chlorite, the presence of magnesium-rich siderite, and significant amounts of ankerite and sericite. Pyrite is present in some places. This assemblage is transitional between the carbonate rhomb alteration and sheared carbonate- and sericite-rich rocks of the CLSZ. In areas of less intense deformation, flow contacts and pillow selvages are locally preserved. Rocks that have been subjected to this "incipient" alteration contain anomalous gold, and form envelopes 8 to 10 m wide along the edges of the CLSZ.

In the mafic intrusive rocks, iron-rich magnesite occurs rather than siderite, and pyrite and gold are rarely present. These gabbroic rocks commonly have "speckled" textures resulting from the contrast between coarse-grained carbonate and chlorite. An emerald green mica, and hematitic staining, are also locally present.

Alteration assemblage 4 occurs in sheared basaltic rocks spatially associated with the gold-bearing breccia veins. This type of alteration contains high gold grades and generally occurs in the centre of high strain zones (Figure 323.2). It is characterized by the absence of calcite and chlorite, and the presence of ankerite, siderite, sericite, and pyrite. The disseminated pyrite euhedra are spatially associated with breccia veins in the CLSZ, and occur in highest concentrations adjacent to them. Locally, diffuse patches of disseminated pyrite occur along the strike or dip extensions of breccia veins. This type of alteration is equivalent to the "pervasive" alteration described in drill core.

The breccia veins are a fundamental local control on the distribution of sulphide minerals and gold (Melling *et al.* 1986). They represent a specific gold-bearing rock type which commonly contains greater than 0.3 ounces gold per ton. The breccia veins have a wide range of morphologies and textures. The veins consist of angular to subrounded, pervasively altered fragments in a matrix of quartz, with lesser amounts of albite and carbonate. The breccias are both framework- and clast-supported types. Fragments have a wide range of shapes and sizes, and may contain internal cleavages or veins which predate brecciation. Individual breccia veins have a continuum of megascopic deformational textures, from undeformed to ribbon textures, which are attributed to ductile deformation postdating brecciation and vein formation.

Pyrite is concentrated within the altered fragments, but rarely in the siliceous matrix; it also occurs in mappable alteration envelopes surrounding the breccia veins. Surface and underground mapping indicate that a gold-bearing shear may, depending on its width, contain one or several breccia veins. Wider shear zones, which in cross-section contain several breccia veins, have incorporated slices up to several metres wide of deformed pervasively altered rocks, between the veins.

Although pyrite rarely exceeds 10 modal percent in any sample, it comprises greater than 98 modal percent of the sulphide minerals present. Pyrite occurs as subhedral to euhedral crystals less than 2 mm in size. Coarse-grained pyrite is sieve textured, due to the presence of abundant inclusions of silicate and carbonate minerals, rutile, chalcopyrite, lesser amounts of gold and pyrrhotite, and traces of hematite and magnetite. The inclusion of all other sulphide phases within pyrite suggests contemporaneous precipitation. Field mapping, core logging, and mineralogical and textural evidence indicate that the precipitation of gold is most closely linked to that of pyrite, rather than to the more extensive development of carbonate minerals and sericite (Melling *et al.* 1986).

ALTERATION LITHOGEOCHEMISTRY

METHODS

In order to determine the relative gains and losses of constituents during hydrothermal alteration, representative samples from different alteration types in diamond-drill hole NC-29 were chemically analyzed at the Bondar–Clegg laboratories in Ottawa. Analytical procedures, and the original major and trace element data, are presented by Melling (1986). The average compositions of the representative lithologies used in the current study are presented in Table 323.1. Based on core logging, surface mapping, and the chemical data, all altered rock types are derived from a basaltic protolith (Melling *et al.* 1986).

These averages were compared by using Grant's (1986) "isocon method"; this provides a simple and direct means of considering changes in mass, volume, and concentration within equivalent units during hydrothermal alteration. This method involves establishing a reference line corresponding to zero concentration change (an isocon or line of equal concentration) as determined statistically by a best fit to the chemical data. The isocon is a graphical simultaneous solution of Gresen's equation (Gresen 1967) for zero concentration change. The advantage of Grant's isocon method (Grant 1986) is that the isocon may be established based on the immobility of one

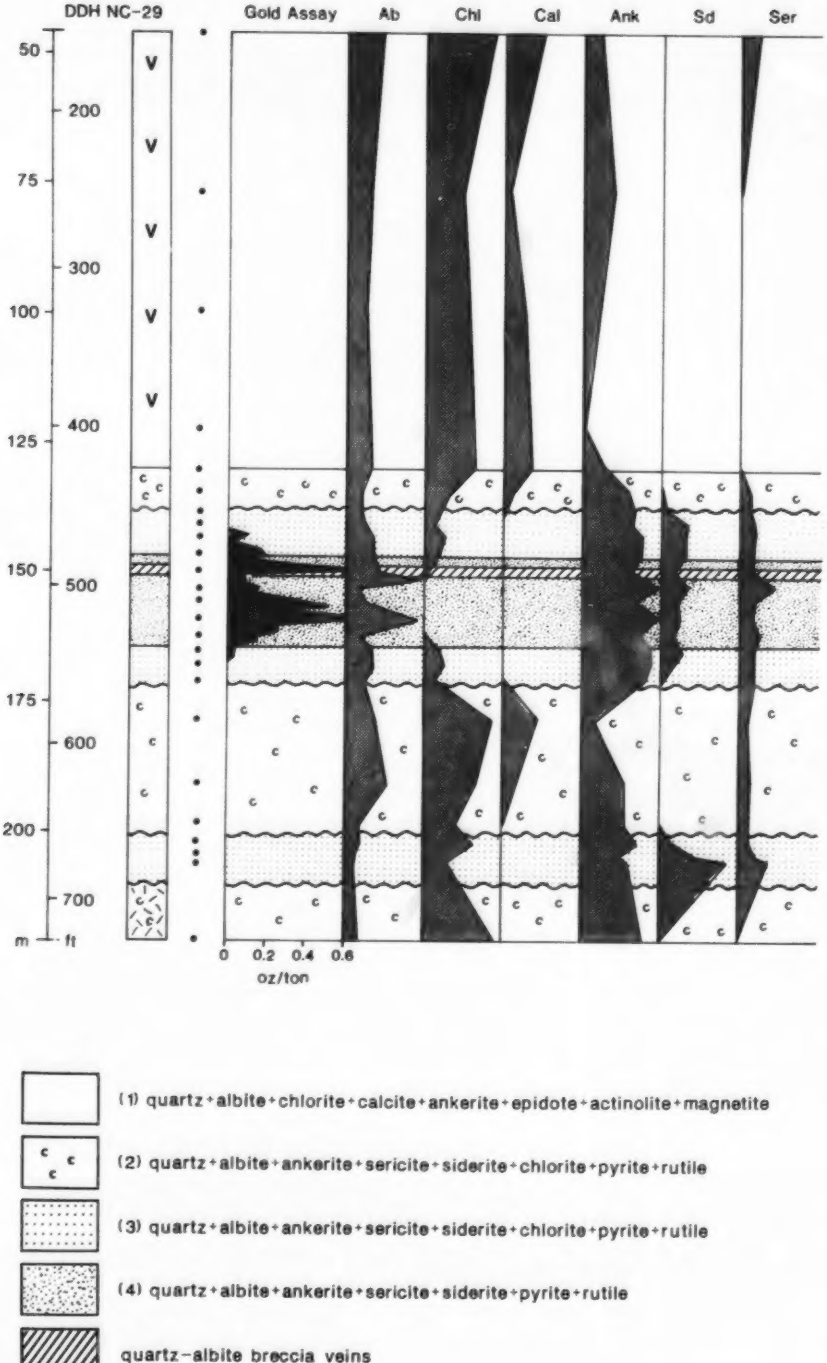

Figure 323.2. *Alteration assemblage profiles from DDH NC-29 illustrating the spatial relationships between hydrothermal alteration, gold concentration, and deformation at Cameron Lake. Mineral data correspond to X-ray diffraction peak heights normalized to quartz. Shear zone boundaries are indicated by the fault symbols. Four symmetrical alteration zones are defined by assemblages (1) through (4). The last assemblage is spatially associated with pyritic quartz-albite breccia veins (modified from Melling et al. 1986). Dots indicate sample locations. Mineral abbreviations after Kretz (1983).*

TABLE 323.1: AVERAGE CHEMICAL COMPOSITIONS OF LEAST DEFORMED LEAST ALTERED (LDLA) AND MOST DEFORMED PERVASIVELY ALTERED (MDPA) MAFIC VOLCANIC ROCKS AND THE CONCENTRATION CHANGES WHICH ACCOMPANIED HYDROTHERMAL ALTERATION.

	LDLA	(n=5)	MDPA	(n=4)	LDLA-MDPA
SiO_2	47.24	(1.21)	41.68	(2.00)	0.00
TiO_2	1.07	(0.05)	0.94	(0.08)	0.00
Al_2O_3	13.02	(0.68)	9.92	(0.44)	-0.13
Fe_2O_3T	13.68	(0.17)	12.08	(0.88)	0.00
MnO	0.20	(0.02)	0.21	(0.05)	0.20
MgO	5.55	(0.50)	4.26	(0.16)	-0.13
CaO	7.71	(1.18)	9.88	(0.55)	0.46
Na_2O	2.44	(0.83)	1.81	(1.56)	-0.16
K_2O	0.14	(0.16)	2.15	(0.78)	16.23
P_2O_5	0.06	(0.08)	0.05	(0.05)	-0.13
CO_2	4.36	(2.35)	16.71	(1.69)	3.36
S	0.10	(0.05)	2.35	(2.09)	26.85
	LDLA	**(n=5)**	**MDPA**	**(n=4)**	**LDLA-MDPA**
Li	12.6	(4.0)	2.5	(2.6)	-0.77
B	9.6	(5.1)	23.8	(9.2)	1.81
Cu	193.6	(15.9)	151.0	(12.7)	-0.11
Zn	129.0	(26.8)	98.0	(6.8)	-0.14
As	29.6	(26.0)	29.5	(29.6)	0.13
Rb	12.4	(6.8)	65.0	(30.6)	4.96
Sr	122.6	(38.3)	183.8	(42.9)	0.70
Ag	0.2	(0.0)	1.4	(1.6)	7.10
Sb	6.2	(3.4)	4.8	(2.3)	-0.13
Ba	26.8	(32.6)	107.0	(33.7)	3.54
W	1.6	(1.2)	3.8	(2.9)	1.66
Au (ppb)	9.0	(5.8)	7103.8	(5560.8)	895.94

Note: LDLA - least deformed, least altered; MDPA - most deformed, pervasively altered. Total Fe as ferric iron (Fe_2O_3T) was used in the isocon calculation, and the concentration changes listed in the column headed LDLA-MDPA are for the best-fit isocon model; n is the number of geochemical analyses averaged; number in parentheses following the abundances is one standard deviation.

component, a group of components, or on mass or volume. Once the isocon, and therefore any change in mass or volume, is selected, the determination of chemical gains and losses relative to concentration in the least altered rocks can be determined graphically, or mathematically, by the amount of displacement from the reference isocon. Isocon diagrams are presented in Figure 323.3. They represent the changes that occurred during the transformation of least deformed, least altered basalts to the most deformed, pervasively altered basalts that contain the highly anomalous gold concentrations.

CHEMICAL GAINS AND LOSSES

The average concentrations of major and trace elements for the least deformed, least altered (LDLA), and the most deformed, pervasively altered (MDPA) mafic volcanics from the Cameron Lake Deposit are presented in Table 323.1. Also listed in Table 323.1 are the relative changes in concentration from the LDLA to MDPA lithologies for the best-fit isocon (Figure 323.3). SiO_2, total iron as Fe_2O_3, and TiO_2 form a linear array that passes through the origin in Figure 323.3; this suggests that these may be considered as "immobile" components for the geochemical system, and are used therefore to define a best-fit isocon (line B in Figure 323.3a). Such an interpretation is supported by the petrographic data, which indicates (1) the persistence, *in situ*, of a titanium-bearing mineral phase (magnetite⟶ilmenite⟶rutile) during the alteration process (Melling *et al.* 1986), and (2) the absence of wall rock silicification (Melling *et al.* 1985). For comparison, the constant mass (line A) and constant Al_2O_3 (line C) isocons are also illustrated in Figure 323.3. Acceptance of the validity of the best-fit isocon requires that a gain in mass of approximately 14 percent (i.e., $M^O/M^A=0.88$, *from* Grant 1986; $C^A_i=(M^O/M^A)C^O_i$, where if C^O_i and C^A_i are the concentrations of an element in the original and altered rock, and if the element is immobile during alteration, then a change in the mass of the rock must occur) accompanied the pervasive hydrothermal alteration. Such a gain in mass is consistent with the pyritization that resulted from the conversion of host rock iron-bearing oxides and silicates.

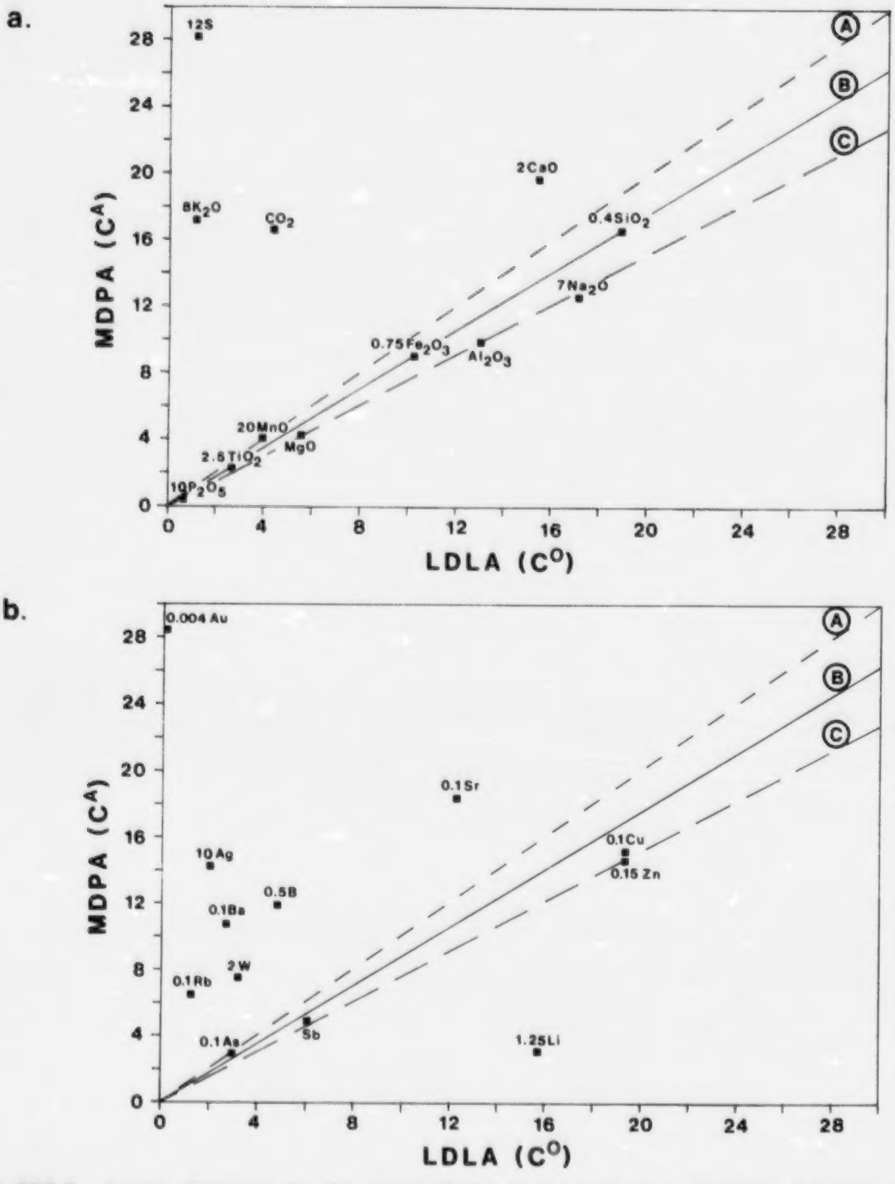

Figure 323.3. *Isocon diagrams for the major elements (a) and trace elements (b) from least deformed, least altered (LDLA) basaltic wall rocks in DDH NC-29 and their most deformed, pervasively altered (MDPA) equivalents. Lines "A", "B", and "C" represent represent respectively the constant mass, best fit, and constant Al_2O_3 isocons. C^O and C^A refer to the original and altered rock compositions.*

On the basis of the best-fit isocon, the mobile components introduced during hydrothermal alteration and gold deposition were (in order of their degree of enrichment; *see* Table 323.1): Au, S, K, Ag, Rb, Ba, CO_2, B, W, Sr, Ca, and Mn. Conversely, the mobile components that were lost were (in order of their degree of depletion; *see* Table 323.1): Li, Na, Zn, Al, Mg, P, Sb, and Cu. The precision for some of the elements of the present study is such that the changes calculated for Mn, P, Sb, Ag, and W should, however, be interpreted with caution. Otherwise the gains and losses are consistent with the mineralogical changes that accompanied the alteration at Cameron Lake: the addition of Ca, CO_2, and K to the host rocks resulted in carbonatization and sericitization, and the addition of S and Au to the system produced the pyritization and gold mineralization.

Of the elements analyzed there are several that, by virtue of their chemical properties (ionic radius, ionic potential, electronegativity), would be expected to exhibit evidence of geochemical coupling during fluid transport and fluid-rock interaction. Consequently, the similar patterns of behaviour of pairs of ele-

TABLE 323.2: SULPHUR ISOTOPE RATIOS IN PYRITES FROM GOLD OCCURRENCES IN THE CAMERON - ROWAN LAKES AREA.

SAMPLE	LITHOLOGY/ALTERATION	d^{34}S$_{CDT}$
Cameron Lake deposit		
RPT-2FPV	breccia vein, fragment	2.1, 2.7
RPT-5WP	pervasively altered basalt	0.2, 0.8
RPT-7FPV	breccia vein, fragment	2.1
RPT-10WP	pervasively altered basalt	1.9
RPT-13WP	pervasively altered basalt	1.8
RPT-21WP	pervasively altered gabbro	0.1
RPT-41WP	pervasively altered basalt	1.4
RPT045FP	breccia vein, fragment	3.2, 3.4
RPT=57WP	breccia vein, fragment	3.7
RPT-63WP	breccia vein, fragment	3.2
Victor Island prospect		
RPT-37WP	breccia vein, fragment	2.3
RPT-38WP	pervasively altered basalt	-0.5
RPT-39WP	breccia vein, fragment	2.3
Monte Cristo prospect		
RPT-31PV	breccia vein, matrix	3.1
RPT-32WP	pervasively altered basalt	2.9
RPT-35WP	pervasively altered basalt	2.9, 3.0
Wampum Lake prospect		
RPT-25FP	breccia vein, fragment	0.9
RPT-26PV	breccia vein, matrix	1.0

Note: all isotopic values are reported in per mil relative to the Canyon Diable meteorite (CDT) international reference standard (O'Neil 1986).

ments such as K and Rb, Ca and Sr, and Ag and Au (Figure 323.3) lend further support to the validity of the interpretations based upon the best-fit isocon.

Similar elemental gains and losses have been recognized in studies of other areas of Archean gold deposits in shear zones, for example: on a deposit scale, Fyon and Crocket (1982) recognized gains in CO_2, and K and Rb, that accompanied pervasive carbonate and alkali metasomatism associated with gold mineralization in the Timmins area; and on a regional scale, Kerrich (1986) and Colvine *et al.* (1988) have documented that the rocks in mineralized faults typically possess enrichments of K, Rb, Cs, B, CO_2, Au, Ag, and W.

SULPHUR ISOTOPE COMPOSITIONS OF PYRITE

Pyrite samples for isotopic analysis were separated from (1) breccia vein fragments, and (2) pervasively altered wall rocks, by microdrilling, and were purified using conventional methods. Sulphur isotope ratio measurements were made at the Ottawa–Carleton Geoscience Centre Stable Isotope Facility using conventional procedures (Faure 1986), after the conversion of the sulphide to SO_2 gas by reaction with CuO at 1000°C. The results of the sulphide analyses are presented in Table 323.2 and include, in addition to the Cameron Lake analyses, some preliminary data from the Victor Island, Monte Cristo, and Wampum Lake gold prospects.

At Cameron Lake, pyrite $\delta^{34}S$ values range from 3.7 to 0.1 per mil, with the breccia vein fragments consistently having heavier $\delta^{34}S$ values (from 3.7 to 2.1 per mil) than the pyrite samples from the pervasively altered basaltic wall rocks (from 1.9 to 0.2 per mil) (Figure 323.4). Mean values for the two groups are: breccia veins ($n=7$, $x=2.9\pm0.6$ per mil) and pervasively altered wallrocks ($n=5$, $x=1.2\pm0.6$ per mil). Although the data for the other gold occurrences located within the Monte Cristo and related shear zones (Figure 323.2) are of a preliminary nature, they show both the same overall range of pyrite $\delta^{34}S$ (from 3.1 to -0.5 per mil), and the trend to higher values in breccia vein samples (Figure 323.4).

CARBON AND OXYGEN ISOTOPE COMPOSITIONS OF CARBONATES

Carbonate samples (typically ankerites) for isotopic analysis were separated by microdrilling from carefully selected samples of vein and alteration material. After separation they were purified by conventional methods, and their composition verified by X-ray diffraction. Carbon and oxygen isotope ratio measurements were made at the Ottawa–Carleton Geoscience Centre Stable Isotope Facility using conventional procedures (Craig 1957; Faure 1986), after a selective chemical separation that involved the sequential extraction of CO_2 at 50°C using 100 percent phosphoric acid (Al-Aasm *et al.* 1988). The results of the carbonate analyses are presented in Table 323.3, and in addition to the Cameron Lake data, include some preliminary data for other gold occurrences in the Cameron–Rowan Lakes area.

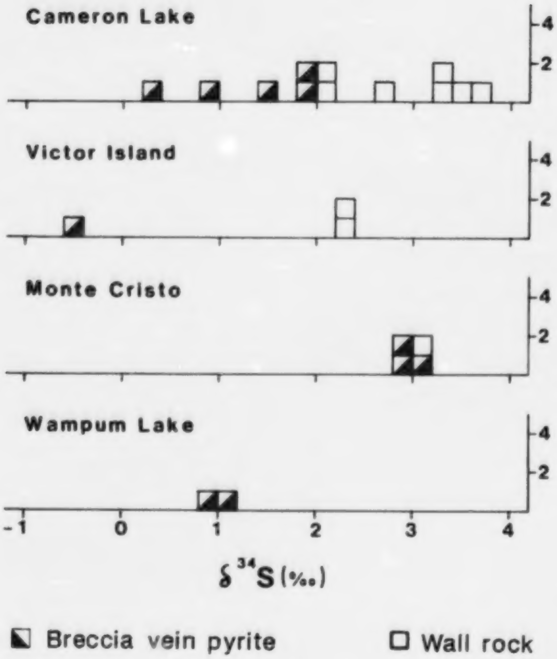

Figure 323.4. *Histogram of $\delta^{34}S$ diagrams (in per mil relative to the CDT international standard) for selected pyrites (see Table 323.2) from the Cameron Lake Deposit and the other gold prospects in the Cameron–Rowan Lakes area.*

Most relevant to the current report are the analyses of ankerite from (1) the matrices of gold-bearing breccia veins, and (2) their enclosing pervasive alteration. These data are illustrated in Figures 323.5 and 323.6. At the Cameron Lake Deposit, the $\delta^{13}C$ values (n=13) show a considerable range from 0.0 to -5.9 per mil. Although the gold-bearing vein samples have a heavier mean $\delta^{13}C$ value (x=-1.9±1.1 per mil, n=7) than their pervasively altered host rocks (x=-3.0±1.3 per mil, n=6), there is a considerable overlap (Figures 323.5 and 323.6) with 10 of the 13 ankerites having values between -1.8 and -3.2 per mil. Fyon *et al.* (1983a) and Fyon (1986) have documented variations in $\delta^{13}C$ of a similar magnitude from alteration zones in the Timmins camp, with the $\delta^{13}C$ of carbonate in wall rocks in discrete zones of carbonatization varying from about -4 per mil adjacent to a quartz vein in the ankerite-bearing rocks, to 0 per mil at the perimeter (chlorite + calcite-bearing rocks) of the zone. Such variations have been attributed to fractionation between reduced and oxidized carbon species and/or to Rayleigh fractionation during fluid-rock interaction (Fyon 1986). Carbonaceous rocks have not been identified in the Cameron Lake area, and therefore it is more likely that the variation in $\delta^{13}C$ is in part related to fluid-rock exchange during alteration. The $\delta^{13}C$ analyses of ankerites from the other gold occurrences fall within the range of values from the Cameron Lake Deposit (Figure 323.5).

In contrast to the $\delta^{13}C$ values, the $\delta^{18}O$ data for the gold-bearing veins and pervasive alteration at Cameron Lake (1) have a much more restricted range, with values from 10.2 to 12.6 per mil; and (2) do not show any degree of separation, with both the gold-bearing veins (x=11.8±0.7 per mil, n=7), and the pervasively altered host rocks (x=11.7±0.3 per mil, n=6) having nearly identical values (Figure 323.6).

DISCUSSION

Both the mineralogical and chemical data for the gold-bearing pervasively altered basaltic host rocks and the gold-bearing breccia veins, that collectively comprise the Cameron Lake Deposit, are consistent with the operation of chemical reactions of the type proposed by Phillips *et al.* (1986) for mafic host rock alteration in Archean gold deposits.

$$\underset{\text{magnetite}}{Fe_3O_4} + \underset{\text{fluid}}{3CO_2} = \underset{\text{siderite}}{3FeCO_3} + \underset{\text{fluid}}{1/2O_2} \qquad (1)$$

$$\underset{\text{fluid}}{H_2S} + 2O_2 = \underset{\text{fluid}}{H_2SO_4} \qquad (2)$$

$$\underset{\text{in wall rock}}{FeO} + \underset{\text{fluid}}{2H_2S} + \underset{\text{fluid}}{1/2O_2} = \underset{\text{pyrite}}{FeS_2} + \underset{\text{fluid}}{2H_2O} \qquad (3)$$

The breakdown of chlorite during hydrothermal alteration produces ankerite and/or siderite without any redox change. In contrast, the carbonatization of magnetite involves the reduction of wall rock iron (Equation 1), leading to fluid oxidation and the conversion of some reduced sulphur to sulphate (Equation 2). Thus the sulphate/sulphide ratio in the fluid will increase during the carbonatization of magnetite-bearing wall rock assemblages and through the deposition of pyrite (i.e. sulphidization; *see* Equation 3). Such reactions, even if accompanied by the removal of iron from ankerite to form pyrite (cf. Phillips and Brown 1987) require no introduction

TABLE 323.3: CARBON AND OXYGEN ISOTOPE RATIOS IN CARBONATES FROM GOLD OCCURRENCES IN THE CAMERON - ROWAN LAKE AREAS.

SAMPLE	LITHOLOGY/ALTERATION	MINERAL	d^{13}C$_{CDT}$	d^{18}O$_{SMOW}$
Cameron Lake deposit				
RPT-1MV	breccia vein, matrix	ankerite	-0.9	12.0
RPT-3FV	breccia vein, matrix	ankerite	0.0	12.0
RPT-4W	pervasively altered basalt	ankerite	-2.6	11.8
RPT-8FV	breccia vein, matrix	ankerite	-1.9	12.3
RPT-9W	pervasively altered basalt	ankerite	-2.4	11.2
RPT-12MV	auriferous vein	ankerite	-3.2	11.5
RPT-17MV	auriferous vein	ankerite	-1.8	12.6
RPT-19W	pervarively altered basalt	ankerite	-2.6	12.1
RPT-20W	pervasively altered gabbro	ankerite	-2.5	11.5
RPT-22W	pervasively altered gabbro	ankerite	-2.1	12.2
RPT-42WC	pervasively altered basalt	ankerite	-5.9	12.0
RPT-48C	incipiently altered basalt	ankerite	-1.5	11.8
RPT-49C	incipiently altered basalt	ankerite	-3.8	8.8
RPT-52WC	altered amygdule in basalt	ankerite	-3.1	12.8
RPT-53WC	pervasively altered basalt	ankerite	-2.3	11.5
RPT-54WC	amygdule in basalt	calcite	-0.2	10.2
RPT-55WC	pervasively altered basalt	ankerite	-2.0	11.4
RPT-58WC	breccia vein, matrix	ankerite	-3.2	10.2
RPT-64WC	breccia vein, matrix	ankerite	-2.6	12.2
Meston prospect				
RPT-67FC	breccia vein, fragment	ankerite	-2.8	12.6
Victor Island prospect				
RPT-36V	post-mineralization vein	ankerite	-4.7	10.5
RPT-44FC	breccia vein, fragment	ankerite	-1.8	11.5
Monte Cristo prospect				
RPT-28V	post-mineralization vein	ankerite	2.4	12.2
RPT-34V	auriferous vein	ankerite	-2.0	11.0
RPT-62WC	incipiently altered basalt	ankerite	-4.5	6.7
Wampum Lake prospect				
RPT-50FC	breccia vein, fragment	ankerite	-1.6	11.1

Note: all isotopic values are reported in per mil relative to either Reedee Belemnite (PDB) or Standard Mean Ocean Water (SMOW) international reference standards (O'Neil 1986). Conversion of d^{18}O from PDB to SMOW was accomplished by using the equation given by Friedman and O'Neil (1977).

$$\begin{aligned} &\text{chlorite} + 1.39\text{albite} + \underset{\text{fluid}}{1.1K^{+}} + \underset{\text{fluid}}{4.7Ca^{+2}} + \underset{\text{fluid}}{2.1(X)^{+2}} + \underset{\text{fluid}}{11.9CO_2} + \underset{\text{fluid}}{3.8H_2O} \\ &= 1.1\text{muscovite} + 3.9\text{quartz} + 5.9\text{ankerite} + \underset{\text{fluid}}{1.4Na^{+}} + \underset{\text{fluid}}{13.3H^{+}} \end{aligned} \tag{4}$$

of iron from an external fluid source. Similarly, although titanium is released during the alteration of magnetite, it is likely to be fixed immediately, *in situ*, in the rutile which is a ubiquitous component of the pervasive alteration at Cameron Lake (Melling *et al.* 1986), rather than be lost to the mobile fluid. Both elements are therefore effectively "immobile" during host rock alteration.

Ankerite and siderite are important minerals which characterize the pervasively altered rocks at Cameron Lake. This is typical of many Archean gold deposits where carbonate minerals display a symmetrical zonation with respect to gold zones; a feature attributed to alteration intensity and the amount of CO_2 available during carbonatization. Calcite is common in less altered rocks furthest from areas of

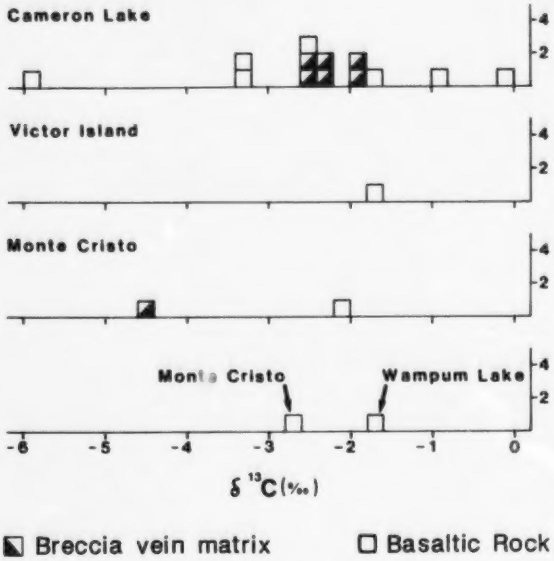

Figure 323.5. *Histogram of $\delta^{13}C$ values (in per mil relative to the PDB international standard) for selected ankerite samples (see Table 323.3) from the Cameron Lake Deposit and the other gold prospects in the Cameron–Rowan Lakes area.*

gold concentration, but gives way to ankerite and siderite in the central portions of the gold zones (Figure 323.2) (Fyon and Crocket 1982; Fyon *et al.* 1983b; Burrows and Spooner 1986).

Together with the iron-bearing carbonates and pyrite, sericite is the other major mineral phase that characterizes the pervasive alteration assemblage surrounding the gold-bearing breccia veins at Cameron Lake (Figure 323.2). Questions remain concerning the relative timing of sericitization and carbonatization in Archean vein-type deposits. At the Kerr–Addison Deposit (Downes 1980), and in the Timmins area (Fyon *et al.* 1983a), "potassic alteration" or the formation of muscovite has been interpreted as postdating "carbonatization". Conversely, many authors (Boyle 1961; Kerrich 1983; Kerrich and Fyfe 1981) consider them to be essentially synchronous in their development.

The paragenetic relationships at Cameron Lake are complex and not yet fully understood; however, there is no evidence to suggest that carbonatization and sericitization were produced by discrete hydrothermal events. Sericite is particularly abundant in areas of highest strain, and does not display any apparent zonation with respect to shear zone geometry, as do the carbonate minerals (Figure 232.2). Kishida and Kerrich (1987), in a detailed study of the textural and mass balance relations of alteration at the Kerr–Addison Deposit, demonstrate the intimate relation of carbonatization and sericitization, and conclude that the formation of muscovite/sericite is simply part of the conversion of chlorite to ankerite.

Reaction 4 requires the addition of large amounts of K^+, Ca^{2+}, and CO_2 from the hydrothermal fluid.

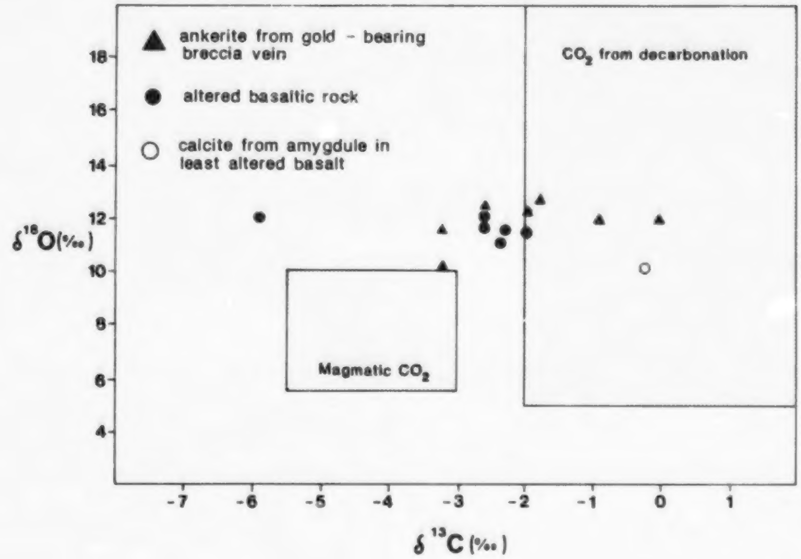

Figure 323.6. *Plot of $\delta^{13}C_{PDB}$ versus $\delta^{18}O_{SMOW}$ for selected carbonate samples (see Table 323.3) from the Cameron Lake Deposit. The shaded fields represent the estimated ranges for magmatic CO_2 (from Taylor 1986) and for CO_2 generated by decarbonation reactions during metamorphism (from Valley 1986).*

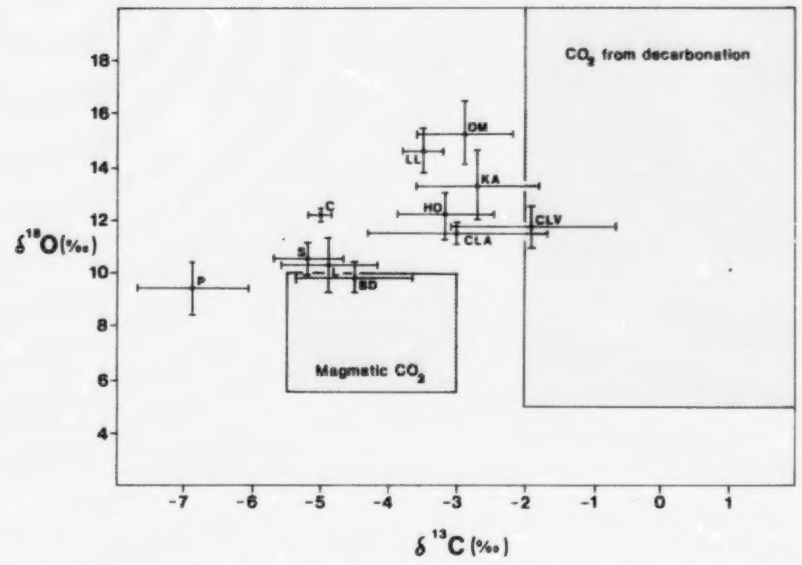

Figure 323.7. *Plot of $\delta^{13}C_{PDB}$ versus $\delta^{18}O_{SMOW}$ showing the mean values for samples of gold-bearing breccia veins (CLV) and pervasively altered basaltic rocks (CLA) from the Cameron Lake Deposit (this study). Also shown for comparison are mean values for ferroan dolomite samples from the Pascalis (P), Sigma (S), Lamaque (L), and Bras D'Or (BD) mines in the Val D'Or district; from the Cheminis (C), Omega (OM), Larder Lake (LL), and Kerr–Addison (KA) mines in the Larder Lake district; and from the Hollinger mine (HO) in the Timmins area (from Kerrich et al. 1987). The bars represent one standard deviation about the mean. The fields for magmatic and metamorphic CO_2 are identical to those in Figure 323.6.* ·

The wall rock alteration process results in the release of H^+ to the fluid, with variable losses or gains of X (Fe, Mg, or Mn) in conjunction with exchanges of K^+ for Na^+ (Kishida and Kerrich 1987). The release of H^+ during progressive alteration acts to reduce fluid pH.

The results of the lithogeochemical study and isocon analysis of the pervasive alteration that surrounds gold mineralization at Cameron Lake are entirely consistent with the processes of hydrothermal alteration of mafic rocks outlined above (equations 1 through 4). Large additions of CO_2, Ca, K, and S accompany the introduction of gold via a fluid of external derivation, with Ti, total Fe, and Si remaining constant during fluid-rock interaction (Figure 323.3). A necessary consequence of such alteration processes is a changing fluid composition, either to lower pH (as a result of carbonate-sericite alteration), and/or to a more oxidized condition (as a result of the sulphidation of magnetite). Assuming T=300°C (cf. Kerrich 1987), and that H_2S dominates sulphide speciation, both processes could result in a significant reduction in the solubility of gold (Seward 1984; Henley *et al.* 1984).

Although little is presently known about the nature and derivation of the ore fluid at Cameron Lake, and also about the influence of boiling on fluid evolution (cf. Drummond and Ohmoto 1985), the results of the sulphur isotope analyses are compatible at least with the oxidation of the hydrothermal fluid during pyrite deposition. The $\delta^{34}S$ values of pyrite from the breccia veins, and their pervasively altered host basalts (Figure 323.4), show a significant variation (from 3.7 to 0.2 per mil), with the altered wall rocks typically having the lighter values. Within the pH range of muscovite/sericite stability, and the fO_2 range of pyrite stability at these temperatures, fluid oxidation could affect such a change in the $\delta^{34}S$ of pyrite (Ohmoto 1972; Rye and Ohmoto 1974); given the close textural relationship between pyrite and gold at Cameron Lake (Melling *et al.* 1986), such a process might also have contributed directly to a reduction in the solubility of gold in the hydrothermal fluid, and hence to gold deposition.

The mean $\delta^{13}C$ value of -2.7 per mil for the ankerites from the Cameron Lake Deposit suggests a carbon isotope signature that is distinct from other Archean gold deposits (Figure 323.7). However, Rayleigh fractionation or mixing with host rock calcite (calcite $\delta^{13}C$=-0.2 per mil; *see* Table 323.3) during fluid-rock interaction may well have produced a trend to ^{13}C-enriched carbonates (Figure 323.6). Consequently, the initial $\delta^{13}C$ value of the hydrothermal fluid at Cameron Lake may have been lighter than -3 per mil, a fact supported by the occurrence of three ankerites with $\delta^{13}C$ values in the range -3.0 to -6.0 per mil (Figure 323.4). Such values are consistent with CO_2 derived from a magmatic reservoir (Figure 323.6), and, given the ambient fluid conditions typical of many Archean gold deposits (cf., Colvine *et al.* 1988), may provide an accurate reflection of the initial composition of the hydrothermal fluid at Cameron Lake.

ACKNOWLEDGMENTS

The authors are indebted to Mr. H.D. Hume and Mr. G.F. Archibald of Nuinsco Resources Limited for allowing this study to be undertaken, and for providing field accommodation and unrestricted access to data on the Cameron Lake gold deposit. Parts of this project were financially supported by Ontario Geoscience Research Grant 323 to R.P. Taylor, and through the generosity of Nuinsco Resources Limited.

REFERENCES

Al-Aasm, I.S., Taylor, B.E., and South, B.
1988: Chemical Separation Techniques Appraisal for Isotopic Analysis of Multiple Carbonate Samples; Geological Association of Canada, Mineralogical Association of Canada, Canadian Society of Petroleum Geologists, Program with Abstracts, Volume 13, p.A2.

Boyle, R.W.
1961: The Geology, Geochemistry, and Origin of Gold Deposits of the Yellowknife District; Canadian Geological Survey Memoir 310, 260p.

Buck, S.
1986: Metallogenetic Studies in the Kakagi–Rowan Lakes Area, District of Kenora; p.261-265 *in* Summary of Field Work and Other Activities, by the Ontario Geological Survey, edited by P.C. Thurston, O.L. White, R.B. Barlow, M.E. Cherry, and A.C. Colvine, Ontario Geological Survey Miscellaneous Paper 132, 435p.

Burrows, D.R., and Spooner, E.T.C.
1986: The McIntyre Cu-Au Deposit, Timmins, Ontario, Canada; p.23-39 *in* Proceedings of Gold '86: An International Symposium on the Geology of Gold, edited by A.J. Macdonald, Toronto, 517p.

Chivers, K.M.
1986: Geology of the Brooks Bay Area, District of Kenora; p.52-56 *in* Summary of Field Work and Other Activities, by the Ontario Geological Survey, edited by P.C. Thurston, O.L. White, R.B. Barlow, M.E. Cherry, and A.C. Colvine, Ontario Geological Survey Miscellaneous Paper 132, 435p.

Colvine, A.C., Fyon, J.A., Heather, K.B., Marmont, S., Smith, P.M., and Troop, D.G.
1988: Archean Lode Gold Deposits in Ontario; Ontario Geological Survey Miscellaneous Paper 139, 136p.

Craig, H.
1957: Isotopic Standards for Carbon and Oxygen and Correction Factors for Mass Spectrometric Analysis of Carbon Dioxide; Geochimica et Cosmochimica Acta, Volume 12, p.133-149.

Downes, M.J.
1980: Structural and Stratigraphic Aspects of Gold Mineralization in the Larder Lake Area, Ontario; p.66-70 *in* Genesis of Archean, Volcanic-Hosted Gold Deposits, Symposium Held at the University of Waterloo, March 7, 1980, Ontario Geological Survey Miscellaneous Paper 97, 175p.

Drummond, S.E., and Ohmoto, H.
1985: Chemical Evolution and Mineral Deposition in Boiling Hydrothermal Systems; Economic Geology, Volume 80, p.126-147.

Faure, G.
1986: Principles of Isotope Geology; John Wiley Sons, New York, 589p.

Friedman, I., and O'Neil, J.R.
1977: Compilation of Stable Isotope Fractionation Factors of Geochemical Interest; Data of Geochemistry, United States Geological Survey Professional Paper 440-KK, 12p.

Fyon, J.A.
1986: Field and Stable Isotope Characteristics of Carbonate Alteration Zones, Timmins Area; Unpublished Ph.D. Thesis, McMaster University, Hamilton, Ontario, 399p.

Fyon, J.A., and Crocket, J.H.
1982: Gold Exploration in the Timmins District Using Field and Lithogeochemical Characteristics of Carbonate Alteration Zones; p.113-129 *in* Geology of Canadian Gold Deposits, edited by R.W. Hodder and W. Petruk, Canadian Institute of Mining and Metallurgy Special Volume 24, 286p.

Fyon, J.A., Crocket, J.N., and Schwarcz, H.P.
1983a: Ontario Geoscience Research Grant Program, Grant No. 49, Application of Stable Isotopes to Gold Metallogeny in the Timmins–Porcupine Camp; Ontario Geological Survey Open File Report 5464, 182p., 9 tables, 23 figures and 16 maps in back pocket.

Fyon, J.A., Crocket, J.N., and Schwarcz, H.P.
1983b: Magnetite Abundance as a Guide to Gold Mineralization Associated with Ultramafic Flows, Timmins Area; Journal of Geochemical Exploration, Volume 18, p.245-266.

Grant, J.A.
1986: The Isocon Diagram—A Simple Solution to the Gresens' Equation for Metasomatic Alteration; Economic Geology, Volume 81, p.1976-1982.

Gresens, R.L.
1967: Composition-Volume Relationships of Metasomatism; Chemical Geology, Volume 2, p.47-55.

Henley, R.W., Truesdell, A.H., and Barton, P.B.
1984: Fluid-Mineral Equilibria in Hydrothermal Systems; Reviews in Economic Geology, Volume 1, 267p.

Johns, G.W.
1986: Kakagi Lake–Rowan Lake Regional Geology, District of Kenora; p.47-51 *in* Summary of Field Work and Other Activities 1986, by the Ontario Geological Survey, edited by P.C. Thurston, O.L. White, R.B. Barlow, M.E. Cherry, and A.C. Colvine, Ontario Geological Survey Miscellaneous Paper 132, 435p.

Kerrich, R.
1983: Geochemistry of Gold Deposits in the Abitibi Greenstone Belt; Canadian Institute of Mining and Metallurgy Special Paper 27, 75p.
1986: Fluid Transport in Lineaments; Philosophical Transactions of the Royal Society of London, Volume A317, p.219-251.

1987: The Stable Isotope Geochemistry of Au-Ag Vein Deposits in Metamorphic Rocks; p.287-336 *in* Short Course in Stable Isotope Geochemistry of Low Temperature Fluids, Mineralogical Association of Canada, Volume 13, 452p.

Kerrich, R., Fryer, B.J., King, R.W., Willmore, L.M., and van Hees, E.

1987: Crustal Outgassing and LILE Enrichment in Major Lithosphere Structures, Archean Abitibi Greenstone Belt: Evidence of Source Reservoir from Strontium and Carbon Isotope Tracers; Contributions to Mineralogy and Petrology, Volume 97, p.156-168.

Kerrich, R., and Fyfe, W.S.

1981: The Gold-Carbonate Association: Source of CO_2, and Fixation of CO_2 *in* Archean Lode Deposits; Chemical Geology, Volume 33, p.265-294.

Kishida, A., and Kerrich, R.

1987: Hydrothermal Alteration Zoning and Gold Concentration at the Kerr–Addison Archean Lode Gold Deposit, Kirkland Lake, Ontario; Economic Geology, Volume 82, p.649-690.

Melling, D.R.

1986: The Geological Setting, Structure, and Alteration Associated With Gold-Pyrite Mineralization at Cameron Lake, Wabigoon Subprovince, Northwestern Ontario; Unpublished M.Sc. Thesis, Carleton University, Ottawa, Ontario, 112p.

1987: The Occurrence of Gold in the Cameron–Rowan Lakes Area: Preliminary Report on the Monte Cristo and Victor Island Gold Prospects in the Monte Cristo Shear Zone; p.252-260 *in* Summary of Field Work and Other Activities 1986, by the Ontario Geological Survey, edited by P.C. Thurston, O.L. White, R.B. Barlow, M.E. Cherry, and A.C. Colvine, Ontario Geological Survey Miscellaneous Paper 132, 435p.

1988: The Geological Setting and Distribution of Gold in the Cameron–Rowan Lakes Area, Northwestern Ontario, With Special Emphasis on the Victor Island and Monte Cristo Gold Prospects; Ontario Geological Survey Open File Report. In Press.

Melling, D.R., Blackburn, C.E., Parker, J.H., and Watkinson, D.H.

1988: The Geological Setting and Distribution of Gold in the Cameron–Rowan Lakes Area: Implications for Exploration Models in the Western Wabigoon Subprovince of the Canadian Shield; Canadian Journal of Earth Sciences. In Press.

Melling, D.R., and Watkinson, D.H.

1986: The Geological Setting and Genesis of the Cameron Lake Gold Deposit; Grant 193, p.27-35 *in* Geoscience Research Grant Program, Summary of Research 1985-1986, edited by V.G. Milne, Ontario Geological Survey Miscellaneous Paper 130, 235p.

Melling, D.R., Watkinson, D.H., Poulsen, K.H., and Chorlton, L.B.

1985: The Geological Setting and Genesis of the Cameron Lake Gold Deposit; Grant 193, p.136-150 *in* Geoscience Research Grant Program, Summary of Research 1984-1985, edited by V.G. Milne, Ontario Geological Survey Miscellaneous Paper 127, 246p.

Melling, D.R., Watkinson, D.H., Poulsen, K.H., Chorlton, L.B., and Hunter, A.D.

1986: The Cameron Lake Gold Deposit, Northwestern Ontario, Canada: Geological Setting, Structure, and Alteration; p.149-169 *in* Proceedings of Gold'86 Symposium, edited by A.J. Macdonald, Toronto, 517p.

Ohmoto, H.

1972: Systematics of Sulphur and Carbon Isotopes in Hydrothermal Ore Deposits; Economic Geology, Volume 67, p.551-578.

O'Neil, J.R.

1986: Terminology and Standards; p.561-570 *in* Stable Isotopes in High Temperature Geological Processes, edited by J.W. Valley, H.P. Taylor, and J.R. O'Neil, Reviews in Mineralogy, Mineralogical Society of America, Volume 16, 570p.

Phillips, G.N., and Brown, I.J.

1987: Host Rock and Fluid Control on Carbonate Assemblages in the Golden Mile Dolerite, Kalgoorlie Gold Deposits, Australia; Canadian Mineralogist, Volume 25, p.265-273.

Phillips, G.N., Groves, D.I., Neall, F.B., Donnelly, T.H., and Lambert, I.B.

1886: Anomalous Sulphur Isotope Compositions in the Golden Mile, Kalgoorlie, Australia; Economic Geology, Volume 81, p.2008-2015.

Rye, R.O., and Ohmoto, H.

1974: Sulphur and Carbon Isotopes and Ore Genesis: A Review; Economic Geology, Volume 69, p.826-842.

Seward, T.M.

1984: The Transport and Deposition of Gold in Hydrothermal Systems; p.165-182 *in* Proceedings of Gold '82: The Geology, Geochemistry, and Genesis of Gold Deposits, edited by R.P. Foster, Geological Society of Zimbabwe, Special Publication Number 1, 753p.

Taylor, B.E.

1986: Magmatic Volatiles: Isotopic Variation of C, H, and S; p.185-225 *in* Stable Isotopes in High Temperature Geological Processes, edited by J.W. Valley, H.P. Taylor, and J.R. O'Neil, Reviews in Mineralogy, Mineralogical Society of America, Volume 16, 570p.

Valley, J.W.

1986: Stable Isotope Geochemistry of Metamorphic Rocks; p.445-489 *in* Stable Isotopes in High Temperature Geological Processes, edited by J.W. Valley, H.P. Taylor and J.R. O'Neil, Reviews in Mineralogy, Mineralogical Society of America, Volume 16, 570p.

MAPS
NOT
FILMED

CARTES
OMISES